

# UC Irvine

## UC Irvine Electronic Theses and Dissertations

### Title

The Total Synthesis of Pleuromutilin and Radical–Polar Crossover Reactions of Allylic Alcohols

### Permalink

<https://escholarship.org/uc/item/96c8272n>

### Author

Foy, Nicholas Jordan

### Publication Date

2022

### Copyright Information

This work is made available under the terms of a Creative Commons Attribution-NonCommercial License, available at <https://creativecommons.org/licenses/by-nc/4.0/>

Peer reviewed|Thesis/dissertation

UNIVERSITY OF CALIFORNIA, IRVINE

The Total Synthesis of Pleuromutilin  
and  
Radical–Polar Crossover Reactions of Allylic Alcohols

DISSERTATION

submitted in partial satisfaction of the requirements  
for the degree of

DOCTOR OF PHILOSOPHY

in Chemistry

By

Nicholas Jordan Foy

Dissertation committee:  
Professor Sergey V. Pronin, Chair  
Professor Larry E. Overman  
Professor Christopher D. Vanderwal

2022

Portions of Chapter 3 were reproduced with permission from: Touney, E.E.; Foy, N. J.; Pronin, S. V. *J. Am. Chem. Soc.* **2018**, *140*, 1692. © 2018 American Chemical Society

All other materials © 2022 Nicholas J. Foy

## **DEDICATION**

To my parents, for their understanding and support.

## TABLE OF CONTENTS

	Page
LIST OF FIGURES	v
LIST OF SCHEMES	vi
LIST OF TABLES	ix
ACKNOWLEDGEMENTS	x
VITA	xi
ABSTRACT OF THE DISSERTATION	xii
CHAPTER 1: THE MUTILIN DITERPENES	1
1.1. Isolation and Structure Determination	1
1.2. Biosynthesis	1
1.3. Biological Activity	4
1.4. Semi-Synthesis	8
1.5. Total Synthesis	14
1.6. References	33
CHAPTER 2: A SYNTHETIC APPROACH TO THE PLEUROMUTILIN DITERPENES	37
2.1. Synthetic Considerations & Analysis of Prior Art	37
2.2. Retrosynthetic Analysis	38
2.3. Synthesis of a Key Tricyclic Sub-Target	39
2.4. Scouting a Synthetic Strategy Relying on Cyclobutanol Oxidation	46
2.5. Scouting a Synthetic Approach Relying on Nucleophilic Addition to C14	54
2.6. Implementation of an Ester as a C14 Functional Handle	62
2.7. Synthesis of Pleuromutilin	74
2.8. Conclusion	89
2.9 Experimental Section	91
2.9.1. Materials & Methods	91
2.9.2. Experimental Procedures	92

2.9.3. Experimental Procedures for Computations in Figure 2.3	189
2.9.4. Experimental Procedures for Table 2.2	190
2.10. References	191
CHAPTER 3: RADICAL–POLAR CROSSOVER REACTIONS OF ALLYLIC ALCOHOLS	197
3.1. Markovnikov-Selective Radical Alkene Hydrofunctionalization	197
3.2. Radical–Polar Crossover Reactions of Allylic Alcohols	199
3.3. Catalyst Control Over Reaction Outcome & Mechanistic Implications	202
3.4. Conclusion	205
3.5. Experimental Section	206
3.5.1. Materials & Methods	206
3.5.2. Experimental Procedures	207
3.6. References	238
APPENDIX A: NMR SPECTRA FOR CHAPTER 2	242
APPENDIX B: COMPUTATIONAL DATA FOR CHAPTER 2	342
APPENDIX C: X-RAY CRYSTALLOGRAPHIC DATA FOR CHAPTER 2	354
APPENDIX D: NMR SPECTRA FOR CHAPTER 3	481

## LIST OF FIGURES

Figure 1.1. Pleuromutilin, mutilin, and the mutilin skeleton with Arigoni's numbering	1
Figure 1.2. A. The pleuromutilin biosynthetic gene cluster B. Biosynthetic intermediates isolated from heterologous expression in <i>A. oryzae</i>	4
Figure 1.3. Retapamulin bound to the bacterial ribosome	6
Figure 1.4. Pleuromutilin derivatives that are approved as antibacterial agents	7
Figure 1.5. Naturally occurring mutilin derivatives	33
Figure 1.6. Natural products with a glycolate function	34
Figure 2.1. Pleuromutilin, mutilin, the cyclooctane domain, and the hydrindanone nucleus	37
Figure 2.2. A. Regioselectivity in cyclobutanol ring-expansions B. Hypothetical cyclobutanol-containing intermediates	47
Figure 2.3. Computed lowest energy conformers of enols <b>2.125</b> and <b>2.126</b>	76
Figure 2.4. Models of relevant conformers	189

## LIST OF SCHEMES

Scheme 1.1. The biosynthesis of mutilin and pleuromutilin	2
Scheme 1.2. Isotopic labelling feeding studies by Arigoni and Birch	3
Scheme 1.3. Substitution of the C22 hydroxyl group	9
Scheme 1.4. Replacement of the C14 glycolate residue	9
Scheme 1.5. Berner, Schulz, and Schneider's 1,5-hydride shift	10
Scheme 1.6. Some ring scission reactions discovered by Arigoni's laboratory	11
Scheme 1.7. Some transannular reactions of the mutilin system	12
Scheme 1.8. Transannular hydride shifts observed by Birch and co-workers	13
Scheme 1.9. Gibbons' synthesis of mutilin and pleuromutilin	16
Scheme 1.10. Paquette and co-workers' synthesis of lactone <b>1.51</b>	17
Scheme 1.11. Paquette and co-workers' attempts to prepare a mutilin cyclooctane	18
Scheme 1.12. Paquette and co-workers' attempts to use photoisomerization to form the C9–C10 bond	19
Scheme 1.13. Boeckman, Springer, and Alessi's synthesis of pleuromutilin	21
Scheme 1.14. Bacque, Pautrat, and Zard's approach to the mutilin skeleton	22
Scheme 1.15. Liu, Lotesta, and Sorensen's RCM approach to the mutilin framework	23
Scheme 1.16. Liu, Lotesta, and Sorensen's second RCM approach to the mutilin framework	24
Scheme 1.17. Sorensen and co-workers' NHK approach to truncated pleuromutilins	25
Scheme 1.18. Fazakerley, Helm, and Procter's synthesis of mutilin and pleuromutilin	27
Scheme 1.19. Murphy, Zeng, and Herzon's synthesis of pleuromutilin	29
Scheme 1.20. Farney, Feng, Schäfers, and Reisman's synthesis of pleuromutilin	32
Scheme 2.1. Comparison of classical and modern approaches to mutilin synthesis	38
Scheme 2.2. Identification of a synthetic strategy	39
Scheme 2.3. Preparation of enone <b>2.9</b> and silyloxydiene <b>2.13</b>	40
Scheme 2.4. Early hit for cycloaddition of enone <b>2.9</b> and silyloxydiene <b>2.13</b>	40
Scheme 2.5. A. Optimized Diels–Alder reaction B. Isomerization of <i>endo</i> and <i>exo</i> diastereomers <b>2.14</b> and <b>2.18</b>	41
Scheme 2.6. A. Reductive cyclization of enone <b>2.18</b> B. Major deleterious pathway C. Radical–polar crossover reactivity	44



Scheme 2.7. Giese cyclization-Mukaiyama hydration cascade	45
Scheme 2.8. Synthesis of homopropargyl ketone <b>2.35</b>	48
Scheme 2.9. A. Synthesis of cyclobutanol <b>2.36</b> and attempted oxidation B. Synthesis of iodide <b>2.38</b> and <i>syn</i> -elimination	49
Scheme 2.10. Synthesis of cyclopropyl ketone <b>2.40</b> and two possible mechanisms	50
Scheme 2.11. Synthesis of hydroxycyclopropane <b>2.44</b> and envisioned ring-expansion to form ketone <b>2.47</b>	51
Scheme 2.12. A. The unexpected formation of tetracyclic ketone <b>2.49</b> B. Proposed mechanism	52
Scheme 2.13. Synthesis of vinylcyclopropane <b>2.54</b> and cyclooctanone <b>2.55</b>	53
Scheme 2.14. A. Steric challenges faced in C14 functionalization B. Plan of action	54
Scheme 2.15. A. Failed oxidative cleavage of the C11-C14 bond B. Synthesis of lactone <b>2.64</b>	55
Scheme 2.16. Methallylation of aldehyde <b>2.64</b> and facile dehydration	56
Scheme 2.17. A. Envisioned cyclobutanediol assembly B. Intramolecular ketone allylation	57
Scheme 2.18. Swern oxidation and synthesis of enoxysilane <b>2.73</b>	58
Scheme 2.19. A. Envisioned Sequence B. Challenges of identifying a suitable nucleophile C. Plan of action	59
Scheme 2.20. Methallylation of ketone <b>2.73</b>	59
Scheme 2.21. Synthesis of diketone <b>2.86</b>	60
Scheme 2.22. Synthesis of homoallylic alcohol <b>2.88</b> and 1,4-silane transfer	61
Scheme 2.23. Synthesis of chloroketone <b>2.90</b>	61
Scheme 2.24. Synthesis of oxasilepine <b>2.91</b> and attempted intramolecular Sakurai addition	62
Scheme 2.25. Carboxylation of enone <b>2.18</b> and unexpected endoperoxide synthesis	63
Scheme 2.26. A. Synthesis of fluoroenone <b>2.98</b> B. Chlorination of ketoester <b>2.93</b> C. Ketalization of ketoester <b>2.93</b>	64
Scheme 2.27. MHAT cyclization of ketoester <b>2.101</b> and synthesis of enol ether <b>2.103</b>	65
Scheme 2.28. Synthesis of lactone <b>2.92</b> and deprotonation studies	66
Scheme 2.29. Synthesis of the ketoester <b>2.108</b> and attempted annulation	67
Scheme 2.30. Synthesis of the cyclobutanol <b>2.113</b>	68

Scheme 2.31. Synthesis of the cyclooctanone <b>2.114</b> and retro-Michael fragmentation	69
Scheme 2.32. A. Envisioned alkylation sequence B. <sup>1</sup> H NMR of cyclobutanol <b>2.113</b> and enone <b>2.114</b>	70
Scheme 2.33. A. Cyclooctane conformers B. Conformers of ketone <b>2.114</b> C. Conformers of ketone <b>2.119</b>	71
Scheme 2.34. A. Synthesis of enone <b>2.119</b> B. <sup>1</sup> H NMR comparison of <b>2.120</b> and <b>2.119</b>	73
Scheme 2.35. Synthesis of ketone <b>2.121</b> and attempted oxidative cleavage	74
Scheme 2.36. Synthesis of the ketone <b>2.124</b>	75
Scheme 2.37. A. Unexpected transannular aldol B. Unexpected formal retro-[2+2]	77
Scheme 2.38. A. Preparation of cyanofornate <b>2.131</b> B. Synthesis of <b>2.136</b>	78
Scheme 2.39. Synthesis of ketoacid <b>2.138</b>	79
Scheme 2.40. Proposed mechanism for the formation of triketone <b>2.140</b>	82
Scheme 2.41. A. Planned epimerization of C10 vs. retro-Michael B. X-ray structure of ketone <b>2.140</b>	83
Scheme 2.42. Synthesis of chlorocyclobutanol <b>2.149</b>	85
Scheme 2.43. Synthesis of chlorotriene <b>2.150</b> and epimerization at C10	86
Scheme 2.44. Synthesis of methoxyketone <b>2.154</b>	87
Scheme 2.45. Synthesis of mutilin <b>2.2</b> and pleuromutilin <b>2.1</b>	88
Scheme 2.46. Preliminary mechanistic hypothesis for reduction of trione <b>2.146</b>	89
Scheme 2.47. Total synthesis of mutilin <b>2.2</b> and pleuromutilin <b>2.1</b>	91
Scheme 3.1. A. Acid-mediated alkene hydrofunctionalization B. MHAT alkene hydrofunctionalization	197
Scheme 3.2. Shigehisa's radical-polar crossover reactions	198
Scheme 3.3. Initial hit for bifurcated reactivity dependent on catalyst structure by Eric Touney	199
Scheme 3.4. Catalyst control over the outcome of MHAT RPC reactions of alcohol <b>3.55</b>	203
Scheme 3.5. Proposed mechanism for the conversion of allylic alcohols into epoxides or semi-pinacol adducts	204
Scheme 3.6. Stereochemical model for ring-expansion stereoselectivity	205

## LIST OF TABLES

Table 2.1. Oxidation of enoxysilanes <b>2.14</b> and <b>2.15</b>	43
Table 2.2. Optimization of a decarboxylative oxygenation of cyclobutanol <b>2.139</b>	81
Table 3.1. Optimization of catalyst-controlled MHAT RPC reactions of allylic alcohols	200
Table 3.2. Scope of catalyst-controlled MHAT RPC reactions of allylic alcohols	202

## ACKNOWLEDGEMENTS

I am deeply indebted to a number of people for their support, guidance, insight, and friendship during the past five years for the completion of this dissertation.

It's been an honor to work with my advisor, Professor Sergey Pronin. I will always be grateful that you accepted me into your research group. I'll carry the approach to chemistry and problem solving you've taught me for the rest of my career. I am leaving UCI with a confidence that I can stand up to whatever challenges may lie ahead because of the high standard you have held me to. Your relentlessness and passion for chemistry are second to none.

I owe no small part of my success to the guidance of my other two committee members, Professors Larry Overman and Chris Vanderwal. As successful and prolific as you both have been over your careers, I am consistently impressed by the attention and care you put into supporting myself and other students in the chemistry program.

There is one person to thank for setting me onto the path of graduate school and pursuit of organic chemistry, my undergraduate mentor Professor Jeff Cannon. I am thankful for you taking a chance on me and showing me what it means to be a dedicated scientist. You are truly excellent at what you do, and there is nobody else who provides the education that you do to undergraduates interested in organic chemistry research.

I would like to thank the many outstanding colleagues I've had in the Pronin lab. When I first joined the group, Chris Discolo, Steve Holmbo, and Eric Kuenstner taught me an incredible amount about how to be a successful researcher. Eric Touney, your willingness to invite me onto your project during my second year will always be appreciated. Chuck Dooley and Will Thomas, your chemistry insights have often helped me to tackle problems on my project, and I have the highest respect for both of you as scientists and people.

I would like to thank my parents, Susan and Kerry, my sister Lauren, and my grandparents Chuck and Peggy, and all the rest of my family for their love and support.

To my friends: thank you for your companionship and for giving me an outlet when I was away from the lab. Whether it was enjoying a fine Nicolas Cage film, playing basketball, or just sitting around and joking, I value every minute I was able to spend with you.

Lastly, I would like to thank my partner, Julia DeRogatis. You made life enjoyable and always cared for me. I wouldn't have made it through graduate school with a positive outlook if it wasn't for you. I'm so proud of how much you've accomplished, and I can't wait to continue our lives together.

I have permissions to use published materials in this dissertation.

**VITA**  
**NICHOLAS J. FOY**

**EDUCATION**

University of California, Irvine Irvine, CA  
Ph.D. Candidate in Chemistry (expected graduation June 2022) 2017-current  
3.88/4.00 GPA

Occidental College Los Angeles, CA  
Bachelor of Arts in Chemistry with Honors and ACS Certification 2013-2017  
3.78/4.00 GPA, *Magna Cum Laude*

**HONORS & AWARDS**

NSF Graduate Research Fellowship Honorable Mention 2017  
ACS Most Outstanding Organic Chemistry Student, Occidental College 2017

**RESEARCH**

Graduate Student in Organic Chemistry, University of California, Irvine 2017-2022  
Supervisor: Prof. Sergey Pronin

Undergraduate Researcher in Organic Chemistry, Occidental College 2015-2017  
Supervisor: Prof. Jeffrey Cannon

**PUBLICATIONS**

Synthesis of Pleuromutilin. Nicholas J. Foy and Sergey V. Pronin\* *Submitted* 2022

Catalytic Radical–Polar Crossover Reactions of Allylic Alcohols. Eric E. Touney, Nicholas J. Foy, and Sergey V. Pronin\* *J. Am. Chem. Soc.* **2018**, *140*, 16982–16987 2018

Dual Lewis Acid/Photoredox-Catalyzed Addition of Ketyl Radicals to Vinylogous Carbonates in the Synthesis of 2,6-Dioxabicyclo[3.3.0]octan-3-ones. Nicholas J. Foy, Katherine C. Forbes, Anne Marie Crooke, Maxwell D. Gruber, and Jeffrey S. Cannon\* *Org. Lett.* **2018**, *20*, 5727–5731 2018

**PROFESSIONAL PRESENTATIONS**

American Chemical Society National Meeting, San Francisco – Poster 2017

**PROFESSIONAL AFFILIATIONS**

Alpha Chi Sigma, Beta Mu Chapter 2017

## ABSTRACT OF THE DISSERTATION

The Total Synthesis of Pleuromutilin  
and  
Radical–Polar Crossover Reactions of Allylic Alcohols

by

Nicholas J. Foy

Doctor of Philosophy in Chemistry

University of California, Irvine, 2022

Professor Sergey V. Pronin, Chair

This dissertation details the development of a synthetic route to the pleuromutilin diterpenes and the discovery of catalyst-controlled radical–polar crossover reactions of allylic alcohols. Chapter one outlines the isolation and structure determination, biosynthesis, and antimicrobial activity of the pleuromutilins. Additionally, analysis of the unique chemistries and existing synthetic approaches to the mutilin diterpenoids is provided. Chapter two delineates our analysis of the pleuromutilin structure and execution of a new synthetic approach. Beginning with our early attempts to assemble the polycyclic architecture, the evolution of our strategy through three distinct phases is described. The culmination of these studies is a 16-step stereocontrolled synthesis of pleuromutilin, the shortest to date. Chapter three is comprised of relevant background to Markovnikov-selective radical hydrofunctionalization reactions and our laboratory's studies on the radical–polar crossover reactions of allylic alcohols. Our observation of previously unprecedented catalyst control over the radical–polar crossover reactions of dialkyl(vinyl)carbinols is outlined.

## CHAPTER 1: THE MUTILIN DITERPENES

### 1.1. Isolation and Structure Determination

The mutilin diterpenoids are a small family of natural products originally isolated in the early 1950s by Kavanagh and co-workers.<sup>1</sup> Kavanagh's team demonstrated that the culture liquids of mycelia from the *Pleurotus* genus of gilled mushrooms inhibited the growth of Gram-positive bacteria. They further isolated the antibacterial substance as a crystalline solid and named it pleuromutilin. Among the observations they reported was the elimination of antibiotic activity that pleuromutilin suffered upon heating in the presence of aqueous base. Though it was unknown to them at the time, the authors were performing hydrolysis of the glycolic acid residue present in pleuromutilin **1.1**, now understood to be essential for antibiotic activity, thereby converting it into its parent diterpene mutilin **1.2** (Figure 1.1).<sup>2,3</sup> Efforts to elucidate the structure of pleuromutilin **1.1** followed shortly, with Anchel reporting in 1952 that it is a neutral substance with two hydroxyl functionalities and the chemical formula  $C_{22}H_{34}O_5$ .<sup>4</sup> It was not until the early 1960s that the groups of Arigoni and Birch independently solved the puzzle of pleuromutilin's structure.<sup>5,6</sup> Their assignment was unambiguously confirmed in 1975, when a bromoacetate derivative of mutilin was characterized by X-ray crystallographic analysis.<sup>7</sup> In the decades since, a large body of literature has grown around the study of mutilins, inspired by the useful bioactivity and exceptionally compelling structure of this small family of natural products.

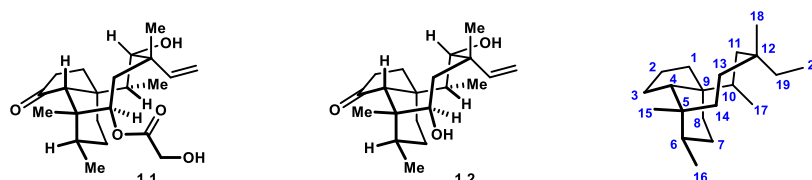


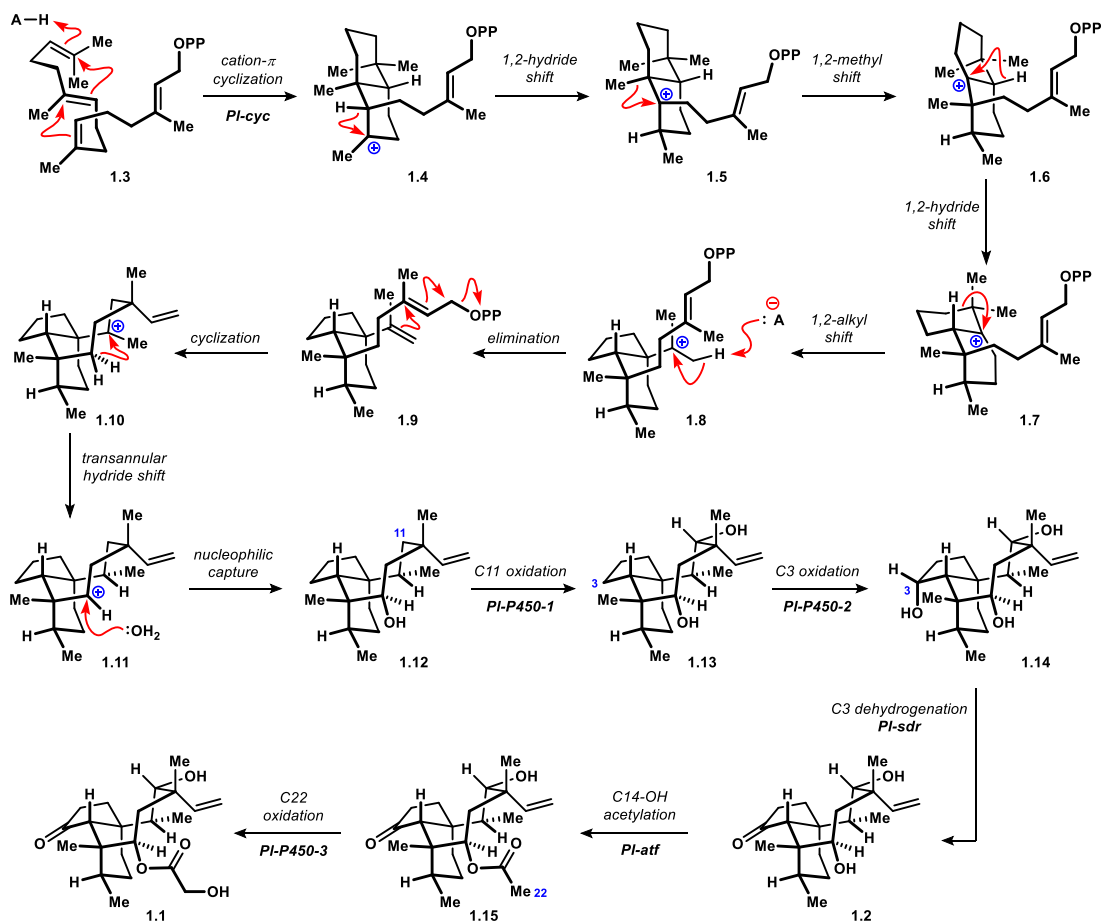
Figure 1.1. Pleuromutilin **1.1**, mutilin **1.2**, and the mutilin skeleton with Arigoni's numbering

### 1.2. Biosynthesis

The groups of both Arigoni and Birch reported feeding studies that provided insights into pleuromutilin's biosynthetic origin.<sup>4,5</sup> More recent work from Foster's laboratory in 2016 identified the gene cluster responsible for the biosynthesis of pleuromutilin.<sup>8</sup> These experiments

culminated in the following biosynthetic proposal: geranylgeranyl pyrophosphate **1.3** initially undergoes a cation- $\pi$  bicyclization mediated by the enzyme pleuromutilin-cyclase (PI-cyc) to afford labdenyl cation **1.4** (Scheme 1.1). A series of rearrangements is initiated by a 1,2-hydride shift, generating intermediate **1.5**. Subsequently, a 1,2-methyl shift and second 1,2-hydride shift

**Scheme 1.1.** The biosynthesis of mutilin **1.2** and pleuromutilin **1.1**

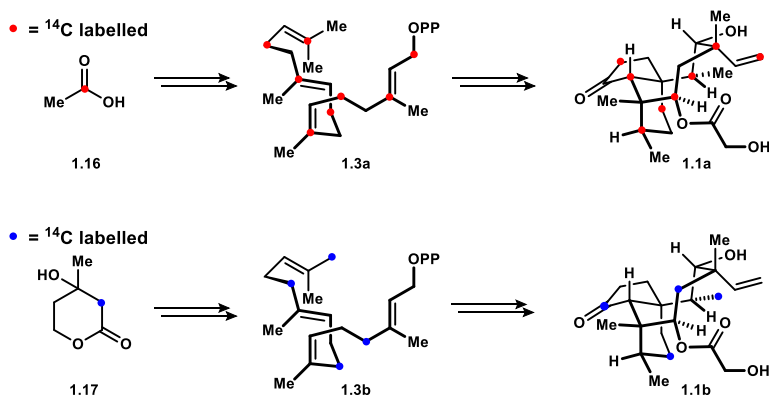


occur to produce a new carbocation **1.7**, setting the stage for ring-contraction. A Wagner–Meerwein shift precedes elimination, quenching the cationic charge and generating perhydroindene **1.9**. The final ring of the pleuromutilin tricyclic core is formed via cyclization initiated at the isopropenyl moiety contained within **1.9**. The tertiary carbocation formed from cyclization undergoes a transannular hydride shift in a contra-thermodynamic fashion. The resulting in the secondary carbocation **1.11** is next captured by water, furnishing so-called premutilin **1.12**. With the mutilin skeleton assembled, several enzymes decorate it with



oxidation. First, C11 is oxidized by pleuromutilin-P450-1 (PI-P450-1) to the produce diol **1.13**. The next site of oxidation (PI-P450-2) is at C3, affording the triol **1.14**, which is further dehydrogenated by pleuromutilin dehydrogenase (PI-sdr) to afford mutilin **1.2**.<sup>9</sup> The C14 hydroxyl group is subsequently adorned with the glycolic ester sidechain by initial acetylation by pleuromutilin-acetyl transferase (PI-attf) and a final C22–H hydroxylation (PI-P450-3) to afford pleuromutilin **1.1**.

**Scheme 1.2.** Isotopic labelling feeding studies by Arigoni and Birch



Initial support for the accepted biosynthetic hypothesis was provided by Arigoni and Birch. Some of the most compelling evidence is derived from feeding studies, wherein both groups employed the same isotopic labelling scheme. In one experiment, <sup>14</sup>C-labelled acetic acid **1.16** was fed to a pleuromutilin-producing organism (Scheme 1.2). According to the biosynthesis outlined above (Scheme 1.1), this feeding study is expected to produce pleuromutilin with carbons isotopically labelled at the sites marked in red on **1.1a**. In another experiment, <sup>14</sup>C-labelled mevalonic lactone **1.17** was used. In this feeding study, the biosynthesis predicts that the pleuromutilin obtained would be labelled at the sites marked in blue on **1.1b**. The laboratories of Arigoni and Birch degraded labelled pleuromutilin to examine the extent of isotopic incorporation at each expected position, lending support to the proposal.<sup>10</sup>

In 2016, the Foster group identified the gene cluster responsible for pleuromutilin biosynthesis and isolated several biosynthetic intermediates (Figure 1.2A).<sup>8</sup> Seven enzymes were found to be upregulated during production of pleuromutilin **1.1** in *C. passeckerianus*: a

geranylgeranyl pyrophosphate synthetase (*Pl-ggs*), a cyclase (*Pl-cyc*), an acetyl transferase (*Pl-atf*), a short-chain dehydrogenase / reductase (*Pl-sdr*), and three cytochrome P450s (*Pl-P450-1*, *Pl-P450-2*, and *Pl-P450-3*). Heterologous expression of the identified gene cluster in *A. oryzae* produced pleuromutilin **1.1**, indicating that the team had accurately identified the pleuromutilin gene cluster. The same group subsequently observed formation of premutilin **1.12** upon expression of *Pl-ggs* and *Pl-cyc* in *A. oryzae*, thereby confirming it to be the first biosynthetic intermediate prepared by the cyclase enzyme.<sup>11</sup> Expression of *Pl-ggs*, *Pl-cyc*, and *Pl-P450-1* in an analogous experiment led to the formation of biosynthetic intermediate **1.13**. Further including *Pl-P450-2* afforded the triol **1.14**. Lastly, incorporating the related dehydrogenase, *Pl-sdr*, led to the production of mutilin **1.2** by *A. oryzae*. To confirm their findings, the authors prepared authentic samples of the purported biosynthetic intermediates **1.12**, **1.13**, and **1.14** from the commercially available mutilin, tiamulin (Figure 1.2B). Remarkably, five genes are responsible for the construction of the complex diterpene scaffold of **1.1**. Finally, the enzymes *Pl-atf* and *Pl-p450-3* were found to be responsible for introduction of the glycolic ester moiety present in pleuromutilin **1.1** by initial acetylation followed by P450-mediated oxidation. Recently, Peters and co-workers observed the formation of tricyclic alcohol **1.12** following expression of pleuromutilin diterpene cyclase enzymes in *Escherichia coli*.<sup>12</sup>

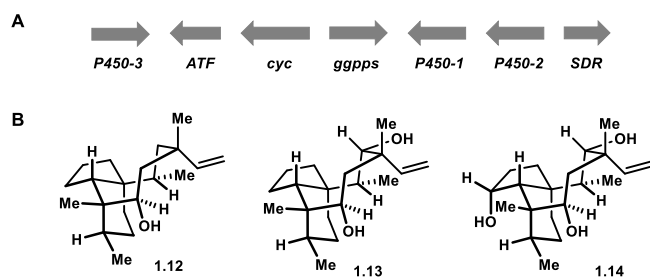


**Figure 1.2.** A. The pleuromutilin biosynthetic gene cluster  
 B. Biosynthetic intermediates isolated from heterologous expression in *A. oryzae*

### 1.3. Biological Activity

Pleuromutilin has received significant attention due to its potent antibiotic activity against Gram-positive bacteria and low mammalian toxicity.<sup>13</sup> Pleuromutilins act by disabling the

bacterial ribosome, inhibiting protein synthesis.<sup>14</sup> Specifically, they target the central part of domain V of the 50s ribosomal subunit at the peptidyl transferase center (PTC).<sup>15</sup> This mode of action is unique among ribosomally targeted inhibitors. X-ray crystallographic structures of pleuromutilins in complex with the 50s ribosomal subunit of *Deinococcus radiodurans* have shed light on the key interactions of pleuromutilins with the PTC (Figure 1.3).<sup>16</sup> The tricyclic diterpenoid core interacts with the ribosomal nucleotides via hydrophobic interactions and van der Waal forces, blocking the A-site of the PTC. Hydrogen bonds from the C11 hydroxyl group with nucleotides G2505 or A2503 have been implicated. Acylation of the C14 hydroxyl as is present in pleuromutilin **1.1** is required for antibacterial activity, as the glycolic ester group, or other suitable C14-appendage, is responsible for blocking the P-site of the PTC. The C21 ester group of the C14-sidechain is seen to hydrogen bond with the nucleotide G2061. Improved activity can be attained by appending hydrogen bond donors to the C14-sidechain. Amino groups have served this role in many pleuromutilin derivatives that have advanced to market as antibacterials (see *below*). The improved binding efficiency in these cases is believed to arise from hydrogen bonding of the amino groups with A2062.<sup>16b,17</sup> The C14 side chains also sterically clash with U2585 and U2506, causing distortions of their native conformation that incurs additional stabilizing interactions between the two nucleotides.

While inhibition of the bacterial ribosome is common to many classes of antibiotics, pleuromutilins exhibit no cross-resistance with macrolide,  $\beta$ -lactam, fluoroquinolone, and tetracycline antibacterial agents, due to their unique binding site. Coupled *in vitro* transcription/translation assays with bacterial ribosomes have demonstrated that pleuromutilins are highly selective for inhibition of bacterial protein translation relative to eukaryotic protein synthesis (>2000 fold activity).<sup>17</sup> This unique property indicates that bacterial resistance against pleuromutilins is much slower to develop when compared with other common antibiotic classes.<sup>14</sup> Resistance to pleuromutilins has, nonetheless, been observed, and the mechanisms of resistance continue to be studied.<sup>18</sup> The three mechanisms of resistance that have been

observed are due to mutations at the 23s rRNA and *rpjC* genes, methylation of the nucleotide A2503, and drug efflux by ATP-binding cassette transporters.<sup>13</sup> Worry has been expressed that the extensive use of pleuromutilins in livestock production will lead to widespread pleuromutilin-resistant bacteria.<sup>19</sup>

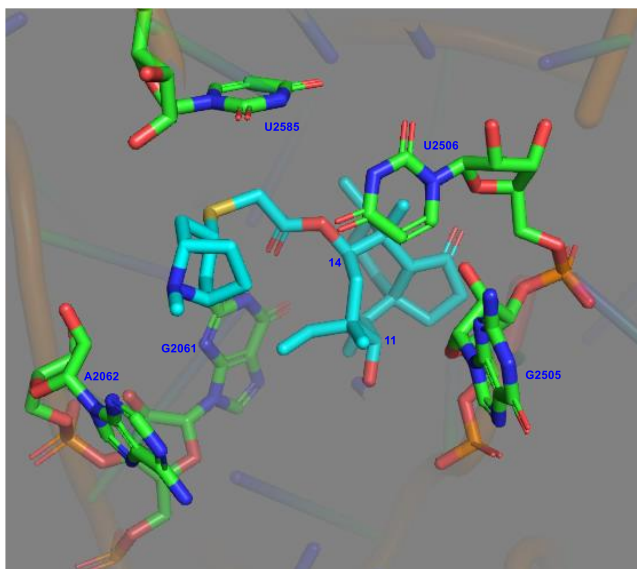


**Figure 1.3.** Retapamulin bound to the bacterial ribosome. Image created with PyMOL from PDB ID "2OGO."

Several semi-synthetic derivatives of natural pleuromutilin are used to treat bacterial infections in clinical settings (Figure 1.4). The first pleuromutilin to see use in medicine was tiamulin **1.18**, the fumaric acid salt of which is marketed as Denegard®. It is deployed as a veterinary antibiotic primarily in swine and poultry, both as a treatment and as a prophylactic, to prevent swine dysentery and conditions arising from mycoplasma infections (e.g., bacterial pneumonia and chronic respiratory disease).<sup>20</sup> Tiamulin **1.18** was first prepared in 1975 by workers at Sandoz Pharmaceutical Company in Austria during a survey of pleuromutilin side-chain derivatives.<sup>21</sup> The structure of the second pleuromutilin to be commercialized, valnemulin **1.19**, first appeared in the patent literature from Sandoz in the 1980s.<sup>22</sup> In the late 1990s, its hydrochloride salt was marketed by Novartis as Econor® and has since been used to combat mycoplasma infections in swine.<sup>23,24</sup> Generally, valnemulin **1.19** exhibits superior activity *in vitro* and *in vivo* than tiamulin **1.18**.<sup>25</sup> Though it is predominantly a veterinary antibiotic, valnemulin

has been successfully used to treat multi-drug resistant mycoplasma infections in immunocompromised human patients.<sup>26</sup> Efforts in the 20<sup>th</sup> century to identify pleuromutilins for use in human medicine were mostly unsuccessful. While one dihydropleuromutilin derivative, the azole azamulin (not shown graphically), did advance to Phase 1 trials with the United States Food and Drug Administration (USFDA) in the 1980s, it failed to advance further when it was found to irreversibly inhibit human cytochrome P450 CYP3A.<sup>27</sup> It wasn't until 2007, with the development of retapamulin **1.20** by GlaxoSmithKline, that a pleuromutilin derivative received approval from the USFDA for human use.<sup>28</sup> Retapamulin, marketed as Altabax®, is effective in topical applications, treating skin and soft tissue infections.<sup>29</sup> One key feature of this therapy is the maintained potency observed by **1.20** against methicillin-, erythromycin-, mupirocin-, and oxacillin-resistant strains of *Staphylococci* and *Streptococci*.<sup>30</sup> Workers at Nabriva have recently developed the first pleuromutilin that is employed as a systemic antibiotic in human medicine.<sup>31</sup> The compound, named lefamulin **1.21**, is marketed as Xenleta® and used to treat community-acquired bacterial pneumonia. It received USFDA approval in 2019.<sup>32</sup>

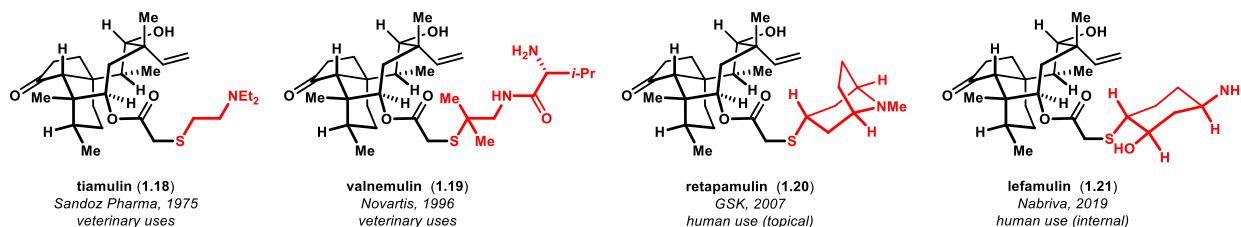


Figure 1.4. Pleuromutilin derivatives that are approved as antibacterial agents

Structurally, all the pleuromutilins that currently see use as therapeutics are derivatized from the natural product only on the glycolic ester side chain at C22 (Figure 1.3, highlighted in red). In all cases, the 1° alcohol that exists in the natural product is replaced with a thioether linkage that appends a new group containing polar functionalities. These C22-substituted derivatives are the most thoroughly explored semi-synthetic pleuromutilins (see below). Pleuromutilin derivatives for systemic use have, until recently with the invention of lefamulin **1.21**, been more elusive. Some have hypothesized that this is due to the proclivity of the

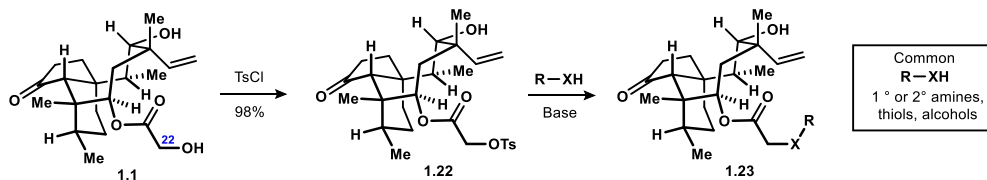
diterpenoid framework to undergo oxidation by cytochrome P450 enzymes *in vivo*, generating hydroxylated derivatives with poor antibiotic activity.<sup>33</sup> Most commonly, C2 and C8 are found to undergo P450-catalyzed hydroxylation, and when isolated, these derivatives do indeed suffer erosion of antibiotic activity. Work from Yang demonstrated that fluorination of the C2 position can modestly improve the activity of pleuromutilins.<sup>34</sup> Further, some semi-synthetic pleuromutilins with an epimeric configuration at the C12 center have been shown to effectively kill Gram-negative pathogens.<sup>35</sup> These two examples demonstrate that improving the therapeutic profile of the pleuromutilins is possible by modifying the diterpenoid core. Despite promising preliminary results, pleuromutilin derivatives containing deep-seated alterations have been slow to develop, presumably due to the challenges posed by their chemical synthesis.

#### **1.4. Semi-Synthesis**

Pleuromutilin semi-synthesis is a rich field of research with a long history stretching back to the 1950s. While Kavanagh and Anchel both disclosed some degradation studies, Arigoni and Birch's pioneering work outlined a large number of semisynthetic reactions that describe many of the key reactivity modes; ring contractions, ring scissions, and transannular hydride shifts being most prevalent among them.<sup>4,5,6</sup> The chemistry outlined by the two academic laboratories set the stage for groups in industry to spearhead pleuromutilin semi-synthesis efforts, with a large number of publications and patents originating from the group at Sandoz Pharmaceuticals during the 1970s and 1980s. Valuable contributions were provided during the 1990s and 2000s by workers at GlaxoSmithKline and Bristol-Myers Squibb, prior to the closure of both companies' programs aimed at the development of antibacterial compounds. Encouragingly, efforts by academic laboratories to investigate manipulations of the pleuromutilin scaffold have increased in recent years. Many of the semi-synthetic manipulations of pleuromutilin were described in an excellent 2014 review by Fazakerley and Procter.<sup>36</sup> The following discussion will outline some of the key contributions and highlight common and

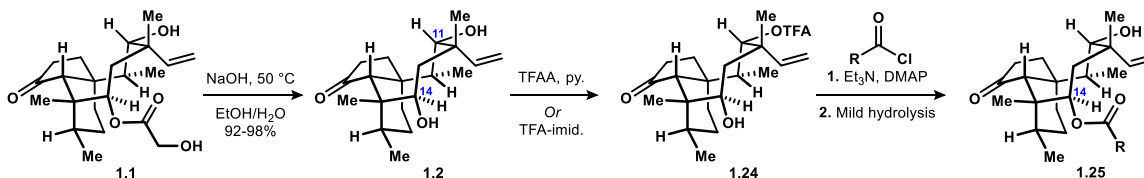
important modes of reactivity within the mutilin scaffold but will not exhaustively examine the mutilin semi-synthetic literature.

**Scheme 1.3.** Substitution of the C22 hydroxyl group



The most extensively studied group of pleuromutilin derivatives are the C22 functionalized compounds (Scheme 1.3). One of the reasons for the prevalence of these structures is their ease of preparation. Additionally, the groups appended to the C22 position have been found to be extremely important to the observed biological activity, as first reported by Egger and Reinshagen.<sup>37</sup> Indeed, modifications of C22 have been the engine behind medicinal chemistry campaigns involving pleuromutilin, as evidenced by the fact that all of the currently approved pleuromutilin-derived antibacterials are modified exclusively at the C22 position. The C22-OH group can be selectively sulfonlated to afford tosylate **1.22**, as was first demonstrated by Riedl.<sup>38</sup> Subsequent reaction with a nucleophile in the presence of base can deliver a host of C22 amines, sulfides, and ether products **1.23**. Similarly, the tosylate can be leveraged into a facile Finkelstein reaction to afford the more reactive iodide when necessary.<sup>39</sup>

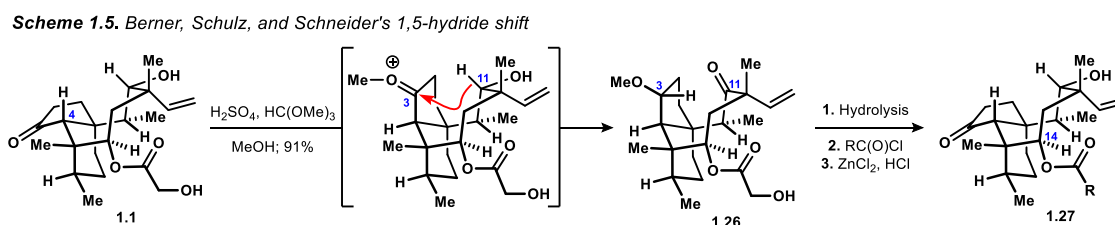
**Scheme 1.4.** Replacement of the C14 glycolate residue



Hydrolysis of pleuromutilin **1.1** to mutilin **1.2** was the first semi-synthetic manipulation of pleuromutilin ever reported (Scheme 1.4). It is still relevant to modifying the core structure, as mutilin can be a valuable starting point for derivatization. The large difference in the relative reactivities of the two remaining hydroxyl moieties positioned at C11 and C14 can be leveraged into selective functionalizations. To this end, the more reactive C11 hydroxyl is typically

substituted with a readily hydrolyzable group, such as trifluoroacetate.<sup>40</sup> Subsequent reaction of the C14–OH group, followed by selective hydrolysis at C11–OH enables the net exchange of the glycolic acid fragment for a group of the chemists' choosing. Notably, workers at SmithKline Beecham leveraged this approach to prepare a number of mutilin C14 carbamates.<sup>40,41</sup>

An alternative approach to the selective derivatization of the C14 hydroxyl group utilizes a powerful transformation first disclosed by Berner, Schulz, and Schneider (Scheme 1.5).<sup>42</sup> The team found that exposure of pleuromutilin to H<sub>2</sub>SO<sub>4</sub> with trimethyl orthoformate produced in high yield the methoxy derivative **1.26**. Presumably, the mechanism includes epimerization of the C4 center followed by 1,5-hydride shift to an intermediate oxocarbenium ion by the C11 methine. Crucially, the reaction proceeds to re-distribute the oxidation states of the C11 and C3 positions, while simultaneously capping the resulting C3 hydroxyl group as its methyl ether. As a result, hydrolysis of the glycolate residue delivers intermediates containing only one reactive hydroxyl group, which resides at C14. In many cases, substitution of the C14–OH functionality proceeds in a straightforward fashion. Next, the hydride shift can be reversed by exposure to ZnCl<sub>2</sub> and HCl in a typically high-yielding process to deliver desired products **1.27**. The same reactivity is observed when mutilin is used as the starting point rather than pleuromutilin. This strategy was employed alongside the approach shown in Scheme 1.4 by the SmithKline workers in their preparation of mutilin C14 carbamates.<sup>43</sup> Additionally, several reports have explored the reactivity of the C11 ketone **1.26** that results from the 1,5-hydride shift.<sup>44</sup>

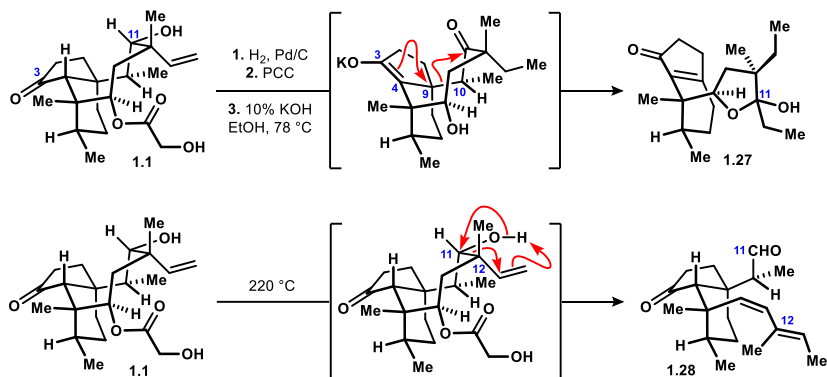


The densely functionalized nature of the mutilin system introduces interactions between the functional groups adorning the tricyclic system, which has led to the identification of some transannular reactions; most prevalent among them have been hydride shifts and some C–C



bond forming processes. Similarly, the ring strain inherent to pleuromutilin's contained 8-membered carbocyclic motif renders it susceptible to ring scission reactions. In addition to the semi-synthetic investigations, these modes of reactivity have played a large role in the total synthesis efforts toward the pleuromutilins. A few notable examples of each type of reactivity are presented here.

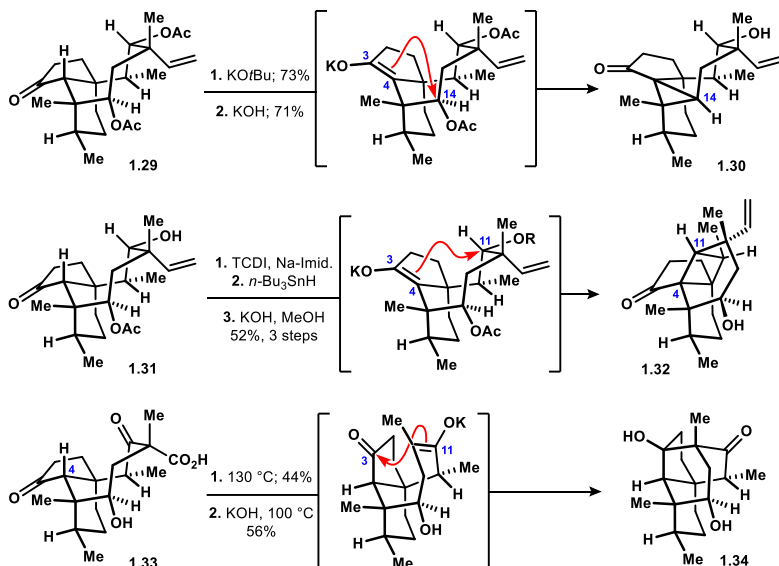
**Scheme 1.6.** Some ring scission reactions discovered by Arigoni's laboratory



The earliest reports of ring scission reactions were described by Arigoni's laboratory in the early 1960s. Most were identified during degradation of the natural product as a part of their studies directed at solving the pleuromutilin structure. Curiously, some of the fascinating reactions discovered in Arigoni's laboratory were never published, to my knowledge, outside of the dissertations of his students Nägeli, Buzzolini, Hasler, and Bonavia.<sup>5</sup> The most commonly observed ring scission reaction in the mutilin system is a retro-Michael process that is available to the 1,5-oxidation pattern connecting the ketone at C3 to the C11 hydroxyl group (Scheme 1.6). Following oxidation of the C11 hydroxyl group of pleuromutilin **1.1**, hydrogenation preceded treatment of the intermediate diketone by Arigoni's team with NaOH and heating. Enolization of the C3 ketone at the C4 position enabled scission of the C9–C10 bond by the retro-Michael process, affording after hemiketalization the tetrahydroindanone **1.27**. Arigoni's group also observed opening of the pleuromutilin eight-membered ring by breaking the C11–C12 bond. Hasler and Buzzolini found that thermolysis of pleuromutilin induced a retro-

carbonyl ene reaction, furnishing the bicyclic aldehyde **1.28** after elimination of the glycolate function. Other related products deriving from the retro-carbonyl ene were also observed.

**Scheme 1.7.** Some transannular reactions of the mutilin system

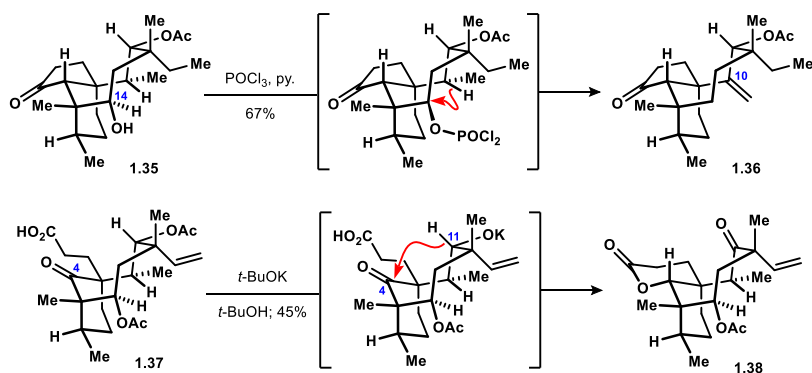


Among the many transannular reactions reported within the mutilin system, some of the most useful ones have been the formation of fused cyclopropane derivatives **1.30** (Scheme 1.7). First identified by the team at SmithKline Beecham, enolization of the C3 ketone at C4 with the C14 hydroxyl group suitably activated as its acetate enabled proximity-induced displacement, generating the cyclopropylketone **1.30**.<sup>43</sup> Some nucleophilic additions to the cyclopropane ring with substitution occurring at C14 were reported, albeit in low yield. Further rearrangements of the system were also disclosed by Hergenrother's laboratory.<sup>45</sup> The enolate of the ketone **1.31** is similarly capable of displacing an acylated derivative of the C11 hydroxyl moiety. First observed by Hasler during his time in Arigoni's lab, attempted deoxygenation by substitution at C11 with thiocarbonyldiimidazole followed by heating in the presence of *n*-Bu<sub>3</sub>SnH led to facile formation of the cyclobutane-containing product **1.32**. The mechanistic details of this ring-contraction are unclear, but it likely proceeds by thermal enolization at the C4 position. Net de-nylation of the mutilin system by decarboxylation of mutilin-derived ketoacid **1.33** enabled another ring-contraction event. In this example, addition of the C12 enolate into the C3 ketone

proceeded to furnish the aldol adduct **1.34**. This transformation unsurprisingly requires forcing conditions (KOH, 100 °C), given the requirement for the C4 position to undergo epimerization and the cyclooctane to distort into the reactive geometry needed for aldolization.

Transannular hydride shifts within the mutilin scaffold have been prevalent since the earliest reports of its reactivity. In addition to the example highlighted earlier in Schemes 1.5 and 1.7, several other transannular interactions between functional groups have been observed. One notable transannular hydride shift was first disclosed by Birch and co-workers in 1966. They found that exposure of the dihydromutilin derivative **1.35**, substituted at C11 with an acetyl group, to POCl<sub>3</sub> afforded the 1,1-disubstituted alkene **1.36**. Likely, activation of the free C14 hydroxyl moiety with POCl<sub>3</sub> enabled a 1,5-hydride shift, resulting in the formation of a 1,1-disubstituted alkene fragment at C10. An oxidative cleavage reaction of the cyclopentanone motif by Birch and co-workers introduced a ketone at the C4 position, enabling access to ketoacid **1.37** in one step from mutilin diacetate. Subsequent exposure to base induced hydrolysis of the acetyl group at C11 followed by transannular hydride shift, furnishing after workup the ketolactone **1.38**.

**Scheme 1.8.** Transannular hydride shifts observed by Birch and co-workers



The field of mutilin semi-synthesis has from the beginning demonstrated fascinating modes of reactivity. Early work from Arigoni and Birch in the 1960s laid a strong foundation for some of the rearrangements and reactivity trends which have come to be prevalent within the synthetic efforts involving mutilins. Even in recent years, new modifications to the core structure

have been explored.<sup>46</sup> The most productive class of semi-synthetic reactions on the pleuromutilin scaffold have been derivatizations of the C14 glycolate residue, as evidenced by the approved antibacterials that were prepared in this manner. Undeniably, the vast majority of operations performed on natural pleuromutilin have been introduction of various sidechains during medicinal chemistry campaigns. Indeed, the medicinal chemists have spent their time wisely, as a large proportion of the core modifications known within the mutilin semi-synthesis literature were reported as unexpected findings. The diverse and unpredictable reactivity of the diterpenoid core has surely in some cases impeded progress toward identifying new mutilin derivatives. Still, other examples exist of chemists cleverly leveraging the unusual reactivity patterns to help fulfill their aims, as demonstrated by some of the excellent work by Berner's team at Sandoz Pharmaceuticals. Despite the substantial amount of research that has been disclosed within the field of mutilin semi-synthesis, one thing that can be stated with certainty is that fascinating new chemistries will be discovered in the future so long as chemists continue to study pleuromutilin and its related structures.

### **1.5. Total Synthesis**

Mutilin and pleuromutilin have been the subject of numerous synthetic efforts. To date, five completed total syntheses and several synthetic efforts have been reported. The first contribution to the field was the disclosure of an annulation reaction to access a simplified pleuromutilin tricyclic ketone by Gibbons in 1980.<sup>47</sup> Later in 1980, Kahn reported an approach to the fused 6-8 bicyclic motif of the pleuromutilins.<sup>48</sup>

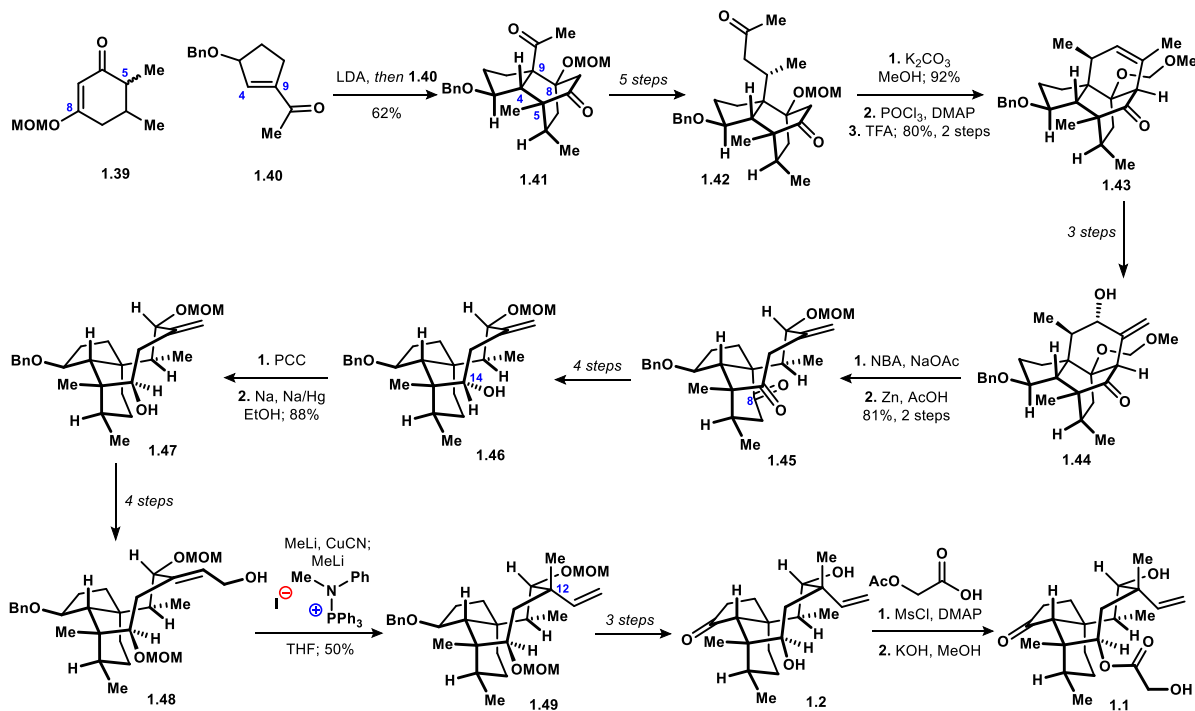
The first completed total synthesis was published in 1982 from Gibbons, who was studying in the laboratories of Woodward at the time of Woodward's unexpected death.<sup>49</sup> Gibbons' synthesis began with an annulation between vinylogous ester **1.39** (available in 2 steps from commercial materials) and cyclopentene **1.40** (available in 4 steps from commercial materials). The annulation proceeded to forge the C8–C9 and C4–C5 bonds of the mutilin skeleton and elegantly established a key stereotetrad in high diastereoselectivity. The product

ketone **1.41** was elaborated over five steps into ketone **1.42**, which was subject to adolization and elimination of the resulting alcohol, furnishing the tetracyclic ketone **1.43**. Manipulations of the alkene contained within **1.43** set the stage for a ring-expansion event to unveil the eight-membered ring. While the ketone **1.44** was resistant to ring-expansion by a retro-aldol reaction, as the author had desired, activation of the alkene with *N*-bromoacetamide induced an irreversible Grob fragmentation, furnishing after dehalogenation the cyclooctanone **1.45**. This tactic enabled ready access to the required tricyclic arrangement but required the introduction of an extraneous carbonyl at C8. Accordingly, reduction of the C8 ketone to the corresponding methylene over four steps afforded the tricyclic alcohol **1.46**, which exhibited the undesired configuration at the C14 hydroxyl group. Gibbons performed epimerization of the C14 stereocenter by an oxidation-reduction sequence, where the author notes that the use of Na<sup>0</sup> in the presence of catalytic Na/Hg amalgam and ethanol were the only effective conditions. The tricyclic alcohol **1.47** obtained in the sequence was elaborated over four steps into the allylic alcohol **1.48**. Gibbons found that exposure of the allylic alcohol **1.48** to an aminophosphonium reagent developed by Murahashi, MeLi, and CuCN introduced the C12 methyl group with high diastereoselectivity.<sup>50</sup> The resulting tricyclic ether **1.49** was converted into mutilin **1.2** over three steps. Lastly, appendage of the C14 glycolate was achieved by double glycolation and selective hydrolysis, furnishing pleuromutilin **1.1**.

Gibbons' 1982 synthesis of pleuromutilin stands as a tremendous achievement. He identified a powerful transformation to access some of the key structural elements in the mutilin system early on in the synthetic sequence in the form of Michael-Michael adduct **1.41**. He introduced the cyclooctane portion by another strategic disconnection, a Grob fragmentation, that generated the cyclooctanone **1.45**. Perhaps his two most lasting contributions to the field of pleuromutilin synthesis were employed after the assembly of the polycyclic skeleton. The first is the reduction of the C14 ketone to the corresponding alcohol using dissolving metal conditions, and the second is the introduction of the methyl group at C12, which he accomplished by S<sub>N</sub>2'-

type displacement of an allylic leaving group. Gibbons' identification of these two transformations has clearly impacted the analysis of the mutilin structure by contemporary chemists, as analogous tactics have been employed in every subsequent synthesis of pleuromutillin. Ultimately, Gibbons' approach culminated in the synthesis of mutilin in 29 steps (LLS, 0.6% overall yield) and pleuromutillin in 31 steps (yield not reported).

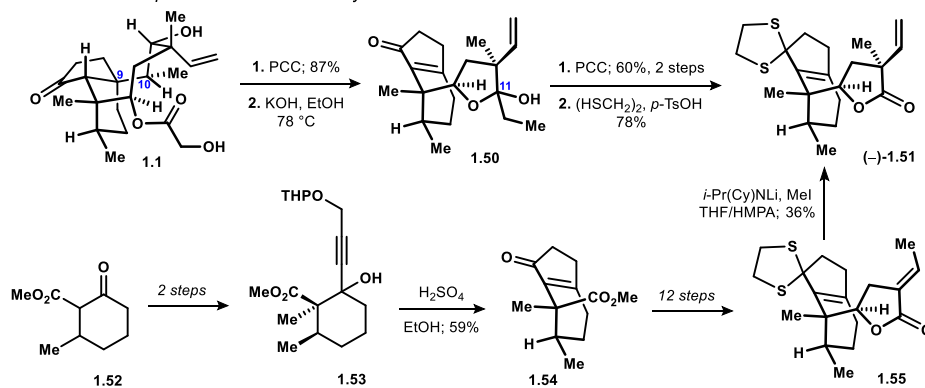
**Scheme 1.9.** Gibbons' synthesis of mutilin and pleuromutillin



Gibbons' completed synthesis of pleuromutillin stood alone in the field until 1985, when Paquette's laboratory revealed some synthetic studies related to pleuromutillins.<sup>51</sup> Then in 1988, Paquette and co-workers published three back-to-back-to-back articles in *The Journal of Organic Chemistry* on their studies toward pleuromutillin.<sup>52</sup> In the first, a synthetic approach to a tetrahydroindanone relevant to the mutilins was disclosed alongside the degradation of natural pleuromutillin to the same intermediate. In the second, Paquette's team outlined attempts induce cyclization of several derivatives of the tetrahydroindanone to forge the cyclooctane portion of the mutilin skeleton. In the third article, their attempts to employ a photochemically-initiated radical cyclization in pursuit of the mutilin cyclooctane were described.

Paquette's team utilized a degradation of pleuromutilin that was first described by Arigoni's laboratory.<sup>5</sup> Namely, oxidation of natural pleuromutilin **1.1** enabled subsequent scission of the cyclooctane ring by a retro-Michael reaction. In this transformation, the C9–C10 bond is cleaved, delivering the intermediate lactol **1.50** (Scheme 1.10).<sup>52a</sup> They next employed a de-ethylative oxidation of the lactol to the corresponding lactone using PCC, as described by Arigoni, followed by conversion of the tetrahydroindanone portion into its dithiane-protected derivative **1.51**. The authors further demonstrated that the same intermediate, available in only four steps from natural pleuromutilin, was accessible by a total synthetic route. Beginning with simple ketoester **1.52**, two straightforward reactions provided access to the propargylic alcohol **1.53**. They next employed a Rupe rearrangement-Nazarov cyclization cascade to assemble the cyclopentenone portion of their sub-target lactone, affording tetrahydroindanone **1.54**. Manipulation of the C14 ester into the desired lactone fragment **1.55** required 12 steps, which included a chiral resolution to access enantiopure material. Lastly, they introduced the C12 methyl group by an enolate alkylation, converging the synthetic material with the semi-synthetic intermediate **1.51**.

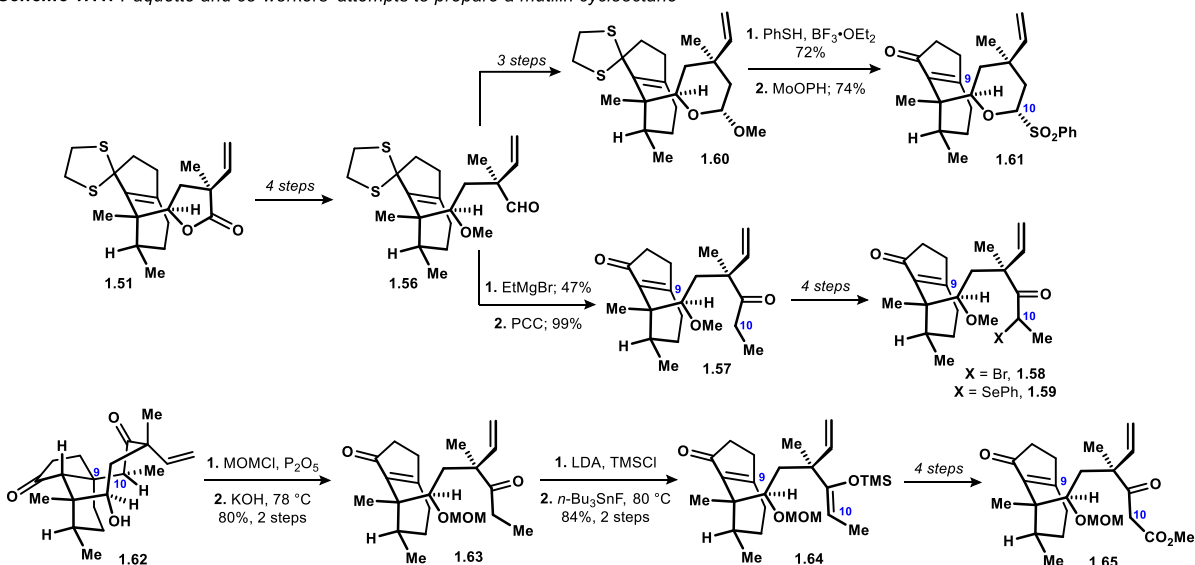
**Scheme 1.10.** Paquette and co-workers' synthesis of lactone **1.51**



Paquette and co-workers next aimed to evaluate formation of the mutilin cyclooctane.<sup>52b</sup> Their synthetic plan necessitated cyclization of a linear fragment onto the appended cyclopentenone moiety, attacking at C9, in an 8-*endo trig* fashion. To this end, they prepared a large number of nucleophiles to evaluate the planned cyclization. Conversion of the lactone **1.51**

into aldehyde **1.56** in 4 steps set the stage for the preparation of ketone **1.57**, whose reactivity toward Michael addition was evaluated (Scheme 1.11). Ketone **1.57** was further elaborated into bromoketone **1.58** and phenylselenenyl ketone **1.59**. Exposure of these derivatives to AIBN and heating showed no signs of cyclization. Homologation of the aldehyde enabled the preparation of tetrahydropyran **1.60** from aldehyde **1.56** over three steps. Substitution of the methoxyacetal with thiophenol in the presence of Lewis acid afforded an intermediate monothioacetal; oxidation with Vedej's reagent (MoOPH) proceeded to introduce the target sulfone. The authors evaluated the ability of sulfonyltetrahydropyran **1.61** to undergo cyclization and reestablish the C9–C10 bond but found it to be an incompetent substrate for the envisioned reaction.

*Scheme 1.11. Paquette and co-workers' attempts to prepare a multilin cyclooctane*

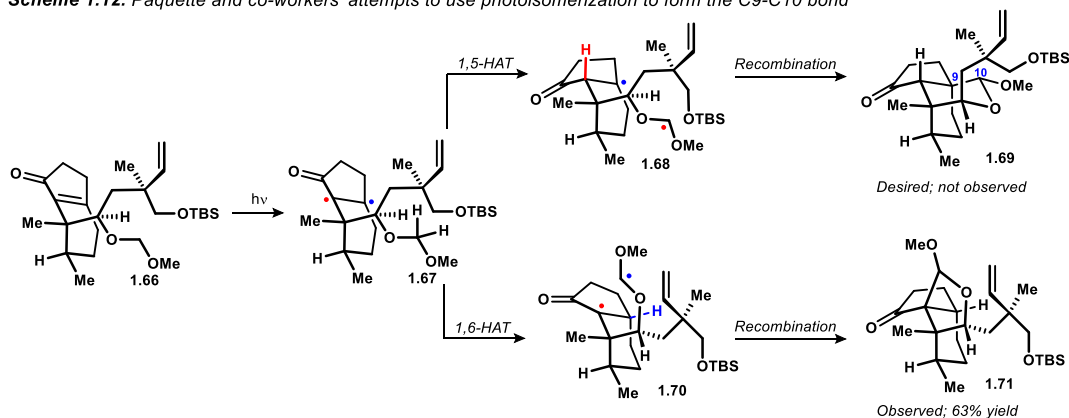


They next developed an alternative sequence beginning with pleuromutilin-derived ketone **1.62**. Protection of the C14 hydroxyl as its methoxymethyl ether and retro-Michael scission afforded the ethyl ketone **1.63**, a key intermediate in the preparation of enoxysilane **1.64**, which was found to be resistant to intramolecular Mukaiyama-Michael. They further elaborated enoxysilane **1.64** into ketoester **1.65** with the hypothesis that a ketoester-derived enolate would be likely to engage in the envisioned cyclization. Once again, the workers found that a variety of conditions were ineffective for the planned addition into the pendant enone.



In the final article of the trilogy, Paquette and co-workers describe their efforts to affect a photoisomerization to forge the challenging C9-C10 bond.<sup>52c</sup> The mechanistic hypothesis the authors relied on began with the excitation of enone **1.66** with light to form the diradical **1.67** (Scheme 1.12). Following a 1,5-HAT between the  $\alpha$ -radical and the appended methoxymethyl acetal, stabilized radical **1.68** would be formed. Following inter-system crossing, recombination of the diradical would forge the C9–C10 bond in the form of tetrahydropyran **1.69**. The authors reasoned that the C10 acetal of **1.69** could be unpoled by substitution of the methoxy group with a sulfone (as above, **1.60**→**1.61**, Scheme 1.11). In this way, the C10–C11 bond could be forged, and the direct construction of a cyclooctane could be avoided by breaking it into two six-membered ring formation events. The expected pathway was found to be inoperable, and the authors discovered that irradiation of enone **1.66** with light from a 450 W Hg-lamp furnished the regioisomeric tetrahydrofuran **1.71** in 63% yield. They posit that the unexpected product arises from initial 1,6-HAT of the  $\beta$ -radical **1.67** to intermediate diradical **1.70**. Following inter-system crossing and recombination, the observed cyclization can be rationalized. It should be noted that intermediate diradical obtained from initial 1,5-HAT (**1.68**) may undergo a second 1,5-HAT event to intercept the diradical **1.70**, formally the product of 1,6-HAT.

**Scheme 1.12.** Paquette and co-workers' attempts to use photoisomerization to form the C9-C10 bond



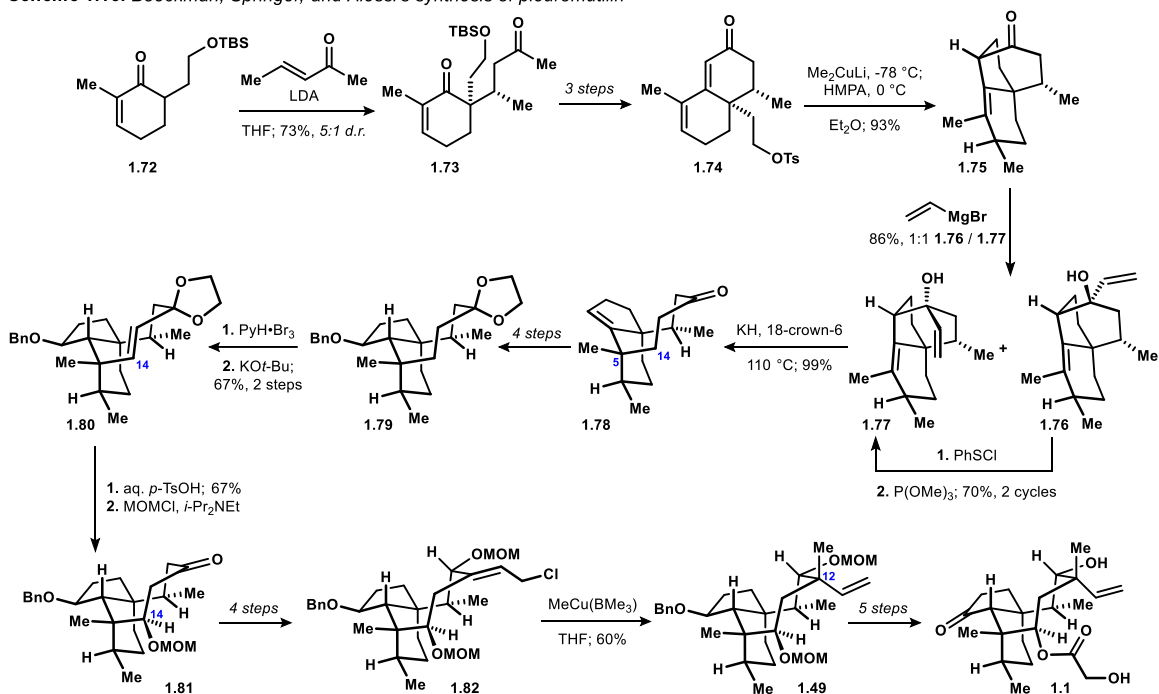
Paquette's team evaluated several approaches to the mutilin scaffold that all relied on a bold but ill-fated disconnection: formation of the C9–C10 bond by an intramolecular cyclization. They ultimately found that the reactivity of the tetrahydroindanone system related to the mutilins

is biased against the envisioned cyclization event. Regardless, they cleverly employed semi-synthetic techniques to prepare valuable frontline intermediates, enabling them to scout many distinct approaches to C9–C10 bond formation. Further, their efforts resulted in valuable insight for the community of chemists pursuing the mutilin structure. Most notably, their work outlined that the disconnection of the late-stage introduction of the C9–C10 bond should be avoided.

The second completed total synthesis of pleuromutilin **1.1** was reported by Boeckman, Springer, and Alessi in 1989.<sup>53</sup> Boeckman's approach hinged on a transform-based strategy wherein an anionic oxy-Cope rearrangement enabled rapid assembly of a pleuromutilin skeleton. The sequence began with 1,4-addition of the lithium enolate of enone **1.72** to (*E*)-pent-3-en-2-one, that proceeded in a 5:1 ratio favoring the desired diastereomer **1.73** (Scheme 1.13). Three additional steps including an intramolecular condensation delivered the bicyclic tosylate **1.74**. Diastereo- and regioselective 1,6-addition of methyl cuprate followed by treatment with excess HMPA and warming to 0 °C promoted intramolecular displacement of the primary tosylate by the intermediate enolate, producing tricyclic ketone **1.75** in 93% yield. Addition of vinylmagnesium bromide to the ketone was found to be unselective, generating a 1:1 mixture of diastereomeric allylic alcohols **1.76** and **1.77** in 86% yield. The authors discovered that a 70% overall yield of the desired epimer **1.77** could be obtained by equilibration of the undesired diastereomer **1.76** by a sulfenate-sulfoxide rearrangement, requiring two cycles. With the 1,5-diene motif in place, the stage was set for the key anionic oxy-Cope rearrangement. Heating the potassium alkoxide of **1.77** to 110 °C initiated the desired [3,3] sigmatropic rearrangement, delivering cyclooctanone **1.78** in nearly quantitative yield. With the mutilin skeleton in hand, the authors set about introducing the needed functionalities decorating the cyclooctane. Four manipulations of ketone **1.78** furnished the dioxolane **1.79**, which was cleverly engaged in a bromination-elimination sequence to deliver the *trans*-cyclooctene **1.80** (Scheme 1.13). Ketal hydrolysis with aqueous *p*-TsOH proceeded with concomitant hydration of the cyclooctene function, introducing the C14 hydroxyl group with the desired diastereoselectivity. Four

additional steps including a Rubottom oxidation sequence afforded the allylic chloride **1.82**. The authors next engaged the allylic chloride moiety in a  $\gamma$ -methylation reaction with  $\text{MeCu}(\text{BMe})_3$  to furnish the tricyclic ether **1.49** in 60% yield over three steps, thereby converging their sequence to one of Gibbons' key intermediates. Boeckman and co-workers elaborated the protected triol **1.49** into target structures mutilin **1.2** and pleuromutilin **1.1** using Gibbons' conditions (5 steps, Scheme 1.9).

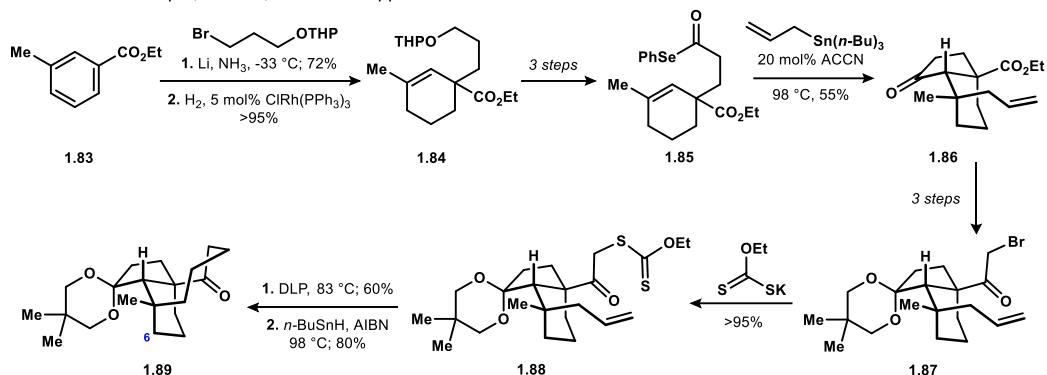
**Scheme 1.13.** Boeckman, Springer, and Alessi's synthesis of pleuromutilin



Boeckman and co-workers identified an exceptionally elegant synthetic sequence to mutilin and pleuromutilin. Their assembly of the tricyclic core of the mutilins leveraged a creative 1,6-conjugate addition / enolate trapping sequence to set the stage for a facile anionic oxy-Cope reaction. While the approach offered access to a sparsely decorated tricyclic core, the central placement of the one ketone functional handle at C12 enabled straightforward elaboration into the natural products. Notably, Boeckman's team relied on the  $\gamma$ -methylation of an allylic leaving group at C12 to establish the quaternary stereocenter, in accord with Gibbons' approach. In total, the sequence required 27 synthetic steps (LLS) to access mutilin **1.2** in 1% overall yield

from enone **1.72**. They converted mutilin into pleuromutilin **1.1** by Gibbons' protocol, for a 29 step, 0.4% overall yielding route. Interestingly, the lead student author, Dane Springer, went on to lead Bristol Myers Squibb's program investigating pleuromutilins.

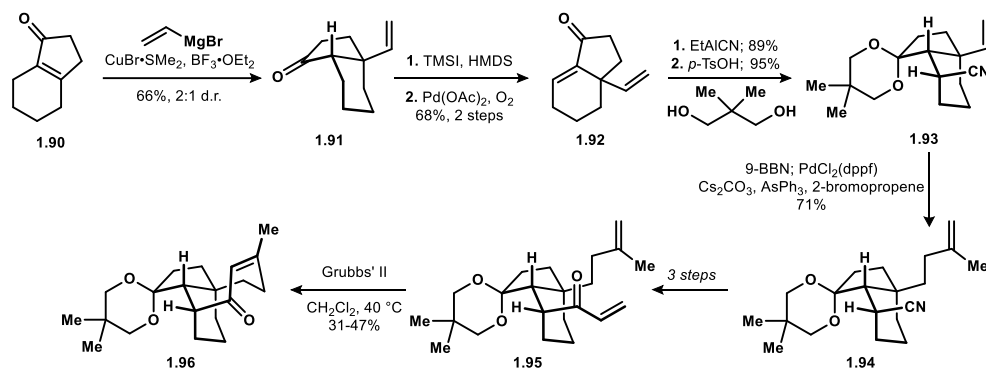
**Scheme 1.14.** Bacque, Pautrat, and Zard's approach to the mutilin skeleton



The next contribution to the field was reported by Zard and co-workers in 2003, wherein they disclosed a radical cyclization approach to the pleuromutilin framework.<sup>54</sup> Beginning with ethyl *m*-toluate **1.83**, Birch reduction followed by trapping of the resultant enolate with an alkyl bromide delivered, following Rh-catalyzed reduction of the 1,2-disubstituted alkene, ester **1.84** (Scheme 1.14). The authors prepared acylselenide **1.85** over three steps, setting the stage for a radical difunctionalization reaction. To this end, a 5-*exo*-trig cyclization was initiated by heating in the presence of catalytic 1,1'-azobis(cyclohexanecarbonitrile), and the resulting tertiary radical was trapped with allyltributyltin to furnish hydriindane **1.86**; three further manipulations afforded the bromoketone **1.87**. Displacement of the bromide with potassium xanthate furnished the ketoxanthate **1.88** quantitatively. Heating xanthate **1.88** in the presence of dilauroyl peroxide (DLP) initiated the key 8-*endo* cyclization wherein the alkyl radical resulting from C-S bond homolysis reacts with the appended allyl fragment. The product xanthate was reduced to the corresponding hydrocarbon by treatment with tributyltin hydride and AIBN to furnish the cyclooctanone **1.89** in 80% yield. Notably, the tricyclic products available by Zard and co-workers' sequence lacks some of the structural features present in the natural structures, including the methyl group at C6.

The Sorensen lab maintained a program studying truncated synthetic pleuromutilin derivatives that culminated in two articles describing their findings. In the first, a ring-closing alkene metathesis (RCM) approach was taken to form the key cyclooctene.<sup>55</sup> Beginning with known tetrahydroindanone **1.90** (available in two steps from commercially available materials), cuprate addition to the tetrasubstituted enone delivered perhydroindanone **1.91** as an inconsequential 2:1 mixture of diastereomers (Scheme 1.15). Preparation of the enoxysilane followed by Saegusa–Ito dehydrogenation furnished the bicyclic enone **1.92**. Nagata hydrocyanation and ketalization of the product ketone produced the bicyclic nitrile **1.93** in high diastereoselectivity. The vinyl fragment was next engaged in a *B*-alkyl Suzuki coupling with 2-bromopropene to provide the 1,1-disubstituted alkene **1.94** in good yield.

**Scheme 1.15.** Liu, Lotesta, and Sorensen's RCM approach to the mutilin framework

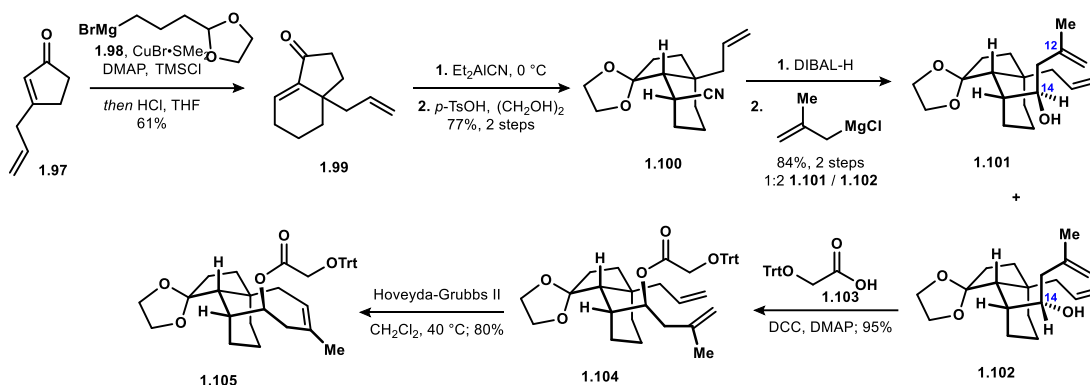


Preparation of the substrate for RCM studies was accomplished over three synthetic steps, furnishing the enone **1.95**. Subjection of diene **1.95** to RCM condition with 30 mol% of Grubbs' II catalyst afforded the desired cyclooctene **1.96** in modest yield, completing a short synthesis of a truncated pleuromutilin skeleton. The authors note that substrates containing C11 oxidation (as present in the natural product) failed to undergo RCM when subjected to standard conditions. Notably, the tricyclic compound **1.96** synthesized by the described route lacks several key structural elements of the pleuromutilin system, including the C15, C16, and C17 methyl groups.

The authors' second approach to the pleuromutilin skeleton featured a similar RCM-based strategy to assemble the eight-membered ring. Beginning with 3-allylcyclopent-2-enone

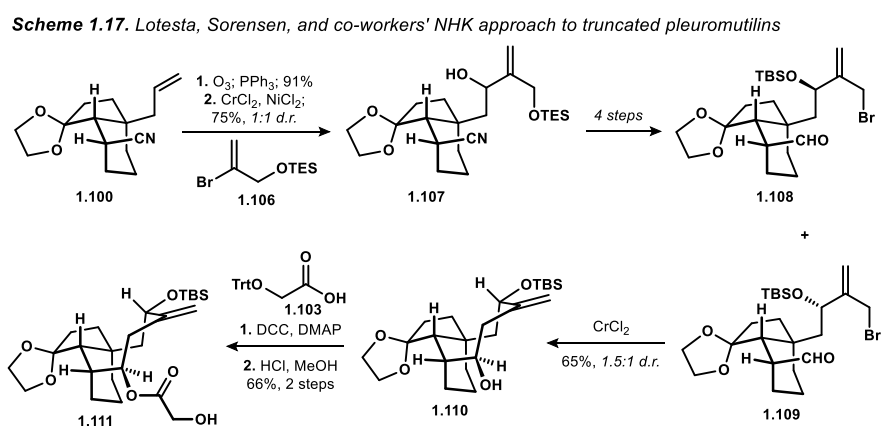
**1.97**, 1,4-addition with the cuprate related to Grignard reagent **1.98** followed by aldol condensation delivered the bicyclic enone **1.99** (Scheme 1.16). Nagata hydrocyanation proceeded in high diastereoselectivity, and subsequent ketalization with ethylene glycol provided hydrindane **1.100**. Diisobutylaluminum hydride reduction of the nitrile enabled addition of methallylmagnesium chloride to the product aldehyde, which proceeded with modest diastereoselection. The major product, homoallylic alcohol **1.102** was subject to glycolation with *O*-tritylglycolic acid, furnishing diene **1.104**. Application of the Hoveyda-Grubbs second generation catalyst induced the desired RCM reaction, affording cyclooctene **1.105**. The authors further established that increasing the bulk of the C14-OH substituent increased the rate of RCM, which they attribute to a biasing of the conformation toward reactive rotamers.

**Scheme 1.16.** Liu, Lotesta, and Sorensen's second RCM-based approach to the mutilin framework



The minor diastereomer from carbonyl addition **1.101** and its glycolate, wherein the C14 stereochemistry matched the natural product, were found to be incompetent in the RCM reaction. The authors posit that a conformational effect prohibits the two alkene components from achieving the requisite proximity to one another, inhibiting RCM. The authors propose that any substituent appended to the C14 hydroxyl group introduces a steric interaction with the neighboring methyl group during formation of the key ruthenacyclobutane intermediate required for successful metathesis. Similarly, the authors suggest that the relative C14 stereochemistry can dictate the conformation of the diene precursor, where the natural epimer **1.101** effectively fails to enter a reactive conformation.

Sorensen and co-workers disclosed a second synthetic route to access truncated pleuromutilin scaffolds in 2011.<sup>56</sup> Their second-generation strategy hinged on a double allylation transform wherein a two-carbon fragment was introduced via sequential nucleophilic allylation reactions as a means for closure of the cyclooctane ring system (Scheme 1.17). Beginning with nitrile **1.100** whose synthesis was described earlier, high yielding ozonolysis delivered an intermediate aldehyde which readily underwent addition under Nozaki–Hiyama–Kishi (NHK)-type conditions with bromide **1.106** to afford a 1:1 mixture of diastereomeric alcohols **1.107**.



Four straightforward steps enabled access to the mixture of diastereomeric allylic bromides **1.108** and **1.109**, which were separated along the sequence. The authors first explored chromium-mediated intramolecular cyclization of the allylic bromide **1.109** exhibiting the natural C11 configuration onto the appended aldehyde proceeded in good yield, albeit with poor diastereoselectivity to deliver pleuromutilin-like tricyclic **1.110**. DCC coupling with trityl-protected glycolic acid and acidic hydrolysis of the protecting groups delivered their target compound **1.111**. The authors also describe the preparation of unnatural epimers that arose from their unselective NHK additions, enabling more pleuromutilin-like chemical space to be probed for potential biological activity. The assay of various epimers uncovered that a C11-epimeric pleuromutilin derivative obtained from their synthetic route displayed comparable (12-25  $\mu\text{g/mL}$ ) inhibitory activity against *M. tuberculosis* as tiamulin **1.18**, the semisynthetic pleuromutilin derivative used as a veterinary antibiotic.

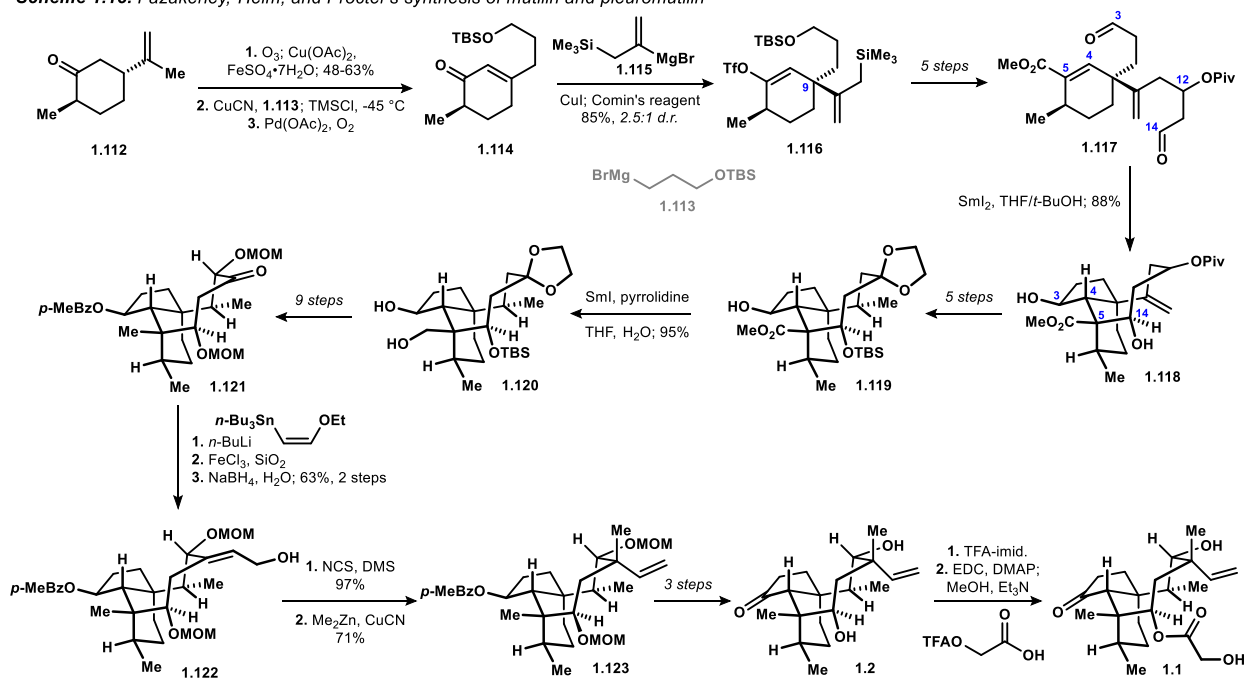
The third, and first enantioselective, synthesis of pleuromutilin **1.1** was disclosed by Fazakerley, Helm, and Procter in 2013.<sup>57</sup> In 2009, the group had previously demonstrated the feasibility of their key step: a  $\text{SmI}_2$ -initiated ketyl cyclization/aldol cascade bicyclization to forge the tricyclic core from a dialdehyde precursor.<sup>58</sup> Procter's total synthesis commenced with a known conversion of *trans*-dihydrocarvone **1.112** (commercially available as a 4:1 chromatographically separable mixture of *cis* and *trans* isomers) to the corresponding  $\alpha,\beta$ -enone via oxidative cleavage of the isopropenyl fragment. Subsequent conjugate addition of the cuprate derived from Grignard reagent **1.113** followed by Saegusa–Ito oxidation efficiently delivered enone **1.114** (95% ee). A second cuprate addition using Grignard reagent **1.115** followed by trapping of the enolate with Comin's reagent provided the vinyl triflate **1.116** in a 2.5:1 mixture of diastereomers. Five more steps provided access to the dialdehyde **1.117**, setting the stage for their key step. Treatment of **1.117** with 2.5 equivalents of  $\text{SmI}_2$  in a THF/*t*BuOH solvent mixture cleanly forged the C3–C4 and C5–C14 bonds, furnishing the tricyclic cyclooctanol **1.118** in excellent yield. The selective synthesis of the observed product is proposed to occur due to the reversibility of ketyl radical formation. In this way, the rapid 5-*exo trig* cyclization available to the C3 aldehyde enables the desired connectivity pattern, despite little meaningful difference in reduction potential of the two aldehydes at C3 and C14.

With the tricyclic skeleton quickly assembled, elaboration to the natural product required extensive decoration of the cyclooctane core and removal of extraneous functionalities. Five manipulations from the diol **1.118** afforded the ketal **1.119**. Subsequently, the authors sought to fully reduce the C15 ester to the corresponding methyl group by initial hydride reduction followed by radical deoxygenation. Surprisingly, the C15 ester was found to be resistant to reduction with ordinary hydride reagents (*i.e.*, alkylaluminum hydrides,  $\text{LiAlH}_4$ ), apparently due to its sterically congested nature. After experimentation, the authors discovered that the desired reduction could be affected by  $\text{SmI}_2$  in the presence of amine additives, with pyrrolidine delivering the highest efficiency to furnish alcohol **1.120** in 95% yield. Nine steps including a



Rubottom oxidation sequence delivered the ketone **1.121**, which was engaged by (*Z*)-lithio ethyl vinyl ether, affording after transposition and reduction the allylic alcohol **1.122**. Chlorination and  $\gamma$ -methylation proceeded smoothly, delivering **1.123**, and three additional steps provided mutilin **1.2**. Selective protection of the C11 hydroxyl as the corresponding trifluoroacetate was accomplished by treatment of mutilin with trifluoroacetoxyimidazolide (TFA-imid). The C14 hydroxyl was next decorated with the glycolate side chain, affording pleuromutilin **1.1** in 75% yield over two steps after mild hydrolysis of the C11 trifluoroacetate.

**Scheme 1.18.** Fazakerley, Helm, and Procter's synthesis of mutilin and pleuromutilin



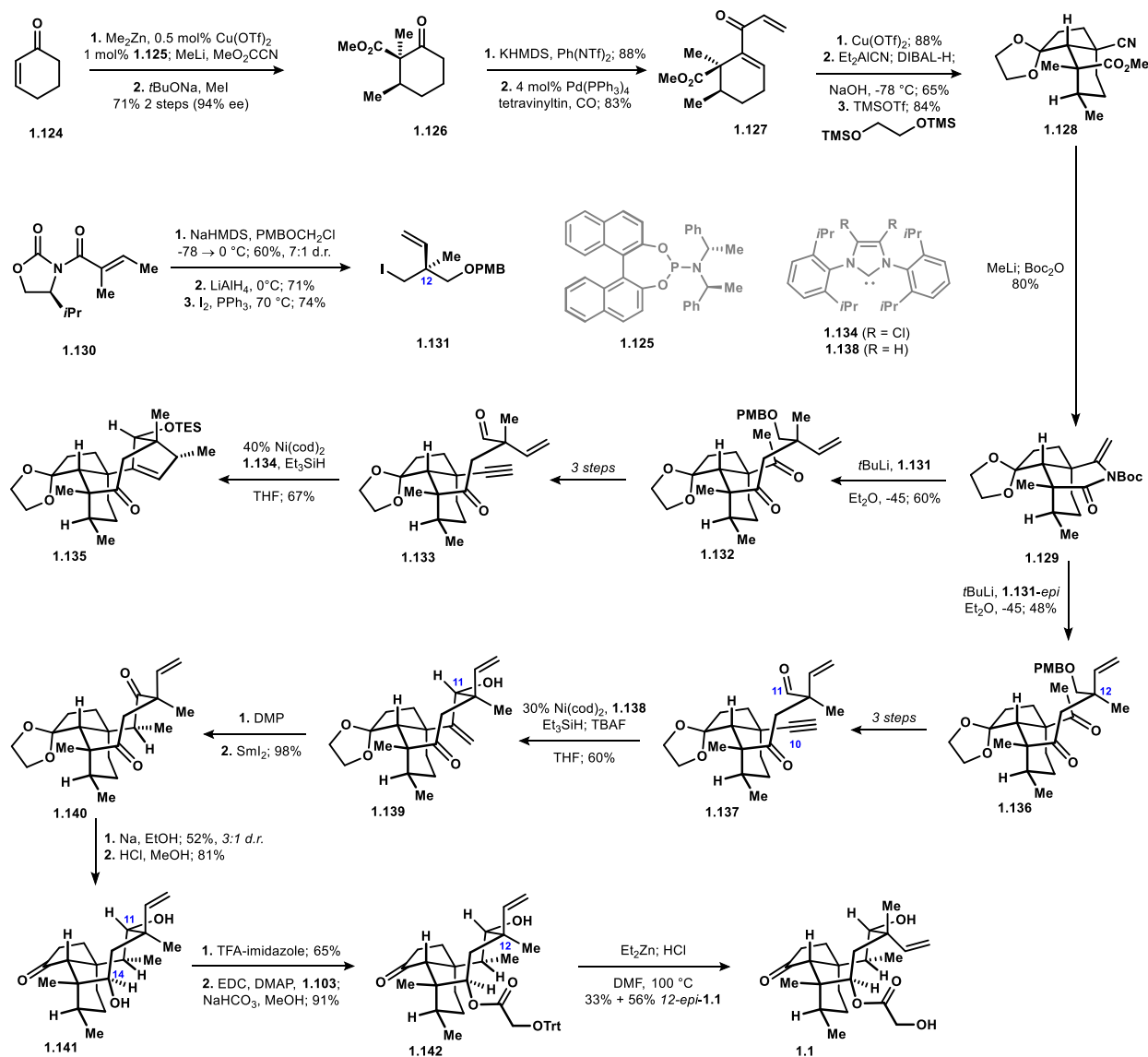
Procter and co-workers approach to the synthesis of pleuromutilin hinged on an impressive key step: the  $\text{Sml}_2$ -initiated bicyclization to prepare the mutilin skeleton from dialdehyde **1.118**. The assembly of the dialdehyde substrate for their key step was concise, relying on sequential enone conjugate addition reactions. Furthermore, the starting point for their synthetic route began with 6-(*R*)-methylcyclohex-2-enone, readily available from the chiral pool. Following the construction of the mutilin polycycle, Procter and co-worker's approach necessitated a large number of operations to access the natural product. The tactics used to introduce the many substituents adorning the cyclooctane core followed suit with those

disclosed by Gibbons and Boeckman, but in the case of Procter's work, the ablation of the C15 ester group required additional manipulations. In total, Procter's team completed the first asymmetric synthesis of the mutilin diterpenoids, requiring 32 steps (LLS) to mutilin, 0.3% overall yield, and 34 steps, 0.2% overall yield to pleuromutilin.

The fourth completed total synthesis of pleuromutilin was reported by Murphy, Zeng, and Herzon in 2017.<sup>59</sup> Beginning with asymmetric conjugate addition of dimethylzinc to cyclohexenone **1.124** catalyzed by low loadings of Cu(OTf)<sub>2</sub> and phosphoramidite ligand **1.125**, carboxylation was achieved in the same pot by addition of MeLi and Mander's reagent (Scheme 1.19). Following methylation of the ketoester with MeI and NaOtBu, ketone **1.126** was prepared in 71% over two steps. Alkenyl triflate synthesis followed by a carbonylative Stille reaction with tetravinyltin delivered dienone **1.127** in good yield. Subsequent Nazarov cyclization and Nagata hydrocyanation of the resultant enone produced a 3:1 mixture of diastereomers which were inseparable on preparative scale. Fortunately, the authors discovered that the minor diastereomer could be selectively reduced in the same pot with DIBAL-H to furnish a single diastereomeric product in 65% yield. Noyori ketalization of the product cyclopentanone delivered hydrindane **1.128**. Addition of methyllithium to the nitrile induces lactam formation, furnishing **1.129** in good yield upon addition of Boc<sub>2</sub>O. With 14 of the carbons of the target in place, introduction of a six-carbon fragment was required to complete the diterpenoid core. To prepare a suitable pronucleophile, the authors utilized an Evans alkylation of tiglic acid-derived oxazolidinone **1.130** with PMBOCH<sub>2</sub>Cl. Following reductive cleavage of the auxiliary and an Appel reaction, alkyl iodide **1.131** was prepared in good yield. Lithium-halogen exchange of **1.131** followed by addition of lactam **1.129** forged the C13-C14 bond to deliver ketone **1.132** in 60% yield following acidic hydrolysis. The authors prepared target alkyne **1.133** over three steps. In their attempts to perform cyclization of the alkyne onto the pendant aldehyde, they discovered that Montgomery's conditions enabled the desired bond formation.<sup>60</sup> However, the C12 vinyl fragment was engaged during the reaction, affording cyclopentene **1.135** as the major

product.<sup>61</sup> Given the unavoidable reactivity of the C12 vinyl fragment during their planned cyclization, Herzon's team identified a solution.

**Scheme 1.19.** Murphy, Zeng, and Herzon's synthesis of pleuromutilin



Returning to the lactam **1.129**, they opted to employ the C12 epimer of the alkyllithium derived from iodide **1.131** and determined that the addition proceeded as before to afford the diketone **1.136**. Once again, three straightforward manipulations provided access to the alkyne **1.137**. They found that applying slightly modified Nickel-catalyzed conditions furnished the desired tricyclic ketone **1.139**. An oxidation-reduction sequence introduced the C17 methyl group with the desired configuration, delivering ketone **1.140**. The authors discovered that the

cyclooctanedione could be reduced with the desired diastereoselectivity using conditions closely related to those employed by Gibbons: Na<sup>0</sup> in EtOH. While the hydroxyl group at C14 was set with immaculate diastereoselectivity, they found that the C11 stereocenter was formed in an acceptable 3:1 mixture. Having established access to C12-*epi* mutilin **1.141**, they set about introducing the glycolate side chain using Procter's approach: selective trifluoroacetylation of the C11 hydroxyl group followed by appendage of *O*-trityl glycolic acid, furnishing C12-*epi* pleuromutilin derivative **1.142**. They completed the synthesis by using Berner's C12 epimerization reaction, affording pleuromutilin in 33% yield alongside 56% of C12-*epi* pleuromutilin after acidic hydrolysis of the trityl moiety.<sup>62</sup>

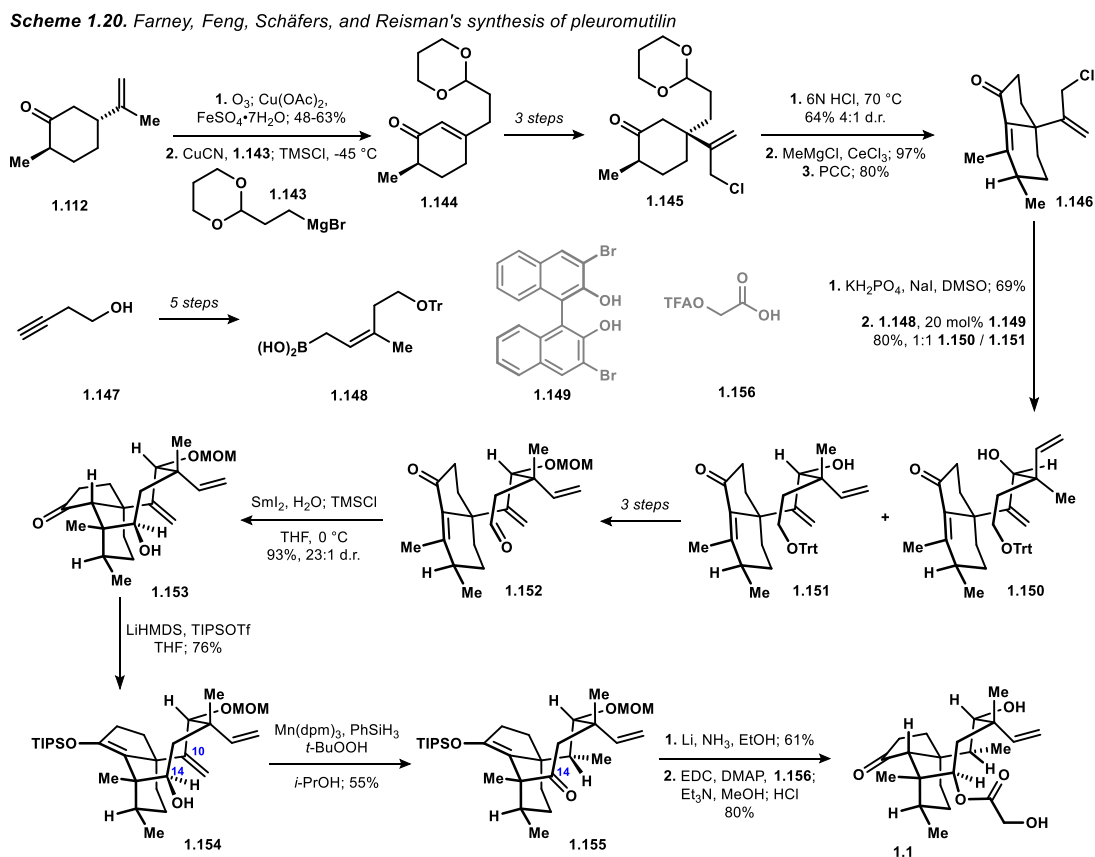
Herzon and co-workers' total synthesis of pleuromutilin represented a leap forward in the synthetic approaches to the mutilin diterpenes. In many ways, the strategy was an evolution of the early work from Paquette. Following an assembly of the tetrahydroindanone portion of the mutilin system that capitalized on strategies outlined by Paquette and Sorensen, Herzon's team identified a very powerful set of disconnections. The key improvement was the strategic choice to assemble the C10–C11 bond, rather than the C9–C10 bond, obviating the need for the cyclooctane synthesis to involve addition into the congested mutilin hydrindanone nucleus. Additionally, they recognized that cyclooctane synthesis is hindered by the transannular interactions present during the transition state, and intelligently targeted a cyclization substrate that contained a large number of sp<sup>2</sup> and sp hybridized carbon atoms. Ultimately, despite the concession of the late stage C12 epimerization, Herzon's team accomplished the shortest synthesis to that point, requiring 20 steps (LLS) to access (+)-pleuromutilin in 0.1% overall yield.

The Reisman lab disclosed an enantioselective total synthesis of pleuromutilin in 2018.<sup>63</sup> Their route began with a sequence analogous to the one developed by Procter: oxidative cleavage of the isopropenyl fragment of *trans*-dihydrocarvone **1.112** followed by addition with the cuprate derived from Grignard reagent **1.143** addition and Saegusa–Ito oxidation furnished enone **1.144** in high yield (Scheme 1.20). Next, a three-step sequence provided allylic chloride

**1.145**. Acid-mediated intramolecular aldol condensation followed by methyl Grignard addition delivered an allylic alcohol, primed to undergo Dauben–Michno oxidative transposition to access enone **1.146**. Direct conversion of the chloride to the corresponding enal was accomplished under Kornblum conditions. Reisman’s team next introduced the requisite 6-carbon fragment and assembled the C12 quaternary center by a catalyst-controlled crotylation with boronic acid **1.148** (prepared in five steps from homopropargylic alcohol **1.147**). Of the four possible stereochemical outcomes, BINOL **1.149** induced some selectivity, affording a 1:1 mixture of alcohol **1.151**, containing the desired stereochemical array, and **1.150**, which displayed a C11,C12-di-*epi* arrangement. Proceeding with the desired crotylation product **1.151**, three steps afforded the aldehyde **1.152**, setting the stage for their key step. Exposure of the aldehyde **1.152** to  $\text{SmI}_2$  afforded the desired cyclization product **1.153** in high yield. Having assembled the mutilin core, the authors next pursued the necessary manipulations of the functional groups surrounding the tricyclic system. They first protected the C3 ketone as its TIPS enoxysilane. Next, they engaged the 1,1-disubstituted alkene moiety to radical hydrogenation conditions, furnishing ketone **1.155**. They observed that a 1,5-HAT pathway was operable upon formation of the alkyl radical intermediate, wherein the C14 methine provided the hydrogen atom that was installed at C11. While the 1,5-HAT mechanism delivered exquisite diastereoselectivity to the C11 stereocenter, it required the re-adjustment of the oxidation state at C14. To this end, exposure of the cyclooctanone to dissolving metal conditions afforded the penultimate intermediate in their synthesis. Introduction of the glycolate side chain preceded global hydrolysis, affording pleuromutilin **1.1**.

The Reisman lab’s synthesis of pleuromutilin followed familiar strategic grounds to the approach outlined by Procter in 2013. Several tactical improvements enabled Reisman’s team to accomplish their synthesis in a more efficient and concise fashion. Most notably, they selected a ketyl cyclization substrate that placed all of the functional groups at the desired oxidation state following reductive cyclization. Their assembly of the tetrahydroindanone

precursor **1.152** proceeded over a high-yielding sequence with the exception of the crotylation, wherein the unselective addition reaction was a solitary, necessary concession to execute their synthetic plan. Reisman's synthesis set a new bar for step efficiency within the field, requiring 18 steps (LLS, 24 total steps) to access (+)-pleuromutilin in 0.3% overall yield.



Pleuromutilin total synthesis has been a rich area of research across nearly four decades. Each approach has provided contributions to strategy and unique reactivity. While the number of operations required to synthesize pleuromutilin **1.1** has decreased significantly in recent years, the structures clearly remain a significant synthetic challenge. Recent efforts have highlighted the difficulties associated with introduction of the stereochemical array present in the mutilin system. The reduction of step count seen in recent approaches to pleuromutilin can be attributed to improvements in synthetic strategy, likely informed by earlier approaches to the same targets, as well as the continued development of chemical methods by the synthetic

organic chemistry community as a whole. Interestingly, despite the notable improvements in step count efficiency of more recent synthetic work, the overall yield of modern pleuromutilin syntheses has not seen a similar spike in efficiency. Future improvements in the analysis of the mutilin structure will likely capitalize on the existing findings that have highlighted the interplay between the functional groups that are densely packed into the tricyclic scaffold. Additionally, ideal approaches will leverage stereochemical relay to a greater extent during introduction of mutilin's eight contiguous stereocenters.

## 1.6. References

(1) Kavanagh, F.; Hervey, A.; Robbins, W. J. *Proc. Natl. Acad. Sci. U. S. A.* **1951**, 37, 570. The name for the basidiomycete fungus *Pleurotus mutilis* is used synonymously with *Clitopilus scyphoides f. mutilus*. Similarly, *Pleurotus passeckerianus* is used synonymously with *Clitopilus passeckerianus*.

(2) It is noteworthy that several other mutilin-derived metabolites have been isolated, though they are not typically considered to be distinct natural products. For example, Berner and co-workers isolated the mutilin derivative **1.157** from the aqueous phase of fermentation extracts (Figure 1.5): (a) Berner, H.; Vyplel, H.; Schulz, G.; Stuchlik, P. *Tetrahedron* **1983**, 39, 1317. Knauseder and Brandl found that pleuromutilin derivative **1.158**, acylated with a  $\Delta^9$ -eicosenoic acid fragment, was formed when sperm oil was included in the fermentation broth, albeit in small quantities: (b) Knauseder, F.; Brandl, E. *J. Antibiot.* **1975**, 29, 125. Michel and co-workers found that the pleuromutilin  $\beta$ -xylose glycoside named A40104A (**1.159**) was formed in high titers by *Clitopilus pseudopinsitus* and noted that it possesses greater activity against *S. aureus* than pleuromutilin itself: (c) Michel, K. H.; Dorman, D. E.; Occolowitz, J. L. *Curr. Chemother. Infect. Dis.* **1980**, 1, 479. (d) Vezina, C.; Singh, K. *Fermentation Products: Proceedings of the Sixth International Fermentation Symposium*. London, Canada. **1980**, 1, 187.

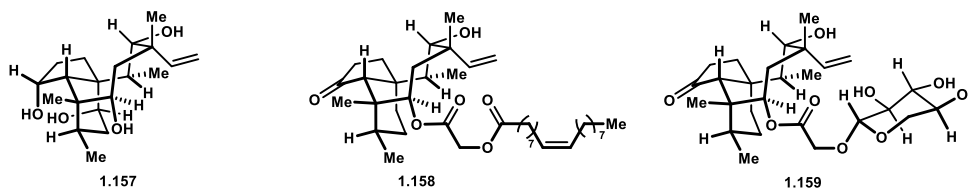
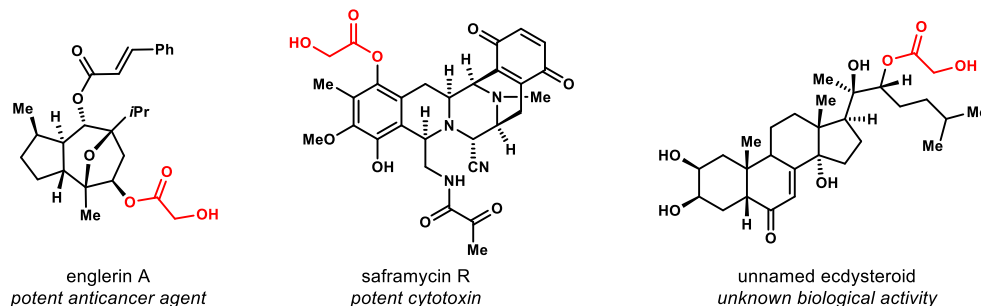


Figure 1.5. Naturally occurring mutilin derivatives

(3) To my knowledge, only four natural products are known to contain a glycolate residue. The structures of the three natural products containing glycolate moieties other than pleuromutilin are shown (Figure 1.6). Englerin A: (a) Ratnayake, R.; Covell, D.; Ransom, T. T.; Gustafson, K. R.; Beutler, J. A. *Org. Lett.* **2009**, 11, 1, 57. Saframycin R: (b) Lown, J. W.; Hanstock, C. C.; Joshua, A. L.; Arai, T.; Takahasi, K. *J. Antibiot.* **1983**, 36, 9, 1184. An unnamed ecdysteroid: (c) Constantino, V.; Dell'Aversano, C.; Fattorusso, E.; Mangoni, A. *Steroids* **2000**, 65, 138.



**Figure 1.6.** Natural products with a glycolate function

- (4) Anchel, M. J. *Biol. Chem.* **1952**, 199, 133.
- (5) (a) Arigoni, D. *Gazz. Chim. Ital.* **1962**, 92, 884. Arigoni, D. *Pure Appl. Chem.* **1968**, 17, 331. (b) Nägeli, P. Ph.D. Thesis, ETH, Zurich **1961**. (c) Buzzolini, M. Ph.D. Thesis, ETH, Zurich **1966**. (d) Bonavia, G. Ph.D. Thesis, ETH, Zurich **1968**. (e) Hasler, H. Ph.D. Thesis, ETH, Zurich **1979**.
- (6) (a) Birch, A. J.; Cameron, D. W.; Holzzapfel, C. W.; Rickards, R. W. *Chem. Ind. (London)* **1963**, 374. (b) Birch, A. J.; Holzzapfel, C. W.; Rickards, R. W. *Tetrahedron* **1966**, 22, 359.
- (7) Dobler, M.; Dürr, B. G. *Cryst. Struct. Commun.* **1975**, 4, 259.
- (8) Bailey, A. M.; Alberti, F.; Kilaru, S.; Collins, C. M.; de Mattos-Shiple, K.; Hartley, A. J.; Hayes, P.; Griffin, A.; Lazarus, C. M.; Cox, R. J.; Willis, C. L.; O'Dwyer, K.; Spence, D. W.; Foster, G. D. *Sci. Rep.* **2016**, 6, 25202.
- (9) Yamane, M.; Minami, A.; Liu, C.; Ozaki, T.; Takeuchi, I.; Tsukagoshi, T.; Tokiwano, T.; Gomi, K.; Oikawa, H. *ChemBioChem.* **2017**, 18, 2317.
- (10) For some insight into pleuromutilin biosynthesis and fermentation: Knauseder, F.; Brandl, E. *J. Antibiot.* **1976**, 29, 125.
- (11) Alberti, F.; Khairudin, K.; Venegas, E. R.; Davis, J. A.; Hayes, P. M.; Willis, C. L.; Bailey, A. M.; Foster, G. D. *Nat. Commun.* **2017**, 8, 1831.
- (12) Xu, M.; Jia, M.; Hong, Y. J.; Yin, X.; Tantillo, D. J.; Proteau, P. J.; Peters, R. J. *Org. Lett.* **2018**, 20, 1200.
- (13) For a comprehensive overview of pleuromutilin biological activity see: Goethe, O.; Heuer, A.; Ma, X.; Wang, Z.; Herzon, S. B. *Nat. Prod. Rep.* **2019**, 36, 220.
- (14) An overview of pleuromutilins, their mode of action, and resistance profile: Paukner, S.; Ridel, R. *Cold Spring Harbor Perspect. Med.* **2017**, 7, a027110.
- (15) Högenauer, G.; Ruf, C. *Antimicrob. Agents Chemother.* **1981**, 19, 260.
- (16) (a) Schlünzen, F.; Pyetan, E.; Fucini, P.; Yonath, A.; Harms, J. H. *Mol. Microbiol.* **2004**, 54, 1287. (b) Davidovich, C.; Bashan, A.; Auerbach-Nevo, T.; Yaggie, R. D.; Gontarek, R. R.; Yonath, A. *Proc. Natl. Acad. Sci., USA* **2007**, 104, 4291.
- (17) Eyal, Z.; Matzov, D.; Krupkin, M.; Paukner, S.; Riedl, R.; Rozenberg, H.; Zimmerman, E.; Bashan, A.; Yonath, A. *Sci. Rep.* **2016**, 6, 39004.
- (18) (a) Pringle, M.; Poehlsgaard, J.; Vester, B.; Long, K. S. *Mol. Microbiol.* **2004**, 54, 1295–1306. (b) Gentry, D. R.; Rittenhouse, S. F.; McCloskey, L.; Holmes, D. J. *Antimicrob. Agents Chemother.* **2007**, 51, 2048. (c) Long, K. S.; Poehlsgaard, J.; Kehrenberg, C.; Schwarz, S.; Vester, B. *Antimicrob. Agents Chemother.* **2006**, 50, 2500. (d) Davidovich, C.; Bashan, A.; Yonath, A. *Proc. Natl. Acad. Sci., USA* **2008**, 105, 20665. (e) Card, R. M.; Stubberfield, E.; Rogers, J.; Nunez-Garcia, J.; Ellis, R. J.; AbuOun, M.; Strugnell, B.; Teale, C.; Williamson, S.; Anjum, M. F. *Front. Microbiol.* **2018**, 9, 1183. (f) Wendlandt, S.; Kadlec, K.; Fessler, A. T.; Schwarz, S. *Vet. Microbiol.* **2015**, 177, 353. (g) Zhang, A.; Xu, C.; Wang, H.; Lei, C.; Liu, B.; Guan, Z.; Yang, C.; Yang, Y.; Peng, L. *Vet. Microbiol.* **2015**, 177, 162.



- (19) Duijkeren, E. V.; Greko, C.; Pringle, M.; Baptiste, K. E.; Catry, B.; Jukes, H.; Moreno, M. A.; Pomba, M. C. M. F.; Pyoralá, S.; Rentala, M.; Ruzauskas, M.; Sanders, P.; Teale, C.; Threfall, E. J.; Torren-Edo, J.; Torneke, K. J. *Antimicrob. Chemother.* **2014**, 69, 2022.
- (20) (a) O'Connor, J. J.; Baughn, C. O.; Pilote, R. R.; Alpaugh, W. C.; Linkenheimer, W. H.; Maplesden, D. C. *J. Anim. Sci.* **1979**, 49, 933. (b) Baughn, C. O.; Alpaugh, W. C.; Linkenheimer, W. H.; Maplesden, D. C. *Avian Dis.* **1978**, 22, 620. (c) Olson, L. D. *J. Am. Vet. Med. Assoc.*, **1986**, 188, 1165. (d) Pickles, R. W. *Vet. Rec.*, **1982**, 110, 403. (e) Burch, D. G.; Goodwin, R. F. *Vet. Rec.* **1984**, 115, 594.
- (21) (a) Drews, J.; Georgopoulos, A.; Laber, G.; Schutze, E.; Unger, J. *Antimicrob. Agents Chemother.*, **1975**, 7, 507. (b) Egger, H.; Reinshagen, H. *J. Antibiot.* **1976**, 29, 915–922 and 923–927. (c) Egger, H.; Reinshagen, H. *US Pat.* **1980**, US4208326A.
- (22) Berner, H.; Vypel, H. *US Pat.* **1987**, US4675330A.
- (23) (a) Burch, D. G. S.; Ripley, P. H.; Zeisl, E. *US Pat.* **2000**, US6130250A. (b) Koller, K.; Schwarz, F. *US Pat.* **2001**, US20010021693 A1.
- (24) (a) Jordan, F. T. W.; Forrester, C. A.; Ripley, P. H.; Burch, D. G. S. *Avian Dis.* **1998**, 42, 738. Windsor, H.M., Ripley, P.H., Hannan, P.C.T., 1996. In: *Proceedings of the 14th IPVS Congress*, Bologna, Italy, p. 226. (b) Aitken, I.A., Morgan, J.H., Dalziel, R., Burch, D.G.S., Ripley, P.H., 1996. In: *Proceedings of the 14th IPVS Congress*, Bologna, Italy, p. 318.
- (25) Hannan, P. C.; Windsor, H. M.; Ripley, P. H. *Res. Vet. Sci.* **1997**, 63, 157.
- (26) Heilmann, C.; Jensen, L.; Jensen, J. S.; Lundstrom, K.; Windsor, D.; Windsor, H.; Webster, D. J. *Infect.* **2001**, 43, 234.
- (27) Stresser, D. M.; Broudy, M. I.; Ho, T.; Cargill, C. E.; Blanchard, A. P.; Sharma, R.; Dandeneau, A. A.; Goodwin, J. J.; Turner, S. D.; Erve, J. C. L.; Patten, C. J.; Dehal, S. S.; Crespi, C. L. *Drug Metabolism and Disposition* **2004**, 32, 105.
- (28) U.S. Food and Drug Administration, Center for Drug Evaluation and Research. Altabax (retapamulin) ointment NDA 22-055 approval letter, May 29, 2007. Retrieved November 11, 2021, from [www.accessdata.fda.gov/drugsatfda\\_docs/nda/2007/022055s000\\_APPROV.pdf](http://www.accessdata.fda.gov/drugsatfda_docs/nda/2007/022055s000_APPROV.pdf).
- (29) Williamson, D. A.; Carter, G. P.; Howden, B. P. *Clin. Microbiol. Rev.* **2017**, 30, 827.
- (30) (a) Jones, R. N.; Fritsche, T. R.; Sader, H. S.; Ross, J. E. *Antimicrob. Agents Chemother.* **2006**, 50, 2583. (b) Candel, F. J.; Morales, G.; Picazo, J. J. *Rev. Esp. Quimioter.* **2011**, 24, 127.
- (31) (a) Alexander, E.; Goldberg, L.; Das, A. F. *JAMA* **2019**, 322, 1661. (b) File, T. M.; Goldberg, L.; Das, A.; Sweeney, C.; Saviski, J.; Gelone, S. P.; Seltzer, E.; Paukner, S.; Wicha, W. W.; Talbot, G. H.; Gasink, L. B. *Clin. Infect. Dis.* **2019**, 69, 1856. (c) Falcó, V.; Burgos, J.; Almirante, B. *Expert Opin. Pharmacother.* **2020**, 21, 629–636. DOI = 10.1080/14656566.2020.1714592.
- (32) U.S. Food and Drug Administration, Center for Drug Evaluation and Research. XENLETA (lefamulin) tablets, NDA 211672; injection NDA 211673 approval letter, August 19, 2019. Retrieved November 11, 2021, from [www.accessdata.fda.gov/drugsatfda\\_docs/nda/2019/211672Orig1s000,%20211673Orig1s000Approv.pdf](http://www.accessdata.fda.gov/drugsatfda_docs/nda/2019/211672Orig1s000,%20211673Orig1s000Approv.pdf)
- (33) (a) Berner, H.; Vypel, H.; Schulz, G.; Fischer, G. *Monatsh. Chem.* **1985**, 1165. (b) Sun, F.; Zhang, H.; Gonzales, G. B.; Zhou, J.; Li, Y.; Zhang, J.; Jin, Y.; Wang, Z.; Li, Y.; Cao, X.; Zhang, S.; Yang, S. *Antimicrob. Agents Chemother.* **2018**, 62, e02388–17.
- (34) Fu, L. Q.; Guo, X. S.; Liu, X.; He, H. L.; Wang, Y. L.; Yang, Y. S. *Chin. Chem. Lett.* **2010**, 21, 507.
- (35) Thirring, K.; Heilmayer, W.; Riedl, R.; Kollmann, H.; Ivezic-Schoenfeld, Z.; Wicha, W.; Paukner, S.; Strickmann, D. *PCT Int. Appl. WO2015110481*.
- (36) Fazakerley, N. J.; Procter, D. J. *Tetrahedron* **2014**, 70, 6911.
- (37) Egger, H.; Reinshagen, H. *J. Antibiot.* **1976**, 29, 915–922 and 923.
- (38) Riedl, K. *J. Antibiot.* **1976**, 29, 132.

- (39) Ling, Y.; Wang, X.; Wang, H.; Yu, J.; Tang, J.; Wang, D.; Chen, G.; Huang, J.; Li, Y.; Zheng, H. *Arch. Pharm.* **2012**, *345*, 638.
- (40) (a) Aitken, S.; Brooks, G.; Dabbs, S.; Frydrych, C. H.; Howard, S.; Hunt, E. *PCT Int. Appl. WO 2002012199*, **2002**. (b) Hirokawa, Y.; Kato, S.; Kinoshita, H.; Tanaka, T. *PCT Int. Appl. WO 2008117796*, **2008**.
- (41) (a) Yang, J. *PCT Int. Appl. WO 2007062334*, **2007**. (b) Yang, Y.; Jiang, Z.; Fu, L.; Cai, Z.; Li, Z.; Chao, Y.; Ji, R. *PCT Int. Appl. WO 2010028542*, **2010**. (c) Elder, J. S.; Forrest, A. K.; Jarvest, R. L.; Sheppard, R. J. *PCT Int. Appl. WO 2002030929*, **2002**.
- (42) Berner, H.; Schulz, G.; Schneider, H. *Tetrahedron* **1980**, *36*, 1807.
- (43) (a) Brooks, G.; Burgess, W.; Colthurst, D.; Hinks, J. D.; Hunt, E.; Pearson, M. J.; Shea, B.; Takle, A. K.; Wilson, J. M.; Woodnutt, G. *Bioorg. Med. Chem.* **2001**, *9*, 1221. (b) Igo, D. H.; Norton, B. A. *PCT Int. Appl. WO 2007062333*, **2007**. (c) Liu, P. *PCT Int. Appl. WO 2007062332*, **2007**.
- (44) (a) Berner, H.; Schulz, G.; Schneider, H. *Tetrahedron* **1981**, *37*, 915. (b) Sato, T.; Takadoi, M.; Fukuda, Y.; Hayashi, K. *Jpn. Kokai Tokkyo Koho JP 2008280297*, **2008**. (c) Takadoi, M. *Jpn. Kokai Tokkyo Koho JP 2010100582*, **2010**. (d) Fukuda, Y.; Takadoi, M.; Asahina, Y.; Sato, T.; Kurasaki, H.; Ebisu, H.; Takei, M.; Fukuda, H. *PCT Int. Appl. WO 2008143343*, **2008**.
- (45) Llabani, E.; Hicklin, R. W.; Lee, H. Y.; Motika, S. E.; Crawford, L. A.; Weerapana, E.; Hergenrother, P. J. *Nat. Chem.* **2019**, *11*, 521.
- (46) Ma, X.; Kucera, R.; Goethe, O. F.; Murphy, S. K.; Herzon, S. B. *J. Org. Chem.* **2018**, *83*, 6843.
- (47) Gibbons, E. G. *J. Org. Chem.* **1980**, *45*, 1540.
- (48) Kahn, M. *Tetrahedron Lett.* **1980**, 4547.
- (49) Gibbons, E. G. *J. Am. Chem. Soc.* **1982**, *104*, 1767.
- (50) Tanigawa, Y.; Ohta, H.; Sonoda, A.; Murahashi, S.-I. *J. Am. Chem. Soc.* **1978**, *100*, 4610.
- (51) (a) Paquette, L. A.; Wiedeman, P. E. *Tetrahedron Lett.* **1985**, *26*, 1603. (b) Paquette, L. A.; Bulman-Page, P. C. *Tetrahedron Lett.* **1985**, *26*, 1607. (c) Paquette, L. A.; Wiedeman, P. E.; Bulman-Page, P. C. *Tetrahedron Lett.* **1985**, *26*, 1611–1614.
- (52) (a) Paquette, L. A.; Wiedeman, P. E.; Bulman-Page, P. C. *J. Org. Chem.* **1988**, *53*, 1441. (b) Paquette, L. A.; Bulman-Page, P. C.; Pansegrau, P. D.; Wiedeman, P. E. *J. Org. Chem.* **1988**, *53*, 1450. (c) Paquette, L. A.; Pansegrau, P. D.; Wiedeman, P. E.; Springer, J. P. *J. Org. Chem.* **1988**, *53*, 1461.
- (53) Boeckman Jr., R. K.; Springer, D. M.; Alessi, T. R. *J. Am. Chem. Soc.* **1989**, *111*, 8284.
- (54) Bacqué, E.; Pautrat, F.; Zard, S. Z. *Org. Lett.* **2003**, *5*, 325.
- (55) Liu, J.; Lotesta, S. D.; Sorensen, E. J. *Chem. Commun.* **2011**, *47*, 1500.
- (56) Lotesta, S. D.; Liu, J.; Yates, E. V.; Krieger, I.; Sacchettini, J. C.; Freundlich, J. S.; Sorensen, E. J. *Chem. Sci.* **2011**, *2*, 1258.
- (57) Fazakerley, N. J.; Helm, M. D.; Procter, D. J. *Chem. Eur. J.* **2013**, *19*, 6718.
- (58) (a) Helm, M. D.; Da Silva, M.; Sucunza, D.; Findley, T. J. K.; Procter, D. J. *Angew. Chem., Int. Ed.* **2009**, *48*, 9315. (b) Findley, T. J.; Sucunza, D.; Miller, L. C.; Helm, M. D.; Helliwell, M.; Davies, D. T.; Procter, D. J. *Org. Biomol. Chem.* **2011**, *9*, 2433.
- (59) Murphy, S. K.; Zeng, M.; Herzon, S. B. *Science* **2017**, *356*, 956.
- (60) Wang, H.; Negretti, S.; Knauff, A. R.; Montgomery, J. *Org. Lett.* **2015**, *17*, 1493.
- (61) Zeng, M.; Murphy, S. K.; Herzon, S. B. *J. Am. Chem. Soc.* **2017**, *139*, 16377.
- (62) Berner, H.; Vypel, H.; Schulz, G.; Schneider, H. *Monatsh. Chem.* **1985**, 1073.
- (63) Farney, E. P.; Feng, S. S.; Schäfers, F.; Reisman, S. E. *J. Am. Chem. Soc.* **2018**, *140*, 1267.

## CHAPTER 2: A SYNTHETIC APPROACH TO THE PLEUROMUTILIN DITERPENES

### 2.1. Synthetic Considerations & Analysis of Prior Art

In *The Logic of Chemical Synthesis*, Corey describes molecular complexity as a culmination of “molecular size, element and functional-group content, cyclic connectivity, stereocenter content, chemical reactivity, and structural instability [...]”.<sup>1</sup> Following this framework, the natural product pleuromutilin **2.1** is the C<sub>14</sub> monoglycolate of its parent diterpenoid, mutilin **2.2**, and possesses the molecular formula C<sub>22</sub>H<sub>34</sub>O<sub>5</sub> (Figure 2.1).<sup>2</sup> The three sites of oxidation are arranged into two 1,4-oxygenation patterns, but the defining feature of the mutilin structure is its cyclic connectivity. Mutilins are typified by their distinctive tricyclic propellane skeleton decorated with eight contiguous stereocenters, seven of which reside on the cyclooctane portion **2.3**. The severe steric environment imposed by mutilin’s congested polycyclic structure plays a prominent role in controlling the reactivity of its functional groups. The propellane arrangement of the three rings dictates that there are no “exposed” faces, increasing the challenge associated with any planned bimolecular reactions.<sup>3</sup> This effect is most prominent for atoms surrounding the C5–C4–C9 juncture (**2.4**), where two all-carbon quaternary centers flank the point of coincidence for the three rings; it becomes less pronounced at the distal functional groups (*i.e.*, the C11 hydroxyl and the C12 alkene).

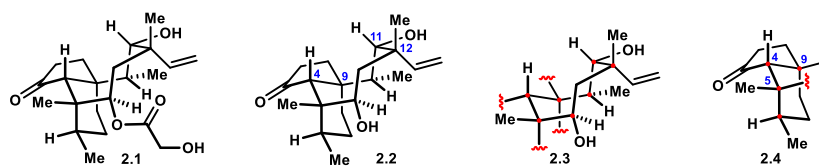
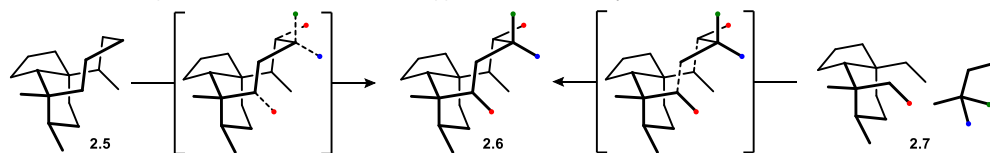


Figure 2.1. Pleuromutilin, mutilin, the cyclooctane domain, and the hydrindanone nucleus

While the assembly of the perhydroindanone portion of the mutilin structure has proven challenging, the evolution of mutilin total synthesis up to this point has been defined by the strategies employed for installation of the highly decorated cyclooctane.<sup>4</sup> Classical approaches, typified by the syntheses of Boeckman and Procter (*see above*), relied on transform-goal based strategies to assemble a sparsely functionalized mutilin tricyclic scaffold represented by model

**2.5** (Scheme 2.1).<sup>5</sup> This design requires the sequential introduction of substituents to the cyclooctane to access mutilin derivatives **2.6**. While these consecutive functionalizations typically benefit from the high diastereoselectivity observed in polycyclic systems, the approach necessitates a large number of linear synthetic steps to realize. Modern analyses of the mutilin structure, exemplified by Herzon and Reisman (*see above*), have prioritized convergency.<sup>6</sup> In this sense, a pair of highly decorated reactive partners represented by fragments **2.7** are coupled. Subsequent cyclization enables direct access to mutilin derivatives **2.6**, reducing the number of steps required to access pleuromutilins. The drawback of the recent approaches has been the low diastereoselectivities observed during fragment coupling and the difficulties of direct cyclooctane synthesis by the cyclization of a linear precursor.

**Scheme 2.1.** Comparison of classical and modern approaches to mutilin synthesis

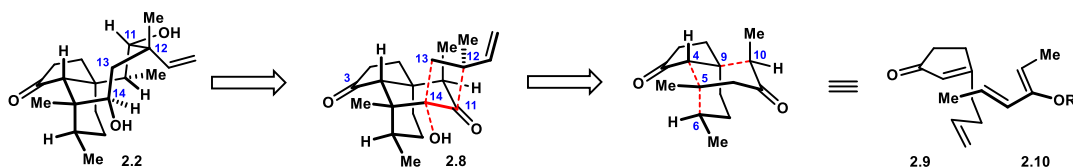


## 2.2. Retrosynthetic Analysis

We initiated synthetic studies toward the mutilin diterpenes in late 2018, aiming to develop a concise, stereocontrolled solution to the challenges posed by mutilin total synthesis. Our analysis of the target structure **2.2** relied on topological, structure-goal, and transform-goal based reasoning (Scheme 2.2). We envisioned establishing the challenging 5-carbon portion of the mutilin cyclooctane system **2.2** spanning C11–C14 by an annulation-ring expansion transform.<sup>7</sup> To this end, we identified the tricyclic ketone **2.8** as a key sub-target. Using the reactivity of the C11 ketone functionality, we envisaged formation of the C13–C14 bond and the C11–C12 bond along with scission of the C11–C14 bond in an oxidative fashion. This set of disconnections addresses two of the most daunting challenges: the formation of the highly decorated cyclooctane motif and one of the 1,4-oxygenation patterns. Another appealing aspect of this synthesis design is the flexibility it affords with respect to executing the requisite bond

constructions in the endgame. Successful implementation of our strategy would therefore require an expedient synthesis of the tricyclic ketone **2.8**. To this end, we identified two key transforms. We planned to employ an intermolecular cycloaddition reaction to initially couple the simple enone **2.9** and diene **2.10**. We next anticipated that the C5–C6 bond could be forged by a radical cyclization.

**Scheme 2.2.** Identification of a synthetic strategy



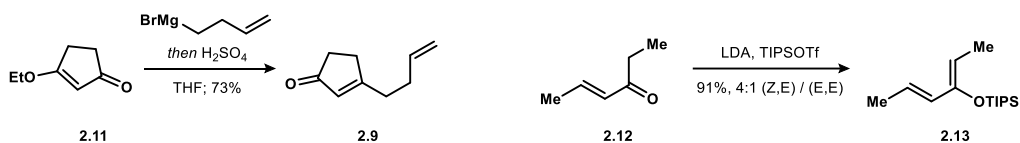
At the outset, we recognized that our selected disconnections did not account for control over all of mutilin's eight stereocenters, but we reasoned that we could devise solutions to these challenges as they should present themselves. Additionally, the presence of ketones at C11 and C3 promised to offer us control over the configuration of adjacent stereocenters at C10 and C4, which could be manipulated as necessary for the success of the synthesis. We were optimistic that our analysis of the mutilin structure would solve the key challenges identified by prior synthetic efforts. Namely, our plan aimed to directly access the cyclooctane motif with the necessary substitution in place, while simultaneously avoiding the preparation of stereochemically complex acyclic intermediates. Depending on the order of bond constructions in the endgame, we hoped to bypass a notoriously challenging cyclooctane synthesis by the cyclization of a polysubstituted linear precursor.

### 2.3. Synthesis of a Key Tricyclic Sub-Target

We began with the synthesis of key sub-target ketone **2.8**. Preparation of cyclopentenone **2.9** followed close literature precedent, with addition of 3-butenylmagnesium bromide to commercially available vinylogous ester **2.12** followed by treatment with aqueous  $\text{H}_2\text{SO}_4$ , completing the Danheiser–Stork transposition (Scheme 2.3).<sup>8</sup> We found that the reaction

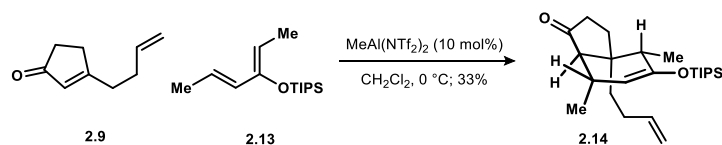
was robust, readily scalable up to 180 mmol, and that the product could be isolated by distillation in 73% yield. Its coupling partner, silyloxydiene **2.13**, was prepared under standard methods: the lithium enolate derived from (*E*)-4-hexen-3-one **2.12** reacted smoothly with TIPSOTf to provide the desired product as a 4:1 mixture of inseparable (*Z,E*) and (*E,E*) isomers in a combined yield of 91%.<sup>9</sup> The lithium enolate was found to be uniquely effective for this transformation when compared with other typical conditions.

**Scheme 2.3.** Preparation of enone **2.9** and silyloxydiene **2.13**



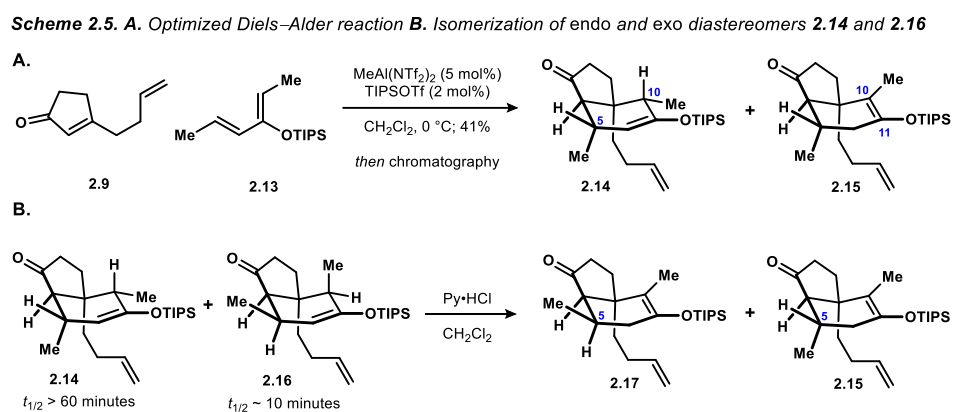
With the coupling partners in hand, we began to investigate the desired intermolecular Diels–Alder reaction. Owing to the high degree of substitution at the reactive positions of the diene and dienophile pair, we anticipated that the cycloaddition reaction would require the use of strong Lewis acids. We turned to the work of Jung, whose group identified several Lewis acids that excelled in catalyzing sterically demanding bimolecular Diels–Alder reactions.<sup>10</sup> While  $\text{AlCl}_3$ ,  $\text{MeAlCl}_2$ , and  $\text{AlBr}_3$  were generally ineffective, we found that alkylaluminum triflimides were competent in catalyzing the desired transformation (Scheme 2.4). Namely, the species  $\text{MeAl}(\text{NTf}_2)_2$ , prepared by combining  $\text{Me}_3\text{Al}$  and  $\text{HNTf}_2$  in a 1:2 stoichiometry, was the most effective, furnishing the bicyclic ketone **2.14** in 33% yield.

**Scheme 2.4.** Early hit for the cycloaddition of enone **2.9** and silyloxydiene **2.13**



While the simple combination of enone **2.9** and silyloxydiene **2.13** with  $\text{MeAl}(\text{NTf}_2)_2$  was initially successful in generating cycloadduct **2.14**, we quickly encountered issues with reproducibility. Under seemingly identical setup procedures, drastic variance in reaction rate

was observed, and in many cases the reaction would not proceed at all. We eventually recognized that the differences in outcome were linked to the batch of silyloxydiene **2.13** used in a given reaction setup. This led us to identify TIPSOTf, which was a contaminant in some batches of silyloxydiene **2.13**, as an active catalyst in the Diels–Alder reaction. Employing 5 mol% MeAl(NTf<sub>2</sub>)<sub>2</sub> and 2 mol% TIPSOTf, we could reproducibly form the cycloadduct in 41% isolated yield (Scheme 2.5A). The reaction does not proceed in the absence of either Lewis acid. We therefore believe this to be an example of Lewis acid-activated Lewis acid catalysis, a phenomenon which was studied by Yamamoto and has been employed by others in total synthesis efforts.<sup>11</sup> During continued use of the cycloaddition to supply material for our synthetic campaign, we encountered another inconsistency in the outcome of the reaction. We observed that in addition to the expected bicyclic ketone **2.14**, variable proportions of the isomerized enoxysilane **2.15** would be obtained following chromatographic purification. These two regioisomers were inseparable, and in some cases the isolated material would be comprised of exclusively the C10 isomer **2.15**. The unintended isomerization would initially hinder our ability to evaluate the next steps but was eventually found to be inconsequential (*see below*).



Another notable facet of the cycloaddition reaction between enone **2.9** and diene **2.13** is the observed *exo* selectivity.<sup>12</sup> Indeed, under our typical procedure, only the cycloadducts **2.14** and **2.15** were obtained, both of which arise from the *exo* attack. However, NMR analysis of the crude material indicated that the *exo* selectivity was far from complete: a set of resonances

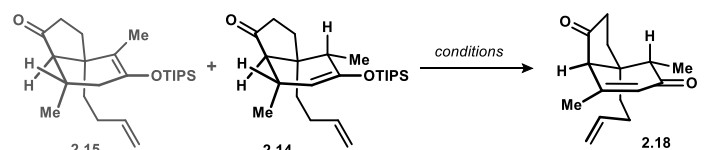
corresponding to a suspected *endo* isomer were present in a 1:2 ratio with ketone **2.14**. We attributed the apparent disappearance of the minor *endo* isomer to hydrolysis during chromatography assisted by trace acid. In this vein, extensively eliminating acidic byproducts by quenching the reaction with saturated aqueous NaHCO<sub>3</sub> and vigorously mixing the resulting emulsion for 14 h afforded a mixture of inseparable isomers **2.14** and **2.16** in 58% yield (Scheme 2.5B). While the *endo* isomer **2.16** proved an ineffective substrate during subsequent steps, we used the mixture of ketones **2.14** and **2.16** to probe the reactivity differences of the two diastereomers. Subjection of enoxysilanes **2.14** and **2.16** to pyridinium hydrochloride induced rapid isomerization of *endo* isomer **2.16** into its regioisomer **2.17**, whereas the *exo* derivative **2.14** isomerized slowly under the reaction conditions. The difference in isomerization rates may correlate to the relatively high reactivity of *endo* product **2.16** to acidic hydrolysis during chromatography. Ultimately, the cycloaddition of enone **2.9** and diene **2.13** proved effective in supplying material for our synthetic campaign. It performed well up to at least 40 mmol scale, permitting us to synthesize >5 g of the desired bicyclic ketones **2.14** and **2.15** in a single pass. Preliminary results aimed at induction of asymmetry to the cycloaddition have been unsuccessful, as Corey's activated oxazaborolidine catalysts failed to promote the reaction.<sup>13</sup>

With access to the mixture of cycloadducts **2.14** and **2.15** established, the next challenge we faced was the oxidation of the enoxysilane moiety to the corresponding  $\alpha,\beta$ -unsaturated ketone. Application of Evans' conditions: ceric ammonium nitrate (CAN) in DMF proved to be uniquely effective in furnishing the bicyclic enone **2.18** (Table 2.1, entry 1).<sup>14</sup> An especially valuable feature of the CAN-mediated reaction is that any mixture of enoxysilanes **2.14** and **2.15** can be used with no effect on the yield. We had found some success implementing Magnus'  $\beta$ -azidonation-elimination protocol, but the product yield failed to exceed 20% (entry 2).<sup>15</sup> In contrast, the palladium-catalyzed reaction such as typical Saegusa-Ito or Stahl's more reactive Pd(OTFA)<sub>2</sub>-catalyzed conditions were completely ineffective (entries 3-



5).<sup>16,17</sup> Attempted selenation led to the formation of complex mixtures (entry 6).<sup>18</sup> Another single-electron oxidant that has been used to prepare  $\alpha,\beta$ -unsaturated carbonyl derivatives from enoxysilanes, DDQ, was similarly unproductive (entries 7-8).<sup>19</sup>

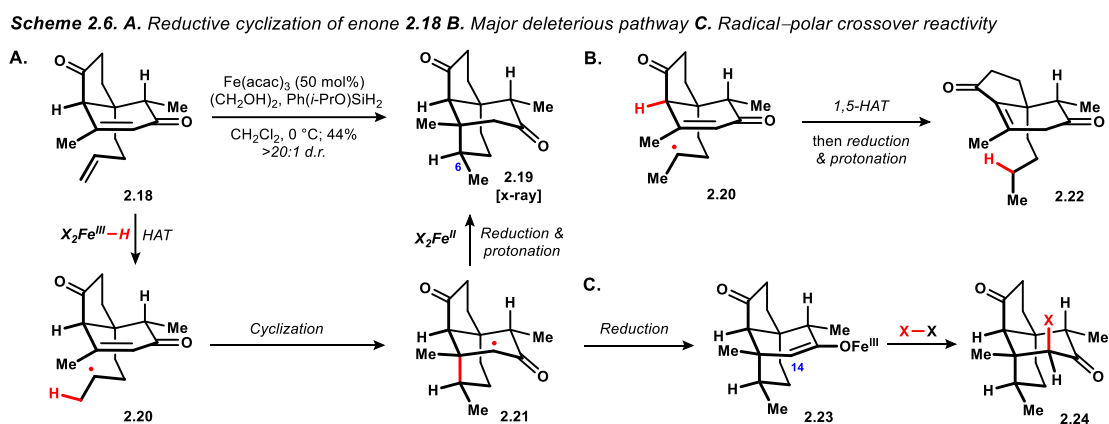
**Table 2.1.** Oxidation of enoxy silanes **2.14** and **2.15**



Entry	Substrate	Conditions	Recovered <b>2.14</b> (%)	Yield <b>2.18</b> (%)
1	<b>2.14</b> + <b>2.15</b>	(NH <sub>4</sub> ) <sub>2</sub> Ce(NO <sub>3</sub> ) <sub>6</sub> , DMF	<5	73
2	<b>2.14</b>	1. TMSN <sub>3</sub> , (PhIO) <sub>n</sub> , 2. TBAF	<5	18
3	<b>2.14</b>	Pd(OTFA) <sub>2</sub> , O <sub>2</sub> , 80 °C	<5	<5
4	<b>2.14</b>	Pd(OTFA) <sub>2</sub> , O <sub>2</sub> , 50 °C	>80	<5
5	<b>2.14</b>	Pd(OAc) <sub>2</sub> , O <sub>2</sub> , 50 °C	>80	<5
6	<b>2.14</b>	PhSeCl, CsF	<5	<5
7	<b>2.14</b>	DDQ, HMDS	>80	<5

Having introduced the  $\alpha,\beta$ -enone moiety, the stage was set for the next key step: an MHAT-initiated Giese cyclization. Baran's group first demonstrated that the alkyl radicals formed from the reaction of relatively electron-rich alkenes with iron hydrides underwent additions to electron deficient alkenes, namely  $\alpha,\beta$ -unsaturated carbonyl derivatives.<sup>20</sup> These processes have been employed to great effect in total synthesis.<sup>21</sup> We found that subjecting the enone **2.18** to 50 mol% iron(III) acetylacetonate in the presence of Shenvi's monoisopropoxy phenylsilane and ethylene glycol in dichloromethane formed the desired tricyclic diketone **2.19** (Scheme 2.6).<sup>22</sup> We were excited to find that the stereocenter at C6 was formed with exquisite diastereoselectivity (>20:1), and our structural assignment was confirmed by X-ray crystallographic analysis. The reaction is presumed to proceed by initial hydrogen-atom transfer (HAT) to the monosubstituted alkene contained within dienone **2.18**, generating an intermediate radical **2.20** (Scheme 2.6A). Subsequent Giese cyclization to form the  $\alpha$ -keto radical **2.21** is believed to precede reduction by iron(II) and protonation of the enolate intermediate to form **2.19**.<sup>23</sup> Alternatively, a mechanism has been suggested where no reduction to an enolate intermediate is involved.<sup>24</sup>

Chromatographic purification of the diketone **2.19** proved to be challenging. A significant impurity, formed in a *ca.* 1:2 ratio with the desired material, consistently co-eluted with the desired product under all of the solvent mixtures we surveyed. While we were unable to isolate it in analytically pure form, we assigned the structure of bicyclic enone **2.22** to the impurity (Scheme 2.6B). The enone **2.22** likely arises from a 1,5-hydrogen atom transfer process of intermediate **2.20** that competes with the Giese cyclization. We required access to pure diketone **2.19** and developed a protocol for its isolation. Initial purification of the crude reaction mixture by chromatography followed by crystallization from 5:1 *n*-hexane/cyclohexane at 4 °C delivered the desired tricyclic diketone **2.19** in 44% overall yield (two crystallizations). The yield of diketone **2.19** by NMR analysis of the crude material was 53%, indicating that the two-step purification protocol we developed proceeded with 83% recovery. This procedure would prove effective in supplying the material required to support our synthetic campaign.

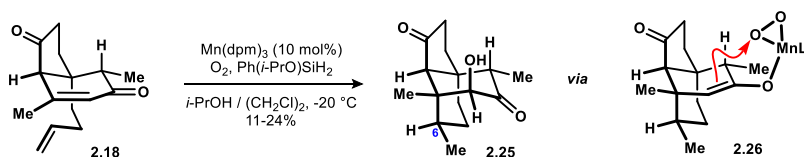


Given the success of the MHAT-initiated radical cyclization, we hoped to extend the reactivity further. Our group had previously observed that the MHAT-initiated Giese cyclization could be coupled to an intramolecular aldol event, enabling the formation of two C–C bonds in one step.<sup>25</sup> On this basis, we imagined a cascade process wherein, rather than undergoing direct protonation, the enolate **2.23** would react with an exogenous electrophile (Scheme 2.6C). We recognized that an alternative mechanism may be available where the keto-radical **2.21**

would be captured by a radicalophile, leading to similar products. This reaction design deviates from the established reactivity in that we hoped to incorporate an electrophile or radicalophile in an intermolecular fashion. We imagined that the functionalized products **2.24** would be useful in our synthetic campaign toward pleuromutilin.

Our initial attempts to leverage the diene **2.18** into the envisioned cyclization cascade reactivity were unsuccessful. We surveyed a number of electrophiles (aldehydes, alkyl halides, sulfonylsulfides, glyoxylates, and cyanosulfonates) and radicalophiles (diazoacetates, nitrites, and halide sources) but never observed the expected functionalized products. Instead, the major product was typically mixtures of starting enone **2.18** and the diketone **2.19**. Implementing other catalysts (*i.e.*, Mn and Co catalysts) and avoiding alcoholic co-solvents did not improve the reaction outcomes. After many failures, we finally realized the envisioned cascade cyclization by employing a particular set of Mukaiyama hydration conditions. Exposure of dienone **2.18** to catalytic Mn(dpm)<sub>3</sub> and Shenvi's silane with continuous sparging of the reaction mixture with O<sub>2</sub> at -20 °C delivered the hydroxyketone **2.25** (Scheme 2.7). The product was formed with high diastereoselectivity at C6, but the yield was low and variable (typically 11-24%). Increasing the scale of the reaction tended to reduce the yield of the desired product. We were not surprised by the variability of the outcome, given the uncertain concentration of oxygen throughout the reaction and the large number of competitive reactions available to the intermediate alkyl radicals.

**Scheme 2.7.** Giese Cyclization-Mukaiyama hydration cascade



Findings from Magnus and co-workers may explain why the Mukaiyama hydration conditions with Mn(dpm)<sub>3</sub> were the only ones to afford the expected C14-functionalized product **2.25**.<sup>26</sup> Magnus' team observed that the pale yellow putative HMn(dpm)<sub>2</sub> would turn to a dark

green-brown color when it was held under an atmosphere of oxygen. This color change could be reversed by evacuating the flask. They concluded that the color change corresponded to the formation of a new manganese complex with oxygen. It seems likely that the HMn peroxo complex delivers the oxygen atom introduced to hydroxyketone **2.25** in an intramolecular fashion via an intermediate resembling **2.26**, overcoming the kinetic barriers associated with bimolecular capture of the enolate or  $\alpha$ -keto radical intermediate (Scheme 2.6). This principal may be more generally applicable in the development of new radical difunctionalization reactions. Interestingly, Magnus and co-workers also note that the yields obtained in the hydration of  $\alpha,\beta$ -unsaturated carbonyl compounds with  $\text{Mn}(\text{dpm})_3 / \text{O}_2$  depended heavily on how the reaction vessel was washed, underscoring the reproducibility challenges these reactions suffer from, even with simple substrates. Washing the reaction vessel with the basic detergent Alconox greatly improved the performance of the reaction for Magnus' team, presumably by deactivating the protic surface of the glassware. We found that the conversion of enone **2.18** to hydroxyketone **2.25** did not improve meaningfully when various detergents were used to wash the reaction flask. Given the inefficient performance of the cyclization-Mukaiyama hydration cascade, we chose for the time being to focus on the elaboration of tricyclic diketone **2.19** into intermediates for the synthesis of mutilin.

#### **2.4. Scouting a Synthetic Strategy Relying on Cyclobutanol Oxidation**

We were intrigued by the promise of a route to pleuromutilins that involved the oxidative fragmentation of a [4.2.0] bicyclic motif, but cognizant of the challenges associated with the planned regioselective cleavage of these cyclobutanol-containing intermediates (Figure 2.2A). Aside from the challenge of establishing the quaternary stereocenter at C12 with the desired diastereoselectivity, we imagined that oxidative opening of an intermediate resembling cyclobutanol **2.29** would likely proceed with scission of the undesired C11–C12 bond (Figure 2.2B, highlighted in red).<sup>27</sup> This expectation arose from our understanding that most ring-

cleavage reactions of small ring cycloalkanols **2.27** proceed through the initial formation of an alkoxy radical. Subsequent  $\beta$ -scission can proceed to cleave either of the adjacent C–C bonds, with the stability of the radical intermediate being formed tending to dictate the observed regioselectivity; in the case of simple cyclobutanol **2.27**, this would lead to scission of the C1–C2 bond, forming the more stabilized radical **2.28**, rather than the alternative pathway where C1–C4 is homolyzed. Some related oxidative cycloalkanol ring-opening reactions are believed to proceed through cationic pathways but follow similar regioselectivity trends to the radical processes. Accordingly, we designed the hypothetical ethylenecyclobutanol **2.30**, which we expected would undergo oxidative cleavage of the desired C11–C14 bond, owing to the relative stability of secondary alkyl radicals when compared with the vinyl radical that would be formed by scission of the undesired C11–C12 bond. Notably, this decision required assembly of the quaternary center at C12 at a later stage in the synthetic sequence. Though it promised to add to the number of linear synthetic steps required, we hoped to leverage cyclic stereocontrol during the introduction of the methyl group at C12.

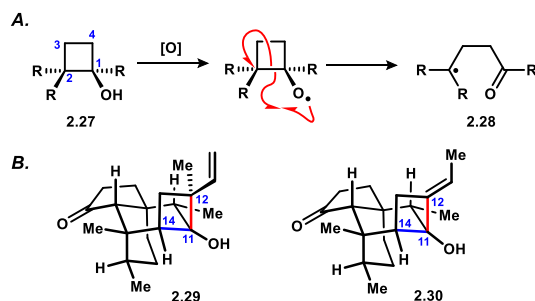
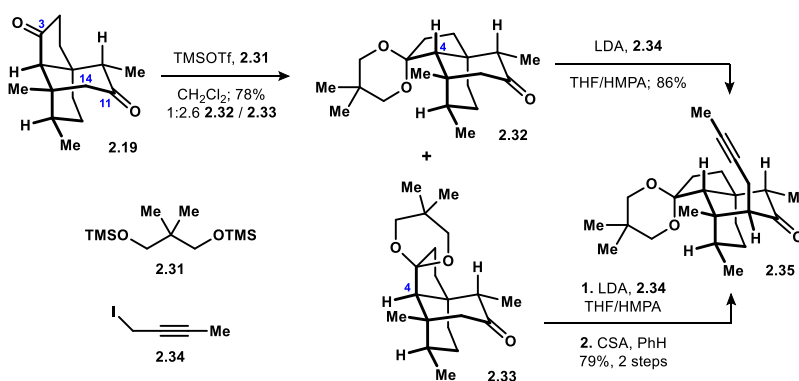


**Figure 2.2.** A. Regioselectivity in cyclobutanol ring-expansions  
B. Hypothetical cyclobutanol-containing intermediates

The C3 ketone was found to be more reactive than the C11 ketone toward deprotonation, and therefore required derivatization before we could proceed. We found that exposure of the diketone **2.19** to Noyori's conditions for acetalization with silyl ether **2.31** was highly effective (Scheme 2.8).<sup>28,29</sup> To our surprise, the reaction proceeded with some epimerization of the C4 stereocenter and afforded a mixture of monoketals **2.32** and **2.33**.

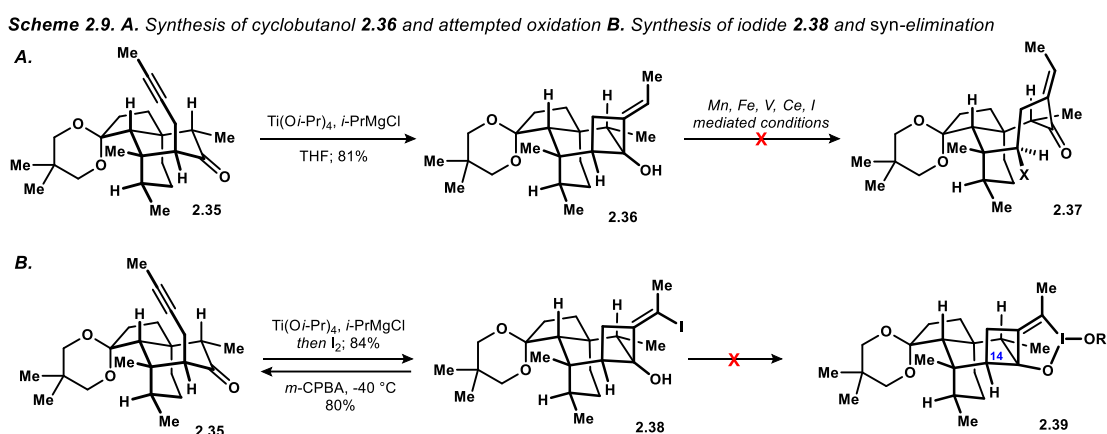
Presumably, the epimerization is enabled by an equilibrium that exists between the ketal and the corresponding enol ether in the presence of Lewis acid. The major product was the diastereomer **2.33**, which displayed the same C4 stereochemistry as its precursor **2.19**. The minor product was its C4 epimer **2.32**, which exhibited C4 stereochemistry matching mutilin. The mixture was found to be a thermodynamic ratio, but we still hoped to leverage this unanticipated epimerization. To this end, we directly alkylated the lithium enolate derived from minor ketone **2.32** with 1-iodo-2-butyne **2.34**, furnishing the alkyne **2.35** in good yield. We reasoned that following introduction of a substituent to the C14 position, the major diastereomer **2.33** should be prone to epimerization at C4, as the inversion of configuration would alleviate a *syn*-pentane interaction. To this end, the major diastereomer **2.33** reacted under similar alkylation conditions, and exposure of the alkylated material to anhydrous acid (CSA, benzene) cleanly epimerized the C4 stereocenter, thereby converging it to the ketone **2.35** in 79% yield across two steps.

**Scheme 2.8.** Synthesis of homopropargyl ketone **2.35**



With the ketoalkyne **2.35** in hand, we turned our attention to the synthesis of the requisite [4.2.0] bicyclic motif. We were encouraged by a single example from Marek's group that demonstrated the use of a titanium-alkyne complex for the addition to an adjacent ketone to form a cyclobutanol.<sup>30</sup> Additionally, the reactivity of titanium-alkyne complexes has been thoroughly explored and used impressively in the context of total synthesis.<sup>31,32</sup> To this end, we generated Sato's reagent ( $\text{Ti}(\text{O}i\text{-Pr})_4$ ,  $i\text{-PrMgCl}$ ) at  $-78\text{ }^\circ\text{C}$  in THF before introducing the alkynyl

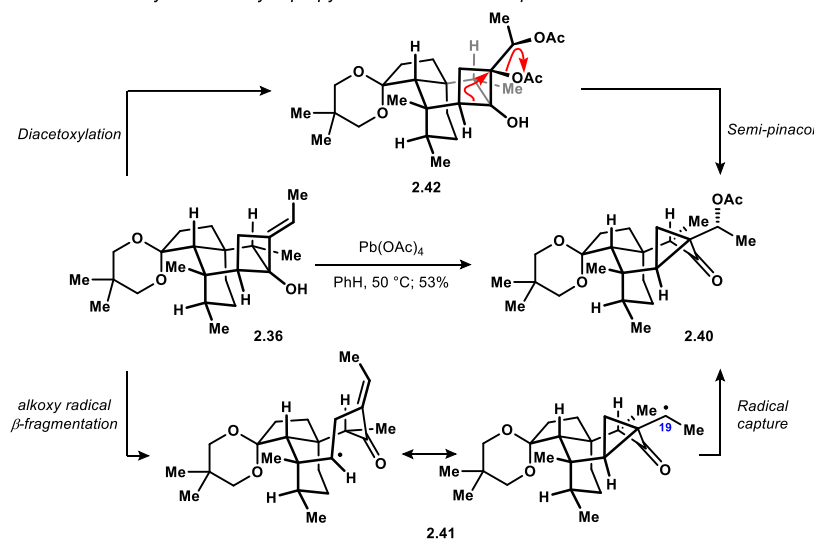
ketone **2.35** (Scheme 2.9A). Upon warming to 0 °C, we were excited to observe clean conversion of the material into the cyclobutanol **2.36**. With an efficient route to the key sub-target **2.36** in hand, we turned our attention to the fragmentation of the contained cyclobutanol. We first investigated manganese(III) based oxidants, developed and used extensively by Snider, to no success.<sup>33</sup> The use of other oxidants that have been employed in the fragmentation of small ring cycloalkanols, namely iron(III), vanadium(V), cerium(IV), and I(III) was no more effective.<sup>34-37</sup>



We attributed the poor reactivity of cyclobutanol **2.36** toward oxidative ring-expansion to its sterically congested nature (Scheme 2.9). In many cases, interaction between the cycloalkanol with the metal oxidant is required, as ring-expansion is initiated by an inner-sphere oxidation to form an alkoxy radical. As such, we wondered if the barrier associated with coordination of the congested alcohol **2.36** with the metal oxidant could be obviated by incorporating the oxidant into the substrate. To this end, application of Sato's reagent and quenching with iodine furnished the iodocyclobutanol **2.38** in good yield (Scheme 2.9B). We had envisioned that oxidation at the iodine center could form a cyclic iodane **2.39**, which was expected to activate the C14 position to attack by a nucleophile in the reaction mixture.<sup>39</sup> Disappointingly, treatment of iodide **2.38** with oxidants furnished exclusively the alkyne **2.35**. The orbital interactions involved in this unusual *syn* elimination are not clear.

We finally observed the formation of a rearranged product when we exposed cyclobutanol **2.36** to  $\text{Pb}(\text{OAc})_4$  in benzene.<sup>40</sup> To our dismay, we found that the reaction had not furnished the expected ring-expanded cyclooctanone derivative. Instead, we identified the major product as the cyclopropyl ketone **2.40** (Scheme 2.10). A plausible mechanism for this transformation begins with oxidation of the substrate by  $\text{Pb}(\text{OAc})_4$  to form an alkoxy radical.  $\beta$ -fragmentation of the endocyclic bond of the [4.2.0] bicyclic moiety, as designed, affords the radical **2.41**. The delocalized cyclopropylcarbinyl radical is captured preferentially at the undesired C19 site, affording the observed product **2.40**. An alternative mechanism could consist of diacetoxylation of the trisubstituted alkene **2.36** followed by a semi-pinacol rearrangement of diacetate **2.42**.

**Scheme 2.10.** Synthesis of cyclopropyl ketone **2.40** and two possible mechanisms

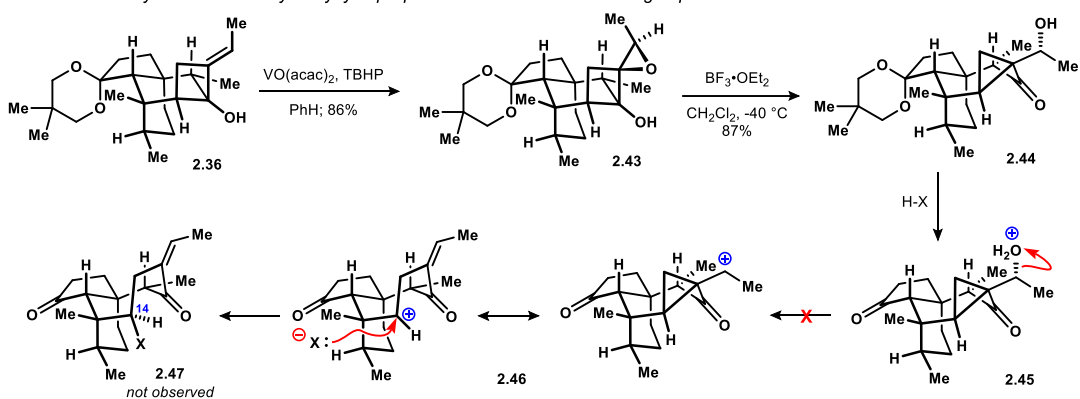


We were surprised by the facile formation of the cyclopropylketone **2.40** but recognized that similar cyclopropane-containing structures may be viable intermediates to produce the desired cyclooctane scaffold. We viewed the acetoxycyclopropane **2.40** as a non-ideal intermediate toward this aim, but we found that similar rearrangements of the bicyclo[4.2.0]octane system of allylic alcohol **2.36** could be initiated by activation of the trisubstituted alkene moiety (Scheme 2.11). For example, hydroxyl-directed epoxidation of **2.36**



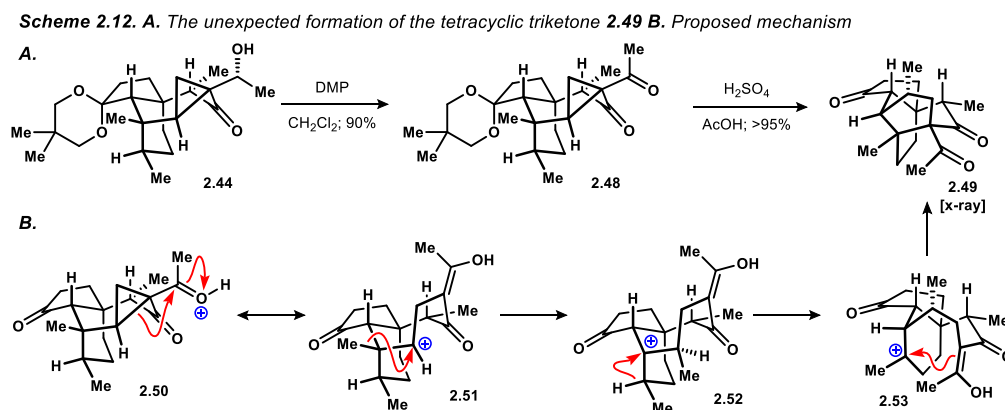
furnished an intermediate epoxyalcohol **2.43** that underwent rearrangement in the presence of Lewis acid to afford the hydroxycyclopropane **2.44** in good yield. We envisioned that an acid-mediated rearrangement of hydroxycyclopropane **2.44** may be initiated by protonation of the alcohol functionality to afford a delocalized cyclopropylcarbinyl carbocation **2.46**. An alternative process in which the ketone is protonated would presumably lead to similarly productive ring-expansion. Intermolecular capture of the carbocation **2.46** would furnish the desired 5-6-8 tricyclic structure **2.47**, complete with the required functionality at the C14 position. Notably, the bimolecular capture of a similar C14 carbocation is implicated in the biosynthesis of mutilin (see *above*, Chapter 1). Furthermore, some bicyclo[4.2.0]octane systems had been shown to undergo similar ring-expansion events.<sup>40</sup> Unfortunately, the hydroxycyclopropane **2.44** was not prone to ring-expansion under the acidic conditions we surveyed, and the cyclopropane moiety was intact following exposure to acid.

**Scheme 2.11.** Synthesis of the hydroxycyclopropane **2.44** and envisioned ring expansion to form ketone **2.47**



We further pursued our designed ring-expansion reaction by modifying the cyclopropane-containing substrate. To this end, oxidation of the hydroxycyclopropane **2.44** afforded the cyclopropanedione **2.48** (Scheme 2.12). We imagined that a similar ring expansion as depicted in Scheme 2.11 may be plausible, with the reactivity of the cyclopropane toward fragmentation being increased by the presence of the 1,3-diketone motif. We soon found that the diketone **2.48** was prone to rearrangement upon exposure to  $\text{H}_2\text{SO}_4$  in AcOH. To our

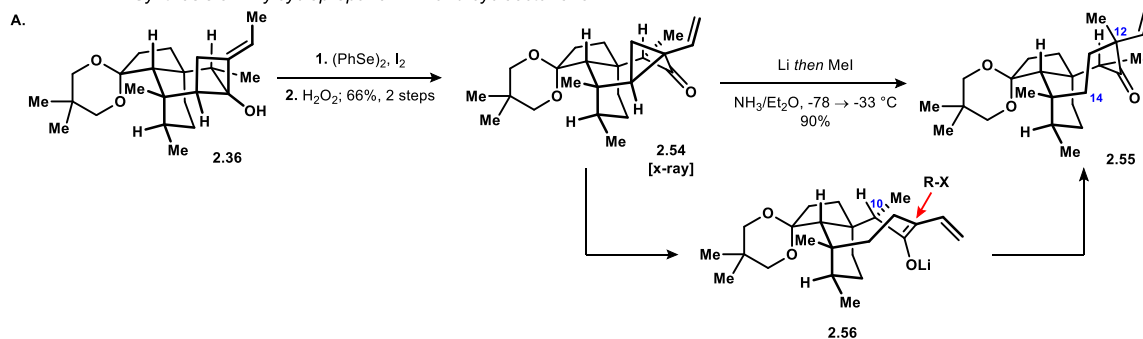
disappointment, rather than the desired cyclooctanone being formed, we isolated in quantitative yield the tetracyclic triketone **2.49**. A likely mechanism for the formation of this product begins with the protonation of the ketone, forming a delocalized cationic system with reactivity that can be rationalized by the two alternative forms of protonated cyclopropyl ketone **2.50** and hypothetical secondary carbocation **2.51** (Scheme 2.12B). Rather than participating in intermolecular capture by a nucleophile, as desired, the initially formed cation **2.51** undergoes a 1,2-methyl shift, generating the intermediate **2.52**. Subsequent 1,2-hydride shift forms the tertiary carbocation **2.53**. Finally, the appended enol of the 1,3-diketone captures the carbocation, affording after proton transfer the observed tetracyclic triketone **2.49**. We initially assigned the structure by 2D NMR experiments and were able to corroborate the structure by X-ray crystallographic analysis. While the unexpected rearrangement was fascinating to discover, we recognized that the facile 1,2-shifts and ring-contraction observed would likely impede us from accessing the desired architecture by cationic ring-expansion processes.



We turned our attention to scission of the cyclopropane moiety by single-electron reduction of the C11 ketone, beginning with the preparation of a new bicyclo[5.1.0]octane substrate. Exposing the ethylenecyclobutanol **2.36** to Kim's conditions, diphenyl diselenide and  $\text{I}_2$  in ethanol, initiated a seleniranium ion-promoted semi-pinacol rearrangement.<sup>41</sup> Subsequent selenoxide elimination of the product alkylselenide under standard conditions furnished the vinylcyclopropane **2.54** in 66% yield over two steps (Scheme 2.13). With a

suitable substrate in hand, we hoped to probe the regioselectivity of cyclopropane opening following single-electron reduction of the neighboring ketone. Though many cyclic ketocyclopropanes undergo reduction to the ketyl radical with subsequent scission of the less substituted bond, we believed that the orbital alignment of ketone **2.54** would favor the alternative ring-expansion process, as desired.<sup>42</sup> This belief was anchored in bonding alignments observed in the X-ray structure of cyclopropane **2.54**. We further hoped to capture the enolate formed during the reduction with a methylating agent, thereby installing the twentieth and final skeletal carbon of the mutilin scaffold. We predicted on the basis of molecular models that the stereochemical outcome of the enolate methylation would provide the desired configuration at C12. We expected that the configuration of the methyl group at C10 would exhibit control over the conformational preference of the enolate intermediate **2.56**. Computational evaluation of a similar substrate would support this hypothesis (*see below*). To this end, dissolving metal reduction of the ketocyclopropane **2.54** followed by addition of iodomethane induced the clean formation of the cyclooctanone **2.55**. We were especially excited to find that the methyl group was incorporated at C12 with high diastereoselectivity (>20:1) for the desired isomer, as determined by NOESY analysis.

**Scheme 2.13.** Synthesis of vinylcyclopropane **2.54** and cyclooctanone **2.55**



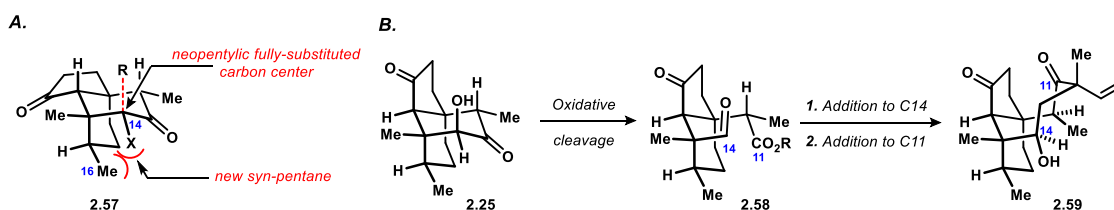
While the synthesis of the cyclooctanone **2.55** was a large step forward in our synthetic campaign, we recognized that ketone **2.55** itself would not be a viable intermediate toward mutilin. The lack of functional handle at the C14 position meant that the introduction of the

requisite oxidation would be challenging. After considering C-H oxidation approaches, we opted at this juncture to pursue a slightly modified synthetic sequence that would establish a functional handle at the C14 position at an earlier stage.

## 2.5. Scouting a Synthetic Approach Relying on Nucleophilic Addition to C14

Having resolved to prepare a C14-functionalized tricyclic intermediate, we set about devising a plan of action. We recognized that the incorporation of a functional handle at the desired site would be challenged by the demanding steric environment surrounding the C14 carbon atom (Scheme 2.14A). The position is neopentyllic and resides within a congested tricyclic system. Evidently, we were able to overcome these steric challenges by employing enolate alkylation chemistry with reactive electrophiles (see above), but the proposed difunctionalization introduced additional obstacles. During the bond formation C14–R of hypothetical ketone **2.57**, a fully substituted center is assembled. Furthermore, the TS during bond formation was expected to be especially high in energy due to a new *syn*-pentane interaction that is induced between the group already present at C14 (X) and the C16 methyl group on the adjacent ring during rehybridization at C14. In view of these concerns, we reasoned that a reordering of events could be the most direct route forward. To this end, oxidative cleavage of hydroxyketone **2.25** was imagined to produce a dicarbonyl derivative **2.58** (Scheme 2.14B). Sequential nucleophilic additions to the C14 and C11 carbonyls would then assemble the requisite cyclooctane motif **2.59**.

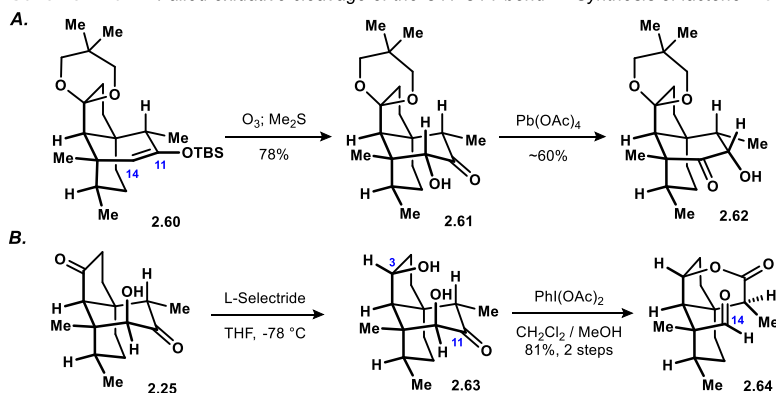
**Scheme 2.14. A.** Steric challenges faced in C14 functionalization **B.** Plan of action



With a plan in mind, we began evaluating the reactivity of relevant intermediates. Previously attempted oxidative cleavage of the C11–C14 bond had proven challenging, as

subjection of enoxysilane **2.60**, prepared in one step from monoketal **2.33**, to ozonolysis afforded the hydroxyketone **2.61** (Scheme 2.15A). The observed Rubottom-type reactivity is not without precedent; some reports of epoxidation predominating during ozonolysis of sterically hindered alkenes exist.<sup>43</sup> Further attempts to cleave the resulting  $\alpha$ -ketol moiety with  $\text{Pb}(\text{OAc})_4$  were ineffective, instead affording the product of acyloin rearrangement **2.62**. Indeed, application of typical oxidative cleavage conditions to the hydroxyketone **2.25** were equally ineffective (Scheme 2.15B). We overcame this challenge by first reducing the C3 ketone, furnishing an intermediate diol **2.63**. We hypothesized that, given the rigidity of the tricyclic framework, the pseudoaxial C3 alcohol would participate in significant  $n \rightarrow \pi^*$  donation with the C11 ketone, increasing the reactivity of the hydroxyketone system toward cleavage. Accordingly, dihydroxyketone **2.63** underwent facile oxidative cleavage under mild conditions to furnish the lactone **2.64**. The selection of an appropriate nucleophile required judicious planning (see *below*), but we first hoped to evaluate readily available organometallic nucleophiles to probe the reactivity of lactone **2.64**. Preliminary results aimed at addition to the C14 aldehyde indicated that application of Grignard or organolithium reagents led to enolization of the lactone and aldol addition into the pendant aldehyde.

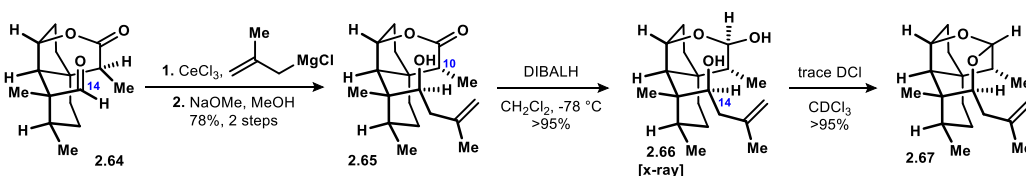
**Scheme 2.15. A. Failed oxidative cleavage of the C11-C14 bond B. Synthesis of lactone 2.64**



Continued evaluation of simple nucleophiles led us to apply the organocerate derived from methallylmagnesium chloride and  $\text{CeCl}_3$ .<sup>44</sup> To our delight, chemoselective addition to the

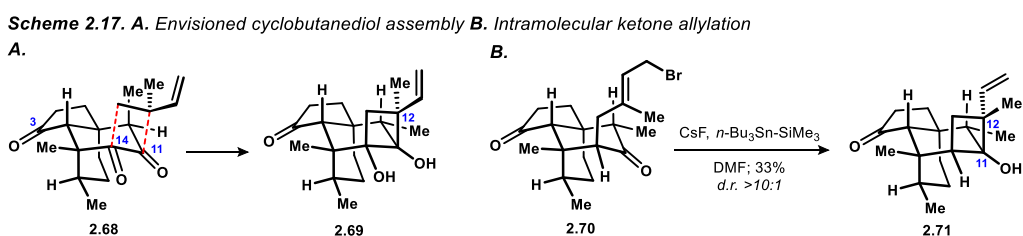
C14 aldehyde **2.64** was observed (Scheme 2.16). However, analysis of the crude mixture obtained from the reaction indicated that at least two compounds were present. We inferred that the homoallylic alcohol formed during the carbonyl addition was participating in trans-lactonization, producing a mixture of isomers. Gratifyingly, the mixture could be resolved into a single compound **2.65** by treatment with base. We rationalized that epimerization of the C10 stereocenter, arranging the methyl group equatorially, rendered the observed lactone isomer **2.65** to be the most thermodynamically stable. Notably, the C10 epimerization was a productive step, as it corrected the configuration at that site to match mutilin **2.2**. We still faced a challenge in complete structural assignment; given the free rotation of bonds possible within the linear homoallylic alcohol fragment, we recognized that NMR analysis would fail to unambiguously assign the relative stereochemistry at the newly formed C14 stereocenter. Reduction of lactone **2.65** cleanly afforded the crystalline lactol **2.66**, which proved suitable for X-ray analysis. Disappointingly, the X-ray structure clearly demonstrated that the relative stereochemistry at C14 was set with the undesired configuration. Interestingly, the lactol **2.66** underwent facile dehydration to the hemiacetal **2.67** upon exposure to trace acid (i.e., attempted NMR analysis in CDCl<sub>3</sub>). While the formation of the C14-*epi* derivative **2.65** was not viewed as an insurmountable obstacle, we were simultaneously investigating an alternative approach which appeared to be a more promising direction.

**Scheme 2.16.** Methallylation of aldehyde **2.64** and facile dehydration



Though it required the preparation of congested tricyclic intermediates **2.69**, we reasoned that direct addition of an isoprenoid fragment into C14 and C11 carbonyls preceding oxidative cleavage of the C11–C14 bond warranted evaluation (Scheme 2.17A). The advantages to this order of events were clear: substrate-controlled diastereoselectivity during

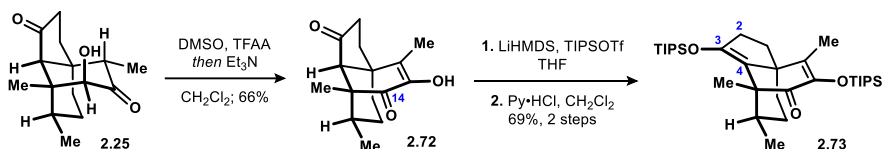
addition to C14 would be avoided, and it obviated the need to directly form the cyclooctane ring by cyclization. In the unfunctionalized system, we had prepared an ethylenecyclobutanol **2.36** since inclusion of the requisite quaternary carbon at C12 was expected to bias oxidative cleavage bicyclo[4.2.0]octane motif toward an undesired regioselectivity (see *above*). Introduction of a functional handle at C14 erased this concern. Consequently, the most direct path forward included preparation of a dihydroxycyclobutane **2.69** that already contained the quaternary center at C12. Therefore, before directing our attention to the difunctionalization of the C14 position, we first pursued a simpler model system. We considered this to be a valuable endeavor since it would validate our ability to form the C11–C12 bond by an intramolecular nucleophilic addition and shed light on the diastereoselectivity observed during a relevant allylation event (Scheme 2.17B). To this end, we prepared the allylic bromide **2.70** (see SI for details) and found that the method of Kinoshita and Mori, CsF and *n*-Bu<sub>3</sub>Sn-SiMe<sub>3</sub>, induced the desired cyclization, furnishing the cyclobutanol **2.71**.<sup>45</sup> The product was formed with high diastereoselectivity, but disappointingly, 2D NMR analysis revealed that the C12 center was formed with the undesired configuration. Clearly, we needed to identify a means of controlling the stereochemical outcome at C12 during cyclobutanol synthesis.



Before we could devise a specific plan, we required access to a suitable tricyclic intermediate that contained an electrophilic carbonyl at C14. Returning to hydroxyketone **2.25**, we found that Swern oxidation proceeded smoothly, affording the trione **2.72** (Scheme 2.18). The planned nucleophilic addition to the C14 ketone required protection of the two reactive groups at C3 and C11, which was accomplished by double silylation. However, we discovered

that C–C bond formation at C14 was not feasible until the enoxysilane, kinetically formed at C2, was isomerized to the C3–C4 position. To this end, isomerization of the enoxysilane with pyridinium hydrochloride afforded the ketone **2.73**. Planarization of the ring juncture is believed to lessen the steric burden surrounding C14, enabling approach by the nucleophile.

**Scheme 2.18.** Swern oxidation and synthesis of enoxy silane **2.73**

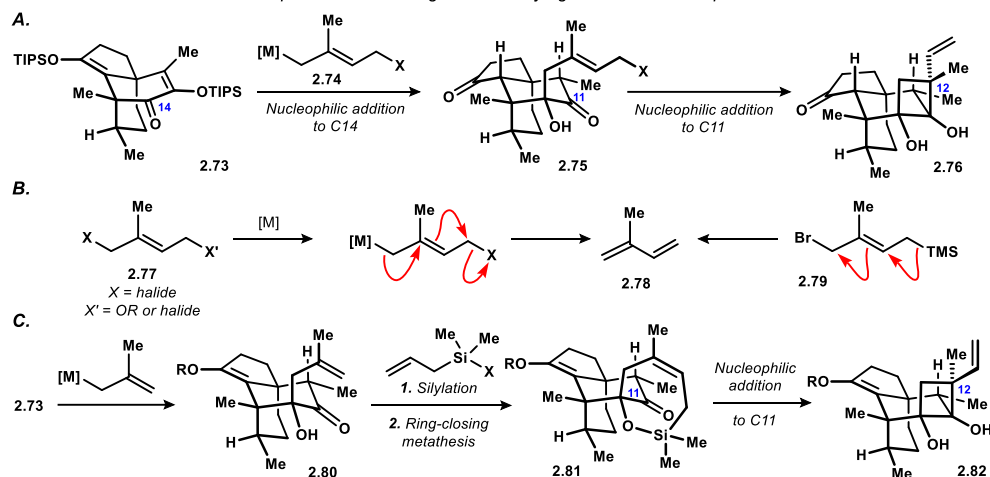


With a suitable C14 ketone in hand, we devised a course of action. Ideally, the ketone **2.73** would react with a 5-carbon nucleophile **2.74** to afford, after hydrolysis of the silanes, the hydroxydione **2.75** (Scheme 2.19A). A fundamental challenge related to this transformation was the selection of an adequate nucleophile. We reasoned that a dihalide or haloether **2.77** could serve as a precursor to an organometallic nucleophile (Scheme 2.19B). However, upon formation of the organometallic species, we expected that elimination of the vinylogous β-leaving group would be unavoidable, generating isoprene **2.78**. As an alternative, we aimed to employ allylic silane **2.79** as a nucleophile precursor. In this design, the product allylic silane **2.75** (X = TMS) was expected to be competent for addition to the C11 ketone. However, our attempts to prepare these derivatives revealed a similar issue: the allylic silane **2.79** was prone to elimination of the vinylogous β-halogen, required for organometallic formation, and our attempts to purify it by distillation or chromatography were unsuccessful. Presuming we could identify a suitable nucleophile and access the hydroxydione **2.75**, we planned to execute an intramolecular allylation of the C11 ketone to afford the cyclobutanediol **2.76**.<sup>46</sup> The envisioned allylation step introduced a second problem: we expected on the basis of our prior findings that the C12 stereocenter would be formed with the undesired configuration. We arrived at a plan that promised to address the two significant pitfalls outlined in Scheme 2.19A. We imagined that the ketone **2.73** could react with a methallyl nucleophile, affording after hydrolysis the



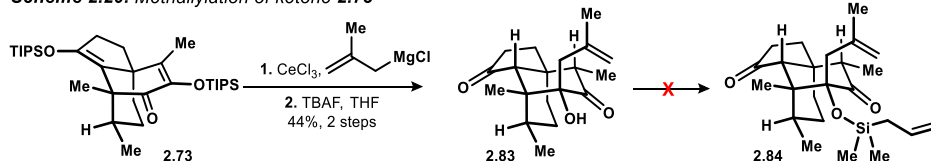
hydroxyketone **2.80** (Scheme 2.19C). Substitution of the hydroxyl group with an allyldialkylsilane group would offer a handle to functionalize the methallyl fragment by ring-closing metathesis, affording the oxasilepine **2.81**. We surmised that the spirocyclic nucleophile should attack the C11 ketone to form the cyclobutanediol **2.82**. Crucially, we expected to obtain the desired configuration at C12, as the hydroxyl group at C14 should tether the allyl nucleophile into a favorable geometry.

**Scheme 2.19.** A. Envisioned sequence B. Challenges of identifying a suitable nucleophile C. Plan of action



Satisfied with our analysis of the next steps, we began evaluating the addition of nucleophiles into the ketone **2.73** (Scheme 2.16). We soon found that methallylcerate performed the desired addition into the C14 ketone and afforded the hydroxydione **2.83** after fluoride treatment. We were disappointed to find that the C14–OH functionality was not reactive under a survey of conditions for silylation and silyl ether **2.84** was not observed.

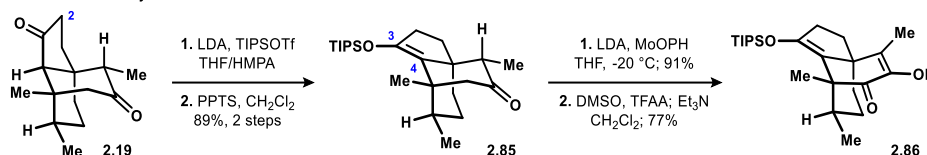
**Scheme 2.20.** Methallylation of ketone **2.73**



We wondered if an intramolecular silane transfer from the adjacent C11 ketone could circumvent the need for intermolecular silylation of the encumbered C14 hydroxyl group and enable the straightforward introduction of the requisite allyldialkylsilane fragment. The existing

route to ketone **2.73** did not offer us the ability to differentially substitute the ketones at C3 and C11, which would be a highly attractive feature when pursuing this strategy. Therefore, we developed an analogous sequence that, crucially, began with the tricyclic diketone **2.19**, the synthesis of which was more robust than the hydroxyketone **2.25** (Scheme 2.21). The difunctionalization of C14 once again required planarization of the C3–C4 bond. We discovered that the enolate formed from the reaction of diketone **2.19** with 1 equivalent of LDA could be efficiently silylated with TIPSOTf. The intermediate enoxysilane is formed selectively at C2, and is subject to isomerization with anhydrous acid, which furnished the ketone **2.85** in 89% yield across two steps. We next introduced the 1,2-diketone motif by enolate hydroxylation using Vedejs' reagent (MoOPH) and Swern oxidation of the hydroxyketone, affording 1,2-dione **2.86**.<sup>47</sup>

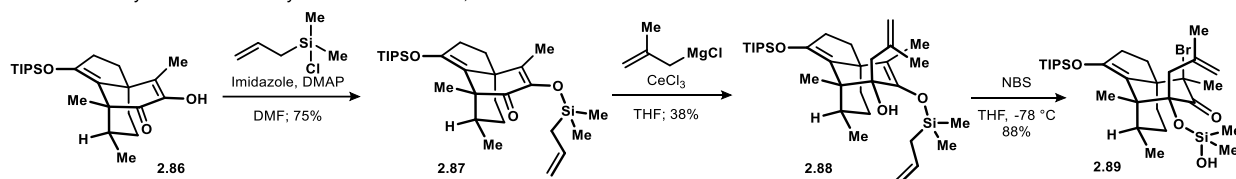
**Scheme 2.21.** Synthesis of diketone **2.86**



The 1,2-dione **2.86** reacted smoothly under standard conditions to afford the enoxysilane **2.87** and nucleophilic addition with methallylcerate furnished the homoallylic alcohol **2.88** in modest yield (Scheme 2.22). We hypothesized that deprotonation of the alcohol could initiate a 1,4-silane transfer and were disappointed when the potassium and lithium alkoxides of **2.88** failed to rearrange in THF, instead only returning starting material. We next envisioned that the desired 1,4-silane transfer could alternatively be initiated by activation of the enoxysilane portion (the nucleofuge), rather than by activation of the alcohol (nucleophile). We were immediately aware of the potential chemoselectivity challenges that may arise from treatment of the tetraene **2.88** with reactive acids or electrophiles, as any of the four contained electron-rich alkenes could react competitively. Still, we were inspired by a solitary report of a 1,4-silane transfer initiated by NBS within a much less densely functionalized system containing an  $\alpha$ -ketol derived enoxysilane.<sup>48</sup> Along these lines, treatment of the tetraene **2.88** with NBS in THF cleanly

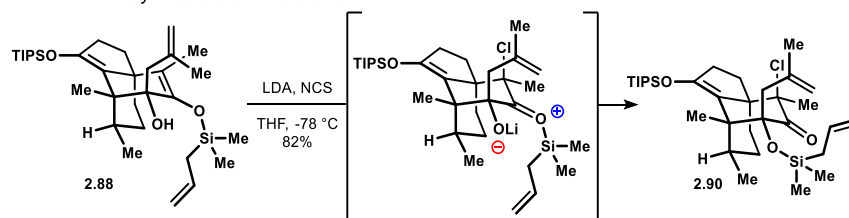
induced the desired 1,4-silane transfer. Unfortunately, NBS proceeded to react with the allylic silane moiety, affording the de-allylated silanol **2.89**. Limiting the quantity of NBS to less than two equivalents only led to mixtures of the silanol **2.89** and starting material, even at -78 °C.

**Scheme 2.22.** Synthesis of homoallylic alcohol **2.88** and 1,4-silane transfer



We imagined that a combination of the two strategies, simultaneous activation of the alcohol (nucleophile) and the enoxysilane (nucleofuge), could enable the selective transfer of the silane group without initiating the undesired de-allylation reaction. We expected that the intermediate alkoxide formed by treatment with base would be in equilibrium with the corresponding silicate by a Lewis acid-Lewis base interaction with the neighboring enoxysilane. We believed that the intermediate anion could react with an electrophile to initiate an irreversible silane transfer. To this end, we treated the tetraene **2.88** with base followed by addition of *N*-chlorosuccinimide (Scheme 2.23). We were pleased to observe that the reaction proceeded as designed, and the product chloroketone **2.90** was formed in good yield.

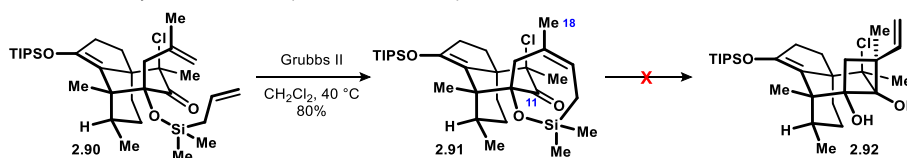
**Scheme 2.23.** Synthesis of chloroketone **2.90**



Having finally identified a route to the C14-OH substituted derivative **2.90**, we were excited to proceed with the next steps. Application of Grubbs' 2<sup>nd</sup> generation catalyst was successful in catalyzing ring-closing alkene metathesis, furnishing the product oxasilepine **2.91** in 80% yield (Scheme 2.24). We envisioned that a Sakurai-type addition of the allylic silane moiety onto the pendant C11 ketone would afford a valuable cyclobutane-containing product

**2.92.** A survey of Lewis acids and activation of the silane with fluoride have failed, up to this point, to deliver observable quantities of cyclobutanol **2.92**. It is unsurprising that the envisioned carbonyl addition has been challenging to realize, as the rigid nature of the oxasilepine moiety likely precludes necessary orbital overlaps between the allylic silane and ketone  $\pi^*$ . Steric interactions between the C18 methyl group and the axial chloride likely increase the energy of the TS, hindering bond formation. While we were still optimistic that intermediate **2.91** could be leveraged in the synthesis of mutilin, we halted our studies involving **2.91** to pursue an alternative route that we were developing concurrently and appeared to be more promising.

**Scheme 2.24.** Synthesis of oxasilepine **2.91** and attempted intramolecular Sakurai addition



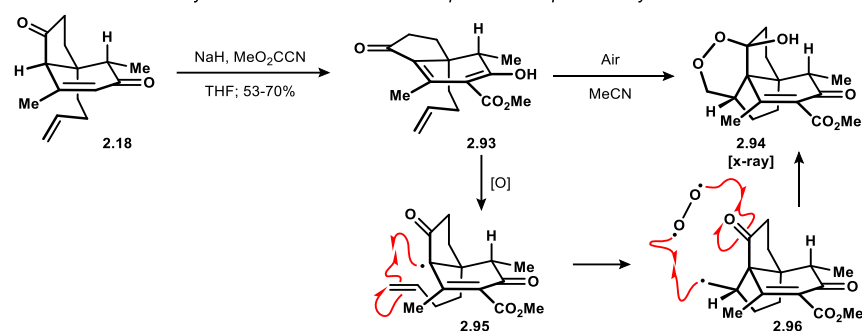
## 2.6. Implementation of an Ester as a C14 Functional Handle

We identified the carboxylate ester as a valuable C14 functional handle to enable our synthetic aims. First, it promised to permit the use of enolate alkylation chemistry to introduce the requisite isoprene fragment. Further, following assembly of the fused bicyclo[4.2.0]octane motif, we envisioned that the presence of the ester group would enable us to employ a retro-aldol reaction to unveil the cyclooctane portion of the mutilin skeleton. Finally, the abundance of decarboxylative oxygenation methods known, many of which operate under distinct mechanistic underpinnings, gave us confidence that we could exchange the carboxylate function for the corresponding oxidation following the synthesis of the carbocyclic core of mutilin.<sup>49</sup>

We hoped to install the ester group at a stage prior to the MHAT-initiated radical cyclization, as we reasoned that the added electron-withdrawing group may increase the facility of the carbon-carbon bond formation. Additionally, the ketoester function may allow us to avoid unwanted protecting group manipulations. To this end, we began by functionalizing the bicyclic enone **2.18** directly (Scheme 2.25). We found that we could form an extended enolate from the

the vinylogous 1,5-diketone system by treatment with sodium hydride (NaH). Subsequent introduction of Mander's reagent generated the ketoester **2.80**, which existed exclusively as the bright-yellow enol tautomer.<sup>50</sup> The isolated yield was found to be variable, presumably due to the instability of ketoester **2.93** on silica gel, but synthetically useful. The enolic nature of the highly conjugated tricarbonyl **2.93** rendered it a poor substrate for the planned radical cyclization. We imagined that several strategies could be available to interrupt the conjugation of the three carbonyl groups, which would likely provide a suitable diene for the MHAT-initiated Giese cyclization.

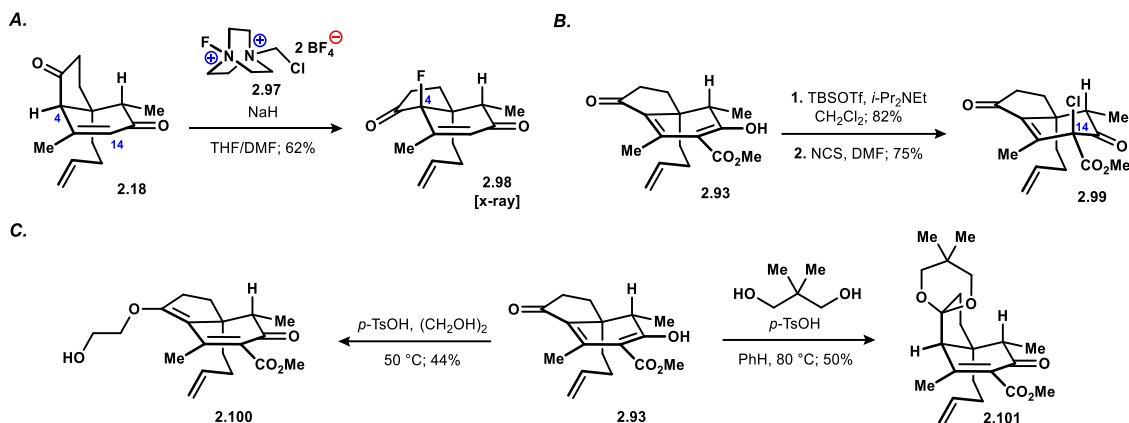
**Scheme 2.25.** Carboxylation of enone **2.18** and unexpected endoperoxide synthesis



As we were evaluating the reactivity of ketoester **2.93**, we at one point prepared a solution in acetonitrile under an atmosphere of air (Scheme 2.25). To our surprise, we observed that a spontaneous reaction occurred. A crystalline product was formed to which we assigned the structure of endoperoxide **2.94** using 2D NMR experiments. We further corroborated the assignment by single crystal X-ray diffraction analysis. Remarkably, the spontaneous reaction with oxygen proceeded to form a new all-carbon quaternary center and an unusual propellane tricyclic architecture. Formally a [2+2+2] cycloadduct, we can only speculate that the mechanism starts with oxidation of the ketoester enol to the corresponding radical **2.95**. Following a 5-*exo trig* cyclization, the resulting alkyl radical **2.96** is presumably captured by triplet oxygen, which undergoes addition into the pendant ketone.<sup>51</sup> Related transformations

have been disclosed in the literature, although all existing reports required the use of an exogenous catalyst or oxidant, to our knowledge.<sup>52</sup>

**Scheme 2.26.** A. Synthesis of fluoroenone **2.98** B. Chlorination of ketoester **2.93** C. Ketalization of ketoester **2.93**

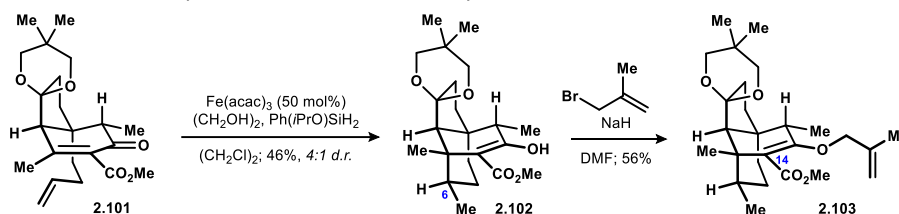


We continued to explore manipulations of the ketoester **2.93**, hoping to identify a suitable substrate for the MHAT-initiated Giese cyclization. We had previously discovered that the extended enolate of enone **2.18** reacted with Selectfluor® **2.97** at C4 to form the fluoroenone **2.98** (Scheme 2.26A). Notably, fluorination was the only process we identified that reacted selectively at C4; all other electrophiles were incorporated at C14. The same conditions were ineffective with ketoester **2.93**, but we wondered if a functionally similar reaction could be realized by chlorination at C4. Disappointingly, we found that both the sodium enolate and enoxysilane of ketoester **2.93** underwent chlorination exclusively at C14 (Scheme 2.26B).<sup>53</sup> In another attempt to interrupt the conjugation between the three carbonyl groups of ketoester **2.93**, we evaluated ketalization of the C3 cyclopentanone (Scheme 2.26C). While the use of ethylene glycol delivered predominantly the alkenyl ether **2.100**, employing 2,2-dimethyl-1,3-propanediol delivered the corresponding ketal **2.101** in 50% yield under standard conditions.

With the unsaturated ketoester **2.101** in hand, we were prepared to attempt the planned MHAT-initiated radical cyclization. We discovered that under our previously developed conditions the expected cyclization product **2.102** was formed in 46% yield (Scheme 2.27). Disappointingly, the diastereoselectivity was greatly eroded when compared to the cyclization of

the parent bicyclic enone **2.18** into its Giese adduct **2.19** (see above). In the prior case, complete diastereoselectivity (>20:1) was observed, whereas ketoester **2.101** cyclized to form the tricyclic product **2.102** as a 4:1 mixture of inseparable diastereomers at C6. We hypothesize that the diminished stereoselectivity results from the addition of the second electron-withdrawing substituent onto the acceptor alkene. The accompanying decrease in the energy of the LUMO likely improves the electronic matching between the SOMO of the electron-rich alkyl radical intermediate and the acceptor system. Naturally, the improved electronic matching leads to an earlier transition state and lower stereoselectivity, according to the Hammond postulate. An alternative explanation would state that the avoidance of a new *syn*-pentane interaction between the ester and C6 methyl substituent is avoided. However, our studies with other groups at C14 suggest that the decrease in diastereoselectivity observed with **2.101** is linked to the electron-withdrawing nature of the substituent. Regardless, we hoped to leverage the ketoester **2.102** by engaging it in enolate alkylation chemistry. We never observed the desired C-alkylation process but found that we could perform straightforward O-methallylation, furnishing the enol ether **2.103**. Disappointingly, the 1,5-diene **2.103** was resistant to Claisen rearrangement, underscoring the demanding steric environment surrounding the C14 position.

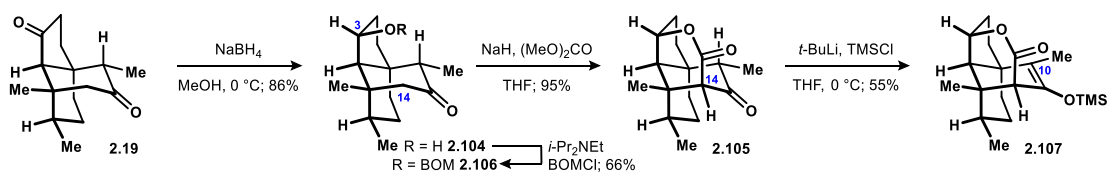
**Scheme 2.27.** MHAT cyclization of ketoester **2.101** and synthesis of enol ether **2.103**



We next pursued the direct carboxylation of the tricyclic ketone **2.19** (Scheme 2.28). We identified a convenient synthesis of a carboxyl derivative that began with selective reduction of the diketone **2.19** to the corresponding ketoalcohol **2.104**. Treatment of this intermediate with dimethylcarbonate and sodium hydride smoothly delivered the lactone **2.105** at ambient temperature. In contrast, the benzyloxymethyl (BOM) ether derivative **2.106** failed to react under

identical conditions, even up to reflux temperature in THF or with protic additives. Clearly, the free alcohol at C3 serves a vital role in delivering the electrophile to the crowded C14 position, enabling the lactone formation to proceed. Aiming to leverage the intermediate into productive reactivity, we imagined that the ketolactone **2.105** may be prone to deprotonation at the C14 bridgehead position.<sup>54</sup> If realized, alkylation of the corresponding anion could deliver synthetically valuable intermediates. Despite the presumed poor overlap of the bridgehead methine C–H  $\sigma$  bond orbital with the  $\pi^*$  orbitals of the two adjacent carbonyl groups, we were guided by the <sup>1</sup>H NMR spectrum of the ketolactone **2.105**, in which the signal for the C14 bridgehead methine was downfield shifted (3.47 ppm) relative to the competitively acidic C10 methine (2.33 ppm). We initiated quenching studies with MeOH-*d* and TMSCl to find that the ketolactone **2.105** was resistant to deprotonation under the action of typical amide bases. Under the action of *tert*-butyllithium we did observe silylation of the substrate but found that the deprotonation had occurred preferentially at the C10 position, evidenced by the formation of enoxysilane **2.107**, which was inert to further deprotonation. Attempted methanolysis of the lactone **2.105** to the corresponding methyl ester derivative cleanly decarboxylated the lactone, furnishing the ketoalcohol **2.104** as the major product.

**Scheme 2.28.** Synthesis of lactone **2.92** and deprotonation studies

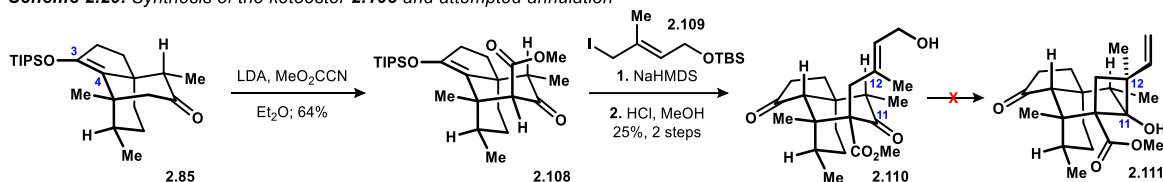


We chose at this juncture to pursue the derivatization of TIPS enoxysilane derivative **2.85**, as it was straightforward to prepare up to 1g scale and was seen as the most likely intermediate to participate in sequential enolate alkylation reactions at C14 (Scheme 2.29). Alkoxyacylation of the lithium enolate derived from ketone **2.85** proceeded smoothly with Mander's reagent to deliver the ketoester product **2.108** in moderate yield. The use of  $\text{Et}_2\text{O}$  as the solvent was essential to reduce the large proportion of *O*-substituted derivatives formed in



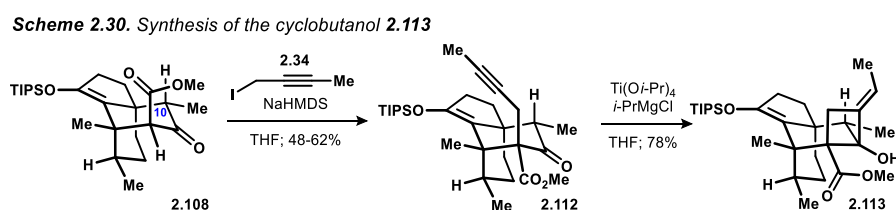
THF.<sup>55</sup> While the chromatographic purification of ketoester **2.108** could not reliably deliver analytically pure material, straightforward recrystallization from methanol proceeded in 88% recovery. Despite our earlier findings that the intramolecular allylation of the C11 ketone preferred the undesired configuration at C12 when under substrate control, we determined that the approach warranted a re-evaluation in the context of ketoester **2.108**. Consequently, we pursued allylation of the enolate derived from ketoester **2.108**. When allylic bromides were employed as the electrophilic species, DMF was required as a co-solvent with THF, and O-alkylated products predominated. We found success returning to reactive alkyl iodide electrophiles. Exposure of the sodium enolate derived from ketoester **2.108** to the allylic iodide **2.109** followed by acidic hydrolysis of the silanes afforded the allylic alcohol **2.110**.

**Scheme 2.29.** Synthesis of the ketoester **2.108** and attempted annulation



In pursuit of the cyclobutanol **2.111**, the intermediate **2.110** enabled us to evaluate two mechanistically distinct approaches to the formation of the C11–C12 bond (Scheme 2.29). First, we engaged the trisubstituted alkene contained in tricyclic ketone **2.110** under MHAT conditions, aiming to induce radical cyclization onto the pendant ketone.<sup>56</sup> Second, following an Appel reaction of the allylic alcohol, we subjected the resulting bromide to the stannyl anion conditions that had successfully forged the C11–C12 bond during our prior approach.<sup>57</sup> In both cases, extrusion of the 5-carbon fragment derived from **2.109** was observed, delivering enolic products. In combination with our earlier findings that substrate control favored the undesired configuration at C12 during intramolecular allylation, the failure of ketone **2.110** to undergo cyclization under anionic or radical conditions encouraged us to evaluate a propargylation-reductive cyclization sequence that followed suit with our earlier successful assembly of the [4.2.0]-containing polycyclic architecture.

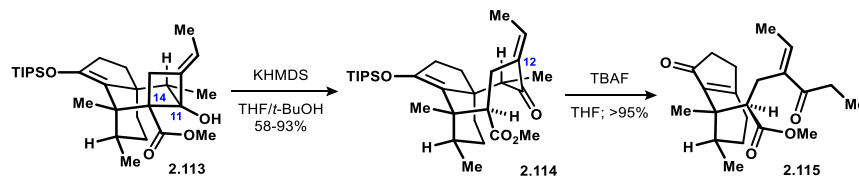
Treatment of the sodium enolate derived from ketoester **2.108** with 1-iodobut-2-yne **2.34** effectively furnished the desired homopropargylic ketone **2.112** (Scheme 2.30). The yield of the reaction was inconsistent, as a regioisomeric alkylation product was formed in variable quantities. The deleterious pathway proceeded with alkylation at C10, presumably through an extreme Curtin–Hammett kinetic scenario. Regardless, with access to useful quantities of the required alkynyl ketone **2.112**, we pursued nucleophilic addition to the pendant ketone. Once again, we employed Sato's reagent to perform the reductive cyclization, furnishing the ethylidenecyclobutanol **2.113** in good yield.



With cyclobutanol **2.113** in hand, we sought to induce a retro-aldol event to cleave the C11–C14 bond and unveil the target cyclooctanone (Scheme 2.31). We were surprised to find that, despite the significant ring strain of the system, the desired retro-aldol product was not observed following formation of the Li, Na, or K alkoxide of **2.113** in THF across a range of temperatures.<sup>58</sup> We eventually found that exposure of the cyclobutanol **2.113** to basic conditions with a protic solvent additive (*t*-BuOH) effectively furnished the tricyclic ketone **2.114** as a single diastereomer. We consider it likely that the observed stereoselectivity arises from the kinetic protonation of an ester enolate intermediate. The product was found to be sensitive to the reaction conditions, leading to some variability in the isolated yield. We further found that attempted hydrolysis of the C3 enoxysilane with fluoride or acid invariably led to formation of a retro-Michael adduct **2.115**. This type of reactivity was described earlier by Nägeli and Arigoni within the natural pleuromutilin system and described in Chapter 1 (*see above*).<sup>59</sup> The deleterious retro-Michael reaction would prove to be extremely general during attempted or incidental hydrolysis of the TIPS enoxysilane on all of the intermediates we prepared during our

synthetic studies that contained the 5-6-8 tricyclic architecture, permitting that C11 was at the ketone oxidation state and the C10 methyl substituent was in the unnatural configuration.

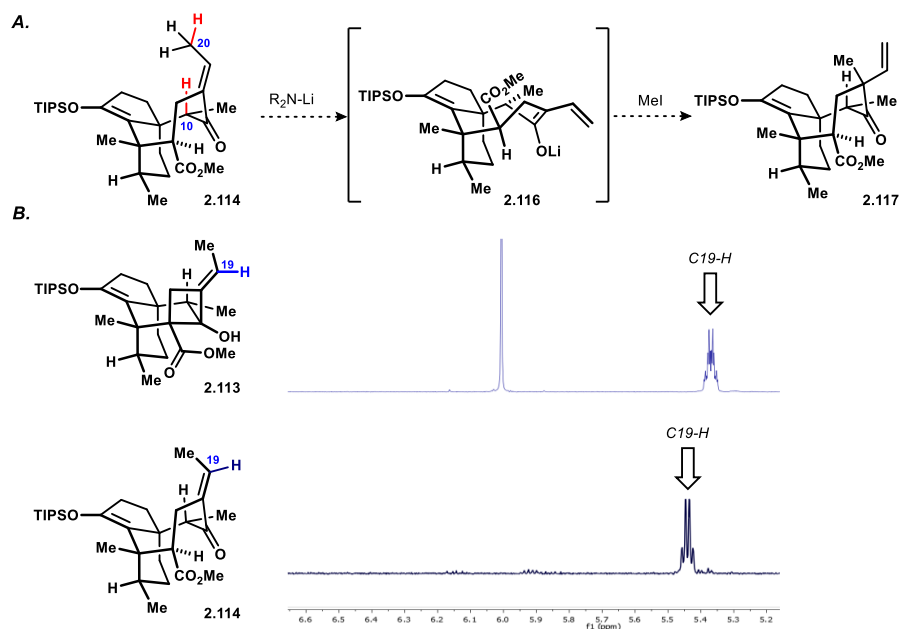
**Scheme 2.31.** Synthesis of the cyclooctanone **2.114** and retro-Michael fragmentation



The synthesis of the tricyclic ketone **2.114** represented a large step forward in our campaign; we had at last prepared an intermediate with the required cyclic connectivity that featured a functional handle at the C14 position. The next hurdle we faced was the installation of the final carbon atom of the mutilin skeleton, a methyl group at C12, by an enolate alkylation reaction (Scheme 2.32A). We envisioned that ketone **2.114** could be selectively deprotonated at the vinylogous  $\gamma$ -position, C20–H, as the competitively acidic  $\alpha$ -position was the sterically hindered C10 methine. Following deprotonation, we hoped to alkylate the enolate intermediate **2.116** with iodomethane, furnishing the ketoester **2.117**. We began by studying the reactivity of ketone **2.114** in the presence of amide bases and quenching with MeOH-*d*. We were initially surprised to find that no deuterium incorporation was observed under typical conditions (*i.e.*, LDA, LiTMP, KHMDS, or LiNEt<sub>2</sub> in THF). Detailed analysis of the <sup>1</sup>H NMR spectrum of the ketone **2.114** corroborated our experimental observations (Scheme 2.32B). We noted that the signal corresponding to the vinylic C19–H bond of the cyclobutanol precursor **2.113** appeared at 5.37 ppm (CDCl<sub>3</sub>). Following retro-aldol, the enone product **2.114** exhibited a signal for the same vinylic C19–H bond at 5.44 ppm, a very modest downfield shift (0.07 ppm). This observation stood in contrast to the expectation that conversion of an allylic alcohol into the corresponding  $\alpha,\beta$ -unsaturated ketone would be accompanied by a significant downfield shift of the <sup>1</sup>H NMR signals of protons at the  $\beta$ -position. The underlying reason for the observed downfield shift in typical cases is linked to the conjugation of the C=C double bond to the ketone, resulting in significant electronic de-shielding of the  $\beta$ -position. We surmised that the

conformational preference of the cyclooctanone **2.114** forced the enone motif to adopt a geometry where the overlap between the  $\pi$ -systems of the ketone and neighboring alkene is minimized, leading to poor acidification of the C20–H protons. These findings erased our belief that the envisioned alkylation reaction could be brought to fruition on the ketone **2.114**.

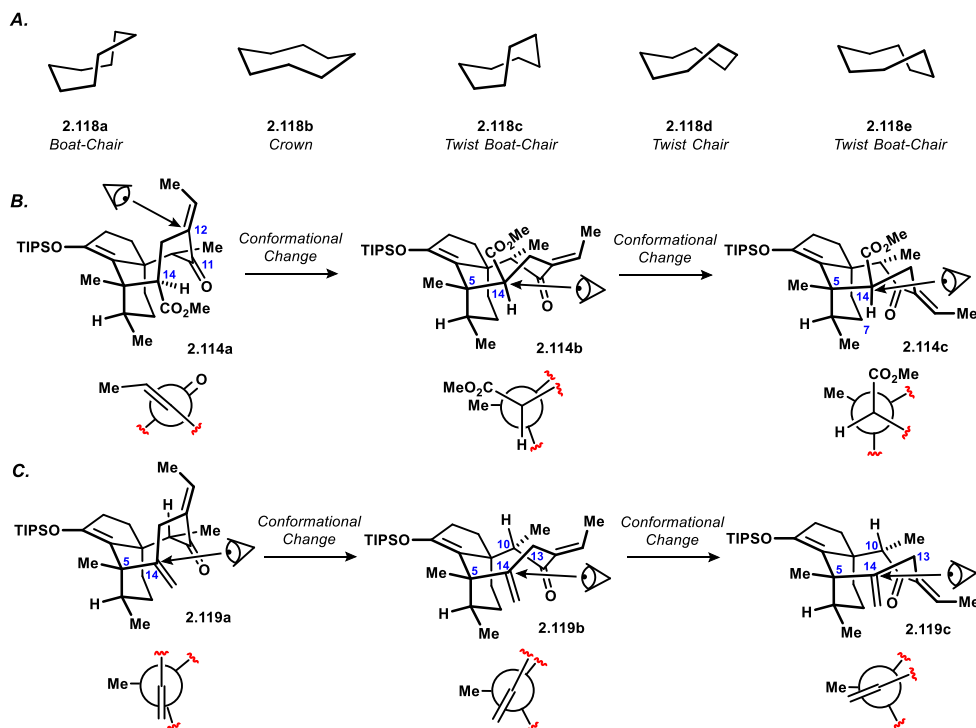
**Scheme 2.32.** A. Envisioned alkylation sequence B.  $^1\text{H}$  NMR of cyclobutanol **2.113** and enone **2.114**



In order to access a substrate that would exhibit suitable acidification at C20 to perform the desired  $\gamma$ -deprotonation-alkylation sequence, we required an understanding of the origin for the poor conjugation observed in enone **2.114**. Accordingly, we resorted to a detailed analysis of the conformations available to the highly decorated cyclooctane **2.114**. Nine conformations of cyclooctane are known. Of these nine, cyclooctane itself exists as a mixture of two conformers in solution, roughly 94% as the boat-chair conformer **2.118a** and the remainder as the crown **2.118b** (Scheme 2.33A).<sup>60</sup> The relative stability of the conformers is dictated chiefly by the minimization of transannular interactions, sometimes called flagpole interactions, that are present in all cyclooctane conformers. Adding substituents, changing the hybridization of carbon atoms, and introducing heteroatoms to the eight-membered ring can drastically change its

conformational preference. Some of the other conformations that are relevant to the present work are the twist boat-chair conformers **2.118c** and **2.118e** and the twist chair **2.118d**.

**Scheme 2.33. A. Cyclooctane conformers B. Conformers of ketone 2.114 C. Conformers of ketone 2.119**



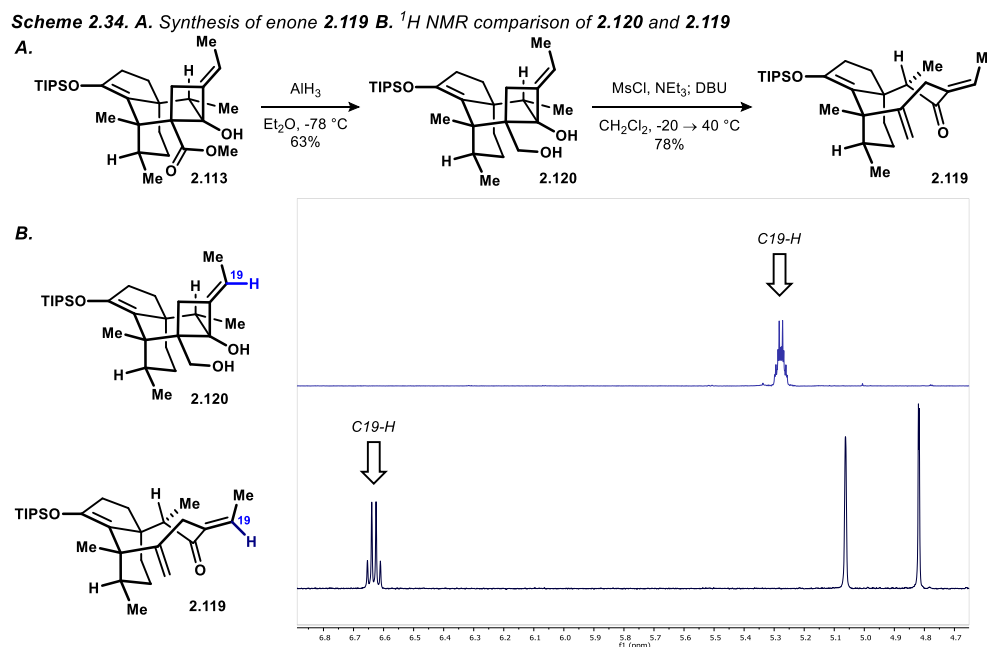
Our analysis began with enone **2.114** and we soon identified three reasonable conformers **2.114a**, **2.114b**, and **2.114c** (Scheme 2.33B). From these we determined that the twist boat-chair conformer **2.114a** was the most stable form, on the basis of minimizing transannular interactions and eclipsing interactions. Notably, poor conjugation is observed within the  $\alpha,\beta$ -enone system in conformer **2.114a**, as exhibited by the Newman projection aimed down the C12–C11 bond, explaining the observed phenomena outlined above. Manipulating the conformation to twist chair **2.114b** places the  $\pi$ -systems of the alkene and ketone into the same plane, as desired, but also introduces several unfavorable interactions. Most notably, it incurs eclipsing interactions between the ester substituent at C14 and the adjacent methyl group at C5, as demonstrated by the Newman projection directed down the C14–C5 bond. The change also appears to introduce a more costly flagpole interaction (C13 to C10) when compared with the

twist boat-chair conformer **2.114a**, in which the energetic penalty was minimized by placing the  $sp^2$  hybridized C11 opposite the inward-facing C14–H methine. Further conformational change to the twist boat-chair **2.114c** maintained the strong conjugation within the  $\alpha,\beta$ -enone system while alleviating the eclipsing interactions observed in twist chair **2.114b** (Newman projection). However, it further exacerbated the flagpole interaction between C10 and C13 and brought the C10-C12 fragment of the cyclooctane ring into direct contact with the C7–H<sub>axial</sub> on the adjacent cyclohexane portion of the tricyclic system.

With an understanding of the factors that contribute to the conformational preferences of cyclooctanone **2.114**, we hoped to manipulate the substrate to favor one of the conformers in which the alkene moiety and ketone would exist in plane with one another. In order to accomplish this, we needed to alleviate the costly steric interactions that disfavor the conformers **2.114b** and **2.114c**, both of which exhibited strong conjugation within the  $\alpha,\beta$ -enone motif. The only reasonable change we could identify was the avoidance of the eclipsing interactions present between the C14 and C5 substituents in twist chair **2.114b**. We reasoned that replacing the ester moiety with an  $sp^2$ -hybridized carbon atom at C14, as exemplified by the 1,1-disubstituted alkene-containing ketone **2.119**, may result in the most stable conformer being the desired twist chair **2.119b** (Scheme 2.33C). Analysis of the three conformers **2.119a**, **2.119b**, and **2.119c** demonstrated that the costly eclipsing interaction was nullified, and perhaps even minimized in the desired twist chair form **2.119b** (Newman projections of the C14–C5 bond). We were hopeful that the favorable  $\pi$ -conjugation introduced by the desired conformer would be sufficient to override the energetic penalty of a more costly flagpole interaction (C10–H to C13–H) compared with the undesired twist boat-chair conformer **2.119a**.

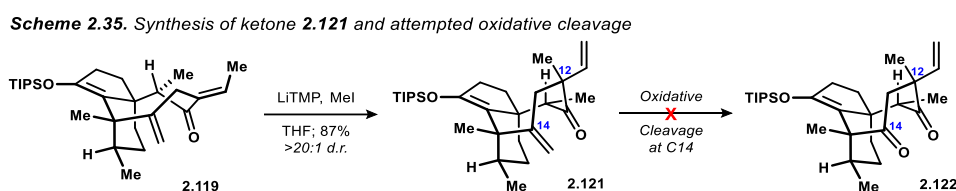
In order to test our hypothesis, we sought access to the cyclooctanone **2.119**. We reasoned that reduction of the ester **2.113** would enable a Grob fragmentation to access the 1,1-disubstituted alkene-containing product **2.119** (Scheme 2.34A). To this end, we evaluated

conditions for the reduction of the ester **2.113**. To our dismay, it was found to be unreactive toward lithium triethylborohydride (LiEt<sub>3</sub>BH), and the application of lithium aluminum hydride (LiAlH<sub>4</sub>) or diisobutylaluminum hydride (DIBAL-H) led predominantly to the formation of over-reduced ring-expansion products. We ascribed the undesired reactivity in the presence of aluminum hydride reagents to the high temperatures needed to engage the sterically encumbered ester ( $\geq 0$  °C for LiAlH<sub>4</sub> and  $\geq -20$  °C for DIBAL-H). Accordingly, we chose to employ alane (AlH<sub>3</sub>), which promised to serve as a hydride source with minimal steric burden.<sup>61</sup> Gratifyingly, we found that AlH<sub>3</sub> reduced the ester moiety at cryogenic temperature and furnished the primary alcohol **2.120** in satisfactory yield (63%). A one-pot mesylation/Grob fragmentation sequence afforded the cyclooctanone **2.119** in 78% yield. Upon inspection of the <sup>1</sup>H NMR spectrum of the enone **2.119**, we were extremely pleased to find that the signal corresponding to C19–H exhibited a significant downfield shift (1.36 ppm) relative to C19–H signal of the allylic alcohol precursor **2.120** (Scheme 2.34B).



With access to a tricyclic ketone **2.119** that exhibited conjugation within the enone motif, we aimed to execute the envisioned  $\gamma$ -deprotonation-alkylation sequence. To our delight,

enolization with lithium 2,2,6,6-tetramethylpiperidide (LiTMP) followed by addition of iodomethane cleanly furnished the desired alkylation product **2.121** as a single diastereomer (Scheme 2.35).<sup>62</sup> The enolate methylation introduced the 20<sup>th</sup> skeletal carbon of the mutilin system. However, we soon found that the 1,1-disubstituted alkene at C14 was not a viable functional handle for the required oxidative cleavage to the corresponding dione **2.122**. Application of some electrophilic oxidants indicated that the C12 monosubstituted alkene was more reactive toward oxidation than the C14 1,1-disubstituted alkene.

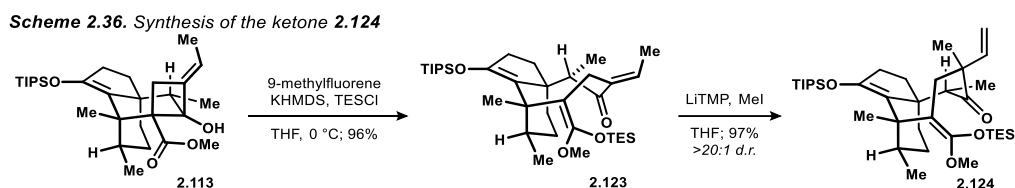


## 2.7. Synthesis of Pleuromutilin

Given the success of the enolate methylation reaction and the challenges associated with the oxidative cleavage of the 1,1-disubstituted alkene motif, we altered our approach slightly. We aimed to prepare a substrate that would contain an sp<sup>2</sup>-hybridized carbon atom at C14, as required for the enolate methylation, but also feature a more reactive functional handle at the C14 position. Returning to the ester-substituted ethylidenecyclobutanol **2.113**, we recognized that capture of the ester enolate formed by retro-aldol ring-expansion with a silyl electrophile would afford a ketene silyl acetal intermediate (Scheme 2.36). Presumably, the increased electron density of the ketene silyl acetal would enable straightforward chemoselective oxidation in the presence of the monosubstituted alkene fragment. Exposing cyclobutanol **2.113** to basic conditions in the presence of chlorotrialkylsilanes resulted in the formation of ketene silyl acetal products. However, the reaction was found to be sensitive to the equivalence of base employed, and the traces of HCl present in the freshly distilled chlorotriethylsilane (TESCI) caused the addition of precisely 1.0 equivalent of KHMDS relative to the cyclobutanol substrate **2.113** to be challenging. We found that including 10 mol % of 9-



methylfluorene as an indicator within the reaction mixture enabled us to consistently reach the equivalence point and to cleanly furnish the desired ketene silyl acetal **2.123**.<sup>63</sup> To our great surprise, we found that the product was readily purified by chromatography without any observed hydrolysis of the ketene silyl acetal group, affording the product in 96% yield. Methylation of the enone **2.123** proceeded smoothly, furnishing the ketone **2.124**, which was similarly stable during chromatography, in high yield and diastereoselectivity.



With the continued success of the enolate methylation reaction to assemble the C12 quaternary stereocenter, we hoped to probe the origins of the observed high diastereoselectivity. Prior to our investigation into the assembly of the C12 quaternary center by enolate alkylation, analysis of molecular models indicated that the C10 methyl group, which was oriented in the unnatural C10-*epi* orientation throughout our synthetic sequence, dictated the conformational preference of the intermediate enolate during the reaction. On this basis, the observed stereoselectivity was expected to be the consequence of facial selectivity observed within the polycyclic architecture. To evaluate this hypothesis, we performed computational analysis of the lowest energy conformers (both silanes = TMS) of the enol within the C10-*epi* series as well as the epimeric enol with a natural configuration at C10. The computations were performed by an initial conformer search using molecular mechanics MMFF and subsequently refined, with the final level of analysis being performed at the  $\omega$ B97X-D / 6-31G(d) level. We found that the lowest energy conformer for the enol with the C10-*epi* configuration **2.125** existed, as expected, with the *re* face exposed (as modeled, Figure 2.3). This result is in line with our experimental observations. Analysis of the enol containing the natural configuration at C10 **2.126** revealed the opposite conformational preference, leaving the *si* face exposed during

a hypothetical alkylation event. The lowest energy conformer in which the opposite facial selectivity was expected for enol **2.126** was computed to be 1.7 kcal/mol higher in energy than the lowest energy conformer. We believe that these computed lowest energy conformers strongly indicate that the C10 methyl group exhibits control over the stereoselectivity of the alkylation reaction during the synthesis of ketone **2.124** as well as related alkylations at C12 used throughout our synthetic campaign. A more sophisticated analysis of relative transition state energies would be required to further evaluate this effect.

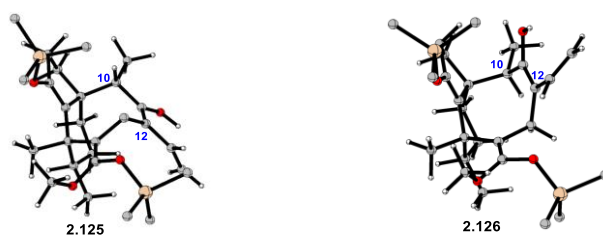
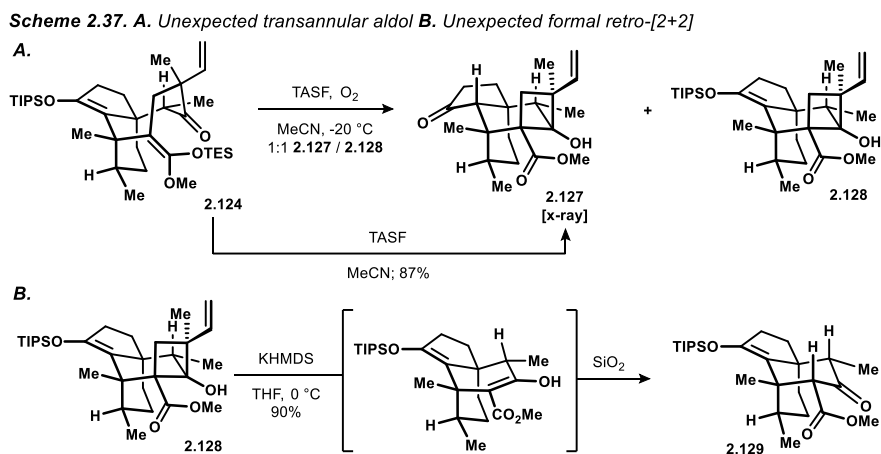


Figure 2.3. Computed lowest energy conformers of enols **2.125** and **2.126** computed at the  $\omega$ B97X-D / 6-31G(d) level

Satisfied with our analysis of the stereoselectivity during the alkylation event and having the ketone **2.124** in hand, we sought to effect the oxidative cleavage of the ketene silyl acetal moiety. In a typical case, the selective oxidation of a ketene silyl acetal in the presence of other alkenes is straightforward. We soon found that the triene **2.124** exhibits unusual reactivity patterns, and the application of oxidants ideal for the direct cleavage of the electron-rich alkenes led only to complex mixtures (*i.e.*, nitrosobenzene, ozone, or “RuO<sub>4</sub>”).<sup>64</sup> Further evaluation of oxidants led us to employ osmium tetroxide (OsO<sub>4</sub>). To our surprise, we found that the triene **2.124** exhibited low reactivity when subjected to superstoichiometric quantities of OsO<sub>4</sub>, and application of forcing conditions (OsO<sub>4</sub> at 50 °C for 16 h) or highly reactive oxidants (TFDO, -78 °C) resulted in exclusive oxidation of the monosubstituted alkene fragment. We ascribe the low reactivity of the ketene silyl acetal group to the energetic cost of rehybridizing the C14 position.

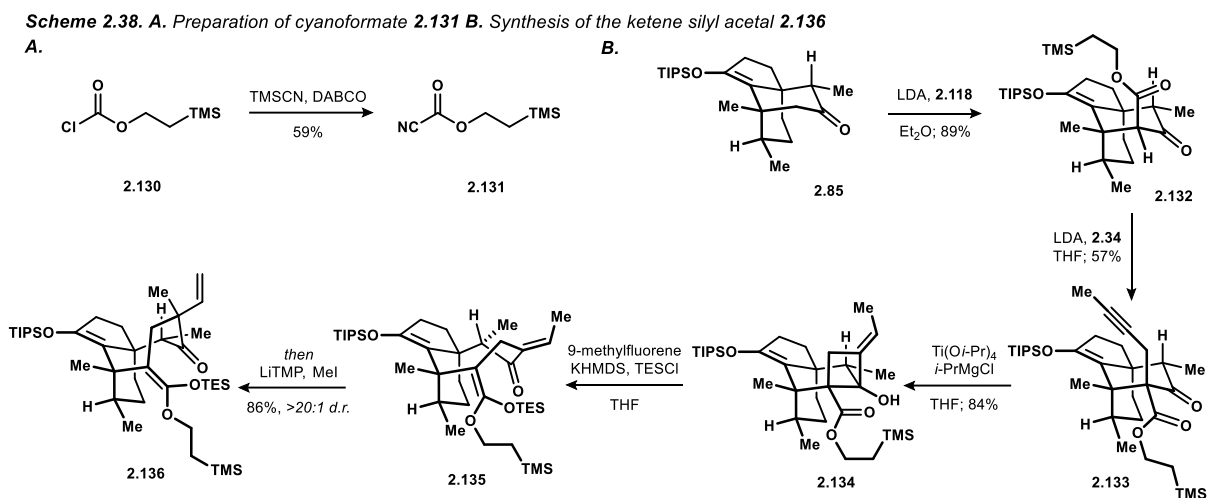
Given the reluctance of ketene silyl acetal **2.124** to undergo oxidation under typical conditions, we resolved to generate the corresponding ester enolate by treatment with fluoride. We reasoned that the increased reactivity of the enolate should enable us to selectively oxidize

the desired position. To this end, we exposed the ketene silyl acetal **2.124** to fluoride at  $-20\text{ }^{\circ}\text{C}$  with continuous sparging of dry  $\text{O}_2$  (Scheme 2.37A).<sup>65</sup> To our surprise, the major products from the reaction were a mixture of transannular aldol adducts **2.128** and **2.127**, the structure of which we later confirmed by X-ray analysis.<sup>66</sup> We were surprised by this outcome, as we employed the inverse process, the corresponding retro-aldol, two steps prior in the synthesis of cyclooctanone **2.123** (see above). Clearly, an equilibrium between these two aldol forms existed, favoring the bicyclo[4.2.0]octane aldol adducts in the absence of a trapping agent for the ester enolate. Treatment of the ketene silyl acetal **2.124** with TASF in the absence of oxygen demonstrated the facility of the aldol event, rapidly furnishing cyclobutanol **2.127**.



We were curious about the equilibrium that existed between ring-expanded cyclooctane derivatives and the corresponding cyclobutanol **2.128** (Scheme 2.37B). Accordingly, we evaluated its behavior in the presence of base, expecting that the retro-aldol adduct may be formed in some proportion. In another incidence of unexpected reactivity, we found that reaction of cyclobutanol **2.128** with base did not afford the anticipated ring-expanded cyclooctanone. Instead, the major product was a ketoester enol which underwent tautomerization during chromatography to afford the ketoester **2.129**.<sup>67</sup> Formally, the ketoester arises from a formal cycloreversion reaction, extruding isoprene. We reason that the mechanism is likely a stepwise process rather than a concerted retro-[2+2]. This outcome was surprising to us, but further

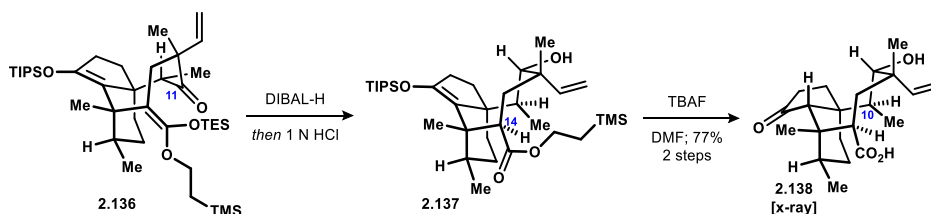
support for our proposed structure of the ketoester **2.129** was obtained by subjecting ketoester **2.108** to basic conditions. Following aqueous workup,  $^1\text{H}$  NMR signals corresponding to the same enolic product present in the crude NMR of the conversion of cyclobutanol **2.128** into ketoester **2.129** were evident.



Having found little success with the direct oxidation of the ketene silyl acetal moiety, we sought to explore decarboxylative oxygenation of the corresponding carboxylic acid derivative. Following some preliminary studies in which we evaluated saponification of the methyl ester derived from ketene silyl acetal **2.124**, we surmised that the methyl ester was unlikely to offer us straightforward access to the desired carboxylic acid. Consequently, we returned to the ketone **2.85** to install an ester functionality that could be readily transformed into the corresponding acid at a late stage in the synthetic sequence (Scheme 2.38B). Of the available options, we opted to introduce the 2-trimethylsilylethyl (TMSE) substituted derivative. In contrast to commercially available methyl cyanoformate, the use of the TMSE cyanoformate has scarcely been reported in the literature.<sup>68</sup> We chose to prepare the TMSE cyanoformate **2.131** from the corresponding acid chloride **2.130** by exposure to neat TMSCN with catalytic DABCO (Scheme 2.38A).<sup>69</sup> Deprotonation of the ketone **2.85** was accomplished with LDA at  $-78$  °C over 30 minutes. Concomitantly, distillation of the cyanoformate **2.131** directly from its reaction mixture afforded it

in pure form prior to introduction into the reaction vessel containing the lithium enolate. We observed that the cyanofomate, initially a colorless liquid, would rapidly develop a dark orange color upon storage, hinting at its poor stability. Regardless, the procedure outlined above enabled the preparation of ketoester **2.132** in high yield (89%). Alkylation of the TMSE-substituted ketoester **2.132** required a re-evaluation of conditions, but we soon found that employing the lithium enolate of ketoester **2.132** enabled us to prepare the homopropargylic ketone **2.133** in 57% yield. Subsequent cyclobutanol synthesis, ring-expansion, and methylation proceeded smoothly as before, affording the ketene silyl acetal **2.136**. Notably, we found that the retro-aldol and enolate methylation processes could be carried out in one reaction flask, affording the product in 86% yield. The alternative two-step protocol proceeded in 91% overall yield.

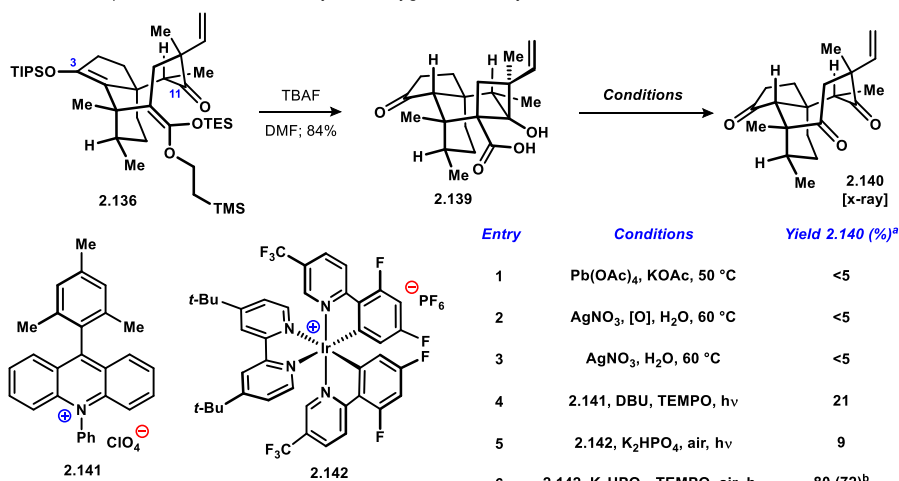
**Scheme 2.39.** Synthesis of ketoacid **2.138**



With access to the TMSE-substituted ketene silyl acetal **2.136** established, we aimed to attain a suitable carboxylic acid-containing substrate for the planned decarboxylative oxygenation reaction. We found that the order of desilylations under treatment with fluoride was as follows: 1. TES-substituted ketene silyl acetal, 2. TIPS substituted enoxysilane, 3. TMSE-substituted carboxylate ester. Consequently, access to the free carboxylic acid required the hydrolysis of the C3 TIPS enoxysilane. Removal of the C3 enoxysilane in prior systems wherein C11 resided at the ketone oxidation state was inevitably coupled with the deleterious retro-Michael reaction, fragmenting the 8-membered ring (see above, Scheme 2.31). Furthermore, we reasoned that the stereochemical outcome at C14 obtained from hydrolysis of the ketene silyl acetal would be essential for the eventual introduction of the hydroxyl group at that site.

However, previous studies indicated that nondiastereoselective hydrolysis was observed in most cases. In order to avoid the retro-Michael process and establish the C14 stereocenter with high selectivity, we identified the following sequence: hydride reduction of the C11 ketone **2.136** followed by exposure to aqueous acid produced an intermediate ester **2.137** (Scheme 2.39). The diastereoselectivity of hydrolysis at C14 may arise from a directing effect of the C11 hydroxyl group. Subsequent treatment with fluoride induced desilylation, affording the ketoacid **2.138**. We were surprised to find that X-ray crystallographic analysis of the structure indicated that the central cyclooctane motif existed as its boat-chair conformer, which forces the C10 methyl group into the midst of the concave ring system, as drawn. The sequence provided access to the carboxylic acid but suffered from a significant drawback. The requirement of reducing the C11 ketone to access the desired functional array necessitated several sacrificial steps to later epimerize the C10 center, which would certainly require the C11 position to reside at the ketone oxidation state. As such, we developed a more streamlined approach.

**Table 2.2.** Optimization of a decarboxylative oxygenation of cyclobutanol **2.139**



<sup>a</sup> Yield determined by <sup>1</sup>H NMR comparison to an internal standard. <sup>b</sup> Isolated yield.

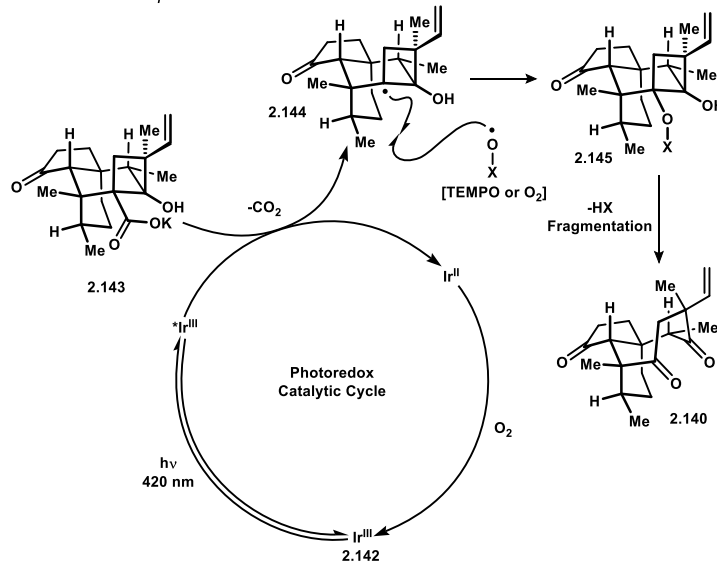
Rather than adjusting the redox state of C11, we aimed to avoid the deleterious retro-Michael fragmentation by leveraging the unexpected transannular aldol reaction observed during treatment of ketene silyl acetal **2.124** with fluoride (see above). We reasoned that exposure of *tris*-silane **2.136** to fluoride would initiate the facile transannular aldol event before

triggering hydrolysis of the enoxysilane at C3, and further anticipated that the cyclobutanol moiety would be resistant to the retro-Michael fragmentation. The reaction performed as designed and we found that treatment of the ketene silyl acetal **2.136** with TBAF delivered the cyclobutanecarboxylic acid **2.139** in good efficiency (84% yield, Table 2.2). With access to the carboxylic acid **2.139** established, we considered our options for the envisioned decarboxylative oxidation. We viewed radical decarboxylation as a favorable approach, which is most commonly executed by the Barton protocol.<sup>70</sup> However, we surmised that the reactivity patterns of cyclobutanol **2.139** precluded the application of this method. Consequently, we explored metal oxidants that have commonly been employed for similar transformations and soon found that the typical conditions (*i.e.*, Kochi conditions, Ag-mediated oxidative decarboxylations) led to complex mixtures of products (Table 2.2, entries 1-3).<sup>71,72</sup> The silver-mediated conditions in some cases led to cleavage of the C11–C12 bond. Accordingly, we resolved to attempt single electron oxidation of the corresponding carboxylate under photocatalytic conditions. We first found success employing acridinium catalyst **2.141** in the presence of DBU and TEMPO under irradiation with visible light (entry 4).<sup>73,74</sup> These conditions formed the tricyclic triketone **2.140** directly in 23% yield as determined by <sup>1</sup>H NMR. We established that iridium catalyst **2.142** was competent in the decarboxylation chemistry and furnished the same triketone, albeit in low yield (9%, entry 5) alongside several side products.<sup>75</sup> The yield was found to be optimal when TEMPO was included in the iridium-catalyzed reaction, ultimately affording the triketone **2.140** in 80% yield by <sup>1</sup>H NMR (entry 6, 72% isolated yield).

In line with the photocatalytic decarboxylation mechanisms proposed in the literature, we presume that the excited state of iridium catalyst **2.142** formed during exposure to light is competent at engaging the potassium carboxylate **2.143** in single electron oxidation (Scheme 2.40).<sup>76</sup> Decarboxylation of the carboxyl radical affords the 3° alkyl radical **2.144**. As the reaction is performed under an atmosphere of air and in the presence of TEMPO, the identity of the

species that traps the alkyl radical is ambiguous at this point.<sup>77</sup> Regardless, capture of the radical by TEMPO or O<sub>2</sub> produces intermediate **2.145** (X = O· or TMP). Fragmentation of the peroxide or oxylamine cleaves the [4.2.0] bicyclic motif, affording the triketone **2.140**. Though the mechanistic details of the fragmentation are unclear, it likely resembles a Grob- or Criegee-type process.

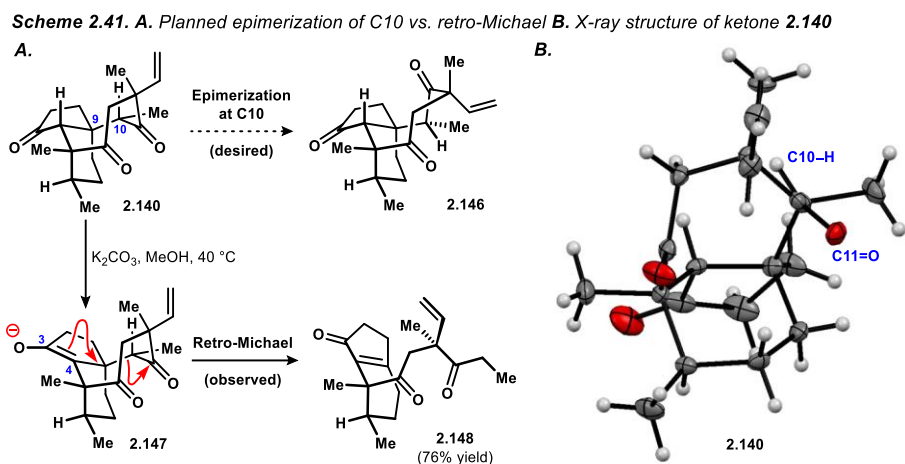
**Scheme 2.40.** Proposed mechanism for the formation of triketone **2.140**



Having achieved the desired decarboxylative oxidation, we were compelled to pursue epimerization of the C10 stereocenter. We imagined that the desired epimer **2.146** would be the more stable diastereomer and accordingly we hoped to induce the epimerization by equilibrating the triketone **2.140** in the presence of base (Scheme 2.41A). Two features of the triketone **2.140** prevented the straightforward execution of the reaction as described. First, the X-ray crystal structure **2.140** demonstrated that the C10–H bond is positioned in a nearly antiperiplanar orientation to the C11=O double bond in the solid state (Scheme 2.41B). A similar conformation is likely in solution. Consequently, the  $\sigma$  C10–H bonding orbital resides between the two lobes of the C11 ketone  $\pi^*$  orbital, minimizing the necessary overlap for acidification of the C10 methine. Accordingly, exposure of trione **2.140** a variety of basic conditions followed by



quenching with MeOH-*d* revealed no deuterium incorporation at C10. All related derivatives surveyed in a wide range of deuterium quenching studies exhibited the same behavior.



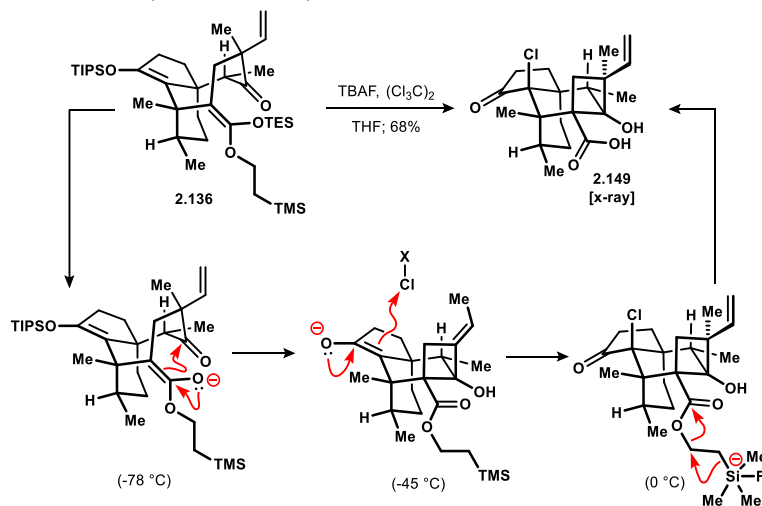
Our first inclination when faced with the poor orbital overlap challenge was to introduce flexibility to the rigid tricyclic system by heating. However, the reactivity patterns of the tricyclic system **2.140** impeded us from solving the orbital overlap issue in this fashion. Application of base, even under relatively mild heating, induced the familiar retro-Michael reaction of the 1,5-dione motif (Scheme 2.41A). In the presence of base, enolization of the C3 ketone at the C4 position initiates the deleterious reaction, fragmenting the cyclooctane by scission of the C9–C10 bond, presumably by the intermediacy of enolate **2.147**. For example, exposure of the triketone **2.140** to  $K_2CO_3$  in MeOH at  $40\text{ }^\circ\text{C}$  resulted in facile formation of bicyclic enone **2.148**. Similar retro-Michael reactions within the mutilin system have been described previously, typically requiring relatively forcing conditions (*i.e.*, KOH in refluxing EtOH). Our studies revealed that no reaction was observed with  $K_2CO_3$ , MeOH,  $40\text{ }^\circ\text{C}$  even after several days in the case of mutilin trione. The apparent increased reactivity within the C10-*epi* series toward retro-Michael can be attributed to the excellent orbital alignment that is enforced by the rigid polycyclic skeleton, as the  $\sigma_{C9-C10}$  bond overlaps strongly with the  $\pi^*_{C11=O}$ , a structural feature that was evident in the solid state by analysis of the X-ray structure of ketone **2.140**. In contrast, the natural mutilin tricyclic system exists in a conformation where the corresponding

orbital interactions appear minimal, thus requiring forcing conditions to accomplish the retro-Michael process.

Taking stock of the two obstacles that impaired our ability to affect the desired epimerization at C10, we devised a structural modification that promised to impede the retro-Michael reaction. We envisioned that introducing a substituent at the C4 position would prevent the enolization from occurring at that site, thereby inhibiting the deleterious fragmentation process. This change should allow us to perform reactions with heating in the presence of base, introducing flexibility to the system, conceivably solving the orbital overlap challenge. According to our considerations, an ideal blocking group at C4 must be readily removable under reductive conditions that we planned to employ in the conclusion to our synthetic sequence. We recognized that the global silane hydrolysis reaction we employed in the synthesis of cyclobutanol **2.139** offered an opportunity to introduce a blocking group at C4 directly, as an enolate intermediate is formed at that site during the reaction of the C3 enoxysilane with fluoride. With a reaction design in mind, we sought conditions to introduce a chlorine atom at C4 during the course of the desilylative cyclobutanol synthesis. We soon identified two sets of conditions to accomplish the desired reaction, both of which relied on the use of temperature control to induce sequential desilylation reactions. Treatment of ketene silyl acetal **2.136** with an excess of TBAF at -78 °C for 2 minutes induced the transannular aldol event (Scheme 2.42). Subsequent introduction of N-chlorosuccinimide (NCS) and warming to -45 °C for 1 hour promoted desilylation of the TIPS functionality, unveiling an enolate that reacted with NCS to form the chloroketone moiety. Notably, when NCS was present at the beginning of the reaction,  $\alpha$ -chlorination of the ester was observed instead of the expected transannular aldolization. Performing the desilylation of the TIPS group at higher temperatures led to significant proportions of a diastereomeric product. Finally, warming the reaction mixture to 0 °C initiated cleavage of the TMSE functionality, revealing the free carboxylic acid. More conveniently, we

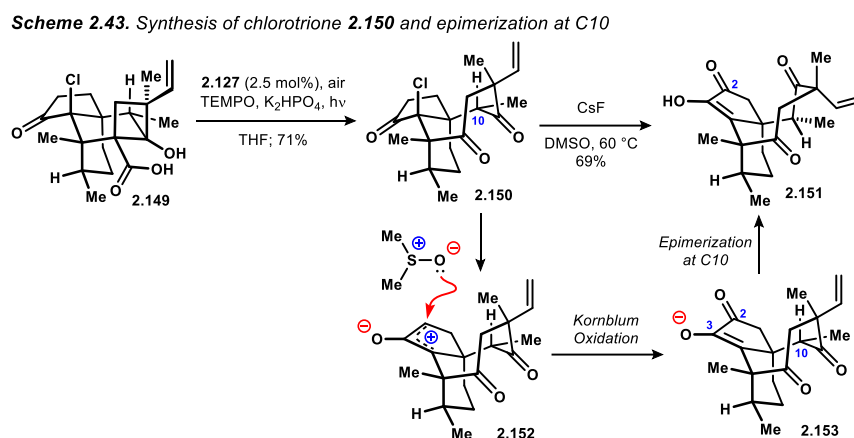
found that the initial transannular aldol event was tolerant of the milder electrophilic chlorine source hexachloroethane ( $\text{Cl}_6\text{C}_2$ ), which enabled us to add TBAF to a THF solution of ketene acetal **2.136** and  $\text{Cl}_6\text{C}_2$  at  $-78\text{ }^\circ\text{C}$ . Sequential increases in the temperature as described above afforded the chlorocyclobutanol **2.149** in 68% yield. A minor diastereomer was also formed during the reaction in a ca. 1:5 ratio with **2.149**, but was found to be incompetent during subsequent synthetic steps and was therefore purified from the crude mixture. The behavior of cyclobutanol **2.149** on silica gel caused purification of the desired product to be challenging under typical conditions. TLC analysis of the material demonstrated significant streaking and attempted chromatography offered the material in poor purity. We discovered that pre-treating a TLC plate with 1% AcOH solution in  $\text{Et}_2\text{O}$  and drying of the plate at ambient temperature for several minutes prior to spotting the material and running the TLC plate resulted in well-defined spots and no signs of streaking. Chromatography under analogous conditions enabled the isolation of the chlorocyclobutanol **2.149** in high purity. We rigorously confirmed the C4 stereochemistry and the overall structure by X-ray crystallographic analysis.

**Scheme 2.42.** Synthesis of chlorocyclobutanol **2.149**



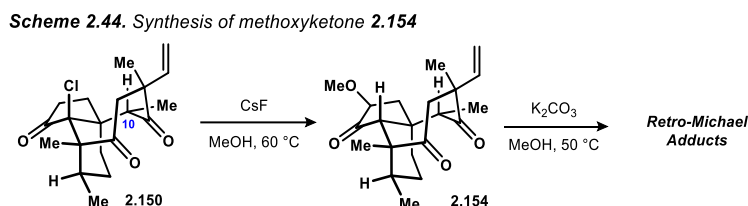
With access to the chlorocyclobutanol **2.149** established, we sought to execute the decarboxylative oxidation. The previously identified conditions, Ir catalyst **2.142**,  $\text{KH}_2\text{PO}_4$ , TEMPO, air, and 420 nm irradiation, performed well, affording the chlorotrione **2.150** in good

yield (Scheme 2.43). We were initially dismayed to find subjecting chlorotrione **2.150** to basic conditions (*i.e.*, *t*-BuOK, basic Al<sub>2</sub>O<sub>3</sub> with heating, LiTMP at -20 °C, or DBU with heating) led to the formation of complex mixtures. Clearly, the chloroketone moiety was not, as we had hoped, an innocent bystander under the conditions we employed. In a last effort before we sought to explore alternative solutions, we subjected chlorotrione **2.150** to CsF in DMSO and found, to our great excitement, that the major product was the tetraketone **2.151**. Most crucially, the reaction had proceeded with the desired epimerization at C10.



We believe that the chloroketone undergoes facile ionization under the reaction conditions to form the corresponding oxyallyl cation **2.152**, which is rapidly captured by DMSO; a Kornblum-type process affords the 1,2-dione **2.153** (Scheme 2.43).<sup>78</sup> The presence of the C2 carbonyl appears to be essential to the success of the reaction, as it draws electron density and stabilizes the C3 enolate of **2.153**, slowing the deleterious retro-Michael reaction that plagued our previous attempts to epimerize C10. Subsequently, epimerization of the C10 position via the corresponding enolate furnishes the observed product **2.151**. We were able to lend some experimental support to our proposed mechanism and analysis of the epimerization reaction. We found that exchanging the solvent for MeOH afforded the methoxyketone **2.154** (Scheme 2.44). The introduction of the methoxy group likely proceeds by a mechanism similar to the one outlined in Scheme 2.42, pointing to facile oxyallyl cation formation under the reaction

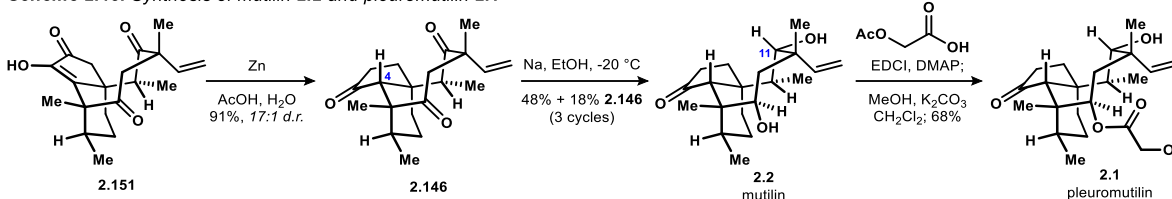
conditions. Notably, NOESY analysis indicated that under these conditions, epimerization had not occurred at C10, precluding enolization of the ketones. Likely, the protic solvent renders CsF too weakly basic to induce deprotonation of the ketones. To probe this hypothesis, we subjected the methoxyketone **2.154** to  $K_2CO_3$  in MeOH with heating to 50 °C and observed the facile formation of retro-Michael adducts.



The tetraketone **2.151** was removed from mutilin only by the oxidation states of its functional groups (Scheme 2.45). We sought to reduce the tetraketone by the most direct means to the natural structure and immediately began investigating its behavior under various reducing conditions. Previous syntheses of pleuromutilin had demonstrated that dissolving metal conditions were most effective for the stereoselective reduction of the two ketones at C11 (Herzon) and C14 (Gibbons, Herzon, and Reisman).<sup>79</sup> We first aimed to reduce the extraneous ketone at C2, and soon found that exposure of tetraketone **2.151** to Zn in a mixture of AcOH and  $H_2O$  led to slow but clean reduction of the 1,2-dione motif, delivering mutilin trione **2.146**.<sup>80,81</sup> Notably, the efficiency of the reduction was found to be contingent on the use of freshly activated Zn. Aging the Zn used in the reaction led to increasing proportions of a minor diastereomer, which was nearly entirely suppressed (1:17) when freshly activated Zn was used. With straightforward access to the mutilin trione **2.146**, we employed the conditions first described by Gibbons:  $Na^0$  in EtOH. To our delight, we found that the natural product mutilin **2.2** was formed as a minor component of the reaction mixture alongside over-reduced mutilin triol and starting material. Lowering the reaction temperature to  $-20$  °C facilitated a clean reaction but attempts to increase the conversion led to the formation of over-reduced products. We found that recycling the trione **2.146** enabled us to prepare mutilin **2.2** in 48% overall yield, alongside

18% recovered trione **2.146** (three cycles). Notably, the use of thinly rolled (*ca.* 0.5 mm) Na<sup>0</sup> was found to be essential to obtain meaningful conversion at -20 °C. Any deviation from the stated conditions (*i.e.*, Li, Mg, or Ca in place of Na, or *i*-PrOH, MeOH, (CH<sub>2</sub>OH)<sub>2</sub>, *n*-PrOH, or NH<sub>3</sub> in place of EtOH) led to decreased efficiency or a complete erosion of the desired reactivity. With mutilin **2.2** in hand, we prepared pleuromutilin **2.1** using conditions that were inspired by Gibbons: glycolation with acetoxyacetic acid and selective hydrolysis in one pot.

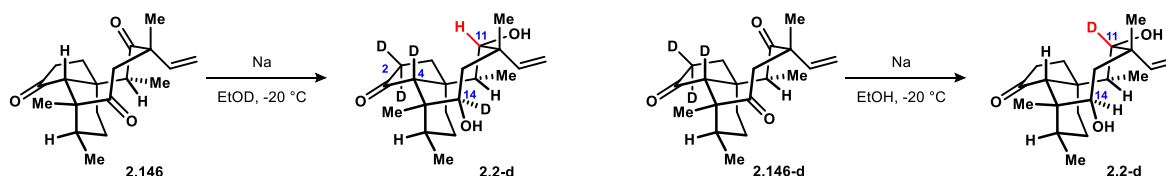
Scheme 2.45. Synthesis of mutilin **2.2** and pleuromutilin **2.1**



Following the completion of our synthetic sequence, we were still curious about the reactivity observed during the reduction of trione **2.146** into mutilin **2.2** (Scheme 2.46). There were two elements of selectivity that we found to be noteworthy. First, we were interested in understanding the chemoselectivity observed, wherein reduction of the two cyclooctanones at C11 and C14 was found to be more rapid than reduction of the cyclopentanone at C3. Second, we aimed to understand the origins of the high stereoselectivity observed during reductions at C11 and C14. Herzon and co-workers employed similar conditions during their synthesis of pleuromutilin, wherein reduction of the analogous ketone at C14 was performed with high selectivity, but the hydroxyl group at C11 was formed with modest diastereoselectivity (see *above*, Chapter 1). In contrast, both the C11 and C14 centers were formed with high diastereoselectivity during the reduction of trione **2.146**. The notable difference between the two ketone substrates is that Herzon's system featured a ketal-protected ketone at C3. We found that employing ethanol-d<sub>6</sub> as solvent in the reduction of trione **2.146** led to extensive deuteration surrounding the C3 ketone at all enolizable sites (C2 and C4), indicating that enolization of the C3 ketone may contribute to the observed chemoselectivity. Additionally, C14 contained a new

deuterium atom, as expected. Interestingly, we found that the C11 methine contained a new C–H bond, likely implicating an intramolecular HAT process. To corroborate the hypothesized intramolecular HAT process, we prepared a deuterated derivative of mutilin trione **2.146-d** and subjected it to the typical reaction conditions. As expected, the C11-monodeuterated mutilin was formed as the major product.

**Scheme 2.46.** Deuterium incorporation studies for reduction of mutilin trione **2.146** to mutilin **2.2**



## 2.8. Conclusion

The entire synthetic sequence for the preparation of pleuomutilin from cyclopentenone **2.9** and silyloxydiene **2.13** (each prepared in one step from commercially available material) is shown below (Scheme 2.47). The cornerstone of the approach was the rapid preparation of the tricyclic diketone intermediate **2.19** by a challenging bimolecular cycloaddition and diastereoselective MHAT-initiated radical cyclization. Subsequent elaboration to mutilin **2.2** relied on the strategic use of a carboxylate ester as a surrogate for the oxidation at C14. The TMSE ester was introduced and further enabled a second alkylation at C14 with iodide **2.34**. A reductive cyclization was used to forge the C12–C11 bond, in turn setting the stage for the planned ring-expansion reaction, which once again relied on the carboxylate ester to establish a retro aldol pathway to cleave the desired C11–C14 bond. One of the unanticipated challenges of the approach was the managing of the equilibrium between cyclooctanone products and the corresponding bicyclo[4.2.0]octane aldol adduct. Ultimately, we made use of the reversibility of the aldol event to first introduce a methyl group at C12 on the ring-expanded ketene silyl acetal **2.136** before leveraging the transannular aldol to protect the C11 ketone from participating in a deleterious retro-Michael process during the unveiling of the carboxylic acid moiety. Notably, the

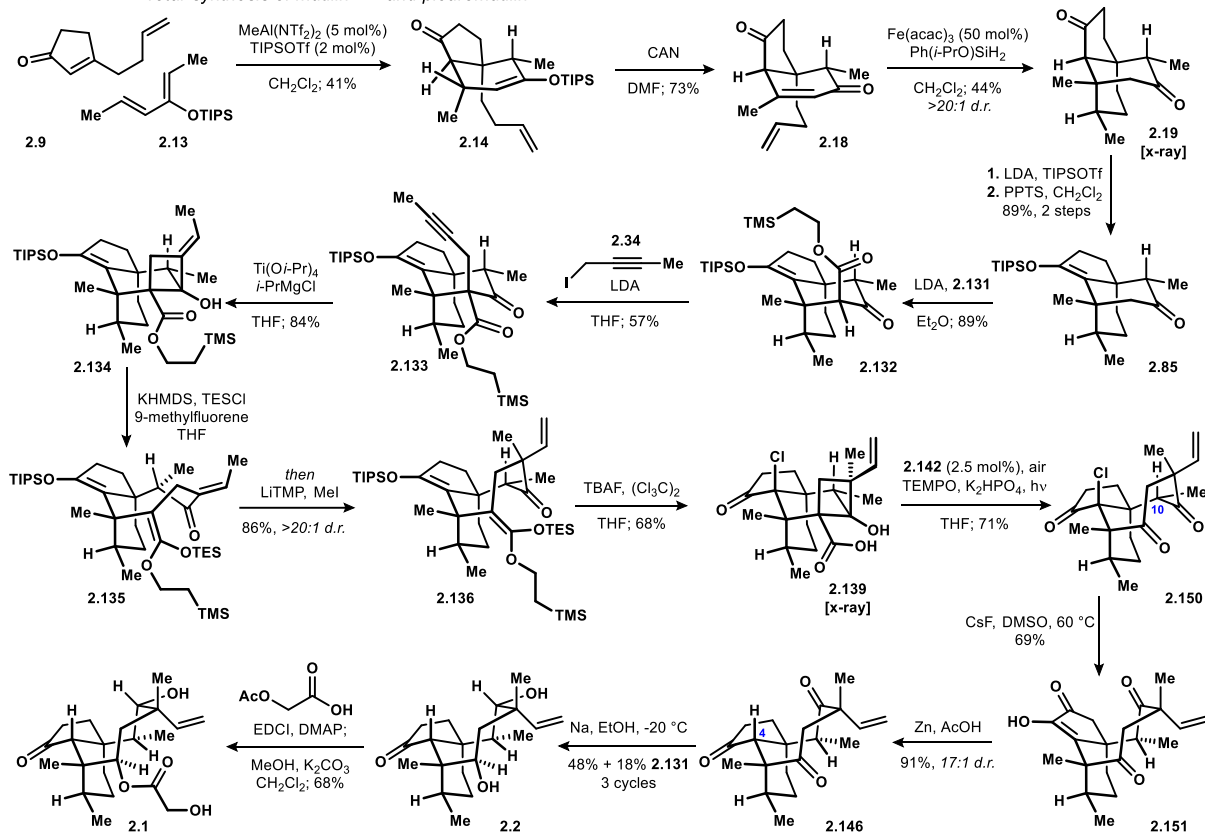
configuration of the methyl group at C10 was found to have a profound effect over the conformational preference of the cyclooctane portion, likely exhibiting control over the stereoselectivity observed during the assembly of the C12 quaternary center. Chlorination of the C4 position enabled late-stage manipulations of the C10-*epi* mutilin scaffold that were otherwise inaccessible. An oxidative decarboxylation reaction to introduce the requisite C14 oxidation spontaneously fragmented the fused bicyclic system to arrive at the C10-*epi* chlorotriene **2.150**. Subsequent epimerization of C10 in the presence of CsF and DMSO benefitted from a fortuitous Kornblum oxidation that retards a deleterious retro-Michael process furnished the tetraketone **2.151**. Finally, a Zn-mediated reduction of the 1,2-dione motif and a selective reduction of the cyclooctanedione portion of the mutilin trione **2.146** using Na<sup>0</sup> in EtOH afforded mutilin **2.2**. Preliminary results indicate that the reduction of the C11 ketone under the action of Na<sup>0</sup> in EtOH proceeds by an intramolecular HAT mechanism. Lastly, appendage of the glycolate side chain was accomplished by diglycolation and selective hydrolysis, providing pleuromutilin **2.1**.

The developed synthetic route required 15 steps (LLS, 17 total steps) to mutilin **2.2** in an overall yield of 0.5% and 16 steps (LLS, 18 total steps) to pleuromutilin **2.1** with an overall yield of 0.3%. Notably, complete stereochemical relay was achieved through the sequence, which had never been accomplished in pleuromutilin total synthesis in fewer than 30 steps LLS. While they are not significantly ahead of prior art, these figures mark the most efficient synthesis of pleuromutilins to date. Regardless, the impact of the work should be derived from the unique and fascinating modes of reactivity we uncovered within the medicinally relevant mutilin scaffold. While many of the chemistries developed were specifically tailored for the problem at hand, other applications for them may arise in unrelated areas of research. Future development of our approach to pleuromutilin synthesis should include the introduction of enantioselectivity to the initial cycloaddition. Further, we hope that some of the intermediates accessible by our synthetic sequence can enable the functionalization of sites within the pleuromutilin scaffold that have been otherwise inaccessible by semi-synthesis. Indeed, the tetraketone **2.151** appears



well functionalized to enable selective modification at C2 and C8, sites of interest to studying the metabolism of pleuromutilins *in vivo*. The developed sequence also appears well suited for the preparation of C10-*epi* pleuromutilin analogs, should interest in these derivatives arise.

**Scheme 2.47.** Total synthesis of mutilin 2.2 and pleuromutilin 2.1



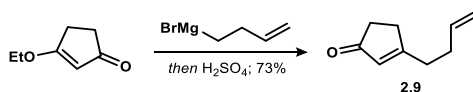
## 2.9. Experimental Section

### 2.9.1. Materials & Methods

All reactions were carried out in flame-dried glassware under positive pressure of dry nitrogen unless otherwise noted. Reaction solvents including dichloromethane ( $\text{CH}_2\text{Cl}_2$ , Fisher, HPLC Grade), diethyl ether ( $\text{Et}_2\text{O}$ , Fisher, HPLC grade), and *N,N*-dimethylformamide (DMF, Fisher, HPLC Grade) were dried by percolation through a column packed with neutral alumina and a column packed with a supported copper catalyst for scavenging oxygen (Q5) under positive pressure of argon. Tetrahydrofuran (THF, Fisher, HPLC Grade) was freshly distilled over sodium-benzophenone ketyl under pressure of  $\text{N}_2$ . Hexamethylphosphoramide (HMPA, Chem-Impex Int'l, 99%) was distilled over calcium hydride and stored under inert atmosphere in a sealed flask. Ethanol ( $\text{EtOH}$ , Gold Shield Dist., 200 proof) and dimethylsulfoxide (DMSO, Sigma Aldrich, reagent grade) were stored over 3 Å molecular sieves under inert atmosphere in a

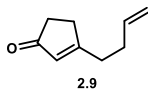
sealed flask. Pyridine (Py), triethylamine (Et<sub>3</sub>N), 2,2,6,6-tetramethylpiperidine (TMP), and diisopropylamine (*i*-Pr<sub>2</sub>NH) were distilled over calcium hydride under inert atmosphere immediately before use. Solvents for extraction, thin layer chromatography (TLC), and flash column chromatography were purchased from Fischer (ACS Grade) and VWR (ACS Grade) and used without further purification. Chloroform-*d*, methanol-*d*<sub>4</sub>, and benzene-*d*<sub>6</sub> for NMR analysis were purchased from Cambridge Isotope Laboratories and used without further purification. Commercially available reagents were used without further purification unless otherwise noted. Reactions were monitored by thin layer chromatography (TLC) using precoated silica gel plates (EMD Chemicals, Silica gel 60 F<sub>254</sub>). Flash column chromatography was performed according to the method of Still and co-workers<sup>82</sup> over silica gel (Acros Organics, 60 Å, particle size 0.04-0.063 mm). <sup>1</sup>H NMR and <sup>13</sup>C NMR spectra were recorded on Bruker DRX-500 (BBO probe), Bruker DRX-500 (TCI cryoprobe), Bruker AVANCE600 (TBI probe), and Bruker AVANCE600 (BBFO cryoprobe) spectrometers using residual solvent peaks as internal standards (CHCl<sub>3</sub> at 7.26 ppm <sup>1</sup>H NMR, 77.16 ppm <sup>13</sup>C NMR; C<sub>6</sub>H<sub>6</sub> at 7.16 ppm <sup>1</sup>H NMR, 128.00 ppm <sup>13</sup>C NMR; CD<sub>3</sub>OD at 3.34 ppm <sup>1</sup>H NMR, 49.00 ppm <sup>13</sup>C NMR). NMR data were collected at 25 °C unless otherwise stated. High-resolution mass spectra (HRMS) were recorded on Waters LCT Premier TOF spectrometer with ESI and CI sources.

### 2.9.2. Experimental Procedures



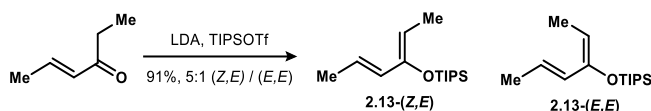
**Cyclopentenone 2.9.** Prepared according to a procedure that was modified from the report of Coote, O'Brien, and Whitwood.<sup>83</sup> A 500 mL two-necked flask fitted with a Vigreux condenser and rubber septum was charged with a magnetic stir bar and magnesium turnings (15.1 g, 0.621 mol) and flame dried under vacuum. After cooling to ambient temperature under N<sub>2</sub>, THF (320 mL) was added. The resulting suspension was sonicated for 20 minutes then stirred vigorously at ambient temperature during the addition of 4-bromobutene as one portion (5.8 mL, 57 mmol). (**Caution: possible exotherm**). The mixture was heated to 60 °C until the reaction showed signs of initiation: a darkening of the initially colorless solution to grey and boiling of the solvent local to the magnesium surface. The flask was transferred to a water bath at ambient temperature and the remainder of the 4-bromobutene (23.2 mL, 0.228 mol for a total of 29.0 mL, 0.285 mol) was added dropwise at such a rate as to maintain a controlled reflux. Subsequently, the suspension was heated to 60 °C for 1 h before cooling to 0 °C. The Grignard reagent solution thus formed was treated dropwise with a solution of 3-ethoxycyclopent-2-en-1-one (23.30 g, 0.185 mol, commercially available or prepared in one step from 1,3-

cyclopentanedione<sup>84</sup>) in THF (50 mL) and warmed to ambient temperature. After 3 h, the solution was cannulated into a separate flask containing ice (300 g) and concentrated sulfuric acid (15 mL). The transfer was quantitated with two portions of Et<sub>2</sub>O (30 mL) and the resulting orange mixture was stirred vigorously for 1 h before the THF was removed by rotary evaporation (ca. 300 mL in the collection flask) and diluting with Et<sub>2</sub>O (150 mL). The phases were separated, and the aqueous component was extracted with Et<sub>2</sub>O (3x 150 mL). The combined organics were washed with saturated aqueous NaHCO<sub>3</sub> and brine, dried over anhydrous MgSO<sub>4</sub>, and concentrated under reduced pressure. The crude product was purified by distillation using a short path distillation apparatus from an 80-95 °C bath (58-64 °C, ca. 0.2 mm Hg) to afford 18.35 g of the known enone **2.9** as a yellow oil (73% yield).



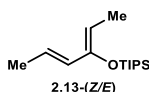
<sup>1</sup>H NMR (500 MHz, CDCl<sub>3</sub>)

δ 5.97 (p, J = 1.6 Hz, 1H)	2.62 – 2.56 (m, 2H)
5.81 (ddt, J = 16.8, 10.2, 6.5 Hz, 1H)	2.52 (t, J = 7.6 Hz, 2H)
5.08 (dq, J = 17.1, 1.7 Hz, 1H)	2.43 – 2.39 (m, 2H)
5.03 (dq, J = 10.2, 1.4 Hz, 1H)	2.39 – 2.32 (m, 2H)



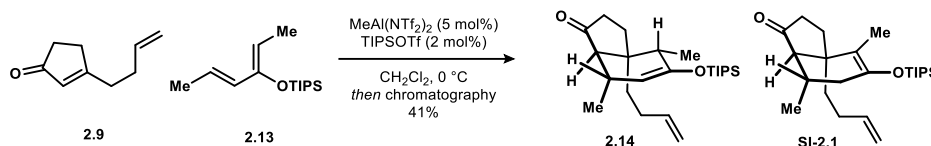
**Siloxydiene 2.13.** Prepared according to a procedure that was modified from the report of Nakashima and Yamamoto.<sup>85</sup> A solution of *i*-Pr<sub>2</sub>NH (8.83 mL, 63.0 mmol) in THF (120 mL) was cooled to -78 °C and treated dropwise with *n*-BuLi (26.0 mL of a 2.35 M solution in hexanes, 61.2 mmol). The solution was warmed to 0 °C for 10 minutes and cooled to -78 °C. (E)-hex-4-en-3-one (6.84 mL, 60.0 mmol) was added dropwise, and the reaction was maintained at the same temperature for 30 minutes. The solution was treated dropwise with TIPSOTf (17.0 mL, 63.0 mmol, distilled from CaH<sub>2</sub> at ca. 0.2 mm Hg). The reaction was stirred for 1 h at -78 °C and 30 minutes at ambient temperature before quenching at 0 °C under vigorous stirring by the rapid addition of saturated aqueous NaHCO<sub>3</sub> (120 mL). The resulting emulsion was stirred for an additional 12 h at ambient temperature, then diluted with Et<sub>2</sub>O (200 mL) and water (30 mL). The phases were separated, and the aqueous layer was extracted with Et<sub>2</sub>O (2x 150 mL). The combined organics were washed with brine, dried over anhydrous MgSO<sub>4</sub>, and concentrated

under reduced pressure. The crude product was purified by flash column chromatography over silica gel slurry-packed with 1% v/v Et<sub>3</sub>N in hexanes. Elution with 1% v/v Et<sub>3</sub>N in hexanes afforded 13.90 g of the known diene **2.13** (91% yield, 4:1 ratio of (*Z,E*) to (*E,E*) isomers). (*Z,E*) / (*E,E*) ratio = 4:1 determined by <sup>1</sup>H NMR: (500 MHz, CDCl<sub>3</sub>) δ 1.81 (d, *J* = 6.1 Hz, 3H, (*E,E*)) vs. 1.73 (d, *J* = 6.1 Hz, 3H, (*Z,E*)). For use in the subsequent step, the pure silyloxydiene **2.13** was rigorously concentrated by stirring and heating to 35 °C under vacuum (0.2 mm Hg) for 8 h.

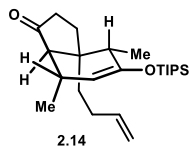


<sup>1</sup>H NMR (500 MHz, CDCl<sub>3</sub>)

δ 5.85 (d, <i>J</i> = 15.6 Hz, 1H)	1.64 (d, <i>J</i> = 7.0 Hz, 3H) – overlaps with ( <i>E,E</i> )
5.82 – 5.73 (m, 1H)	1.25 – 1.16 (m, 3H) – overlaps with ( <i>E,E</i> )
4.67 (q, <i>J</i> = 7.0 Hz, 1H)	1.11 (d, <i>J</i> = 7.0 Hz, 18H)
1.73 (d, <i>J</i> = 6.3 Hz, 3H)	



**Enoxysilane 2.14.** Me<sub>3</sub>Al (0.83 mL of a 2.0 M solution, 1.65 mmol) was added dropwise to a solution of HNTf<sub>2</sub> (0.93 g, 3.3 mmol) in CH<sub>2</sub>Cl<sub>2</sub> (200 mL) at ambient temperature. After 15 minutes, the flask was cooled to 0 °C and silyloxydiene **2.13** (12.73 g, 50.0 mmol), enone **2.9** (4.59 mL, 33.0 mmol), and TIPSOTf (0.2 mL, 0.72 mmol) were added sequentially. The reaction was maintained at the same temperature for 10 h then quenched with pyridine (2 mL). The resulting solution was filtered over a plug of silica gel which was washed with CH<sub>2</sub>Cl<sub>2</sub> until TLC analysis of the eluting solvent indicated that all of the desired adduct had been collected. The combined organics were concentrated and purified by flash column chromatography over silica gel. Elution with 5-10% v/v Et<sub>2</sub>O in hexanes afforded 5.25 g of enoxysilane **2.14** as a viscous oil (41% yield). Variable proportions of the isomerized enoxysilane **SI-2.1** were formed during the chromatography, with no effect on the outcome of the next step.



<sup>1</sup>H NMR (600 MHz, CDCl<sub>3</sub>)

δ 5.81 (ddt, <i>J</i> = 16.8, 10.2, 6.5 Hz, 1H)	2.02 (q, <i>J</i> = 7.1 Hz, 1H)
5.03 (dq, <i>J</i> = 17.1, 1.6 Hz, 1H)	1.86 – 1.78 (m, 2H)

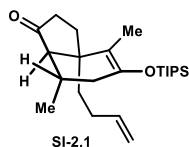
4.96 (dq, J = 10.1, 1.1 Hz, 1H)	1.75 (d, J = 5.2 Hz, 1H)
4.56 (dd, J = 3.5, 1.1 Hz, 1H)	1.54 – 1.47 (m, 1H)
2.42 (dddd, J = 7.1, 5.4, 3.5, 1.9 Hz, 1H)	1.41 – 1.33 (m, 1H)
2.35 – 2.19 (m, 2H)	1.21 – 1.13 (m, 3H)
2.12 – 2.05 (m, 2H)	1.11 – 1.05 (m, 24H)

<sup>13</sup>C NMR (151 MHz, CDCl<sub>3</sub>)

δ 218.6	45.1	27.0
151.8	37.6	22.2
138.5	33.9	18.3
114.7	32.8	18.3
104.2	28.1	14.8
57.2	27.8	12.9

TLC R<sub>f</sub> = 0.42 (10% v/v Et<sub>2</sub>O in hexanes). Modestly UV active.

HRMS (ES<sup>+</sup>) calculated for C<sub>24</sub>H<sub>42</sub>O<sub>2</sub>SiH [M+H]: 391.3032, found: 391.3017



<sup>1</sup>H NMR (499 MHz, CDCl<sub>3</sub>)

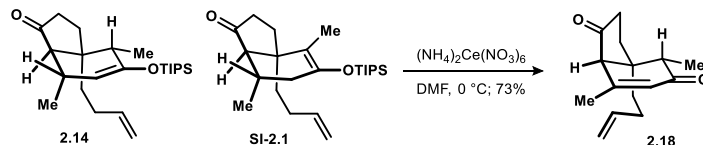
δ 5.76 (ddt, J = 16.9, 10.3, 6.6 Hz, 1H)	2.11 – 1.77 (m, 9H)
4.97 (dq, J = 17.1, 1.7 Hz, 1H)	1.65 – 1.58 (m, 4H)
4.91 (dq, J = 10.1, 1.3 Hz, 1H)	1.43 – 1.33 (m, 1H)
2.34 – 2.21 (m, 2H)	1.15 – 1.06 (m, 23H)

<sup>13</sup>C NMR (151 MHz, CDCl<sub>3</sub>)

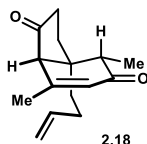
δ 220.8	47.5	28.2
144.0	38.4	19.2
138.7	36.6	18.2
114.5	35.1	18.2
113.8	33.8	17.8
58.2	29.0	13.3

TLC R<sub>f</sub> = 0.42 (10% v/v Et<sub>2</sub>O in hexanes). Modestly UV active.

HRMS (ES<sup>+</sup>) calculated for C<sub>24</sub>H<sub>42</sub>O<sub>2</sub>SiNa [M+Na]: 413.2852, found: 413.2865



**Enone 2.18.** A solution of enoxysilanes **2.14** and **SI-2.1** (5.25 g, 13.40 mmol) in DMF (130 mL) was cooled to 0 °C. With stirring under inert atmosphere, ceric ammonium nitrate (CAN, 5.5 g, 10.0 mmol) was added as a single portion. Three additional portions of CAN (5.5 g, 10.0 mmol, for a total of 22.0 g, 40.1 mmol) were added at 5-minute intervals. The reaction was stirred at the same temperature for 1.5 h, then diluted with Et<sub>2</sub>O (150 mL) and H<sub>2</sub>O (150 mL). The phases were separated, and the aqueous portion was extracted with Et<sub>2</sub>O (3x 150 mL). The combined organics were washed with saturated aqueous NaHCO<sub>3</sub>, H<sub>2</sub>O, and brine, then dried over anhydrous MgSO<sub>4</sub> and concentrated under reduced pressure. The crude product was purified by flash column chromatography over silica gel. Elution with 14% v/v EtOAc in hexanes afforded 2.27 g of enone **2.18** as a light-yellow oil (73% yield) contaminated with small proportions (<1:10) of a regioisomer.



<sup>1</sup>H NMR (500 MHz, CDCl<sub>3</sub>)

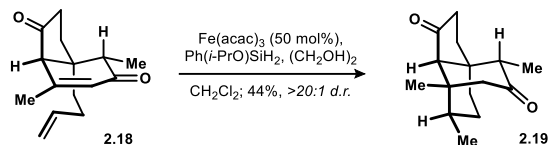
δ 5.90 (s, 1H)	2.11 (d, J = 1.4 Hz, 3H)
5.01 (dq, J = 17.1, 1.6 Hz, 1H)	2.07 – 1.97 (m, 2H)
4.96 (dq, J = 10.2, 1.4 Hz, 1H)	1.93 – 1.85 (m, 2H)
2.78 (s, 1H)	1.54 – 1.49 (m, 2H)
2.47 (dddd, J = 19.7, 9.6, 2.9, 1.1 Hz, 1H)	1.12 (d, J = 6.8 Hz, 3H)
2.41 – 2.31 (m, 2H)	

<sup>13</sup>C NMR (126 MHz, CDCl<sub>3</sub>)

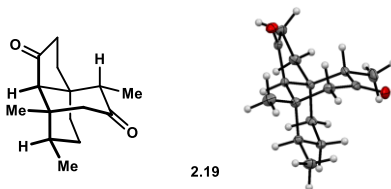
δ 213.9	115.3	33.1
200.0	59.9	29.1
153.7	49.4	28.5
137.9	44.6	23.9
126.4	36.1	8.6

TLC R<sub>f</sub> = 0.53 (30% v/v EtOAc in hexanes). UV active.

HRMS (ES<sup>+</sup>) calculated for C<sub>15</sub>H<sub>20</sub>O<sub>2</sub>H [M+H]: 233.1542, found: 233.1532



**Diketone 2.19.** A solution of enone **2.18** (2.14 g, 9.21 mmol) and  $\text{Fe}(\text{acac})_3$  (1.63 g, 4.61 mmol) in  $\text{CH}_2\text{Cl}_2$  (180 mL) was treated with ethylene glycol (2.4 mL, 42.9 mmol). The resulting suspension was sparged with Ar under continuous sonication for 1 h, then cooled to 0 °C. With good stirring,  $\text{Ph}(i\text{-PrO})\text{SiH}_2$  (3.30 mL, 18.42 mmol, prepared according to the known method<sup>86</sup>) was added over 3 minutes. After 3 h, the reaction mixture appeared yellow and heterogeneous and was treated with 1 N HCl (180 mL) with vigorous stirring. The stirring was continued until much of the orange-red color had faded (ca. 40 minutes) at which point the mixture was transferred to a separatory funnel and the phases separated. The aqueous layer was extracted with  $\text{CH}_2\text{Cl}_2$  (3x 150 mL). The combined organics were washed  $\text{NaHCO}_3$  and brine, dried over  $\text{Na}_2\text{SO}_4$  and concentrated under reduced pressure. The crude product was purified by flash column chromatography over silica gel. Elution with 12% v/v EtOAc in hexanes afforded 1.61 g of the tricyclic diketone **2.19** alongside an impurity (ca. 2.4:1). The mixture was dissolved in a minimal quantity of hot 20% v/v cyclohexane in hexane and allowed to slowly cool to room temperature over 1 h. The crystallization was continued at 4 °C for 14 h, resulting in 735 mg of crystals of diketone **2.19** (34% yield) which were collected by filtration and washed with a small portion of cold pentane. The filtrate was concentrated, and the residue was subjected to the same crystallization procedure, affording a second 216 mg crop of crystals (10% yield) for an overall yield of 44%. The crystals were suitable for x-ray diffraction analysis.



$^1\text{H}$  NMR (500 MHz,  $\text{CDCl}_3$ )

$\delta$  2.41 (ddt,  $J = 19.5, 10.3, 1.5$  Hz, 1H)

2.32 (d,  $J = 1.8$  Hz, 2H)

2.24 (dt,  $J = 19.4, 9.3$  Hz, 1H)

2.10 – 2.02 (m, 2H)

1.97 (s, 1H)

1.82 (q,  $J = 6.6$  Hz, 1H)

$^{13}\text{C}$  NMR (151 MHz,  $\text{CDCl}_3$ )

$\delta$  215.9

43.7

30.8

1.64 – 1.57 (m, 1H)

1.48 (dtd,  $J = 15.3, 4.7, 2.3$  Hz, 1H)

1.38 – 1.28 (m, 5H)

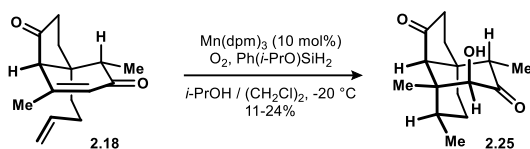
1.08 (d,  $J = 6.6$  Hz, 3H)

0.94 – 0.83 (m, 4H)

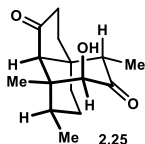
212.8	43.3	29.5
63.6	38.8	23.0
46.9	35.0	14.3
45.7	34.7	8.6

TLC  $R_f$  = 0.51 (30% v/v EtOAc in hexanes). Not UV active.

HRMS (ES+) calculated for  $C_{15}H_{22}O_2Na$  [M+Na]: 257.1518, found: 257.1517



**Diketone 2.25.** A solution of enone **2.18** (92.9 mg, 0.40 mmol) and  $Mn(dpm)_3$  (24.2 mg, 0.04 mmol) in  $i-PrOH$  (10 mL) was cooled to  $-20\text{ }^\circ\text{C}$  and sparged continuously with  $O_2$  for 10 minutes. With maintained sparging with  $O_2$  and good stirring,  $Ph(i-PrO)SiH_2$  (0.16 mL, 0.8 mmol, prepared according to the known method<sup>86</sup>) was added over 3 minutes. After 5 h, the reaction mixture was treated saturated aqueous  $Na_2S_2O_3$  (2 mL),  $H_2O$  (8 mL), and  $Et_2O$  (15 mL). The aqueous layer was extracted with  $Et_2O$  (3x 8 mL). The combined organics were washed  $NH_4OH$  and brine, dried over  $MgSO_4$  and concentrated under reduced pressure. The crude product was purified by flash column chromatography over silica gel. Elution with 25% v/v EtOAc in hexanes afforded 15.7 mg of the tricyclic diketone **2.25** (16% yield).



$^1H$  NMR (600 MHz,  $CDCl_3$ )

$\delta$ 3.74 (s, 1H)	1.57 (dt, $J = 13.4, 10.1$ Hz, 1H)
3.10 (bs, 1H)	1.50 – 1.46 (m, 4H)
2.51 (q, $J = 6.6$ Hz, 1H)	1.45 – 1.40 (m, 1H)
2.44 (ddt, $J = 19.6, 9.9, 1.4$ Hz, 1H)	1.30 (td, $J = 13.3, 4.6$ Hz, 1H)
2.36 (ddd, $J = 19.6, 10.1, 8.9$ Hz, 1H)	1.10 (d, $J = 6.6$ Hz, 3H)
2.10 (dddd, $J = 27.8, 13.5, 5.6, 1.6$ Hz, 2H)	1.00 – 0.95 (m, 1H)
1.92 (s, 1H)	0.91 (d, $J = 6.8$ Hz, 3H)

$^{13}C$  NMR (151 MHz,  $CDCl_3$ )

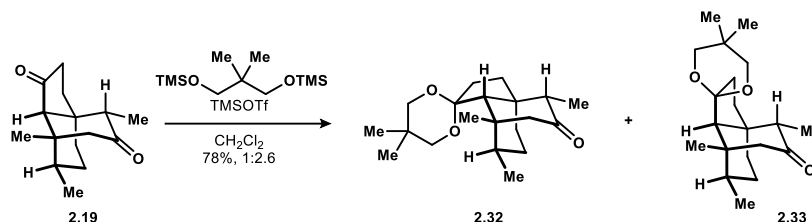
$\delta$ 219.5	42.9	31.1
----------------	------	------



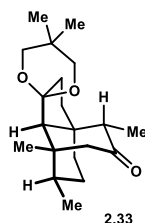
211.5	42.895	29.0
77.0	40.8	19.5
62.8	35.1	14.7
47.1	34.9	8.1

TLC  $R_f$  = 0.40 (40% v/v EtOAc in hexanes). Not UV active.

HRMS (ES+) calculated for  $C_{15}H_{22}O_3Na$  [M+Na]: 273.1467, found: 273.1471



**Monoketals 2.32 and 2.33.** A solution of diketone **2.19** (780 mg, 3.33 mmol) and 1,3-*bis*(trimethylsilyloxy)-2,2-dimethylpropane (5.8 mL, 19.36 mmol, prepared according to the known method<sup>87</sup> and distilled under vacuum) in  $CH_2Cl_2$  (33 mL) was cooled to 0 °C and treated with TMSOTf (1.75 mL, 9.68 mmol, distilled over  $CaH_2$  under vacuum). The reaction was warmed to ambient temperature and stirred for 15 h, then cooled back to 0 °C. Pyridine (2.0 mL) was added, followed immediately by saturated aqueous  $NaHCO_3$  (30 mL) with vigorous stirring. The emulsion was stirred for 20 minutes, then the phases were separated. The aqueous portion was extracted with  $CH_2Cl_2$  (2x 20 mL). The combined organics were washed with brine, dried over  $MgSO_4$ , and concentrated under reduced pressure. The crude product was purified by flash column chromatography over silica gel. Elution with 8% v/v EtOAc in hexanes afforded 615 mg of monoketal **2.33** as a yellow oil (58% yield) and 218 mg of diastereomer **2.32** as a white solid (20% yield). To achieve good performance in the subsequent enolate alkylation, the major monoketal **2.33** required a second chromatographic purification over silica gel. Elution with 1.6-2% EtOAc in  $CH_2Cl_2$  delivered 602 mg of monoketal **2.33** as a white solid in high purity (56% yield).



$^1H$  NMR (600 MHz,  $CDCl_3$ )

$\delta$  3.65 (d,  $J$  = 11.4 Hz, 1H)

1.87 (ddd,  $J$  = 13.0, 8.7, 1.4 Hz, 1H)

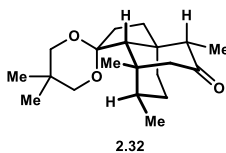
3.60 (d, J = 11.4 Hz, 1H)	1.57 (d, J = 1.9 Hz, 1H)
3.48 (dd, J = 11.4, 2.7 Hz, 1H)	1.41 – 1.29 (m, 3H)
3.38 (dd, J = 11.4, 2.7 Hz, 1H)	1.28 (d, J = 4.3 Hz, 6H)
2.85 (d, J = 16.3 Hz, 1H)	1.09 (td, J = 13.4, 4.7 Hz, 1H)
2.38 (q, J = 6.7 Hz, 1H)	1.00 (d, J = 6.8 Hz, 3H)
2.25 – 2.15 (m, 2H)	0.88 – 0.80 (m, 4H)
2.07 (ddd, J = 13.9, 10.7, 8.7 Hz, 1H)	0.73 (s, 3H)
1.94 (ddd, J = 13.4, 4.5, 2.2 Hz, 1H)	

<sup>13</sup>C NMR (126 MHz, CDCl<sub>3</sub>)

δ 216.5	44.8	29.3
110.7	44.6	24.2
73.0	39.8	23.9
71.1	35.5	22.9
63.2	34.6	14.7
48.0	30.0	8.6
45.0	29.9	

TLC R<sub>f</sub> = 0.51 (20% v/v EtOAc in hexanes). Not UV active.

HRMS (ES<sup>+</sup>) calculated for C<sub>20</sub>H<sub>32</sub>O<sub>3</sub>H [M+H]: 321.2430, found: 321.2426



<sup>1</sup>H NMR (600 MHz, CDCl<sub>3</sub>)

δ 3.64 (d, J = 11.3 Hz, 1H)	1.63 – 1.56 (m, 1H)
3.57 (d, J = 11.2 Hz, 1H)	1.48 – 1.32 (m, 3H)
3.42 (ddd, J = 17.6, 11.3, 2.7 Hz, 2H)	1.29 (s, 3H)
2.49 (d, J = 16.3 Hz, 1H)	1.25 (s, 3H)
2.30 – 2.18 (m, 2H)	1.03 (d, J = 6.8 Hz, 3H)
2.09 – 1.99 (m, 2H)	0.83 – 0.73 (m, 4H)
1.94 – 1.85 (m, 2H)	0.73 (s, 3H)
1.68 (ddd, J = 12.4, 8.7, 1.2 Hz, 1H)	

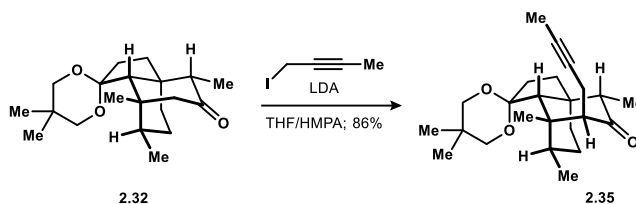
<sup>13</sup>C NMR (126 MHz, CDCl<sub>3</sub>)

δ 214.2	46.8	26.3
110.5	38.8	25.6
72.8	36.1	24.0

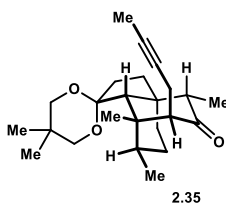
71.3	35.0	22.7
64.5	30.5	15.7
56.3	30.0	9.2
50.8	29.1	

TLC  $R_f$  = 0.44 (20% v/v EtOAc in hexanes). Not UV active.

HRMS (CI+) calculated for  $C_{20}H_{32}O_3H$  [ $M^+$ ]: 320.2351, found: 320.2344



**Alkyne 2.35.** A solution of *i*-Pr<sub>2</sub>NH (0.16 mL, 1.16 mmol) in THF (1.6 mL) was cooled to -78 °C and treated dropwise with *n*-BuLi (0.42 mL of a 2.44 M solution in hexanes, 1.02 mmol). The mixture was warmed to 0 °C for 10 minutes, then cooled back to -78 °C. The LDA solution was treated dropwise with a solution of ketone **2.32** (218.0 mg, 0.68 mmol) in THF (3.0 mL). The reaction was maintained at the same temperature for 30 minutes, then treated with HMPA (0.35 mL, 2.04 mmol). After 5 minutes, 1-iodobut-2-yne (0.27 mL, 2.72 mmol, prepared according to the known method<sup>88</sup> and distilled over CaH<sub>2</sub> under N<sub>2</sub> atmosphere) was added as a single portion. After 30 minutes, the reaction was warmed to ambient temperature and stirred for 2.5 h, prior to the addition of ½-saturated aqueous NH<sub>4</sub>Cl (20 mL) and Et<sub>2</sub>O (20 mL) with stirring. The phases were separated, and the aqueous portion was extracted with Et<sub>2</sub>O (2x 10 mL). The combined organics were washed with brine, dried over anhydrous MgSO<sub>4</sub>, and concentrated under reduced pressure. The crude product was purified by flash column chromatography over silica gel. Elution with 8% EtOAc in pentane furnished 218.0 mg of alkyne **2.35** as a light-yellow solid (86% yield).



<sup>1</sup>H NMR (500 MHz, CDCl<sub>3</sub>)

δ 3.60 (d, <i>J</i> = 11.3 Hz, 1H)	1.55 (td, <i>J</i> = 13.7, 5.1 Hz, 1H)
3.56 (d, <i>J</i> = 11.3 Hz, 1H)	1.42 – 1.34 (m, 2H)
3.41 (ddd, <i>J</i> = 19.1, 11.3, 2.7 Hz, 2H)	1.32 – 1.26 (m, 4H)

2.52 – 2.42 (m, 2H)

2.38 – 2.16 (m, 5H)

2.08 – 1.98 (m, 1H)

1.75 (t, J = 2.5 Hz, 3H)

1.68 – 1.64 (m, 1H)

$^{13}\text{C}$  NMR (151 MHz,  $\text{CDCl}_3$ )

$\delta$  215.2

53.8

25.7

110.8

46.7

24.0

78.9

39.9

22.7

76.5

36.6

22.5

72.8

36.1

19.7

71.2

30.4

15.3

57.8

29.9

9.2

53.8

28.4

3.8

1.23 (s, 3H)

1.02 (d, J = 6.7 Hz, 3H)

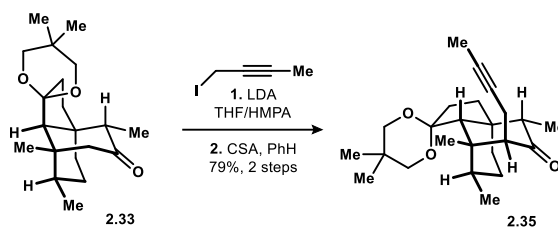
0.98 – 0.87 (m, 1H)

0.78 (d, J = 7.0 Hz, 3H)

0.71 (s, 3H)

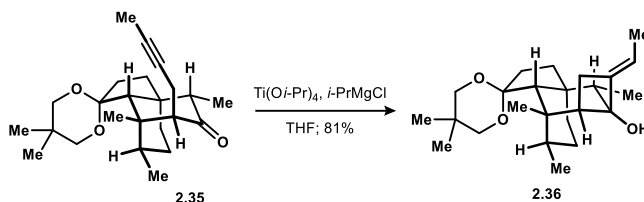
TLC  $R_f$  = 0.53 (20% v/v EtOAc in hexanes).

HRMS (CI+) calculated for  $\text{C}_{24}\text{H}_{36}\text{O}_3\text{H}$  [M+H]: 373.2743, found: 373.2740

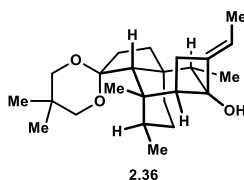


**Alkyne 2.35.** A solution of *i*-Pr<sub>2</sub>NH (0.26 mL, 1.84 mmol) in THF (2.4 mL) was cooled to -78 °C and treated dropwise with *n*-BuLi (0.66 mL of a 2.44 M solution in hexanes, 1.62 mmol). The mixture was warmed to 0 °C for 10 minutes, then cooled back to -78 °C. The LDA solution was treated dropwise with a solution of ketone **2.33** (346.0 mg, 1.08 mmol) in THF (5.0 mL). The reaction was maintained at the same temperature for 30 minutes, then treated with HMPA (0.56 mL, 3.24 mmol). After 5 minutes, 1-iodobut-2-yne (0.43 mL, 4.32 mmol, prepared according to the known method<sup>88</sup> and distilled over CaH<sub>2</sub> under N<sub>2</sub> atmosphere) was added as a single portion. After 30 minutes, the reaction was warmed to ambient temperature and stirred for 16 h, prior to the addition of ½-saturated aqueous NH<sub>4</sub>Cl (30 mL) and Et<sub>2</sub>O (30 mL) with stirring. The phases were separated, and the aqueous portion was extracted with Et<sub>2</sub>O (2x 20 mL). The combined organics were washed with brine, dried over anhydrous MgSO<sub>4</sub>, and concentrated under reduced pressure. The crude residue was taken up in dry PhH (5 mL) and treated with

camphorsulfonic acid (160 mg, 0.69 mmol). After 15 minutes, the reaction was quenched by the addition of Et<sub>3</sub>N (0.1 mL), then loaded directly onto a silica gel column. Elution with 8% EtOAc in pentane furnished 318 mg of ketone **2.35** as a light-yellow solid (79% yield). Characterization for the alkyne **2.35** is presented above on page 101.



**Cyclobutanol 2.36.** A solution of (*i*-PrO)<sub>4</sub>Ti (0.85 mL, 2.87 mmol) in THF (3 mL) was cooled to -78 °C and treated dropwise with a solution of *i*-PrMgCl (2.87 mL of a 2.0 M solution in THF, 5.74 mmol). After 5 minutes, a solution of alkyne **2.35** (267 mg, 0.717 mmol) in THF (4 mL) was added dropwise to the yellow solution. After 30 minutes, the reaction was warmed to ambient temperature and the mixture soon developed a red-brown color. After 20 minutes, the reaction was quenched at 0 °C by the addition of aqueous 1 N HCl (20 mL) with stirring for 5 minutes, and then diluted with Et<sub>2</sub>O (20 mL). The phases were separated, and the aqueous component was extracted with Et<sub>2</sub>O (2x 20 mL). The organics were washed with saturated aqueous NaHCO<sub>3</sub> (20 mL) and brine, dried over anhydrous MgSO<sub>4</sub>, and concentrated under reduced pressure. The crude product was purified by flash column chromatography over silica gel. Elution with 5-7% v/v EtOAc in pentane afforded 217 mg of cyclobutanol **2.36** as a white solid (81% yield).



<sup>1</sup>H NMR (500 MHz, CDCl<sub>3</sub>)

δ 5.38 (qd, J = 6.7, 3.8 Hz, 1H)	1.43 – 1.30 (m, 2H)
3.60 (d, J = 11.6 Hz, 1H)	1.27 – 1.19 (m, 5H)
3.54 (d, J = 11.5 Hz, 1H)	1.13 (td, J = 11.9, 9.3 Hz, 1H)
3.39 (ddd, J = 11.6, 5.8, 2.7 Hz, 2H)	1.08 (s, 3H)
2.40 – 2.15 (m, 5H)	0.90 (d, J = 7.3 Hz, 3H)
2.02 – 1.87 (m, 2H)	0.79 (d, J = 6.9 Hz, 3H)
1.71 – 1.63 (m, 2H)	0.70 (s, 3H)

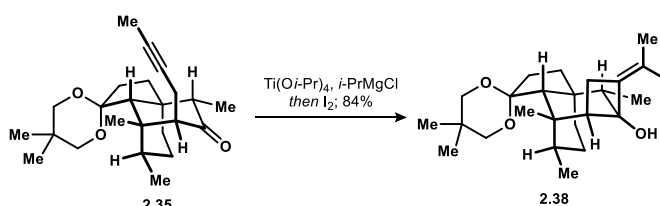
1.56 – 1.48 (m, 4H)

<sup>13</sup>C NMR (126 MHz, CDCl<sub>3</sub>)

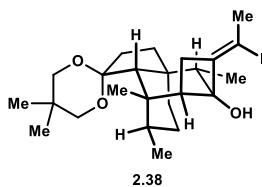
δ 148.4	50.0	24.6
112.1	43.7	23.8
111.4	37.1	23.5
78.4	36.9	22.7
72.8	33.5	21.3
71.3	30.1	16.0
60.2	29.9	13.0
50.1	27.8	8.8

TLC R<sub>f</sub> = 0.63 (20% v/v EtOAc in hexanes). Modestly UV active.

HRMS (CI+) calculated for C<sub>24</sub>H<sub>38</sub>O<sub>3</sub>H [M+H]: 375.2899, found: 375.2889



**Cyclobutanol 2.38.** A solution of (*i*-PrO)<sub>4</sub>Ti (30 μL, 0.10 mmol) in THF (0.8 mL) was cooled to -78 °C and treated dropwise with a solution of *i*-PrMgCl (0.10 mL of a 2.0 M solution in THF, 0.20 mmol). After 5 minutes, a solution of alkyne **2.35** (18.6 mg, 0.05 mmol) in THF (0.6 mL) was added dropwise to the yellow solution. After 30 minutes, the reaction was warmed to ambient temperature and the mixture soon developed a red-brown color. After 20 minutes, the reaction was treated with I<sub>2</sub> (76 mg, 0.30 mmol) and stirred for an additional 2 h. The mixture was partitioned between 1 N HCl (6 mL) and Et<sub>2</sub>O (6 mL), and the phases were separated. The aqueous component was extracted with Et<sub>2</sub>O (2x 6 mL). The organics were washed with saturated aqueous NaHCO<sub>3</sub>, 5% aqueous Na<sub>2</sub>S<sub>2</sub>O<sub>3</sub>, and brine, dried over anhydrous MgSO<sub>4</sub>, and concentrated under reduced pressure. The crude product was purified by flash column chromatography over silica gel. Elution with 5-7% v/v EtOAc in pentane afforded 21.1 mg of cyclobutanol **2.38** as a white solid (84% yield).



<sup>1</sup>H NMR (500 MHz, CDCl<sub>3</sub>)

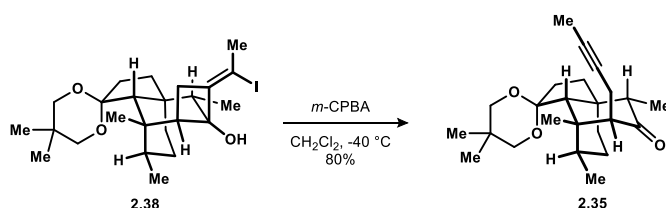
$\delta$ 3.60 (d, $J$ = 11.4 Hz, 1H)	1.80 (q, $J$ = 7.3 Hz, 1H)
3.54 (d, $J$ = 11.4 Hz, 1H)	1.59 – 1.53 (m, 2H)
3.42 – 3.35 (m, 2H)	1.37 (dd, $J$ = 12.0, 4.9 Hz, 2H)
2.77 (s, 1H)	1.24 – 1.19 (m, 7H)
2.56 – 2.36 (m, 3H)	1.15 (td, $J$ = 11.9, 9.4 Hz, 1H)
2.33 – 2.25 (m, 4H)	1.06 (s, 3H)
2.18 (dd, $J$ = 13.7, 9.2 Hz, 1H)	0.80 (d, $J$ = 6.9 Hz, 3H)
1.99 – 1.88 (m, 2H)	0.70 (s, 3H)

$^{13}\text{C}$  NMR (126 MHz,  $\text{CDCl}_3$ )

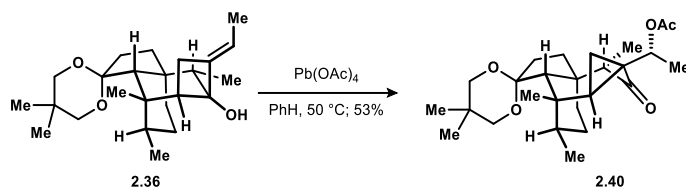
$\delta$ 148.1	44.1	24.8
111.9	37.2	23.8
79.4	36.8	22.7
72.8	33.6	21.0
71.3	30.0	15.9
59.2	28.7	12.2
49.6	28.5	
47.3	27.4	

TLC  $R_f$  = 0.49 (10% v/v EtOAc in hexanes). Not UV active.

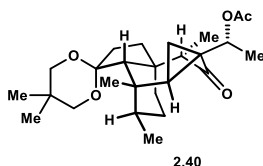
HRMS ( $\text{CI}^+$ ) calculated for  $\text{C}_{24}\text{H}_{37}\text{O}_3\text{I}$   $[\text{M}]^+$ : 500.1787, found: 500.1786



**Alkyne 2.35.** A solution of vinyl iodide **2.38** (1.2 mg, 2.4  $\mu\text{mol}$ ) in  $\text{CH}_2\text{Cl}_2$  (0.4 mL) was cooled to  $-40\text{ }^\circ\text{C}$  and treated with  $m\text{-CPBA}$  (2.0 mg of a 65 wt% suspension in  $m\text{-chlorobenzoic acid}$  and  $\text{H}_2\text{O}$ , 7.5  $\mu\text{mol}$ ). The reaction was maintained at the same temperature for 3 h, then treated with dimethylsulfide (10  $\mu\text{L}$ ). The mixture was partitioned between  $\text{H}_2\text{O}$  (6 mL) and  $\text{Et}_2\text{O}$  (6 mL), and the phases were separated. The aqueous portion was extracted with  $\text{Et}_2\text{O}$  (6 mL). The organics were washed with saturated aqueous  $\text{NaHCO}_3$ , 5% aqueous  $\text{Na}_2\text{S}_2\text{O}_3$ , and brine, dried over anhydrous  $\text{MgSO}_4$ , and concentrated under reduced pressure. The crude product was purified by flash column chromatography over silica gel. Elution with 18% v/v EtOAc in pentane afforded 0.7 mg of alkyne **2.35** as a white film (80% yield). Characterization data for **2.35** are presented above on page 101.



**Acetoxycyclopropane 2.40.** A solution of cyclobutanol **2.36** (10.0 mg, 27  $\mu$ mol) in PhH (0.8 mL) in a dry vial was treated  $\text{Pb}(\text{OAc})_4$  (36.0 mg, 80  $\mu$ mol). The vial was sealed and heated to 50  $^{\circ}\text{C}$  for 2 h. The reaction mixture was cooled to ambient temperature, diluted with  $\text{Et}_2\text{O}$  (10 mL), and washed with saturated aqueous  $\text{Na}_2\text{S}_2\text{O}_3$  (8 mL). The phases were separated, and the aqueous component was extracted with  $\text{Et}_2\text{O}$  (2x 6 mL). The organics were washed with saturated aqueous  $\text{NaHCO}_3$  (8 mL) and brine, dried over anhydrous  $\text{MgSO}_4$ , and concentrated under reduced pressure. The crude product was purified by flash column chromatography over silica gel. Elution with 15% v/v  $\text{EtOAc}$  in pentane afforded 6.1 mg of acetoxycyclopropane **2.40** as a white solid (53% yield).



$^1\text{H}$  NMR (600 MHz,  $\text{CDCl}_3$ )

$\delta$ 5.51 (q, $J = 6.1$ Hz, 1H)	1.33 – 1.28 (m, 1H)
3.67 (d, $J = 11.6$ Hz, 1H)	1.25 (s, 3H)
3.56 (d, $J = 11.6$ Hz, 1H)	1.23 – 1.17 (m, 2H)
3.46 – 3.39 (m, 2H)	1.15 (d, $J = 6.4$ Hz, 3H)
2.40 – 2.30 (m, 2H)	1.14 – 1.06 (m, 1H)
2.26 (ddd, $J = 14.1, 6.9, 4.5$ Hz, 1H)	1.01 (dd, $J = 9.8, 5.6$ Hz, 1H)
1.99 (s, 3H), 1.78 – 1.70 (m, 2H)	0.96 (d, $J = 6.6$ Hz, 3H)
1.60 (s, 3H)	0.89 (d, $J = 7.0$ Hz, 3H)
1.49 – 1.37 (m, 4H)	0.72 (s, 3H)

$^{13}\text{C}$  NMR (151 MHz,  $\text{CDCl}_3$ )

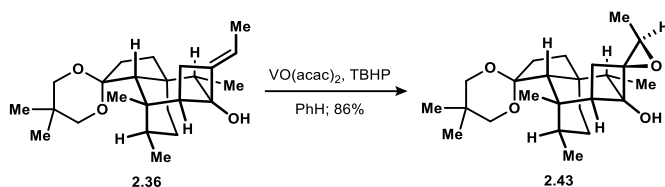
$\delta$ 211.2	37.6	24.6
170.3	36.6	23.0
112.3	35.4	21.4
72.5	34.5	17.3



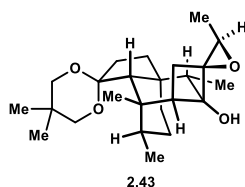
71.4	29.7	15.3
62.3	28.7	14.9
51.4	28.1	11.9
44.0	26.7	
41.6	24.6	

TLC  $R_f$  = 0.35 (20% v/v EtOAc in hexanes).

HRMS (ES+) calculated for  $C_{26}H_{40}O_5Na$  [M+Na]: 455.2773, found: 455.2774



**Epoxycyclobutanol 2.43.** A solution of cyclobutanol **2.36** (259 mg, 0.691 mmol) in PhH (6.9 mL) was treated with *t*-BuOOH (0.26 mL of a 5.5 M solution in decane, 1.43 mmol) and  $VO(acac)_2$  (37 mg, 0.14 mmol). After 1 h, TLC analysis indicated full consumption of starting material. The reaction mixture was loaded directly onto a silica gel column. Elution with 8-10% v/v EtOAc in hexanes afforded 232 mg of epoxycyclobutanol **2.43** as a white solid (86% yield).



$^1H$  NMR (600 MHz,  $CDCl_3$ )

$\delta$ 3.63 (d, $J$ = 11.5 Hz, 1H)	1.51 – 1.45 (m, 2H)
3.55 (d, $J$ = 11.6 Hz, 1H)	1.62 – 1.56 (m, 2H)
3.41 (ddd, $J$ = 11.7, 7.8, 2.7 Hz, 2H)	1.43 – 1.35 (m, 2H)
3.08 (q, $J$ = 5.3 Hz, 1H)	1.23 (s, 3H)
2.55 (t, $J$ = 10.5 Hz, 1H)	1.22 – 1.16 (m, 5H)
2.43 (s, 1H)	1.07 (s, 3H)
2.38 – 2.20 (m, 3H)	0.81 (d, $J$ = 6.9 Hz, 3H)
1.99 – 1.89 (m, 2H)	0.79 (d, $J$ = 7.2 Hz, 3H)
1.81 – 1.74 (m, 2H)	0.71 (s, 3H)

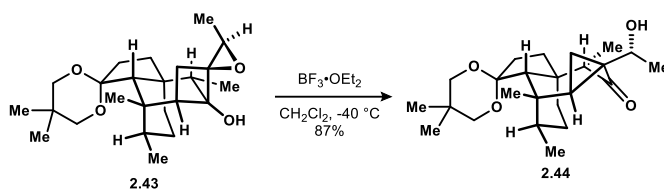
$^{13}C$  NMR (126 MHz,  $CDCl_3$ )

$\delta$ 111.9	49.1	24.9
75.0	44.1	23.8

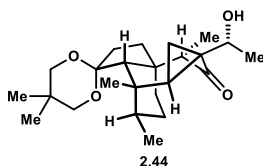
72.8	37.0	23.5
71.8	36.8	22.7
71.4	33.8	21.2
59.9	30.1	15.9
55.0	29.9	15.4
49.1	27.5	10.0

TLC  $R_f$  = 0.43 (20% v/v EtOAc in hexanes).

HRMS (ES+) calculated for  $C_{24}H_{38}O_4Na$  [M+Na]: 413.2668, found: 413.2660



**Hydroxycyclopropane 2.44.** A solution of epoxycyclobutanol **2.43** (232 mg, 0.594 mmol) in  $CH_2Cl_2$  (10 mL) was cooled to  $-40\text{ }^\circ C$  treated with  $BF_3 \cdot OEt_2$  (0.37 mL, 3 mmol). (**note: temperature control is essential to preserve the ketal**). After 4 h, the reaction was quenched under vigorous stirring by the addition of saturated aqueous  $NaHCO_3$  (10 mL). The mixture was further diluted with additional  $NaHCO_3$  (10 mL) and  $CH_2Cl_2$  (20 mL). The phases were separated, and the aqueous component was extracted with  $CH_2Cl_2$  (2x 20 mL). The combined organics were washed with brine, dried over  $MgSO_4$ , and concentrated under reduced pressure. The crude product was purified by flash column chromatography over silica gel. Elution with 16-20% v/v EtOAc in hexanes afforded 198 mg of hydroxycyclopropane **2.44** as a white solid (87% yield).



$^1H$  NMR (600 MHz,  $CDCl_3$ )

$\delta$ 3.74 – 3.65 (m, 2H)	1.45 – 1.39 (m, 1H)
3.55 (d, $J$ = 11.6 Hz, 1H)	1.34 – 1.29 (m, 2H)
3.42 (ddd, $J$ = 11.7, 5.6, 2.5 Hz, 2H)	1.25 (t, $J$ = 3.3 Hz, 7H)
3.18 (d, $J$ = 7.3 Hz, 1H)	1.21 (t, $J$ = 4.9 Hz, 1H)
2.36 (td, $J$ = 8.7, 4.5 Hz, 2H)	1.16 – 1.07 (m, 1H)
2.28 (ddd, $J$ = 12.7, 6.9, 4.2 Hz, 1H)	0.99 (dd, $J$ = 9.8, 5.7 Hz, 1H)

1.77 (d, J = 1.9 Hz, 1H)                      0.97 (d, J = 6.6 Hz, 3H)  
 1.73 (td, J = 13.3, 8.1 Hz, 1H)            0.94 (d, J = 7.0 Hz, 3H)  
 1.59 (s, 3H)                                    0.72 (s, 3H)

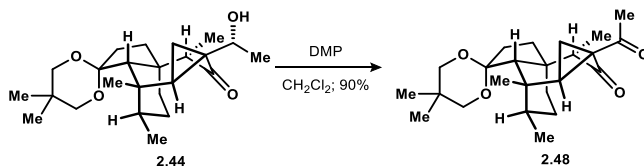
1.51 – 1.45 (m, 2H)

<sup>13</sup>C NMR (126 MHz, CDCl<sub>3</sub>)

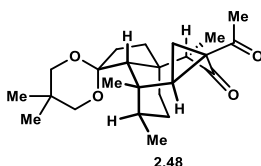
δ 215.6	37.5	24.8
112.2	36.8	24.5
72.5	35.4	23.0
71.4	34.9	19.5
62.2	29.7	17.8
52.0	28.7	15.5
44.0	28.2	11.7
43.3	26.6	

TLC R<sub>f</sub> = 0.63 (40% v/v EtOAc in hexanes).

HRMS (ES<sup>+</sup>) calculated for C<sub>24</sub>H<sub>38</sub>O<sub>4</sub>Na [M+Na]: 413.2668, found: 413.2679



**Cyclopropanedione 2.48.** A solution of hydroxycyclopropane **2.44** (5 mg, 12.8 μmol) in CH<sub>2</sub>Cl<sub>2</sub> (1.0 mL) was cooled to 0 °C treated with Dess-Martin periodinane (16.3 mg, 38.4 μmol). After 2 h, the reaction was diluted with saturated aqueous Na<sub>2</sub>S<sub>2</sub>O<sub>3</sub> (1 mL), H<sub>2</sub>O (5 mL) and CH<sub>2</sub>Cl<sub>2</sub> (5 mL). The phases were separated, and the aqueous component was extracted with CH<sub>2</sub>Cl<sub>2</sub> (2x 6 mL). The combined organics were washed with brine, dried over MgSO<sub>4</sub>, and concentrated under reduced pressure. The crude product was purified by flash column chromatography over silica gel. Elution with 15% v/v EtOAc in pentane afforded 4.5 mg of cyclopropanedione **2.48** as a colorless oil (90% yield).



<sup>1</sup>H NMR (600 MHz, CDCl<sub>3</sub>)

δ 3.67 (d, J = 11.7 Hz, 1H)                    1.54 – 1.41 (m, 3H)  
 3.56 (d, J = 11.7 Hz, 1H)                    1.37 – 1.31 (m, 1H)

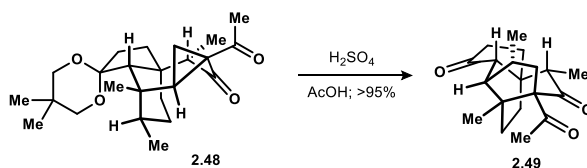
3.43 (ddd, J = 11.5, 4.3, 2.4 Hz, 2H)      1.29 – 1.24 (m, 5H)  
 2.42 – 2.33 (m, 5H)      1.09 (dd, J = 12.9, 4.6 Hz, 1H)  
 2.29 (ddd, J = 13.3, 6.7, 4.3 Hz, 1H)      1.01 (d, J = 6.6 Hz, 3H)  
 1.81 – 1.71 (m, 3H)      0.91 (d, J = 7.0 Hz, 3H)  
 1.66 (dd, J = 8.4, 5.2 Hz, 1H)      0.72 (s, 3H)  
 1.60 (s, 3H)

<sup>13</sup>C NMR (151 MHz, CDCl<sub>3</sub>)

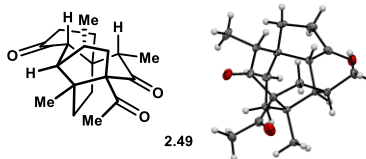
δ 210.4	44.1	28.6
204.8	38.9	26.3
112.2	37.9	24.6
72.6	36.7	24.6
71.4	35.4	23.0
61.8	30.1	18.1
52.0	29.7	15.8
50.8	28.7	11.6

TLC R<sub>f</sub> = 0.60 (30% v/v EtOAc in hexanes).

HRMS (ES<sup>+</sup>) calculated for C<sub>24</sub>H<sub>36</sub>O<sub>4</sub>Na [M+Na]: 411.2511, found: 411.2519



**Triketone 2.49.** A solution of cyclopropanedione **2.48** (4.5 mg, 11.6 μmol) in AcOH (0.4 mL) was cooled to 0 °C treated with concentrated H<sub>2</sub>SO<sub>4</sub> (8 μL, 0.15 mmol). The reaction was allowed to warm to ambient temperature and stirred for 12 h, at which point the reaction was diluted with H<sub>2</sub>O (5 mL) and Et<sub>2</sub>O (5 mL). The phases were separated, and the aqueous component was extracted with Et<sub>2</sub>O (2x 6 mL). The combined organics were washed with saturated aqueous NaHCO<sub>3</sub> (5 mL) and brine, dried over MgSO<sub>4</sub>, and concentrated under reduced pressure. The crude product was purified by flash column chromatography over silica gel. Elution with 20% v/v EtOAc in pentane afforded 3.7 mg of trione **2.49** as a white solid (>95% yield). Crystals suitable for x-ray diffraction analysis were grown by slow evaporation of a 2 mg sample of pure product from PhH.



$^1\text{H}$  NMR (600 MHz,  $\text{CDCl}_3$ )

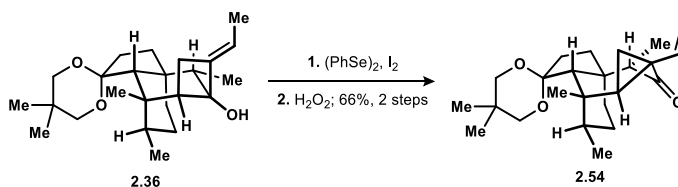
$\delta$ 3.13 (ddd, $J = 15.0, 8.7, 1.4$ Hz, 1H)	1.78 – 1.67 (m, 2H)
2.71 (qd, $J = 7.0, 1.9$ Hz, 1H)	1.62 – 1.56 (m, 1H)
2.62 – 2.52 (m, 1H)	1.31 – 1.26 (m, 1H)
2.43 (ddt, $J = 19.8, 10.1, 1.4$ Hz, 1H)	1.21 (d, $J = 7.0$ Hz, 3H)
2.27 – 2.17 (m, 2H)	1.07 (dd, $J = 14.9, 10.7$ Hz, 1H)
2.15 (s, 3H)	0.98 (d, $J = 6.7$ Hz, 3H)
2.13 – 2.07 (m, 2H)	0.94 (s, 3H)
1.93 (ddd, $J = 12.9, 9.2, 1.4$ Hz, 1H)	

$^{13}\text{C}$  NMR (151 MHz,  $\text{CDCl}_3$ )

$\delta$ 218.3	44.3	29.7
213.1	41.3	27.6
204.4	38.8	22.8
79.6	34.3	14.9
55.5	34.0	11.5
55.1	33.0	
50.2	30.1	

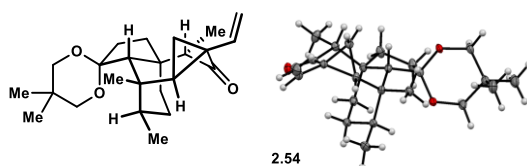
TLC  $R_f = 0.68$  (50% v/v EtOAc in hexanes).

HRMS (ES+) calculated for  $\text{C}_{19}\text{H}_{26}\text{O}_3\text{Na}$  [ $\text{M}+\text{Na}$ ]: 325.1780, found: 325.1782



**Vinylcyclopropane 2.54.** A solution of cyclobutanol **2.36** (50.0 mg, 0.133 mmol) in EtOH (2.5 mL) and  $\text{H}_2\text{O}$  (0.5 mL) was treated with diphenyl diselenide (125 mg, 0.400 mmol) and  $\text{I}_2$  (205 mg, 0.810 mmol). The mixture was stirred for 1 h, then diluted with  $\text{H}_2\text{O}$  (10 mL) and  $\text{Et}_2\text{O}$  (10 mL). The phases were separated, and the aqueous portion was extracted with  $\text{Et}_2\text{O}$  (2x 10 mL). The combined organics were washed with saturated aqueous  $\text{Na}_2\text{S}_2\text{O}_3$  (10 mL) and brine, dried over  $\text{MgSO}_4$ , and concentrated under reduced pressure. The crude product was purified by flash column chromatography over silica gel. Elution with 6-12% v/v EtOAc in pentane afforded

an intermediate alkyl selenide ( $R_f = 0.55$  in 20% v/v EtOAc in hexanes) that was immediately subjected to the next step. The selenide was dissolved in  $\text{CH}_2\text{Cl}_2$  (2 mL), stirred vigorously, and treated with  $\text{H}_2\text{O}_2$  (0.2 mL of a 35% aqueous solution). After 1 h, TLC analysis indicated full conversion. The reaction mixture was diluted with  $\text{H}_2\text{O}$  (8 mL), saturated aqueous  $\text{Na}_2\text{S}_2\text{O}_3$  (2 mL), and  $\text{CH}_2\text{Cl}_2$  (10 mL). The phases were separated, and the aqueous portion was extracted with  $\text{CH}_2\text{Cl}_2$  (2x 10 mL). The combined organics were washed with brine, dried over anhydrous  $\text{MgSO}_4$ , and concentrated under reduced pressure. The crude product was purified by flash column chromatography over silica gel. Elution with 10% v/v EtOAc in pentane afforded 32.5 mg of the vinylcyclopropane **2.54** as a white solid (66% over two steps). Crystals suitable for x-ray diffraction analysis were grown by slow evaporation of a 2 mg sample of pure product from PhH.



$^1\text{H}$  NMR (600 MHz,  $\text{CDCl}_3$ )

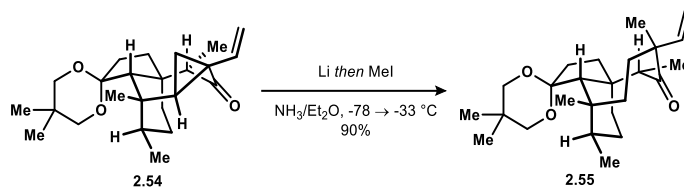
$\delta$ 6.84 (dd, $J = 17.5, 10.7$ Hz, 1H)	1.58 (s, 3H)
4.91 (d, $J = 10.7$ Hz, 1H)	1.49 (dd, $J = 12.6, 8.1$ Hz, 1H)
4.78 (d, $J = 17.4$ Hz, 1H)	1.45 – 1.40 (m, 1H)
3.68 (d, $J = 11.4$ Hz, 1H)	1.35 (d, $J = 7.6$ Hz, 1H)
3.56 (d, $J = 11.3$ Hz, 1H)	1.32 – 1.28 (m, 1H)
3.46 – 3.40 (m, 2H)	1.24 (d, $J = 12.5$ Hz, 6H)
2.42 – 2.32 (m, 2H)	1.04 – 0.97 (m, 4H)
2.25 (ddd, $J = 13.1, 6.9, 4.4$ Hz, 1H)	0.84 (d, $J = 6.9$ Hz, 3H)
1.80 (s, 1H)	0.72 (s, 3H)
1.78 – 1.68 (m, 2H)	

$^{13}\text{C}$  NMR (151 MHz,  $\text{CDCl}_3$ )

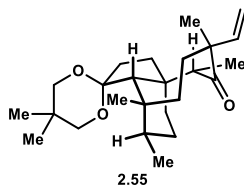
$\delta$ 211.3	44.0	28.7
139.4	43.6	26.4
112.3	41.1	24.6
109.6	38.1	24.5
72.5	36.6	23.0
71.4	35.5	18.8
62.0	29.7	16.1
51.1	28.7	12.0

TLC  $R_f = 0.57$  (20% v/v EtOAc in hexanes).

HRMS (ES+) calculated for C<sub>24</sub>H<sub>36</sub>O<sub>3</sub>Na [M+Na]: 395.2562, found: 325.2569



**Cyclooctanone 2.55.** Anhydrous ammonia (ca. 3 mL) was condensed into a flame-dried two-necked flask in a -78 °C cooling bath fitted with a condenser at -78 °C and a rubber septum. Under positive pressure of Ar, lithium wire (21 mg, 3.04 mmol) was added. A solution of vinylcyclopropane **2.54** (18 mg, 48 μmol) in Et<sub>2</sub>O (2 mL) was added dropwise with stirring to the dark blue Li-ammonia mixture. After 40 minutes, the reaction was treated with iodomethane (0.30 mL, 4.8 mmol). Following 30 minutes at the same temperature, the cooling bath was removed. The reaction was maintained at -33 °C for an additional 30 minutes, then the condenser was removed, allowing the ammonia to evaporate for 1 h. The mixture was diluted with ½-saturated aqueous NH<sub>4</sub>Cl (6 mL) and Et<sub>2</sub>O (6 mL). The phases were separated, and the aqueous portion was extracted with Et<sub>2</sub>O (2x 6 mL). The combined organics were washed with brine, dried over anhydrous MgSO<sub>4</sub>, and concentrated under reduced pressure. The crude product was purified by flash column chromatography over silica gel. Elution with 6-10% v/v EtOAc in pentane afforded 16.8 mg of the cyclooctanone **2.55** as a colorless oil (90% yield).



<sup>1</sup>H NMR (600 MHz, CDCl<sub>3</sub>)

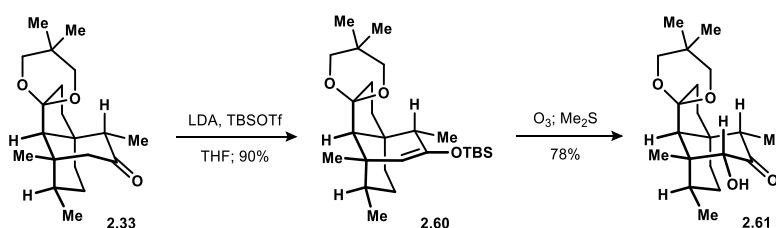
δ 6.25 (ddd, J = 17.7, 11.0, 0.7 Hz, 1H)	1.98 – 1.86 (m, 2H)
5.11 (dd, J = 11.0, 1.2 Hz, 1H)	1.75 – 1.60 (m, 2H)
4.99 (dd, J = 17.7, 1.3 Hz, 1H)	1.57 – 1.50 (m, 1H) – overlaps with H <sub>2</sub> O
3.70 (d, J = 11.6 Hz, 1H)	1.37 (s, 3H)
3.56 (d, J = 11.5 Hz, 1H)	1.30 (ddd, J = 13.2, 11.7, 7.6 Hz, 3H)
3.46 – 3.37 (m, 2H)	1.22 (s, 3H)
2.80 (q, J = 6.9 Hz, 1H)	1.21 – 1.15 (m, 6H)
2.45 (dd, J = 13.5, 7.5 Hz, 1H)	1.01 (d, J = 6.9 Hz, 3H)
2.14 (dt, J = 11.1, 5.9 Hz, 1H)	0.71 (s, 3H)
2.03 (s, 1H)	0.64 (d, J = 6.9 Hz, 3H)

<sup>13</sup>C NMR (151 MHz, CDCl<sub>3</sub>)

δ 219.4	46.9	26.2
142.0	38.24	24.5
113.1	36.4	24.3
112.2	34.4	23.2
72.4	32.3	22.9
71.6	29.7	15.6
63.1	28.1	15.0
56.3	28.1	
50.9	26.8	

TLC R<sub>f</sub> = 0.67 (20% v/v EtOAc in hexanes).

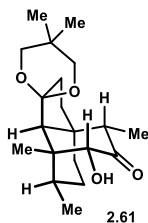
HRMS (ES<sup>+</sup>) calculated for C<sub>25</sub>H<sub>40</sub>O<sub>3</sub>Na [M+Na]: 411.2875, found: 411.2887



**Hydroxyketone 2.61.** A 0.5 M solution of LDA was prepared as follows: *i*-Pr<sub>2</sub>NH (0.154 mL, 1.1 mmol) in THF (1.44 mL) was cooled to -78 °C and treated dropwise with *n*-BuLi (0.41 mL of a 2.42 M solution in hexanes, 1.0 mmol). The mixture was warmed to 0 °C and stirred for 10 minutes before use. A solution of ketone **2.33** (20 mg, 0.062 mmol) in THF (0.8 mL) was cooled to -78 °C and treated dropwise with the freshly prepared LDA solution (0.25 mL of a 0.5 M solution, 0.125 mmol). After 30 minutes, TBSOTf (60 μL, 0.248 mmol) was added over 1 minute. The reaction was stirred for an additional 1 h at the same temperature, then slowly warmed to 0 °C for 30 minutes. The solution was stirred vigorously and treated with saturated aqueous NaHCO<sub>3</sub> (2 mL). The resulting emulsion was stirred for 30 minutes, then diluted with Et<sub>2</sub>O (6 mL) and H<sub>2</sub>O (4 mL). The phases were separated, and the aqueous portion was extracted with Et<sub>2</sub>O (2x 6 mL). The combined organics were washed with brine, dried over anhydrous MgSO<sub>4</sub>, and concentrated under reduced pressure. The crude residue was purified by flash column chromatography over silica gel. Elution with 1% Et<sub>3</sub>N, 3% v/v Et<sub>2</sub>O in hexanes afforded 24.2 mg of enoxysilane **2.60** (90% yield) as a white amorphous solid. R<sub>f</sub> = 0.44 (20% v/v EtOAc in hexanes).



A flask was charged with enoxysilane **2.60** (8.0 mg, 18  $\mu$ mol) and  $\text{CH}_2\text{Cl}_2$  (1.0 mL), then cooled to  $-78^\circ\text{C}$ . The mixture was ozonized until the light blue color became persistent, at which point ozonization was ceased. The reaction was maintained for 1 minute, then treated with dimethylsulfide (80  $\mu$ L). The mixture was warmed to ambient temperature, then concentrated under reduced pressure. The crude product was purified by flash column chromatography over silica gel. Elution with 20% v/v EtOAc in pentane afforded 4.7 mg of the hydroxyketone **2.61** as a white solid (78% yield).



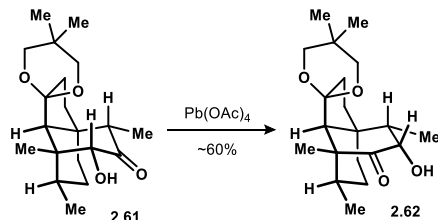
$^1\text{H}$  NMR (600 MHz,  $\text{CDCl}_3$ )

$\delta$ 5.60 (d, $J = 10.9$ Hz, 1H)	1.92 (ddd, $J = 13.3, 8.8, 2.3$ Hz, 1H)
3.74 (d, $J = 11.5$ Hz, 1H)	1.76 (s, 1H)
3.67 (d, $J = 11.5$ Hz, 1H)	1.49 – 1.37 (m, 3H)
3.60 – 3.54 (m, 2H)	1.35 (s, 3H)
3.50 (dd, $J = 11.5, 2.7$ Hz, 1H)	1.30 (s, 3H)
2.71 (q, $J = 6.7$ Hz, 1H)	1.12 (td, $J = 13.5, 5.2$ Hz, 1H)
2.24 (ddd, $J = 14.1, 9.9, 2.3$ Hz, 1H)	1.03 (d, $J = 6.7$ Hz, 3H)
2.11 (ddd, $J = 14.1, 10.2, 8.8$ Hz, 1H)	0.98 – 0.87 (m, 4H)
1.98 (ddd, $J = 13.4, 4.8, 1.9$ Hz, 1H)	0.77 (s, 3H)

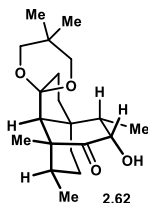
$^{13}\text{C}$  NMR (151 MHz,  $\text{CDCl}_3$ )

$\delta$ 213.4	45.0	29.3
109.8	43.3	23.9
74.3	41.5	22.5
72.9	35.4	20.1
71.9	34.5	15.6
64.5	30.0	8.1
47.8	29.5	

TLC  $R_f = 0.57$  (40% v/v EtOAc in hexanes). Not UV active.



**Hydroxyketone 2.62.** A vial was charged with hydroxyketone **2.61** (2.6 mg, 7.7  $\mu$ mol), PhH (0.6 mL) and MeOH (0.2 mL). The solution was treated with Pb(OAc)<sub>4</sub> (6.1 mg, 13.8  $\mu$ mol) and stirred at ambient temperature for 25 minutes. The mixture was partitioned between H<sub>2</sub>O (6 mL) and Et<sub>2</sub>O (6 mL) and the phases were separated. The aqueous portion was extracted with Et<sub>2</sub>O (2x 6 mL). The combined organics were washed with saturated aqueous Na<sub>2</sub>S<sub>2</sub>O<sub>3</sub> and brine, dried over anhydrous MgSO<sub>4</sub>, and concentrated under reduced pressure. The crude residue was purified by flash column chromatography over silica gel. Elution with 18% v/v EtOAc in pentane afforded 1.7 mg of hydroxyketone **2.62** as a white film in *ca.* 85% purity (*ca.* 60% yield).



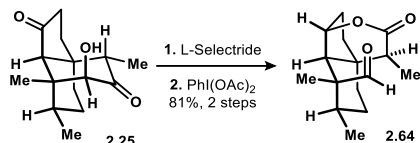
<sup>1</sup>H NMR (500 MHz, CDCl<sub>3</sub>)

$\delta$ 3.82 (s, 1H)	1.79 (s, 1H)
3.58 – 3.49 (m, 3H)	1.68 – 1.58 (m, 1H) – overlaps with H <sub>2</sub> O
3.41 (dd, J = 11.4, 2.6 Hz, 1H)	1.45 (s, 3H)
3.26 (dd, J = 11.5, 2.6 Hz, 1H)	1.32 – 1.19 (m, 7H)
2.13 (ddt, J = 14.0, 10.4, 6.0 Hz, 2H)	1.11 (d, J = 6.8 Hz, 3H)
2.04 – 1.93 (m, 2H)	0.76 (d, J = 6.8 Hz, 3H)
1.85 (ddd, J = 12.9, 9.0, 1.4 Hz, 1H)	0.67 (s, 3H)

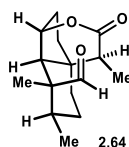
<sup>13</sup>C NMR (151 MHz, CDCl<sub>3</sub>)

$\delta$ 212.3	44.0	29.0
108.9	41.9	24.3
79.4	41.3	23.0
73.1	34.6	19.4
70.7	34.2	15.8
66.6	31.3	14.4
50.2	29.7	

TLC R<sub>f</sub> = 0.68 (40% v/v EtOAc in hexanes). Not UV active.



**Lactone 2.64.** A solution of hydroxydione **2.25** (15.0 mg, 60  $\mu\text{mol}$ ) in THF (0.8 mL) was cooled to  $-78^\circ\text{C}$  and treated dropwise with L-selectride (90  $\mu\text{L}$  of a 1.0 M solution in THF, 90  $\mu\text{mol}$ ). After 10 minutes, the reaction was quenched by the addition of  $\frac{1}{2}$ -saturated aqueous  $\text{NH}_4\text{Cl}$  (2 mL) under vigorous stirring. The mixture was warmed to ambient temperature and partitioned between  $\text{Et}_2\text{O}$  (6 mL) and  $\text{H}_2\text{O}$  (4 mL). The phases were separated, and the aqueous portion was extracted with  $\text{Et}_2\text{O}$  (2x 6 mL). The combined organics were washed with brine, dried over anhydrous  $\text{MgSO}_4$ , and concentrated under reduced pressure. The crude residue was taken up in  $\text{CH}_2\text{Cl}_2$  (0.4 mL) and  $\text{MeOH}$  (0.8 mL) and treated with  $\text{PhI(OAc)}_2$  (29.0 mg, 90  $\mu\text{mol}$ ). The reaction was stirred at ambient temperature for 8 h, then partitioned between 5% aqueous  $\text{Na}_2\text{S}_2\text{O}_3$  (6 mL) and  $\text{Et}_2\text{O}$  (6 mL). The phases were separated, and the aqueous portion was extracted with  $\text{Et}_2\text{O}$  (2x 6 mL). The combined organics were washed with brine, dried over anhydrous  $\text{MgSO}_4$ , and concentrated under reduced pressure. The crude product was purified by flash column chromatography over silica gel. Elution with 12% v/v  $\text{EtOAc}$  in pentane afforded 12.2 mg of lactone **2.64** as a white solid (81% yield).



$^1\text{H NMR}$  (600 MHz,  $\text{CDCl}_3$ )

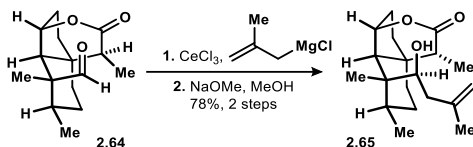
$\delta$ 9.68 (d, $J = 1.3$ Hz, 1H)	1.61 (dtd, $J = 14.7, 4.3, 2.7$ Hz, 2H)
4.93 (dd, $J = 5.9, 2.6$ Hz, 1H)	1.48 – 1.39 (m, 6H)
2.67 – 2.59 (m, 1H)	1.36 (d, $J = 2.6$ Hz, 1H)
2.29 – 2.20 (m, 2H)	1.32 (s, 3H)
2.02 – 1.89 (m, 2H)	0.99 (d, $J = 7.0$ Hz, 3H)
1.84 (ddd, $J = 10.9, 8.8, 1.8$ Hz, 1H)	

$^{13}\text{C NMR}$  (151 MHz,  $\text{CDCl}_3$ )

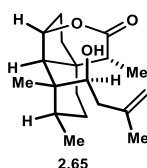
$\delta$ 204.8	45.5	30.3
174.1	42.6	21.3
60.1	41.6	15.8
50.8	34.2	13.9
46.0	31.5	

TLC  $R_f = 0.37$  (40% v/v  $\text{EtOAc}$  in hexanes). Not UV active.

HRMS (ES+) calculated for C<sub>15</sub>H<sub>20</sub>O<sub>3</sub>Na [M+Na]: 273.1467, found: 23.1465



**Homoallylic alcohol 2.65.** A dry Schlenk tube was charged with CeCl<sub>3</sub> (50.0 mg, 0.20 mmol) and THF (0.8 mL). The suspension was sonicated for 30 minutes, then cooled to 0 °C and treated dropwise with methallylmagnesium chloride (0.82 mL of a 0.245 M solution in THF, 0.20 mmol). The yellow suspension was stirred for an additional 1.5 h, then treated with a solution of lactone **2.64** (11.5 mg, 46 μmol) in THF (0.6 mL). After 2 h, the reaction mixture was treated with ½-saturated aqueous NH<sub>4</sub>Cl (2 mL). The mixture was partitioned between H<sub>2</sub>O (4 mL) and Et<sub>2</sub>O (6 mL). The phases were separated, and the aqueous portion was extracted with Et<sub>2</sub>O (2x 6 mL). The combined organics were washed with brine, dried over anhydrous MgSO<sub>4</sub>, and concentrated under reduced pressure. The crude residue was taken up in MeOH (0.5 mL) and treated with NaOMe (8 mg, 0.148 mmol). After 2 h, the reaction was diluted with ½-saturated aqueous NH<sub>4</sub>Cl (6 mL) and Et<sub>2</sub>O (6 mL). The phases were separated, and the aqueous portion was extracted with Et<sub>2</sub>O (2x 6 mL). The combined organics were washed with brine, dried over anhydrous MgSO<sub>4</sub>, and concentrated under reduced pressure. The crude product was purified by flash column chromatography over silica gel. Elution with 15% v/v EtOAc in pentane afforded 11.0 mg of homoallylic alcohol **2.65** as a white solid (78% yield).



<sup>1</sup>H NMR (600 MHz, CDCl<sub>3</sub>)

δ 4.94 (dd, J = 2.2, 1.4 Hz, 1H)

4.88 (dq, J = 2.0, 0.9 Hz, 1H)

4.78 (dd, J = 4.9, 1.9 Hz, 1H)

3.70 – 3.58 (m, 2H)

2.70 – 2.60 (m, 1H)

2.14 – 2.06 (m, 2H)

2.03 – 1.85 (m, 5H)

<sup>13</sup>C NMR (151 MHz, CDCl<sub>3</sub>)

δ 176.3

43.3

29.8

1.72 (s, 3H)

1.36 – 1.30 (m, 2H)

1.29 (s, 1H)

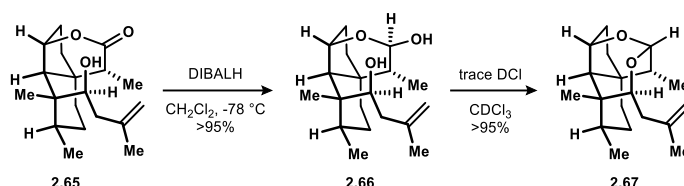
1.19 – 1.11 (m, 5H)

1.05 (d, J = 6.9 Hz, 3H)

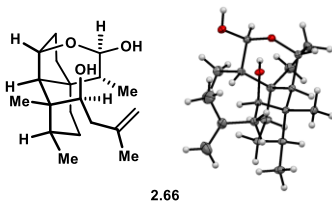
1.02 (s, 3H)

142.8	42.8	28.7
115.7	40.2	22.3
78.0	39.7	16.0
68.7	35.6	12.1
57.3	32.7	
46.6	32.3	

TLC  $R_f$  = 0.58 (30% v/v EtOAc in hexanes). Not UV active.



**Lactol 2.66.** A solution of lactone **2.65** (3.5 mg, 11.4  $\mu\text{mol}$ ) in  $\text{CH}_2\text{Cl}_2$  (1.2 mL) was cooled to  $-78^\circ\text{C}$  and treated dropwise with DIBAL-H (0.45 mL of a 0.1 M solution in  $\text{CH}_2\text{Cl}_2$ , 45  $\mu\text{L}$ ). The reaction was maintained at the same temperature for 1 h, then stirred vigorously and treated with saturated aqueous Rochelle's salt (2 mL). The emulsion was warmed to ambient temperature and stirred vigorously for 3 h, then diluted with  $\text{H}_2\text{O}$  (4 mL) and  $\text{CH}_2\text{Cl}_2$  (4 mL). The phases were separated, and the aqueous portion was extracted with  $\text{CH}_2\text{Cl}_2$  (2x 6 mL). The combined organics were washed with brine, dried over anhydrous  $\text{Na}_2\text{SO}_4$ , and concentrated under reduced pressure. The crude product was purified by flash column chromatography over silica gel. Elution with 25% v/v EtOAc in pentane afforded 3.5 mg of lactol **2.66** as a white solid (quantitative). Crystals suited for X-ray diffraction analysis were grown by slow evaporation of 3 mg of lactol **2.66** from PhH. Dissolving the lactol **2.66** in unpurified  $\text{CDCl}_3$  led to facile dehydration, forming the hemiacetal **2.67** quantitatively.



$^1\text{H NMR}$  (600 MHz,  $\text{C}_6\text{D}_6$ )

$\delta$  5.08 (dd,  $J = 2.4, 1.3$  Hz, 1H)

5.00 – 4.93 (m, 2H)

4.36 – 4.28 (m, 3H)

2.83 (d,  $J = 5.7$  Hz, 1H)

2.60 (dd,  $J = 13.6, 10.0$  Hz, 1H)

1.64 – 1.51 (m, 3H)

1.34 (dddd,  $J = 15.7, 8.1, 5.6, 3.5$  Hz, 2H)

1.15 – 1.06 (m, 2H)

1.05 (s, 3H)

1.02 (d,  $J = 7.0$  Hz, 3H)

2.45 (d,  $J = 13.6$  Hz, 1H) 0.85 – 0.77 (m, 4H)

2.30 (dq,  $J = 8.4, 6.6, 1.7$  Hz, 1H) 0.74 – 0.68 (m, 2H)

1.94 – 1.88 (m, 4H)

$^{13}\text{C}$  NMR (151 MHz,  $\text{C}_6\text{D}_6$ )

$\delta$  145.4 45.5 28.7

112.2 43.9 23.3

96.4 42.7 23.2

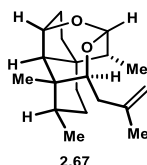
74.7 38.8 18.7

70.6 36.2 11.0

60.8 32.1

45.8 29.7

TLC  $R_f = 0.48$  (40% v/v EtOAc in hexanes). Not UV active.



$^1\text{H}$  NMR (600 MHz,  $\text{CDCl}_3$ )

$\delta$  4.82 – 4.75 (m, 2H) 1.85 – 1.76 (m, 4H)

4.62 (s, 1H) 1.66 – 1.61 (m, 2H)

4.40 (q,  $J = 2.0$  Hz, 1H) 1.48 (dddd,  $J = 14.8, 5.6, 3.7, 1.9$  Hz, 1H)

4.12 (dd,  $J = 6.7, 4.9$  Hz, 1H) 1.36 – 1.27 (m, 2H)

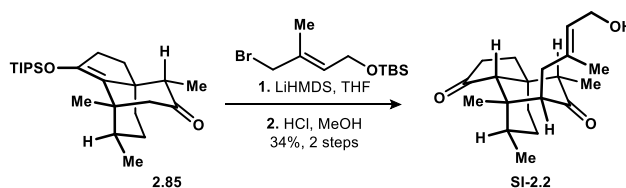
2.39 (q,  $J = 7.3$  Hz, 1H) 1.13 – 1.08 (m, 4H)

2.20 (d,  $J = 6.0$  Hz, 2H) 0.95 (d,  $J = 7.2$  Hz, 3H)

2.02 – 1.96 (m, 1H) 0.93 (d,  $J = 7.1$  Hz, 3H)

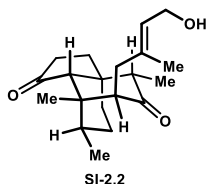
1.93 (ddd,  $J = 13.4, 5.1, 1.9$  Hz, 1H)

TLC  $R_f = 0.38$  (10% v/v EtOAc in hexanes). Not UV active.



**Ketone SI-2.2.** A 0.5 M solution of LiHMDS was prepared: HMDS (0.23 mL, 1.1 mmol) in THF (1.36 mL) was cooled to 0 °C and treated dropwise with *n*-BuLi (0.41 mL of a 2.44 M solution in hexanes, 1.0 mmol). The mixture was maintained at the same temperature for 10 minutes

before use. A separate, flame-dried flask was charged with ketone **2.85** (18 mg, 46  $\mu\text{mol}$ , see page 127 for preparation) and THF (1.0 mL). The solution was cooled to  $-78\text{ }^{\circ}\text{C}$  and treated with the LiHMDS solution (0.18 mL of a 0.5 M solution in THF / hexanes, 92  $\mu\text{mol}$ ). After 30 minutes at the same temperature, (*E*)-((4-bromo-3-methylbut-2-en-1-yl)oxy)(*tert*-butyl)dimethylsilane (36 mg, 0.129 mmol, prepared according to the known procedure<sup>89</sup>) was added dropwise. The reaction was stirred for 1 h at  $-78\text{ }^{\circ}\text{C}$  and 4 h at ambient temperature, then quenched by the addition of  $\frac{1}{2}$ -saturated aqueous  $\text{NH}_4\text{Cl}$  (2 mL). The mixture was partitioned between  $\text{Et}_2\text{O}$  (6 mL) and  $\text{H}_2\text{O}$  (4 mL). The phases were separated, and the aqueous portion was extracted with  $\text{Et}_2\text{O}$  (2x 6 mL). The combined organics were washed with brine, dried over anhydrous  $\text{MgSO}_4$ , and concentrated under reduced pressure. The crude product was taken up in anhydrous  $\text{MeOH}$  (1.0 mL), cooled to  $0\text{ }^{\circ}\text{C}$ , and treated with concentrated  $\text{HCl}$  (ca. 10  $\mu\text{L}$ ). The reaction was monitored by TLC, hydrolysis of the *tert*-butyldimethylsilyl ether was evident within minutes. Once TLC analysis indicated complete hydrolysis (ca. 1 h), solid  $\text{NaHCO}_3$  was added to the mixture with stirring. Following dilution with  $\text{EtOAc}$  (2 mL), anhydrous  $\text{MgSO}_4$  was added, and the mixture was filtered over celite. The flask and filter cake were washed thoroughly with  $\text{EtOAc}$ . The organics were concentrated, and the resulting crude product was purified by flash column chromatography over silica gel. Elution with 50% v/v  $\text{EtOAc}$  in pentane afforded 5.0 mg of the hydroxydione **SI-2.2** as a colorless oil (34%, 2 steps).



$^1\text{H}$  NMR (600 MHz,  $\text{CDCl}_3$ )

$\delta$ 5.28 (tt, $J = 7.0, 1.5$ Hz, 1H)	1.73 – 1.67 (m, 5H)
4.15 – 4.01 (m, 2H)	1.61 – 1.56 (m, 1H)
2.56 (dd, $J = 11.9, 5.2$ Hz, 1H)	1.33 – 1.28 (m, 2H)
2.46 (s, 1H)	1.27 (s, 3H)
2.42 – 2.28 (m, 5H)	1.16 – 1.06 (m, 2H)
2.06 (dd, $J = 13.2, 11.9$ Hz, 1H)	1.02 (d, $J = 6.7$ Hz, 3H)
1.83 (ddd, $J = 12.7, 9.1, 1.9$ Hz, 1H)	0.85 (d, $J = 6.9$ Hz, 3H)

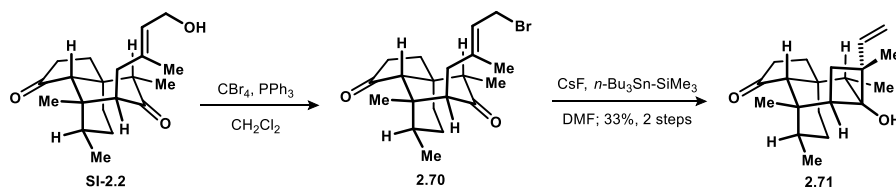
$^{13}\text{C}$  NMR (151 MHz,  $\text{CDCl}_3$ )

$\delta$ 215.6	51.9	27.9
214.4	46.2	26.8
137.1	40.0	22.5

126.3	39.3	15.8
59.8	37.5	15.0
59.2	36.1	8.2
52.7	32.3	

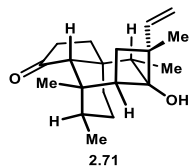
TLC  $R_f$  = 0.40 (70% v/v EtOAc in hexanes). Not UV active.

HRMS (ES+) calculated for  $C_{20}H_{30}O_3Na$  [M+Na]: 341.2093, found: 341.2094



**Cyclobutanol 2.71.** A solution of allylic alcohol **SI-2.2** (5.0 mg, 16  $\mu$ mol) in  $CH_2Cl_2$  (0.8 mL) was treated with  $Ph_3P$  (6.2 mg, 24  $\mu$ mol) and  $CBr_4$  (7.8 mg, 24  $\mu$ mol). After 12 h, TLC analysis indicated incomplete conversion. Additional portions of  $Ph_3P$  (6.2 mg, 24  $\mu$ mol) and  $CBr_4$  (7.8 mg, 24  $\mu$ mol) were added. After 6 h, the reaction was diluted with pentane (2 mL). The insoluble material was removed by filtration over celite, and the flask and filter cake were washed thoroughly with pentane (12 mL total). The combined organics were concentrated, then purified by flash column chromatography over silica gel. Elution with 8% v/v EtOAc in pentane afforded 4.6 mg of the allylic bromide **2.70** in moderate purity. A flame-dried flask was charged with allylic bromide **2.70** (4.6 mg, ca. 12  $\mu$ mol) and  $CsF$  (3.6 mg, 24  $\mu$ mol). DMF (0.6 mL) was added, and the mixture was cooled to 0  $^{\circ}C$ . A solution of  $n-Bu_3SnSiMe_3$  (8.7 mg, 24  $\mu$ mol, prepared according to the known procedure<sup>90</sup>) in THF (0.1 mL) was added by syringe pump over 30 minutes. The reaction was stirred for an additional 30 minutes, then diluted with  $H_2O$  (6 mL) and  $Et_2O$  (6 mL). The phases were separated, and the aqueous portion were extracted with  $Et_2O$  (2x 6 mL). The combined organics were washed with brine, dried over anhydrous  $MgSO_4$ , and concentrated under reduced pressure. The crude product was purified by flash column chromatography over silica gel. Elution with 7% v/v EtOAc in pentane afforded the cyclobutanol **2.71** in moderate purity. A second purification by preparative thin-layer chromatography (15% v/v EtOAc in pentane) afforded 1.6 mg of the cyclobutanol **2.71** as a colorless oil (33% yield over two steps).





<sup>1</sup>H NMR (600 MHz, CDCl<sub>3</sub>)

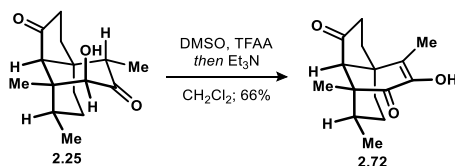
δ 5.94 (dd, J = 17.3, 10.6 Hz, 1H)	1.68 (s, 1H)
5.05 (dd, J = 10.6, 1.5 Hz, 1H)	1.65 – 1.57 (m, 3H)
4.93 (dd, J = 17.2, 1.5 Hz, 1H)	1.36 (ddd, J = 11.3, 9.6, 2.5 Hz, 2H)
2.33 – 2.29 (m, 1H)	1.23 – 1.19 (m, 4H)
2.26 – 2.18 (m, 2H)	1.06 – 1.00 (m, 4H)
2.01 – 1.89 (m, 2H)	0.85 (d, J = 7.2 Hz, 4H)
1.81 (s, 1H)	0.81 (d, J = 6.8 Hz, 3H)
1.72 – 1.69 (m, 1H)	

<sup>13</sup>C NMR (151 MHz, CDCl<sub>3</sub>)

δ 219.1	45.3	25.4
143.2	43.1	25.0
113.3	36.5	22.3
78.2	36.1	20.4
62.1	34.6	15.6
46.8	32.9	9.0
45.9	27.9	

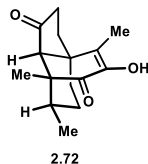
TLC R<sub>f</sub> = 0.55 (20% v/v EtOAc in hexanes). Not UV active.

HRMS (CI<sup>+</sup>) calculated for C<sub>20</sub>H<sub>30</sub>O<sub>2</sub>NH<sub>4</sub> [M+NH<sub>4</sub>]: 320.2589, found: 320.2576



**Triketone 2.72.** A solution of DMSO (50 μL, 0.70 mmol) in CH<sub>2</sub>Cl<sub>2</sub> (1.0 mL) was cooled to -78 °C and treated with trifluoroacetic anhydride (70 μL, 0.50 mmol). After 15 minutes at the same temperature, hydroxyketone **2.25** (24.0 mg, 0.096 mmol) was added as a solution in CH<sub>2</sub>Cl<sub>2</sub> (1.0 mL). The reaction was stirred for 1 h, treated with Et<sub>3</sub>N (0.14 mL, 1.0 mmol), then warmed to ambient temperature. After 30 minutes, The mixture was diluted with saturated aqueous NaHCO<sub>3</sub> (8 mL) and CH<sub>2</sub>Cl<sub>2</sub> (8 mL). The phases were separated, and the aqueous portion was extracted with CH<sub>2</sub>Cl<sub>2</sub> (2x 6 mL). The combined organics were washed with brine, dried over

MgSO<sub>4</sub>, and concentrated under reduced pressure. The crude product was taken up in PhH (1 mL) and allowed to stand over SiO<sub>2</sub> (ca. 100 mg) for 20 minutes, then purified by flash column chromatography over silica gel. Elution with 12% v/v EtOAc in pentane afforded 15.6 mg of triketone **2.72** as a white solid (66% yield).



<sup>1</sup>H NMR (600 MHz, CDCl<sub>3</sub>)

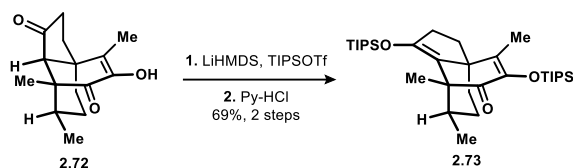
δ 6.31 (s, 1H)	1.55 – 1.47 (m, 4H)
2.35 – 2.24 (m, 2H)	1.40 (dtd, J = 13.3, 6.8, 4.6 Hz, 1H)
2.01 – 1.88 (m, 3H)	1.16 (dtd, J = 14.4, 12.8, 4.7 Hz, 1H)
1.80 (s, 3H)	0.81 (d, J = 6.7 Hz, 3H)
1.63 – 1.58 (m, 2H)	

<sup>13</sup>C NMR (151 MHz, CDCl<sub>3</sub>)

δ 214.5	46.9	30.3
194.5	45.7	29.3
148.0	40.9	18.0
126.0	35.786	15.1
63.4	32.8	11.6

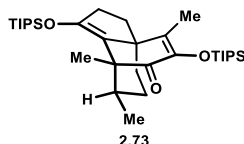
TLC R<sub>f</sub> = 0.48 (30% v/v EtOAc in hexanes). UV active. Does not stain well in *p*-anisaldehyde or KMnO<sub>4</sub>

HRMS (ES<sup>+</sup>) calculated for C<sub>15</sub>H<sub>20</sub>O<sub>3</sub>Na [M+Na]: 271.1310, found: 271.1308



**Enoxysilane 2.73.** A flame-dried flask was charged with HMDS (45 μL, 0.22 mmol) and THF (0.5 mL) and cooled to 0 °C. *n*-BuLi (0.13 mL of a 1.57 M solution, 0.20 mmol) was added dropwise. After 10 minutes, the solution was cooled to -78 °C and treated dropwise with a solution of triketone **2.72** (12.2 mg, 49 μmol) in THF (0.5 mL). The reaction was maintained for 30 minutes, then treated with TIPSOTf (40 μL, 0.15 mmol) and warmed to 0 °C. The reaction was stirred for 4 h, then quenched with vigorous stirring by the rapid addition of saturated aqueous NaHCO<sub>3</sub> (2 mL). The stirring was maintained for 30 minutes, then the mixture was

diluted with additional saturated aqueous NaHCO<sub>3</sub> (5 mL) and Et<sub>2</sub>O (7 mL). The phases were separated, and the aqueous portion was extracted with Et<sub>2</sub>O (2x 5 mL). The combined organics were washed with brine, dried over anhydrous MgSO<sub>4</sub>, and concentrated under reduced pressure. The crude product was taken up in CH<sub>2</sub>Cl<sub>2</sub> (1 mL), and treated with pyridinium hydrochloride (50 mg, 0.43 mmol). After 30 minutes, the mixture was concentrated, and the crude product was loaded onto a silica gel column with pentane. Elution with 1.5% v/v Et<sub>2</sub>O in pentane afforded 18.9 mg of the enoxysilane **2.73** as a white solid (69% yield).



<sup>1</sup>H NMR (600 MHz, CDCl<sub>3</sub>)

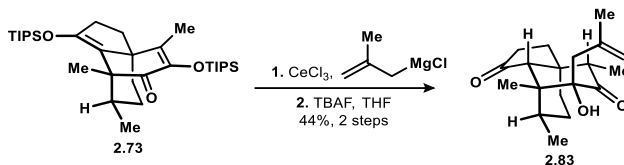
δ 2.51 (dt, J = 15.1, 8.9 Hz, 1H)	1.53 – 1.45 (m, 6H)
2.34 – 2.23 (m, 1H)	1.30 – 1.25 (m, 3H)
1.83 (ddd, J = 12.7, 10.2, 8.9 Hz, 1H)	1.15 – 1.09 (m, 4H)
1.79 (s, 3H)	1.07 – 1.02 (m, 36H)
1.68 (ddd, J = 12.7, 8.9, 2.2 Hz, 1H)	0.78 (d, J = 6.6 Hz, 3H)
1.60 – 1.56 (m, 1H)	

<sup>13</sup>C NMR (151 MHz, CDCl<sub>3</sub>)

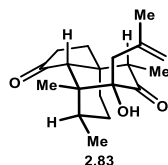
δ 195.1	41.4	18.2
147.1	33.4	18.2
142.5	32.4	16.1
139.7	30.4	14.4
119.2	30.0	13.5
63.5	18.8	12.3
51.1	18.5	12.2
49.6	18.5	

TLC R<sub>f</sub> = 0.62 (3% v/v Et<sub>2</sub>O in hexanes). UV active. Does not stain well in *p*-anisaldehyde or KMnO<sub>4</sub>

HRMS (ES<sup>+</sup>) calculated for C<sub>33</sub>H<sub>60</sub>O<sub>3</sub>Si<sub>2</sub>Na [M+Na]: 583.3979, found: 583.3976



**Diketone 2.83.**  $\text{CeCl}_3$  (63 mg, 0.255 mmol) was heated under vacuum until it became a free-flowing powder. After cooling to ambient temperature, THF (0.5 mL) was added with stirring. The suspension was sonicated for 20 minutes, then cooled to 0 °C and treated dropwise with a solution of methallylmagnesium chloride (0.94 mL of a 0.245 M solution in THF, 0.230 mmol). The reaction was maintained at the same temperature for 1 h, at which point a solution of ketone **2.73** (13.0 mg, 0.023 mmol) in THF (0.6 mL) was added dropwise. The resulting suspension was stirred for 1.5 h, then quenched by the addition of saturated aqueous  $\text{NaHCO}_3$  (2 mL). The mixture was diluted with  $\text{Et}_2\text{O}$  (6 mL) and  $\text{H}_2\text{O}$  (6 mL) and the phases were separated. The aqueous portion was extracted with  $\text{Et}_2\text{O}$  (2x 6 mL). The combined organics were washed with brine, dried over anhydrous  $\text{MgSO}_4$ , and concentrated under reduced pressure. The crude residue was taken up in THF (1.0 mL), cooled to 0 °C, and treated with TBAF (0.1 mL of a 1.0 M solution in THF, 0.100 mmol). After 30 minutes, the reaction was quenched by the addition of 1 N HCl (2 mL), then partitioned between  $\text{Et}_2\text{O}$  (6 mL) and 1 N HCl (4 mL). The phases were separated, and the aqueous portion was extracted with  $\text{Et}_2\text{O}$  (2x 6 mL). The combined organics were washed with brine, dried over anhydrous  $\text{MgSO}_4$ , and concentrated under reduced pressure. The crude product was purified by flash column chromatography over silica gel. Elution with 12% v/v EtOAc in pentane afforded the product diketone **2.83** in moderate purity. Subsequent purification by preparative thin-layer chromatography (20% EtOAc in pentane) afforded 3.1 mg of the diketone **2.83** as a colorless oil (44% yield)



$^1\text{H NMR}$  (600 MHz,  $\text{CDCl}_3$ )

$\delta$ 4.80 (p, $J = 1.6$ Hz, 1H)	1.74 – 1.65 (m, 3H)
4.60 (s, 1H)	1.65 (s, 3H)
3.78 (s, 1H)	1.47 (s, 3H)
2.62 (q, $J = 6.7$ Hz, 1H)	1.29 (dddd, $J = 15.1, 5.8, 4.0, 1.9$ Hz, 1H)
2.52 (d, $J = 13.2$ Hz, 1H)	1.21 – 1.14 (m, 1H)
2.48 (t, $J = 1.8$ Hz, 1H)	1.13 (d, $J = 6.6$ Hz, 3H)

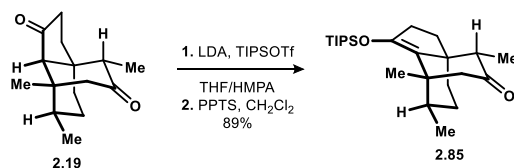
2.43 – 2.36 (m, 2H) 1.07 (d, J = 7.1 Hz, 3H)  
 2.35 – 2.26 (m, 1H) 1.06 – 0.98 (m, 1H)  
 1.86 (ddd, J = 12.6, 9.0, 1.8 Hz, 1H)

<sup>13</sup>C NMR (151 MHz, CDCl<sub>3</sub>)

215.5	47.0	27.4
214.5	46.0	24.1
140.9	45.3	19.2
115.8	39.2	18.2
84.8	36.0	8.2
62.3	32.3	
52.5	27.9	

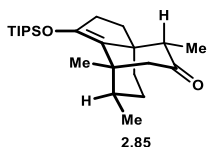
TLC R<sub>f</sub> = 0.68 (30% v/v EtOAc in hexanes). Not UV active.

HRMS (ES<sup>+</sup>) calculated for C<sub>19</sub>H<sub>28</sub>O<sub>3</sub>Na [M+Na]: 327.1936, found: 327.1922



**Ketone 2.85.** A 0.5 M solution of LDA was prepared as follows: *i*-Pr<sub>2</sub>NH (1.08 mL, 7.7 mmol) in THF (10.1 mL) was cooled to -78 °C and treated dropwise with *n*-BuLi (2.85 mL of a 2.46 M solution in hexanes, 7.0 mmol). The mixture was warmed to 0 °C and stirred for 10 minutes before use. A solution of diketone **2.19** (761 mg, 3.25 mmol) in THF (33 mL) was cooled to -78 °C and treated dropwise with the freshly prepared LDA solution (7.0 mL of a 0.5 M solution, 3.50 mmol). After 30 minutes, HMPA (1.24 mL, 7.15 mmol) was added over 1 minute. Following dissolution of the frozen HMPA (ca. 5 minutes), TIPSOTf (0.98 mL, 3.64 mmol) was added over 1 minute. The resulting slurry was stirred for an additional 1 h at the same temperature, then slowly warmed to 0 °C for 30 minutes. The resulting light-yellow solution was stirred vigorously and treated with saturated aqueous NaHCO<sub>3</sub> (30 mL). The resulting emulsion was stirred for 30 minutes, then diluted with Et<sub>2</sub>O (40 mL) and H<sub>2</sub>O (10 mL). The phases were separated, and the aqueous portion was extracted with Et<sub>2</sub>O (2x 40 mL). The combined organics were washed with brine, dried over anhydrous MgSO<sub>4</sub>, and concentrated under reduced pressure. The crude residue was taken up in CH<sub>2</sub>Cl<sub>2</sub> (22 mL) and treated with pyridinium *p*-toluenesulfonate (PPTS, 550 mg, 2.19 mmol). After 1.5 h, the mixture was concentrated and directly purified by flash

column chromatography over silica gel, loading with hexanes. Elution with 5% v/v Et<sub>2</sub>O in hexanes afforded 1.13 g of ketone **2.85** (89% yield) as a white amorphous solid.



<sup>1</sup>H NMR (500 MHz, CDCl<sub>3</sub>)

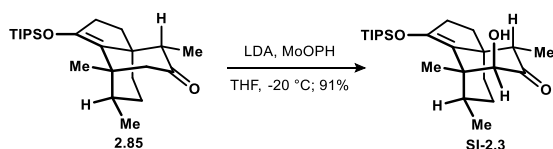
δ 2.54 – 2.40 (m, 3H)	1.35 – 1.24 (m, 1H)
2.14 (q, J = 7.1 Hz, 1H)	1.21 – 1.13 (m, 3H)
2.09 (d, J = 15.2 Hz, 1H)	1.14 – 1.08 (m, 18H)
1.82 (ddd, J = 13.2, 4.3, 2.3 Hz, 1H)	1.02 (d, J = 6.8 Hz, 3H)
1.70 (ddd, J = 13.1, 9.1, 7.3 Hz, 1H)	0.97 – 0.91 (m, 1H)
1.59 – 1.51 (m, 2H) – overlaps with H <sub>2</sub> O	0.82 (d, J = 6.8 Hz, 3H)
1.41 (m, 4H)	

<sup>13</sup>C NMR (126 MHz, CDCl<sub>3</sub>)

δ 214.7	42.6	24.9
143.1	40.7	18.3
121.9	35.1	15.3
54.8	33.5	13.6
51.5	33.3	8.9
48.6	30.4	

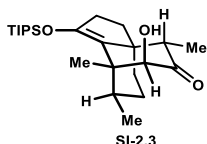
TLC R<sub>f</sub> = 0.41 (10% v/v Et<sub>2</sub>O in hexanes). Modestly UV active.

HRMS (CI<sup>+</sup>) calculated for C<sub>24</sub>H<sub>42</sub>O<sub>2</sub>Si [M<sup>+</sup>]: 390.2954, found: 390.2938



**Hydroxyketone SI-2.3.** A solution of *i*-Pr<sub>2</sub>NH (88 μL, 0.626 mmol) in THF (2 mL) was cooled to -78 °C and treated dropwise with *n*-BuLi (0.24 mL of a 2.42 M solution in hexanes, 0.587 mmol). The mixture was warmed to 0 °C for 10 minutes before cooling back to -78 °C. The LDA solution was treated with ketone **2.85** (153 mg, 0.391 mmol) in THF (2 mL). The reaction was maintained at the same temperature for 30 minutes, then warmed to -20 °C. Under positive pressure of N<sub>2</sub>, MoOPH (374 mg, 0.861 mmol, prepared according to the known method<sup>91</sup>) was added as one portion. The reaction was stirred for 1.5 h, then quenched by the addition of saturated aqueous Na<sub>2</sub>S<sub>2</sub>O<sub>3</sub> (2 mL) and H<sub>2</sub>O (8 mL). The mixture was partitioned between Et<sub>2</sub>O

(20 mL) and additional H<sub>2</sub>O (10 mL). The phases were separated, and the aqueous portion was extracted with Et<sub>2</sub>O (2x 20 mL). The combined organics were washed with brine, dried over anhydrous MgSO<sub>4</sub>, and concentrated under reduced pressure. The crude product was purified by flash column chromatography over silica gel. Elution with 16% Et<sub>2</sub>O in pentane afforded 144 mg of the hydroxyketone **SI-2.3** as a white solid (91% yield).



<sup>1</sup>H NMR (500 MHz, CDCl<sub>3</sub>)

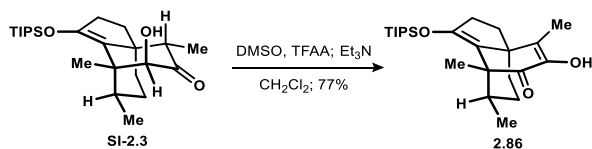
δ 3.63 (d, J = 8.7 Hz, 1H)	1.49 (s, 3H)
2.61 (q, J = 6.7 Hz, 1H)	1.42 (dtd, J = 14.6, 4.8, 4.3, 2.7 Hz, 1H)
2.55 – 2.50 (m, 2H)	1.30 (td, J = 13.3, 5.0 Hz, 1H)
1.94 (d, J = 8.7 Hz, 1H)	1.22 – 1.15 (m, 3H)
1.80 (ddd, J = 13.2, 4.6, 2.1 Hz, 1H)	1.11 (d, J = 5.6 Hz, 18H)
1.73 (ddd, J = 13.2, 9.2, 7.8 Hz, 1H)	1.08 – 0.96 (m, 5H)
1.69 – 1.57 (m, 2H)	0.89 (d, J = 7.0 Hz, 3H)

<sup>13</sup>C NMR (126 MHz, CDCl<sub>3</sub>)

δ 213.4	45.9	20.8
149.2	41.2	18.3
117.3	34.4	18.3
78.4	33.7	15.5
51.4	33.2	13.6
50.0	29.6	8.4

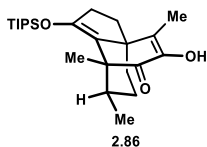
TLC R<sub>f</sub> = 0.60 (40% v/v Et<sub>2</sub>O in hexanes). Not UV active.

HRMS (ES<sup>+</sup>) calculated for C<sub>24</sub>H<sub>42</sub>O<sub>3</sub>SiNa [M+Na]: 429.2801, found: 429.2809



**Ketone 2.86.** A solution of DMSO (0.10 mL, 1.37 mmol) in CH<sub>2</sub>Cl<sub>2</sub> (2.0 mL) was cooled to -78 °C and treated with trifluoroacetic anhydride (0.16 μL, 1.15 mmol). After 15 minutes at the same temperature, hydroxyketone **SI-2.3** (144.0 mg, 0.35 mmol) was added as a solution in CH<sub>2</sub>Cl<sub>2</sub> (2.0 mL). The reaction was stirred for 1 h, treated with Et<sub>3</sub>N (0.30 mL, 2.12 mmol), then warmed to ambient temperature. After 30 minutes, The mixture was diluted with saturated aqueous

NaHCO<sub>3</sub> (10 mL) and CH<sub>2</sub>Cl<sub>2</sub> (10 mL). The phases were separated, and the aqueous portion was extracted with CH<sub>2</sub>Cl<sub>2</sub> (2x 10 mL). The combined organics were washed with brine, dried over MgSO<sub>4</sub>, and concentrated under reduced pressure. The crude product was taken up in hexanes (1 mL) and allowed to stand over SiO<sub>2</sub> (ca. 100 mg) for 20 minutes, then purified by flash column chromatography over silica gel. Elution with 6% v/v Et<sub>2</sub>O in pentane afforded 108 mg of diketone **2.86** as a white solid (77% yield).



<sup>1</sup>H NMR (500 MHz, CDCl<sub>3</sub>)

δ 6.18 (s, 1H)	1.61 – 1.56 (m, 1H)
2.51 (dt, J = 15.2, 8.9 Hz, 1H)	1.54 (s, 3H) – overlaps with H <sub>2</sub> O
2.29 (ddd, J = 15.2, 10.2, 2.2 Hz, 1H)	1.53 – 1.44 (m, 3H)
1.88 (ddd, J = 12.8, 10.2, 8.7 Hz, 1H)	1.24 – 1.10 (m, 4H)
1.80 (s, 3H)	1.10 – 1.03 (m, 18H)
1.70 (ddd, J = 12.8, 9.0, 2.3 Hz, 1H)	0.76 (d, J = 6.5 Hz, 3H)

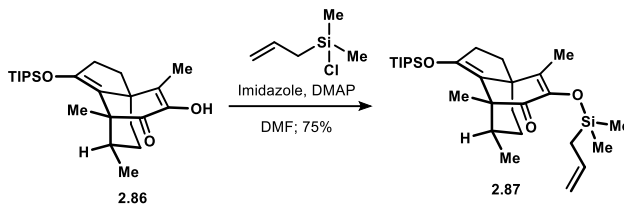
<sup>13</sup>C NMR (151 MHz, CDCl<sub>3</sub>)

δ 195.6	49.0	18.3
145.6	41.3	18.2
143.3	33.3	16.1
133.0	32.3	13.5
118.7	30.0	11.3
50.4	29.8	

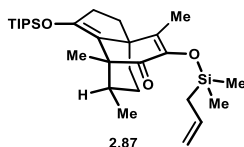
TLC R<sub>f</sub> = 0.65 (15% v/v Et<sub>2</sub>O in hexanes). UV active. Does not stain well in *p*-anisaldehyde or KMnO<sub>4</sub>

HRMS (ES<sup>+</sup>) calculated for C<sub>24</sub>H<sub>40</sub>O<sub>3</sub>SiNa [M+Na]: 427.2644, found: 427.2657





**Enoxysilane 2.87.** A flame-dried flask was charged with 1,2-dione **2.86** (48.4 mg, 0.120 mmol), imidazole (35.0 mg, 0.514 mmol), and DMAP (6.5 mg, 0.053 mmol). To the solids was added DMF (1.0 mL, freshly distilled at *ca.* 0.2 mmHg). Subsequently, allyl(dimethyl)chlorosilane (60  $\mu$ L, 0.39 mmol) was added dropwise. The mixture was stirred at ambient temperature for 1 h, then treated with saturated aqueous  $\text{NaHCO}_3$  (2 mL) and stirred for 15 minutes. The mixture was partitioned between  $\text{Et}_2\text{O}$  (8 mL) and additional saturated aqueous  $\text{NaHCO}_3$  (6 mL). The phases were separated, and the aqueous portion was extracted with  $\text{Et}_2\text{O}$  (2x 8 mL). The combined organics were washed with brine, dried over  $\text{MgSO}_4$ , and concentrated under reduced pressure. The crude product was purified by flash column chromatography over silica gel. Elution with 2-3% v/v  $\text{Et}_2\text{O}$  in pentane afforded 45.0 mg of enoxysilane **2.87** as a colorless oil (75% yield).



$^1\text{H}$  NMR (600 MHz,  $\text{C}_6\text{D}_6$ )

$\delta$ 6.00 (ddt, $J = 17.0, 10.1, 8.1$ Hz, 1H)	1.73 – 1.65 (m, 4H)
5.04 (ddt, $J = 16.9, 2.5, 1.4$ Hz, 1H)	1.46 – 1.25 (m, 6H)
5.01 – 4.95 (m, 1H)	1.09 – 0.99 (m, 21H)
2.38 (dt, $J = 15.1, 8.9$ Hz, 1H)	0.89 (d, $J = 6.7$ Hz, 3H)
2.15 (ddd, $J = 15.1, 10.3, 2.2$ Hz, 1H)	0.42 (s, 3H)
1.96 – 1.89 (m, 2H)	0.41 (s, 3H)
1.82 (s, 3H)	

$^{13}\text{C}$  NMR (151 MHz,  $\text{C}_6\text{D}_6$ )

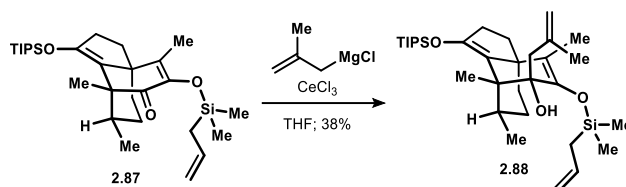
$\delta$ 194.6	49.6	18.2
146.8	41.7	16.3
142.7	33.6	13.6
139.6	32.6	11.9
135.2	30.3	-0.2
119.8	30.1	-0.2

113.6 26.8

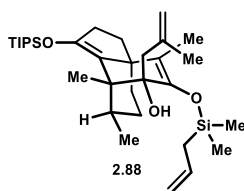
51.3 19.1

TLC  $R_f$  = 0.58 (5% v/v Et<sub>2</sub>O in hexanes). UV active.

HRMS (ES+) calculated for C<sub>29</sub>H<sub>50</sub>O<sub>3</sub>Si<sub>2</sub>Na [M+Na]: 525.3196, found: 525.3199



**Homoallylic alcohol 2.88.** CeCl<sub>3</sub> (40 mg, 0.162 mmol) was heated under vacuum until it became a free-flowing powder. After cooling to ambient temperature, THF (0.8 mL) was added with stirring. The suspension was sonicated for 20 minutes, then cooled to 0 °C and treated dropwise with a solution of methallylmagnesium chloride (0.43 mL of a 0.245 M solution in THF, 0.146 mmol). The reaction was maintained at the same temperature for 1 h, at which point a solution of ketone **2.87** (22.5 mg, 0.045 mmol) in THF (1.0 mL) was added dropwise. The resulting suspension was stirred for 1.0 h, then quenched by the addition of saturated aqueous NaHCO<sub>3</sub> (2 mL). The mixture was diluted with Et<sub>2</sub>O (6 mL) and H<sub>2</sub>O (6 mL) and the phases were separated. The aqueous portion was extracted with Et<sub>2</sub>O (2x 6 mL). The combined organics were washed with brine, dried over anhydrous MgSO<sub>4</sub>, and concentrated under reduced pressure. The crude product was purified by flash column chromatography over silica gel. Elution with 1% v/v Et<sub>2</sub>O in pentane afforded 9.6 mg of the homoallylic alcohol **2.88** as a colorless oil (38% yield).



<sup>1</sup>H NMR (600 MHz, C<sub>6</sub>D<sub>6</sub>)

δ 5.88 (ddt, J = 17.0, 10.1, 8.1 Hz, 1H)

5.04 – 4.94 (m, 2H)

4.85 (s, 1H)

4.76 (s, 1H)

2.65 (d, J = 12.6 Hz, 1H)

2.52 – 2.43 (m, 2H)

2.26 – 2.17 (m, 1H)

1.80 (dq, J = 8.1, 1.3 Hz, 2H)

1.76 (s, 3H)

1.74 – 1.66 (m, 2H)

1.54 – 1.50 (m, 4H)

1.49 (s, 3H)

1.47 – 1.40 (m, 4H)

1.13 – 1.04 (m, 21H)

1.91 – 1.83 (m, 3H) 0.30 (s, 3H)

1.83 (s, 3H) 0.29 (s, 3H)

<sup>13</sup>C NMR (151 MHz, C<sub>6</sub>D<sub>6</sub>)

δ 147.6 50.6 24.6

145.0 49.5 21.2

142.4 47.7 18.9

134.5 46.5 18.3

121.2 35.0 13.7

115.0 33.0 10.9

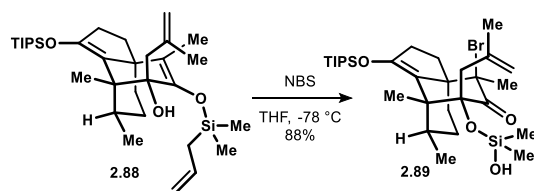
114.2 31.0 -0.3

113.5 30.9 -0.4

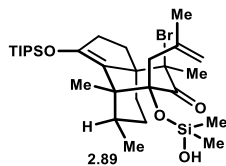
78.4 26.3

TLC R<sub>f</sub> = 0.45 (2% v/v Et<sub>2</sub>O in hexanes). Modestly UV active.

HRMS (ES<sup>+</sup>) calculated for C<sub>33</sub>H<sub>58</sub>O<sub>3</sub>Si<sub>2</sub>Na [M+Na]: 581.3822, found: 581.3812



**Bromoketone 2.89.** A solution of enoxysilane **2.88** (1.9 mg, 3.4 μmol) in THF (0.4 mL) was cooled to -78 °C. A solution of *N*-bromosuccinimide (1.34 mg, 7.6 μmol) in THF (0.10 mL) was added dropwise to the reaction mixture. After 30 minutes, the reaction was warmed to 0 °C and quenched by the addition of saturated aqueous Na<sub>2</sub>S<sub>2</sub>O<sub>3</sub> (1 mL). The mixture was diluted with H<sub>2</sub>O (5 mL) and Et<sub>2</sub>O (6 mL). The phases were separated, and the aqueous portion was extracted with Et<sub>2</sub>O (2x 6 mL). The combined organics were washed with brine, dried over anhydrous MgSO<sub>4</sub>, and concentrated under reduced pressure. The crude product was purified by flash column chromatography over silica gel. Elution with 12% v/v Et<sub>2</sub>O in pentane afforded 1.8 mg of the product bromoketone **2.89** as a white film (88% yield).



<sup>1</sup>H NMR (600 MHz, CDCl<sub>3</sub>)

δ 5.01 (s, 1H) 1.79 (s, 3H)

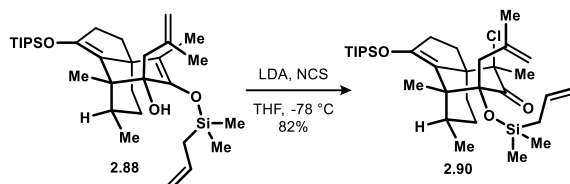
4.93 (s, 1H)	1.67 (s, 3H)
3.03 (d, J = 15.2 Hz, 1H)	1.64 – 1.56 (m, 3H)
2.92 (d, J = 15.3 Hz, 1H)	1.39 – 1.35 (m, 1H)
2.73 – 2.63 (m, 2H)	1.18 – 1.13 (m, 4H)
2.38 – 2.29 (m, 2H)	1.11 (dt, J = 7.3, 4.4 Hz, 22H)
2.07 (dt, J = 13.5, 3.0 Hz, 1H)	0.18 (s, 3H)
1.85 (s, 3H)	0.16 (s, 3H)

<sup>13</sup>C NMR (151 MHz, CDCl<sub>3</sub>)

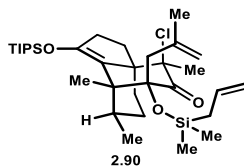
δ 210.1	49.6	25.0
148.1	48.3	20.8
143.4	47.1	18.3
115.4	40.3	18.2
115.2	35.1	17.8
89.8	33.1	13.7
75.6	28.7	1.9
55.3	27.0	1.8

TLC R<sub>f</sub> = 0.46 (20% v/v Et<sub>2</sub>O in hexanes). Modestly UV active.

HRMS (ES<sup>+</sup>) calculated for C<sub>30</sub>H<sub>53</sub>BrO<sub>4</sub>Si<sub>2</sub>Na [M+Na]: 637.2549, found: 637.2563



**Chloroketone 2.90.** A solution of enoxysilane **2.88** (10 mg, 17.9 μmol) in THF (0.6 mL) was cooled to -78 °C. A solution of *N*-bromosuccinimide (14 mg, 0.107 mmol) in THF (0.4 mL) was added dropwise to the reaction mixture. After 30 minutes, the reaction was quenched by the addition of saturated aqueous Na<sub>2</sub>S<sub>2</sub>O<sub>3</sub> (1 mL) with vigorous stirring. The mixture was warmed to ambient temperature and diluted with H<sub>2</sub>O (5 mL) and Et<sub>2</sub>O (6 mL). The phases were separated, and the aqueous portion was extracted with Et<sub>2</sub>O (2x 6 mL). The combined organics were washed with brine, dried over anhydrous MgSO<sub>4</sub>, and concentrated under reduced pressure. The crude product was purified by flash column chromatography over silica gel. Elution with 1% v/v Et<sub>2</sub>O in pentane afforded 8.7 mg of the product chloroketone **2.90** as a colorless oil (82% yield).



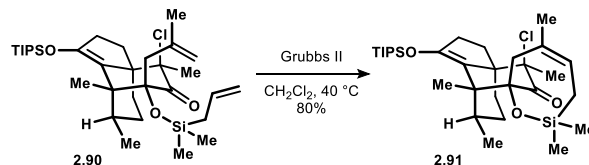
<sup>1</sup>H NMR (600 MHz, C<sub>6</sub>D<sub>6</sub>)

δ 6.08 (ddt, J = 16.6, 10.0, 8.2 Hz, 1H)	1.83 (s, 3H)
5.23 (s, 1H)	1.72 (dt, J = 13.4, 3.0 Hz, 1H)
5.10 (ddt, J = 16.9, 2.6, 1.5 Hz, 1H)	1.58 (s, 3H)
5.01 (ddt, J = 10.0, 2.2, 1.1 Hz, 1H)	1.52 (ddd, J = 12.6, 7.3, 3.7 Hz, 1H)
4.99 (dt, J = 2.5, 1.2 Hz, 1H)	1.28 – 1.25 (m, 1H)
3.16 (d, J = 15.4 Hz, 1H)	1.23 (d, J = 7.3 Hz, 3H)
2.98 (d, J = 15.4 Hz, 1H)	1.09 (dd, J = 6.9, 3.6 Hz, 20H)
2.65 – 2.56 (m, 1H)	1.07 – 0.99 (m, 4H)
2.26 – 2.17 (m, 2H)	0.53 (s, 3H)
1.99 (qdt, J = 13.1, 8.2, 1.3 Hz, 2H)	0.48 (s, 3H)
1.86 (s, 3H)	

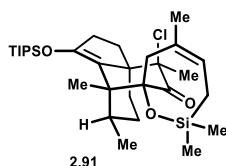
<sup>13</sup>C NMR (151 MHz, C<sub>6</sub>D<sub>6</sub>)

δ 209.1	50.1	23.2
148.0	47.9	21.3
141.7	47.3	18.2
136.6	40.5	18.2
117.1	35.5	18.1
115.6	30.9	13.8
113.0	30.4	2.2
89.2	28.7	1.9
78.4	28.5	
55.3	26.3	

TLC R<sub>f</sub> = 0.63 (3% v/v Et<sub>2</sub>O in hexanes). Modestly UV active.



**Oxasilepine 2.91.** A vial was charged with chloroketone **2.90** (8.7 mg, 14.7  $\mu\text{mol}$ ),  $\text{CH}_2\text{Cl}_2$  (0.6 mL), and Grubbs 2<sup>nd</sup> generation catalyst (2.5 mg, 3.0  $\mu\text{mol}$ ). The vial was sealed and heated to 40 °C for 1.5 h, then cooled to ambient temperature. The mixture was concentrated under reduced pressure and purified by flash column chromatography over silica gel. Elution with 2% v/v  $\text{Et}_2\text{O}$  in pentane afforded 6.6 mg of the product oxasilepine **2.91** as a colorless oil (80% yield).



$^1\text{H}$  NMR (600 MHz,  $\text{C}_6\text{D}_6$ )

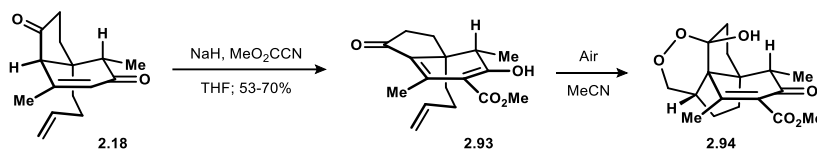
$\delta$ 5.66 (tdd, $J = 5.0, 4.0, 3.5, 2.0$ Hz, 1H)	1.58 – 1.50 (m, 1H)
3.14 (d, $J = 15.7$ Hz, 1H)	1.36 – 1.25 (m, 3H)
2.98 (d, $J = 15.8$ Hz, 1H)	1.23 (d, $J = 7.1$ Hz, 3H)
2.60 (dtd, $J = 17.4, 9.0, 8.3, 3.8$ Hz, 1H)	1.22 – 1.17 (m, 2H)
2.30 – 2.20 (m, 2H)	1.11 (dd, $J = 6.8, 3.8$ Hz, 18H)
1.92 (d, $J = 1.3$ Hz, 4H)	1.08 – 1.04 (m, 3H)
1.82 (s, 3H)	0.54 (s, 3H)
1.74 (dt, $J = 13.2, 3.0$ Hz, 1H)	0.23 (s, 3H)
1.63 (s, 3H)	

$^{13}\text{C}$  NMR (151 MHz,  $\text{C}_6\text{D}_6$ )

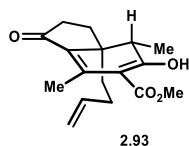
$\delta$ 207.4	49.7	22.8
147.6	47.5	20.0
131.5	45.0	19.4
124.4	40.2	18.9
115.8	35.3	18.3
88.3	30.8	13.8
78.2	29.1	1.7
55.4	28.0	1.1

TLC  $R_f = 0.51$  (4% v/v  $\text{Et}_2\text{O}$  in hexanes). Modestly UV active.

HRMS (CI+) calculated for C<sub>30</sub>H<sub>53</sub>ClO<sub>4</sub>Si<sub>2</sub>Na [M–Cl]: 528.3455, found: 528.3452



**Ketoester 2.93.** To a solution of enone **2.18** (46.5 mg, 0.20 mmol) in THF (2.0 mL) at 0 °C was added NaH (40 mg of a 60 wt% suspension in mineral oil, 1.0 mmol). The suspension was stirred for 1 h, then treated with methyl cyanofornate (48  $\mu$ L, 0.60 mmol). The reaction was warmed to ambient temperature and stirred for 14 h, then treated with  $\frac{1}{2}$ -saturated aqueous NH<sub>4</sub>Cl (2 mL). The mixture was partitioned between H<sub>2</sub>O (2 mL) and Et<sub>2</sub>O (8 mL). The phases were separated, and the aqueous portion was extracted with Et<sub>2</sub>O (2x 8 mL). The combined organics were washed with brine, dried over anhydrous MgSO<sub>4</sub>, and concentrated under reduced pressure. The crude product was purified by flash column chromatography over silica gel. Elution with 10% v/v EtOAc in hexanes afforded 40.7 mg of the product ketoester **2.93** as a bright yellow film (70% yield). Dissolving ketoester **2.93** in MeCN under an atmosphere of air for 10 h led to the spontaneous formation of the endoperoxide **2.94**, which was isolated by flash column chromatography over silica gel. Elution with 50% v/v EtOAc in pentane afforded 11.1 mg of the endoperoxide **2.94**. A crystal for x-ray diffraction analysis was grown by slow evaporation of a 5 mg sample of endoperoxide **2.94** from benzene.



<sup>1</sup>H NMR (600 MHz, CDCl<sub>3</sub>)

$\delta$  14.37 (s, 1H)

5.67 (ddt, J = 16.8, 10.1, 6.5 Hz, 1H)

4.97 – 4.86 (m, 2H)

3.85 (s, 3H)

2.78 (q, J = 7.1 Hz, 1H)

2.52 – 2.46 (m, 1H)

2.44 (s, 3H)

<sup>13</sup>C NMR (151 MHz, CDCl<sub>3</sub>)

$\delta$  206.3

114.6

33.6

2.39 (ddd, J = 19.1, 10.0, 1.8 Hz, 1H)

2.01 (ddd, J = 12.9, 9.5, 1.8 Hz, 1H)

1.93 – 1.83 (m, 2H)

1.74 – 1.68 (m, 1H)

1.59 (td, J = 13.1, 4.6 Hz, 1H)

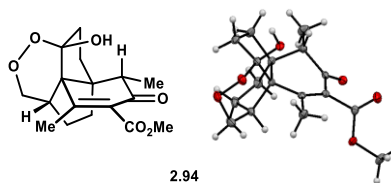
1.36 (ddd, J = 13.6, 12.4, 4.7 Hz, 1H)

1.20 (d, J = 7.1 Hz, 3H)

184.7	102.1	32.2
173.1	52.0	29.8
143.6	46.8	17.5
138.8	44.7	7.9
130.1	38.8	

TLC  $R_f$  = 0.34 (20% v/v EtOAc in hexanes). UV active.

HRMS (ES+) calculated for  $C_{17}H_{22}O_4Na$  [M+Na]: 313.1416, found: 313.1409



$^1H$  NMR (600 MHz,  $CDCl_3$ )

$\delta$ 4.57 (dd, $J$ = 12.9, 7.0 Hz, 1H)	2.16 (s, 3H)
4.07 (dd, $J$ = 12.9, 2.8 Hz, 1H)	1.94 – 1.85 (m, 3H)
3.80 (s, 3H)	1.81 – 1.74 (m, 1H)
3.11 (s, 1H)	1.73 – 1.64 (m, 2H)
2.72 (q, $J$ = 6.7 Hz, 1H)	1.38 – 1.31 (m, 1H)
2.66 – 2.55 (m, 1H)	1.13 (d, $J$ = 6.7 Hz, 3H)
2.26 (dtd, $J$ = 10.3, 7.4, 2.8 Hz, 1H)	

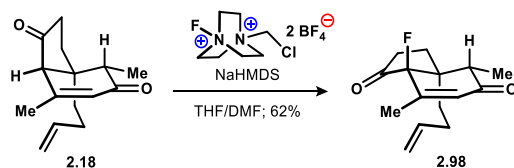
$^{13}C$  NMR (151 MHz,  $CDCl_3$ )

$\delta$ 197.1	57.7	34.8
167.7	57.0	34.4
158.5	52.3	30.1
131.7	48.3	19.1
111.3	46.4	9.4
73.6	37.6	

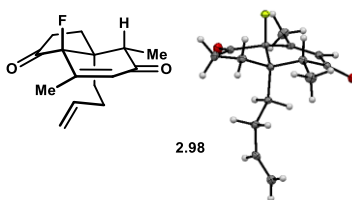
TLC  $R_f$  = 0.39 (60% v/v EtOAc in hexanes). UV active.

HRMS (ES+) calculated for  $C_{17}H_{22}O_6Na$  [M+Na]: 345.1314, found: 345.1324





**Fluoroenone 2.98.** To a solution of enone **2.18** (23.2 mg, 0.10 mmol) in THF (0.8 mL) at 0 °C was added NaHMDS (20 mg 0.11 mmol). The solution was stirred for 20 minutes, then treated with a DMF (0.4 mL) solution of Selectfluor (43 mg, 0.12 mmol). The reaction was warmed to ambient temperature and stirred for 14 h, then treated with ½-saturated aqueous NH<sub>4</sub>Cl (2 mL). The mixture was partitioned between H<sub>2</sub>O (2 mL) and Et<sub>2</sub>O (8 mL). The phases were separated, and the aqueous portion was extracted with Et<sub>2</sub>O (2x 8 mL). The combined organics were washed with brine, dried over anhydrous MgSO<sub>4</sub>, and concentrated under reduced pressure. The crude product was purified by flash column chromatography over silica gel. Elution with 5% v/v EtOAc in hexanes afforded 14.0 mg of the product fluoroenone **2.98** as a white solid (62% yield). Crystals suitable for x-ray diffraction analysis were grown by slow evaporation from benzene.



<sup>1</sup>H NMR (500 MHz, CDCl<sub>3</sub>)

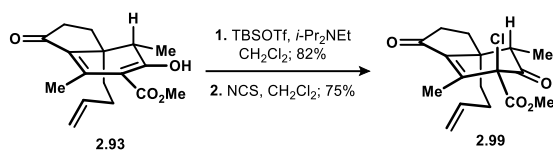
δ 6.03 (dd, J = 6.1, 1.8 Hz, 1H)	2.20 – 2.12 (m, 2H)
5.61 (ddt, J = 16.8, 10.1, 6.5 Hz, 1H)	2.09 – 2.02 (m, 2H)
5.04 – 4.90 (m, 2H)	1.86 (tt, J = 12.8, 5.8 Hz, 1H)
2.99 (q, J = 7.1 Hz, 1H)	1.35 – 1.23 (m, 2H)
2.67 (ddt, J = 19.5, 9.9, 1.8 Hz, 1H)	1.19 (d, J = 7.1 Hz, 3H)
2.32 – 2.25 (m, 1H)	1.08 – 0.99 (m, 1H)

2.24 (dd, J = 4.8, 1.7 Hz, 3H)

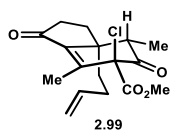
<sup>13</sup>C NMR (126 MHz, CDCl<sub>3</sub>)

δ 207.04 (d, J = 24.6 Hz)	115.85	32.28 (d, J = 1.9 Hz)
200.59 (d, J = 4.5 Hz)	94.85 (d, J = 166.8 Hz)	30.47, 25.63 (d, J = 2.9 Hz)
148.50 (d, J = 13.3 Hz)	49.32 (d, J = 17.6 Hz)	25.63 (d, J = 2.9 Hz)
136.94	46.95 (d, J = 3.8 Hz)	18.61
133.83 (d, J = 9.6 Hz)	33.57 (d, J = 3.1 Hz)	9.06

TLC R<sub>f</sub> = 0.55 (20% v/v EtOAc in hexanes). UV active.



**Chloroketone 2.99.** A solution of ketoester **2.93** (8.7 mg, 30  $\mu\text{mol}$ ) in  $\text{CH}_2\text{Cl}_2$  (1.0 mL) was treated with *i*-Pr<sub>2</sub>NEt (15  $\mu\text{L}$ , 88  $\mu\text{mol}$ ) and TBSOTf (8  $\mu\text{L}$ , 34  $\mu\text{mol}$ ). The reaction was stirred for 1 h, at which point saturated aqueous NaHCO<sub>3</sub> (2 mL) was added under vigorous stirring. The emulsion was stirred vigorously for an additional 12 h, then diluted with  $\text{CH}_2\text{Cl}_2$  (5 mL) and saturated aqueous NaHCO<sub>3</sub> (4 mL). The phases were separated, and the aqueous portion was extracted with  $\text{CH}_2\text{Cl}_2$  (2x 6 mL). The combined organics were washed with brine, dried over anhydrous MgSO<sub>4</sub>, and concentrated under reduced pressure. The crude product (10.0 mg, *ca.* 82% yield) was of sufficient purity for use in the subsequent step. The crude enoxysilane (5.0 mg, 12  $\mu\text{mol}$ ) was dissolved in DMF (0.4 mL), cooled to 0 °C, and treated with NCS (2.0 mg, 15  $\mu\text{mol}$ , recrystallized from AcOH before use). The reaction was warmed to ambient temperature for 10 h, then diluted with Et<sub>2</sub>O (6 mL) and H<sub>2</sub>O (6 mL). The phases were separated, and the aqueous portion was extracted with Et<sub>2</sub>O (2x 6 mL). The combined organics were washed with saturated aqueous Na<sub>2</sub>S<sub>2</sub>O<sub>3</sub> (6 mL) and brine, dried over anhydrous MgSO<sub>4</sub>, and concentrated under reduced pressure. The crude product was purified by flash column chromatography over silica gel. Elution with 15% v/v EtOAc in pentane afforded 2.9 mg of the chloroketone **2.99** as a colorless oil (75% yield).



<sup>1</sup>H NMR (600 MHz, CDCl<sub>3</sub>)

$\delta$  5.64 (ddt, *J* = 16.8, 10.0, 6.4 Hz, 1H)

4.98 – 4.89 (m, 2H)

3.81 (s, 3H)

3.15 (q, *J* = 6.7 Hz, 1H)

2.60 – 2.43 (m, 2H)

2.21 (s, 3H)

<sup>13</sup>C NMR (151 MHz, CDCl<sub>3</sub>)

$\delta$  206.7

200.5

115.2

77.4

2.16 (ddd, *J* = 13.0, 8.7, 2.5 Hz, 1H)

1.99 – 1.90 (m, 2H)

1.87 – 1.78 (m, 1H)

1.62 – 1.55 (m, 1H)

1.41 (td, *J* = 13.2, 4.6 Hz, 1H)

1.21 (d, *J* = 6.6 Hz, 3H)

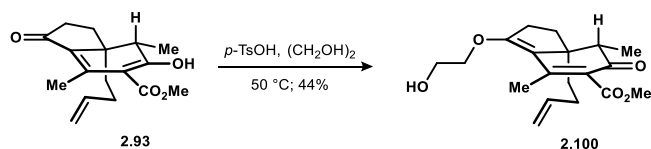
36.5

33.0

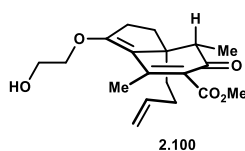
165.8	54.3	29.3
140.5	50.2	14.3
140.2	50.0	7.8
137.7	37.6	

TLC  $R_f$  = 0.39 (20% v/v EtOAc in hexanes). UV active.

HRMS (ES+) calculated for  $C_{17}H_{21}ClO_4Na$  [M+Na]: 347.1026, found: 347.1023



**Dienol ether 2.100.** A solution of ketoester **2.93** (72.6 mg, 0.25 mmol) in ethylene glycol (1.8 mL) was treated with  $p$ -TsOH (4.8 mg, 0.025 mmol) and trimethylorthoformate (0.2 mL). The reaction mixture was heated to 50 °C for 25 minutes, then cooled to ambient temperature. The components were partitioned between saturated aqueous  $NaHCO_3$  (8 mL) and  $Et_2O$  (8 mL), and the phases were separated. The aqueous portion was extracted with  $Et_2O$  (2x 8 mL). The combined organics were washed with brine, dried over anhydrous  $MgSO_4$ , and concentrated under reduced pressure. The crude product was purified by flash column chromatography over silica gel. Elution with 60% v/v EtOAc in hexanes afforded 37.2 mg of the dienol ether **2.100** as a white solid (44% yield).



$^1H$  NMR (600 MHz,  $CDCl_3$ )

$\delta$ 5.71 (ddt, $J$ = 16.7, 10.2, 6.5 Hz, 1H)	2.52 (q, $J$ = 6.9 Hz, 1H)
4.95 (dq, $J$ = 17.1, 1.7 Hz, 1H)	2.22 (s, 3H)
4.89 (dq, $J$ = 10.2, 1.5 Hz, 1H)	2.01 (t, $J$ = 5.9 Hz, 1H)
4.14 – 4.04 (m, 2H)	1.97 – 1.84 (m, 4H)
3.86 (q, $J$ = 4.9 Hz, 2H)	1.56 – 1.46 (m, 1H)
3.80 (s, 3H)	1.44 – 1.35 (m, 1H)
2.78 – 2.67 (m, 2H)	1.05 (d, $J$ = 6.9 Hz, 3H)

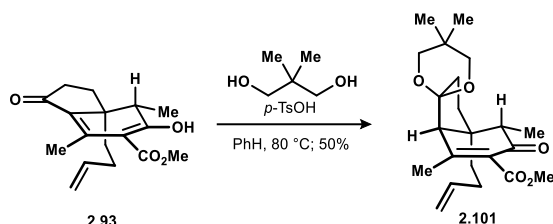
$^{13}C$  NMR (151 MHz,  $CDCl_3$ )

$\delta$ 197.7	114.4	32.5
168.4	71.3	31.3

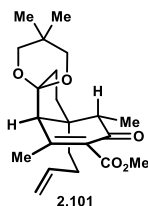
161.0	61.8	29.4
148.7	54.1	18.9
138.9	52.1	8.0
128.4	51.3	
114.5	32.9	

TLC  $R_f$  = 0.29 (60% v/v EtOAc in hexanes). UV active.

HRMS (ES+) calculated for  $C_{19}H_{26}O_5Na$  [M+Na]: 357.1678, found: 357.1674



**Ketal 2.101.** A flame-dried flask fitted with a reflux condenser was charged with ketoester **2.93** (53 mg, 0.183 mmol) and PhH (3.7 mL). 2,2-dimethyl-1,3-propanediol (190.7 mg, 1.83 mmol) and *p*-TsOH (17.3 mg, 0.091 mmol) were added as a single portion. The reaction was heated to reflux for 1 h, then cooled to ambient temperature. The mixture was partitioned between saturated aqueous  $NaHCO_3$  (8 mL) and  $Et_2O$  (8 mL), and the phases were separated. The aqueous portion was extracted with  $Et_2O$  (2x 8 mL). The combined organics were washed with brine, dried over anhydrous  $MgSO_4$ , and concentrated under reduced pressure. The crude product was purified by flash column chromatography over silica gel. Elution with 25% v/v EtOAc in hexanes afforded 34.0 mg of the ketal **2.101** as a white solid (50% yield).



$^1H$  NMR (500 MHz,  $CDCl_3$ )

$\delta$ 5.71 (ddt, $J$ = 16.8, 10.1, 6.4 Hz, 1H)	2.20 (ddd, $J$ = 13.1, 9.1, 3.7 Hz, 1H)
4.97 (dq, $J$ = 17.1, 1.6 Hz, 1H)	2.14 (s, 3H)
4.92 (dq, $J$ = 10.1, 1.4 Hz, 1H)	2.09 (ddd, $J$ = 13.6, 9.7, 8.0 Hz, 1H)
3.81 (s, 3H)	1.98 – 1.81 (m, 2H)
3.64 (d, $J$ = 11.4 Hz, 1H)	1.79 – 1.63 (m, 2H)
3.56 (d, $J$ = 11.4 Hz, 1H)	1.40 (dd, $J$ = 9.2, 7.5 Hz, 2H)

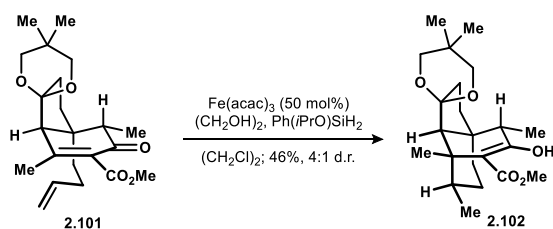
3.46 (dd, J = 11.4, 2.7 Hz, 1H)                      1.18 (s, 3H)  
 3.39 (dd, J = 11.4, 2.7 Hz, 1H)                      1.03 (d, J = 6.9 Hz, 3H)  
 2.80 (q, J = 6.8 Hz, 1H)                                0.73 (s, 3H)  
 2.60 (s, 1H)

<sup>13</sup>C NMR (126 MHz, CDCl<sub>3</sub>)

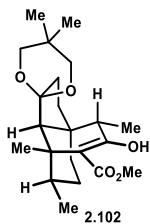
δ 198.3	71.3	29.9
167.7	59.2	29.1
154.8	52.1	23.5
138.4	48.6	22.5
133.6	44.4	21.8
114.9	33.2	7.8
109.6	32.0	
73.1	30.0	

TLC R<sub>f</sub> = 0.30 (20% v/v EtOAc in hexanes). UV active.

HRMS (ES<sup>+</sup>) calculated for C<sub>22</sub>H<sub>32</sub>O<sub>5</sub>Na [M+Na]: 399.2148, found: 399.2137



**Ketoester 2.102.** A flame-dried flask was charged with enone **2.101** (17.0 mg, 45 μmol), Fe(acac)<sub>3</sub> (8.0 mg, 23 μmol), 1,2-dichloroethane (1.0 mL), and ethylene glycol (25 μL, 0.45 mmol). The mixture was sparged with Ar with continuous sonication for 15 minutes, then cooled to -20 °C. Ph(*i*-PrO)SiH<sub>2</sub> (18 μL, 90 μmol, prepared according to the known method<sup>x</sup>) was added dropwise to the stirred suspension. After 6 h, the reaction was treated with aqueous 1 N HCl (2 mL) and stirred vigorously for 40 minutes. The resulting biphasic mixture was diluted with CHCl<sub>3</sub> (6 mL) and additional 1 N HCl (4 mL). The phases were separated, and the aqueous portion was extracted with CHCl<sub>3</sub> (2x 6 mL). The combined organics were washed with brine, dried over anhydrous MgSO<sub>4</sub>, and concentrated under reduced pressure. The crude product was purified by flash column chromatography over silica gel. Elution with 6% v/v EtOAc in hexanes afforded 7.9 mg of the ketoester **2.102** as a white film (46% yield).



<sup>1</sup>H NMR (600 MHz, CDCl<sub>3</sub>)

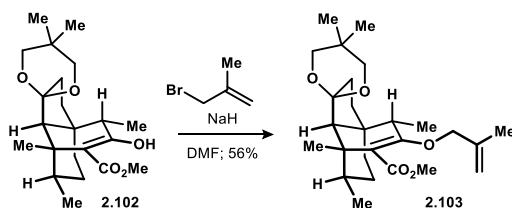
δ 13.90 (s, 1H)	1.78 – 1.68 (m, 1H)
3.72 (s, 3H)	1.62 (s, 3H)
3.57 (d, J = 11.4 Hz, 1H)	1.34 – 1.22 (m, 4H)
3.45 (d, J = 11.4 Hz, 1H)	1.20 (s, 3H)
3.41 (dd, J = 11.3, 2.7 Hz, 1H)	1.17 (d, J = 8.9 Hz, 1H)
3.28 (dd, J = 11.4, 2.6 Hz, 1H)	1.12 (d, J = 7.3 Hz, 3H)
2.37 (q, J = 7.3 Hz, 1H)	1.06 – 0.97 (m, 2H)
2.09 – 1.97 (m, 2H)	0.70 (d, J = 6.5 Hz, 3H)
1.94 – 1.88 (m, 1H)	0.67 (s, 3H)

<sup>13</sup>C NMR (151 MHz, CDCl<sub>3</sub>)

δ 180.0	44.9	28.9
175.4	42.0	24.2
110.0	38.9	23.2
98.3	37.3	22.9
73.1	35.8	16.7
70.9	35.2	11.5
66.0	29.9	
50.8	29.2	

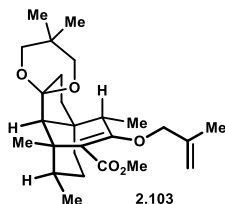
TLC R<sub>f</sub> = 0.48 (10% v/v EtOAc in hexanes). Modestly UV active.

HRMS (ES<sup>+</sup>) calculated for C<sub>22</sub>H<sub>34</sub>O<sub>5</sub>Na [M+Na]: 401.2304, found: 401.2305



**Ketoester 2.103.** A solution of ketoester **2.102** (7.9 mg, 20.9 μmol) in DMF (0.5 mL) was cooled to 0 °C. NaH (4.8 mg, 0.20 mmol) was added as one portion. After 20 minutes, methyl acrylate (20 μL, 0.20 mmol, freshly distilled over CaH<sub>2</sub> under N<sub>2</sub> atmosphere) was added

dropwise. The reaction was maintained at the same temperature for 3 h, then treated with  $\frac{1}{2}$ -saturated aqueous  $\text{NH}_4\text{Cl}$  (1 mL). The mixture was diluted with  $\text{H}_2\text{O}$  (5 mL) and  $\text{Et}_2\text{O}$  (6 mL) and the phases separated. The aqueous portion was extracted with  $\text{Et}_2\text{O}$  (2x 6 mL). The combined organics were washed with water and brine, dried over anhydrous  $\text{MgSO}_4$ , and concentrated under reduced pressure. The crude product was purified by flash column chromatography over silica gel. Elution with 5% v/v  $\text{EtOAc}$  in pentane afforded 5.0 mg of the enol ether **2.103** as a white film (56% yield).



<sup>1</sup>H NMR (600 MHz,  $\text{CDCl}_3$ )

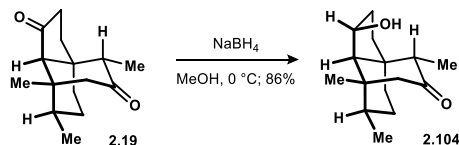
$\delta$ 4.95 (dt, $J = 2.2, 1.1$ Hz, 1H)	2.34 (q, $J = 7.3$ Hz, 1H)
4.90 – 4.81 (m, 1H)	2.15 – 1.93 (m, 3H)
4.07 (d, $J = 11.3$ Hz, 1H)	1.78 – 1.68 (m, 4H)
3.82 (d, $J = 11.4$ Hz, 1H)	1.40 (s, 3H)
3.67 (s, 3H)	1.37 (ddd, $J = 10.0, 4.8, 2.6$ Hz, 3H)
3.58 (d, $J = 11.3$ Hz, 1H)	1.33 – 1.22 (m, 7H)
3.53 (d, $J = 11.2$ Hz, 1H)	1.03 (d, $J = 7.4$ Hz, 4H)
3.44 (dd, $J = 11.3, 2.7$ Hz, 1H)	0.87 (d, $J = 6.3$ Hz, 3H)
3.35 (dd, $J = 11.1, 2.7$ Hz, 1H)	0.70 (s, 3H)

<sup>13</sup>C NMR (151 MHz,  $\text{CDCl}_3$ )

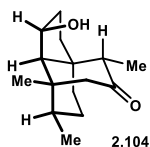
$\delta$ 170.2	63.9	29.5
158.8	51.2	29.0
142.2	45.1	24.1
119.0	43.2	23.0
112.3	39.9	20.9
109.6	36.4	19.8
74.0	35.5	15.8
73.2	33.9	11.1
70.5	29.9	

TLC  $R_f = 0.48$  (10% v/v  $\text{EtOAc}$  in hexanes). Modestly UV active.

HRMS (ES<sup>+</sup>) calculated for  $\text{C}_{26}\text{H}_{40}\text{O}_5\text{Na}$  [ $\text{M}+\text{Na}$ ]: 455.2773, found: 455.2773



**Alcohol 2.104.** A solution of diketone **2.19** (70.3 mg, 0.30 mmol) in MeOH (1.5 mL) was cooled to 0 °C and treated with small portions (ca. 10 mg / 30 s; gas evolution) of NaBH<sub>4</sub> (total of 56.7 mg, 1.5 mmol). The reaction was maintained for 1 h, then treated dropwise with ½-saturated aqueous NH<sub>4</sub>Cl (3 mL). The mixture was partitioned between H<sub>2</sub>O (6 mL) and Et<sub>2</sub>O (10 mL), and the phases separated. The aqueous portion was extracted with Et<sub>2</sub>O (2x 10 mL). The combined organics were washed with brine and dried over anhydrous MgSO<sub>4</sub>, then concentrated under reduced pressure. The crude product was purified by flash column chromatography over silica gel. Elution with 15% v/v EtOAc in hexanes afforded 61.0 mg of ketoalcohol **2.104** (86% yield).



<sup>1</sup>H NMR (500 MHz, CDCl<sub>3</sub>)

δ 4.72 – 4.64 (m, 1H)	1.33 (dt, J = 11.8, 5.7 Hz, 1H)
2.82 (d, J = 16.4 Hz, 1H)	1.26 (dd, J = 6.0, 2.1 Hz, 1H)
2.68 (q, J = 6.8 Hz, 1H)	1.23 – 1.16 (m, 1H)
2.33 – 2.21 (m, 2H)	1.13 (s, 3H)
2.04 – 1.92 (m, 2H)	1.07 – 0.99 (m, 4H)
1.69 (dtd, J = 14.7, 8.9, 1.8 Hz, 1H)	0.92 – 0.85 (m, 1H)
1.49 (s, 1H)	0.84 (d, J = 6.8 Hz, 3H)
1.40 (ddd, J = 9.2, 5.3, 2.3 Hz, 1H)	

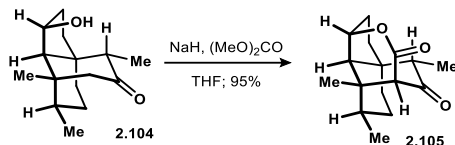
<sup>13</sup>C NMR (151 MHz, CDCl<sub>3</sub>)

δ 216.9	45.1	35.1
74.5	44.4	30.2
59.8	39.5	24.4
48.7	36.6	14.8
46.7	35.5	9.1

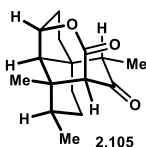
TLC R<sub>f</sub> = 0.44 (30% v/v EtOAc in hexanes). Not UV active.

HRMS (ES<sup>+</sup>) calculated for C<sub>15</sub>H<sub>24</sub>O<sub>2</sub>Na [M+Na]: 259.1674, found: 256.1673





**Lactone 2.105.** A dry flask was charged with NaH (7.2 mg, 0.3 mmol, stored in a dry glovebox) and THF (0.4 mL), then cooled to 0 °C. A solution of ketoalcohol **2.104** (14.2 mg, 0.06 mmol) in THF (0.6 mL) was added dropwise to the suspension followed by dimethyl carbonate (50  $\mu$ L, 0.60 mmol). The reaction was warmed to ambient temperature and stirred for 3 h prior to addition of  $\frac{1}{2}$ -saturated aqueous  $\text{NH}_4\text{Cl}$  (2 mL). The mixture was partitioned between  $\text{H}_2\text{O}$  (4 mL) and  $\text{Et}_2\text{O}$  (6 mL), and the phases separated. The aqueous portion was extracted with  $\text{Et}_2\text{O}$  (2x 6 mL). The combined organics were washed with brine and dried over anhydrous  $\text{MgSO}_4$ , then concentrated under reduced pressure. The crude product was purified by flash column chromatography over silica gel. Elution with 25% v/v  $\text{EtOAc}$  in hexanes afforded 15.2 mg of lactone **2.105** (96% yield).



$^1\text{H}$  NMR (600 MHz,  $\text{CDCl}_3$ )

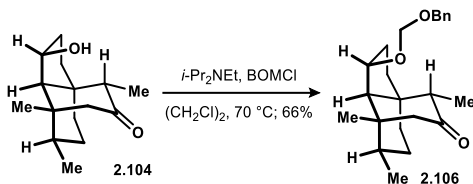
$\delta$ 5.14 (ddd, $J = 8.0, 6.0, 2.0$ Hz, 1H)	1.60 – 1.50 (m, 2H) – overlaps with $\text{H}_2\text{O}$
3.47 (d, $J = 2.4$ Hz, 1H)	1.34 (dt, $J = 13.0, 10.0$ Hz, 1H)
2.47 (dddd, $J = 15.8, 9.8, 7.8, 1.3$ Hz, 1H)	1.23 – 1.15 (m, 4H)
2.33 (q, $J = 6.5$ Hz, 1H)	1.08 (d, $J = 6.5$ Hz, 3H)
2.17 (dddd, $J = 16.0, 10.0, 8.8, 2.0$ Hz, 1H)	1.00 – 0.94 (m, 1H)
2.06 – 2.00 (m, 2H)	0.92 (d, $J = 6.7$ Hz, 3H)

$^{13}\text{C}$  NMR (151 MHz,  $\text{CDCl}_3$ )

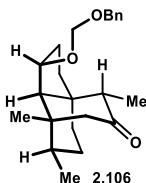
$\delta$ 205.5	45.2	29.2
166.9	41.7	24.3
82.0	40.2	13.9
63.5	36.5	9.0
54.1	33.3	
49.4	31.5	

TLC  $R_f = 0.31$  (30% v/v  $\text{EtOAc}$  in hexanes). Not UV active.

HRMS (ES+) calculated for  $\text{C}_{16}\text{H}_{22}\text{O}_3\text{Na}$  [ $\text{M}+\text{Na}$ ]: 285.1467, found: 285.1472



**Benzyloxymethyl ether 2.106.** A dry vial was charged with ketoalcohol **2.104** (14.2 mg, 0.06 mmol) and placed under an atmosphere of N<sub>2</sub>. 1,2-dichloroethane (0.8 mL) was added to the vial, followed by *i*-Pr<sub>2</sub>NEt (51 μL, 0.3 mmol) and BOMCl (25 μL, 0.18 mmol). The vial was sealed and heated to 70 °C for 22 h, then cooled to ambient temperature. Additional portions of *i*-Pr<sub>2</sub>NEt (51 μL, 0.3 mmol) and BOMCl (25 μL, 0.18 mmol) were added, and the reaction heated to 70 °C for 14 h, then cooled to ambient temperature. The mixture was partitioned between saturated aqueous NaHCO<sub>3</sub> (6 mL) and CH<sub>2</sub>Cl<sub>2</sub> (6 mL). The phases were separated, and the aqueous portion was extracted with CH<sub>2</sub>Cl<sub>2</sub> (2x 6 mL). The combined organics were washed with brine, dried over anhydrous Na<sub>2</sub>SO<sub>4</sub>, then concentrated under reduced pressure. The crude product was purified by flash column chromatography over silica gel. Elution with 25% v/v EtOAc in hexanes afforded 14.1 mg of ketone **2.106** (66% yield).



<sup>1</sup>H NMR (600 MHz, CDCl<sub>3</sub>)

δ 7.36 – 7.27 (m, 5H)	1.95 (ddd, J = 12.5, 9.3, 2.6 Hz, 1H)
4.80 (d, J = 7.0 Hz, 1H)	1.87 (dddd, J = 14.7, 9.5, 8.2, 1.9 Hz, 1H)
4.71 (d, J = 7.0 Hz, 1H)	1.44 – 1.39 (m, 1H)
4.63 (d, J = 11.7 Hz, 1H)	1.38 (dd, J = 6.1, 1.9 Hz, 1H)
4.57 (d, J = 11.8 Hz, 1H)	1.33 (ddd, J = 11.8, 6.8, 4.8 Hz, 1H)
4.53 (td, J = 6.5, 1.8 Hz, 1H)	1.21 (ddd, J = 12.8, 10.8, 8.2 Hz, 1H)
2.83 (d, J = 16.3 Hz, 1H)	1.11 (s, 3H)
2.59 (q, J = 6.8 Hz, 1H)	1.08 – 1.01 (m, 4H)
2.28 (dd, J = 16.3, 1.9 Hz, 1H)	0.92 – 0.86 (m, 1H)
2.15 (dddd, J = 14.7, 11.1, 6.8, 2.6 Hz, 1H)	0.85 (d, J = 6.8 Hz, 3H)
2.01 (ddd, J = 13.3, 4.5, 2.3 Hz, 1H)	

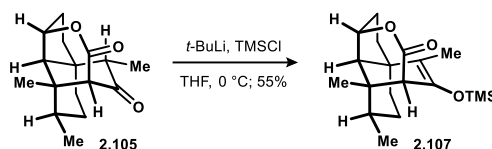
<sup>13</sup>C NMR (151 MHz, CDCl<sub>3</sub>)

δ 216.8	70.7	36.6
137.8	59.5	35.5

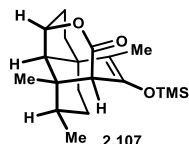
128.6	48.7	30.9
127.9	46.6	30.1
127.9	44.9	24.2
94.1	44.4	14.9
80.3	39.4	9.1

TLC  $R_f$  = 0.32 (10% v/v EtOAc in hexanes). Not UV active.

HRMS (ES+) calculated for  $C_{23}H_{32}O_3Na$  [M+Na]: 379.2249, found: 379.2249



**Enoxysilane 2.107.** A  $-78\text{ }^\circ\text{C}$  solution of lactone **2.105** (5.2 mg, 0.02 mmol) in THF (0.5 mL) was treated dropwise with  $t\text{-BuLi}$  (22  $\mu\text{L}$  of a 1.37 M solution in hexanes, 0.03 mmol). The reaction was maintained at the same temperature for 1 h, then treated with  $\text{TMSCl}$  (8  $\mu\text{L}$ , 0.06 mmol, freshly distilled over  $\text{CaH}_2$  under an atmosphere of  $\text{N}_2$ ). After 10 minutes, the mixture was warmed to  $0\text{ }^\circ\text{C}$  for 1 h, then quenched by the addition of saturated aqueous  $\text{NaHCO}_3$  (2 mL). The mixture was partitioned between  $\text{H}_2\text{O}$  (4 mL) and  $\text{Et}_2\text{O}$  (6 mL), and the phases were separated. The aqueous portion was extracted with  $\text{Et}_2\text{O}$  (2x 6 mL). The combined organics were washed with brine and dried over anhydrous  $\text{MgSO}_4$ , then concentrated under reduced pressure. The crude product was purified by flash column chromatography over silica gel. Elution with 8% v/v EtOAc in pentane afforded 3.8 mg of enoxysilane **2.107** (60% yield).



$^1\text{H NMR}$  (600 MHz,  $\text{CDCl}_3$ )

$\delta$ 4.88 (td, $J = 8.1, 4.6\text{ Hz}$ , 1H)	1.48 – 1.46 (m, 3H)
2.84 (s, 1H)	1.44 (d, $J = 4.8\text{ Hz}$ , 1H)
2.27 (dt, $J = 14.0, 8.0\text{ Hz}$ , 1H)	1.36 – 1.28 (m, 1H) – overlaps with grease
2.05 (dd, $J = 12.4, 7.5\text{ Hz}$ , 1H)	1.23 – 1.17 (m, 3H)
1.82 (ddd, $J = 12.6, 4.9, 2.0\text{ Hz}$ , 1H)	1.08 (s, 3H)
1.71 – 1.65 (m, 1H)	0.95 (d, $J = 6.8\text{ Hz}$ , 3H)
1.55 – 1.51 (m, 1H)	0.22 (s, 9H)

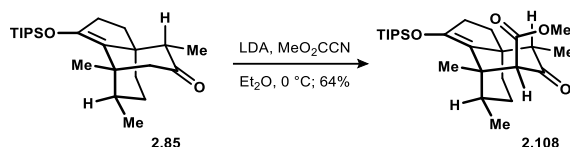
$^{13}\text{C NMR}$  (151 MHz,  $\text{CDCl}_3$ )

$\delta$ 170.1	47.5	30.8
----------------	------	------

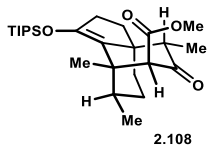
141.9	41.1	24.8
115.8	36.9	15.3
81.1	35.8	10.3
53.2	32.7	1.1
52.2	32.6	

TLC  $R_f$  = 0.52 (20% v/v EtOAc in hexanes). Not UV active.

HRMS (ES+) calculated for  $C_{19}H_{30}O_3SiNa$  [M+Na]: 357.1862, found: 357.1865



**Ketoester 2.108.** An  $Et_2O$  (15 mL) solution of  $i\text{-Pr}_2\text{NH}$  (0.44 mL, 3.14 mmol) was cooled to  $-78$  °C and treated dropwise with  $n\text{-BuLi}$  (1.16 mL of a 2.44 M solution in hexanes, 2.84 mmol), at which point the mixture was warmed to  $0$  °C. After 10 minutes, the LDA solution was cooled back to  $-78$  °C, and a solution of ketone **2.85** (529 mg, 1.35 mmol) in  $Et_2O$  (4 mL) was added dropwise with stirring. The mixture was maintained for 30 minutes at the same temperature, at which point methyl cyanofornate (0.54 mL, 6.77 mmol, freshly distilled over  $CaH_2$  under an atmosphere of  $N_2$ ) was added dropwise to the enolate solution, and the resulting mixture was stirred for 1 h at  $-78$  °C, then 1 h at  $0$  °C. The resulting suspension was stirred vigorously and treated with  $\frac{1}{2}$ -saturated aqueous  $NH_4Cl$  (30 mL). The phases were separated, and the aqueous component was extracted with  $Et_2O$  (2x 30 mL). (**caution: the aqueous waste contains HCN**). The combined organics were washed with brine and dried over anhydrous  $MgSO_4$ , then concentrated under reduced pressure. The crude product was purified by flash column chromatography over silica gel. Elution with 5% v/v  $Et_2O$  in hexanes afforded 405 mg of ketoester **2.108** in moderate purity. The material was recrystallized from hot MeOH to afford, after two crystallizations, 356 mg of ketoester **2.108** as a white solid (64% yield).



$^1H$  NMR (500 MHz,  $CDCl_3$ )

$\delta$ 3.62 (s, 3H)	1.29 (td, $J$ = 13.3, 4.8 Hz, 1H)
3.37 (s, 1H)	1.20 – 1.12 (m, 3H)
2.84 (q, $J$ = 6.7 Hz, 1H)	1.10 (dd, $J$ = 6.3, 3.5 Hz, 18H)
2.55 – 2.43 (m, 2H)	1.02 (d, $J$ = 6.8 Hz, 3H)

1.85 – 1.71 (m, 2H)

0.96 – 0.89 (m, 1H)

1.62 – 1.55 (m, 2H)

0.87 (d, J = 6.8 Hz, 3H)

1.45 – 1.36 (m, 4H)

<sup>13</sup>C NMR (151 MHz, CDCl<sub>3</sub>)

δ 210.6

51.3

22.4

169.8

44.3

18.2

145.4

43.7

15.3

117.8

34.7

13.6

61.8

33.4

8.8

52.9

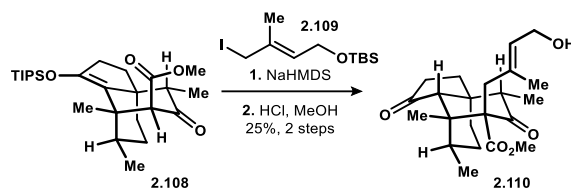
33.3

52.0

29.9

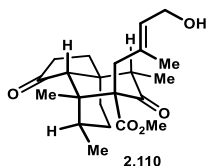
TLC R<sub>f</sub> = 0.58 (20% v/v Et<sub>2</sub>O in hexanes). Modestly UV active.

HRMS (ES<sup>+</sup>) calculated for C<sub>26</sub>H<sub>44</sub>O<sub>4</sub>Si<sub>2</sub>Na [M+Na]: 471.2906, found: 471.2907



**Ketoester 2.110.** A flame-dried flask was charged with ketone **2.108** (11.9 mg, 26.5 μmol) and THF (0.6 mL). The solution was cooled to -78 °C and treated with a NaHMDS (6.4 mg, 35 μmol) solution in THF (0.5 mL). After 30 minutes at the same temperature, (*E*)-((4-iodo-3-methylbut-2-en-1-yl)oxy)(*tert*-butyl)dimethylsilane (**2.109**, 26 mg, 80 μmol, prepared according to the known procedure<sup>90</sup>) was added dropwise. The reaction was stirred for 1 h at -78 °C and 2 h at ambient temperature, then quenched by the addition of ½-saturated aqueous NH<sub>4</sub>Cl (2 mL). The mixture was partitioned between Et<sub>2</sub>O (6 mL) and H<sub>2</sub>O (4 mL). The phases were separated, and the aqueous portion was extracted with Et<sub>2</sub>O (2x 6 mL). The combined organics were washed with brine, dried over anhydrous MgSO<sub>4</sub>, and concentrated under reduced pressure. The crude product was taken up in anhydrous MeOH (1.0 mL), cooled to 0 °C, and treated with concentrated HCl (*ca.* 10 μL). The reaction was monitored by TLC, hydrolysis of the *tert*-butyldimethylsilyl ether was evident within minutes. Once TLC analysis indicated complete hydrolysis (*ca.* 1 h), solid NaHCO<sub>3</sub> was added to the mixture with stirring. Following dilution with EtOAc (2 mL), anhydrous MgSO<sub>4</sub> was added, and the mixture was filtered over celite. The flask and filter cake were washed thoroughly with EtOAc. The organics were concentrated, and the resulting crude product was purified by flash column chromatography over silica gel. Elution with

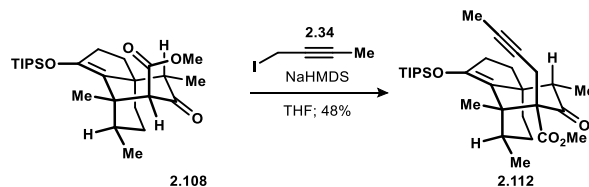
50-80% v/v EtOAc in pentane afforded 2.9 mg of the hydroxydione **2.110** as a colorless oil (29%, 2 steps).



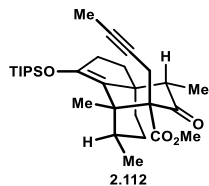
<sup>1</sup>H NMR (500 MHz, CDCl<sub>3</sub>)

δ 5.31 (t, J = 6.8 Hz, 1H)	1.77 (dtd, J = 14.7, 7.4, 3.2 Hz, 1H)
4.04 (qd, J = 12.4, 6.8 Hz, 2H)	1.72 – 1.67 (m, 1H)
3.71 (s, 3H)	1.63 – 1.57 (m, 1H) – overlaps with H <sub>2</sub> O
3.21 (d, J = 13.4 Hz, 1H)	1.56 – 1.51 (m, 2H)
2.45 (s, 1H)	1.49 (d, J = 6.9 Hz, 6H)
2.42 – 2.27 (m, 2H)	1.35 – 1.29 (m, 1H)
2.23 (d, J = 13.5 Hz, 1H)	1.17 (td, J = 13.9, 5.2 Hz, 1H)
2.21 – 2.15 (m, 1H)	1.08 (d, J = 6.6 Hz, 3H)
1.86 (ddd, J = 12.5, 8.7, 1.8 Hz, 1H)	0.75 (d, J = 7.3 Hz, 3H)

TLC R<sub>f</sub> = 0.58 (100% EtOAc). Modestly UV active.



**Alkyne 2.112.** A flame-dried flask was charged with ketoester **2.108** (356 mg, 0.79 mmol) and THF (6 mL), cooled to 0 °C, and treated with a THF (2 mL) solution of NaHMDS (138 mg, 0.75 mmol) over 4 minutes. After 15 minutes, 1-iodobut-2-yne **11** (0.16 mL, 1.59 mmol, prepared according to the known method<sup>8</sup> and distilled over CaH<sub>2</sub>) was added dropwise. The reaction was allowed to gradually warm to ambient temperature and maintained for 18 h, then partitioned between ½-saturated aqueous NH<sub>4</sub>Cl (20 mL) and Et<sub>2</sub>O (20 mL). The phases were separated, and the aqueous portion was extracted with Et<sub>2</sub>O (2x 20 mL). The combined organics were washed with brine, dried over anhydrous MgSO<sub>4</sub>, and concentrated under reduced pressure. The crude product was purified by flash column chromatography over silica gel. Elution with 14-25% Et<sub>2</sub>O in pentane furnished 87 mg of recovered ketoester **2.108** (24% recovery) alongside 189 mg of alkyne **2.112** as a white solid (48% yield).



<sup>1</sup>H NMR (500 MHz, CDCl<sub>3</sub>)

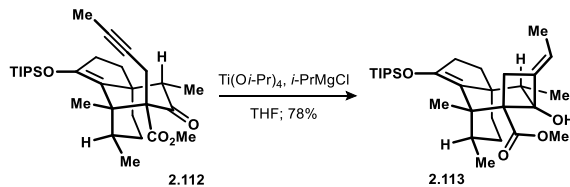
δ 3.73 (s, 3H)	1.45 (s, 3H)
3.27 (dq, J = 16.3, 2.5 Hz, 1H)	1.42 – 1.36 (m, 1H)
2.60 (dq, J = 16.6, 2.6 Hz, 1H)	1.29 – 1.23 (m, 1H) – overlaps with grease
2.51 – 2.40 (m, 2H)	1.18 – 1.12 (m, 3H)
2.28 (q, J = 6.6 Hz, 1H)	1.10 (d, J = 6.0 Hz, 18H)
1.90 (ddd, J = 13.1, 3.9, 2.4 Hz, 1H)	1.07 (d, J = 6.7 Hz, 3H)
1.75 – 1.65 (m, 5H)	0.79 (d, J = 7.3 Hz, 3H)
1.56 – 1.46 (m, 2H)	

<sup>13</sup>C NMR (151 MHz, CDCl<sub>3</sub>)

δ 207.2	51.8	26.8
170.9	50.5	20.0
145.2	48.6	18.3
119.5	46.4	18.3
79.7	35.5	15.3
74.0	33.2	13.6
65.7	33.2	9.3
51.9	28.9	3.9

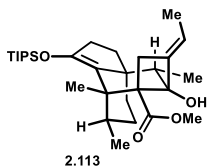
TLC R<sub>f</sub> = 0.51 (20% v/v EtOAc in hexanes). Modestly UV active.

HRMS (ES<sup>+</sup>) calculated for C<sub>30</sub>H<sub>48</sub>O<sub>4</sub>Si<sub>2</sub>H [M+H]: 501.3400, found: 501.3388



**Cyclobutanol 2.113.** A solution of (*i*-PrO)<sub>4</sub>Ti (0.14 mL, 0.473 mmol) in THF (3 mL) was cooled to -78 °C and treated dropwise with a solution of *i*-PrMgCl (0.48 mL of a 2.0 M solution in THF, 0.96 mmol). After 5 minutes, a solution of alkyne **2.112** (157 mg, 0.313 mmol) in THF (4 mL) was added dropwise to the yellow solution. After 30 minutes, the reaction was warmed to 0 °C and it soon adopted a red-brown coloration. After 30 minutes, the reaction was quenched at 0

°C by the introduction of aqueous 1 N HCl (7 mL) with stirring for 10 minutes. The biphasic mixture was with Et<sub>2</sub>O (20 mL) and additional 1 N HCl (13 mL), and the phases were separated. The aqueous component was extracted with Et<sub>2</sub>O (2x 20 mL). The combined organics were washed with saturated aqueous NaHCO<sub>3</sub> (20 mL) and brine, dried over anhydrous MgSO<sub>4</sub>, and concentrated under reduced pressure. The crude product was purified by flash column chromatography over silica gel. Elution with 3% v/v Et<sub>2</sub>O in pentane afforded 122 mg of cyclobutanol **2.113** as a white solid (78% yield).



<sup>1</sup>H NMR (600 MHz, CDCl<sub>3</sub>)

δ 6.01 (s, 1H)	1.61 – 1.56 (m, 2H)
5.37 (qt, J = 6.7, 2.2 Hz, 1H)	1.53 (s, 3H)
3.70 (s, 3H)	1.48 (d, J = 6.7 Hz, 3H)
2.61 – 2.52 (m, 2H)	1.39 – 1.30 (m, 2H)
2.41 – 2.33 (m, 2H)	1.19 – 1.13 (m, 4H)
2.22 (qd, J = 13.4, 5.1 Hz, 1H)	1.10 (d, J = 5.9 Hz, 18H)
2.01 – 1.94 (m, 1H)	0.96 (d, J = 7.1 Hz, 3H)
1.72 (q, J = 7.1 Hz, 1H)	0.72 (d, J = 7.3 Hz, 3H)

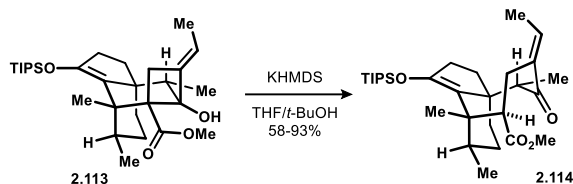
<sup>13</sup>C NMR (126 MHz, CDCl<sub>3</sub>)

δ 180.5	47.7	29.3
145.8	47.2	20.1
143.7	45.1	18.3
122.1	43.4	15.6
110.1	33.9	13.7
79.9	33.6	13.0
58.3	33.4	8.5
51.8	33.3	

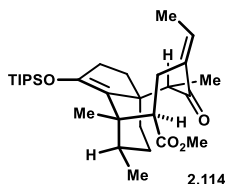
TLC R<sub>f</sub> = 0.52 (10% v/v Et<sub>2</sub>O in hexanes). Modestly UV active.

HRMS (ES<sup>+</sup>) calculated for C<sub>30</sub>H<sub>50</sub>O<sub>4</sub>SiNa [M+Na]: 525.3376, found: 525.3381





**Cyclooctanone 2.114.** A solution of cyclobutanol **2.113** (11.4 mg, 22.7  $\mu\text{mol}$ ) in THF (1.2 mL) and *t*-BuOH (0.2 mL) was cooled to 0 °C and treated dropwise with KHMDS (50  $\mu\text{L}$  of a 0.53 M solution in toluene, 27  $\mu\text{mol}$ ). After 1 h, the reaction was stirred vigorously and quenched by the addition of  $\frac{1}{2}$ -saturated aqueous  $\text{NH}_4\text{Cl}$  (2 mL). The mixture was diluted with  $\text{H}_2\text{O}$  (4 mL) and  $\text{Et}_2\text{O}$  (6 mL), then the phases separated. The aqueous component was extracted with  $\text{Et}_2\text{O}$  (2x 6 mL). The combined organics were washed with brine, dried over anhydrous  $\text{MgSO}_4$ , and concentrated under reduced pressure. The crude product was purified by flash column chromatography over silica gel. Elution with 10% v/v  $\text{Et}_2\text{O}$  in pentane afforded 10.6 mg of cyclooctanone **2.114** as a colorless oil (93% yield). Some  $^{13}\text{C}$  NMR signals were absent, but visible by HMBC.



$^1\text{H}$  NMR (600 MHz,  $\text{CDCl}_3$ )

$\delta$  5.44 (q,  $J = 6.8, 6.4$  Hz, 1H)

3.66 (s, 3H)

3.27 (dd,  $J = 13.4, 3.6$  Hz, 1H)

3.15 (q,  $J = 6.5$  Hz, 1H)

2.85 (t,  $J = 13.7$  Hz, 1H)

2.70 – 2.64 (m, 1H)

2.52 (ddd,  $J = 15.9, 10.9, 5.5$  Hz, 1H)

2.05 – 1.93 (m, 3H)

1.68 (d,  $J = 6.8$  Hz, 3H)

1.47 (s, 3H)

1.41 – 1.34 (m, 2H)

1.29 (q,  $J = 5.0$  Hz, 1H)

1.19 – 1.15 (m, 4H)

1.11 (dt,  $J = 6.2, 2.9$  Hz, 24H)

1.03 – 0.99 (m, 1H)

$^{13}\text{C}$  NMR (151 MHz,  $\text{CDCl}_3$ )

$\delta$  175.4

51.3

18.4

150.2

50.7

18.3

145.6

41.4

17.8

124.4

39.7

17.2

123.6

32.4

15.4

66.0

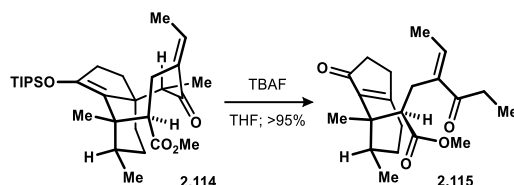
31.8

13.7

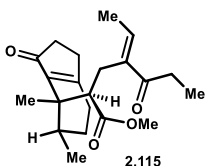
53.4	28.7	13.2
53.2	18.4	11.7

TLC R<sub>f</sub> = 0.41 (10% v/v EtOAc in hexanes). Modestly UV active.

HRMS (ES+) calculated for C<sub>30</sub>H<sub>50</sub>O<sub>4</sub>SiH [M+H]: 503.3557, found: 503.3552



**Tetrahydroindanone 2.115.** A solution of cyclooctanone **2.114** (7.0 mg, 13.9 μmol) in THF (0.6 mL) was cooled to 0 °C and treated dropwise with TBAF (50 μL of a 1.0 M solution in toluene, 50 μmol). After 15 min, the reaction was stirred vigorously and quenched by the addition of ½-saturated aqueous NH<sub>4</sub>Cl (2 mL). The mixture was diluted with H<sub>2</sub>O (4 mL) and Et<sub>2</sub>O (6 mL), then the phases separated. The aqueous component was extracted with Et<sub>2</sub>O (2x 6 mL). The combined organics were washed with brine, dried over anhydrous MgSO<sub>4</sub>, and concentrated under reduced pressure. The crude product was purified by flash column chromatography over silica gel. Elution with 30% v/v EtOAc in pentane afforded 4.6 mg of enone **2.115** as a colorless oil (95% yield).



<sup>1</sup>H NMR (600 MHz, CDCl<sub>3</sub>)

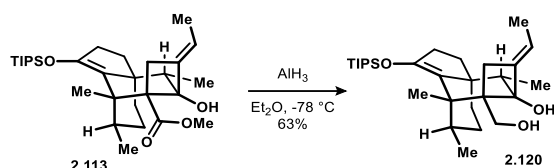
δ 6.69 (q, J = 7.0 Hz, 1H)	1.75 (dd, J = 7.0, 0.9 Hz, 3H)
3.43 (s, 3H)	1.54 (dd, J = 6.9, 3.5 Hz, 1H)
2.84 – 2.72 (m, 3H)	1.51 (s, 3H)
2.71 – 2.51 (m, 2H)	1.36 – 1.30 (m, 1H)
2.50 – 2.36 (m, 4H)	1.09 (d, J = 6.9 Hz, 3H)
2.29 (dd, J = 7.6, 2.5 Hz, 2H)	1.07 (t, J = 7.3 Hz, 3H)

<sup>13</sup>C NMR (151 MHz, CDCl<sub>3</sub>)

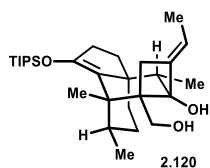
δ 209.0	50.9	29.0
202.3	48.6	26.6
175.9	42.2	26.6
175.5	40.5	22.2

141.6	35.6	15.7
140.6	30.6	14.9
139.1	29.6	9.0

TLC  $R_f$  = 0.47 (50% v/v EtOAc in hexanes). UV active.



**Diol 2.120.** A dry Schlenk flask was charged with  $\text{AlCl}_3$  (38.8 mg, 0.291 mmol, stored in a dry glovebox) and  $\text{Et}_2\text{O}$  (2.0 mL). The solution was cooled to 0 °C and treated with  $\text{LiAlH}_4$  (0.22 mL of a 4.0 M solution in  $\text{Et}_2\text{O}$ , 0.873 mmol), leading to immediate formation of a white precipitate. The suspension was stirred for 15 minutes, then cooled to -78 °C. A solution of cyclobutanol **2.113** (60.0 mg, 0.120 mmol) in  $\text{Et}_2\text{O}$  (1.0 mL) was added dropwise. The reaction was maintained at the same temperature for 3 h, then warmed to 0 °C for 15 minutes, stirred vigorously and treated with saturated aqueous Rochelle's salt (3 mL). The emulsion was warmed to ambient temperature and stirred vigorously for 3 h, then diluted with  $\text{H}_2\text{O}$  (6 mL) and  $\text{Et}_2\text{O}$  (6 mL). The phases were separated, and the aqueous portion was extracted with  $\text{Et}_2\text{O}$  (2x 9 mL). The combined organics were washed with brine, dried over anhydrous  $\text{MgSO}_4$ , and concentrated under reduced pressure. The crude product was purified by flash column chromatography over silica gel. Elution with 25% v/v  $\text{Et}_2\text{O}$  in pentane afforded 35.6 mg of diol **2.120** as a white solid (63%).



$^1\text{H}$  NMR (600 MHz,  $\text{CDCl}_3$ )

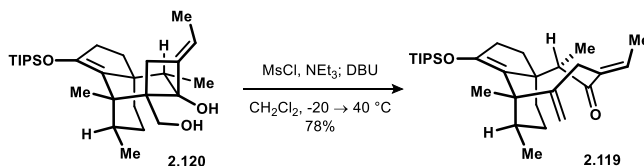
$\delta$ 5.28 (qt, $J$ = 6.7, 2.4 Hz, 1H)	1.52 (dt, $J$ = 6.8, 1.5 Hz, 3H)
4.11 (d, $J$ = 11.3 Hz, 1H)	1.35 – 1.32 (m, 1H)
3.81 (d, $J$ = 11.2 Hz, 1H)	1.30 (s, 3H)
2.91 (s, 1H)	1.16 – 1.12 (m, 3H)
2.41 – 2.28 (m, 4H)	1.09 (d, $J$ = 6.1 Hz, 18H)
1.95 – 1.85 (m, 3H)	0.97 (d, $J$ = 7.3 Hz, 3H)
1.57 (ddd, $J$ = 12.0, 9.2, 4.7 Hz, 3H)	0.95 (d, $J$ = 7.4 Hz, 3H)

$^{13}\text{C}$  NMR (151 MHz,  $\text{CDCl}_3$ )

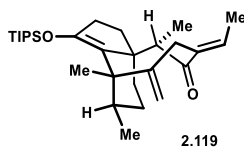
$\delta$ 150.3	47.5	18.6
142.0	44.4	18.3
123.6	43.6	18.3
108.8	34.6	18.0
78.5	34.2	13.7
65.0	33.3	13.0
55.3	29.4	8.6
48.0	29.1	

TLC  $R_f$  = 0.49 (50% v/v Et<sub>2</sub>O in hexanes). Not UV active.

HRMS (ES+) calculated for C<sub>29</sub>H<sub>50</sub>O<sub>3</sub>SiNa [M+Na]: 497.3427, found: 497.3421



**Enone 2.119.** A solution of diol **2.120** (39.0 mg, 82  $\mu$ mol) in CH<sub>2</sub>Cl<sub>2</sub> (3 mL) at -20 °C was treated with Et<sub>3</sub>N (0.20 mL, 1.44 mmol) and MsCl (30  $\mu$ L, 0.388 mmol). After 1 h, the reaction was treated with DBU (0.10 mL, 0.67 mmol) and transferred to a 30 °C bath. The reaction was maintained at the same temperature for 1.5 h, then treated with an additional portion of DBU (0.10 mL, 0.67 mmol). After 45 minutes, the mixture was cooled to ambient temperature and partitioned between saturated aqueous NaHCO<sub>3</sub> (9 mL) and CH<sub>2</sub>Cl<sub>2</sub> (6 mL). The phases were separated, and the aqueous portion was extracted with CH<sub>2</sub>Cl<sub>2</sub> (2x 9 mL). The combined organics were washed with brine, dried over anhydrous MgSO<sub>4</sub>, and concentrated under reduced pressure. The crude product was purified by flash column chromatography over silica gel. Elution with 4-6% v/v Et<sub>2</sub>O in pentane afforded 29.4 mg of enone **2.119** as a white solid (78%).



<sup>1</sup>H NMR (500 MHz, CDCl<sub>3</sub>)

$\delta$ 6.63 (q, J = 7.2 Hz, 1H)	2.09 – 2.00 (m, 2H)
5.06 (d, J = 1.3 Hz, 1H)	1.80 (d, J = 7.2 Hz, 3H)
4.82 (d, J = 1.5 Hz, 1H)	1.59 (s, 3H)
3.33 (d, J = 13.9 Hz, 1H)	1.47 – 1.28 (m, 2H)

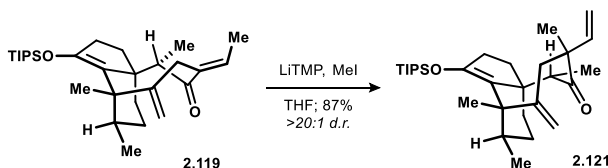
3.15 (q, $J = 6.6$ Hz, 1H)	1.19 – 1.11 (m, 4H)
3.09 (d, $J = 14.0$ Hz, 1H)	1.09 (d, $J = 6.5$ Hz, 21H)
2.52 (ddd, $J = 15.1, 11.4, 5.3$ Hz, 1H)	1.06 – 1.01 (m, 2H)
2.19 (dd, $J = 11.8, 5.2$ Hz, 1H)	0.74 (d, $J = 6.8$ Hz, 3H)

$^{13}\text{C}$  NMR (126 MHz,  $\text{CDCl}_3$ )

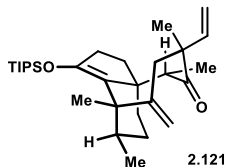
$\delta$ 208.7	49.7	30.6
150.3	45.0	18.3
150.0	41.5	18.2
139.5	40.4	17.5
134.9	36.9	15.1
126.2	33.7	14.3
114.8	32.2	13.6
51.5	31.0	

TLC  $R_f = 0.55$  (10% v/v  $\text{Et}_2\text{O}$  in hexanes). UV active.

HRMS (ES+) calculated for  $\text{C}_{29}\text{H}_{48}\text{O}_2\text{SiH}$  [M+H]: 457.3502, found: 457.3506



**Ketone 2.121.** A solution of LiTMP was prepared: 2,2,6,6-tetramethylpiperidine (TMP, 185  $\mu\text{L}$ , 1.1 mmol, freshly distilled over  $\text{CaH}_2$  under  $\text{N}_2$  atmosphere) in THF (1.40 mL) was cooled to 0  $^\circ\text{C}$  and treated with *n*-BuLi (0.41 mL of a 2.42 M solution in hexanes, 1.0 mmol), and stirred for 10 minutes before use. A separate flask was charged with enone **2.119** (6.0 mg, 13  $\mu\text{mol}$ ) and THF (0.6 mL), and cooled to -78  $^\circ\text{C}$ . The solution was treated dropwise with the freshly prepared LiTMP solution (0.12 mL of a 0.5 M solution in THF / hexanes, 60  $\mu\text{mol}$ ). After 30 minutes at the same temperature, iodomethane (20  $\mu\text{L}$ , 0.32 mmol, distilled over  $\text{CaH}_2$  under  $\text{N}_2$  atmosphere) was added dropwise. The reaction was stirred for 1 h at -78  $^\circ\text{C}$  and 30 minutes at 0  $^\circ\text{C}$ , then treated with saturated aqueous  $\text{NaHCO}_3$  (2 mL). The mixture was diluted with  $\text{H}_2\text{O}$  (4 mL) and  $\text{Et}_2\text{O}$  (6 mL), and the phases were separated. The aqueous portion was extracted with  $\text{Et}_2\text{O}$  (2x 6 mL). The combined organics were washed with brine, dried over anhydrous  $\text{MgSO}_4$ , and concentrated under reduced pressure. The crude product was purified by flash column chromatography over silica gel. Elution with 5% v/v  $\text{Et}_2\text{O}$  in pentane afforded 5.4 mg of the ketone **2.121** as a colorless oil (87% yield). The presence of rotamers led to broadening of  $^1\text{H}$  NMR signals and some  $^{13}\text{C}$  NMR signals to be absent.

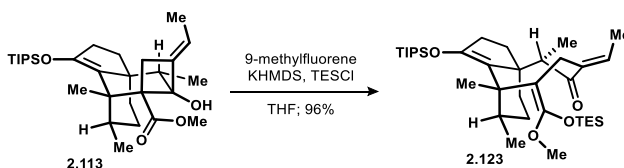


<sup>1</sup>H NMR (600 MHz, CDCl<sub>3</sub>)

δ 6.24 (dd, J = 17.8, 11.0 Hz, 1H)	1.57 (s, 3H)
5.33 – 5.12 (m, 1H)	1.42 – 1.34 (m, 2H)
5.09 – 4.95 (m, 3H)	1.20 – 1.13 (m, 7H)
3.13 (q, J = 6.7 Hz, 1H)	1.11 (t, J = 6.3 Hz, 18H)
3.02 (d, J = 13.6 Hz, 1H)	1.07 – 1.01 (m, 4H)
2.53 (ddd, J = 15.1, 11.5, 5.6 Hz, 1H)	0.97 (d, J = 7.0 Hz, 3H)
2.20 – 2.12 (m, 2H)	0.93 – 0.83 (m, 1H)
2.12 – 1.94 (m, 2H)	

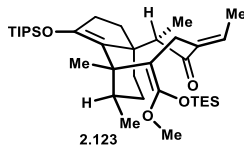
TLC R<sub>f</sub> = 0.59 (10% v/v Et<sub>2</sub>O in hexanes). Not UV active.

HRMS (ES<sup>+</sup>) calculated for C<sub>30</sub>H<sub>50</sub>O<sub>2</sub>SiH [M+H]: 471.3658, found: 471.3637



**Enone 2.123.** A flame-dried flask was charged with an over-sized magnetic stir bar, 9-methylfluorene (1.3 mg, 7 μmol, prepared according to the known method<sup>9</sup> and recrystallized from MeOH), cyclobutanol **2.113** (34.9 mg, 69 μmol), and THF (1.5 mL), and cooled to -20 °C. Chlorotriethylsilane (50 μL, 0.30 mmol, freshly distilled over CaH<sub>2</sub> under N<sub>2</sub> atmosphere) was added. The solution was treated with KHMDS (0.53 M solution in PhMe) until a pink-orange coloration indicating the equivalence point was persistent for >50 seconds (final volume: 0.16 mL). The reaction was warmed to 0 °C and stirred for 1 h, then saturated aqueous NaHCO<sub>3</sub> (6 mL) was added with vigorous stirring. (**note: an efficient quench is essential to obtain the product in high yield**). After 15 minutes, the mixture was partitioned between saturated aqueous NaHCO<sub>3</sub> (9 mL), and Et<sub>2</sub>O (15 mL) were added, and the phases separated. The aqueous portion was extracted with Et<sub>2</sub>O (2x 15 mL). The combined organics were washed with brine, dried over anhydrous MgSO<sub>4</sub>, and concentrated under reduced pressure. The crude product was purified by flash column chromatography over silica gel. Elution with 5-6% v/v Et<sub>2</sub>O in pentane furnished 41.0 mg of the enone **2.123** as a colorless oil as a 14:1 mixture of ketene

silyl acetal stereoisomers (96% yield). Peak-broadening was observed in the  $^1\text{H}$  NMR of **2.123** and many  $^{13}\text{C}$  NMR signals were absent when the spectra were collected at 25 °C. Consequently, NMR data were collected at 50 °C.



$^1\text{H}$  NMR (600 MHz,  $\text{C}_6\text{D}_6$ , 50 °C)

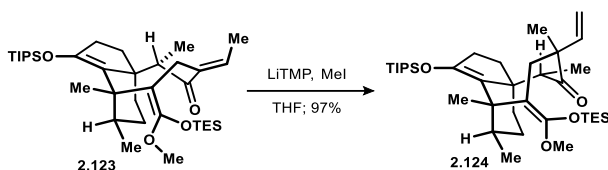
$\delta$ 6.87 (q, $J = 7.1$ Hz, 1H)	1.84 (d, $J = 7.3$ Hz, 3H)
3.56 (d, $J = 14.5$ Hz, 1H)	1.62 – 1.56 (m, 1H)
3.28 (s, 3H)	1.52 – 1.46 (m, 1H)
3.17 (q, $J = 6.6$ Hz, 1H)	1.41 – 1.28 (m, 3H)
3.10 (d, $J = 14.5$ Hz, 1H)	1.24 (d, $J = 6.6$ Hz, 3H)
2.45 (ddd, $J = 14.8, 11.7, 5.3$ Hz, 1H)	1.20 – 1.11 (m, 21H)
2.24 (ddd, $J = 13.6, 6.1, 3.7$ Hz, 1H)	1.04 (t, $J = 7.9$ Hz, 9H)
2.12 (dd, $J = 11.6, 5.2$ Hz, 1H)	1.00 (d, $J = 6.9$ Hz, 3H)
2.02 (s, 3H)	0.79 (q, $J = 7.8$ Hz, 6H)
1.94 (dd, $J = 14.8, 7.5$ Hz, 1H)	

$^{13}\text{C}$  NMR (151 MHz,  $\text{C}_6\text{D}_6$ , 50 °C)

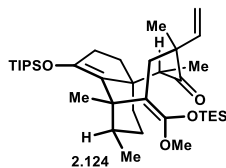
$\delta$ 206.5	49.4	18.5
150.8	44.8	18.5
149.8	42.6	18.2
142.6	40.5	15.7
134.5	32.6	14.7
129.2	31.6	14.1
100.9	31.5	7.0
55.2	30.3	5.5
51.0	28.8	

TLC  $R_f = 0.51$  (10% v/v  $\text{Et}_2\text{O}$  in hexanes). UV active.

HRMS (ES+) calculated for  $\text{C}_{36}\text{H}_{64}\text{O}_4\text{Si}_2\text{H}$  [M+H]: 617.4421, found: 617.4401



**Ketene silyl acetal 2.124.** A solution of LiTMP was prepared: 2,2,6,6-tetramethylpiperidine (TMP, 185  $\mu\text{L}$ , 1.1 mmol, freshly distilled over  $\text{CaH}_2$  under  $\text{N}_2$  atmosphere) in THF (1.40 mL) was cooled to 0  $^\circ\text{C}$  and treated with *n*-BuLi (0.41 mL of a 2.42 M solution in hexanes, 1.0 mmol), and stirred for 10 minutes before use. A separate flask was charged with enone **2.123** (41.0 mg, 66.0  $\mu\text{mol}$ ) and THF (1.5 mL), and cooled to -78  $^\circ\text{C}$ . The solution was treated dropwise with the freshly prepared LiTMP solution (0.40 mL of a 0.5 M solution in THF / hexanes, 0.20 mmol). After 30 minutes at the same temperature, iodomethane (40  $\mu\text{L}$ , 0.64 mmol, distilled over  $\text{CaH}_2$  under  $\text{N}_2$  atmosphere) was added dropwise. The reaction was stirred for 1 h at -78  $^\circ\text{C}$  and 30 minutes at 0  $^\circ\text{C}$ , then treated with saturated aqueous  $\text{NaHCO}_3$  (8 mL). The mixture was diluted with  $\text{H}_2\text{O}$  (4 mL) and  $\text{Et}_2\text{O}$  (12 mL), and the phases were separated. The aqueous portion was extracted with  $\text{Et}_2\text{O}$  (2x 12 mL). The combined organics were washed with brine, dried over anhydrous  $\text{MgSO}_4$ , and concentrated under reduced pressure. The crude product was purified by flash column chromatography over silica gel. Elution with 5% v/v  $\text{Et}_2\text{O}$  in pentane afforded 40.4 mg of the ketene silyl acetal **2.124** as a colorless oil (97% yield).



$^1\text{H}$  NMR (600 MHz,  $\text{C}_6\text{D}_6$ , 50  $^\circ\text{C}$ )

$\delta$ 6.62 (dd, $J = 17.7, 11.0$ Hz, 1H)	2.07 – 1.94 (m, 5H)
5.23 (dd, $J = 11.0, 1.6$ Hz, 1H)	1.90 – 1.78 (m, 1H)
5.10 (dd, $J = 17.7, 1.7$ Hz, 1H)	1.56 – 1.27 (m, 4H)
3.30 (s, 3H)	1.21 (s, 3H)
3.16 (q, $J = 6.7$ Hz, 1H)	1.18 – 1.11 (m, 24H)
2.81 (d, $J = 14.4$ Hz, 1H)	1.09 (d, $J = 7.3$ Hz, 4H)
2.49 (d, $J = 14.3$ Hz, 1H)	1.02 (t, $J = 7.9$ Hz, 9H)
2.48 – 2.37 (m, 2H)	0.74 (q, $J = 7.9$ Hz, 6H)

$^{13}\text{C}$  NMR (151 MHz,  $\text{C}_6\text{D}_6$ , 50  $^\circ\text{C}$ )

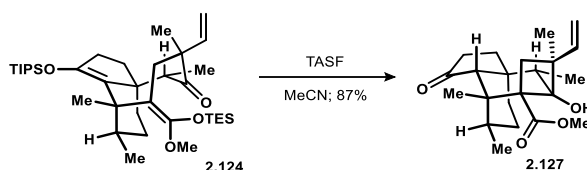
$\delta$ 217.7	51.8	23.7
152.47	46.1	18.7
148.9	45.0	18.4



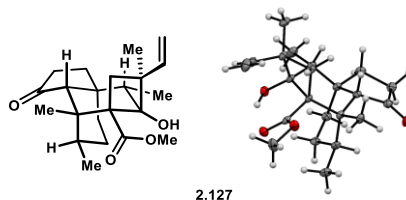
143.8	42.4	18.4
128.9	40.0	16.4
111.3	38.5	14.0
97.6	32.5	6.9
55.1	30.2	5.7
54.8	29.3	

TLC  $R_f$  = 0.60 (10% v/v Et<sub>2</sub>O in hexanes). Not UV active.

HRMS (ES+) calculated for C<sub>37</sub>H<sub>66</sub>O<sub>4</sub>Si<sub>2</sub>H [M+H]: 631.4578, found: 631.4604



**Cyclobutanol 2.127.** A solution of ketene silyl acetal **2.124** (13.0 mg, 20.6  $\mu$ mol) in THF (0.5 mL) was cooled to 0 °C and treated dropwise with a solution of TASF (17 mg, 61.8  $\mu$ mol) in MeCN (0.7 mL). After 1 h, the reaction was quenched by the addition of aqueous 1 N HCl (2 mL) with vigorous stirring. The mixture was warmed to ambient temperature, then diluted with Et<sub>2</sub>O (6 mL) and additional 1 N HCl (4 mL), and the phases were separated. The aqueous portion was extracted with Et<sub>2</sub>O (2x 6 mL). The combined organics were washed with brine, dried over anhydrous MgSO<sub>4</sub>, and concentrated under reduced pressure. The crude product was purified by flash column chromatography over silica gel. Elution with 4% v/v Et<sub>2</sub>O in pentane afforded 6.5 mg of the cyclobutanol **2.127** as a white solid (87% yield). Some signals were absent from the <sup>13</sup>C NMR spectra due to the presence of rotamers; HMBC revealed the missing <sup>13</sup>C signals. Crystals suitable for X-ray diffraction analysis were grown by slow evaporation of a pentane solution of 2 mg of cyclobutanol **2.127**.



<sup>1</sup>H NMR (600 MHz, CDCl<sub>3</sub>, 50 °C)

$\delta$  6.23 – 5.97 (m, 2H)

5.24 – 4.92 (m, 2H)

3.60 (s, 3H)

2.38 (d, J = 12.2 Hz, 1H)

1.75 (d, J = 1.1 Hz, 1H)

1.68 (dtt, J = 14.3, 7.2

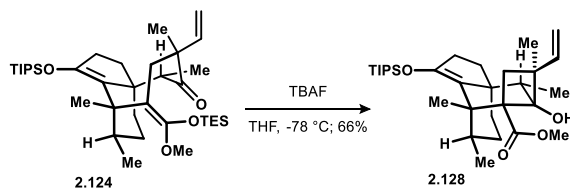
3.6 Hz, 1H)

1.39 (dt, J = 12.7, 10.0 Hz, 1H)

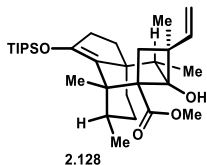
2.30 – 2.22 (m, 2H)		1.35 (s, 3H)
2.07 (ddt, J = 26.2, 13.8, 6.4 Hz, 2H)		1.26 – 1.22 (m, 1H)
1.91 – 1.85 (m, 2H)		1.12 – 1.03 (m, 7H)
1.79 (ddd, J = 12.7, 7.3, 3.5 Hz, 1H)		0.67 (d, J = 7.3 Hz, 3H)
13C NMR (151 MHz, CDCl <sub>3</sub> , 50 °C)		
δ 218.0	42.8	25.9
142.9	42.3	24.2
113.0	36.1	18.0
64.2	33.4	14.9
52.0	33.1	9.4
48.5	29.9	
48.0	27.6	

TLC R<sub>f</sub> = 0.39 (20% v/v Et<sub>2</sub>O in hexanes). Not UV active.

HRMS (ES<sup>+</sup>) calculated for C<sub>31</sub>H<sub>52</sub>O<sub>4</sub>SiNa [M+Na]: 383.2198, found: 383.2206



**Cyclobutanol 2.128.** A solution of ketene silyl acetal **2.124** (13.0 mg, 20.6 μmol) in THF (0.7 mL) was cooled to -78 °C and treated dropwise with tetrabutylammonium fluoride (50 μL of a 1.0 M solution in THF, 50 μmol). After 2 minutes, the reaction was quenched by the addition of aqueous 1 N HCl (2 mL) with vigorous stirring. The mixture was warmed to ambient temperature, then diluted with Et<sub>2</sub>O (6 mL) and additional 1 N HCl (4 mL), and the phases were separated. The aqueous portion was extracted with Et<sub>2</sub>O (2x 6 mL). The combined organics were washed with brine, dried over anhydrous MgSO<sub>4</sub>, and concentrated under reduced pressure. The crude product was purified by flash column chromatography over silica gel. Elution with 4% v/v Et<sub>2</sub>O in pentane afforded 7.0 mg of the cyclobutanol **2.128** as a white solid (66% yield). Some signals were absent from the <sup>13</sup>C NMR spectra due to the presence of rotamers; HMBC revealed the missing <sup>13</sup>C signals.



<sup>1</sup>H NMR (600 MHz, CDCl<sub>3</sub>)

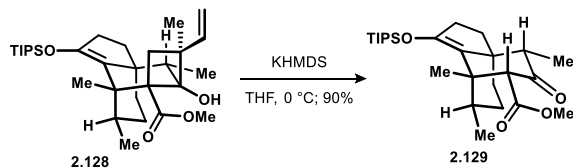
δ 6.17 (dd, J = 17.6, 10.8 Hz, 2H)	1.60 – 1.53 (m, 1H) – overlaps with H <sub>2</sub> O
5.09 – 4.99 (m, 2H)	1.44 – 1.36 (m, 4H)
3.58 (s, 3H)	1.30 – 1.25 (m, 1H)
2.45 – 2.35 (m, 3H)	1.19 – 1.13 (m, 4H)
2.14 (qd, J = 13.4, 5.1 Hz, 1H)	1.11 (d, J = 6.1 Hz, 18H)
2.03 (ddd, J = 13.2, 5.1, 1.7 Hz, 1H)	0.98 (s, 3H)
1.97 (q, J = 7.0 Hz, 1H)	0.97 (d, J = 7.0 Hz, 3H)
1.74 – 1.64 (m, 2H)	0.66 (d, J = 7.4 Hz, 3H)

<sup>13</sup>C NMR (151 MHz, CDCl<sub>3</sub>)

δ 143.2	45.5	24.0
142.8	44.2	19.3
122.9	43.7	18.3
112.7	34.5	18.3
79.7	34.3	15.0
51.8	33.9	13.7
49.1	33.4	9.9
47.5	29.0	

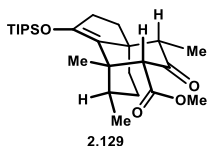
TLC R<sub>f</sub> = 0.51 (10% v/v Et<sub>2</sub>O in hexanes). Modestly UV active.

HRMS (ES<sup>+</sup>) calculated for C<sub>31</sub>H<sub>52</sub>O<sub>4</sub>SiNa [M+Na]: 539.3533, found: 539.3510



**Ketoester 2.129.** A solution cyclobutanol **2.128** (6.9 mg, 13.4 μmol) in THF (0.7 mL) was cooled to 0 °C and treated dropwise with KHMDS (50 μL of a 0.53 M solution in toluene, 26.5 μmol). After 30 minutes, the reaction was quenched by the addition of saturated aqueous NH<sub>4</sub>Cl (2 mL). The mixture was warmed to ambient temperature, then diluted with Et<sub>2</sub>O (6 mL) and H<sub>2</sub>O (5 mL), and the phases were separated. The aqueous portion was extracted with Et<sub>2</sub>O (2x 6 mL). The combined organics were washed with brine, dried over anhydrous MgSO<sub>4</sub>, and

concentrated under reduced pressure. The crude product was purified by flash column chromatography over silica gel. Elution with 12% v/v Et<sub>2</sub>O in pentane afforded 5.4 mg of the ketoester **2.129** as a colorless oil (90% yield). Further support for the identified structure was obtained as follows: treatment of ketoester **2.108** with KHMDS in THF followed by workup with saturated aqueous NH<sub>4</sub>Cl provided a crude product. <sup>1</sup>H NMR analysis of the crude material showed signals for an enolic product that matched the crude NMR taken in the conversion of **2.128** to **2.129**.



<sup>1</sup>H NMR (600 MHz, CDCl<sub>3</sub>)

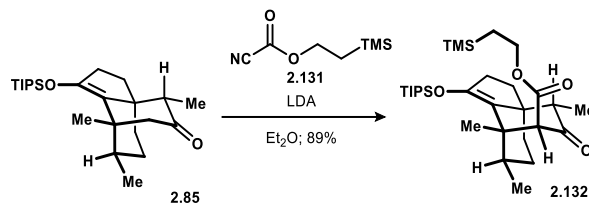
δ 3.70 (s, 3H)	1.49 – 1.43 (m, 1H)
3.44 (d, J = 1.2 Hz, 1H)	1.31 – 1.24 (m, 2H)
2.47 (t, J = 7.8 Hz, 2H)	1.19 – 1.14 (m, 3H)
2.23 (q, J = 6.7 Hz, 1H)	1.11 (d, J = 6.5 Hz, 18H)
1.95 – 1.86 (m, 1H)	1.06 (d, J = 6.8 Hz, 3H)
1.73 – 1.64 (m, 2H)	1.03 (d, J = 7.3 Hz, 3H)
1.58 – 1.54 (m, 4H) – overlaps with H <sub>2</sub> O	

<sup>13</sup>C NMR (151 MHz, CDCl<sub>3</sub>)

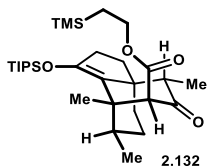
δ 208.4	51.4	23.8
169.5	45.8	18.3
142.7	44.2	16.7
121.7	35.8	13.6
65.5	33.4	9.1
54.5	33.2	
51.6	30.2	

TLC R<sub>f</sub> = 0.43 (20% v/v Et<sub>2</sub>O in hexanes). Modestly UV active.

HRMS (CI+) calculated for C<sub>26</sub>H<sub>44</sub>O<sub>4</sub>Si [M<sup>+</sup>]: 448.3009, found: 448.3025



**Ketoester 2.132.** Cyanofornate **2.131** was prepared as follows: A flame-dried 25 mL round bottom flask was charged with TeocCl (1.34 g, 7.42 mmol, prepared according to the known method<sup>92</sup>), trimethylsilylcyanide (TMSCN, 0.93 mL, 7.42 mmol), and 1,4-diazabicyclo[2.2.2]octane (DABCO, 9.5 mg, 0.08 mmol). The mixture was stirred at ambient temperature for 12 h. In a separate flask, a Et<sub>2</sub>O (10 mL) solution of *i*-Pr<sub>2</sub>NH (0.23 mL, 1.66 mmol) was cooled to -78 °C and treated dropwise with *n*-BuLi (0.61 mL of a 2.50 M solution in hexanes, 1.54 mmol), at which point the mixture was warmed to 0 °C. After 10 minutes, the LDA solution was cooled back to -78 °C, and a solution of ketone **2.85** (500 mg, 1.28 mmol) in Et<sub>2</sub>O (4 mL) was added dropwise with stirring. The mixture was maintained for 30 minutes at the same temperature. Meanwhile, the flask containing the crude cyanofornate **2.131** was fitted with a short-path distillation head. The product was distilled (*ca.* 0.2 mm Hg, 34 °C) from a 50 °C bath into a 0 °C collection flask, affording 749 mg of the known cyanofornate **2.131**<sup>93</sup> (59% yield) as a colorless oil that was not stable upon storage. Cyanofornate **2.131** (0.31 mL, 1.66 mmol) was added dropwise to the separate enolate solution, and the resulting mixture was stirred for 1 h at -78 °C, then 40 minutes at 0 °C. The resulting suspension was stirred vigorously and treated with ½-saturated aqueous NH<sub>4</sub>Cl (30 mL). Et<sub>2</sub>O (16 mL) was added, the phases were separated, and the aqueous component was extracted with Et<sub>2</sub>O (2x 30 mL). **(caution: the aqueous waste contains HCN)**. The combined organics were washed with brine and dried over anhydrous MgSO<sub>4</sub>, then concentrated under reduced pressure. The crude product was purified by flash column chromatography over silica gel. Elution with 4% v/v Et<sub>2</sub>O in pentane afforded 608 mg of ketoester **2.132** (89% yield) as a colorless oil contaminated with 7 mol% (31 mg) of ketone **2.85**. The material was sufficiently pure for use in the subsequent step, and an analytically pure sample of ketoester **2.132** was obtained from a second chromatographic purification of 15 mg of the sample.



<sup>1</sup>H NMR (500 MHz, CDCl<sub>3</sub>)

δ 4.16 – 4.04 (m, 2H)

1.31 – 1.24 (m, 1H)

3.33 (s, 1H)	1.19 – 1.12 (m, 4H)
2.85 (q, J = 6.7 Hz, 1H)	1.10 (dd, J = 6.4, 3.4 Hz, 18H)
2.55 – 2.43 (m, 2H)	1.01 – 0.95 (m, 2H)
1.85 – 1.72 (m, 2H)	0.94 – 0.89 (m, 1H)
1.59 – 1.51 (m, 2H) – overlaps with H <sub>2</sub> O	0.87 (d, J = 6.8 Hz, 3H)
1.62 – 1.52 (m, 2H)	0.02 (s, 9H)

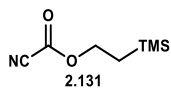
1.39 (m, 4H)

<sup>13</sup>C NMR (151 MHz, CDCl<sub>3</sub>)

δ 210.8	44.3	18.3
169.5	43.7	17.6
145.3	34.8	15.3
118.0	33.5	13.6
63.4	33.3	8.8
62.1	29.9	-1.5
52.8	22.5	
51.2	18.3	

TLC R<sub>f</sub> = 0.44 (10% v/v Et<sub>2</sub>O in hexanes). Modestly UV active.

HRMS (ES<sup>+</sup>) calculated for C<sub>30</sub>H<sub>54</sub>O<sub>4</sub>Si<sub>2</sub>H [M+H]: 535.3639, found: 535.3624



<sup>1</sup>H NMR (500 MHz, CDCl<sub>3</sub>)

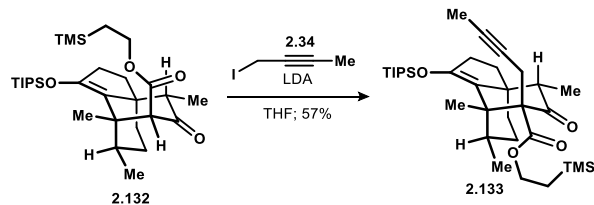
δ 4.49 – 4.38 (m, 2H)

1.18 – 1.08 (m, 2H)

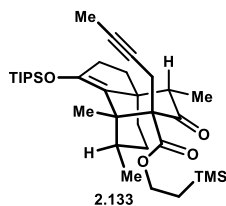
0.07 (s, 9H)

<sup>13</sup>C NMR (126 MHz, CDCl<sub>3</sub>)

δ 144.6	68.3	-1.5
109.6	17.4	



**Ketoester 2.133.** A 0.7 M solution of LDA was prepared: a solution of *i*-Pr<sub>2</sub>NH (0.62 mL, 4.4 mmol) in THF (3.5 mL) at -78 °C was treated with *n*-BuLi (1.6 mL of a 2.50 M solution in hexanes, 4.0 mmol). The mixture was warmed to 0 °C for 10 minutes before use. A separate flame-dried flask was charged with ketoester **2.132** (608 mg, 1.14 mmol) and THF (11 mL), cooled to -78 °C, and treated with the freshly prepared LDA (2.1 mL of a 0.7 M solution in THF / hexanes, 1.48 mmol) over 4 minutes. After 45 minutes, 1-iodobut-2-yne **2.34** (0.57 mL, 5.7 mmol, prepared according to the known method<sup>88</sup> and distilled over CaH<sub>2</sub>) was added dropwise. The reaction was allowed to gradually warm to ambient temperature and maintained for 14 h, then partitioned between ½-saturated aqueous NH<sub>4</sub>Cl (30 mL) and Et<sub>2</sub>O (30 mL). The phases were separated, and the aqueous portion was extracted with Et<sub>2</sub>O (2x 30 mL). The combined organics were washed with brine, dried over anhydrous MgSO<sub>4</sub>, and concentrated under reduced pressure. The crude product was purified by flash column chromatography over silica gel. Elution with 10-14% v/v Et<sub>2</sub>O in pentane furnished 379 mg of alkyne **2.133** as a colorless oil (57% yield).



<sup>1</sup>H NMR (600 MHz, CDCl<sub>3</sub>)

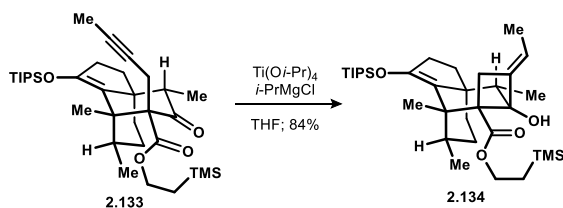
δ 4.31 (ddd, J = 12.5, 10.9, 5.4 Hz, 1H)	1.46 (s, 3H)
4.11 (ddd, J = 12.5, 10.9, 5.3 Hz, 1H)	1.38 (ddt, J = 15.0, 5.2, 2.7 Hz, 1H)
3.25 (dq, J = 16.8, 2.6 Hz, 1H)	1.30 – 1.20 (m, 2H)
2.57 (dq, J = 16.6, 2.5 Hz, 1H)	1.17 – 1.13 (m, 3H)
2.50 – 2.40 (m, 2H)	1.10 (d, J = 6.4 Hz, 18H)
2.28 (q, J = 6.6 Hz, 1H)	1.06 (d, J = 6.7 Hz, 3H)
1.90 (ddd, J = 13.2, 4.0, 2.3 Hz, 1H)	1.05 – 1.00 (m, 1H)
1.74 – 1.65 (m, 5H)	0.84 (d, J = 7.3 Hz, 3H)
1.59 – 1.50 (m, 2H) – overlaps with H <sub>2</sub> O	0.04 (s, 9H)

<sup>13</sup>C NMR (151 MHz, CDCl<sub>3</sub>)

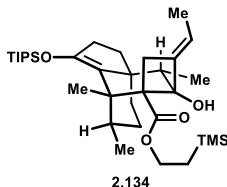
δ 207.0	50.5	18.3
170.4	48.5	18.3
144.9	46.6	17.3
119.7	35.6	15.5
79.5	33.2	13.6
74.3	33.2	9.4
65.6	28.8	3.9
63.1	26.7	-1.4
51.8	20.0	

TLC  $R_f$  = 0.44 (10% v/v Et<sub>2</sub>O in hexanes). Modestly UV active.

HRMS (ES+) calculated for C<sub>34</sub>H<sub>58</sub>O<sub>4</sub>Si<sub>2</sub>H [M+H]: 587.3952, found: 587.3955



**Cyclobutanol 2.134.** A solution of (*i*-PrO)<sub>4</sub>Ti (0.14 mL, 0.473 mmol, distilled at ca. 2 mm Hg before use) in THF (3 mL) was cooled to -78 °C and treated dropwise with a solution of *i*-PrMgCl (0.48 mL of a 2.0 M solution in THF, 0.96 mmol). After 5 minutes, a solution of alkyne **2.133** (175 mg, 0.297 mmol) in THF (4 mL) was added dropwise to the yellow solution. After 40 minutes, the reaction was warmed to 0 °C and the mixture soon developed a red-brown color. After 15 minutes, the reaction was quenched at 0 °C by the addition of aqueous 1 N HCl (4 mL) with stirring for 10 minutes, and then diluted with Et<sub>2</sub>O (12 mL) and additional 1 N HCl (8 mL). The phases were separated, and the aqueous portion was extracted with Et<sub>2</sub>O (2x 12 mL). The organics were washed with saturated aqueous NaHCO<sub>3</sub> and brine, dried over anhydrous MgSO<sub>4</sub>, then concentrated under reduced pressure. The crude product was purified by flash column chromatography over silica gel. Elution with 3% v/v Et<sub>2</sub>O in pentane afforded 147 mg of cyclobutanol **2.134** as a colorless oil (84% yield).



<sup>1</sup>H NMR (500 MHz, CDCl<sub>3</sub>)

δ 6.12 (s, 1H)

1.54 (s, 3H)



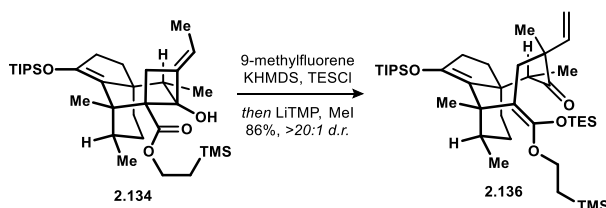
5.37 (qt, J = 6.6, 2.1 Hz, 1H)  
4.23 (td, J = 11.3, 6.3 Hz, 1H)  
4.13 (td, J = 11.4, 5.2 Hz, 1H)  
2.57 (s, 2H)  
2.39 – 2.32 (m, 2H)  
2.24 (qd, J = 13.4, 4.9 Hz, 1H)  
1.97 (dd, J = 13.2, 3.8 Hz, 1H)  
1.72 (q, J = 7.1 Hz, 1H)  
1.62 – 1.55 (m, 2H)  
1.48 (d, J = 6.7 Hz, 3H)  
1.39 – 1.28 (m, 2H)  
1.20 – 1.13 (m, 4H)  
1.11 (d, J = 5.8 Hz, 18H)  
1.08 – 0.98 (m, 2H)  
0.96 (d, J = 7.1 Hz, 3H)  
0.75 (d, J = 7.3 Hz, 3H)  
0.06 (s, 9H)

$^{13}\text{C}$  NMR (126 MHz,  $\text{CDCl}_3$ )

$\delta$ 180.2	47.3	18.3
146.0	45.2	17.3
143.5	43.6	15.8
122.3	33.9	13.7
109.9	33.7	13.0
79.9	33.5	8.5
63.3	33.4	-1.4
58.2	29.4	
47.7	20.2	

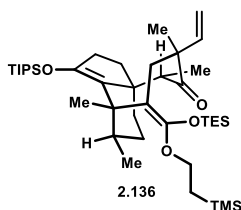
TLC  $R_f$  = 0.67 (10% v/v  $\text{Et}_2\text{O}$  in hexanes). Modestly UV active.

HRMS (ES+) calculated for  $\text{C}_{34}\text{H}_{60}\text{O}_4\text{Si}_2\text{Na}$  [ $\text{M}+\text{Na}$ ]: 611.3928, found: 611.3911



**Ketene silyl acetal 2.136.** A flame-dried flask was charged with 9-methylfluorene (0.8 mg, 4  $\mu\text{mol}$  prepared according to the known method<sup>9</sup> and recrystallized from MeOH), cyclobutanol **2.134** (25.0 mg, 42  $\mu\text{mol}$ ), and THF (0.7 mL), and cooled to  $-20$  °C. Chlorotriethylsilane (14  $\mu\text{L}$ , 84  $\mu\text{mol}$ , freshly distilled over  $\text{CaH}_2$  under  $\text{N}_2$  atmosphere) was added. The solution was treated with KHMDS (0.53 M solution in PhMe) until a pink-orange coloration indicating the equivalence point was persistent for >50 seconds (final volume: 95  $\mu\text{L}$ ). The reaction was warmed to 0 °C and stirred for 1 h. Meanwhile, a solution of LiTMP was prepared: a dry flask was charged with 2,2,6,6-tetramethylpiperidine (TMP, 185  $\mu\text{L}$ , 1.1 mmol, freshly distilled over  $\text{CaH}_2$  under  $\text{N}_2$

atmosphere) and THF (1.40 mL). The solution was cooled to 0 °C and treated with *n*-BuLi (0.41 mL of a 2.42 M solution in hexanes, 1.0 mmol), and stirred for 10 minutes before use. The reaction was cooled to -78 °C and treated dropwise with the freshly prepared LiTMP solution (0.42 mL of a 0.5 M solution in THF / hexanes, 0.21 mmol). After 30 minutes at the same temperature, the reaction was warmed to 0 °C for 10 minutes, then re-cooled to -78 °C. Iodomethane (50  $\mu$ L, 0.84 mmol, distilled over CaH<sub>2</sub> under N<sub>2</sub> atmosphere) was added dropwise. The reaction was stirred for 1 h at -78 °C and 30 minutes at 0 °C, then treated with saturated aqueous NaHCO<sub>3</sub> (5 mL). The mixture was diluted with H<sub>2</sub>O (5 mL) and Et<sub>2</sub>O (10 mL), and the phases were separated. The aqueous portion was extracted with Et<sub>2</sub>O (2x 10 mL). The combined organics were washed with brine, dried over anhydrous MgSO<sub>4</sub>, and concentrated under reduced pressure. The crude product was purified by flash column chromatography over silica gel. Elution with 3% v/v Et<sub>2</sub>O in pentane afforded 25.9 mg of the ketene silyl acetal **2.136** as a colorless oil as a ca. 14:1 mixture of ketene silyl acetal stereoisomers (86% yield). Peak-broadening was observed in the <sup>1</sup>H NMR of **2.136** and many <sup>13</sup>C NMR signals were absent when the spectra were collected at 25 °C. Consequently, NMR data were collected at 50 °C.



<sup>1</sup>H NMR (600 MHz, C<sub>6</sub>D<sub>6</sub>, 50 °C)

$\delta$ 6.70 (dd, J = 17.7, 11.0 Hz, 1H)	2.07 (s, 3H)
5.23 (dd, J = 11.0, 1.6 Hz, 1H)	2.06 – 1.95 (m, 3H)
5.10 (dd, J = 17.8, 1.6 Hz, 1H)	1.56 (t, J = 12.2 Hz, 1H)
4.06 – 3.98 (m, 1H)	1.49 – 1.37 (m, 2H)
3.96 – 3.84 (m, 1H)	1.23 (s, 3H)
3.16 (q, J = 6.7 Hz, 1H)	1.20 – 1.13 (m, 27H)
2.84 (d, J = 14.3 Hz, 1H)	1.08 (t, J = 7.9 Hz, 12H)
2.54 (d, J = 14.3 Hz, 1H)	0.82 (q, J = 7.8 Hz, 6H)
2.51 – 2.37 (m, 2H)	-0.02 (s, 9H)

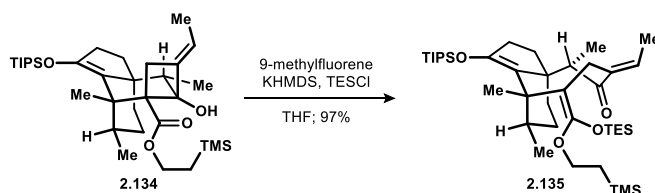
<sup>13</sup>C NMR (151 MHz, C<sub>6</sub>D<sub>6</sub>, 50 °C)

$\delta$ 217.7	51.9	23.6
152.2	46.2	18.5
148.8	44.9	18.4

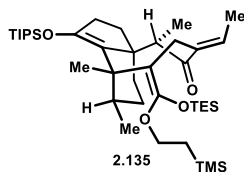
143.9	42.3	16.3
128.8	40.0	14.0
111.3	38.3	7.0
97.7	32.4	5.8
65.2	30.3	-1.6
55.2	29.0	

TLC  $R_f$  = 0.61 (10% v/v Et<sub>2</sub>O in hexanes). Not UV active.

HRMS (ES+) calculated for C<sub>41</sub>H<sub>76</sub>O<sub>4</sub>Si<sub>3</sub>H [M+H]: 716.5130, found: 716.5132



**Enone 2.135.** A flame-dried flask was charged with an over-sized magnetic stir bar, 9-methylfluorene (2.3 mg, 12.8  $\mu$ mol, prepared according to the known method<sup>9</sup> and recrystallized from MeOH), cyclobutanol **2.134** (77.0 mg, 0.13 mmol), and THF (2.0 mL), and cooled to -20 °C. Chlorotriethylsilane (80  $\mu$ L, 0.48 mmol, freshly distilled over CaH<sub>2</sub> under N<sub>2</sub> atmosphere) was added. The solution was treated with KHMDS (0.53 M solution in PhMe) until a pink-orange coloration indicating the equivalence point was persistent for >50 seconds (final volume: 0.28 mL). The reaction was warmed to 0 °C and stirred for 1 h, then saturated aqueous NaHCO<sub>3</sub> (4 mL) was added with vigorous stirring. (**note: an efficient quench is essential to obtain the product in high yield**). After 15 minutes, the mixture was partitioned between H<sub>2</sub>O (2 mL), additional saturated aqueous NaHCO<sub>3</sub> (6 mL), and Et<sub>2</sub>O (12 mL). The phases were separated, and the aqueous portion was extracted with Et<sub>2</sub>O (2x 12 mL). The combined organics were washed with brine, dried over anhydrous MgSO<sub>4</sub>, and concentrated under reduced pressure. The crude product was purified by flash column chromatography over silica gel. Elution with 4-6% v/v Et<sub>2</sub>O in pentane furnished 89.6 mg of the enone **2.135** as a colorless oil as a 14:1 mixture of ketene silyl acetal stereoisomers (97% yield). Peak-broadening was observed in the <sup>1</sup>H NMR of **2.135** and many <sup>13</sup>C NMR signals were absent when the spectra were collected at 25 °C. Consequently, NMR data were collected at 50 °C.



<sup>1</sup>H NMR (600 MHz, C<sub>6</sub>D<sub>6</sub>, 50 °C)

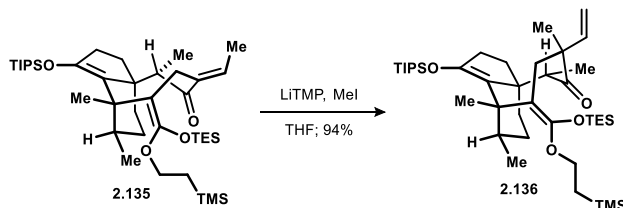
δ 6.81 (q, J = 7.0 Hz, 1H)	1.86 (d, J = 7.3 Hz, 3H)
4.14 – 4.01 (m, 1H)	1.77 – 1.64 (m, 1H)
3.79 (td, J = 9.6, 8.0 Hz, 1H)	1.52 (dtd, J = 13.5, 9.7, 3.7 Hz, 1H)
3.63 (d, J = 14.6 Hz, 1H)	1.45 – 1.37 (m, 2H)
3.25 – 3.11 (m, 2H)	1.25 (d, J = 6.6 Hz, 3H)
2.47 (ddd, J = 14.8, 11.6, 5.3 Hz, 1H)	1.16 (dd, J = 5.8, 2.2 Hz, 21H)
2.26 (ddd, J = 13.6, 7.0, 3.7 Hz, 1H)	1.12 – 1.05 (m, 15H)
2.11 (s, 4H)	0.91 – 0.85 (m, 6H)
1.96 (dd, J = 14.8, 7.5 Hz, 1H)	-0.04 (s, 9H)

<sup>13</sup>C NMR (151 MHz, C<sub>6</sub>D<sub>6</sub>, 50 °C)

δ 206.9	49.5	18.5
150.5	44.8	18.5
149.7	42.5	18.0
143.1	40.3	15.6
134.0	32.6	14.7
129.1	31.5	14.1
101.0	30.1	7.1
65.8	28.7	5.6
51.1	18.5	-1.6

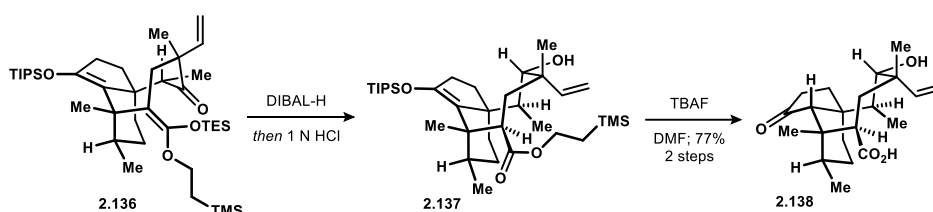
TLC R<sub>f</sub> = 0.55 (10% v/v Et<sub>2</sub>O in hexanes). UV active.

HRMS (ES<sup>+</sup>) calculated for C<sub>40</sub>H<sub>74</sub>O<sub>4</sub>Si<sub>3</sub>Na [M+Na]: 725.4792, found: 725.4797

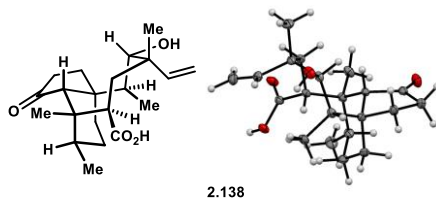


**Ketene silyl acetal 2.136.** A solution of LiTMP was prepared: 2,2,6,6-tetramethylpiperidine (TMP, 185 μL, 1.1 mmol, freshly distilled over CaH<sub>2</sub> under N<sub>2</sub> atmosphere) in THF (1.40 mL) was cooled to 0 °C and treated with *n*-BuLi (0.41 mL of a 2.42 M solution in hexanes, 1.0 mmol),

and stirred for 10 minutes before use. A separate flask was charged with enone **2.135** (89.6 mg, 0.127 mmol) and THF (2.0 mL), and cooled to  $-78\text{ }^{\circ}\text{C}$ . The solution was treated dropwise with the freshly prepared LiTMP solution (0.76 mL of a 0.5 M solution in THF / hexanes, 0.382 mmol). After 30 minutes at the same temperature, iodomethane (80  $\mu\text{L}$ , 1.27 mmol, distilled over  $\text{CaH}_2$  under  $\text{N}_2$  atmosphere) was added dropwise. The reaction was stirred for 1 h at  $-78\text{ }^{\circ}\text{C}$  and 30 minutes at  $0\text{ }^{\circ}\text{C}$ , then treated with saturated aqueous  $\text{NaHCO}_3$  (8 mL). The mixture was diluted with  $\text{H}_2\text{O}$  (7 mL) and  $\text{Et}_2\text{O}$  (15 mL), and the phases were separated. The aqueous portion was extracted with  $\text{Et}_2\text{O}$  (2x 15 mL). The combined organics were washed with brine, dried over anhydrous  $\text{MgSO}_4$ , and concentrated under reduced pressure. The crude product was purified by flash column chromatography over silica gel. Elution with 3% v/v  $\text{Et}_2\text{O}$  in pentane afforded 85.5 mg of the ketene silyl acetal **2.136** as a colorless oil (94% yield). Characterization data presented above on page 172.



**Ketoacid 2.138.** A solution of ketene silyl acetal **2.136** (10 mg, 13.9  $\mu\text{mol}$ ) in THF (1.8 mL) was cooled to  $-78\text{ }^{\circ}\text{C}$  and treated dropwise with DIBAL-H (50  $\mu\text{L}$  of a 1.0 M solution in toluene, 50  $\mu\text{mol}$ ). After 1.5 h, the reaction treated with aqueous 1 N HCl (2 mL) with vigorous stirring and warmed to ambient temperature for 1 h. The mixture was diluted with  $\text{Et}_2\text{O}$  (6 mL) and additional 1 N HCl (4 mL), and the phases were separated. The aqueous portion was extracted with  $\text{Et}_2\text{O}$  (2x 6 mL). The combined organics were washed with brine, dried over anhydrous  $\text{MgSO}_4$ , and concentrated under reduced pressure. The crude residue was taken up in DMF (0.4 mL, freshly distilled at ca. 0.2 mmHg, ambient temperature) and cooled to  $0\text{ }^{\circ}\text{C}$ , then treated with TBAF (50  $\mu\text{L}$  of a 1.0 M solution in THF, 50  $\mu\text{mol}$ ). After 2 h, the reaction was quenched by the addition of 1 N HCl (2 mL). The mixture was diluted with  $\text{Et}_2\text{O}$  (6 mL) and additional 1 N HCl (4 mL), and the phases were separated. The aqueous portion was extracted with  $\text{Et}_2\text{O}$  (3x 6 mL). The combined organics were washed with brine, dried over anhydrous  $\text{MgSO}_4$ , and concentrated under reduced pressure. The crude product was purified by flash column chromatography over silica gel. Elution with 40% v/v  $\text{EtOAc}$  in pentane afforded 3.7 mg of ketoacid **2.138** as a white solid (77% yield). Crystals suitable for x-ray diffraction analysis were grown by vapor diffusion of pentane into a benzene solution of 2 mg of ketoacid **2.138**.



2.138

<sup>1</sup>H NMR (600 MHz, CD<sub>3</sub>OD)

δ 6.14 (ddd, J = 17.6, 10.9, 0.9 Hz, 1H)

5.15 (dd, J = 17.6, 1.3 Hz, 1H)

5.06 (dd, J = 10.8, 1.3 Hz, 1H)

3.04 (d, J = 12.6 Hz, 1H)

2.89 (q, J = 6.8 Hz, 1H)

2.63 (ddd, J = 19.6, 9.5, 1.5 Hz, 1H)

2.43 (d, J = 12.5 Hz, 1H)

2.31 (ddd, J = 19.6, 9.0, 7.9 Hz, 1H)

<sup>13</sup>C NMR (151 MHz, CD<sub>3</sub>OD)

δ 206.4

49.2

31.1

183.2

48.5

29.2

144.0

46.6

27.6

113.8

39.7

25.2

96.2

39.1

16.8

81.1

35.2

16.8

57.7

33.5

9.2

2.21 (td, J = 13.2, 12.6, 6.2 Hz, 1H)

2.17 – 2.07 (m, 2H)

1.74 (ddd, J = 12.5, 9.5, 7.9 Hz, 1H)

1.53 (s, 4H), 1.27 – 1.16 (m, 2H)

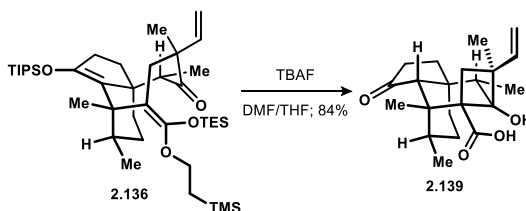
1.11 (s, 3H)

1.03 (d, J = 7.0 Hz, 3H)

0.89 (d, J = 7.1 Hz, 3H)

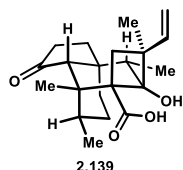
TLC R<sub>f</sub> = 0.55 (60% v/v EtOAc in hexanes). Not UV active.

HRMS (ES<sup>-</sup>) calculated for C<sub>21</sub>H<sub>31</sub>O<sub>4</sub> [M-H]: 347.2222, found: 347.2232



**Cyclobutanol 2.139.** A solution of ketene silyl acetal **2.136** (66.5 mg, 92.7 μmol) in DMF (0.9 mL, freshly distilled at ambient temperature under vacuum ca. 0.2 mm Hg) was cooled to -30 °C and treated dropwise with TBAF (0.30 mL of a 1.0 M solution in THF, 0.30 mmol). After 1 h, the reaction was warmed to 0 °C. After 1.5 h, the reaction was quenched by the addition of aqueous 1 N HCl (2 mL). The mixture was diluted with Et<sub>2</sub>O (6 mL) and additional 1 N HCl (6 mL), and the phases were separated. The aqueous portion was extracted with Et<sub>2</sub>O (3x 6 mL). The

combined organics were washed with water, brine, dried over anhydrous  $\text{MgSO}_4$ , and concentrated under reduced pressure. (Note: TLC plates used for analysis were soaked in a 1% v/v AcOH in  $\text{Et}_2\text{O}$  solution and allowed to dry under ambient conditions for 5 minutes before use). The crude product was purified by flash column chromatography over silica gel slurry-packed with 1% AcOH, 20% v/v  $\text{Et}_2\text{O}$  in pentane. Elution with 1% AcOH, 20% v/v  $\text{Et}_2\text{O}$  in pentane afforded 27.0 mg of the cyclobutanol **2.139** as a white solid (84% yield).



$^1\text{H}$  NMR (600 MHz,  $\text{CD}_3\text{OD}$ )

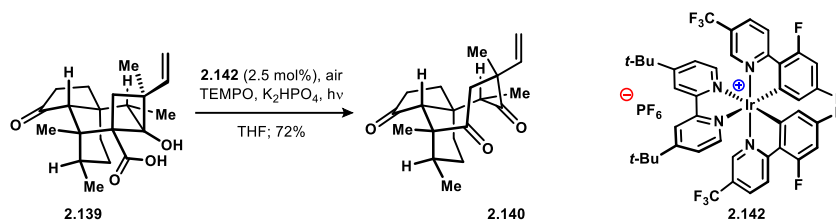
$\delta$ 6.16 (dd, $J = 17.5, 10.8$ Hz, 1H)	1.75 (ddd, $J = 12.5, 8.7, 2.0$ Hz, 1H)
5.19 (dd, $J = 17.6, 1.4$ Hz, 1H)	1.64 (ddq, $J = 14.5, 7.2, 3.2$ Hz, 1H)
5.07 (dd, $J = 10.9, 1.3$ Hz, 1H)	1.53 – 1.44 (m, 1H)
2.41 – 2.37 (m, 1H)	1.40 (s, 3H)
2.31 – 2.20 (m, 2H)	1.24 – 1.19 (m, 1H)
2.20 – 2.15 (m, 1H)	1.16 – 1.09 (m, 1H)
2.14 (s, 1H)	1.07 (s, 3H)
2.09 (tt, $J = 13.4, 6.7$ Hz, 1H)	1.01 (d, $J = 7.0$ Hz, 3H)
1.86 (d, $J = 12.2$ Hz, 1H)	0.82 (d, $J = 7.3$ Hz, 3H)
1.82 (dd, $J = 14.5, 5.6$ Hz, 1H)	

$^{13}\text{C}$  NMR (151 MHz,  $\text{CD}_3\text{OD}$ )

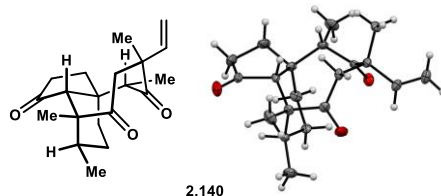
$\delta$ 220.8	49.2	33.6
183.7	48.3	28.6
143.5	43.7	26.7
114.3	42.9	24.5
81.1	37.6	18.3
64.5	36.8	15.5
57.7	34.0	9.7

TLC  $R_f = 0.40$  (1% AcOH, 30% v/v  $\text{Et}_2\text{O}$  in hexanes). TLC plates pre-treated with 1% v/v AcOH in  $\text{Et}_2\text{O}$  and dried under ambient conditions for 5 minutes. Not UV active.

HRMS (ES $^-$ ) calculated for  $\text{C}_{21}\text{H}_{29}\text{O}_4$  [M-H]: 345.2066, found: 345.2065



**Trione 2.140.** A vial was charged with cyclobutanol **2.139** (5.0 mg, 14.4  $\mu\text{mol}$ ),  $[\text{Ir}(\text{dF}(\text{CF}_3)\text{ppy})_2(\text{dtbpy})]\text{PF}_6$  **2.142** (0.7 mg, 6.2  $\mu\text{mol}$ ), TEMPO (6.8 mg, 43.3  $\mu\text{mol}$ ),  $\text{K}_2\text{HPO}_4$  (5.0 mg, 28.9  $\mu\text{mol}$ ), and THF (0.8 mL). The vial was sealed under air and irradiated with 420 nm LEDs for 1.5 h with vigorous stirring, then diluted with 1 N HCl (5 mL) and  $\text{Et}_2\text{O}$  (5 mL). The phases were separated, and the aqueous portion was extracted with  $\text{Et}_2\text{O}$  (2x 5 mL). The combined organics were washed with brine, dried over  $\text{MgSO}_4$ , and concentrated under reduced pressure. The crude product was purified by flash column chromatography over silica gel. Elution with 20% v/v  $\text{EtOAc}$  in pentane furnished 3.3 mg of the trione **2.140** as a white solid (72% yield). Crystals for x-ray diffraction analysis were grown by slow evaporation of a 1 mg sample from pentane.



$^1\text{H}$  NMR (600 MHz,  $\text{CDCl}_3$ )

$\delta$ 6.54 (dd, $J = 17.8, 11.1$ Hz, 1H)	1.87 (ddd, $J = 12.7, 8.6, 1.7$ Hz, 1H)
5.25 (dd, $J = 11.1, 1.0$ Hz, 1H)	1.56 – 1.49 (m, 4H)
5.11 (dd, $J = 17.8, 1.0$ Hz, 1H)	1.42 (s, 3H)
3.33 (d, $J = 12.4$ Hz, 1H)	1.32 – 1.25 (m, 2H)
3.17 (q, $J = 6.8$ Hz, 1H)	1.20 (dd, $J = 14.2, 5.5$ Hz, 1H)
2.53 (s, 1H)	1.17 (d, $J = 6.9$ Hz, 3H)
2.39 – 2.25 (m, 2H)	1.14 (d, $J = 6.8$ Hz, 3H)
2.24 – 2.16 (m, 2H)	1.12 – 1.03 (m, 1H)

$^{13}\text{C}$  NMR (151 MHz,  $\text{CDCl}_3$ )

$\delta$ 218.4	52.9	28.9
214.7	50.5	26.5
213.0	47.0	23.0
140.2	44.6	22.1
113.1	38.8	17.5

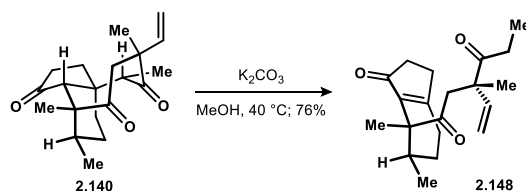


64.5 36.2 15.0

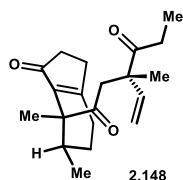
54.1 34.3

TLC  $R_f$  = 0.50 (40% v/v EtOAc in hexanes). Not UV active.

HRMS (ES+) calculated for  $C_{20}H_{28}O_3Na$  [M+Na]: 339.1936, found: 339.1947



**Enone 2.148.** A solution of trione **2.140** (3.3 mg, 10.4  $\mu$ mol) in MeOH (0.8 mL) was treated with  $K_2CO_3$  (20.2 mg, 0.146 mmol). The reaction mixture was heated to 40 °C for 30 minutes, then cooled to ambient temperature and quenched by the addition of  $\frac{1}{2}$ -saturated aqueous  $NH_4Cl$  (5 mL) and  $Et_2O$  (5 mL). The phases were separated, and the aqueous portion was extracted with  $Et_2O$  (2x 5 mL). The combined organics were washed with brine, dried over anhydrous  $MgSO_4$ , and concentrated under reduced pressure. The crude product was purified by flash column chromatography over silica gel. Elution with 20% v/v EtOAc in pentane furnished 2.5 mg of the enone **2.148** as a colorless oil (76% yield).



$^1H$  NMR (600 MHz,  $CDCl_3$ )

$\delta$ 5.91 (dd, $J$ = 17.5, 10.7 Hz, 1H)	1.70 – 1.61 (m, 2H)
5.16 – 5.06 (m, 2H)	1.47 (s, 3H)
3.00 (s, 2H)	1.29 (s, 3H)
2.60 – 2.46 (m, 4H)	0.99 (t, $J$ = 7.2 Hz, 3H)
2.43 – 2.30 (m, 4H)	0.97 (d, $J$ = 7.0 Hz, 3H)
1.80 – 1.73 (m, 1H)	

$^{13}C$  NMR (151 MHz,  $CDCl_3$ )

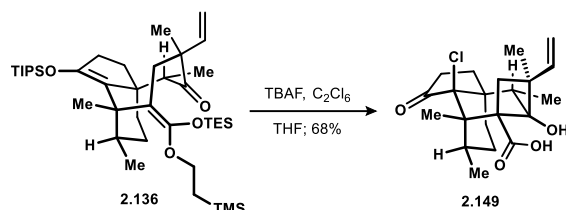
$\delta$ 213.1	51.8	28.1
210.7	51.6	27.2
207.5	49.8	21.5
174.4	40.3	20.5
142.2	34.8	15.8

141.7 31.4 7.9

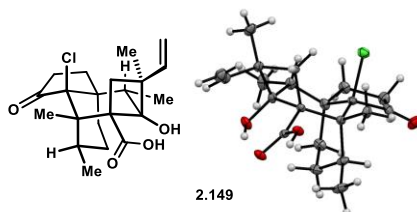
114.5 30.0

TLC  $R_f$  = 0.46 (40% v/v EtOAc in hexanes). UV active.

HRMS (CI+) calculated for  $C_{20}H_{28}O_3$  [ $M^+$ ]: 316.2039, found: 316.2043



**Chlorocyclobutanol 2.149.** A solution of ketene silyl acetal **2.136** (41.0 mg, 57  $\mu$ mol) and hexachloroethane (63.0 mg, 0.263 mmol) in THF (1.8 mL) was cooled to  $-78$   $^{\circ}C$  and treated dropwise with tetrabutylammonium fluoride (TBAF, 0.31 mL of a 1.0 M solution in THF, 0.31 mmol). After 2 minutes, the reaction was warmed to  $-45$   $^{\circ}C$ . After 1.5 h, the reaction was warmed to  $0$   $^{\circ}C$  for 1 h, at which point it was quenched by the addition of aqueous 1 N HCl (2 mL). The mixture was diluted with  $Et_2O$  (10 mL) and additional 1 N HCl (8 mL), and the phases were separated. The aqueous portion was extracted with  $Et_2O$  (3x 10 mL). The combined organics were washed with brine, dried over anhydrous  $MgSO_4$ , and concentrated under reduced pressure. (Note: TLC plates used for analysis were soaked in a 1% v/v AcOH in  $Et_2O$  solution and allowed to dry under ambient conditions for 5 minutes before use). The crude product was purified by flash column chromatography over silica gel slurry-packed with 1% AcOH, 15% v/v  $Et_2O$  in pentane. Elution with 1% AcOH, 15% v/v  $Et_2O$  in pentane afforded 14.7 mg of the chlorocyclobutanol **2.149** as a white solid (68% yield). Crystals suitable for x-ray diffraction analysis were grown by slow evaporation of a MeOH- $Et_2O$  (2:1) solution of chlorocyclobutanol **2.149**.



$^1H$  NMR (600 MHz,  $CD_3OD$ )

$\delta$  6.14 (ddd,  $J$  = 17.6, 10.9, 0.9 Hz, 1H)

5.15 (dd,  $J$  = 17.6, 1.3 Hz, 1H)

5.06 (dd,  $J$  = 10.8, 1.3 Hz, 1H)

2.21 (td,  $J$  = 13.2, 12.6, 6.2 Hz, 1H)

2.17 – 2.07 (m, 2H)

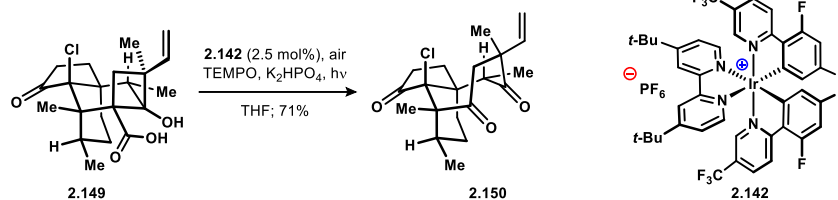
1.74 (ddd,  $J$  = 12.5, 9.5, 7.9 Hz, 1H)

3.04 (d, J = 12.6 Hz, 1H)                      1.53 (s, 4H), 1.27 – 1.16 (m, 2H)  
 2.89 (q, J = 6.8 Hz, 1H)                      1.11 (s, 3H)  
 2.63 (ddd, J = 19.6, 9.5, 1.5 Hz, 1H)                      1.03 (d, J = 7.0 Hz, 3H)  
 2.43 (d, J = 12.5 Hz, 1H)                      0.89 (d, J = 7.1 Hz, 3H)  
 2.31 (ddd, J = 19.6, 9.0, 7.9 Hz, 1H)  
<sup>13</sup>C NMR (151 MHz, CD<sub>3</sub>OD)

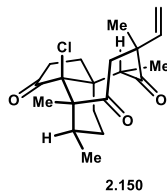
δ 206.4	49.2	31.1
183.2	48.5	29.2
144.0	46.6	27.6
113.8	39.7	25.2
96.2	39.1	16.8
81.1	35.2	16.8
57.7	33.5	9.2

TLC R<sub>f</sub> = 0.47 (1% AcOH, 30% v/v Et<sub>2</sub>O in hexanes). TLC plates pre-treated with 1% v/v AcOH in Et<sub>2</sub>O and dried under ambient conditions for 5 minutes. Not UV active.

HRMS (ES<sup>-</sup>) calculated for C<sub>21</sub>H<sub>28</sub>ClO<sub>4</sub> [M-H]: 379.1676, found: 379.1691



**Chlorotrione 2.150.** A vial was charged with chlorocyclobutanol **2.149** (14.5 mg, 38 μmol), [Ir(dF(CF<sub>3</sub>)ppy)<sub>2</sub>(dtbpy)]PF<sub>6</sub> **2.142** (1.1 mg, 1.0 μmol), TEMPO (11.9 mg, 76 μmol), K<sub>2</sub>HPO<sub>4</sub> (13.2 mg, 76 μmol), and THF (1.2 mL). The vial was sealed under air and irradiated with 420 nm LEDs for 1.5 h with vigorous stirring, then the mixture was partitioned between 1 N HCl (6 mL) and Et<sub>2</sub>O (6 mL). The phases were separated, and the aqueous portion was extracted with Et<sub>2</sub>O (2x 6 mL). The combined organics were washed with brine, dried over MgSO<sub>4</sub>, and concentrated under reduced pressure. The crude product was purified by flash column chromatography over silica gel. Elution with 10-14% v/v EtOAc in pentane furnished 9.5 mg of the chlorotrione **2.150** as a white solid (71% yield).



<sup>1</sup>H NMR (600 MHz, CDCl<sub>3</sub>)

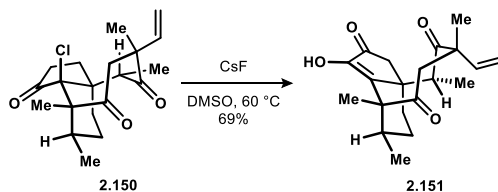
δ 6.21 (dd, J = 17.6, 11.1 Hz, 1H)	1.78 (ddq, J = 13.7, 6.9, 3.8 Hz, 1H)
5.28 (dd, J = 11.1, 0.9 Hz, 1H)	1.70 – 1.62 (m, 4H)
5.17 (dd, J = 17.6, 0.9 Hz, 1H)	1.37 (s, 3H)
4.30 (bd, J = 11.7 Hz, 1H)	1.27 – 1.23 (m, 1H) – overlaps with grease
3.88 (q, J = 6.8 Hz, 1H)	1.19 (dd, J = 14.1, 5.6 Hz, 1H)
2.65 (ddd, J = 20.1, 10.0, 1.4 Hz, 1H)	1.15 (d, J = 6.9 Hz, 3H)
2.35 – 2.27 (m, 3H)	1.14 (d, J = 6.9 Hz, 3H)
1.98 (dt, J = 12.8, 9.6 Hz, 1H)	0.86 (qd, J = 13.7, 4.6 Hz, 1H)

<sup>13</sup>C NMR (151 MHz, CDCl<sub>3</sub>)

δ 215.9	53.1	29.3
211.5	52.5	28.7
207.4	49.1	23.8
139.3	41.8	20.9
114.4	41.1	18.7
85.9	31.7	15.6
58.9	30.5	

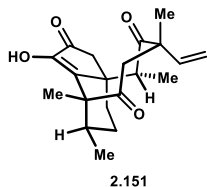
TLC R<sub>f</sub> = 0.47 (20% v/v EtOAc in hexanes). Not UV active.

HRMS (CI+) calculated for C<sub>20</sub>H<sub>27</sub>ClO<sub>3</sub> [M<sup>+</sup>]: 350.1649, found: 350.1661



**Tetraketone 2.151.** A flame-dried flask was charged with chlorotrione **2.150** (9.5 mg, 27 μmol) and CsF (15.2 mg, 0.10 mmol). Dry DMSO (0.8 mL) was added, and the mixture was heated to 60 °C for 1.5 h. The reaction was cooled to ambient temperature and diluted with H<sub>2</sub>O (6 mL) and Et<sub>2</sub>O (6 mL). The phases were separated, and the aqueous portion was extracted with Et<sub>2</sub>O (3x 6 mL). The combined organics were washed with H<sub>2</sub>O (6 mL) and brine, dried over anhydrous MgSO<sub>4</sub>, and concentrated under reduced pressure. The crude product was purified

by flash column chromatography over silica gel. Elution with 20% v/v EtOAc in pentane afforded 6.2 mg of the tetraketone **2.151** as a white solid (69% yield).



<sup>1</sup>H NMR (600 MHz, CDCl<sub>3</sub>)

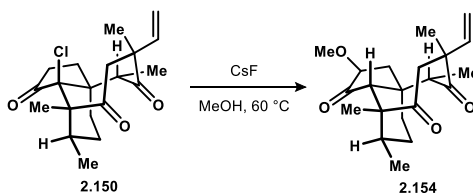
δ 6.46 (dd, J = 17.7, 10.9 Hz, 1H)	1.93 – 1.82 (m, 2H)
5.56 (s, 1H)	1.69 (s, 3H)
5.27 (d, J = 10.9 Hz, 1H)	1.56 – 1.48 (m, 2H)
5.08 (d, J = 17.7 Hz, 1H)	1.36 (d, J = 6.9 Hz, 3H)
3.22 (d, J = 19.3 Hz, 1H)	1.20 (td, J = 13.7, 4.0 Hz, 1H)
3.07 (q, J = 6.5 Hz, 1H)	1.10 (s, 3H)
2.71 (d, J = 11.8 Hz, 1H)	1.06 (d, J = 6.5 Hz, 3H)
2.25 – 2.18 (m, 2H)	

<sup>13</sup>C NMR (151 MHz, CDCl<sub>3</sub>)

212.4	56.2	37.9
211.3	55.7	27.1
201.5	47.8	24.0
148.1	45.3	21.5
143.6	43.5	16.1
138.2	43.2	15.8
118.2	41.1	

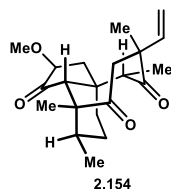
TLC R<sub>f</sub> = 0.47 (30% v/v EtOAc in hexanes). UV active. Does not stain well in *p*-anisaldehyde or KMnO<sub>4</sub>.

HRMS (CI<sup>+</sup>) calculated for C<sub>20</sub>H<sub>26</sub>O<sub>4</sub>H [M+H]: 331.1909, found: 331.1924



**Methoxyketone 2.154.** A flame-dried flask was charged with chlorotrione **2.150** (1.5 mg, 4.3 μmol) and CsF (7.6 mg, 50 μmol). MeOH (0.4 mL) was added, and the mixture was heated to 60 °C for 1.5 h. The reaction was cooled to ambient temperature and diluted with H<sub>2</sub>O (6 mL)

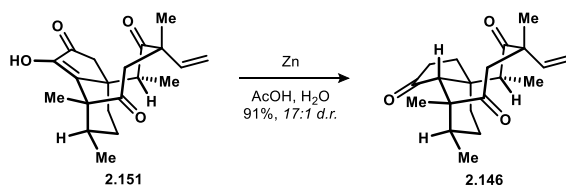
and Et<sub>2</sub>O (6 mL). The phases were separated, and the aqueous portion was extracted with Et<sub>2</sub>O (3x 6 mL). The combined organics were washed with H<sub>2</sub>O (6 mL) and brine, dried over anhydrous MgSO<sub>4</sub>, and concentrated under reduced pressure. The crude product was purified by flash column chromatography over silica gel. Elution with 25% v/v EtOAc in pentane afforded 0.9 mg of the methoxyketone **2.154** as a white solid (61% yield).



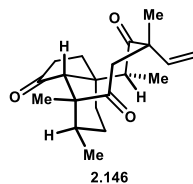
<sup>1</sup>H NMR (600 MHz, CDCl<sub>3</sub>)

δ 6.46 (dd, J = 17.7, 10.9 Hz, 1H)	1.93 – 1.82 (m, 2H)
5.56 (s, 1H)	1.69 (s, 3H)
5.27 (d, J = 10.9 Hz, 1H)	1.56 – 1.48 (m, 2H)
5.08 (d, J = 17.7 Hz, 1H)	1.36 (d, J = 6.9 Hz, 3H)
3.22 (d, J = 19.3 Hz, 1H)	1.20 (td, J = 13.7, 4.0 Hz, 1H)
3.07 (q, J = 6.5 Hz, 1H)	1.10 (s, 3H)
2.71 (d, J = 11.8 Hz, 1H)	1.06 (d, J = 6.5 Hz, 3H)
2.25 – 2.18 (m, 2H)	

TLC R<sub>f</sub> = 0.52 (40% v/v EtOAc in hexanes). Not UV active.



**Mutilin trione 2.146.** A vial was charged with tetraketone **2.151** (6.2 mg, 19 μmol), glacial AcOH (0.8 mL) and H<sub>2</sub>O (0.1 mL). Under vigorous stirring, freshly activated Zn<sup>10</sup> (100 mg, 1.53 mmol) was added. After 17 h, a second portion of Zn (100 mg, 1.53 mmol) was added, and the reaction was stirred for an additional 25 h. (**note: freshly activated Zn is required to obtain the product with high diastereoselectivity**). The mixture was diluted with Et<sub>2</sub>O (2 mL), a small scoop of anhydrous MgSO<sub>4</sub> was added, and the mixture was filtered over a plug of celite. The vial and filter cake were washed with Et<sub>2</sub>O (total volume of 16 mL) and the combined organics were concentrated. The crude product was purified by flash column chromatography over silica gel. Elution with 12% v/v EtOAc in pentane afforded 5.4 mg of mutilin trione **2.146** as a white film as a 17:1 mixture of diastereomers at C4 (91% yield).



<sup>1</sup>H NMR (600 MHz, CDCl<sub>3</sub>)

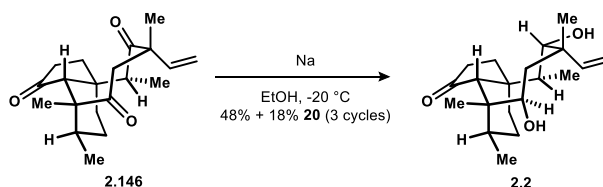
δ 6.54 (dd, J = 17.7, 10.9 Hz, 1H)	1.80 (qd, J = 13.8, 3.8 Hz, 1H)
5.28 (d, J = 10.9 Hz, 1H)	1.64 (dq, J = 14.5, 2.6 Hz, 1H)
5.11 (d, J = 17.7 Hz, 1H)	1.55 – 1.48 (m, 5H)
2.92 (q, J = 6.6 Hz, 1H)	1.37 – 1.31 (m, 1H)
2.73 (d, J = 12.1 Hz, 1H)	1.22 (s, 3H)
2.35 (dt, J = 13.0, 10.2 Hz, 1H)	1.20 (d, J = 7.0 Hz, 3H)
2.28 – 2.18 (m, 3H)	1.16 (td, J = 14.1, 4.6 Hz, 1H)
2.16 (d, J = 2.6 Hz, 1H)	1.03 (d, J = 6.7 Hz, 3H)

<sup>13</sup>C NMR (151 MHz, CDCl<sub>3</sub>)

δ 216.6	51.3	26.4
214.3	46.1	25.0
212.1	45.6	24.3
138.7	43.8	21.1
117.9	36.8	16.2
58.7	34.7	14.0
56.0	30.4	

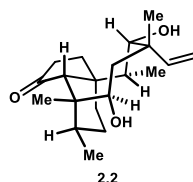
TLC R<sub>f</sub> = 0.55 (20% v/v EtOAc in hexanes). Not UV active.

HRMS (ES<sup>+</sup>) calculated for C<sub>20</sub>H<sub>28</sub>O<sub>3</sub>H [M+H]: 317.2117, found: 317.2111



**Mutillin 2.2.** A solution of mutilin trione **2.146** (6.0 mg, 19 μmol) in dry EtOH (1.2 mL) was cooled to -20 °C. A piece of Na<sup>0</sup> (55 mg, 2.39 mmol), stored in mineral oil, was washed thoroughly with hexanes, and weighed in a tared vial of hexanes. The Na<sup>0</sup> was rolled to a ca. 0.5 mm thickness using a clean culture tube on a smooth, clean surface, and immediately added to the solution of trione **2.146** with stirring. (**caution: exothermic reaction occurs between Na<sup>0</sup> and EtOH.**) Significant bubbling was observed on the bright silver-colored surface of the Na<sup>0</sup>. After 1 h, the

Na<sup>0</sup> was completely consumed. The reaction was quenched by the addition of ½-saturated aqueous NH<sub>4</sub>Cl (5 mL), warmed to ambient temperature, diluted with EtOAc (5 mL), and the phases separated. The aqueous portion was extracted with EtOAc (3x 5 mL). The combined organics were washed with brine, dried over anhydrous MgSO<sub>4</sub>, and concentrated under reduced pressure. The crude product was purified by flash column chromatography over silica gel. Elution with 12-35% v/v EtOAc in pentane afforded 3.9 mg of recovered mutilin trione **2.146** (65% yield) alongside 2.0 mg mutilin **2.2** in moderate purity (ca. 32% yield). The recovered trione **2.146** was subjected to the same reaction conditions two additional times. Following the last cycle, the crude product was combined with the mutilin **2.2** isolated from the first two cycles. The mixture was purified by preparative thin-layer chromatography (30% v/v EtOAc in pentane) to afford 3.0 mg mutilin **2.2** (48% yield) with 1.1 mg recovered mutilin trione **2.146** (18% yield).



<sup>1</sup>H NMR (600 MHz, CDCl<sub>3</sub>)

δ 6.15 (ddd, J = 17.9, 11.2, 0.9 Hz, 1H)	1.63 – 1.56 (m, 4H)
5.47 – 5.14 (m, 2H)	1.53 – 1.43 (m, 3H)
4.35 (dd, J = 7.7, 5.5 Hz, 1H)	1.36 (s, 4H)
3.41 (t, J = 6.6 Hz, 1H)	1.25 (d, J = 5.5 Hz, 1H)
2.29 – 2.13 (m, 3H)	1.15 (s, 3H)
2.05 (s, 1H)	1.16 – 1.08 (m, 4H)
1.91 (dd, J = 15.9, 7.7 Hz, 1H)	0.96 (d, J = 7.1 Hz, 3H)
1.74 (dq, J = 14.5, 3.1 Hz, 1H)	0.92 (d, J = 7.1 Hz, 3H)
1.67 (dtd, J = 14.2, 7.1, 3.7 Hz, 1H)	

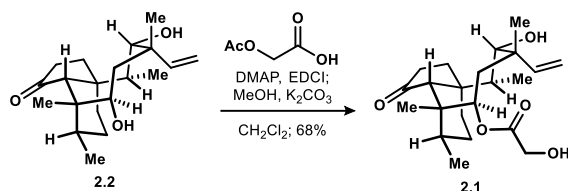
<sup>13</sup>C NMR (151 MHz, CDCl<sub>3</sub>)

δ 217.7	45.4	28.7
139.5	45.2	27.3
116.2	42.5	25.3
75.3	37.0	18.3
66.9	36.6	13.6
59.3	34.6	11.4
45.5	30.5	

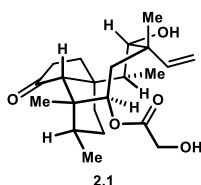
TLC R<sub>f</sub> = 0.40 (40% v/v EtOAc in hexanes). Not UV active.



HRMS (ES+) calculated for C<sub>20</sub>H<sub>32</sub>O<sub>3</sub>Na [M+Na]: 343.2249, found: 343.2251



**Pleuromutilin 2.1.** A flame-dried flask was charged with mutilin **2.2** (3.0 mg, 9.4  $\mu$ mol), acetoxyacetic acid (8.1 mg, 68.6  $\mu$ mol, commercially available or prepared in one step<sup>94</sup>), EDC (13.1 mg, 68.3  $\mu$ mol), and DMAP (4.8 mg, 39.3  $\mu$ mol). The atmosphere was exchanged with N<sub>2</sub>, then the CH<sub>2</sub>Cl<sub>2</sub> (0.5 mL) was added to the reaction flask. After 2 h at ambient temperature, TLC analysis of the reaction mixture indicated complete consumption of the starting material (new spot = R<sub>f</sub> 0.57 in 40% v/v EtOAc in hexanes), and the reaction was treated with MeOH (0.5 mL) and K<sub>2</sub>CO<sub>3</sub> (33.1 mg, 0.239 mmol). After 24 h, additional portions of K<sub>2</sub>CO<sub>3</sub> (13.0 mg, 94.1  $\mu$ mol) and MeOH (0.3 mL) were added. After 8 h, the reaction was cooled to 0 °C and treated slowly with 1 N HCl (2 mL). The mixture was partitioned between CHCl<sub>3</sub> (6 mL) and additional 1 N HCl (4 mL). The phases were separated, and the aqueous portion was extracted with CHCl<sub>3</sub> (3x 4 mL). The combined organics were washed with brine, dried over anhydrous MgSO<sub>4</sub>, and concentrated under reduced pressure. The crude product was purified by flash column chromatography over silica gel. Elution with 30-45% v/v EtOAc in pentane afforded 2.4 mg of pleuromutilin **2.1** as a white film (68% yield).



<sup>1</sup>H NMR (600 MHz, CDCl<sub>3</sub>)

$\delta$ 6.50 (dd, J = 17.4, 11.0 Hz, 1H)	1.72 – 1.63 (m, 2H)
5.84 (d, J = 8.5 Hz, 1H)	1.56 – 1.46 (m, 3H)
5.37 (dd, J = 11.0, 1.5 Hz, 1H)	1.44 (s, 3H)
5.22 (dd, J = 17.4, 1.5 Hz, 1H)	1.39 (dq, J = 14.5, 3.6 Hz, 1H)
4.04 (q, J = 17.1 Hz, 2H)	1.32 (d, J = 16.1 Hz, 1H)
3.37 (d, J = 6.5 Hz, 1H)	1.20 – 1.11 (m, 4H)
2.43 – 2.15 (m, 4H)	0.90 (d, J = 7.1 Hz, 3H)
2.13 – 2.07 (m, 2H)	0.71 (d, J = 7.1 Hz, 3H)
1.78 (dq, J = 14.4, 3.0 Hz, 1H)	

$^{13}\text{C}$  NMR (151 MHz,  $\text{CDCl}_3$ )

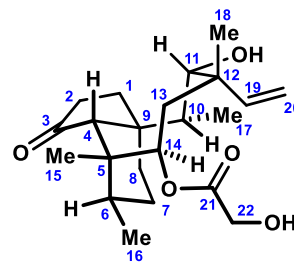
$\delta$ 217.0	45.4	26.8
172.2	44.7	26.3
138.8	44.0	24.8
117.4	41.8	16.6
74.6	36.6	14.8
69.8	36.0	11.5
61.3	34.4	
58.1	30.4	

TLC  $R_f$  = 0.54 (60% v/v EtOAc in hexanes). Not UV active.

HRMS ( $\text{ES}^-$ ) calculated for  $\text{C}_{22}\text{H}_{34}\text{O}_5\text{Cl}$  [ $\text{M}+\text{Cl}$ ]: 413.2095, found: 413.2097

Comparison of  $^{13}\text{C}$  NMR shifts of synthetic pleuromutilin with the reported values (Schulz and Berner<sup>95</sup>, 90 MHz,  $\text{CDCl}_3$  calibrated to 77.0 ppm).

Carbon #	Synthetic 1	Natural 1	$\Delta$
3	$\delta$ 217.0	216.8	+0.2
21	172.2	172.2	0
19	138.8	138.9	-0.1
20	117.4	117.3	+0.1
11	74.6	74.7	-0.1
14	69.8	69.9	-0.1
22	61.3	61.3	0
4	58.1	58.2	-0.1
9	45.4	45.5	-0.1
13	44.7	44.9	-0.2
12	44.0	44.1	-0.1
5	41.8	41.9	-0.1
6	36.6	36.7	-0.1
10	36.0	36.1	-0.1
2	34.4	34.5	-0.1
8	30.4	30.4	0
7	26.8	26.9	-0.1
18	26.3	26.5	-0.2
1	24.8	24.9	-0.1
16	16.6	16.6	0
15	14.8	14.8	0
17	11.5	11.5	0



### 2.9.3. Experimental Procedures for Computations in Figure 2.3

All calculations were performed using Spartan 18 in the gas phase.<sup>96</sup> Two enol epimers **2.125** and **2.126** were subjected to the same analysis. To simplify calculations, the triisopropylsilyl and triethylsilyl groups present in enone **2.123** were replaced with trimethylsilyl groups and the TMSE portion was replaced with methyl group. A conformers search was performed using Molecular Mechanics MMFF, wherein the “flip” option was enabled under torsions for the C10 and C13 positions. Of the resulting conformers, all of those exceeding 8 kcal/mol in energy above the lowest energy conformer were discarded. The remaining conformers were subjected to a geometry optimization calculation using Hartree–Fock HF/3-21G, and then assigned an alignment score. Duplicate conformers were discarded. Additionally, all conformers exceeding 5 kcal/mol were discarded. All of the remaining conformers were subjected to geometry optimization at the  $\omega$ B97X-D/6-31G(d) level. The resulting single point energies of the remaining conformers were compared. Images were processed with CYLView.<sup>97</sup>

The conformers were analyzed for expected facial selectivity during an alkylation event. The lowest energy conformer corresponding to the enolate of enone **2.123** prepared during our synthetic route was enol **2.125-a**, which exhibited an exposed face in accord with our experimental results. The lowest energy conformer of enol **2.125** that presented the opposite exposed face to lowest energy conformer **2.125-a** was **2.125-b**, which was 4.67 kcal/mol higher in energy than **2.125-a**. The enol **2.126-a**, which is the C10 epimer of **2.125**, exhibited the opposite expected facial selectivity during a hypothetical alkylation event to **2.125-a**. The lowest energy conformer of enol **2.126** that presented the opposite exposed face to its lowest energy conformer **2.126-a** was **2.126-b**, which was 1.68 kcal/mol higher in energy than **2.126-a**. We concluded that in the absence of an extreme Curtin–Hammett scenario, the enolate corresponding to enol **2.126** should be expected to engage in an alkylation event with the opposite diastereoselectivity from the enolate of enone **2.123**.

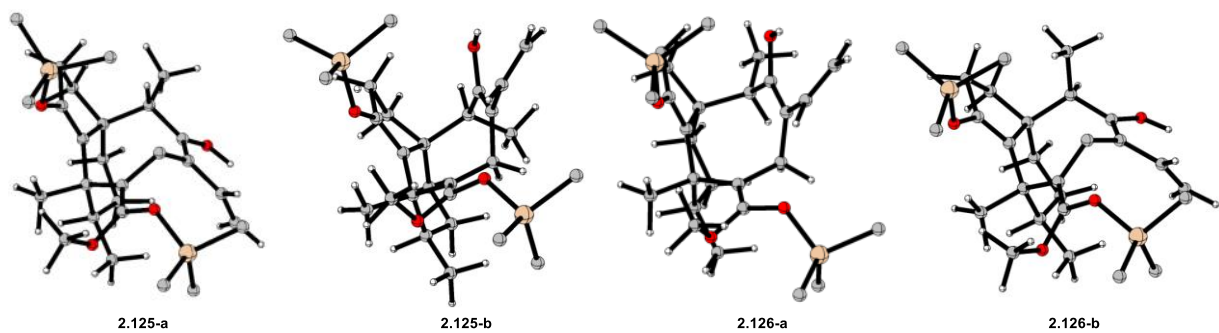


Figure 2.4. Models of relevant conformers. Selected hydrogen atoms omitted for clarity.

#### 2.9.4. Experimental Procedures for Table 2.2

Entry 1: A vial was charged with cyclobutanol **2.139** (2.7 mg, 7.8  $\mu\text{mol}$ ), KOAc (12.0 mg, 122.3  $\mu\text{mol}$ ), and  $\text{Pb}(\text{OAc})_4$  (11.5 mg, 25.9  $\mu\text{mol}$ ). The mixture was dissolved in glacial AcOH (0.8 mL) and the solution was heated to 50 °C. After 1 h, the reaction was cooled to ambient temperature, diluted with  $\text{H}_2\text{O}$  (5 mL) and  $\text{Et}_2\text{O}$  (5 mL). The phases were separated, and the aqueous portion was extracted with  $\text{Et}_2\text{O}$  (2x 5 mL). The combined organics were washed with saturated aqueous  $\text{NaHCO}_3$ , brine, dried over anhydrous  $\text{MgSO}_4$ , and concentrated under reduced pressure. Analysis of the crude NMR indicated that the proportion of triketone **2.140** formed was <5%.

Entry 2-3: A vial was charged with cyclobutanol **2.139** (2.7 mg, 7.8  $\mu\text{mol}$ ) and  $\text{AgNO}_3$  (25.0 mg, 147.2  $\mu\text{mol}$ ). The mixture was dissolved in  $\text{H}_2\text{O}$  (0.4 mL) and  $\text{Me}_2\text{CO}$  (0.4 mL), and the solution was heated to 60 °C. After 1 h, the reaction was cooled to ambient temperature, diluted with  $\text{H}_2\text{O}$  (5 mL) and  $\text{Et}_2\text{O}$  (5 mL). The phases were separated, and the aqueous portion was extracted with  $\text{Et}_2\text{O}$  (2x 5 mL). The combined organics were washed with brine, dried over anhydrous  $\text{MgSO}_4$ , and concentrated under reduced pressure. Analysis of the crude NMR indicated that the proportion of triketone **2.140** formed was <5%.

Entry 4: A vial was charged with cyclobutanol **2.139** (5.0 mg, 14.4  $\mu\text{mol}$ ), acridinium photocatalyst **2.141** (0.6 mg, 1.5  $\mu\text{mol}$ ), DBU (4.3 mg, 28.9  $\mu\text{mol}$ ), TEMPO (4.7 mg, 30.0  $\mu\text{mol}$ ) and MeCN (0.8 mL). The vial was sealed under air and irradiated with 420 nm LEDs for 1.5 h with vigorous stirring, then diluted with 1 N HCl (5 mL) and  $\text{Et}_2\text{O}$  (5 mL). The phases were separated, and the aqueous portion was extracted with  $\text{Et}_2\text{O}$  (2x 5 mL). The combined organics were washed with brine, dried over  $\text{MgSO}_4$ , and concentrated under reduced pressure. Yield of ketone **2.140** was determined by  $^1\text{H}$  NMR analysis of the crude mixture with 1.0 equivalent of mesitylene from a stock solution (100  $\mu\text{L}$  of a 0.144 M solution in  $\text{CDCl}_3$ ) added as an internal standard. Comparison of the integrations of mesitylene peak (s, 6.80 ppm, integration = 3.0) and a cleanly resolved peak corresponding to triketone **2.140** (3.33 d,  $J = 12.4$  Hz, integration = 0.23) determined the yield to be 23%.

Entry 5: A vial was charged with cyclobutanol **2.139** (5.0 mg, 14.4  $\mu\text{mol}$ ),  $[\text{Ir}(\text{dF}(\text{CF}_3)\text{ppy})_2(\text{dtbpy})]\text{PF}_6$  **2.142** (0.7 mg, 6.2  $\mu\text{mol}$ ),  $\text{K}_2\text{HPO}_4$  (5.0 mg, 28.9  $\mu\text{mol}$ ), and THF (0.8 mL). The vial was sealed under air and irradiated with 420 nm LEDs for 1.5 h with vigorous stirring, then diluted with 1 N HCl (5 mL) and  $\text{Et}_2\text{O}$  (5 mL). The phases were separated, and the aqueous portion was extracted with  $\text{Et}_2\text{O}$  (2x 5 mL). The combined organics were washed with

brine, dried over MgSO<sub>4</sub>, and concentrated under reduced pressure. Yield of ketone **2.140** was determined by <sup>1</sup>H NMR analysis of the crude mixture with 1.0 equivalent of mesitylene from a stock solution (100 μL of a 0.144 M solution in CDCl<sub>3</sub>) added as an internal standard. Comparison of the integrations of mesitylene peak (s, 6.80 ppm, integration = 3.0) and a cleanly resolved peak corresponding to triketone **2.140** (3.33 d, J = 12.4 Hz, integration = 0.09) determined the yield to be 9%.

Entry 6: See above, page 178. Yield determined by <sup>1</sup>H NMR was 80%.

## 2.10. References

- (1) Corey, E. J.; Cheng, X.-M. *The Logic of Chemical Synthesis*; John Wiley & Sons, 1989.
- (2) For isolation and structural elucidation, see above, Chapter 1 page 1.
- (3) For an overview of the chemical reactivity of mutilins: Fazakerley, N. J.; Procter, D. J. *Tetrahedron* **2014**, *70*, 6911.
- (4) For a detailed discussion of prior synthetic efforts, see above, Chapter 1 pages 14–33.
- (5) (a) Boeckman Jr., R. K.; Springer, D. M.; Alessi, T. R. *J. Am. Chem. Soc.* **1989**, *111*, 8284. (b) Fazakerley, N. J.; Helm, M. D.; Procter, D. J. *Chem. Eur. J.* **2013**, *19*, 6718.
- (6) (a) Murphy, S. K.; Zeng, M.; Herzon, S. B. *Science* **2017**, *356*, 956. (b) Zeng, M.; Murphy, S. K.; Herzon, S. B. *J. Am. Chem. Soc.* **2017**, *139*, 16377. (c) Farney, E. P.; Feng, S. S.; Schäfers, F.; Reisman, S. E. *J. Am. Chem. Soc.* **2018**, *140*, 1267.
- (7) Some classic examples of ring-expansion to prepare cyclooctanoid natural products: (a) Paton, R. M.; Ross, J. F.; Crosby, J. *J. Chem. Soc. Chem. Commun.* **1980**, 11945. (b) Paquette, L. A.; Ham, W. H. *J. Am. Chem. Soc.* **1987**, *109*, 3025. A synthetic study toward taxol (c) Winkler, J. D.; Subrahmanyam, D. *Tetrahedron* **1992**, *48*, 7049. A more recent example: (d) Maimone, T. J.; Shi, J.; Ashida, S.; Baran, P. S. *J. Am. Chem. Soc.* **2009**, *131*, 17066.
- (8) Coote, S. C.; O'Brien, P.; Whitwood, A. C. *Org. Biomol. Chem.* **2008**, *6*, 4299.
- (9) Nakashima, D.; Yamamoto, H. *J. Am. Chem. Soc.* **2006**, *128*, 9626.
- (10) (a) Jung, M. E.; Ho, D.; Chu, H. V. *Org. Lett.* **2005**, *7*, 1649. (b) Jung, M. E.; Guzaev, M. *Org. Lett.* **2012**, *14*, 5169. Early report of alkylaluminum triflimide as a catalyst: Marx, A.; Yamamoto, H. *Angew. Chem., Int. Ed.* **2000**, *39*, 178.
- (11) Relevant review: Yamamoto, H.; Futatsugi, K. *Angew. Chem., Int. Ed.* **2005**, *44*, 1924. Application in total synthesis: Jewett, J. C.; Rawal, V. H. *Angew. Chem., Int. Ed.* **2007**, *46*, 6502.
- (12) For an excellent example of an *exo*-selective Diels–Alder reaction: Jung, M. E.; Davidov, P. *Angew. Chem., Int. Ed.* **2002**, *41*, 4125. For an outline of mechanistic details: Lam, Y.; Cheong, P. H.-Y.; Mata, J. M. B.; Stanway, S. J.; Gouverneur, V.; Houk, K. N. *J. Am. Chem. Soc.* **2009**, *131*, 1947.
- (13) Some enantioselective Diels–Alder reactions we evaluated: Ryu, D. H.; Corey, E. J. *J. Am. Chem. Soc.* **2003**, *125*, 6388. Liu, D.; Canales, E.; Corey, E. J. *J. Am. Chem. Soc.* **2007**, *129*, 1498.
- (14) (a) Evans, P. A.; Longmire, J. M.; Modi, D. P. *Tetrahedron Lett.* **1995**, *36*, 3985. For an application in synthesis: (b) Liu, J. F.; Heathcock, C. H. *J. Org. Chem.* **1999**, *64*, 8263.

- (15) Magnus, P.; Evans, A.; Lacour, J. *Tetrahedron Lett.* **1992**, *33*, 2933. Magnus, P.; Lacour, J.; Evans, P. A.; Rigollier, P.; Tobler, H. *J. Am. Chem. Soc.* **1998**, *120*, 12486.
- (16) (a) Ito, Y.; Hirao, T.; Saegusa, T. *J. Org. Chem.* **1978**, *43*, 1011.
- (17) (a) Diao, T.; Stahl, S. S. *J. Am. Chem. Soc.* **2011**, *133*, 14566. (b) Yu, J-Q.; Wu, H-C.; Corey, E. J. *Org. Lett.* **2005**, *7*, 1415.
- (18) Selenation of TIPS enoxysilane derivatives in total synthesis: (a) Boeckman Jr., R. K.; del Rosario Ferreira, M. R.; Mitchell, L. H.; Shao, P.; Neeb, M. J. Fang, Y. *Tetrahedron* **2011**, *67*, 9787. (b) Woo, C. M.; Gholap, S. L.; Lu, L.; Kaneko, M.; Li, Z.; Ravikumar, P. C.; Herzon, S. B. *J. Am. Chem. Soc.* **2012**, *134*, 17262.
- (19) Use of DDQ to oxidize TIPS enoxysilane: Corey, E. J.; Guzman-Perez, A.; Loh, T-P. *J. Am. Chem. Soc.* **1994**, *116*, 3611.
- (20) (a) Lo, J. C.; Yabe, Y.; Baran, P. S. *J. Am. Chem. Soc.* **2014**, *136*, 1304. (b) Lo, J. C.; Gui, J.; Yabe, Y.; Pan, C.-M.; Baran, P. S. *Nature* **2014**, *516*, 343. (c) Lo, J. C.; Kim, D.; Pan, C-M.; Edwards, J. T.; Yabe, Y.; Gui, J.; Qin, T.; Gutierrez, S.; Giacoboni, J.; Smith, M. W.; Holland, P. L.; Baran, P. S. *J. Am. Chem. Soc.* **2017**, *139*, 2484.
- (21) (a) George, D. T.; Kuenstner, E. J.; Pronin, S. V. *J. Am. Chem. Soc.* **2015**, *137*, 15410. (b) Deng, H.; Cao, W.; Liu, R.; Zhang, Y.; Liu, B. *Angew. Chem. Int. Ed.* **2017**, *56*, 5849. (c) Lu, Z.; Zhang, X.; Guo, Z.; Chen, Y.; Mu, T.; Li, A. *J. Am. Chem. Soc.* **2018**, *140*, 9211. (d) Godfrey, N. A.; Schatz, D. J.; Pronin, S. V. *J. Am. Chem. Soc.* **2018**, *140*, 12770. (e) Thomas, W. P.; Schatz, D. J.; George, D. T.; Pronin, S. V. *J. Am. Chem. Soc.* **2019**, *141*, 12246. (f) Xu, G.; Wu, J.; Li, L.; Lu, Y.; Li, C. *J. Am. Chem. Soc.* **2020**, *142*, 15240. (g) Thomas, W. P.; Pronin, S. V. *J. Am. Chem. Soc.* **2022**, *144*, 118.
- (22) Obradors, C.; Martinez, R. M.; Shenvi, R. A. *J. Am. Chem. Soc.* **2016**, *138*, 4962.
- (23) For a review of MHAT-initiated reactions: Crossley, S. W. M.; Martinez, R. M.; Obradors, C.; Shenvi, R. A. *Chem. Rev.* **2016**, *116*, 8912.
- (24) Kim, D.; Rahaman, S. M. W.; Mercado, B. Q.; Poli, R.; Holland, P. *J. Am. Chem. Soc.* **2019**, *141*, 7473.
- (25) See ref 21a,d,e,g.
- (26) (a) Magnus, P.; Payne, A. H.; Waring, M. J.; Scott, D. A.; Lynch, V. *Tetrahedron Lett.* **2000**, *41*, 9725. (b) Magnus, P.; Scott, D. A.; Fielding, M. R. *Tetrahedron Lett.* **2001**, *42*, 4127.
- (27) Hirao, T. *Small Ring Compounds in Organic Synthesis V* pp. 99–147. Springer-Verlag Berlin. See also refs. 33-37 for related mechanistic proposals.
- (28) Tsunoda, T.; Noyori, R. *Tetrahedron Lett.* **1980**, *21*, 1357.
- (29) Note: the application of *bis*-trimethylsilyl ethylene glycol proceeded in a similar fashion but the resulting mixture of epimeric ketals were inseparable by chromatography.
- (30) Morlender-Vais, N.; Solodovnikova, N.; Marek, I. *Chem. Commun.* **2000**, 1849.
- (31) Initial report of Sato's reagent: (a) Harada, K.; Urabe, H.; Sato, F. *Tetrahedron Lett.* **1995**, *36*, 3203. Review of low-valent titanium / C–C multiple bond complexes: (b) Sato, F.; Urabe, H.; Okamoto, S. *Chem. Rev.* **2000**, *100*, 2835.
- (32) Applications of relevant titanium-alkyne complexes in total synthesis: (a) Belardi, J. K.; Micalizio, G. C. *Angew. Chem., Int. Ed.* **2008**, *47*, 4005. (b) Du, K.; Kier, M. J.; Stempel, Z. D.; Jeso, V.; Rheingold, A. L.; Micalizio, G. C. *J. Am. Chem. Soc.* **2020**, *142*, 12937.

- (33) (a) Snider, B. B.; Vo, N. H.; Foxman, B. M. *J. Org. Chem.* **1993**, *25*, 7228. Analogous Mn-catalyzed ring-expansion of cyclopropanols: (b) Nobuharu, I.; Masahiro, F.; Satoshi, H.; Koichi, N. *Chem. Lett.* **1993**, *22*, 545. (c) Snider, B. B.; Kwon, T.; *J. Org. Chem.* **1992**, *57*, 2399.
- (34) (b) Ito, Y.; Fujii, S.; Saegusa, T. *J. Org. Chem.* **1976**, *41*, 2073. (b) Booker-Milburn, K. I.; Thompson, D. F. *Tetrahedron Lett.* **1993**, *34*, 7291.
- (35) Hirao, T.; Fujii, T.; Tanaka, T.; Oshiro, Y. *Synlett* **1994**, 845.
- (36) Meyer, K.; Roček, J. *J. Am. Chem. Soc.* **1972**, *94*, 1209.
- (37) Fujioka, H.; Komatsu, H.; Miyoshi, A.; Murai, K.; Kita, Y. *Tetrahedron Lett.* **2011**, *52*, 973.
- (38) Similar cyclic arene-fused iodanes have been prepared: (a) Brand, J. P.; Chevalley, C.; Scopelliti, R.; Waser, J. *Chem. Eur. J.* **2012**, *18*, 5655. (b) Moss, R. A.; Wilk, B.; Krogh-Jespersen, K.; Blair, J. T.; Westbrook, J. D. *J. Am. Chem. Soc.* **1989**, *111*, 250.
- (39) Cyclopropanol oxidative cleavage with Pb(OAc)<sub>4</sub>: Rubottom, G. M.; Krueger, M. D. S.; Schreiner, J. L. *Tetrahedron Lett.* **1977**, *18*, 4013.
- (40) Hwang, C.-S.; Reusch, W. *Synthesis* **1989**, 428.
- (41) Kim, Y.; Kim, D. Y. *Tetrahedron Lett.* **2019**, *60*, 1538.
- (42) Dissolving metal reduction of a bicyclo[5.1.0] ketone proceeding with scission of the exocyclic bond: Gampe, C. M.; Carreira, E. M. *Angew. Chem., Int. Ed.* **2011**, *50*, 2962.
- (43) (a) Yamakoshi, H.; Kawamura, S.-I.; Nojima, M.; Mayr, H.; Baran, J. *J. Org. Chem.* **1996**, *61*, 5939. (b) Bailey, P. S.; Hwang, H. H.; Chiang, C. Y. *J. Org. Chem.* **1985**, *50*, 231.
- (44) Imamoto, T.; Takiyama, N.; Nakamura, K.; Hatajima, T.; Kamiya, Y. *J. Am. Chem. Soc.* **1989**, *111*, 4392.
- (45) Kinoshita, A.; Mori, M. *Chem. Lett.* **1994**, 1475.
- (46) (a) Rieke, R. D.; Xiong, H. *J. Org. Chem.* **1991**, *56*, 3109. (b) Tamao, K.; Akita, M.; Kanatani, R.; Ishida, N.; Kumada, M. *J. Organomet. Chem.* **1982**, *226*, C9.
- (47) Vedejs, E. *J. Am. Chem. Soc.* **1974**, *96*, 5944.
- (48) He, J.; Tchabanenko, K.; Adlington, R. M.; Cowley, A. R.; Baldwin, J. E. *Eur. J. Org. Chem.* **2006**, *17*, 4003.
- (49) A relevant review of decarboxylative functionalizations: Zeng, Z.; Feceu, A.; Sivendran, N.; Gooßen, L. *Adv. Synth. Catal.* **2021**, *363*, 2678.
- (50) Mander, L. N.; Sethi, S. P. *Tetrahedron Lett.* **1983**, *24*, 5425.
- (51) Yoshida, J.-I.; Nakatani, S.; Sakaguchi, K.; Isoe, S. *J. Org. Chem.* **1989**, *54*, 3383.
- (52) (a) Yang, W.; Cao, J.; Zhang, M.; Lan, R.; Zhu, L.; Du, G.; He, S.; Lee, C.-S. *J. Org. Chem.* **2015**, *80*, 836. (b) Parrish, J. D.; Ischay, M. A.; Lu, Z.; Guo, S.; Peters, N. R.; Yoon, T. P. *Org. Lett.* **2012**, *14*, 1640. (c) Tamai, T.; Mizuno, K.; Hashida, I.; Otsuji, Y. *Tetrahedron Lett.* **1993**, *34*, 2641. (d) Yin, J.; Wang, C.; Kong, L.; Cai, S.; Gao, S. *Angew. Chem., Int. Ed.* **2012**, *51*, 7786. (e) see also ref. 51.
- (53) The structure was inferred by subjecting the chlorinated product **2.99** to MHAT conditions, which led to an alternative cyclization product.
- (54) Wakamatsu, K.; Tan, H.; Ban, N.; Uchiyama, N.; Niwa, H.; Yamada, K. *Chem. Lett.* **1987**, 121.
- (55) Crabtree, S. R.; Chu, W. L. A.; Mander, L. N. *Synlett* **1990**, 169.

- (56) Saladrigas, M.; Bosch, C.; Saborit, G. V.; Bonjoch, J.; Bradshaw, B. *Angew. Chem., Int. Ed.* **2018**, *57*, 182.
- (57) Conditions were the same as employed above in Scheme 2.17B.
- (58) Similar retro-aldol ring expansions have been used in the preparation of cyclooctanes: Lange, G. L.; Organ, M. G. *J. Org. Chem.* **1996**, *61*, 5358. See also ref. 7c.
- (59) Nägeli, P. Ph.D. Thesis, ETH, Zurich 1961.
- (60) Petasis, N. A.; Patane, M. A. *Tetrahedron* **1992**, *48*, 5757.
- (61) Use of alane to avoid ring-opening during azetidione reduction: Jackson, M. B.; Mander, L. N.; Spotswood, T. M. *Aust. J. Chem.* **1983**, *36*, 779.
- (62) The use of LDA in place of LiTMP led to the formation of Mannich adducts.
- (63) Bowen, M. E.; Aavula, B. R.; Mash, E. A. *J. Org. Chem.* **2002**, *67*, 9087.
- (64) Payette, J. N.; Yamamoto, H. *J. Am. Chem. Soc.* **2008**, *130*, 12276.
- (65) Use of TASF for enolate functionalization: Noyori, R.; Nishida, I. Sakata, J. *Tetrahedron Lett.* **1980**, *21*, 2085.
- (66) We could not identify any prior reports of transannular aldolization to form a [4.2.0]bicyclic structure from a cyclooctanoid.
- (67) A related base-mediated fragmentation of an arylcyclobutanol has been reported: (a) Cohen, T.; Bhupathy, M.; Matz, J. R. *J. Am. Chem. Soc.* **1983**, *105*, 520. Additionally, extrusion of allylic organometallics appended to ketoesters during attempted Barbier-type additions has been observed: Molander, G. A.; Etter, J. B.; Zinke, P. W. *J. Am. Chem. Soc.* **1987**, *109*, 453.
- (68) The only reported use of TMSE cyanofornate, to our knowledge: Yamamoto, K.; Hentemann, M. F.; Allen, J. G.; Danishefsky, S. J. *Chem. Eur. J.* **2003**, *9*, 3242.
- (69) A related preparation of allyl cyanofornate: Huber, T.; Preuhs, T. A.; Gerlinger, C. K. G.; Magauer, T. *J. Org. Chem.* **2017**, *82*, 7410.
- (70) (a) Barton, D. H. R.; Crich, D.; Motherwell, W. B. *J. Chem. Soc., Chem. Commun.* **1984**, 242. For an example in total synthesis: (b) Takasu, K.; Mizutani, S.; Noguchi, M.; Makita, K.; Ihara, M. *Org. Lett.* **1999**, *1*, 391. See also ref. 49.
- (71) (a) Mosher, W. A.; Kehr, C. L. *J. Am. Chem. Soc.* **1953**, *75*, 3172. (b) Kochi, J. K. *J. Am. Chem. Soc.* **1965**, *87*, 1811. (c) Snider, B. B.; Kwon, T. *J. Org. Chem.* **1990**, *55*, 1965.
- (72) (a) Firstad, W. E.; Fry, M. A.; Klang, J. A. *J. Org. Chem.* **1983**, *48*, 3575. For a relevant review: (b) Varenikov, A.; Shapiro, E.; Gandelman, M. *Chem. Rev.* **2021**, *121*, 412.
- (73) (a) Song, H.-T.; Ding, W.; Zhou, Q.-Q.; Liu, J.; Lu, L.-Q.; Xiao, W.-J. *J. Org. Chem.* **2016**, *81*, 7250. (b) Okada, K.; Okubo, K.; Oda, M. *Tetrahedron Lett.* **1992**, *33*, 83.
- (74) For a review of photocatalytic decarboxylative processes: Xuan, J.; Zhang, Z.-G.; Xiao, W.-J. *Angew. Chem., Int. Ed.* **2015**, *54*, 15632.
- (75) Khan, S. N.; Zaman, M. K.; Li, R.; Sun, Z. *J. Org. Chem.* **2020**, *85*, 5019.
- (76) Chu, L.; Ohta, C.; Zuo, Z.; MacMillan, D. W. C. *J. Am. Chem. Soc.* **2014**, *136*, 10886.
- (77) Examples of TEMPO serving to trap intermediate alkyl radicals under similar conditions: (a) Cao, H.; Jiang, H.; Feng, H.; Kwan, J. M. C.; Liu, X.; Wu, J. *J. Am. Chem. Soc.* **2018**, *140*, 16360. (b) Wu, Z.; Gockel, S. N.; Hull, K. L. *Nat. Commun.* **2021**, *12*, 5956.



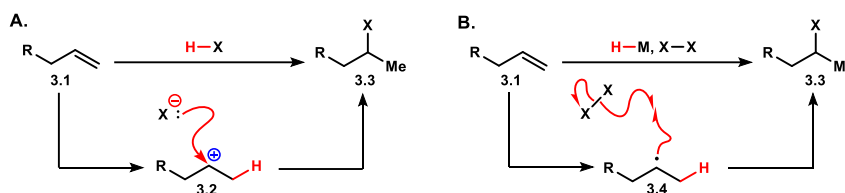
- (78) (a) Fort, A. W. *J. Am. Chem. Soc.* **1962**, *84*, 2620. (b) Fohlisch, B.; Joachimi, R. *Chem. Ber.* **1987**, *120*, 1951. (c) Vander Wal, M. N.; Dilger, A. K.; MacMillan, D. W. C. *Chem. Sci.* **2013**, *4*, 3075.
- (79) (a) Gibbons, E. G. *J. Am. Chem. Soc.* **1982**, *104*, 1767. (b) See also ref. 6a,b,c.
- (80) Majgier-Baranowska, H.; Templeton, J. F. *Tetrahedron* **1999**, *55*, 3717.
- (81) (a) The trione **2.146** was known in the pleuromutilin semi-synthesis literature, being first reported by P. Nägeli in 1961, see ref. 59. (b) It was named mutilin trione in 1966 by Birch: Birch, A. J.; Holzapfel, C. W.; Rickards, R. W. *Tetrahedron* **1966**, *22*, 359. For relevant discussion, see Chapter 1 of this document. No related NMR spectra had ever been reported of the trione **2.146** to our knowledge.
- (82) Still, W. C.; Kahn, M.; Mitra, A. *J. Org. Chem.* **1978**, *43*, 2923.
- (83) Coote, S. C.; O'Brien, P.; Whitwood, A. C. *Org. Biomol. Chem.* **2008**, *6*, 4299.
- (84) Brenninger, C.; Pöthig, A.; Bach, T. *Angew. Chem. Int. Ed.* **2017**, *56*, 4337.
- (85) Nakashima, D.; Yamamoto, H. *J. Am. Chem. Soc.* **2006**, *128*, 9626.
- (86) Obradors, C.; Martinez, R. M.; Shenvi, R. A. *J. Am. Chem. Soc.* **2016**, *138*, 4962.
- (87) Blanchard, C.; Framery, E.; Vaultier, M. *Synthesis* **1996**, 45.
- (88) Fürstner, A.; Grela, K.; Mathes, C.; Lehmann, C. W. *J. Am. Chem. Soc.* **2000**, *122*, 11799.
- (89) Miyaoka, H.; Isaji, Y.; Mitome, H.; Yamada, Y. *Tetrahedron* **2003**, *59*, 61.
- (90) Harrowven, D. C.; Curran, D. P.; Kostiuk, S. L.; Wallis-Guy, I. L.; Whiting, S.; Stenning, K. J.; Tang, B.; Packard, E.; Nanson, L. *Chem. Commun.* **2010**, *46*, 6335.
- (91) Vedejs, E.; Larsen, S. *Org. Synth.* **1986**, *64*, 127.
- (92) Lee, J.; Chen, D. Y. K. *Angew. Chem. Int. Ed.* **2019**, *58*, 488.
- (93) Yamamoto, K.; Hentemann, M. F.; Allen, J. G.; Danishefsky, S. J. *Chem. Eur. J.* **2003**, *9*, 3242.
- (94) Altamura, M.; Cesti, P.; Francalanci, F.; Marchi, M. *J. Chem. Soc. Perkin Trans. 1*, **1989**, 1225.
- (95) Schulz, G.; Berner, H. *Tetrahedron* **1984**, *40*, 905.
- (96) (a) Spartan 18, Wavefunction Inc., Irvine CA. (b) Shao, Y.; Gan, Z.; Epifanovsky, E.; Gilbert, A. T. B.; Wormit, M.; Kussmann, J.; Lange, A. W.; Behn, A.; Deng, J.; Feng, X.; Ghosh, D.; Goldey, M.; Horn, P. R.; Jacobson, L. D.; Kaliman, I.; Khaliullin, R. Z.; Kuś, T.; Landau, A.; Liu, J.; Proynov, E. I.; Rhee, Y. M.; Richard, R. M.; Rohrdanz, M. A.; Steele, R. P.; Sundstrom, E. J.; Woodcock, H. L., III; Zimmerman, P. M.; Zuev, D.; Albrecht, B.; Alguire, E.; Austin, B.; Beran, G. J. O.; Bernard, Y. A.; Berquist, E.; Brandhorst, K.; Bravaya, K. B.; Brown, S. T.; Casanova, D.; Chang, C.-M.; Chen, Y.; Chien, S. H.; Closser, K. D.; Crittenden, D. L.; Diedenhofen, M.; DiStasio, R. A., Jr.; Do, H.; Dutoi, A. D.; Edgar, R. G.; Fatehi, S.; FustiMolnar, L.; Ghysels, A.; Golubeva-Zadorozhnaya, A.; Gomes, J.; Hanson-Heine, M. W. D.; Harbach, P. H. P.; Hauser, A. W.; Hohenstein, E. G.; Holden, Z. C.; Jagau, T.-C.; Ji, H.; Kaduk, B.; Khistyayev, K.; Kim, J.; Kim, J.; King, R. A.; Klunzinger, P.; Kosenkov, D.; Kowalczyk, T.; Krauter, C. M.; Lao, K. U.; Laurent, A. D.; Lawler, K. V.; Levchenko, S. V.; Lin, C. Y.; Liu, F.; Livshits, E.; Lochan, R. C.; Luenser, A.; Manohar, P.; Manzer, S. F.; Mao, S.-P.; Mardirossian, N.; Marenich, A. V.; Maurer, S. A.; Mayhall, N. J.; Neuscammann, E.; Oana, C. M.; Olivares-Amaya, R.; O'Neill, D. P.; Parkhill, J. A.; Perrine, T. M.; Peverati, R.; Prociuk, A.; Rehn, D. R.; Rosta, E.; Russ, N.

J.; Sharada, S. M.; Sharma, S.; Small, D. W.; Sodt, A.; Stein, T.; Stück, D.; Su, Y.-C.; Thom, A. J. W.; Tsuchimochi, T.; Vanovschi, V.; Vogt, L.; Vydrov, O.; Wang, T.; Watson, M. A.; Wenzel, J.; White, A.; Williams, C. F.; Yang, J.; Yeganeh, S.; Yost, S. R.; You, Z.-Q.; Zhang, I. Y.; Zhang, X.; Zhao, Y.; Brooks, B. R.; Chan, G. K. L.; Chipman, D. M.; Cramer, C. J.; Goddard III, W. A.; Gordon, M. S.; Hehre, W. J.; Klamt, A.; Schaefer, H. F., III; Schmidt, M. W.; Sherrill, C. D.; Truhlar, D. G.; Warshel, A.; Xu, X.; Aspuru-Guzik, A.; Baer, R.; Bell, A. T.; Besley, N. A.; Chai, J.-D.; Dreuw, A.; Dunietz, B. D.; Furlani, T. R.; Gwaltney, S. R.; Hsu, C.-P.; Jung, Y.; Kong, J.; Lambrecht, D. S.; Liang, W.; Ochsenfeld, C.; Rassolov, V. A.; Slipchenko, L. V.; Subotnik, J. E.; Van Voorhis, T.; Herbert, J. M.; Krylov, A. I.; Gill, P. M. W.; Head-Gordon, M. Advances in Molecular Quantum Chemistry Contained in the Q-Chem 4 Program Package. *Molecular Physics* **2014**, *113*, 184.  
(97) CYLview20; Legault, C. Y., Université de Sherbrooke, 2020 (<http://www.cylview.org>)

## CHAPTER 3: RADICAL–POLAR CROSSOVER REACTIONS OF ALLYLIC ALCOHOLS

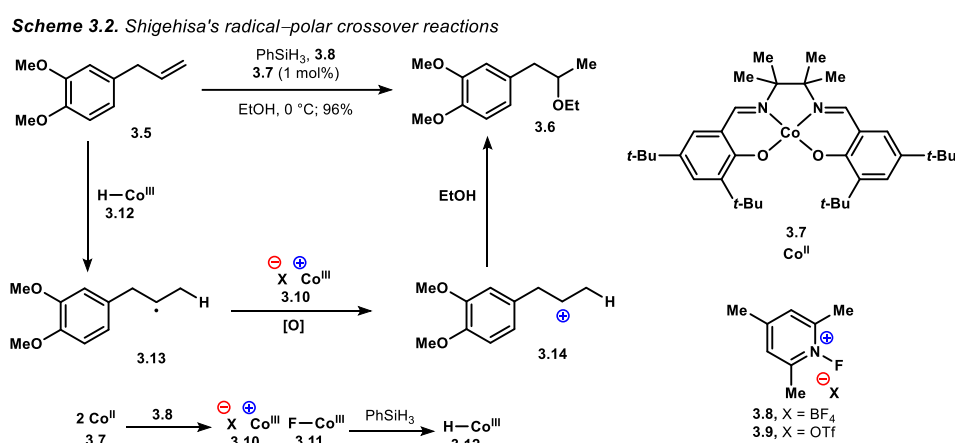
### 3.1. Markovnikov-Selective Radical Alkene Hydrofunctionalization

Scheme 3.1. A. Acid-mediated alkene hydrofunctionalization B. MHAT alkene hydrofunctionalization



Markovnikov-selective alkene hydrofunctionalization has long served as an indispensable tool for synthetic organic chemists. Traditionally, these transformations have been performed by treatment of an alkene **3.1** with a Brønsted acid to generate a carbocation **3.2**, which is next captured by a suitable heteroatom nucleophile, typically the counterion to the acid or solvent, to furnish the hydrofunctionalized product **3.3** (Scheme 3.1A). Owing to their operational simplicity and longstanding utility, Brønsted acid-mediated or catalyzed alkene hydrofunctionalizations are frequently used to this day.<sup>1</sup> The drawbacks of this approach are the poor chemoselectivity associated with the use of strong acids and the numerous deleterious pathways in which highly reactive carbocationic intermediates may participate. As a result, radical alkene hydrofunctionalization reactions have become increasingly valued by synthetic chemists.<sup>2</sup> Typically, these processes are mediated by *in situ*-generated metal hydride species, which react in a hydrogen atom transfer (HAT) reaction with an alkene **3.1** to form alkyl radical intermediates **3.4** (Scheme 3.1B). Therefore, the name for reactions with these mechanistic underpinnings is metal-hydride mediated hydrogen atom transfer (MHAT). As would be expected on the basis of mechanistic differences, MHAT reactions display far superior chemoselectivity to the corresponding acid-mediated processes. One of the first MHAT reactions to see widespread use is the Drago–Mukaiyama hydration, which was first described in the 1980s.<sup>3,4</sup> In the decades since, numerous related transformations have been identified, and some of the relevant mechanistic details have been deciphered.<sup>5</sup> While these two reaction

types are often thought of as analogous, the reactivity of the two key intermediates, carbocation **3.2** and alkyl radical **3.3**, is quite opposite. The empty orbital of the carbocation **3.2** is a viciously reactive electrophile. Conversely, the singly-occupied orbital of alkyl radical **3.5** is an electron rich, nucleophilic species that will react more rapidly with electron-deficient, electrophilic acceptors than the corresponding electron-rich acceptor.<sup>6</sup> This effect has been cleverly leveraged in the MHAT manifold to engage canonical electrophiles, such as  $\alpha,\beta$ -unsaturated carbonyl derivatives or a variety of traditionally electrophilic groups.<sup>7-9</sup>



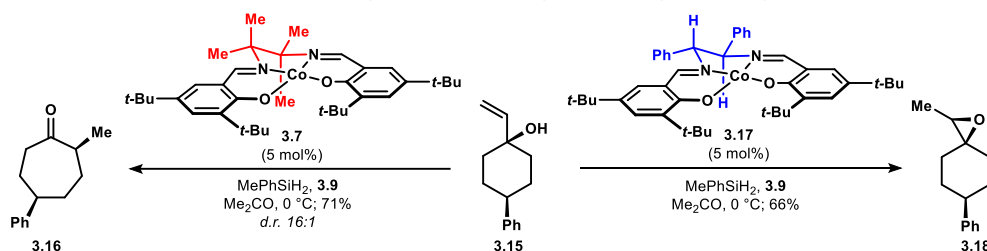
In 2013, Shigehisa's laboratory reported a new mode of reactivity initiated by MHAT. They found that exposure of alkene **3.5** to cobalt salen complex **3.7** in the presence of phenylsilane and *N*-fluorocollidinium **3.8** with alcoholic solvent furnished the hydroetherification product **3.6**.<sup>10</sup> Further exploration of the reactivity underscored a likely mechanism: *in situ*-generated cobalt fluoride species **3.11**, formed by reaction of the salen pre-catalyst **3.7** with the *N*-fluorocollidinium salt **3.8**, reacts with the hydrosilane to generate a cobalt hydride **3.12**. The active cobalt hydride **3.12** then engages the alkene substrate **3.5** in a HAT event, forming the intermediate alkyl radical **3.13**. Subsequent single-electron oxidation of the alkyl radical, presumably by a cobalt(III) complex **3.10**, affords the carbocation intermediate **3.14**. Solvolytic capture of the carbocation **3.14** affords, after proton transfers, the observed product. Shigehisa's group proved the utility of these processes by engaging the electrophilic species

with a host of other nucleophiles.<sup>11</sup> The so-called radical–polar crossover (RPC) reactions offered a unique method for generation of carbocationic species from alkenes that obviated the need for potent Brønsted acids. The MHAT RPC reaction manifold displays high chemoselectivity but enables the formation of electrophilic intermediates, thereby drastically expanding the scope of reactivities available within the MHAT manifold.

### 3.2. Radical–Polar Crossover Reactions of Allylic Alcohols

Our initial interest stemmed from a simple idea: MHAT radical–polar crossover should enable the formation of carbocations from alkenes even in the presence of acid-labile functionalities. As such, we started by evaluating the reactivity of tertiary allylic alcohols under MHAT RPC conditions. Initial work in this area was performed by Eric E. Touney.<sup>12</sup> Eric soon identified an unusual reactivity feature. Exposure of vinyl carbinol **3.15** to the cobalt salen catalyst **3.7** in the presence of *N*-fluorocollidinium **3.9** and PhMeSiH<sub>2</sub> afforded the semi-pinacol adduct **3.16** in 71% yield. Curiously, exchanging the catalyst the cobalt salen **3.17** fitted with a 1,2-diphenyldiamine backbone, but under otherwise identical conditions, afforded a different major product: epoxide **3.18**.

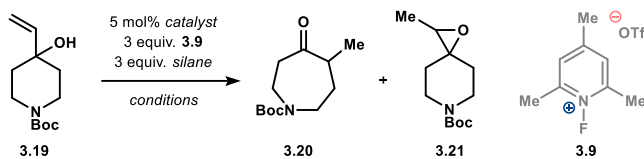
**Scheme 3.3.** Initial hit for bifurcated reactivity dependent on catalyst structure by Eric Touney



We reasoned that the catalyst-dependent reactivity carried mechanistic implications (see *below*), but we first aimed to evaluate the reactivity and optimize the reaction for each outcome. At this point, I joined the efforts and began evaluating the reactivity of piperidone-derived allylic alcohol **3.19** (Table 1). We found that the application of Eric’s conditions with catalyst **3.7** at 0 °C in acetone were optimal for the synthesis of ring-expanded ketone **3.20** (entry 7). Meanwhile, evaluation of a series of other cobalt salen complexes demonstrated that most were effective for

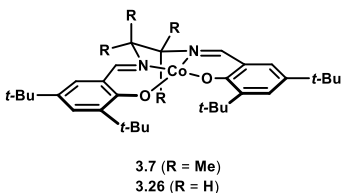
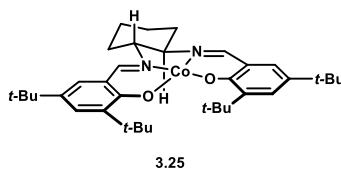
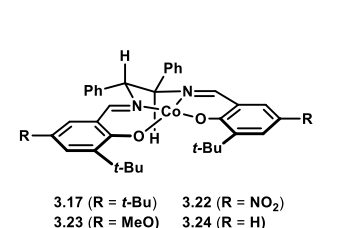
catalyzing the desired reactivity, but the efficiency was lower in all cases (entries 1-6). Eric's epoxidation conditions were quite effective on allylic alcohol **3.19**, furnishing the product **3.21** in a 3.2:1 ratio with the corresponding semi-pinacol adduct **3.20**. While some other catalysts such as cyclohexanediamine-derived salen **3.25** were selective for epoxidation, the diphenyl-substituted derivative **3.17** was superior (entries 1 and 5). One key finding was that reducing the reaction temperature to  $-40\text{ }^{\circ}\text{C}$  greatly improved the epoxide-selective nature of the reaction, increasing the ratio of epoxide **3.21** to ketone **3.20** to 9.3:1 (entry 10). While acetone was found to be the optimal solvent for both processes, dichloromethane was found to be a suitable alternative (entries 12-13). Of the evaluated silanes, tetramethyldisiloxane (TMDS) was the only alternative to  $\text{MePhSiH}_2$  we could identify that afforded comparable yields (entries 14-15). Satisfied with our optimization efforts, we moved to evaluate the scope of the reactivity.

**Table 3.1.** Optimization of catalyst-controlled MHAT RPC reactions of allylic alcohols



entry	catalyst	silane	conditions	3.19 (%) <sup>a</sup>	3.20 (%) <sup>a</sup>	3.21 (%) <sup>a</sup>
1	<b>3.17</b>	$\text{MePhSiH}_2$	$\text{Me}_2\text{CO}$ , $0\text{ }^{\circ}\text{C}$	<1	22	70
2	<b>3.22</b>	$\text{MePhSiH}_2$	$\text{Me}_2\text{CO}$ , $0\text{ }^{\circ}\text{C}$	14	52	10
3	<b>3.23</b>	$\text{MePhSiH}_2$	$\text{Me}_2\text{CO}$ , $0\text{ }^{\circ}\text{C}$	1	33	58
4	<b>3.24</b>	$\text{MePhSiH}_2$	$\text{Me}_2\text{CO}$ , $0\text{ }^{\circ}\text{C}$	1	16	42
5	<b>3.25</b>	$\text{MePhSiH}_2$	$\text{Me}_2\text{CO}$ , $0\text{ }^{\circ}\text{C}$	21	21	54
6	<b>3.26</b>	$\text{MePhSiH}_2$	$\text{Me}_2\text{CO}$ , $0\text{ }^{\circ}\text{C}$	48	5	35
7	<b>3.7</b>	$\text{MePhSiH}_2$	$\text{Me}_2\text{CO}$ , $0\text{ }^{\circ}\text{C}$	<1	63	14
8	<b>3.7</b>	$\text{MePhSiH}_2$	$\text{Me}_2\text{CO}$ , $-40\text{ }^{\circ}\text{C}$	<1	51	20
9	<b>3.7</b>	$\text{MePhSiH}_2$	$\text{Me}_2\text{CO}$ , $20\text{ }^{\circ}\text{C}$	18	53	11
10	<b>3.17</b>	$\text{MePhSiH}_2$	$\text{Me}_2\text{CO}$ , $-40\text{ }^{\circ}\text{C}$	<1	9	84
11	<b>3.17</b>	$\text{MePhSiH}_2$	$\text{Me}_2\text{CO}$ , $20\text{ }^{\circ}\text{C}$	<1	26	66
12	<b>3.17</b>	$\text{MePhSiH}_2$	$\text{CH}_2\text{Cl}_2$ , $-40\text{ }^{\circ}\text{C}$	<1	14	81
13	<b>3.7</b>	$\text{MePhSiH}_2$	$\text{CH}_2\text{Cl}_2$ , $0\text{ }^{\circ}\text{C}$	24	45	13
14	<b>3.17</b>	TMDS	$\text{Me}_2\text{CO}$ , $-40\text{ }^{\circ}\text{C}$	<1	7	78
15	<b>3.7</b>	TMDS	$\text{Me}_2\text{CO}$ , $0\text{ }^{\circ}\text{C}$	<1	66	15

<sup>a</sup>yields determined by  $^1\text{H}$  NMR by comparison to an internal standard



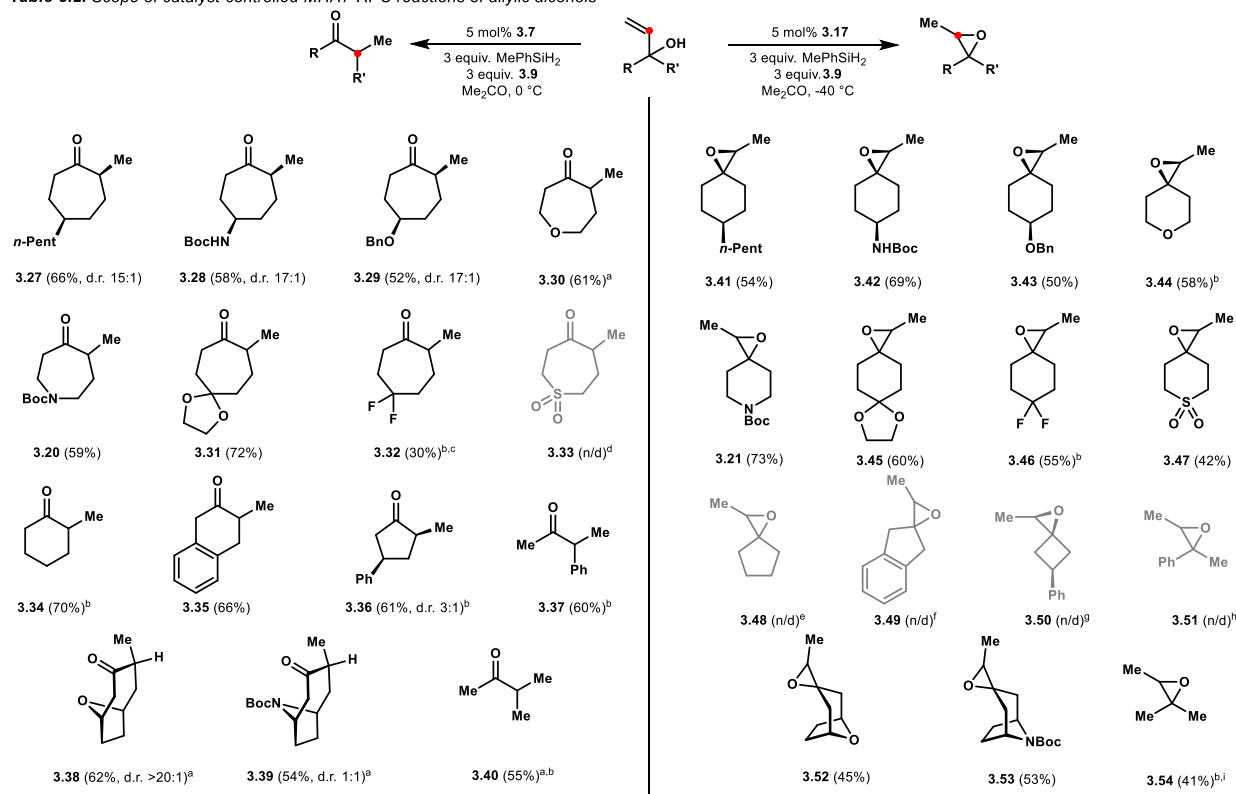
We found that conversion of dialkyl(vinyl)carbinols containing a six-membered cyclic scaffold could be generally converted into the corresponding ring-expanded ketones under the action of catalyst **3.7** (Table 3.2). In the case of 4-substituted derivatives, the products **3.27**,

**3.28**, and **3.29** were formed with high diastereoselectivity for the *cis* isomer. 4,4-disubstituted substrates were also readily engaged in ring-expansion, as exemplified by ketone **3.31**. Installation of a heteroatom within the cyclic system did not impede the selectivity or efficiency of the reaction, as the azepanone **3.20** and oxepanone **3.30** products were effectively prepared. Cyclic sulfonyl ketone **3.33** was not observed, presumably due to the electron-withdrawing nature of the sulfone function. Indeed, this effect was apparent during the synthesis of difluoroketone **3.32**, which was formed as a minor component of the reaction mixture regardless of catalyst structure. The semi-pinacol process was straightforwardly executed with 4- and 5-membered cyclic vinylcarbinols, furnishing ketones **3.34**, **3.35**, and **3.36**. Some bicyclic and acyclic substrates were effectively employed, affording the expected semi-pinacol adducts **3.37**, **3.38**, **3.39**, and **3.40**.

Merely exchanging the catalyst for related cobalt salen **3.17** and lowering the reaction temperature to -40 °C provided straightforward access to the corresponding epoxides in most cases (Table 3.2). To this end, 4-substituted derivatives **3.41**, **3.42**, **3.43** and **3.45** were prepared in moderate yields. Installation of a heteroatom into the 4-position of the cyclic system was well-tolerated, as epoxytetrahydropyran **3.44** and epoxy piperidine **3.21** were furnished in good yields. Including electron-withdrawing substituents on the cyclic substrate did not impede the epoxidation process to the same extent as the ring-expansion reactions; difluoroepoxide **3.46** was prepared in 55% yield, and the cyclic sulfonylepoxide **3.47** was synthesized in 42% yield, whereas the ketone was not observed. The scope of the epoxidation reaction was hindered to a greater extent by the ring size of the substrate. Attempts to extend the catalyst-controlled reactivity to 4- and 5-membered cyclic vinylcarbinols was unsuccessful, and the epoxide products **3.48**, **3.49**, and **3.50** were not observed. Acyclic substrates were effectively engaged in the catalyst-controlled reactivity, as 2-methyl-2-butene oxide **3.54** was prepared in 41% yield. However, linear substrates containing phenyl substituents were not tolerated, presumably due to the higher migratory aptitude of the aryl group, and the 2-methyl-1-

phenylpropene oxide **3.51** was not observed under the optimized conditions. Some more complex, bicyclic substrates performed well in the reaction, affording the epoxides **3.52** and **3.53**. During the course of the studies, Eric found similar trends to be true for substrates to which he applied the method.

**Table 3.2.** Scope of catalyst-controlled MHAT RPC reactions of allylic alcohols



n/d = not detected. Yield corresponds to pure isolated material. Ratio of epoxide to ketone >3:1 in all cases where epoxide is shown, unless otherwise stated. Ratio of ketone to epoxide >4:1 in all cases where ketone is shown, unless otherwise stated. <sup>a</sup>Pre-catalyst **3.22** was used. <sup>b</sup>Yield determined by <sup>1</sup>H NMR by comparison to an internal standard. <sup>c</sup>Major product was epoxide **3.46** (48% by NMR). <sup>d</sup>Major product was epoxide **3.47** (32% by NMR). <sup>e</sup>Major product was ketone **3.34** (90% by NMR). <sup>f</sup>Major product was ketone **3.35** (70% by NMR). <sup>g</sup>Major product was ketone **3.36** (85% isolated yield). <sup>h</sup>Major product was ketone **3.37** (66% isolated yield). <sup>i</sup>Pre-catalyst **3.23** was used. All experimental data obtained by NJF except for ketone **3.40**, which was obtained by EET.

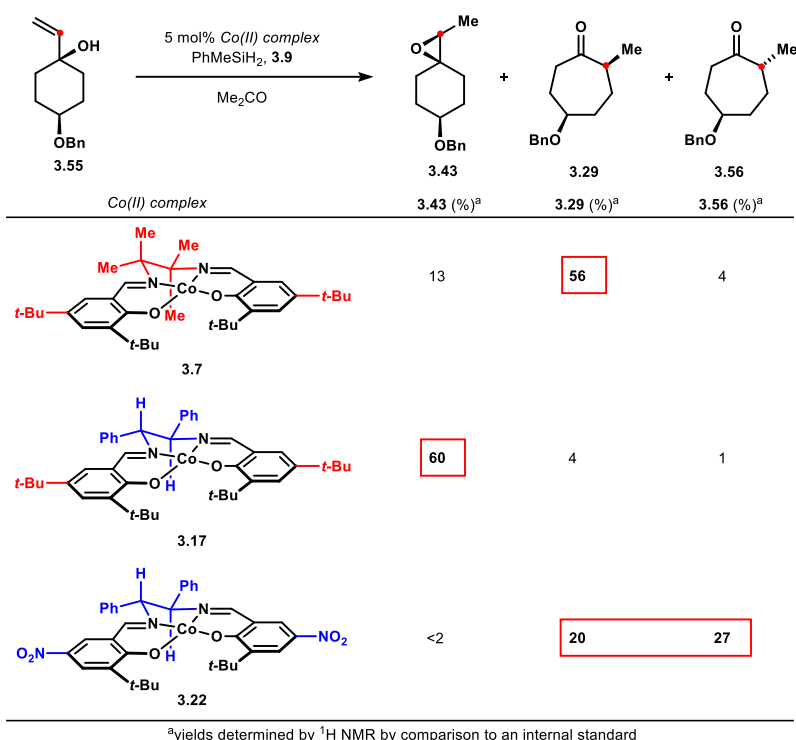
### 3.3. Catalyst Control Over Reaction Outcome & Mechanistic Implications

During our investigation of reaction scope, we identified some aspects of catalyst control over the reaction outcome other than the epoxide- or semi-pinacol-selectivity dependent on catalyst structure. Employing 4-benzyloxy-substituted vinylcarbinol **3.55** can result in the formation of three products: epoxide **3.43**, ring-expanded ketone **3.29** with a *cis* configuration of substituents, or the diastereomeric ketone **3.56** with a *trans* orientation of substituents (Scheme 3.4). As established above, employing the 2,2-dimethylbutanediamine-derived cobalt salen **3.7**, the major product is the *cis* diastereomer of the semi-pinacol process **3.29**, which is formed



alongside small proportions (1:4.3) of the epoxide **3.43** and even smaller quantities of the diastereomeric ketone **3.56** (1:14). Exchanging the catalyst for the 1,2-diphenyldiamine-derived salen **3.17** affords the epoxide **3.43** in high selectivity (12:1 with all semi-pinacol adducts). Implementing the nitro-substituted 1,2-diphenyldiamine-derived salen **3.22** suppresses the epoxidation pathway but curiously generates the semi-pinacol products in a non-diastereoselective fashion (1:1.3 **3.29** to **3.56**).

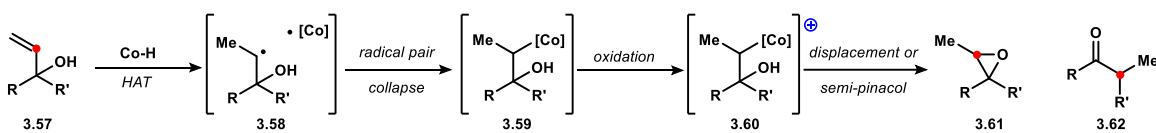
**Scheme 3.4.** Catalyst control over the outcome of MHAT RPC reactions of alcohol **3.55**



From the outset, the catalyst control over reaction outcome carried important implications. The mechanism put forward by Shigehisa precluded catalyst involvement in bond-forming steps, as the reactive intermediates were presumed to be carbocations (see *above*). Our findings clearly demonstrated that the catalyst must be involved in key bond-forming steps in the mechanism, as catalyst structure-dependent reactivity cannot be explained by the reactions of identical carbocationic intermediates. To this end, we surmised that an alkylcobalt electrophilic species is involved in at least one of the reaction pathways we identified (epoxidation or semi-pinacol). Following HAT by a cobalt hydride to the allylic alcohol substrate

**3.57**, we presume that a radical pair **3.58** is formed (Scheme 3.5). Subsequent radical pair collapse to form an alkylcobalt **3.59** is believed to precede oxidation to the corresponding electrophilic alkylcobalt species **3.60**. Subsequent displacement or semi-pinacol affords the observed products. Some prior reports of invertive displacement of so-called alkylcobalt(IV) derivatives have been disclosed.<sup>13</sup> The radical pair **3.58** may in some cases undergo escape from the solvent cage, generating a freely-diffusing alkyl radical, which can be oxidized to the corresponding carbocation, as proposed by Shigehisa.

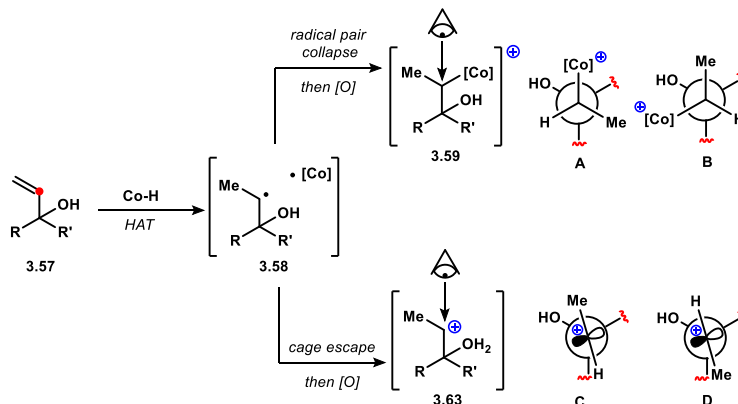
**Scheme 3.5.** Proposed mechanism for conversion of allylic alcohols into epoxides or semi-pinacol adducts



With a mechanistic picture in mind, we could effectively analyze the diverse reaction outcomes observed in the reaction of allylic alcohol **3.55** with the three cobalt salen complexes **3.7**, **3.17**, and **3.22** (Scheme 3.4). We expect that the semi-pinacol selectivity observed under the action of catalyst **3.7** can be explained by the carbocationic pathway. Indeed, similar semi-pinacol processes of bromohydrins mediated by  $\text{I(I)}$ , believed to proceed through carbocationic intermediates, exhibited very similar levels of diastereoselectivity to those we observed in the case of 4-substituted cyclic dialkyl(vinyl)carbinols.<sup>14</sup> Eric found that the  $\text{Ag(I)}$ -mediated ring-expansions of bromohydrins, known to proceed by a displacement mechanism, led to a non-diastereoselective reaction, which aligns closely with our findings employing nitro-salen catalyst **3.22**.<sup>15</sup> We therefore conclude that the semi-pinacol processes catalyzed by salen **3.22** proceeds through an electrophilic alkylcobalt intermediate. The differences in outcome can be linked to the hybridization of the electrophilic carbon participating in ring-expansion. Following formation of the radical pair **3.58**, radical pair collapse and oxidation would generate the electrophilic alkylcobalt species **3.59** (Scheme 3.6.) Newman projection analysis of the two diastereomeric transition states **A** and **B** possible by rotation of the involved C–C bond displays an expected low energetic difference. In contrast, the carbocation intermediate **3.62** that would

arise from cage escape of radical pair **3.58** and oxidation of the alkyl radical contains an  $sp^2$ -hybridized electrophilic carbon. Newman projection analysis of the two possible rotamers **C** and **D** corresponding to diastereomeric outcomes displays an expected large energetic difference; rotamer **D** exhibits a costly eclipsing interaction with the methyl substituent that is avoided in the alternative rotamer **C**. We further attributed the epoxidation process to an electrophilic alkylcobalt pathway, as some enantioselectivity was observed when enantioenriched catalysts were employed. The differences in outcome between 1,2-diphenyldiamine derived catalysts **3.17**, which promotes epoxidation, and **3.22**, which catalyzes non-diastereoselective semi-pinacol, may be attributed to the greater reactivity of the nitro-substituted salen **3.22** as a nucleofuge.

**Scheme 3.6.** Stereochemical model for ring-expansion stereoselectivity



### 3.4. Conclusion

In exploring the reactivity of tertiary allylic alcohols to MHAT RPC conditions, we identified a pair of new synthetic methodologies. The straightforward catalysis of semi-pinacol or epoxidation processes from dialkyl(vinyl)carbinol substrates was achieved, wherein catalyst structure determined the selectivity of the reaction. Additional catalyst-dependent selectivity over the stereoselectivity of the semi-pinacol rearrangements was identified. The catalyst-dependence on reaction outcome further enabled us to propose a new mechanistic proposal for MHAT RPC reactions that invokes alkylcobalt derivatives as electrophilic species. The discovery

of catalyst control over other transition metal-catalyzed processes has been essential to expanding their utility.<sup>16</sup> We believed that catalyst involvement in MHAT RPC reactions could lay the foundation for the identification of new reactivities. In the years since, this has already begun to come to fruition, as several enantioselective MHAT RPC reactions have been disclosed, including from our laboratory.<sup>17</sup>

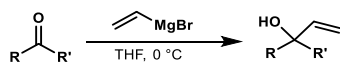
### **3.5. Experimental Section**

#### **3.5.1. Materials & Methods**

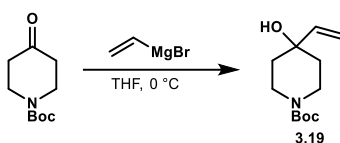
All reactions were carried out in flame-dried glassware under positive pressure of dry nitrogen unless otherwise noted. Reaction solvents including tetrahydrofuran (THF, Fisher, HPLC Grade), dichloromethane (CH<sub>2</sub>Cl<sub>2</sub>, Fisher, HPLC Grade), and toluene (Fisher, HPLC Grade) were dried by percolation through a column packed with neutral alumina and a column packed with a supported copper catalyst for scavenging oxygen (Q5) under positive pressure of argon. Acetone was dried over anhydrous powdered CaSO<sub>4</sub> overnight, distilled into a two-neck round bottom, and then transferred by cannula into a storage Schlenk. Solvents for extraction, thin layer chromatography (TLC), and flash column chromatography were purchased from Fischer (ACS Grade) and VWR (ACS Grade) and used without further purification. Chloroform-d and benzene-d<sub>6</sub> for <sup>1</sup>H and <sup>13</sup>C NMR analysis were purchased from Cambridge Isotope Laboratories and used without further purification. Commercially available reagents were used without further purification unless otherwise noted. Reactions were monitored by thin layer chromatography (TLC) using precoated silica gel plates (EMD Chemicals, Silica gel 60 F<sub>254</sub>). Flash column chromatography was performed over silica gel (Acros Organics, 60 Å, particle size 0.04-0.063 mm). <sup>1</sup>H NMR and <sup>13</sup>C NMR spectra were recorded on Bruker DRX-500 (BBO probe), Bruker DRX-500 (TCI cryoprobe), Bruker AVANCE600 (TBI probe), and Bruker AVANCE600 (BBFO cryoprobe) spectrometers using residual solvent peaks as internal standards (CHCl<sub>3</sub> @ 7.26 ppm <sup>1</sup>H NMR, 77.00 ppm <sup>13</sup>C NMR; C<sub>6</sub>H<sub>6</sub> @ 7.16 ppm <sup>1</sup>H NMR, 128.00 ppm <sup>13</sup>C NMR; (CD<sub>3</sub>)<sub>2</sub>CO @ 2.05 ppm <sup>1</sup>H NMR, 29.84 ppm <sup>13</sup>C NMR; (CD<sub>3</sub>)<sub>2</sub>SO @ 2.50 ppm <sup>1</sup>H NMR, 39.52 ppm <sup>13</sup>C NMR). High-resolution mass spectra (HRMS) were recorded on Waters LCT Premier TOF spectrometer with ESI and CI sources.

### 3.5.2. Experimental Procedures

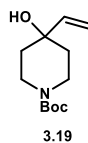
#### General procedure 1: Synthesis of allylic alcohols



**Allylic alcohols.** A solution of vinylmagnesium bromide (2.0 equiv.) in THF (0.6 M w.r.t. Grignard reagent) was cooled to 0 °C. A solution of ketone (1.0 equiv.) in THF (0.6 M w.r.t. ketone, final reaction concentration 0.2 M) was added slowly. After 1 h, the reaction was quenched by the addition of saturated aqueous NH<sub>4</sub>Cl (30 mL). The resulting mixture was extracted with Et<sub>2</sub>O 3x 30 mL. The organics were washed with brine and dried over MgSO<sub>4</sub>. The desired allylic alcohols were purified by flash column chromatography over silica gel.



**Allylic alcohol 3.19.** A solution of vinylmagnesium bromide (50 mL, 1.0 M in THF, 50 mmol) in THF (100 mL) was cooled to 0 °C. A solution of 4-*N*-Boc-piperidone (4.98 g, 25 mmol) in THF (25 mL) was added slowly. After 1 h, the reaction was quenched by the addition of sat. aq. NH<sub>4</sub>Cl (100 mL). The resulting mixture was extracted with Et<sub>2</sub>O 3x 100 mL. The organics were washed with brine and dried over MgSO<sub>4</sub>. The crude material was purified by flash silica chromatography with 15% EtOAc/Hex as the eluting solvent to deliver 5.21 g (92%) of known allylic alcohol **3.19** as a viscous oil.<sup>18</sup>



<sup>1</sup>H NMR (500 MHz, CDCl<sub>3</sub>, 25 °C):

δ 5.94 (dd, *J* = 17.3, 10.7 Hz, 1H)

5.27 (d, *J* = 17.4 Hz, 1H)

5.10 (d, *J* = 10.8 Hz, 1H)

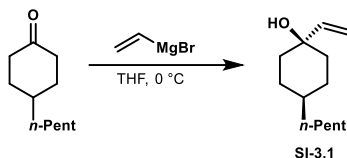
3.82 (d, *J* = 13.4 Hz, 2H)

3.23 (t, *J* = 12.5 Hz, 2H)

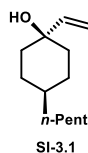
1.67 (td, *J* = 13.1, 12.4, 4.6 Hz, 3H)

1.59 – 1.54 (m, 1H)

1.46 (s, 9H)



**Allylic alcohol SI-3.1.** Prepared according to the general procedure 1 with 2.0 mmol of vinylmagnesium bromide, 1.0 mmol (168.3 mg) of 4-pentylcyclohexanone and 5.0 mL of THF. The reaction produced a 1:1 mixture of diastereomeric alcohols. **SI-3.1** was purified by flash silica chromatography with 10% Et<sub>2</sub>O/Hex as the eluting solvent to yield 69 mg (35%) of the desired alcohol as an oil that solidified upon storage in the freezer.



<sup>1</sup>H NMR (500 MHz, CDCl<sub>3</sub>, 25 °C):

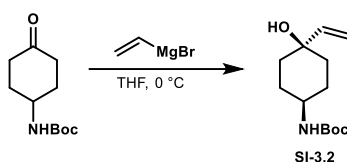
δ 5.94 (dd, <i>J</i> = 17.4, 10.8 Hz, 1H)	1.47 (td, <i>J</i> = 14.2, 13.4, 4.2 Hz, 2H)
5.23 (d, <i>J</i> = 17.3 Hz, 1H)	1.33 – 1.27 (m, 7H)
5.00 (d, <i>J</i> = 10.7 Hz, 1H)	1.26 – 1.22 (m, 5H)
1.63 – 1.58 (m, 4H)	0.88 (t, <i>J</i> = 7.1 Hz, 3H)

<sup>13</sup>C NMR (125 MHz, CDCl<sub>3</sub>, 25 °C):

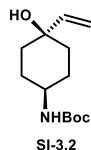
δ 147.05	37.19	32.31	22.84
111.03	37.13	28.21	14.24
71.76	37.00	26.75	

HRMS (ES<sup>+</sup>) calculated for C<sub>13</sub>H<sub>24</sub>ONa [M+Na]: 219.1725, found: 219.1721

TLC: R<sub>f</sub> = 0.35 (10% EtOAc/Hex)



**Allylic alcohol SI-3.2.** Prepared according to the general procedure 1 with 4.0 mmol of vinylmagnesium bromide, 2.0 mmol (426.6 mg) of 4-*N*-boc-aminocyclohexanone and 10.0 mL of THF. The reaction produced a 1.5:1 mixture of diastereomeric alcohols. The crude material was purified by flash column chromatography with 20-40% EtOAc/Hex as the eluting solvent to yield 110.4 mg (23%) of the desired alcohol as a colorless solid. Distortions and peak broadening in the NMR spectra of this compound are due to the presence of the carbamate.



$^1\text{H}$  NMR (500 MHz,  $\text{CDCl}_3$ , 25 °C):

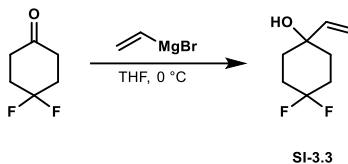
$\delta$ 5.93 (dd, $J = 17.4, 10.7$ Hz, 1H)	3.43 (s, 1H)
5.24 (dd, $J = 17.3, 1.2$ Hz, 1H)	1.86 – 1.80 (m, 2H)
5.04 (dd, $J = 10.7, 1.2$ Hz, 1H)	1.66 – 1.52 (m, 5H)
4.44 (s, 1H)	1.44 (s, 9H)

$^{13}\text{C}$  NMR (125 MHz,  $\text{CDCl}_3$ , 25 °C):

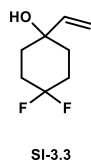
$\delta$ 155.41	79.29	36.09
146.09	70.74	28.58
111.77	49.06	28.49

HRMS (CI<sup>+</sup>) calculated for  $\text{C}_{13}\text{H}_{23}\text{NO}_3\text{Na}$  [ $\text{M}+\text{Na}$ ]: 264.1576, found: 264.1564

TLC:  $R_f = 0.35$  (30% EtOAc/Hex)



**Allylic alcohol SI-3.3.** Prepared according to the general procedure 1 with 2.0 mmol of vinylmagnesium bromide, 1.0 mmol (134 mg) of 4,4-difluorocyclohexanone and 5.0 mL of THF. The crude material was purified by flash column chromatography with 15%  $\text{Et}_2\text{O}$ /Pentane as the eluting solvent to yield 152 mg (94%) of the desired alcohol as a pungent semi-solid.



$^1\text{H}$  NMR (500 MHz,  $\text{CDCl}_3$ , 25 °C):

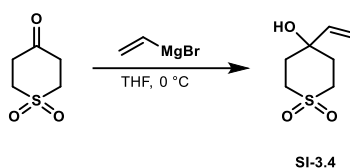
$\delta$ 5.97 (dd, $J = 17.4, 10.8$ Hz, 1H)	1.99 – 1.90 (m, 2H)
5.30 (d, $J = 17.3$ Hz, 1H)	1.80 (td, $J = 13.5, 4.3$ Hz, 2H)
5.11 (d, $J = 10.6$ Hz, 1H)	1.72 – 1.65 (m, 3H)
2.23 – 2.09 (m, 2H)	

$^{13}\text{C}$  NMR (125 MHz,  $\text{CDCl}_3$ , 25 °C):

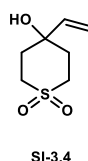
$\delta$ 144.69 (d, $J = 2.4$ Hz)	70.51
123.45 (dd, $J = 242.3, 239.0$ Hz)	34.08 – 33.70 (m)
112.80	29.94 – 29.41 (m)

HRMS (CI+) calculated for  $C_8H_{12}F_2O$   $[M]^+$ : 162.0856, found: 162.0853

TLC: Rf = 0.20 (10% EtOAc/Hex)



**Allylic alcohol SI-3.4.** Prepared according to the general procedure 1 with 2.0 mmol of vinylmagnesium bromide, 1.0 mmol (148 mg) of tetrahydro-4H-thiopyran-4-one and 5.0 mL of THF. The crude material was purified by flash column chromatography with 50-70% EtOAc/Hex as the eluting solvent to yield 129 mg (73%) of the desired alcohol as a colorless solid.



$^1H$  NMR (500 MHz,  $CDCl_3$ , 25 °C):

$\delta$  5.96 (dd,  $J$  = 17.4, 10.8 Hz, 1H) 2.06 – 1.93 (m, 3H)

5.33 (d,  $J$  = 17.4 Hz, 1H)

5.17 (d,  $J$  = 10.9 Hz, 1H)

3.51 – 3.36 (m, 2H)

2.92 – 2.77 (m, 2H)

2.30 (td,  $J$  = 14.1, 3.4 Hz, 2H)

$^{13}C$  NMR (125 MHz,  $CDCl_3$ , 25 °C):

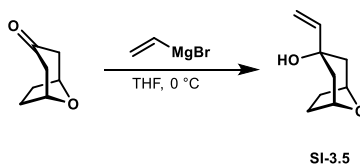
$\delta$  143.29 47.01

113.92 35.283

68.81

HRMS (ES+) calculated for  $C_7H_{12}O_3SNa$   $[M+Na]$ : 199.0405, found: 199.0412

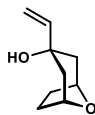
TLC: Rf = 0.42 (70% EtOAc/Hex)



**Allylic alcohol SI-3.5.** Prepared according to the general procedure 1 with 2.0 mmol of vinylmagnesium bromide, 1.0 mmol (126.2 mg) of 8-oxabicyclo[3.2.1]octan-3-one and 5.0 mL of THF. The reaction produced a single diastereomer of the desired alcohol (by  $^1H$  NMR). The crude material was purified by



flash column chromatography with 15% EtOAc/Hex as the eluting solvent to deliver 84 mg (54%) of **SI-3.5** as a colorless oil.



SI-3.5

<sup>1</sup>H NMR (500 MHz, CDCl<sub>3</sub>, 25 °C):

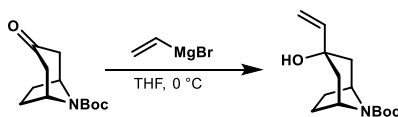
δ 5.83 (dd, <i>J</i> = 17.2, 10.6 Hz, 1H)	1.52 (d, <i>J</i> = 14.6 Hz, 2H)
5.18 (dd, <i>J</i> = 17.1, 1.0 Hz, 1H)	1.30 (bs, 1H)
4.97 (dd, <i>J</i> = 10.6, 1.0 Hz, 1H)	
2.30 – 2.25 (m, 2H)	
2.02 (dd, <i>J</i> = 14.7, 4.4 Hz, 2H)	
1.95 – 1.87 (m, 2H)	

<sup>13</sup>C NMR (125 MHz, CDCl<sub>3</sub>, 25 °C):

δ 147.82	71.13
110.74	42.97
73.84	28.51

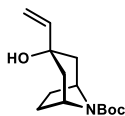
HRMS (CI<sup>+</sup>) calculated for C<sub>9</sub>H<sub>14</sub>O<sub>2</sub> [M]<sup>+</sup>: 154.0994, found: 154.0997

TLC: R<sub>f</sub> = 0.26 (30% EtOAc/Hex)



SI-3.6

**Allylic alcohol SI-3.6.** Prepared according to the general procedure 1 with 2.0 mmol of vinylmagnesium bromide, 1.0 mmol (225.3 mg) of *N*-Boc-nortropinone and 5.0 mL of THF. The reaction produced a single diastereomer of the desired alcohol. The crude material was purified by flash column chromatography with 10-20% EtOAc/Hex as the eluting solvent to deliver 127 mg (50%) of **SI-3.6** as a colorless solid. Distortions and peak broadening in the NMR spectra of this compound are due to the presence of the carbamate.



SI-3.6

<sup>1</sup>H NMR (500 MHz, CDCl<sub>3</sub>, 25 °C):

δ 5.78 (dd, <i>J</i> = 17.2, 10.6 Hz, 1H)	1.98 – 1.86 (m, 3H)
5.18 (d, <i>J</i> = 17.1 Hz, 1H)	1.56 (d, <i>J</i> = 14.5 Hz, 2H)

4.97 (d,  $J = 10.6$  Hz, 1H)                                1.46 (s, 9H)  
 4.22 (d,  $J = 49.5$  Hz, 2H)                                1.29 (bs, 1H)  
 2.22 – 2.14 (m, 2H)  
 2.08 (s, 1H)

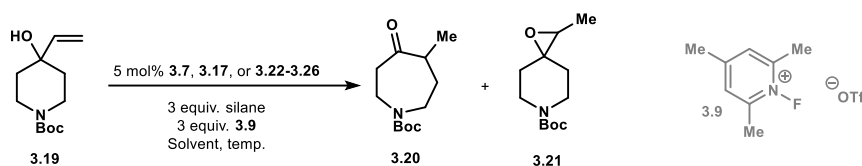
$^{13}\text{C}$  NMR (125 MHz,  $\text{CDCl}_3$ , 25 °C):

$\delta$ 153.64	79.33	42.74 – 42.13 (m)
147.71	72.06	28.64
110.82	53.35 – 52.50 (m)	28.27 – 27.71 (m)

HRMS (ES+) calculated for  $\text{C}_{14}\text{H}_{23}\text{NO}_3\text{Na}$  [M+Na]: 276.1576, found: 276.1565

TLC:  $R_f = 0.43$  (30% EtOAc/Hex)

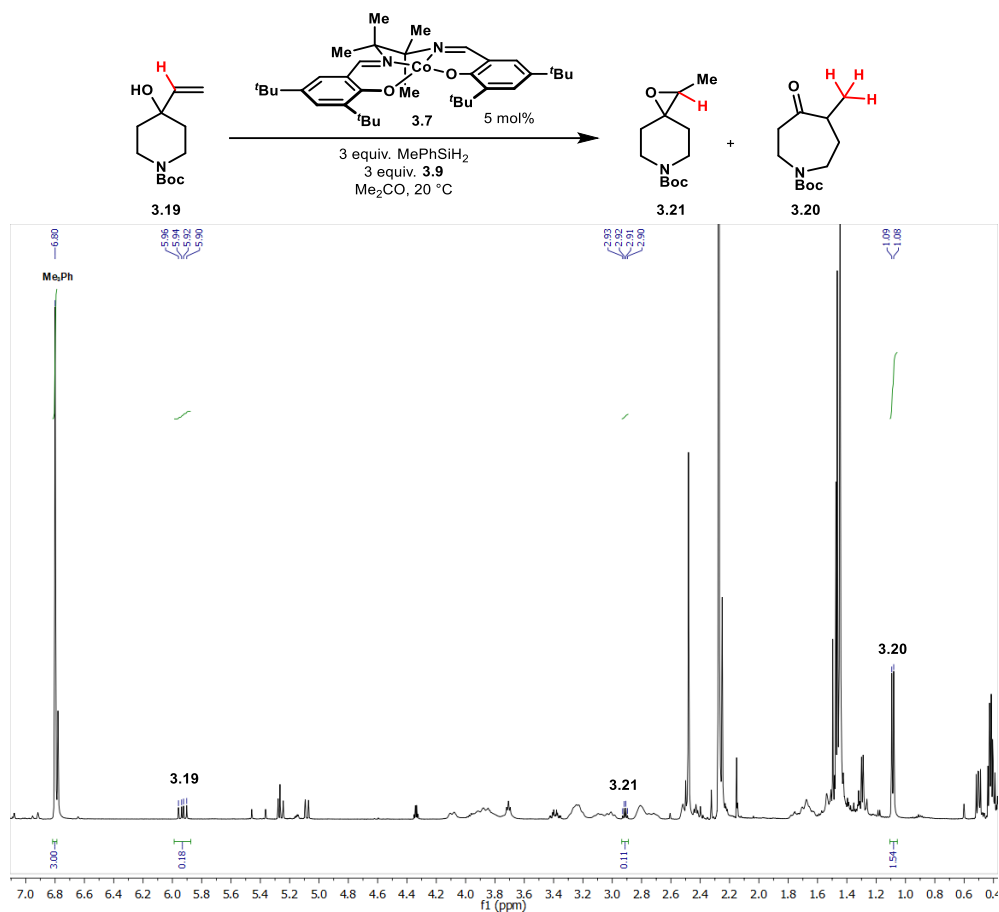
### General procedure for optimization studies (Table 3.1)



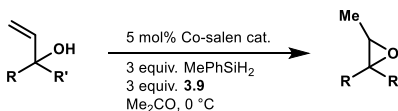
**Experimental Procedure:** To a flame dried roundbottom flask charged with magnetic stir bar was added Co-salen catalyst **3.7**, **3.17**, or **3.22-3.26** (5  $\mu\text{mol}$ ) and oxidant **3.9** (86.8 mg, 0.3 mmol). The roundbottom was placed under an atmosphere of argon. Allylic alcohol **3.19** (22.7 mg, 0.1 mmol) was added as a solution in dry acetone (1.0 mL, 0.1 M) and stirred until homogeneous. The resulting solution was sparged with argon and simultaneously subjected to sonication for 15 min. After cooling to the desired reaction temperature, silane (MePhSiH<sub>2</sub> or TMDS, 0.3 mmol) was added at a rate of 1 drop/10 s. The reaction quickly developed a bright orange color in most cases. After 2 h (12 h for TMDS), the reaction was quenched by the addition of saturated aqueous  $\text{NH}_4\text{Cl}$  (2 mL) and diluted with  $\text{CH}_2\text{Cl}_2$  (3 mL) and  $\text{H}_2\text{O}$  until homogeneous. The aqueous phase was extracted with  $\text{CH}_2\text{Cl}_2$  3x 5 mL. The combined organics were washed with brine and dried over  $\text{Na}_2\text{SO}_4$  and concentrated. To the resulting dark-brown residue was added mesitylene (0.1 mmol, 14  $\mu\text{L}$ ) and 0.7 mL  $\text{CDCl}_3$ .

**Determination of conversion & product ratios by  $^1\text{H}$  NMR analysis:** The entirety of the sample was transferred to an NMR tube and a spectrum collected. The mesitylene singlet was set to 6.80 ppm and was integrated to 3.0. Quantification of the remaining starting allylic alcohol **3.19** was accomplished by integration of the doublet of doublets at 5.94 ppm ( $J = 10.7$  Hz, 1 H). Quantification of the epoxide **3.21** produced was accomplished by integration of the quartet at 2.92 ppm ( $J = 5.5$  Hz, 1H). Quantification of the semi-pinacol adduct **3.20** produced was accomplished by integration of the doublet at 1.08 ppm ( $J = 6.6$  Hz, 3H) and division of the integration by 3.

The example spectrum below (Table 3.1, entry 10) shows 18% starting allylic alcohol **3.19**, 11% epoxide **3.21**, and 51% cycloheptanone **3.22**. The protons corresponding to integrated peaks are highlighted in red.



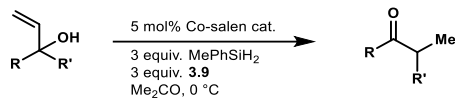
### General procedure 2: MCHAT RPC Epoxidation.



To a flame dried roundbottom flask charged with magnetic stir bar was added Co-salen catalyst **3.17** (0.05 equiv.) and oxidant **3.9** (3.0 equiv.). The roundbottom was placed under an atmosphere of argon. The allylic alcohol (1.0 equiv.) was added as a solution in dry acetone (0.1 M) and stirred until homogeneous. The resulting solution was sparged with argon with concomitant sonication for 15 min. After cooling to -40 °C, MePhSiH<sub>2</sub> (3.0 equiv.) was added at a rate of 1 drop/10 s. The reaction quickly developed a bright orange color. After 1 h, the reaction was quenched by the addition of saturated aqueous NH<sub>4</sub>Cl (2x reaction volume) and diluted with CH<sub>2</sub>Cl<sub>2</sub> (3 mL) and H<sub>2</sub>O until homogeneous. The aqueous phase was extracted with CH<sub>2</sub>Cl<sub>2</sub> 3x 5 mL. The combined organics were washed with brine and dried over Na<sub>2</sub>SO<sub>4</sub>. The products were isolated using flash column chromatography.

*Protocol 1: For epoxides that co-elute on silica with their corresponding semi-pinacol side products.* The crude reaction mixture was dissolved in MeOH (0.1 M) and cooled to 0 °C before treatment with NaBH<sub>4</sub> (10 equiv.). After warming to 20 °C for 30 min the mixture was diluted with H<sub>2</sub>O (10 mL) and extracted with CH<sub>2</sub>Cl<sub>2</sub> 3x 5 mL. The organics were washed with brine and dried over Na<sub>2</sub>SO<sub>4</sub>.

**General procedure 3: MHAT RPC Semi-pinacol.**



To a flame dried roundbottom flask charged with magnetic stir bar was added Co-salen catalyst **3.7** or **3.22** (0.05 equiv.) and oxidant **3.9** (3.0 equiv.). The roundbottom was placed under an atmosphere of argon. The allylic alcohol (1.0 equiv.) was added as a solution in dry acetone (0.1 M) and stirred until homogeneous. The resulting solution was sparged with argon and simultaneously subjected to sonication for 15 min. After cooling to 0 °C, MePhSiH<sub>2</sub> (3.0 equiv.) was added at a rate of 1 drop/10 s. The reaction quickly developed a bright orange color. After 1 h, the reaction was quenched by the addition of saturated aqueous NH<sub>4</sub>Cl (2x reaction volume) and diluted with CH<sub>2</sub>Cl<sub>2</sub> (3 mL) and H<sub>2</sub>O until homogeneous. The aqueous phase was extracted with CH<sub>2</sub>Cl<sub>2</sub> 3x 5 mL. The combined organics were washed with brine and dried over Na<sub>2</sub>SO<sub>4</sub>. The products were isolated using flash column chromatography.

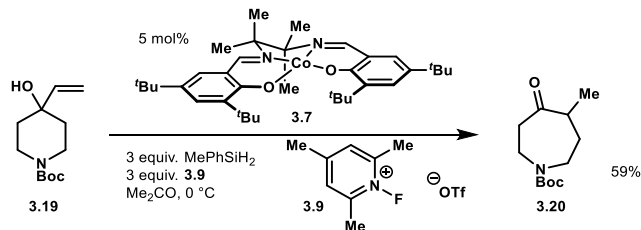
*Protocol 2: For semi-pinacol products that co-elute on silica with their corresponding epoxide side products.* The crude reaction mixture was flushed through a plug of silica using 50% v/v CH<sub>2</sub>Cl<sub>2</sub>/hexanes and concentrated in vacuo. The material was dissolved in THF (0.2 M) and LiBr was added (10 equiv w.r.t epoxide component). The mixture was cooled to 0 °C and glacial acetic acid (12 equiv w.r.t epoxide component) was added. The reaction was left to warm to room temperature overnight then quenched with aqueous saturated NaHCO<sub>3</sub> and extracted with Et<sub>2</sub>O 3x (10 mL portions). The organics were washed with brine, dried over Na<sub>2</sub>SO<sub>4</sub>, and concentrated in vacuo.

*Note 1:* In many cases, separation of the desired products from the silane byproducts was facilitated by including ca. 3 cm neutral alumina on top of the silica substrate during chromatography. For some semi-pinacol adducts this protocol was found to epimerize the α-keto stereocenter.

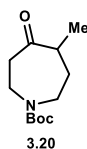
*Note 2:* Variation of solvent mixtures from Hex/EtOAc to CH<sub>2</sub>Cl<sub>2</sub>/EtOAc or CH<sub>2</sub>Cl<sub>2</sub>/Et<sub>2</sub>O often improved separation on silica of the epoxide and semi-pinacol products.

*Note 3:* When silane byproducts are inseparable from the desired products on silica: purified material was dissolved in MeCN (10 mL) and extracted with pentane (10 mL). The pentane layer was extracted 3x with MeCN. The recovery of material from this procedure was found to be variable depending on the compound.

*Note 4:* All product ratios are determined by integration of the crude <sup>1</sup>H NMR spectrum



**Azepanone 3.20.** Prepared according to “**General procedure 3: MHAT RPC Semi-pinacol.**” The reaction was performed with 0.3 mmol (86.8 mg) of **3.9**, 5  $\mu$ mol (3.0 mg) of **3.7**, 0.3 mmol (41  $\mu$ L) of MePhSiH<sub>2</sub>, and 0.1 mmol (22.7 mg) allylic alcohol **3.19** producing a 5.8:1.0 ratio of **3.20** to **3.21**. The crude reaction mixture of inseparable products was dissolved in 1 mL Me<sub>2</sub>CO and treated with PhSH (31  $\mu$ L, 0.3 mmol) and anhydrous K<sub>2</sub>CO<sub>3</sub> (14 mg, 0.1 mmol). The resulting solution was heated to 70 °C for 12 h at which point it was quenched with sat. aq. NH<sub>4</sub>Cl. The aqueous phase was extracted with CH<sub>2</sub>Cl<sub>2</sub> 3x 5 mL. The organics were washed with brine and dried over Na<sub>2</sub>SO<sub>4</sub>. The crude was chromatographed with 3% EtOAc/ CH<sub>2</sub>Cl<sub>2</sub> as the eluting solvent to afford 13.4 mg (59%) of the title compound as a light-yellow oil. Distortions and peak broadening in the NMR spectra of this compound are due to the presence of the carbamate. Heating the NMR sample to 100 °C in DMSO removed the distortions.



<sup>1</sup>H NMR (600 MHz, (CD<sub>3</sub>)<sub>2</sub>SO, 100 °C):

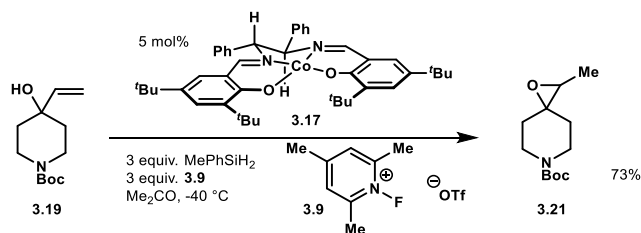
$\delta$ 3.35 (dt, <i>J</i> = 14.2 Hz, 4.2 Hz, 1H)	2.12 – 2.08 (m, 2H)
3.26 (dt, <i>J</i> = 14.5 Hz, 5.0 Hz, 1H)	2.03 (p, <i>J</i> = 1.9 Hz, 1H)
2.89 (ddd, <i>J</i> = 14.7, 9.0, 5.8 Hz, 1H)	1.23 (dq, <i>J</i> = 14.2, 3.8 Hz, 2H)
2.67 (ddd, <i>J</i> = 14.3, 11.0, 3.3 Hz, 1H)	0.93 (s, 9H)
2.42 (dt, <i>J</i> = 13.3, 6.7, 3.3 Hz, 1H)	0.53 (d, <i>J</i> = 6.6 Hz, 3H)

<sup>13</sup>C NMR (151 MHz, (CD<sub>3</sub>)<sub>2</sub>SO, 100 °C):

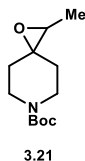
$\delta$ 211.40	46.48	41.27	15.70
153.37	43.74	33.19	
78.35	42.22	27.57	

HRMS (ES<sup>+</sup>) calculated for C<sub>12</sub>H<sub>21</sub>NO<sub>3</sub> [M+Na]: 250.1419, found: 250.1424

R<sub>f</sub> 0.51 (30% EtOAc/Hex), 0.38 (5% EtOAc/CH<sub>2</sub>Cl<sub>2</sub>)



**Epoxide 3.21.** Prepared according to “**General procedure 2: MHAT RPC Epoxidation.**” The reaction was performed with 0.3 mmol (86.8 mg) of **3.9**, 5  $\mu$ mol (3.5 mg) of **3.17**, 0.3 mmol (41  $\mu$ L) of MePhSiH<sub>2</sub>, and 0.1 mmol (22.7 mg) of allylic alcohol **3.19** producing a 9.3:1.0 ratio of **3.21** to **3.20**. The products were found to be inseparable, protocol 1 was employed. The crude mixture was purified on silica with ~3 cm neutral alumina on top of the silica substrate eluting with 10% EtOAc/Hex to afford 16.5 mg (73%) of the title epoxide as a colorless oil. Distortions and peak broadening in the NMR spectra of this compound are due to the presence of the carbamate.



<sup>1</sup>H NMR (500 MHz, CDCl<sub>3</sub>, 25 °C):

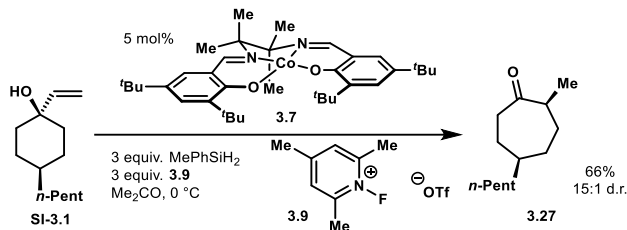
$\delta$ 3.77 – 3.63 (m, 2H)	1.54 – 1.48 (m 1H)
3.38 (dtd, $J$ = 13.5 Hz, 9.9, 3.7 Hz, 2H)	1.46 (s, 9H)
2.92 (q, $J$ = 5.5 Hz, 1H)	1.42 – 1.36 (m 1H)
1.80 – 1.71 (m, 2H)	1.30 (d, $J$ = 5.6 Hz, 3H)

<sup>13</sup>C NMR (151 MHz, CDCl<sub>3</sub>, 25 °C):

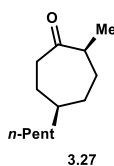
$\delta$ 154.92	42.36 (m)
79.82	34.68
60.86	28.57
59.74	13.57

HRMS (ES<sup>+</sup>) calculated for C<sub>12</sub>H<sub>21</sub>NO<sub>3</sub>Na [M+Na]: 250.1419, found: 250.14216

R<sub>f</sub> 0.56 (30% EtOAc/Hex)



**Cycloheptanone 3.27.** Prepared according to “General procedure 3: MHAT RPC Semi-pinacol.” The reaction was performed with 0.3 mmol (86.8 mg) of **3.9**, 5 μmol (3.0 mg) of **3.7**, 0.3 mmol (41 μL) of MePhSiH<sub>2</sub>, and 0.1 mmol (19.6 mg) vinylcyclohexanol **SI-3.1** producing a 11.0:1.0 ratio of **3.27** to epoxide **3.41**. **3.27** was produced as a 15:1 mixture of diastereomers. The crude was chromatographed with 20% CH<sub>2</sub>Cl<sub>2</sub>/Hex delivering 13.7 mg of desired cycloheptanone contaminated with a small amount (6 mol%, 6 wt% by <sup>1</sup>H NMR) of the epoxide **3.41** (66% yield of **3.27**) as a colorless oil.



<sup>1</sup>H NMR (600 MHz, CDCl<sub>3</sub>, 25 °C):

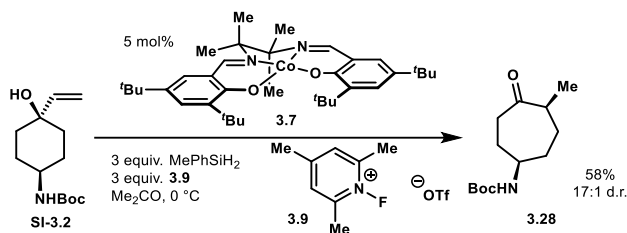
δ 2.59 (h <i>J</i> = 6.8 Hz, 1H)	1.38 (dtd, <i>J</i> = 14.0, 9.2, 3.4 Hz, 1H)
2.52 (ddd, <i>J</i> = 13.2, 9.4, 3.6 Hz, 1H)	1.33 – 1.25 (m, 6H)
2.45 (ddd, <i>J</i> = 13.5, 9.0, 3.3 Hz, 1H)	1.24 – 1.16 (m, 4H)
1.90 – 1.79 (m, 2H)	1.07 (d, <i>J</i> = 6.9 Hz, 3H)
1.71 – 1.64 (m, 1H)	0.87 (t, <i>J</i> = 7.1 Hz, 3H)
1.61 – 1.54 (m, 1H)	

<sup>13</sup>C NMR (151 MHz, CDCl<sub>3</sub>, 25 °C):

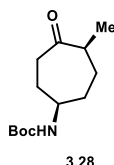
δ 216.61	32.20	22.78
46.02	31.85	16.58
40.43	30.14	14.21
39.19	29.67	
34.95	27.09	

HRMS (ES<sup>+</sup>) calculated for C<sub>13</sub>H<sub>24</sub>ONa [M+Na]: 219.1725, found: 219.1736

R<sub>f</sub> 0.29 (30% CH<sub>2</sub>Cl<sub>2</sub>/Hex)



**Cycloheptanone 3.28.** Prepared according to “General procedure 3: MHAT RPC Semi-pinacol.” The reaction was performed with 0.3 mmol (86.8 mg) of **3.9**, 5 μmol (3.9 mg) of **3.7**, 0.3 mmol (41 μL) of MePhSiH<sub>2</sub>, and 0.1 mmol (24.1 mg) vinylcyclohexanol **SI-3.2** producing a 15.0:1.0 ratio of **3.28** to epoxide **3.42**. The crude was chromatographed with 4% EtOAc/ CH<sub>2</sub>Cl<sub>2</sub> as the eluting solvent, delivering 14.0 mg (58%) of the desired cycloheptanone as a light-yellow solid.



<sup>1</sup>H NMR (500 MHz, CDCl<sub>3</sub>, 25 °C):

δ 4.50 (app bs, 1H)	1.87 (d, <i>J</i> = 52.4 Hz, 2H)
3.83 (app bs, 1H)	1.68 (d, <i>J</i> = 35.1 Hz, 1H)
2.60 (td, <i>J</i> = 7.0, 4.9 Hz, 1H)	1.61 – 1.54 (m, 2H)
2.50 (ddd, <i>J</i> = 17.3, 9.5, 3.5 Hz, 2H)	1.44 (s, 9H)
2.06 – 1.95 (m, 1H)	1.09 (d, <i>J</i> = 6.9 Hz, 3H)

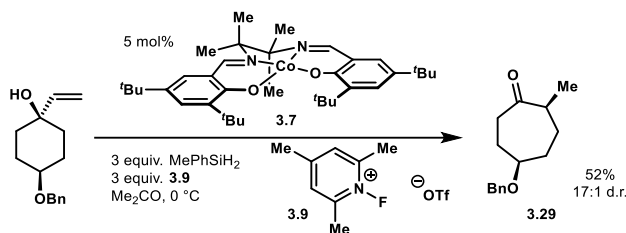
<sup>13</sup>C NMR (126 MHz, CDCl<sub>3</sub>, 25 °C):

δ 215.33	38.16	28.53
155.19	32.50	28.07
50.68	30.23	16.62
46.05	29.84	

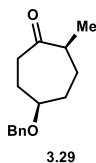
HRMS (ES<sup>+</sup>) calculated for C<sub>13</sub>H<sub>23</sub>NO<sub>3</sub>Na [M+Na]: 264.1576, found: 264.1565

R<sub>f</sub> 0.37 (5% EtOAc/Hex)





**Cycloheptanone 3.29.** Prepared according to “**General procedure 3: MHAT RPC Semi-pinacol.**” The reaction was performed with 0.3 mmol (86.8 mg) of **3.9**, 5  $\mu$ mol (3.0 mg) of **3.7**, 0.3 mmol (41  $\mu$ L) of MePhSiH<sub>2</sub>, and 0.1 mmol (23.2 mg) *cis*-4-(benzyloxy)-1-vinylcyclohexan-1-ol<sup>19</sup> producing a 3.9:1.0 ratio of **3.29** to epoxide **3.43**. Ketone **3.29** was produced as a 17:1 mixture of diastereomers. The crude was chromatographed with 3% Et<sub>2</sub>O/PhMe as the eluting solvent, delivering 12.0 mg (52%) of the desired epoxide as a light-yellow oil.



<sup>1</sup>H NMR (500 MHz, CDCl<sub>3</sub>, 25 °C):

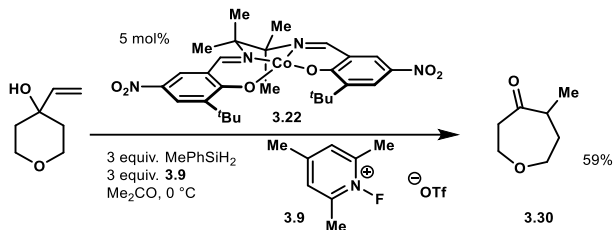
$\delta$ 7.34 (d, $J$ = 5.4 Hz, 4H)	1.38 (dtd, $J$ = 14.0, 9.2, 3.4 Hz, 1H)
7.31 – 7.26 (m, 1H)	2.27 (ddd, $J$ = 14.5, 7.0, 2.7 Hz, 1H)
4.51 (d, $J$ = 1.8 Hz, 2H)	2.16 – 2.04 (m, 2H)
3.77 (dt, $J$ = 5.8, 3.1 Hz, 1H)	1.91 – 1.74 (m, 2H)
2.89 (ddd, $J$ = 14.8, 12.1, 2.8 Hz, 1H)	1.59 – 1.53 (m, 1H)
2.51 (dq, $J$ = 10.6, 6.9, 3.7 Hz, 1H)	1.10 (d, $J$ = 7.0 Hz, 3H)

<sup>13</sup>C NMR (151 MHz, CDCl<sub>3</sub>, 25 °C):

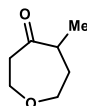
$\delta$ 216.37	74.86	28.87
138.89	70.06	26.24
128.52	47.05	17.91
127.63	36.03	
127.45	32.56	

HRMS (ES<sup>+</sup>) calculated for C<sub>15</sub>H<sub>20</sub>O<sub>2</sub>Na [M+Na]: 255.1361, found: 255.1370

R<sub>f</sub> 0.35 (10% EtOAc/Hex)



**Cycloheptanone 3.30.** Prepared according to “General procedure 3: MHAT RPC Semi-pinacol.” The reaction was performed with 0.6 mmol (173.6 mg) of **3.9**, 10 μmol (6.8 mg) of **3.22**, 0.6 mmol (106 μL) of TMS, and 0.2 mmol (25.6 mg) 4-vinyltetrahydro-2H-pyran-4-ol<sup>20</sup> producing no detectable epoxide **3.44**. The crude was chromatographed once with 20% Et<sub>2</sub>O/Pentane and once with 3% Et<sub>2</sub>O/ CH<sub>2</sub>Cl<sub>2</sub> as the eluting solvent, delivering 15.1 mg (59%) of the desired cycloheptanone **3.30** as a yellow oil. Purification of this compound was found to be more successful when TMS was used in place of MePhSiH<sub>2</sub>.



**3.30**

<sup>1</sup>H NMR (600 MHz, CDCl<sub>3</sub>, 25 °C):

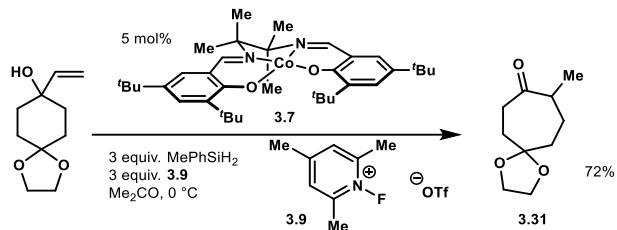
δ 4.06 (dt, <i>J</i> = 12.5, 3.7 Hz, 1H)	2.83 – 2.77 (m, 2H)
4.01 (dt, <i>J</i> = 13.1, 4.4 Hz, 1H)	2.56 (ddd, <i>J</i> = 16.7, 4.3, 2.8 Hz, 1H)
3.70 (ddd, <i>J</i> = 13.2, 10.7, 2.8 Hz, 1H)	1.75 – 1.65 (m, 2H)
3.62 (ddd, <i>J</i> = 12.8, 10.5, 2.6 Hz, 1H)	1.11 (d, <i>J</i> = 6.7 Hz, 3H)

<sup>13</sup>C NMR (151 MHz, CDCl<sub>3</sub>, 25 °C):

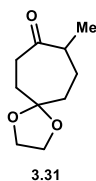
δ 213.03	45.85	16.95
72.35	45.74	
66.37	35.24	

HRMS (CI<sup>+</sup>) calculated for C<sub>7</sub>H<sub>12</sub>O<sub>2</sub> [M]<sup>+</sup>: 128.0837 found: 128.0839

R<sub>f</sub> 0.26 (30% CH<sub>2</sub>Cl<sub>2</sub>/Hex)



**Cycloheptanone 3.31.** Prepared according to “**General procedure 3: MHAT RPC Semi-pinacol.**” The reaction was performed with 0.3 mmol (86.8 mg) of **3.9**, 5  $\mu$ mol (3.0 mg) of **3.7**, 0.3 mmol (41  $\mu$ L) of MePhSiH<sub>2</sub>, and 0.1 mmol (18.4 mg) 8-vinyl-1,4-dioxaspiro[4.5]decan-8-ol<sup>21</sup> producing a 6.0:1.0 ratio of **3.31** to **3.45**. The crude was chromatographed once with 10-20% Et<sub>2</sub>O/Hex and once with 70-100% CH<sub>2</sub>Cl<sub>2</sub>/Hex as the eluting solvent, delivering 13.2 mg (72%) of the cycloheptanone **3.31** as a colorless oil.



<sup>1</sup>H NMR (600 MHz, CDCl<sub>3</sub>, 25 °C):

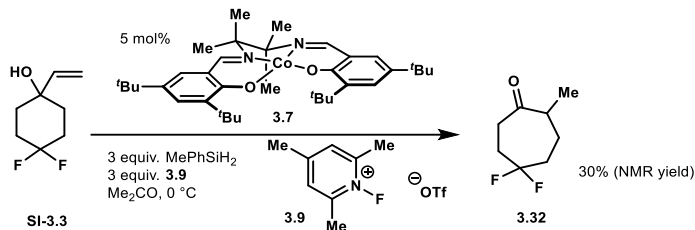
$\delta$ 3.95 (s, 4H)	1.98 – 1.83 (m, 3H)
2.67 (t, <i>J</i> = 13.4 Hz, 1H)	1.83 – 1.64 (m, 3H)
2.59 (s, 1H)	1.09 (d, <i>J</i> = 6.6 Hz, 3H)
2.41 (dd, <i>J</i> = 15.1, 7.4 Hz, 1H)	

<sup>13</sup>C NMR (126 MHz, CDCl<sub>3</sub>, 25 °C):

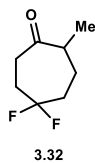
$\delta$ 215.66	46.74	27.73
110.00	37.39	17.41
64.66	36.75	
64.59	33.60	

HRMS (ES<sup>+</sup>) calculated for C<sub>10</sub>H<sub>16</sub>O<sub>3</sub>Na [M+Na]: 207.0997, found: 207.0990

R<sub>f</sub> 0.50 (30% EtOAc/Hex)



**Cycloheptanone 3.32.** Prepared according to “**General procedure 3: MHAT RPC Semi-pinacol.**” The reaction was performed with 0.3 mmol (86.8 mg) of **3.9**, 5 μmol (3.0 mg) of **3.7**, 0.3 mmol (41 μL) of MePhSiH<sub>2</sub>, and 0.1 mmol (16.2 mg) vinylcyclohexanol **SI-3.3** producing a 0.6:1.0 ratio of **3.32** to epoxide **3.46**. The crude was chromatographed with 8% Et<sub>2</sub>O/Pentane as the eluting solvent, delivering 1.8 mg (11%) of the desired cycloheptanone as a sweet-smelling oil. **3.32** is volatile. An analytical sample was obtained from running the reaction on 0.5 mmol scale and implementation of protocol 2.



<sup>1</sup>H NMR (500 MHz, C<sub>6</sub>D<sub>6</sub>, 25 °C):

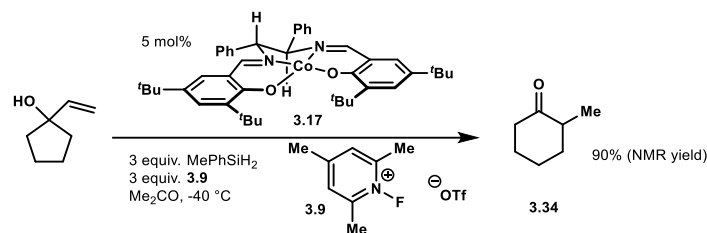
δ 2.24 (t, <i>J</i> = 15.0 Hz, 1H)	1.65 – 1.53 (m, 1H)
1.94 (dd, <i>J</i> = 15.9, 7.2 Hz, 1H)	1.43 – 1.30 (m, 1H)
1.88 – 1.84 (m, 1H)	1.18 – 1.10 (m, 2H)
1.80 – 1.69 (m, 2H)	0.82 (d, <i>J</i> = 7.0 Hz, 3H)

<sup>13</sup>C NMR (126 MHz, C<sub>6</sub>D<sub>6</sub>, 25 °C):

δ 210.79	34.81 (dd, <i>J</i> = 8.4, 4.5 Hz)
124.23 (dd, <i>J</i> = 241.0, 239.2 Hz)	33.19 – 31.59 (m)
17.01	
46.04, 36.25 (t, <i>J</i> = 26.0 Hz)	25.92 (dd, <i>J</i> = 9.5, 3.0 Hz)

HRMS (CI<sup>+</sup>) calculated for C<sub>8</sub>H<sub>12</sub>F<sub>2</sub>O [M]<sup>+</sup>: 162.0856, found: 162.0851

R<sub>f</sub> 0.26 (30% CH<sub>2</sub>Cl<sub>2</sub>/Hex)



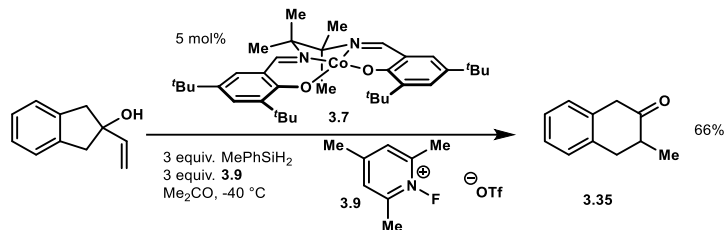
**Cyclohexanone 3.34.** Prepared according to “**General procedure 3: MHAT RPC Semi-pinacol.**” The reaction was performed with 0.3 mmol (86.8 mg) of **3.9**, 5 μmol (3.5 mg) of **3.17**, 0.3 mmol (41 μL) of MePhSiH<sub>2</sub>, and 0.1 mmol (11.2 mg) of 1-vinylcyclopentan-1-ol in 1 mL of (CD<sub>3</sub>)<sub>2</sub>CO producing no detectable epoxide **3.48** by <sup>1</sup>H NMR. 0.1 mmol (14 μL) of mesitylene was added directly to the reaction mixture, which was transferred into an NMR tube for analysis. The NMR yield was determined by integration of relevant peaks (methyl doublet at 0.94 ppm *J* = 6.5 Hz, 3H) and was found to be 90%. A standard of the NMR spectrum of this compound in acetone-*d* was obtained by analysis of a sample from Acros organics, 98%.



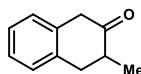
**3.34**

<sup>1</sup>H NMR (500 MHz, (CD<sub>3</sub>)<sub>2</sub>CO, 25 °C):

δ 2.48 – 2.38 (m, 1H)	1.72 (qt, <i>J</i> = 13.2, 3.6 Hz, 1H)
2.38 – 2.29 (m, 1H)	1.59 (qt, <i>J</i> = 12.9, 4.1 Hz, 1H)
2.27 – 2.20 (m, 1H)	1.32 (qd, <i>J</i> = 12.5, 3.9 Hz, 1H)
2.11 – 2.00 (m, 2H)	0.94 (d, <i>J</i> = 6.5 Hz, 3H)
1.81 (dtd, <i>J</i> = 9.0, 3.6, 1.6 Hz, 1H)	



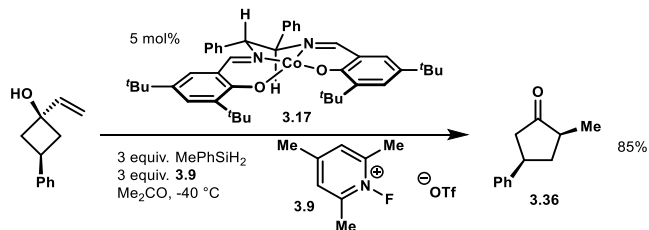
**Cyclohexanone 3.35.** Prepared according to “**General procedure 3: MHAT RPC Semi-pinacol.**” The reaction was performed with 0.3 mmol (86.8 mg) of **3.9**, 5  $\mu$ mol (3.5 mg) of **3.7**, 0.3 mmol (41  $\mu$ L) of MePhSiH<sub>2</sub>, and 0.1 mmol (16.0 mg) of 2-vinyl-2,3-dihydro-1H-inden-2-ol producing no detectable epoxide **3.49** by <sup>1</sup>H NMR. The crude material was purified by column chromatography with 10% EtOAc/Hex as the eluting solvent, delivering 10.5 mg (66%) of the desired semi-pinacol adduct **3.35**. The NMR spectra of this compound matched those reported in the literature.<sup>22</sup>



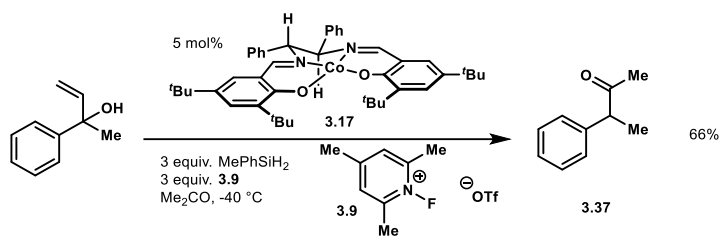
3.35

<sup>1</sup>H NMR (500 MHz, CDCl<sub>3</sub>, 25 °C):

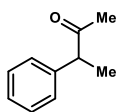
$\delta$ 7.24 – 7.17 (m, 3H)	2.55 (ddq, $J$ = 12.4, 10.6, 6.6 Hz, 1H)
7.14 – 7.11 (m, 1H)	1.20 (d, $J$ = 6.9 Hz, 3H)
3.61 (d, $J$ = 4.3 Hz, 2H)	1.32 (qd, $J$ = 12.5, 3.9 Hz, 1H)
3.09 (dd, $J$ = 15.4, 5.6 Hz, 1H)	0.94 (d, $J$ = 6.5 Hz, 3H)
2.84 (dd, $J$ = 15.4, 10.9 Hz, 1H)	



**Ketone 3.36.** Prepared according to “**General procedure 2: MHAT RPC Epoxidation.**” The reaction was performed with 0.3 mmol (86.8 mg) of **3.9**, 5  $\mu$ mol (3.5 mg) of **3.17**, 0.3 mmol (41  $\mu$ L) of MePhSiH<sub>2</sub>, and 0.1 mmol (17.2 mg) of (1s,3s)-3-phenyl-1-vinylcyclobutan-1-ol; no epoxide **3.50** as detectable by <sup>1</sup>H NMR. The crude material was chromatographed with 8% v/v EtOAc in hexanes as the eluting solvent, delivering 14.6 mg (85%) of the cyclopentanone **3.36** as a colorless oil.<sup>23</sup>



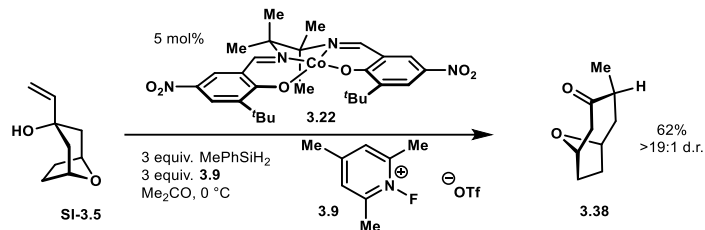
**Ketone 3.37.** Prepared according to “**General procedure 2: MHAT RPC Epoxidation.**” The reaction was performed with 0.3 mmol (86.8 mg) of **3.9**, 5  $\mu$ mol (3.5 mg) of **3.17**, 0.3 mmol (41  $\mu$ L) of MePhSiH<sub>2</sub>, and 0.1 mmol (14.8 mg) of 2-phenylbut-3-en-2-ol<sup>24</sup> producing no detectable epoxide **3.49** by <sup>1</sup>H NMR. The crude material was purified by column chromatography with 10% EtOAc/Hex as the eluting solvent, delivering 12.8 mg of pure material containing some (0.38 mol%, 23 wt%) diethyl ether (66% yield of **3.37**). The NMR spectra of this compound matched those reported in the literature.<sup>25</sup>



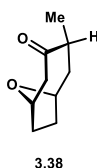
3.37

<sup>1</sup>H NMR (500 MHz, CDCl<sub>3</sub>, 25 °C):

$\delta$ 7.34 (t, $J$ = 7.4 Hz, 2H)	3.74 (q, $J$ = 7.0 Hz, 1H)
7.29 – 7.24 (m, 1H)	2.05 (s, 3H)
7.24 – 7.19 (m, 2H)	1.39 (d, $J$ = 7.0 Hz, 3H)



**Cyclooctanone 3.38.** Prepared according to “**General procedure 3: MHAT RPC Semi-pinacol.**” The reaction was performed with 0.3 mmol (86.8 mg) of **3.9**, 5  $\mu$ mol (3.4 mg) of **3.22**, 0.3 mmol (41  $\mu$ L) of MePhSiH<sub>2</sub>, and 0.1 mmol (15.4 mg) of vinylcyclohexanol **SI-3.5** producing no detectable epoxide **3.54**. Ketone **3.38** was produced as an apparent single diastereomer by <sup>1</sup>H NMR. The crude material was chromatographed with 90% CH<sub>2</sub>Cl<sub>2</sub>/Pentane as the eluting solvent, delivering 9.6 mg (62%) of the desired ketone as a yellow oil.



<sup>1</sup>H NMR (500 MHz, CDCl<sub>3</sub>, 25 °C):

$\delta$ 4.59 – 4.55 (m, 2H)	2.16 – 2.08 (m, 1H)
4.50 (app t, $J = 7.0$ Hz, 1H)	1.99 – 1.91 (m, 1H)
3.02 (dp, $J = 10.4, 6.8$ Hz, 1H)	1.71 – 1.66 (m, 1H)
2.87 (dd, $J = 12.4, 6.5$ Hz, 1H)	1.46 – 1.39 (m, 1H)
2.29 (dd, $J = 12.4, 1.6$ Hz, 1H)	1.08 – 1.03 (m, 4H)
2.28 – 2.22 (m, 1H)	

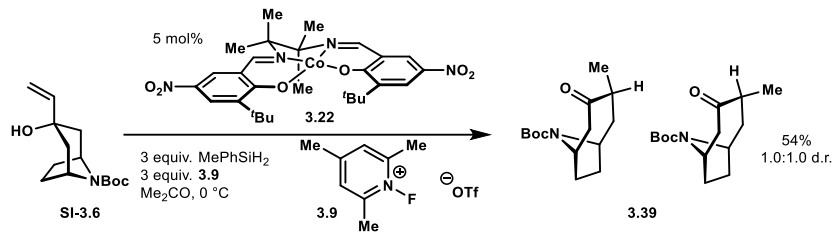
<sup>13</sup>C NMR (126 MHz, CDCl<sub>3</sub>, 25 °C):

$\delta$ 214.11	52.19	32.32
75.86	42.08	29.85
73.79	39.12	15.86

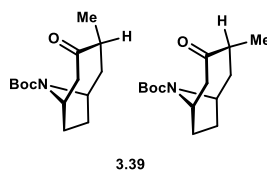
HRMS (ES<sup>+</sup>) calculated for C<sub>9</sub>H<sub>14</sub>O<sub>2</sub>Na [M+Na]: 177.0892, found: 177.0899

R<sub>f</sub> 0.36 (100% CH<sub>2</sub>Cl<sub>2</sub>)





**Ketone 3.39.** Prepared according to “General procedure 3: MHAT RPC Semi-pinacol.” The reaction was performed with 0.3 mmol (86.8 mg) of **3.9**, 5 μmol (3.4 mg) of **3.22**, 0.3 mmol (41 μL) of MePhSiH<sub>2</sub>, and 0.1 mmol (25.3 mg) of vinylcyclohexanol **SI-3.5** producing a >20:1 ratio of ketone **3.39** to epoxide **3.53**. Ketone **3.39** was produced as a 1:1 mixture of diastereomers. The crude material was chromatographed with 2% EtOAc/ CH<sub>2</sub>Cl<sub>2</sub> as the eluting solvent, delivering 13.7 mg (54%) of the desired cyclooctanone as a yellow oil.



<sup>1</sup>H NMR (500 MHz, CDCl<sub>3</sub>, 25 °C):

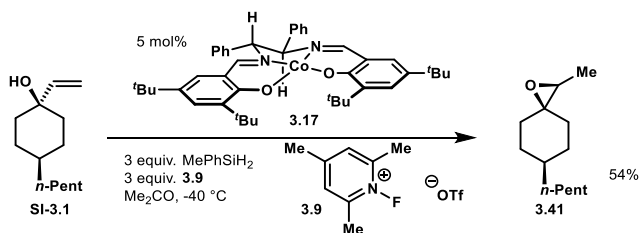
δ 4.39 – 4.33 (m, 2H)	2.29 – 2.17 (m, 4H)
4.30 – 4.22 (m, 2H)	1.98 – 1.86 (m, 2H)
3.01 (dd, <i>J</i> = 12.1, 6.0 Hz, 1H)	1.64 – 1.59 (m, 2H)
2.85 (dd, <i>J</i> = 12.0, 5.9 Hz, 1H)	1.50 (s, 18H)
2.69 – 2.58 (m, 2H)	1.41 – 1.31 (m, 2H)
2.48 (dt, <i>J</i> = 14.3, 7.4 Hz, 1H)	1.08 – 1.01 (m, 8H)
2.32 (dt, <i>J</i> = 14.7, 8.2 Hz, 1H)	

<sup>13</sup>C NMR (126 MHz, CDCl<sub>3</sub>, 25 °C):

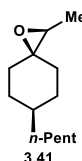
δ 214.41	52.51	42.42	29.07	15.83
79.84	52.20	39.03	28.73	15.80
79.76	50.56	38.09	28.70	
53.56	49.66	31.93	28.66	
53.26	42.57	31.28	28.59	

HRMS (ES<sup>+</sup>) calculated for C<sub>14</sub>H<sub>23</sub>NO<sub>3</sub>Na [M+Na]: 276.1576, found: 276.1577

R<sub>f</sub> 0.44 (20% EtOAc/Hex)



**Epoxide 3.41.** Prepared according to “**General procedure 2: MHAT RPC Epoxidation.**” The reaction was performed with 0.3 mmol (86.8 mg) of **3.9**, 5  $\mu$ mol (3.5 mg) of **3.17**, 0.3 mmol (41  $\mu$ L) of MePhSiH<sub>2</sub>, and 0.1 mmol (19.6 mg) vinylcyclohexanol **SI-3.1** producing a 4.9:1.0 ratio of **3.41** to ketone **3.27**. The inseparable mixture was subjected to protocol 1. The crude was chromatographed with 20% CH<sub>2</sub>Cl<sub>2</sub>/Hex to deliver 10.5 mg (54%) of the desired epoxide as a colorless oil.



<sup>1</sup>H NMR (600 MHz, CDCl<sub>3</sub>, 25 °C):

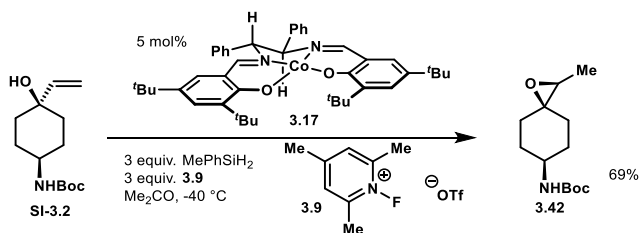
$\delta$ 2.86 (q, $J$ = 5.6 Hz 1H)	1.33 – 1.28 (m, 6H)
1.81 – 1.74 (m, 2H)	1.28 – 1.25 (m 6H)
1.72 – 1.68 (m, 1H)	1.24 – 1.20 (m, 3H)
1.63 (td, $J$ = 13.1, 4.3 1H)	0.88 (t, $J$ = 7.2, 3H)
1.46 (dq, $J$ = 13.7, 3.6 1H)	

<sup>13</sup>C NMR (151 MHz, CDCl<sub>3</sub>, 25 °C):

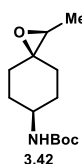
$\delta$ 62.44	32.31	14.24
59.96	30.45	13.56
37.19	28.27	
36.74	26.86	
34.56	22.84	

HRMS (ES<sup>+</sup>) calculated for C<sub>13</sub>H<sub>24</sub>ONa [M+Na]: 219.1725, found: 219.1720

R<sub>f</sub> 0.29 (30% CH<sub>2</sub>Cl<sub>2</sub>/Hex)



**Epoxide 3.42.** Prepared according to “**General procedure 2: MHAT RPC Epoxidation.**” The reaction was performed with 0.3 mmol (86.8 mg) of **3.9**, 5  $\mu$ mol (3.5 mg) of **3.17**, 0.3 mmol (41  $\mu$ L) of MePhSiH<sub>2</sub>, and 0.1 mmol (24.1 mg) vinylcyclohexanol **SI-3.2** producing a 9.5:1.0 ratio of **3.42** to ketone **3.28**. The crude was chromatographed once with 5% EtOAc/ CH<sub>2</sub>Cl<sub>2</sub> and once with 15% EtOAc/Hex as the eluting solvent, delivering 16.6 mg (69%) of the desired epoxide as a colorless solid.



<sup>1</sup>H NMR (500 MHz, CDCl<sub>3</sub>, 25 °C):

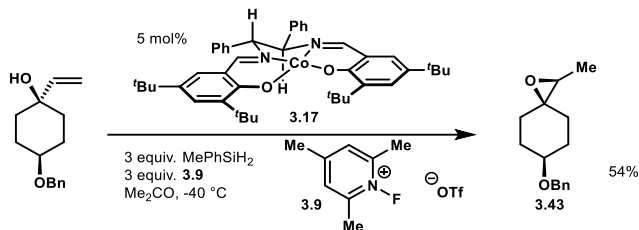
$\delta$ 4.48 (app bs, 1H)	1.73 (td, $J = 13.4, 4.3$ Hz, 1H)
3.58 (app bs, 1H)	1.54 – 1.47 (m, 3H)
2.90 (q, $J = 5.6$ Hz, 1H)	1.45 (s, 9H)
1.97 (dd, $J = 30.9, 12.1$ Hz, 2H)	1.34 – 1.25 (m, 1H)
1.86 (td, $J = 13.2, 4.3$ Hz, 1H)	1.27 (d, $J = 5.5$ Hz, 3H)

<sup>13</sup>C NMR (126 MHz, CDCl<sub>3</sub>, 25 °C):

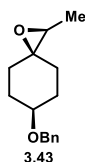
$\delta$ 155.39	48.91	28.57
79.41	33.16	27.01
61.16	30.69	13.69
59.94	29.84	

HRMS (ES<sup>+</sup>) calculated for C<sub>13</sub>H<sub>23</sub>NO<sub>3</sub>Na [M+Na]: 264.1576, found: 264.1566

R<sub>f</sub> 0.31 (5% EtOAc/Hex)



**Epoxide 3.43.** Prepared according to “**General procedure 2: MHAT RPC Epoxidation.**” The reaction was performed with 0.3 mmol (86.8 mg) of **3.9**, 5  $\mu$ mol (3.5 mg) of **3.17**, 0.3 mmol (41  $\mu$ L) of MePhSiH<sub>2</sub>, and 0.1 mmol (23.2 mg) *cis*-4-(benzyloxy)-1-vinylcyclohexan-1-ol<sup>19</sup> producing a 15.0:1.0 ratio of **3.43** to ketone **3.29**. The crude was chromatographed with 3% Et<sub>2</sub>O/PhMe as the eluting solvent, delivering 11.5 mg (50%) of the desired epoxide as a colorless oil.



<sup>1</sup>H NMR (500 MHz, CDCl<sub>3</sub>, 25 °C):

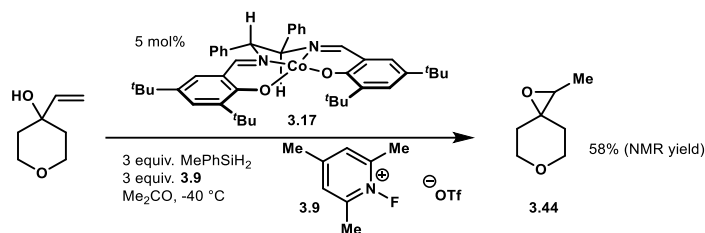
$\delta$ 7.41 – 7.32 (m, 4H)	1.87 – 1.78 (m, 2H)
7.28 (d, <i>J</i> = 6.6 Hz, 1H)	1.77 – 1.70 (m, 2H)
3.53 (tt, <i>J</i> = 7.9, 3.7 Hz, 1H)	1.65 – 1.59 (m, 1H)
2.89 (q, <i>J</i> = 5.5 Hz, 1H)	1.57 – 1.53 (m, 2H)
1.94 – 1.87 (m, 2H)	1.29 (d, <i>J</i> = 5.6 Hz, 3H)
1.87 – 1.78 (m, 2H)	

<sup>13</sup>C NMR (151 MHz, CDCl<sub>3</sub>, 25 °C):

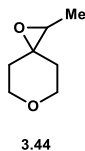
$\delta$ 139.07	75.19	31.91
128.51	69.99	25.63
127.60	61.77	13.90
127.57	59.79	

HRMS (ES<sup>+</sup>) calculated for C<sub>15</sub>H<sub>20</sub>O<sub>2</sub>Na [M+Na]: 255.1361, found: 255.1350

R<sub>f</sub> 0.35 (10% EtOAc/Hex)



**Epoxide 3.44.** Prepared according to “**General procedure 2: MHAT RPC Epoxidation.**” The reaction was performed with 0.6 mmol (173.6 mg) of **3.9**, 10  $\mu$ mol (7.0 mg) of **3.17**, 0.6 mmol (82  $\mu$ L) of MePhSiH<sub>2</sub>, and 0.2 mmol (25.6 mg) 4-vinyltetrahydro-2H-pyran-4-ol<sup>20</sup> producing a 4.8:1.0 ratio of **3.44** to ketone **3.30**. The crude was chromatographed once with 20% Et<sub>2</sub>O/Pentane and once with 2% Et<sub>2</sub>O/CH<sub>2</sub>Cl<sub>2</sub> as the eluting solvent, delivering 4.9 mg (19%) of the desired epoxide in moderate purity. **3.44** is volatile. An analytical sample was obtained by the procedure outlined on page 52.



<sup>1</sup>H NMR (500 MHz, CDCl<sub>3</sub>, 25 °C):

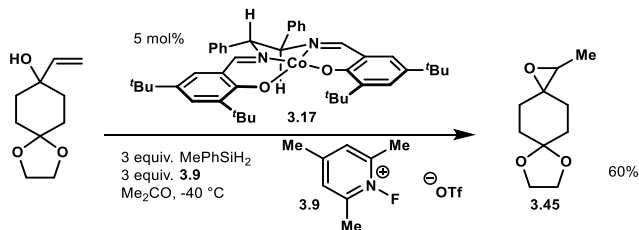
$\delta$ 3.85 – 3.76 (m, 4H)	1.57 – 1.52 (m, 1H)
2.91 (q, $J$ = 5.5 Hz, 1H)	1.49 – 1.44 (m, 1H)
1.87 – 1.82 (m, 2H)	1.29 (d, $J$ = 5.6 Hz, 3H)

<sup>13</sup>C NMR (126 MHz, CDCl<sub>3</sub>, 25 °C):

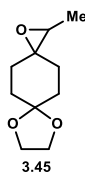
$\delta$ 66.58	59.75	13.48
66.56	35.60	
60.16	29.98	

HRMS (CI<sup>+</sup>) calculated for NH<sub>4</sub>C<sub>7</sub>H<sub>12</sub>O<sub>2</sub> [M+NH<sub>4</sub>]<sup>+</sup>: 146.1181, found: 146.1181

R<sub>f</sub> 0.24 (20% EtOAc/Hex)



**Epoxide 3.45.** Prepared according to “**General procedure 2: MHAT RPC Epoxidation.**” The reaction was performed with 0.3 mmol (86.8 mg) of **3.9**, 5  $\mu$ mol (3.5 mg) of **3.17**, 0.3 mmol (41  $\mu$ L) of MePhSiH<sub>2</sub>, and 0.1 mmol (18.4 mg) 8-vinyl-1,4-dioxaspiro[4.5]decan-8-ol<sup>21</sup> producing a 11.2:1.0 ratio of **3.45** to **3.31**. The crude was chromatographed once with 100% CH<sub>2</sub>Cl<sub>2</sub> to 5% EtOAc/CH<sub>2</sub>Cl<sub>2</sub> as the eluting solvent, delivering 11.1 mg (60%) of the desired epoxide as a colorless oil.



<sup>1</sup>H NMR (500 MHz, CDCl<sub>3</sub>, 25 °C):

$\delta$  4.02 – 3.91 (m, 4H)                      1.30 (d, *J* = 5.6 Hz, 3H)

2.92 (q, *J* = 5.5 Hz, 1H)

1.92 – 1.77 (m, 4H)

1.76 – 1.70 (m, 2H)

1.68 – 1.63 (m, 1H)

1.57 – 1.53 (m, 1H)

<sup>13</sup>C NMR (126 MHz, CDCl<sub>3</sub>, 25 °C):

$\delta$  108.60                      59.83                      25.97

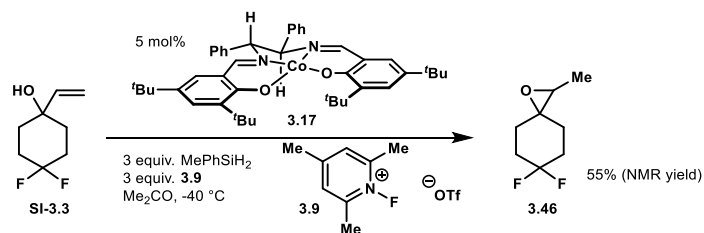
64.55                          33.01                      13.89

64.53                          32.93

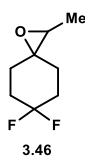
61.45                          32.23

HRMS (ES<sup>+</sup>) calculated for C<sub>10</sub>H<sub>16</sub>O<sub>3</sub>Na [M+Na]: 207.0997, found: 207.0991

R<sub>f</sub> 0.50 (30% EtOAc/Hex)



**Epoxide 3.46.** Prepared according to “**General procedure 2: MHAT RPC Epoxidation.**” The reaction was performed with 0.3 mmol (86.8 mg) of **3.9**, 5  $\mu$ mol (3.5 mg) of **3.17**, 0.3 mmol (41  $\mu$ L) of MePhSiH<sub>2</sub>, and 0.1 mmol (16.2 mg) vinylcyclohexanol **SI-3.3** producing none of the ketone **3.32** as detectable by <sup>1</sup>H NMR. The crude was chromatographed with 20% CH<sub>2</sub>Cl<sub>2</sub>/Pentane as the eluting solvent, delivering 3.5 mg (22%) of the desired epoxide as a sweet-smelling oil. **3.46** is volatile.



<sup>1</sup>H NMR (500 MHz, CDCl<sub>3</sub>, 25 °C):

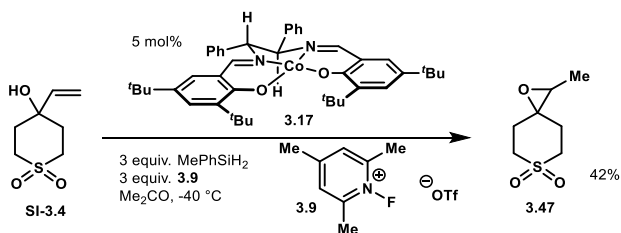
$\delta$ 2.96 (q, $J$ = 5.6 Hz, 1H)	1.66 – 1.61 (m, 1H)
2.14 – 2.03 (m, 4H)	1.52 – 1.47 (m, 1H)
1.95 – 1.84 (m, 2H)	1.31 (d, $J$ = 5.6 Hz, 1H)

<sup>13</sup>C NMR (126 MHz, CDCl<sub>3</sub>, 25 °C):

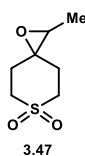
$\delta$ 123.22 (dd, $J$ = 242.4, 239.8 Hz)	30.96 (dd, $J$ = 7.4, 3.1 Hz)
59.81 (d, $J$ = 1.8 Hz)	24.94 (dd, $J$ = 7.5, 3.1 Hz)
31.88 (td, $J$ = 24.6, 3.1 Hz)	13.81

HRMS (CI<sup>+</sup>) calculated for C<sub>8</sub>H<sub>12</sub>F<sub>2</sub>O [M]<sup>+</sup>: 162.0856, found: 162.0849

R<sub>f</sub> 0.26 (30% CH<sub>2</sub>Cl<sub>2</sub>/Hex)



**Epoxide 3.47.** Prepared according to “**General procedure 2: MHAT RPC Epoxidation.**” The reaction was performed with 0.3 mmol (86.8 mg) of **3.9**, 5  $\mu$ mol (3.5 mg) of **3.17**, 0.3 mmol (41  $\mu$ L) of MePhSiH<sub>2</sub>, and 0.1 mmol (17.6 mg) vinylcyclohexanol **SI-3.4** producing none of the ketone **3.33** as detectable by <sup>1</sup>H NMR. The crude was chromatographed with 40% EtOAc/Hex as the eluting solvent, delivering 7.4 mg (42%) of the desired epoxide as a colorless solid.



<sup>1</sup>H NMR (500 MHz, CDCl<sub>3</sub>, 25 °C):

$\delta$ 3.29 (d, $J$ = 54.8 Hz, 2H)	2.43 (ddd, $J$ = 14.4, 12.3, 3.8 Hz, 1H)
3.11 – 3.02 (m, 3H)	1.35 (d, $J$ = 5.6 Hz, 3H)
2.53 (ddd, $J$ = 14.4, 12.3, 3.8 Hz, 1H)	

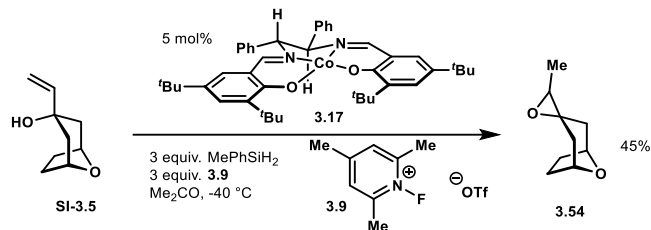
<sup>13</sup>C NMR (126 MHz, CDCl<sub>3</sub>, 25 °C):

$\delta$ 61.02	49.27	13.89
58.31	32.79	
49.30	26.85	

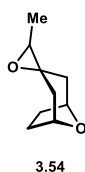
HRMS (ES<sup>+</sup>) calculated for C<sub>7</sub>H<sub>12</sub>O<sub>3</sub>SNa [M+Na]: 199.0405, found: 199.0412

R<sub>f</sub> 0.23 (50% EtOAc/Hex)





**Epoxide 3.54.** Prepared according to “**General procedure 2: MHAT RPC Epoxidation.**” The reaction was performed with 0.3 mmol (86.8 mg) of **3.9**, 5  $\mu$ mol (3.5 mg) of **3.17**, 0.3 mmol (41  $\mu$ L) of MePhSiH<sub>2</sub>, and 0.1 mmol (15.4 mg) of vinylcyclohexanol **SI-3.5** producing a 7.8:1.0 ratio of **3.54** to ketone **3.38**. The crude material was chromatographed with 100% CH<sub>2</sub>Cl<sub>2</sub> to 5% Et<sub>2</sub>O/ CH<sub>2</sub>Cl<sub>2</sub> as the eluting solvent, delivering 7.0 mg (45%) of the desired epoxide as a colorless oil.



<sup>1</sup>H NMR (500 MHz, CDCl<sub>3</sub>, 25 °C):

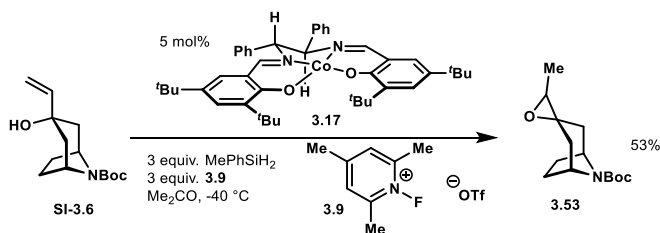
$\delta$ 4.49 (dt, $J = 34.3, 5.1$ Hz, 2H)	2.01 – 1.92 (m, 2H)
2.62 (q, $J = 5.5$ Hz, 1H)	1.29 (d, $J = 14.2$ Hz, 1H)
2.34 (dd, $J = 14.3, 4.0$ Hz, 1H)	1.20 (d, $J = 5.6$ Hz, 3H)
2.21 (dd, $J = 14.2, 4.1$ Hz, 1H)	1.11 (d, $J = 14.2$ Hz, 1H)
2.16 – 2.11 (m, 2H)	

<sup>13</sup>C NMR (126 MHz, CDCl<sub>3</sub>, 25 °C):

$\delta$ 74.69	54.84	28.57
74.53	40.68	28.47
57.99	36.06	12.84

HRMS (ES<sup>+</sup>) calculated for C<sub>9</sub>H<sub>14</sub>O<sub>2</sub>Na [M+Na]: 177.0892, found: 177,0900

R<sub>f</sub> 0.25 (100% CH<sub>2</sub>Cl<sub>2</sub>)



**Epoxide 3.53.** Prepared according to “**General procedure 2: MHAT RPC Epoxidation.**” The reaction was performed with 0.3 mmol (86.8 mg) of **3.9**, 5  $\mu$ mol (3.5 mg) of **3.17**, 0.3 mmol (41  $\mu$ L) of MePhSiH<sub>2</sub>, and 0.1 mmol (25.3 mg) of vinylcyclohexanol **SI-3.6** producing a 10.7:1.0 ratio of epoxide **3.53** to ketone **3.39**. The products were inseparable and subjected to protocol 1. The crude material was chromatographed once with 10% EtOAc/Hex and once with 3% EtOAc/CH<sub>2</sub>Cl<sub>2</sub> as the eluting solvent, delivering 13.4 mg (53%) of the desired epoxide as a colorless oil.



<sup>1</sup>H NMR (500 MHz, CDCl<sub>3</sub>, 25 °C):

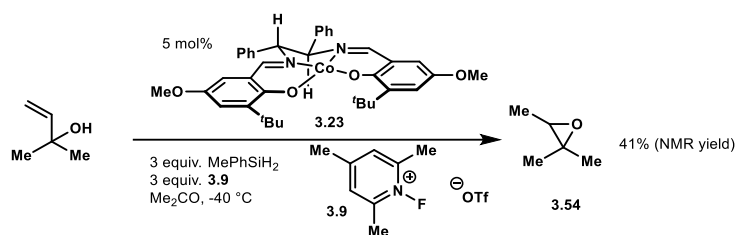
$\delta$ 4.29 (t, $J$ = 35.2 Hz, 2H)	1.47 (s, 9H)
2.62 (q, $J$ = 5.5 Hz, 1H)	1.33 (d, $J$ = 14.2 Hz, 1H)
2.43 – 2.10 (m, 2H)	1.21 (d, $J$ = 5.6 Hz, 3H)
2.05 (app d, $J$ = 10.1 Hz, 2H)	1.14 (d, $J$ = 14.3 Hz, 1H)
2.02 – 1.94 (m, 2H)	

<sup>13</sup>C NMR (126 MHz, CDCl<sub>3</sub>, 25 °C):

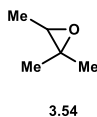
$\delta$ 153.51	40.25 (d, $J$ = 94.9 Hz)
79.49	35.45 (d, $J$ = 107.8 Hz)
58.44	28.67
54.75	28.41 – 27.26 (m)
53.94-52.73 (m)	12.93

HRMS (ES<sup>+</sup>) calculated for C<sub>14</sub>H<sub>23</sub>NO<sub>3</sub>Na [M+Na]: 276.1576, found: 276.1573

R<sub>f</sub> 0.24 (10% EtOAc/Hex)



**Epoxide 3.54.** Prepared according to “**General procedure 2: MHAT RPC Epoxidation.**” The reaction was performed with 0.3 mmol (86.8 mg) of **3.9**, 5  $\mu$ mol (3.2 mg) of **3.23**, 0.3 mmol (41  $\mu$ L) of MePhSiH<sub>2</sub>, and 0.1 mmol (10.4  $\mu$ L) of 3-buten-2-ol producing a 3.4:1.0 ratio of **3.54** to ketone **3.40**. 0.1 mmol (14  $\mu$ L) of mesitylene was added directly to the reaction mixture, which was transferred into an NMR tube for analysis. The NMR yield was determined by integration of relevant peaks (3 methyl multiplet 1.25-1.15, 9H) and was found to be 41%. A standard of the NMR spectrum of this compound in acetone-*d* was obtained by analysis of a sample purchased from Sigma-Aldrich, 97%.

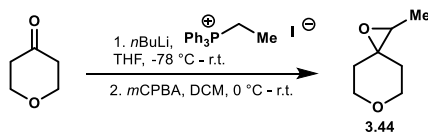


<sup>1</sup>H NMR (500 MHz, (CD<sub>3</sub>)<sub>2</sub>CO, 25 °C):

$\delta$  2.74 (q, *J* = 5.5 Hz, 1H)

1.25 – 1.15 (m, 9H)

#### Synthesis of analytical sample of epoxide 3.44



**Epoxide 3.44.** *n*BuLi (1.83 mL, 2.46 M in hexanes, 4.5 mmol) was added slowly to a -78 °C suspension of ethyltriphenylphosphonium iodide (1.76 g, 4.2 mmol) in THF (12 mL). After 30 min, a solution of tetrahydro-4H-pyran-4-one (300.3 mg, 3.0 mmol) in THF (3 mL) was added slowly. After 15 min, the solution was allowed to warm to 20 °C. After 12 h, the reaction was quenched with saturated aqueous NH<sub>4</sub>Cl. The aqueous phase was extracted with Et<sub>2</sub>O 2x 50 mL. The organics were dried over MgSO<sub>4</sub>. Careful evaporation of the solvent delivered ~1.2 g of crude material which was triturated with pentane (2x 10 mL) and filtered. The filtrate was carefully concentrated and used crude in the following transformation.

Crude alkene from the preceding operation was dissolved in CH<sub>2</sub>Cl<sub>2</sub> (5 mL) and added slowly to a 0 °C solution of *m*CPBA (1.11 g, 6.4 mmol) in CH<sub>2</sub>Cl<sub>2</sub> (45 mL). The clear solution was warmed to 20 °C and stirred for 1 h, at which point TLC analysis indicated complete consumption of the starting material. The

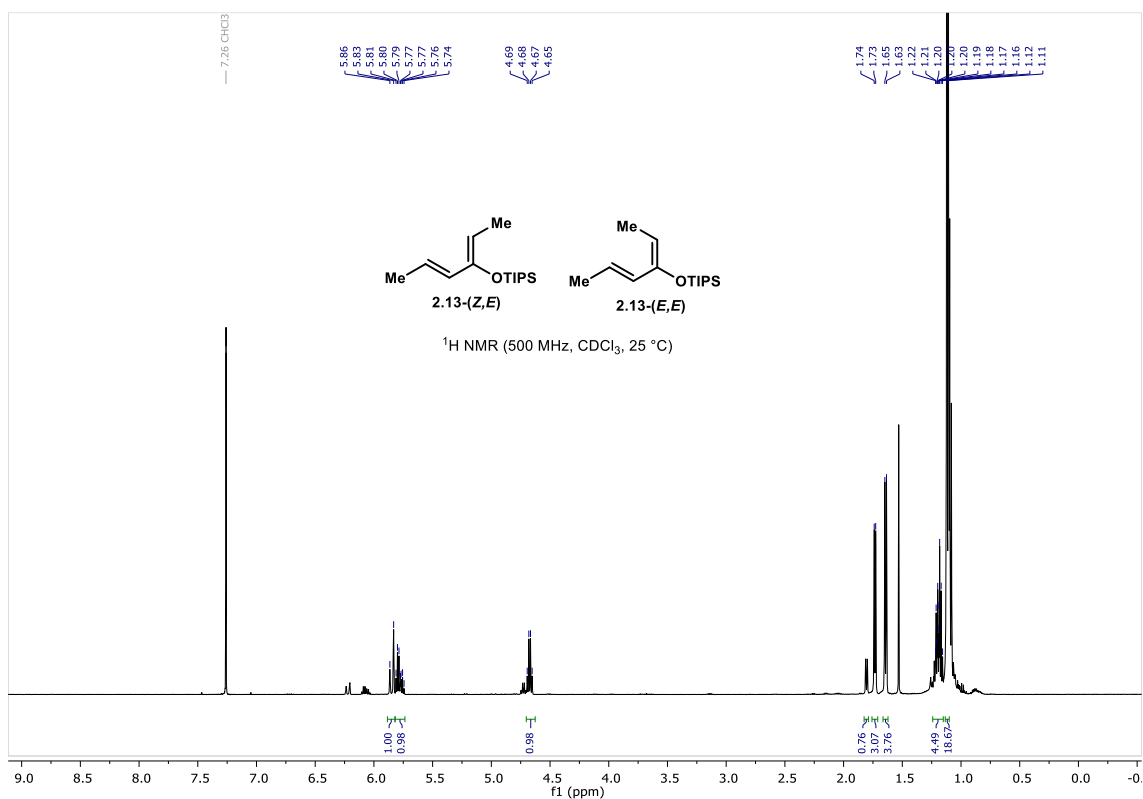
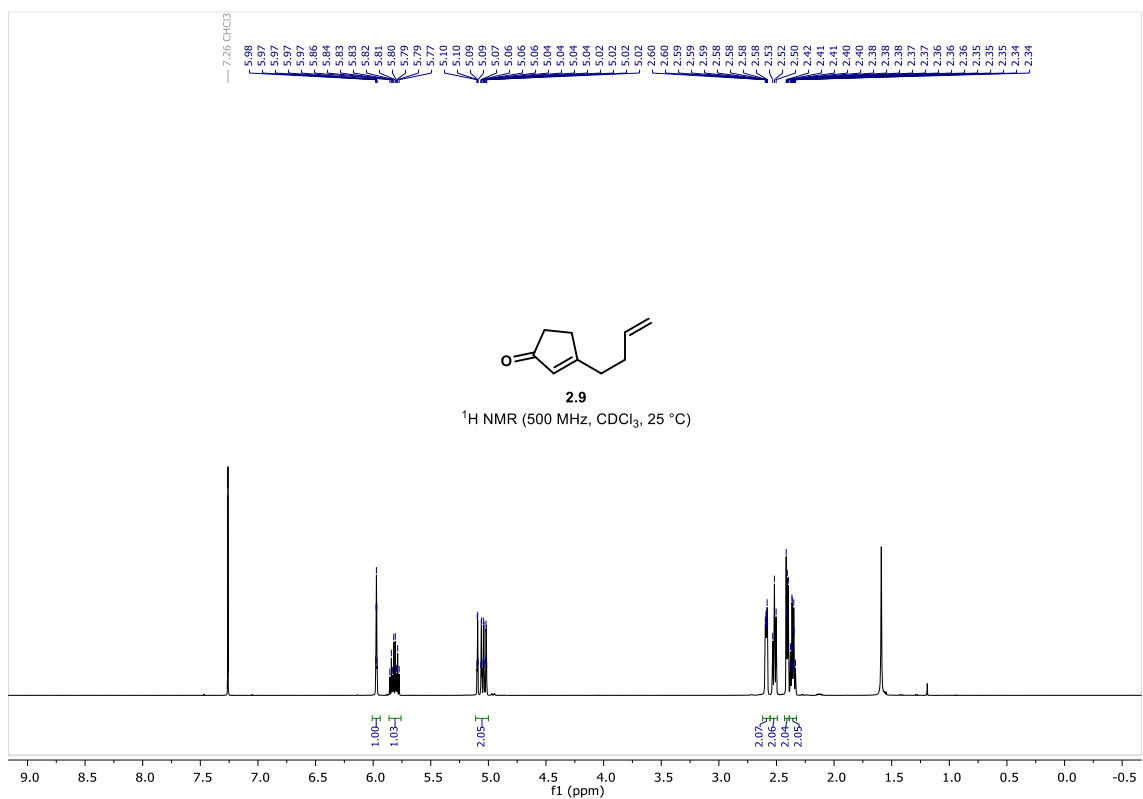
reaction was poured into 25 mL saturated aqueous NaHCO<sub>3</sub> and 25 mL saturated aqueous Na<sub>2</sub>S<sub>2</sub>O<sub>3</sub>. The aqueous layer was extracted with CH<sub>2</sub>Cl<sub>2</sub> 2x 50 mL. The organics were washed with brine and dried over Na<sub>2</sub>SO<sub>4</sub>. Following careful concentration in vacuo, the crude material was purified by flash column chromatography with 20% Et<sub>2</sub>O/pentane as the eluting solvent, delivering 81 mg (21%) of analytically pure epoxide **3.44**.

### 3.6. References

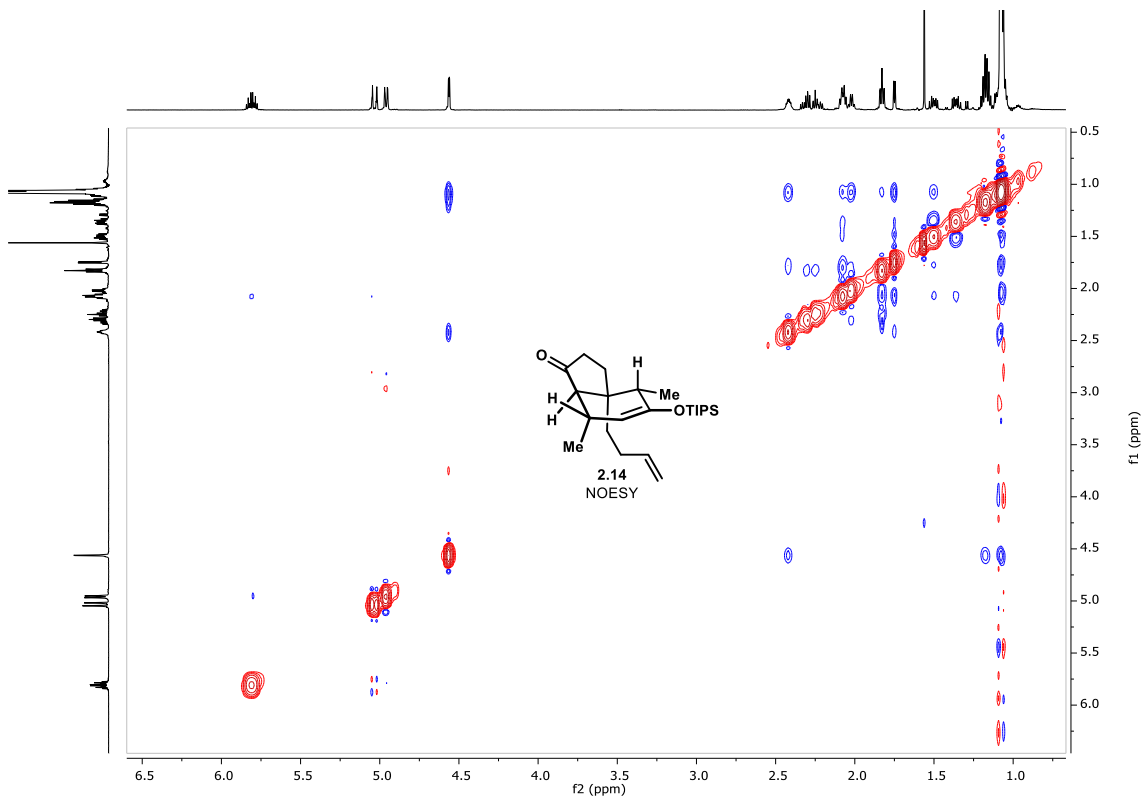
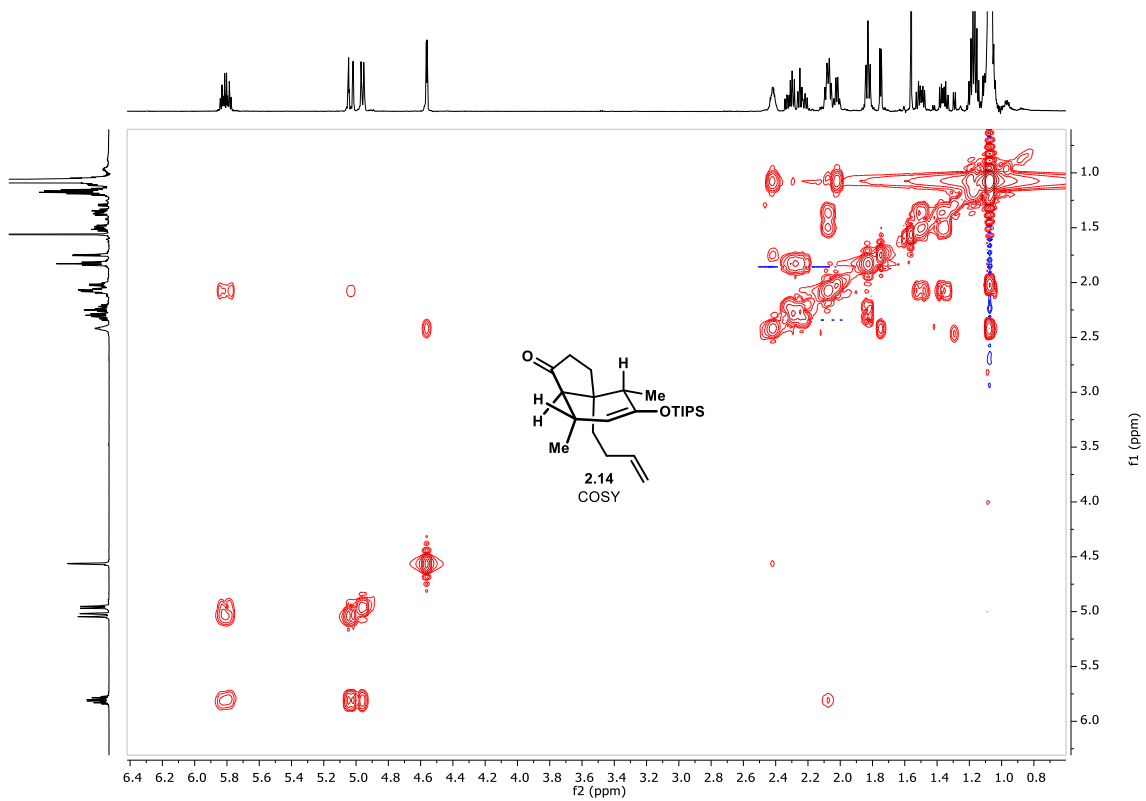
- (1) For a review of carbocation chemistry: Reddy, R. R.; Klumpp, D. A. *Chem. Rev.* **2013**, *113*, 6905.
- (2) For a review of MHAT alkene hydrofunctionalization: Crossley, S. W. M.; Martinez, R. M.; Obradors, C.; Shenvi, R. A. *Chem. Rev.* **2016**, *116*, 8912.
- (3) Drago's initial disclosure: Zombeck, A.; Hamilton, D. E.; Drago, R. S. *J. Am. Chem. Soc.* **1982**, *104*, 6782.
- (4) (a) Mukaiyama's initial disclosure: Mukaiyama, T.; Isayama, S.; Inoki, S.; Kato, K.; Yamada, T.; Takai, T. *Chem. Lett.* **1989**, *18*, 449. (b) An account by Mukaiyama: Mukaiyama, T.; Tohru, Y. *Bull. Chem. Soc. Jpn.* **1995**, *68*, 17.
- (5) (a) Eisenberg, D. C.; Norton, J. R. *Isr. J. Chem.* **1991**, *31*, 55. (b) Hartung, J.; Norton, J. *Catalysis Without Precious Metals*; Bullock, R. M., Ed.; Wiley: Weinheim, Germany, 2010. See also discussions in ref. 2 and ref 8c.
- (6) (a) For an insightful discussion of electronic effects in radical addition reactions: Giese, B. *Angew. Chem. Int. Ed. Engl.* **1983**, *22*, 753. (b) see also: Roberts, B. P. *Chem. Soc. Rev.* **1999**, *28*, 25.
- (7) A sample of canonical radical additions into  $\alpha,\beta$ -unsaturated carbonyl derivatives: (a) Porter, N. A.; Giese, B.; Curran, D. P. *Acc. Chem. Res.* **1991**, *24*, 296. (b) Srikanth, G. S. C.; Castle, S. L.; *Tetrahedron* **2005**, *61*, 10377. (c) Jamison, C. R.; Overman, L. E. *Acc. Chem. Res.* **2016**, *49*, 1578.
- (8) Pioneering MHAT additions into  $\alpha,\beta$ -unsaturated carbonyl derivatives: (a) Lo, J. C.; Yabe, Y.; Baran, P. S. *J. Am. Chem. Soc.* **2014**, *136*, 1304. (b) Lo, J. C.; Gui, J.; Yabe, Y.; Pan, C.-M.; Baran, P. S. *Nature* **2014**, *516*, 343. (c) Lo, J. C.; Kim, D.; Pan, C.-M.; Edwards, J. T.; Yabe, Y.; Gui, J.; Qin, T.; Gutierrez, S.; Giacoboni, J.; Smith, M. W.; Holland, P. L.; Baran, P. S. *J. Am. Chem. Soc.* **2017**, *139*, 2484.
- (9) Some of the many reports from Carreira's laboratory: (a) Waser, J.; Carreira, E. M. *J. Am. Chem. Soc.* **2004**, *126*, 5676. (b) Waser, J.; Gaspar, B.; Nambu, H.; Carreira, E. M. *J. Am. Chem. Soc.* **2006**, *128*, 11693. (c) Gaspar, B.; Carreira, E. M. *Angew. Chem., Int. Ed.* **2007**, *46*, 4519.
- (10) Shigehisa, H.; Aoki, T.; Yamaguchi, S.; Shimizu, N.; Hiroya, K. *J. Am. Chem. Soc.* **2013**, *135*, 10306.
- (11) (a) Shigehisa, H.; Koseki, N.; Shimizu, N.; Fujisawa, M.; Niitsu, M.; Hiroya, K. *J. Am. Chem. Soc.* **2014**, *136*, 13534. (b) Shigehisa, H.; Hayashi, M.; Ohkawa, H.; Suzuki, T.; Okayasu, H.; Mukai, M.; Yamazaki, A.; Kawai, R.; Kikuchi, H.; Satoh, Y.; Fukuyama, A.; Hiroya, K. *J. Am. Chem. Soc.* **2016**, *138*, 10597. (c) Date, S.; Hamasaki, K.; Sunagawa, K.; Koyama, H.; Sebe,

- C.; Hiroya, K.; Shigehisa, H. *ACS Catal.* **2020**, *10*, 2039–2045. (d) Shigehisa, H. *Synlett* **2015**, *26*, 2479. (e) Ohuchi, S.; Koyama, H.; Shigehisa, H. *ACS Catalysis* **2021**, *11*, 900.
- (12) Touney, E. E. Ph.D. Thesis, University of California, Irvine 2021.
- (13) (a) Anderson, S. N.; Ballard, D. H.; Chrzastowski, J. Z.; Dodd, D.; Johnson, M. D. *J. Chem. Soc., Chem. Commun.* **1972**, 685. (b) Magnuson, R. H.; Halpern, J.; Levitin, I. Y.; Vol'pin, M. E. *J. Chem. Soc., Chem. Commun.* **1978**, 44. (c) Vol'pin, M. E.; Levitin, I. Y.; Sigan, A. L.; Halpern, J.; Tom, G. M. *Inorg. Chim. Acta.* **1980**, *41*, 271.
- (14) Tsuji, N.; Kobayashi, Y.; Takemoto, Y. *Chem. Commun.* **2014**, *50*, 13691.
- (15) Touney, E. E.; Foy, N. J.; Pronin, S. V. *J. Am. Chem. Soc.* **2018**, *140*, 16982.
- (16) For a discussion of how catalyst control has impacted the broader field of palladium-catalyzed reactions: Surry, D. S.; Buchwald, S. L. *Angew. Chem., Int. Ed.* **2008**, *47*, 6338.
- (17) (a) Discolo, C. A.; Touney, E. E.; Pronin, S. V. *J. Am. Chem. Soc.* **2019**, *141*, 17527. (b) Ebisawa, K.; Izumi, K.; Ooka, Y.; Kato, H.; Kanazawa, S.; Komatsu, S.; Nishi, E.; Shigehisa, H. *J. Am. Chem. Soc.* **2020**, *142*, 13481. (c) Qin, T.; Lv, G.; Meng, Q.; Zhang, G.; Xiong, T.; Zhang, Q. *Angew. Chem., Int. Ed.* **2021**, *60*, 25949.
- (18) Zheng, H.; Lejkowskia, M. and Hall, D. G. *Chem. Sci.* **2011**, *2*, 1305.
- (19) Quin, L. D.; MacDiarmid, J. E. *J. Org. Chem.* **1982**, *46*, 461.
- (20) Miralles, N.; Alam, R.; Szabo, K. J.; Fernandez, E. *Angew. Chem., Int. Ed.* **2016**, *55*, 4303.
- (21) Williams, R.; Eldridge, G.; Starks, C.; Guzzo, P. R.; Huang, Z. US Pat. App. WO2017044877A1, September 12, 2015.
- (22) Justik, M.; Koser, G. *Molecules* **2005**, *10*, 217.
- (23) Ozaki, S.; Yoshinaga, H.; Matsui, E.; Adachi, M. *J. Org. Chem.* **2001**, *66*, 2503.
- (24) Hu, X.-Q.; Hu, Z.; Trita, A. S.; Zhang, G.; Gooßen, L. J. *Chem. Sci.* **2018**, *9*, 5289.
- (25) Enders, D.; Eichenauer, H.; Baus, U.; Schubert, H.; Kremer, K. A. M. *Tetrahedron* **1984**, *40*, 1345.

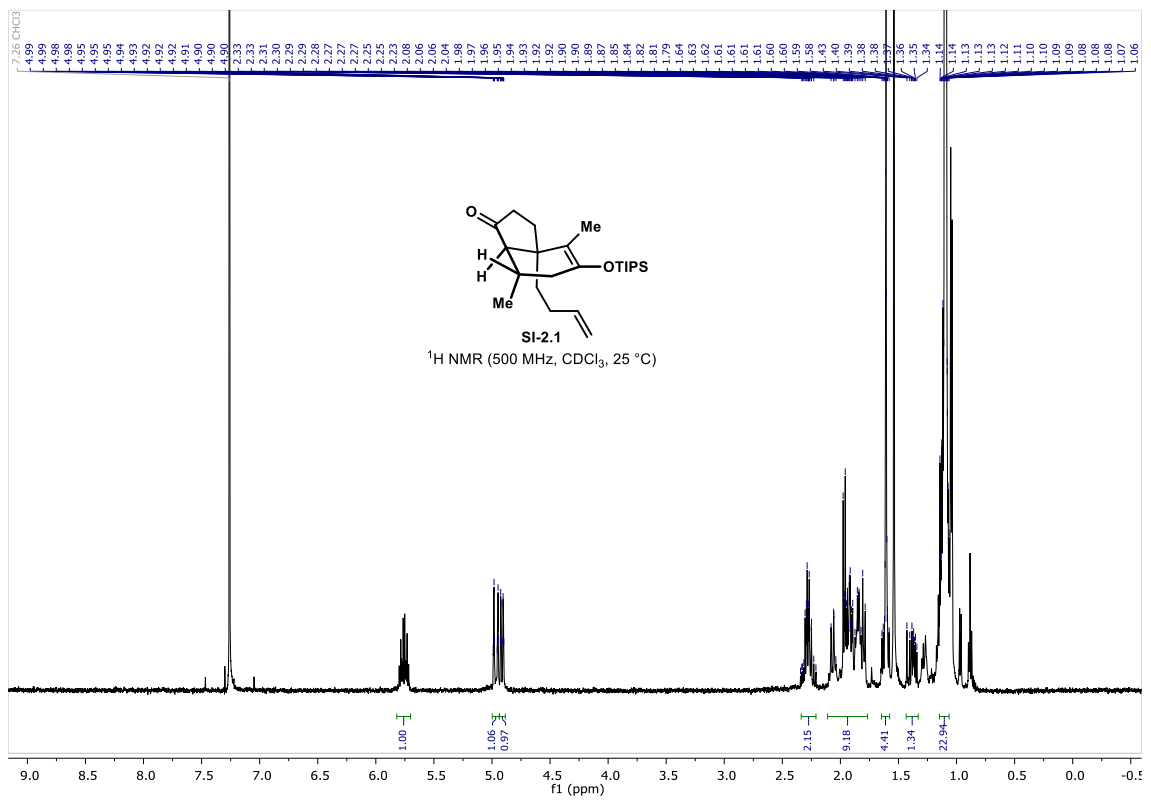
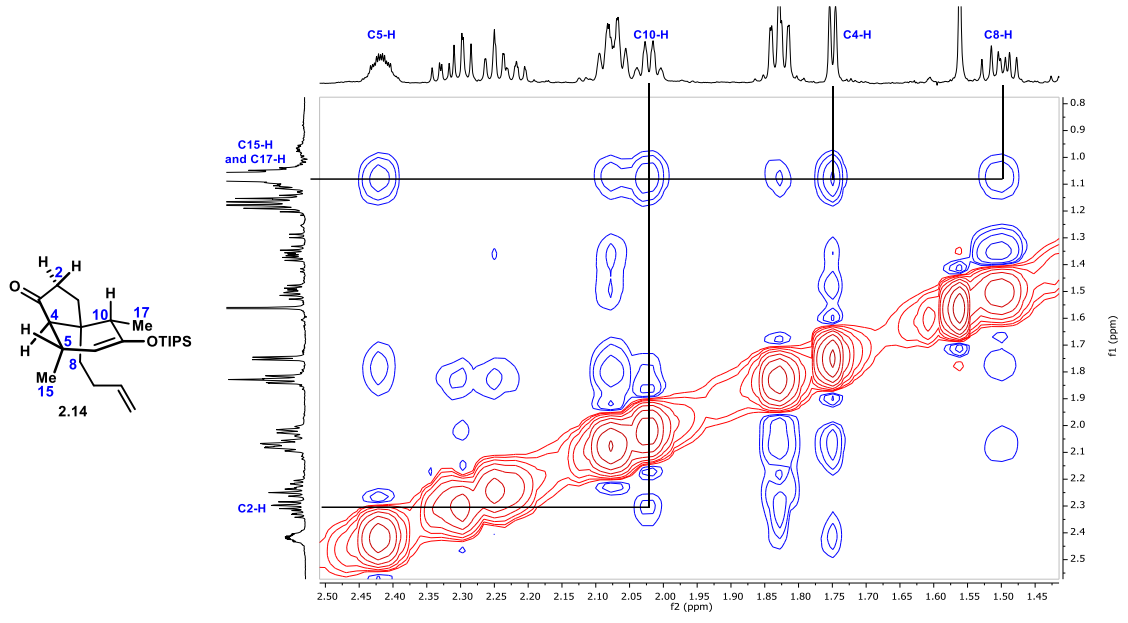
## Appendix A. Spectra for Chapter 2

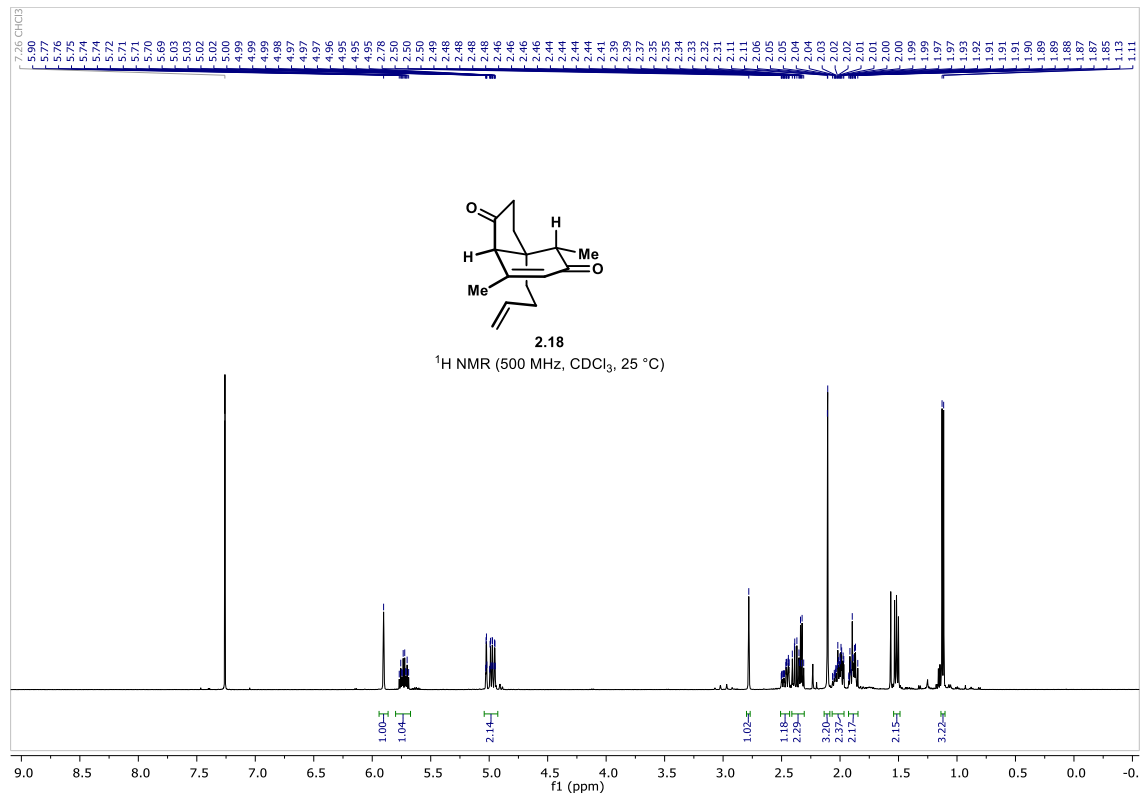
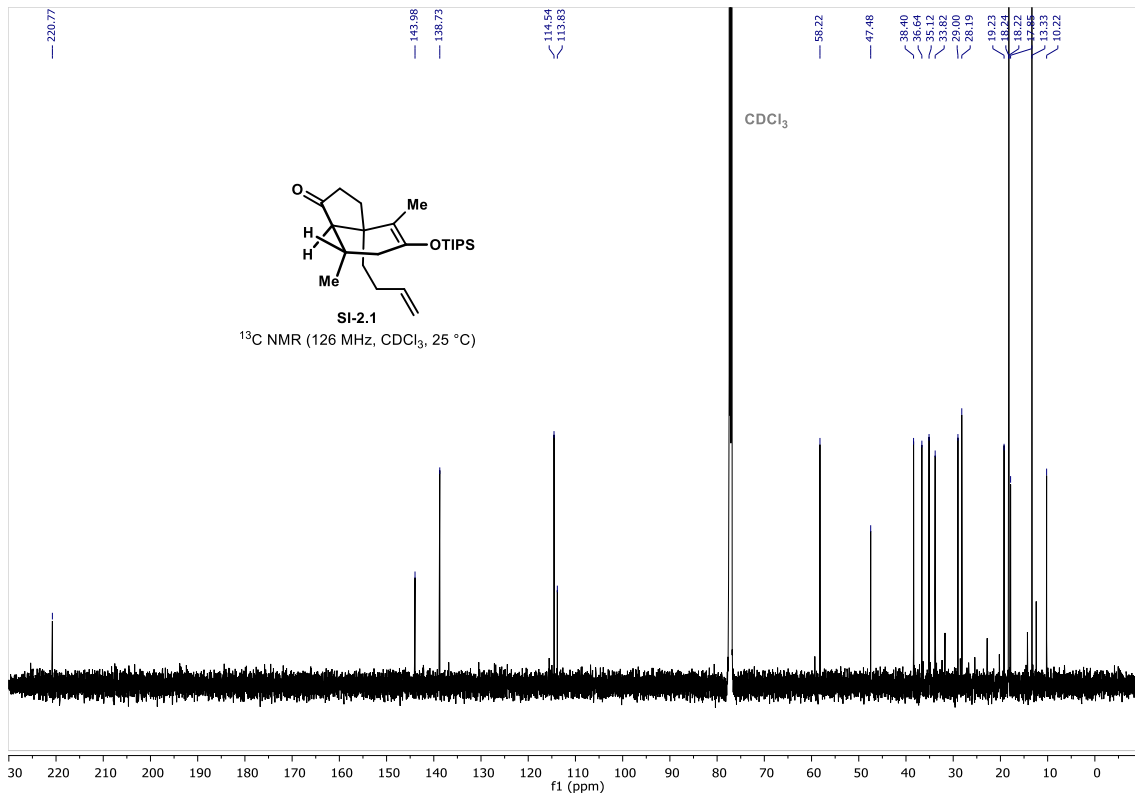


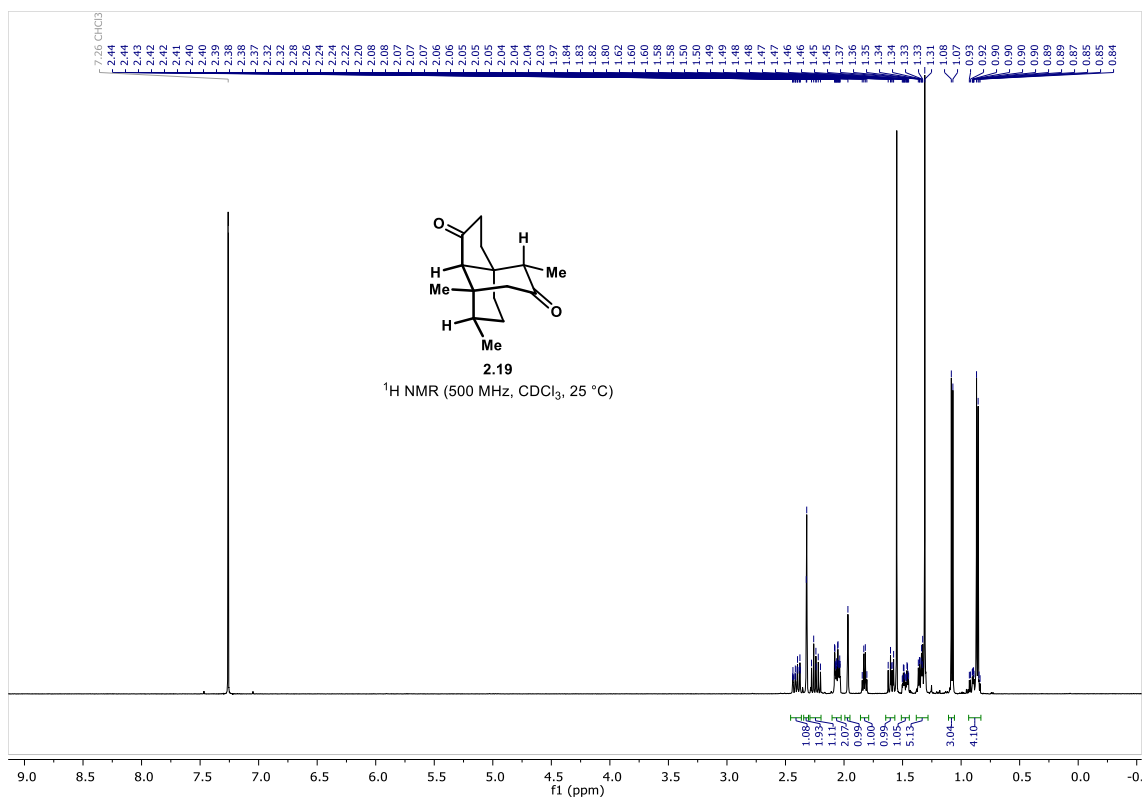
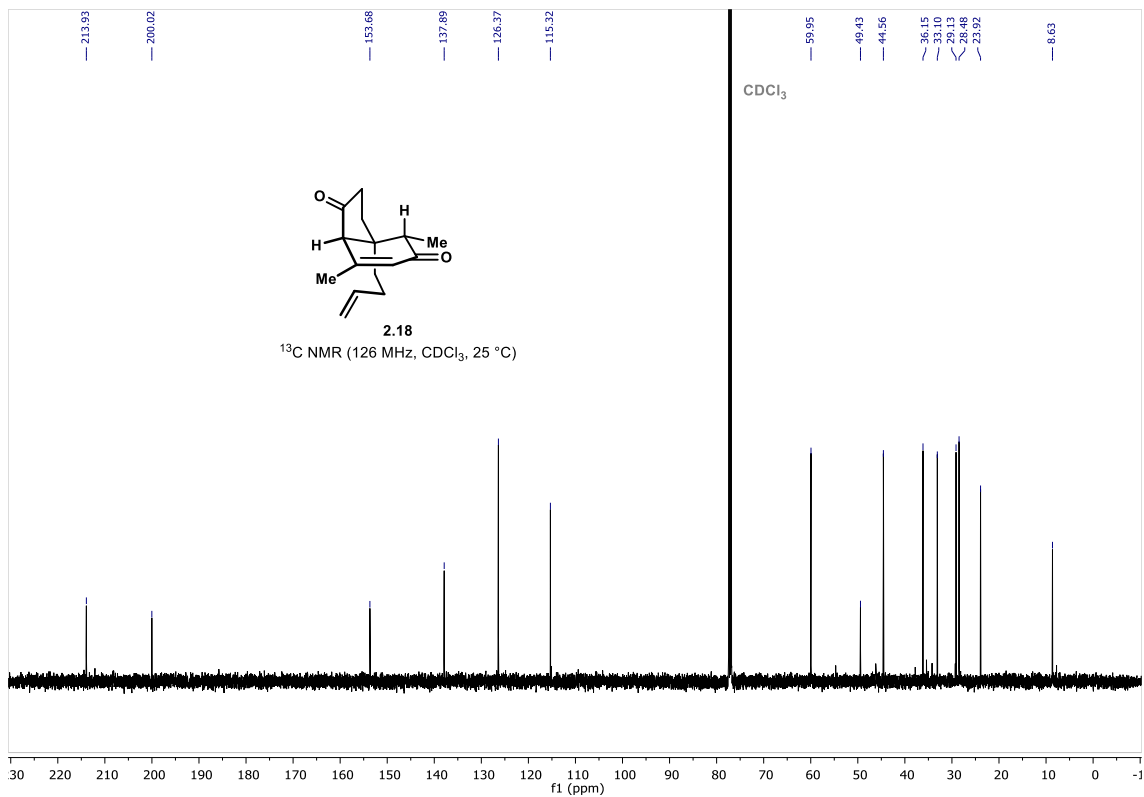




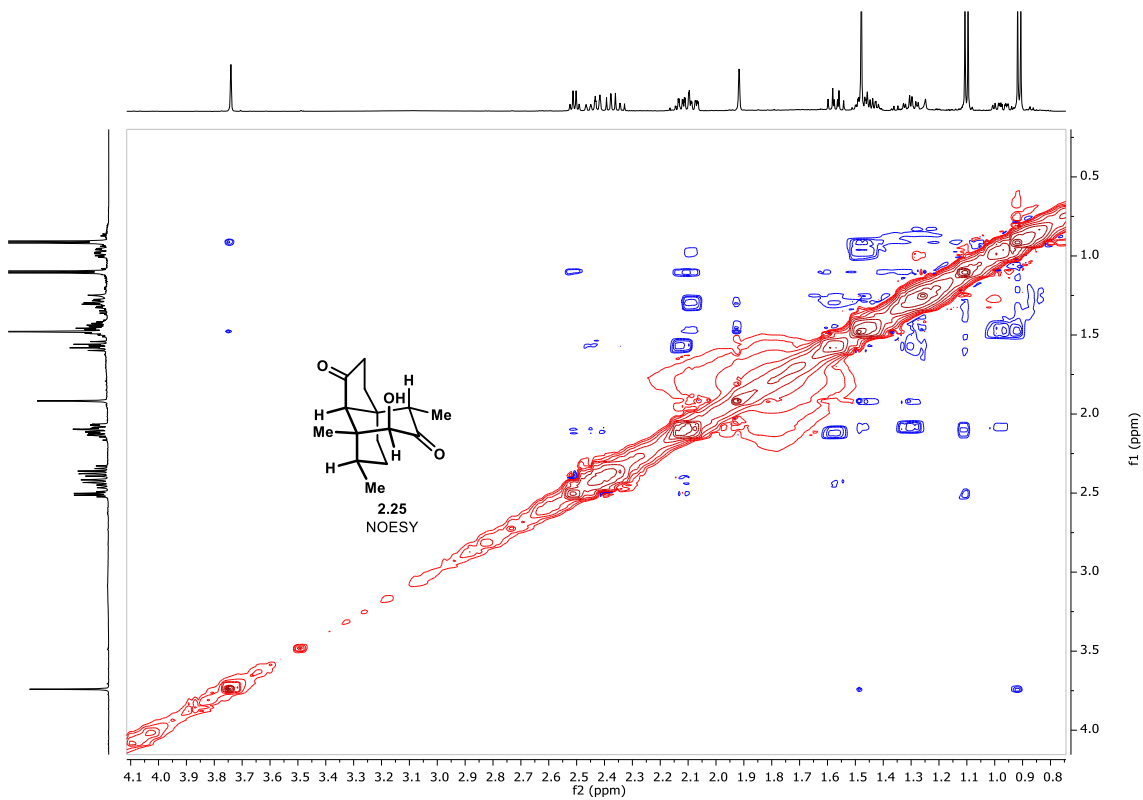
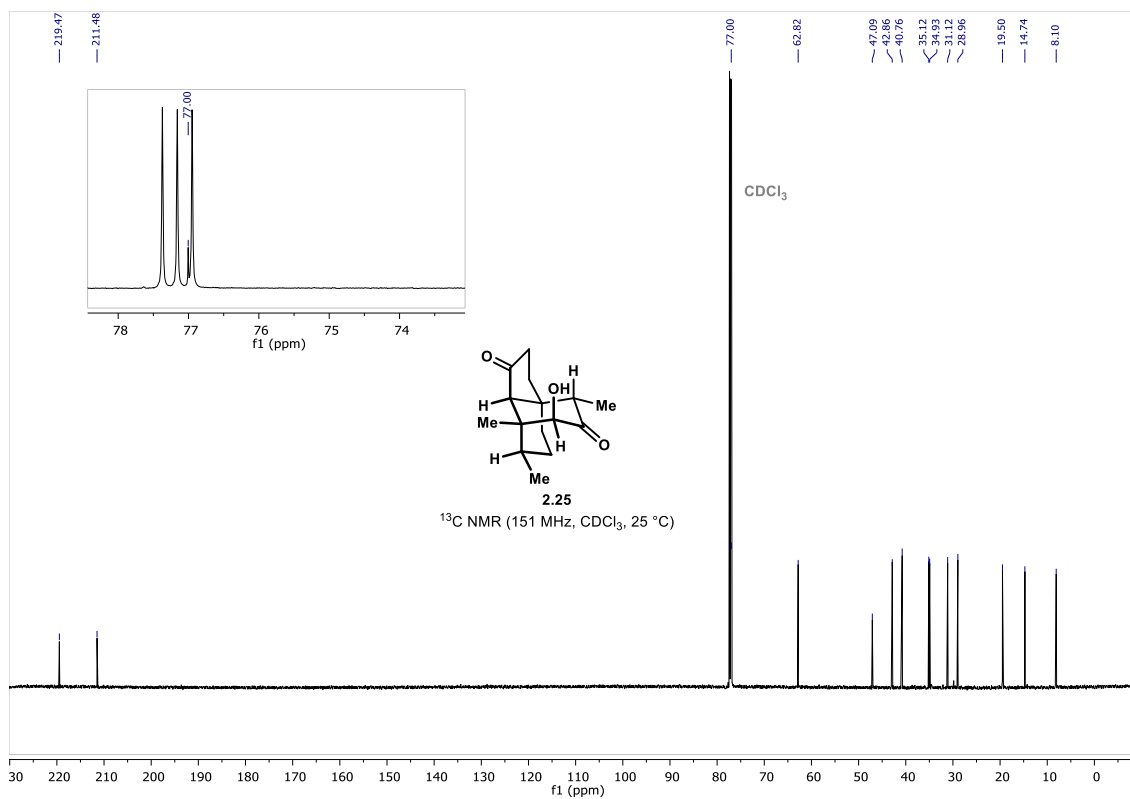


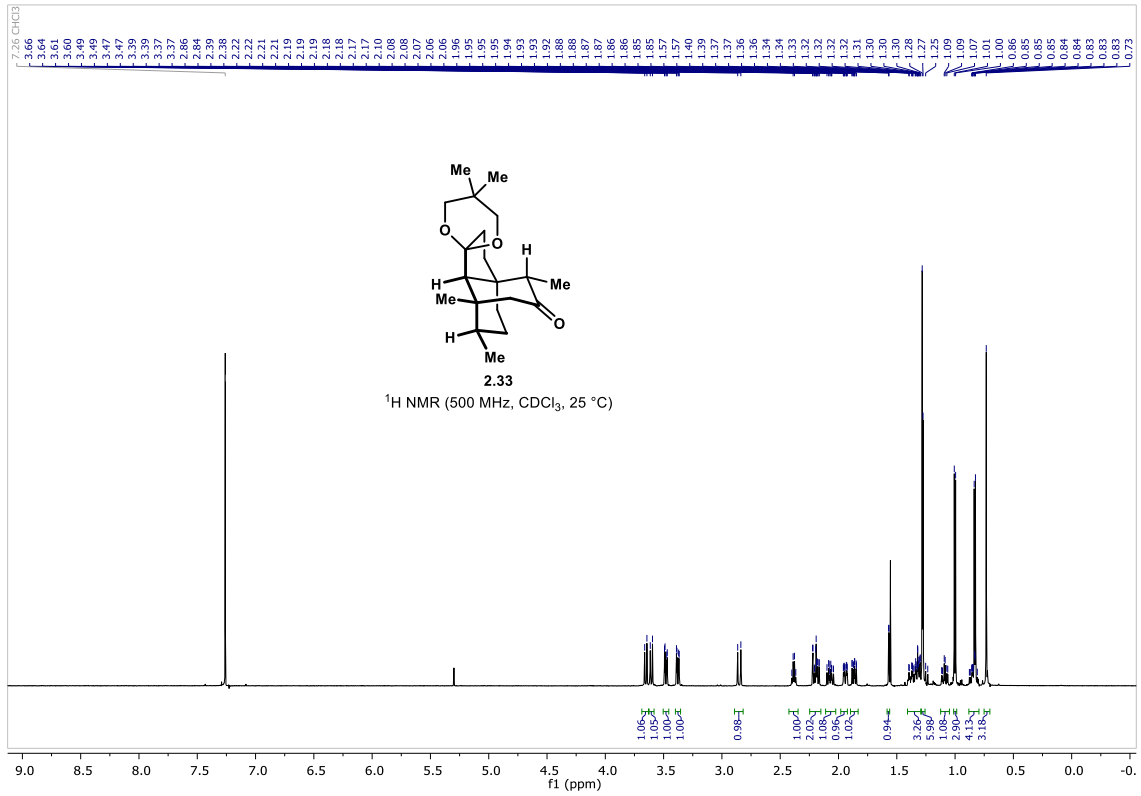
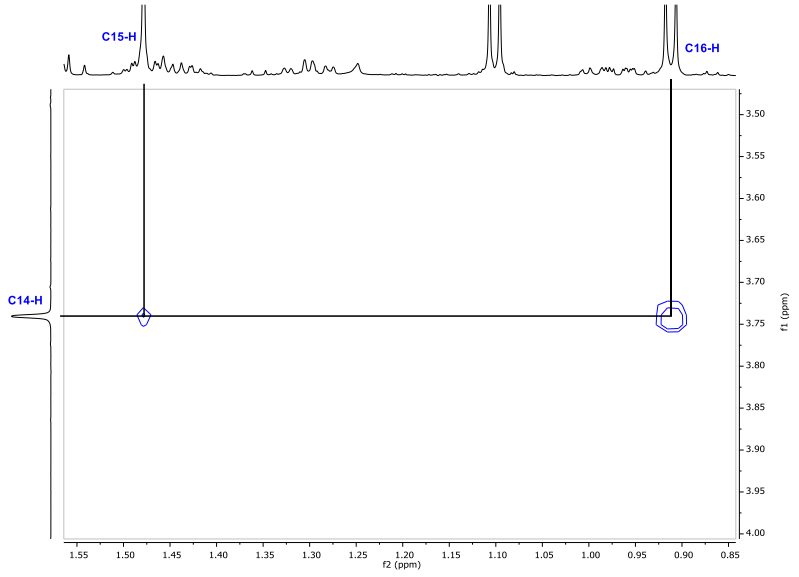
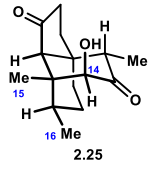


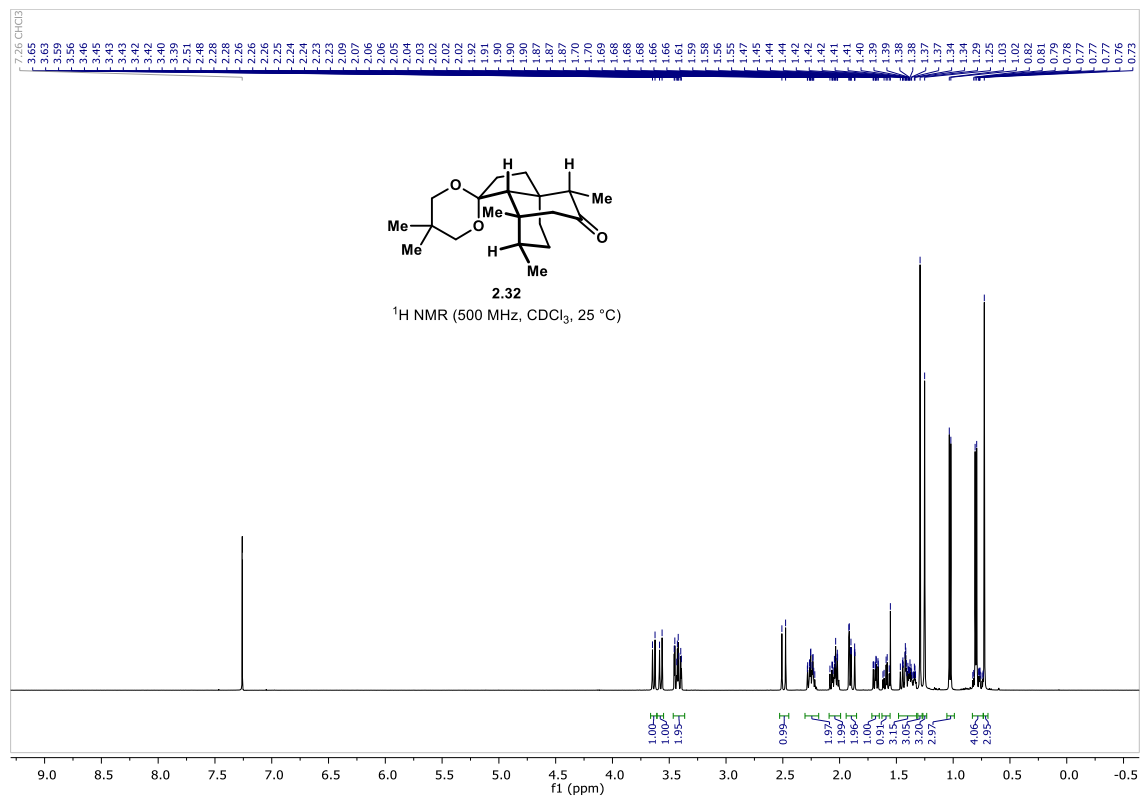
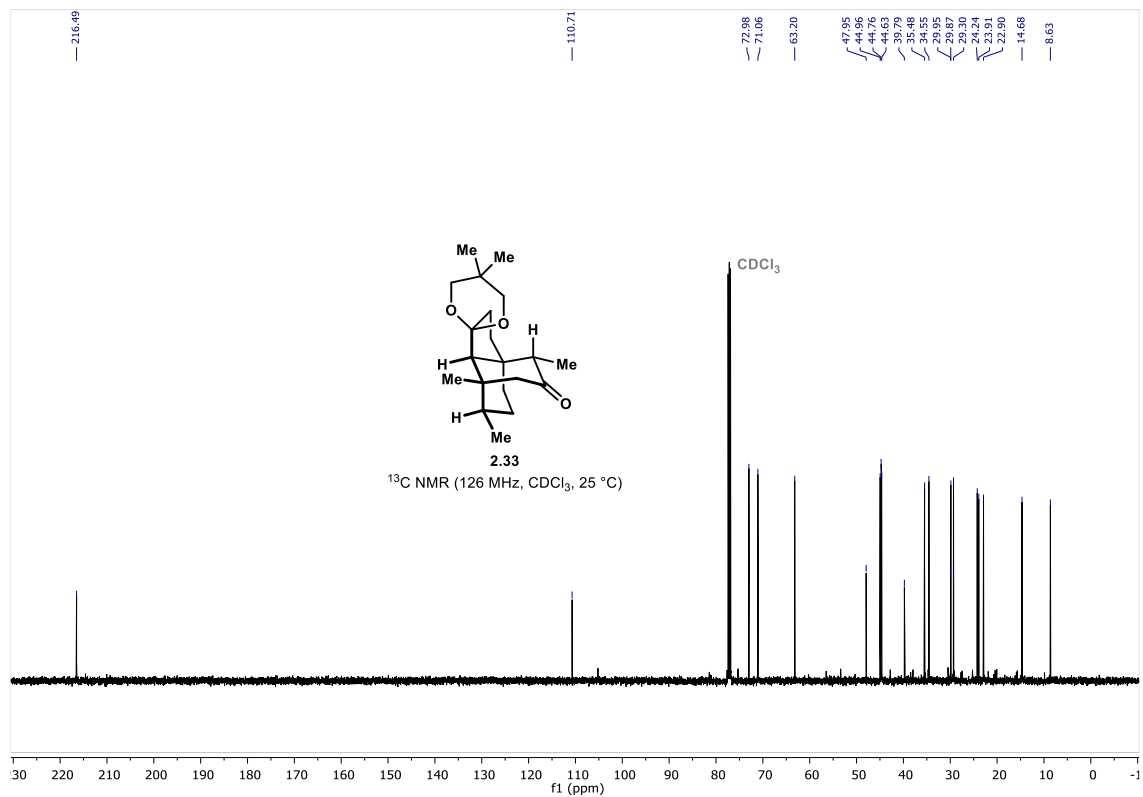


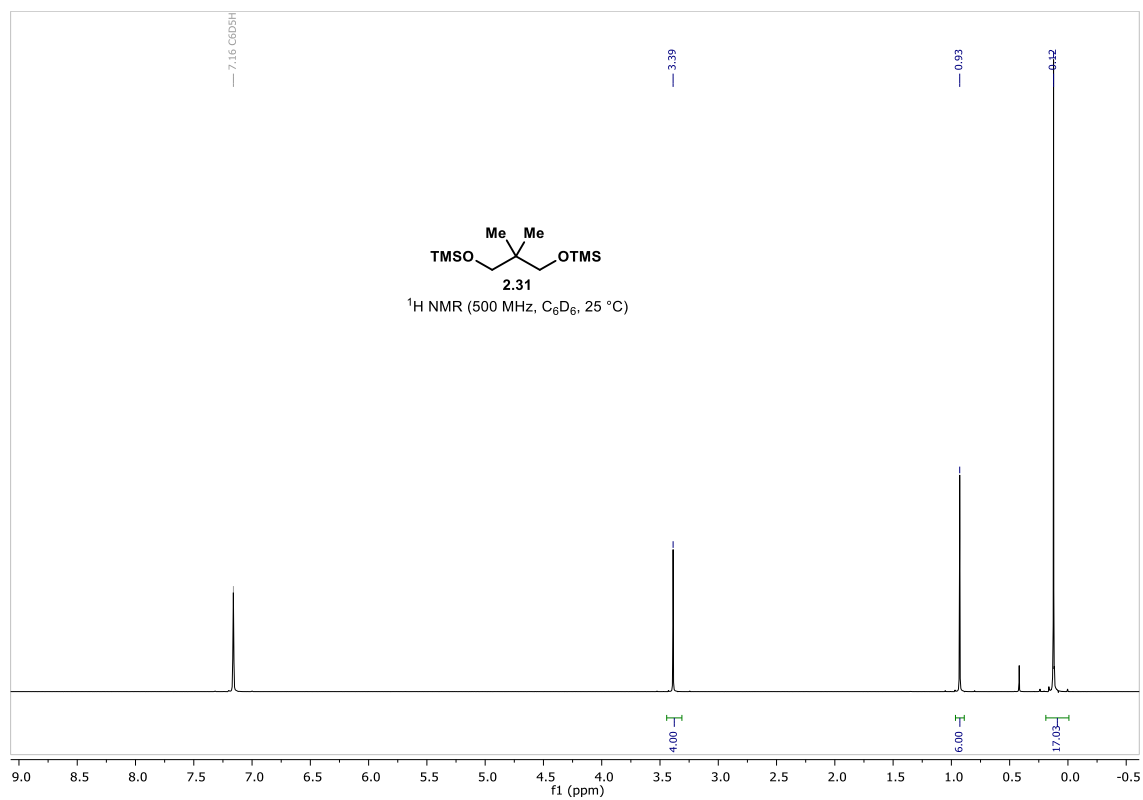
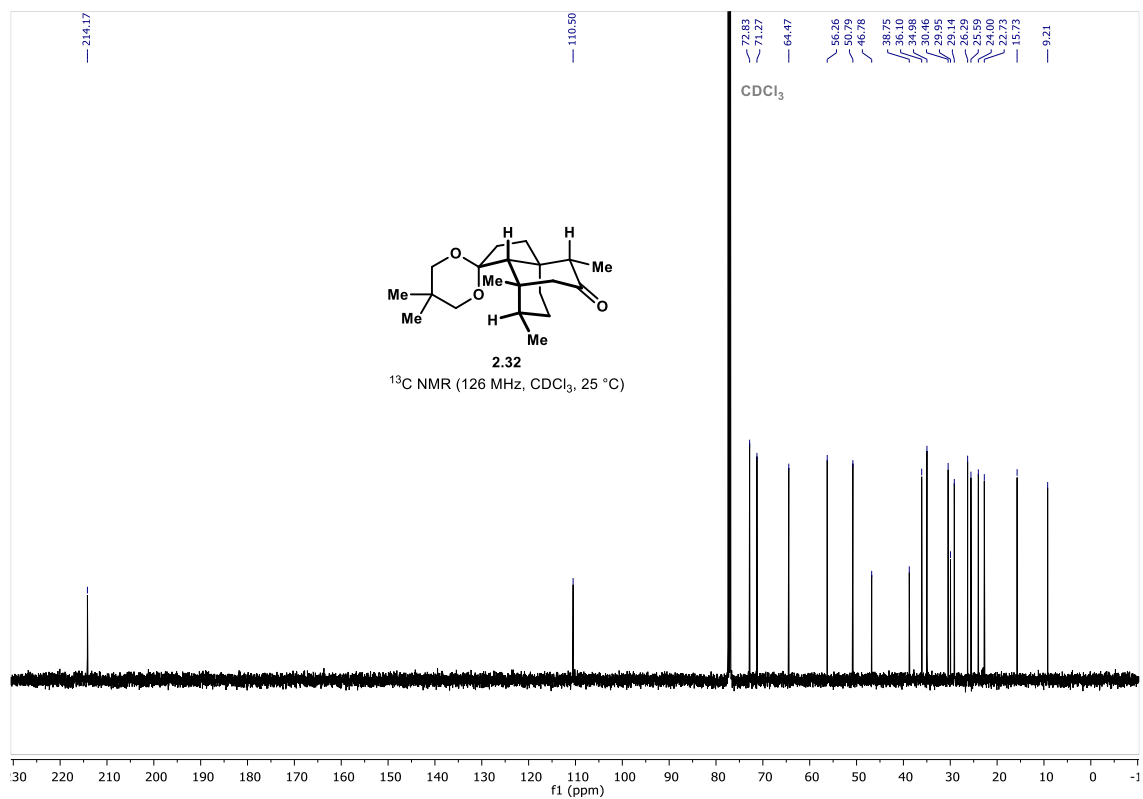




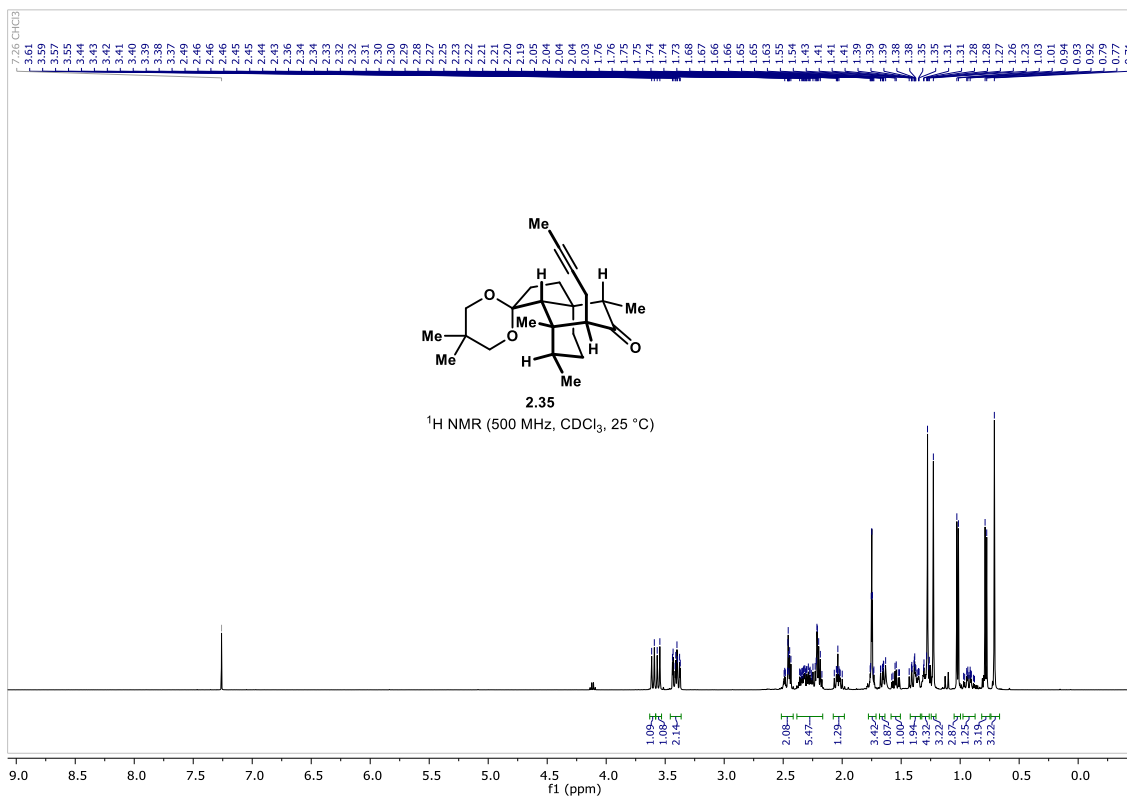
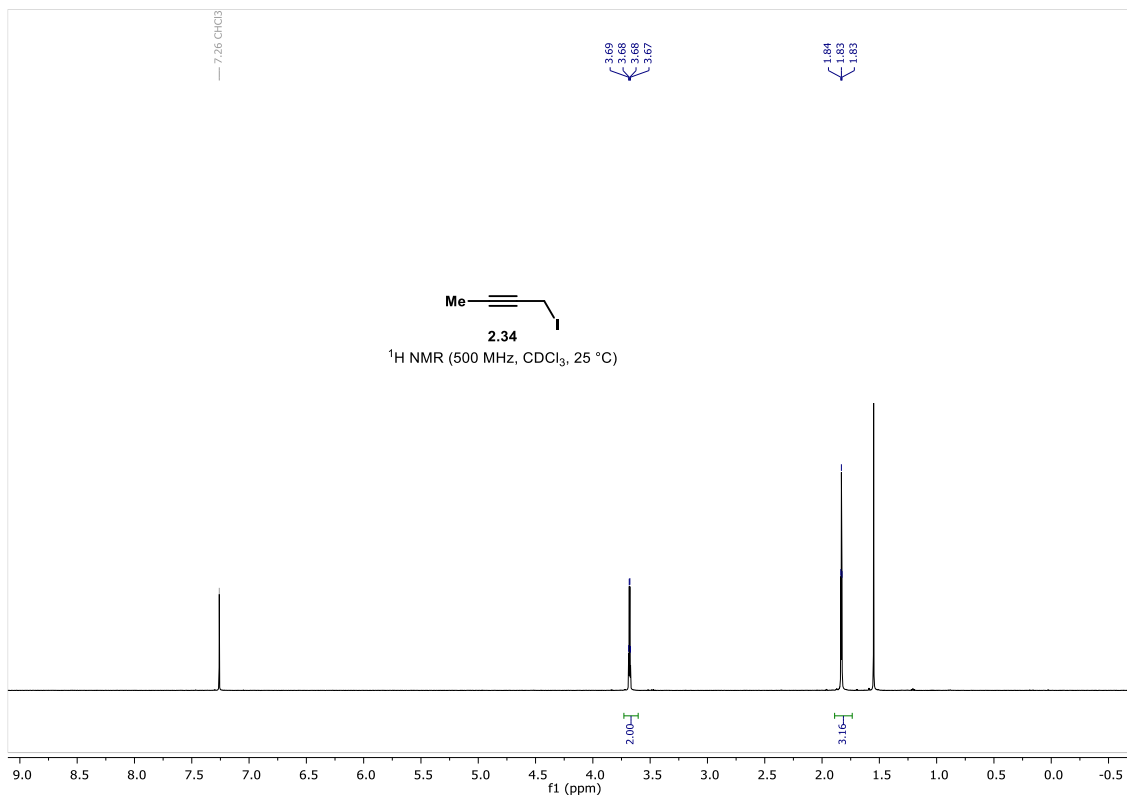


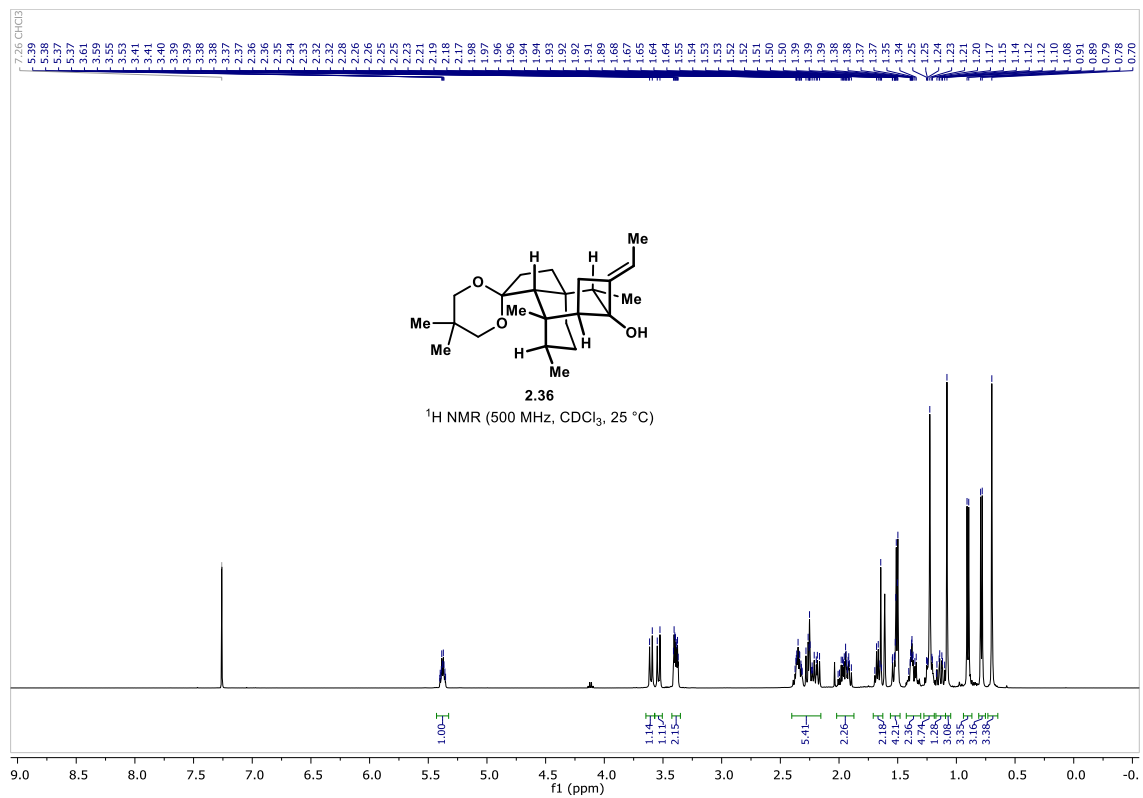
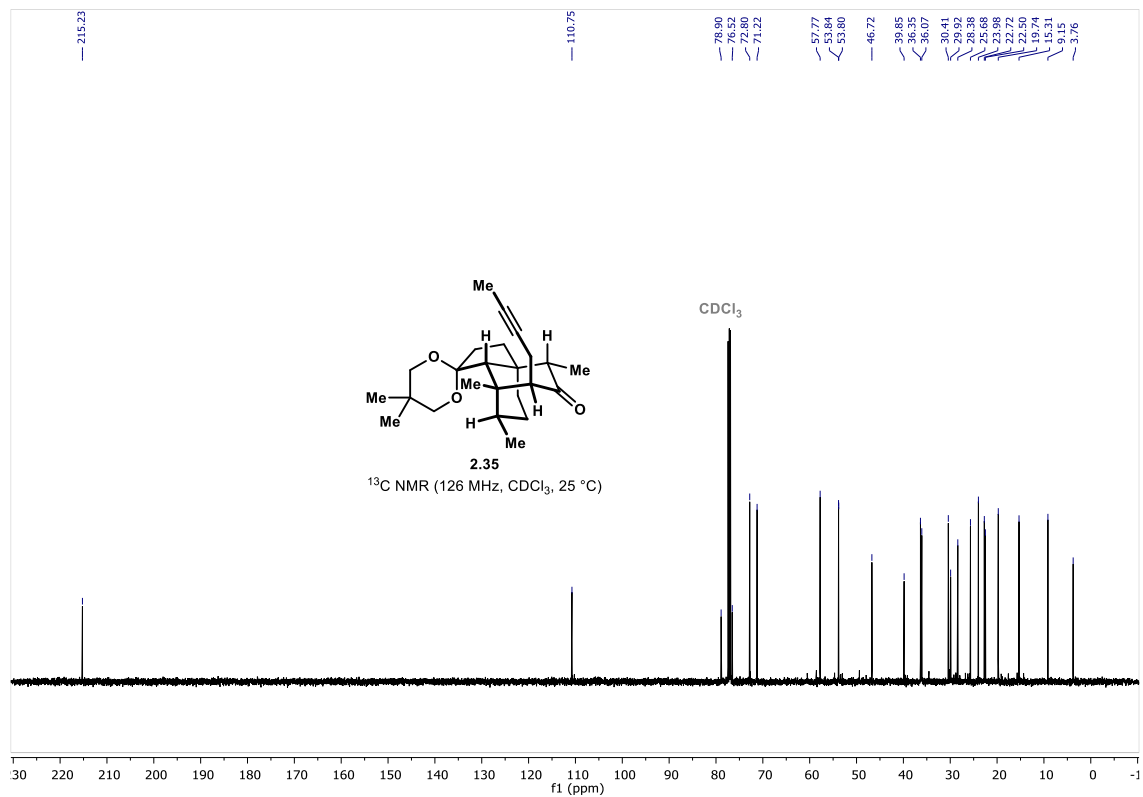


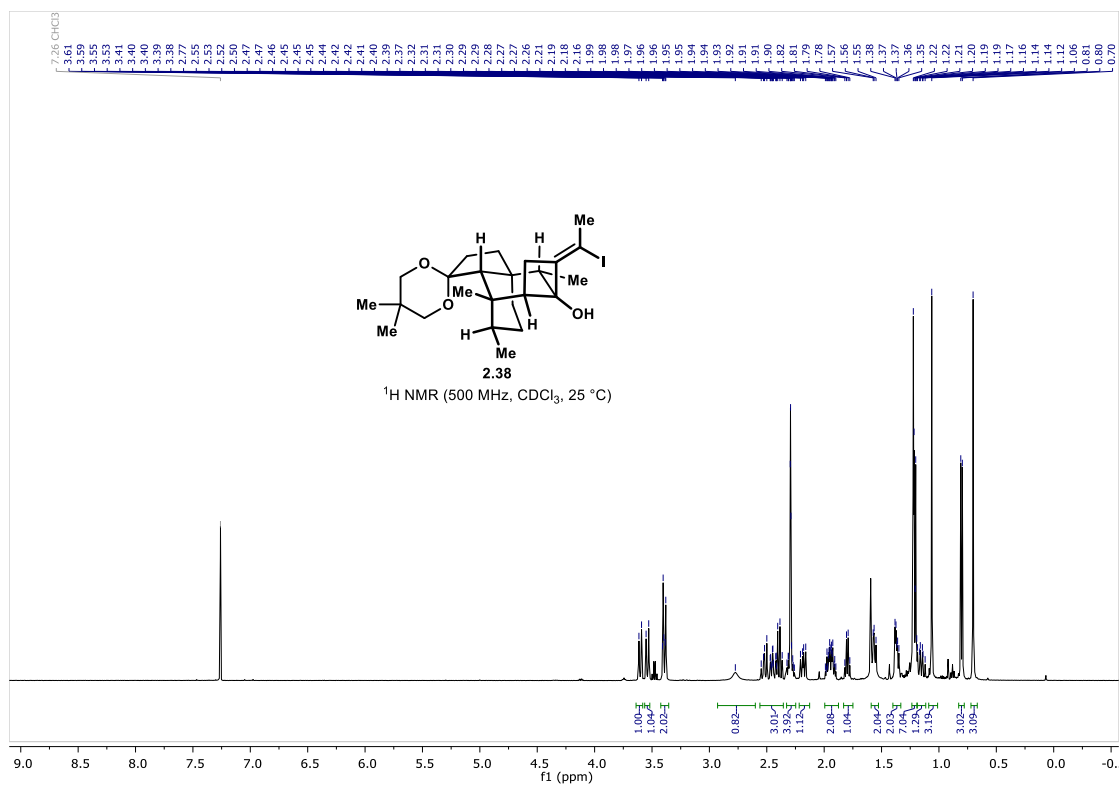
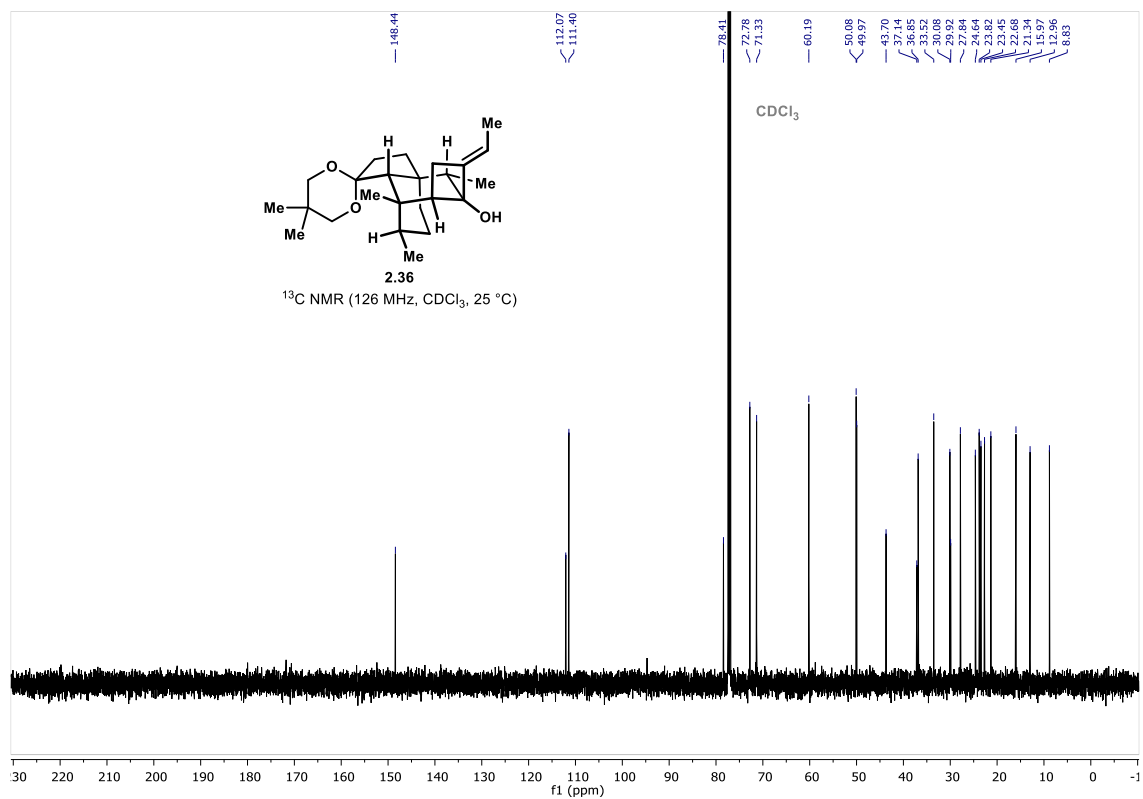


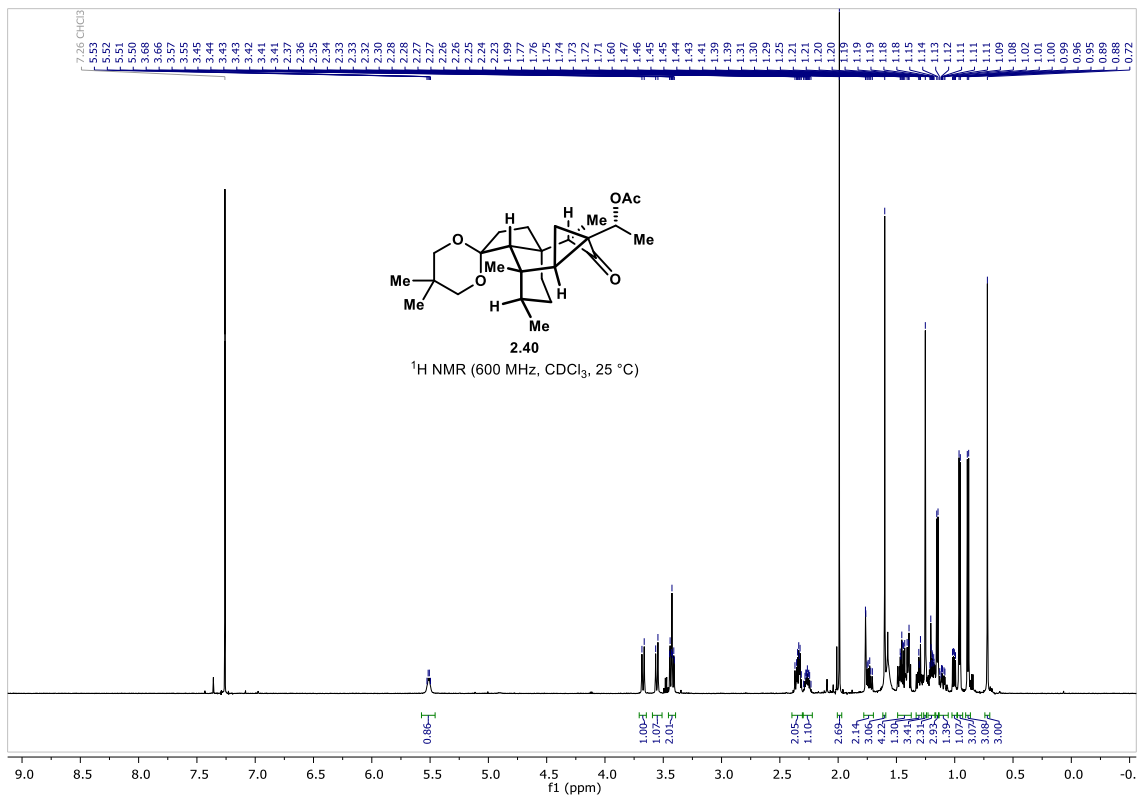
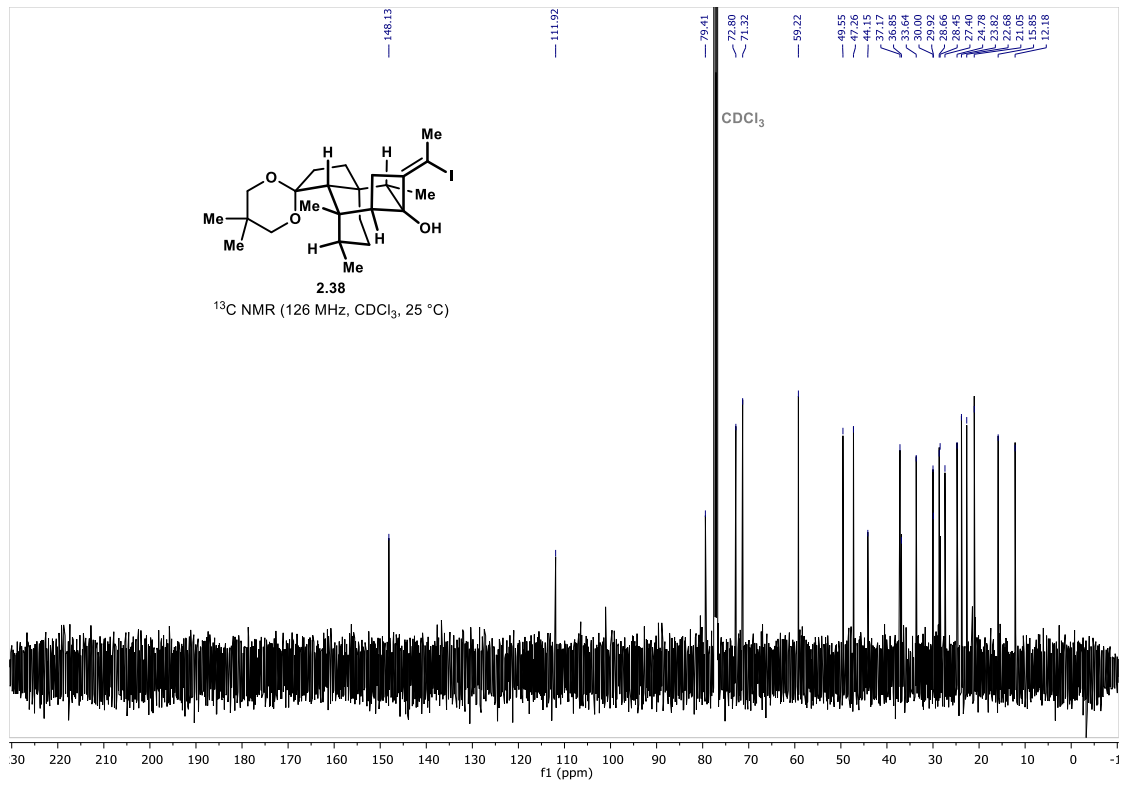


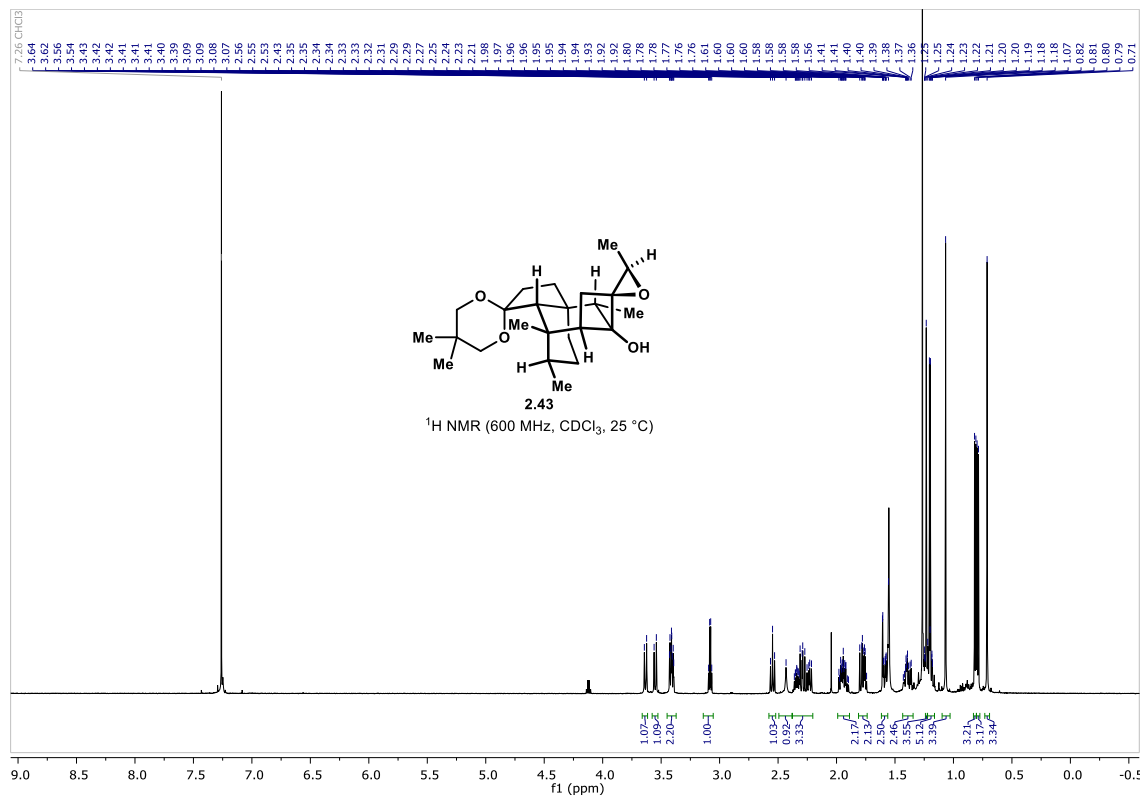
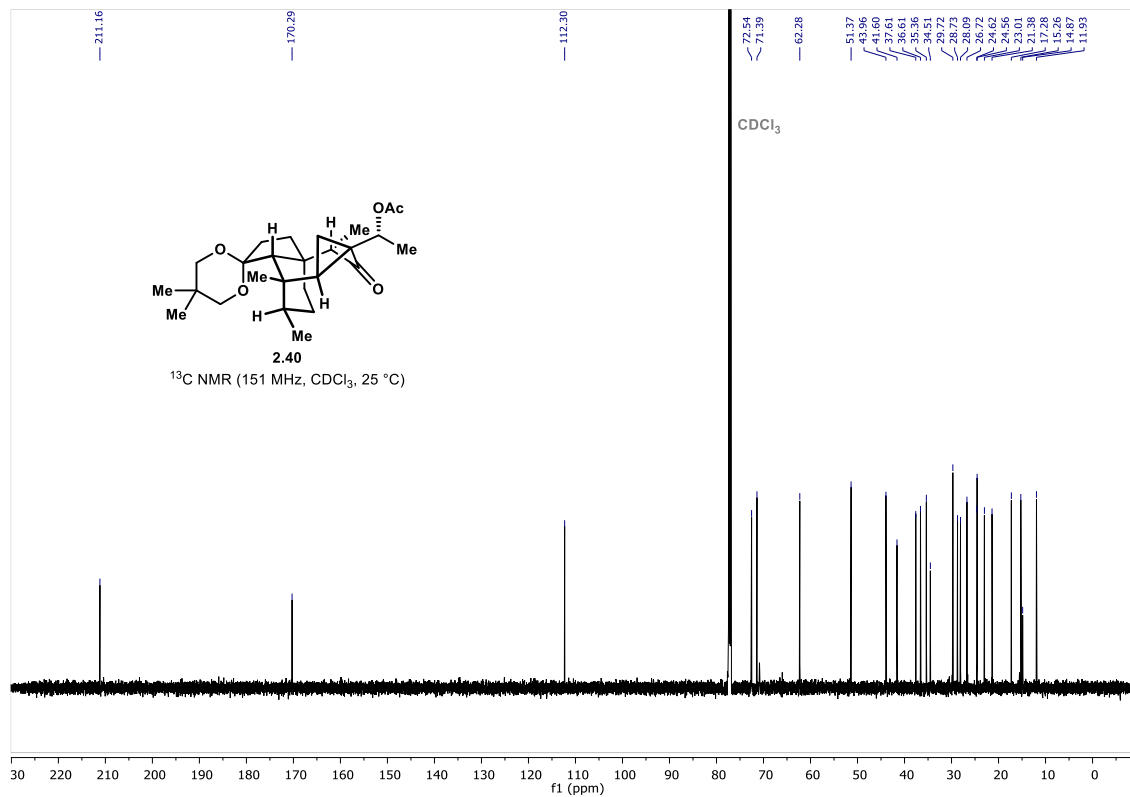


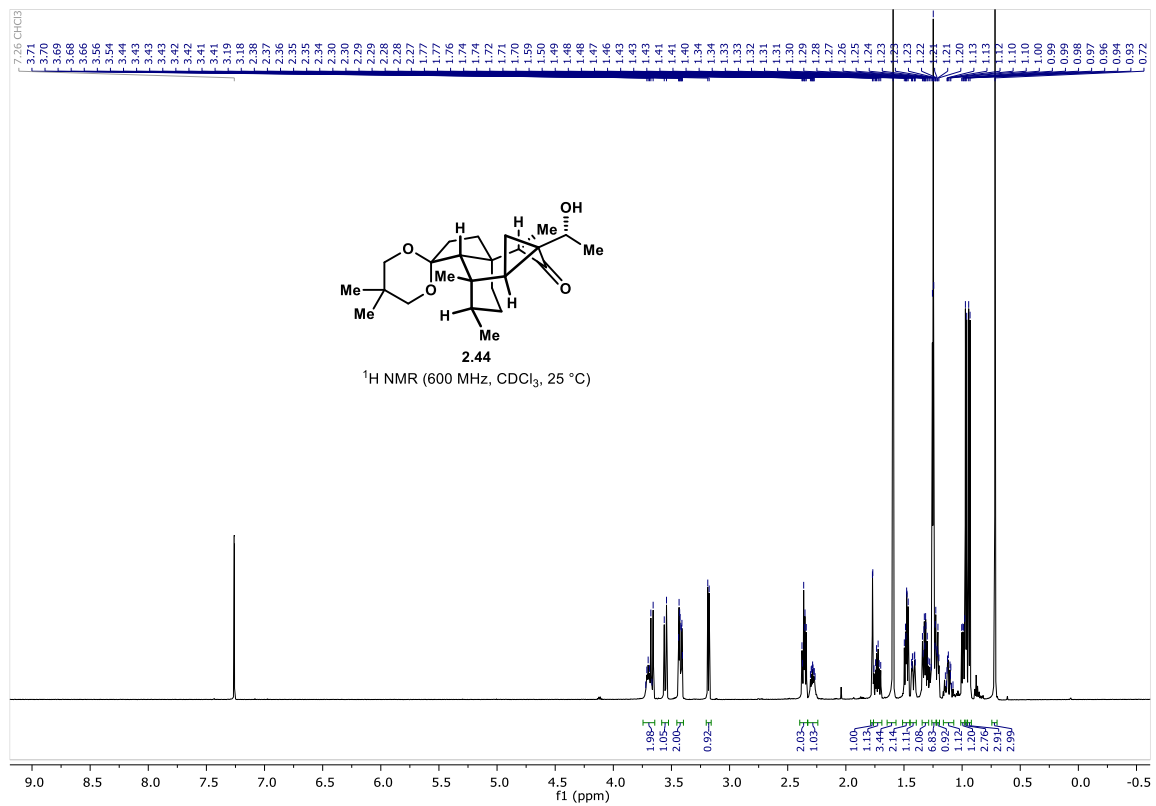
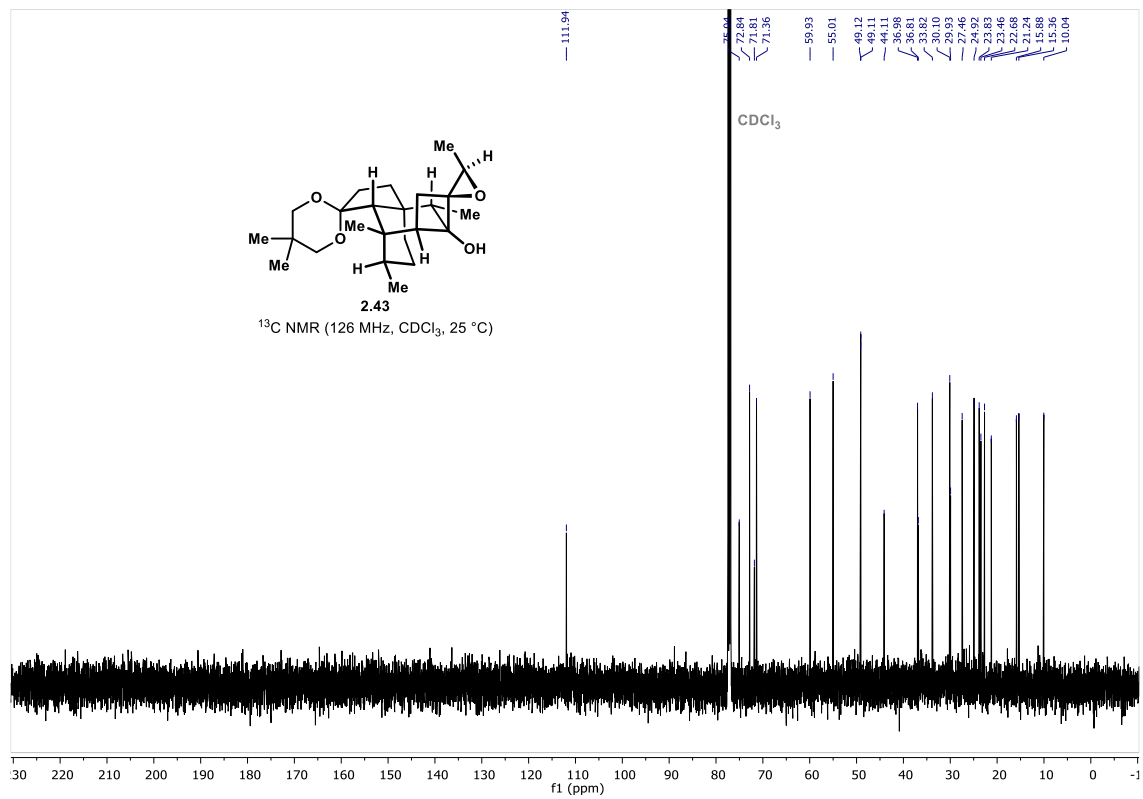


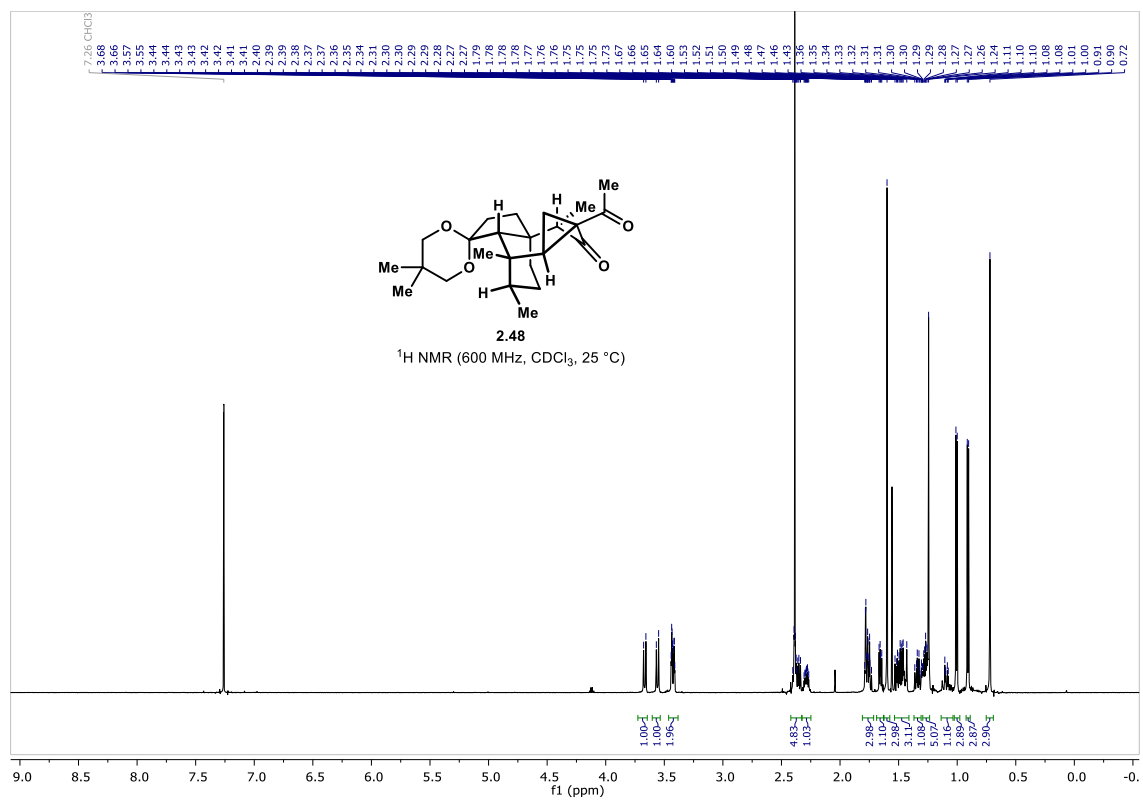
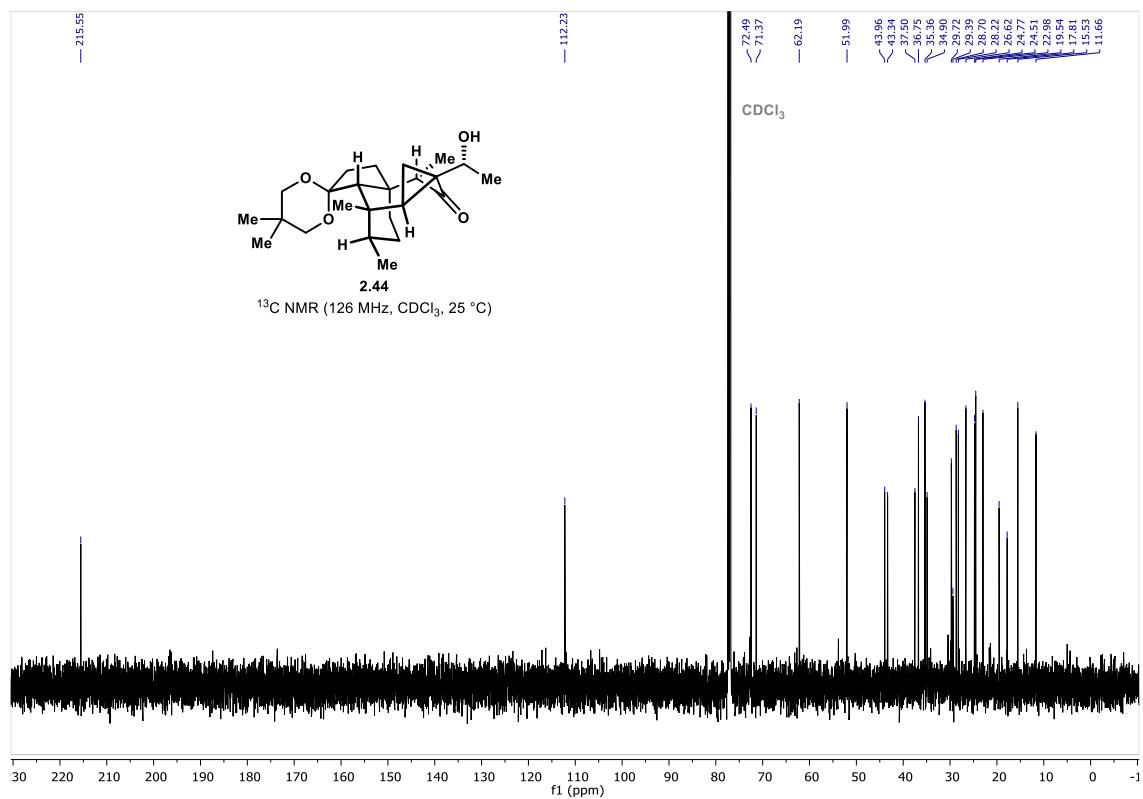


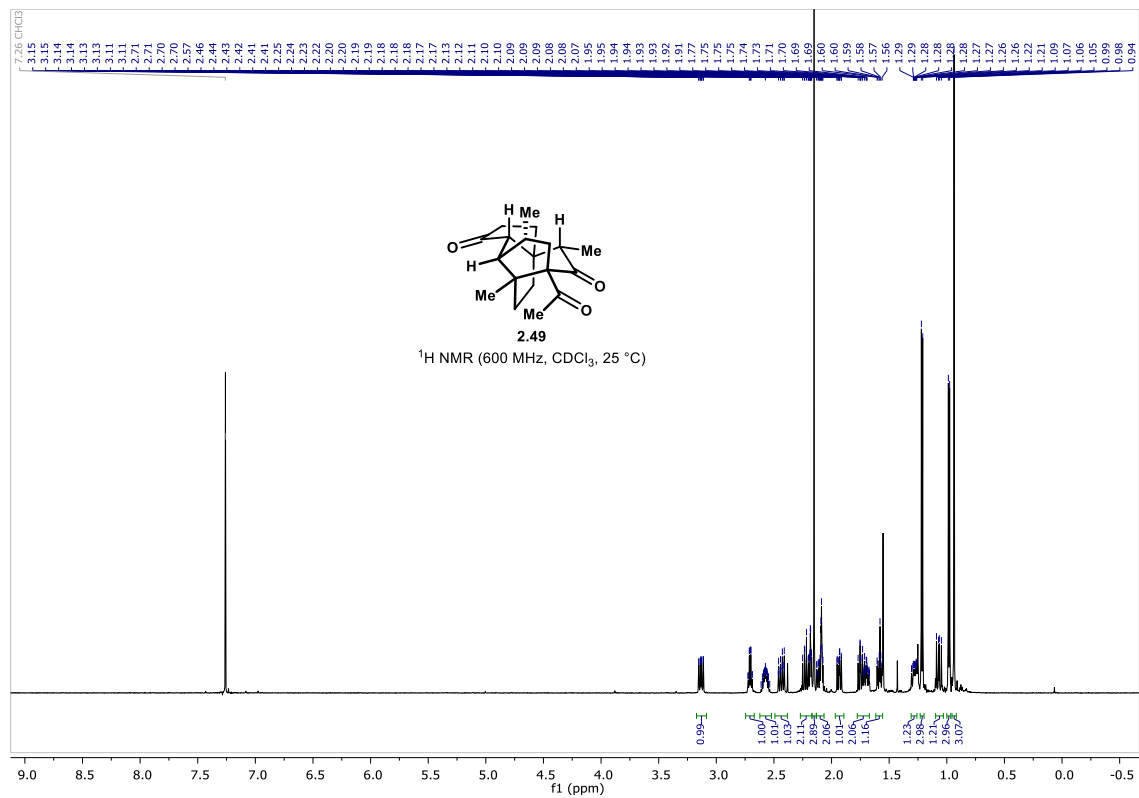
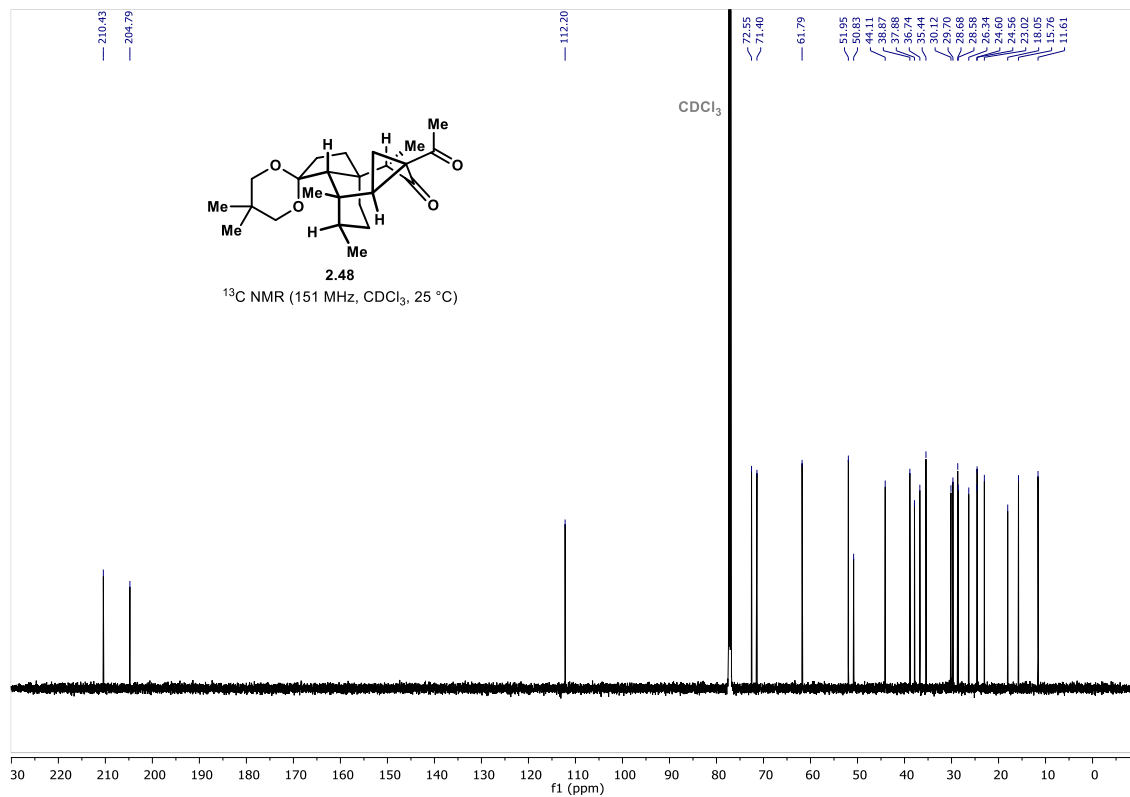




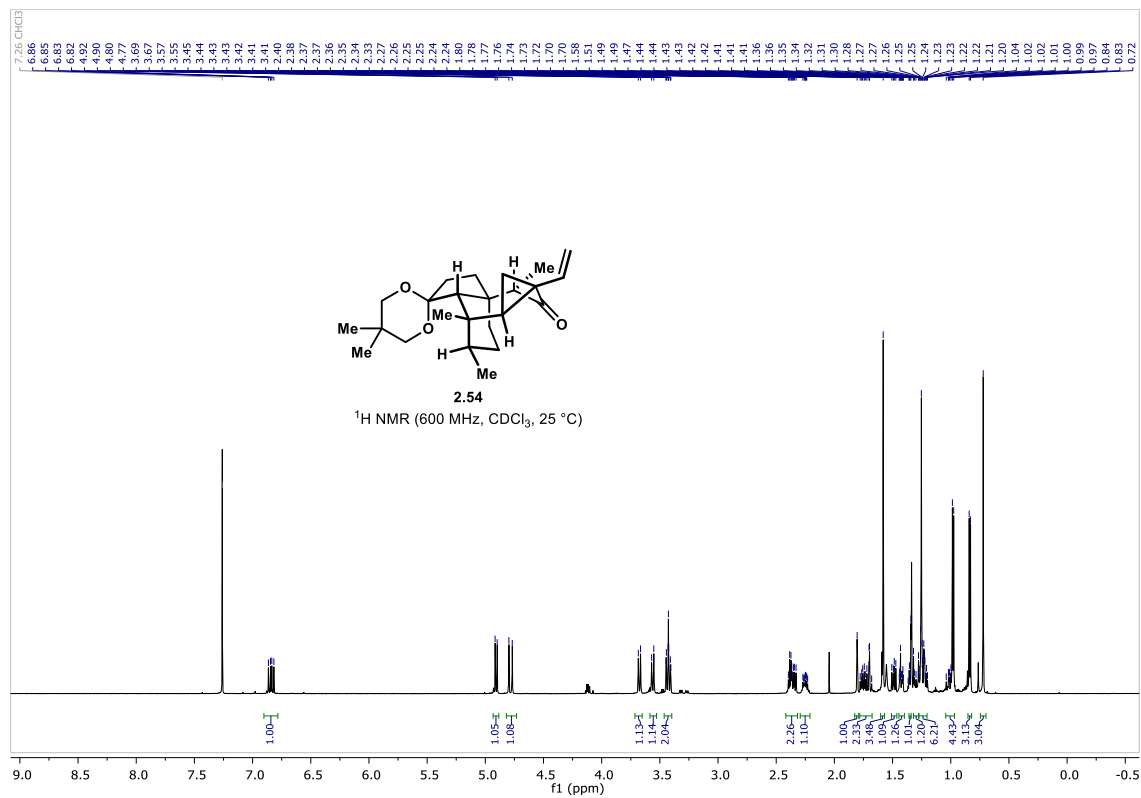
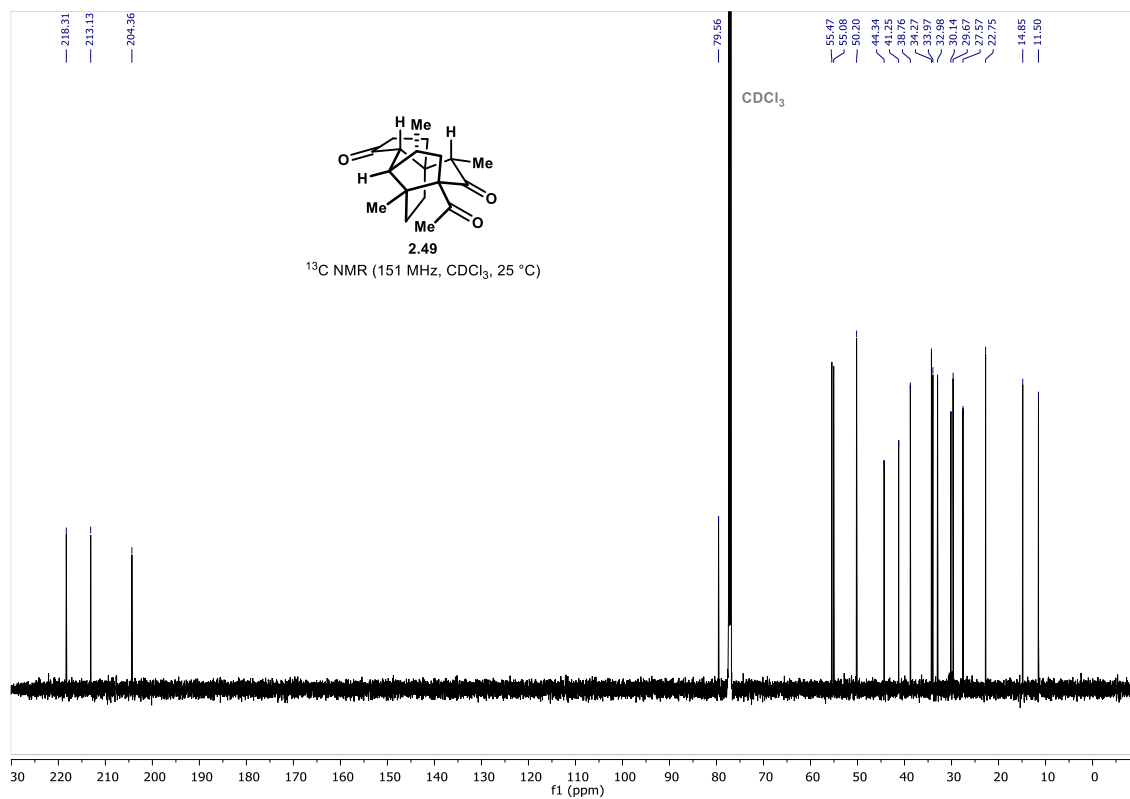


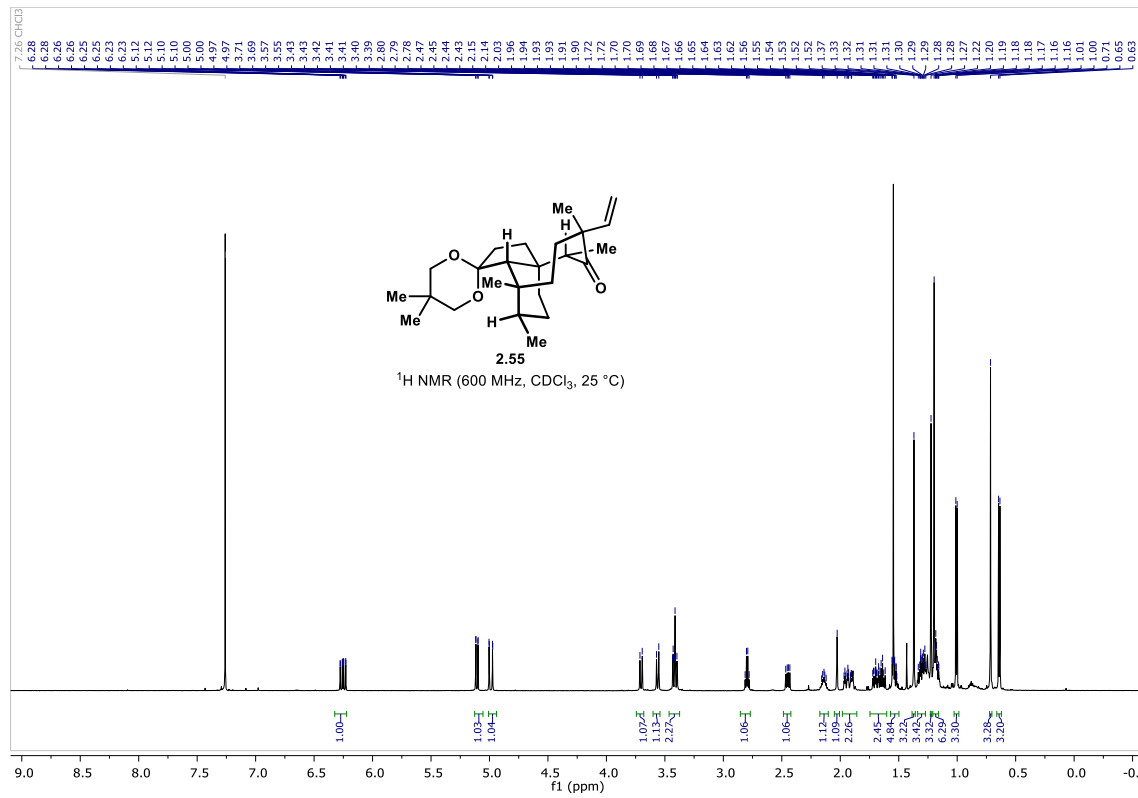
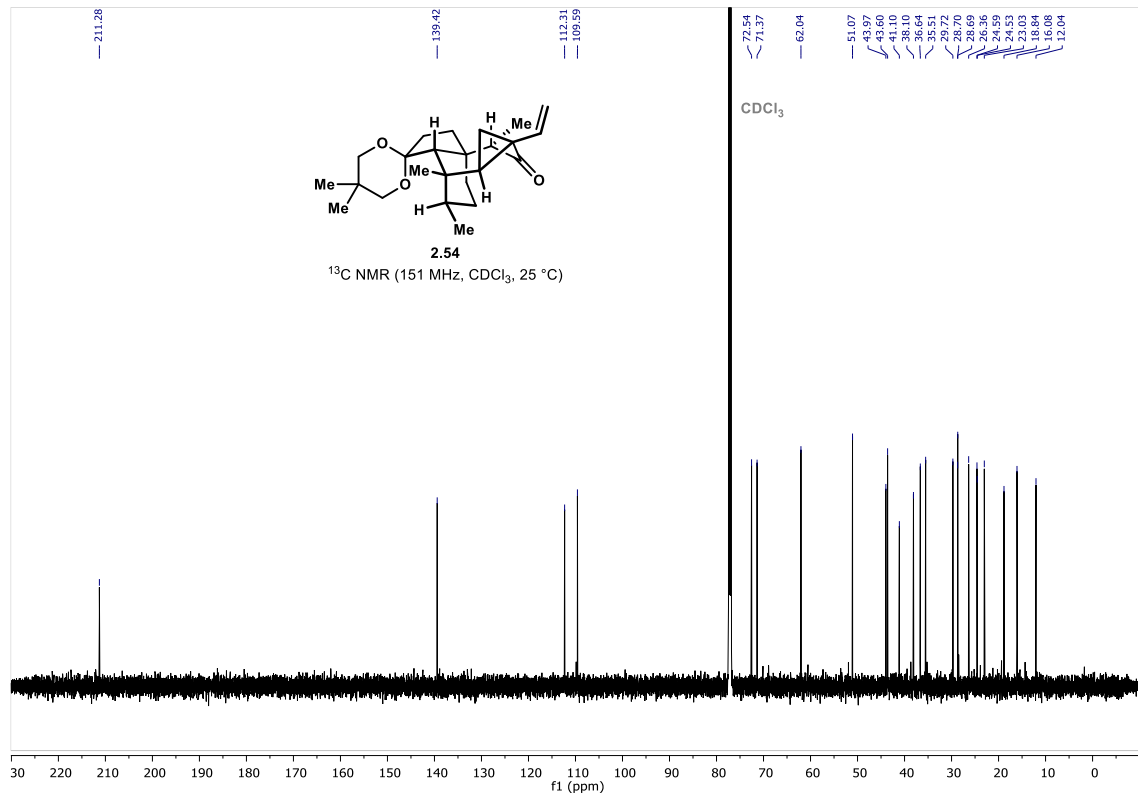


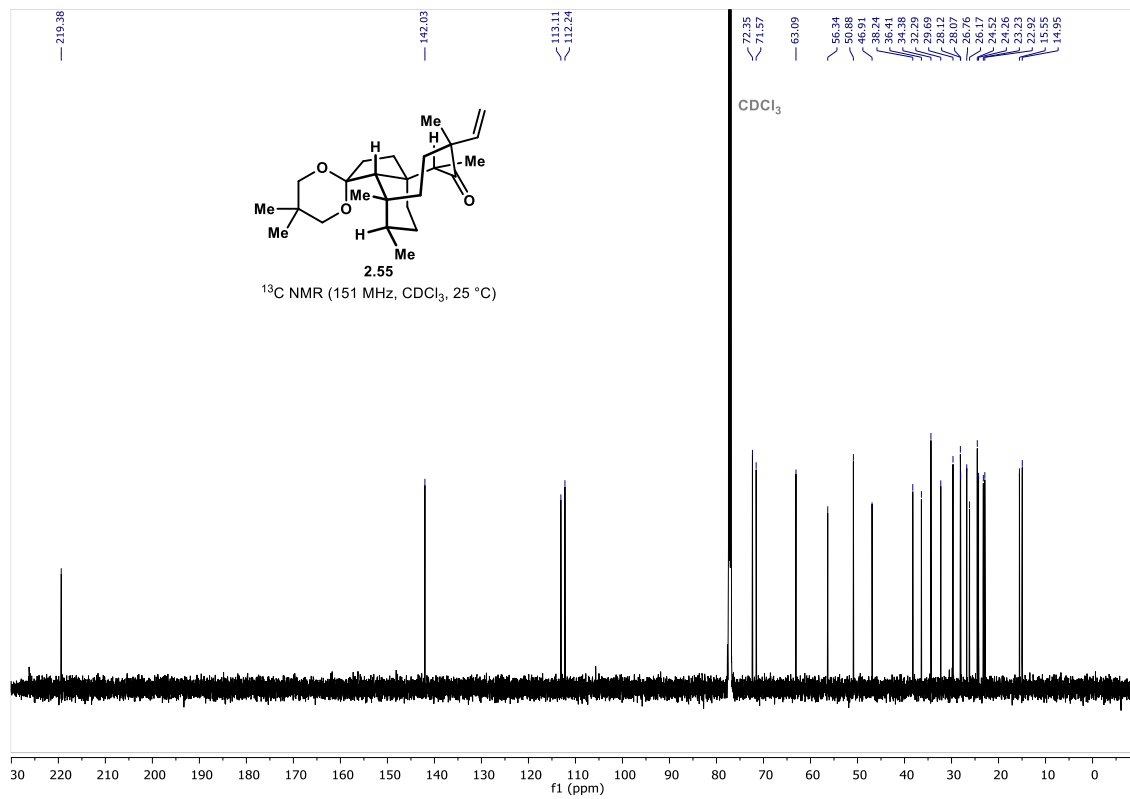


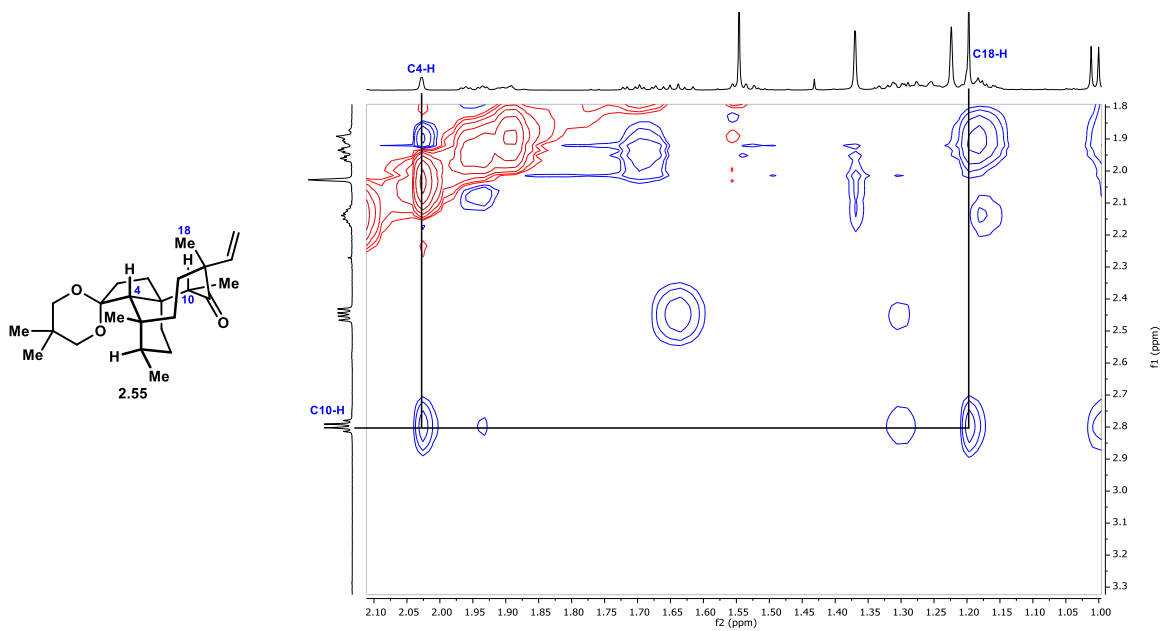
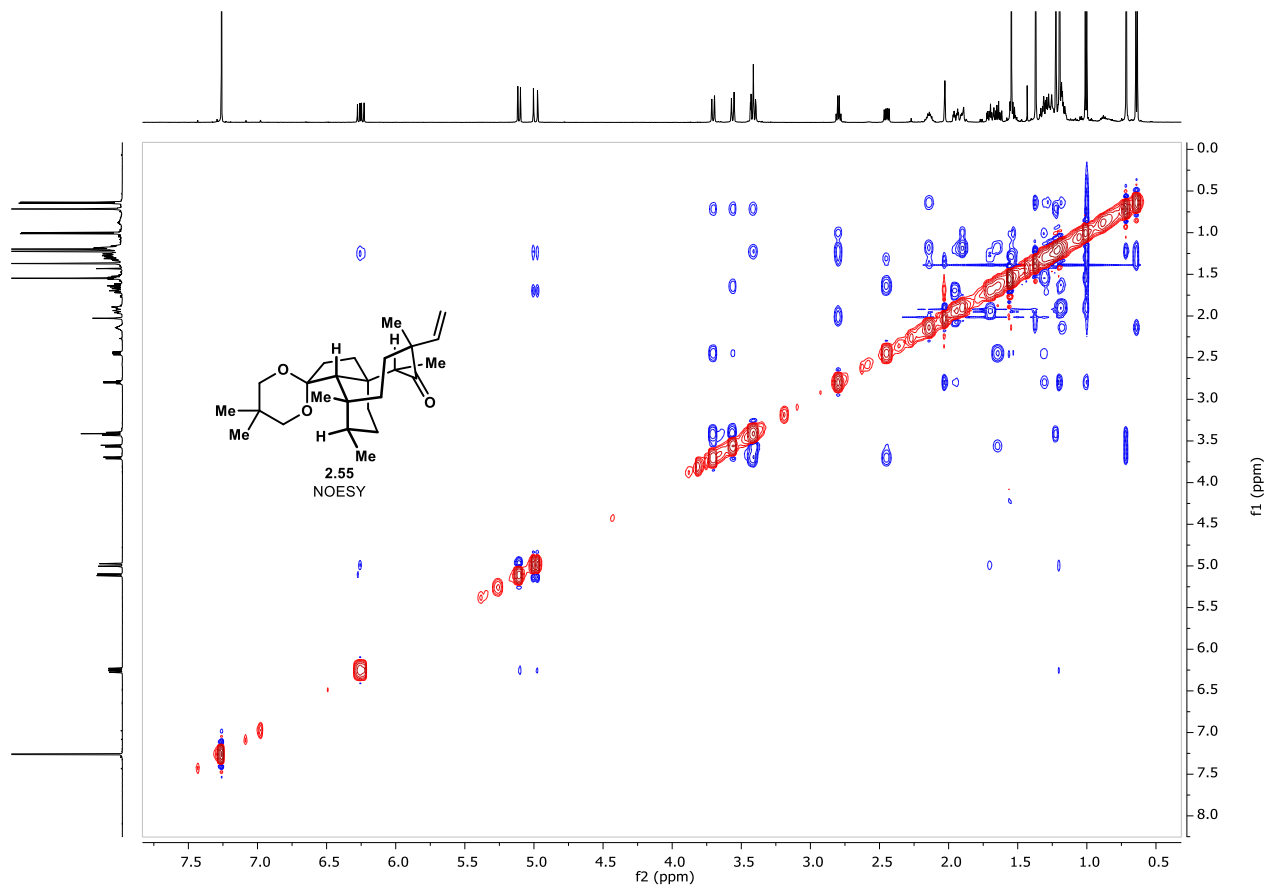


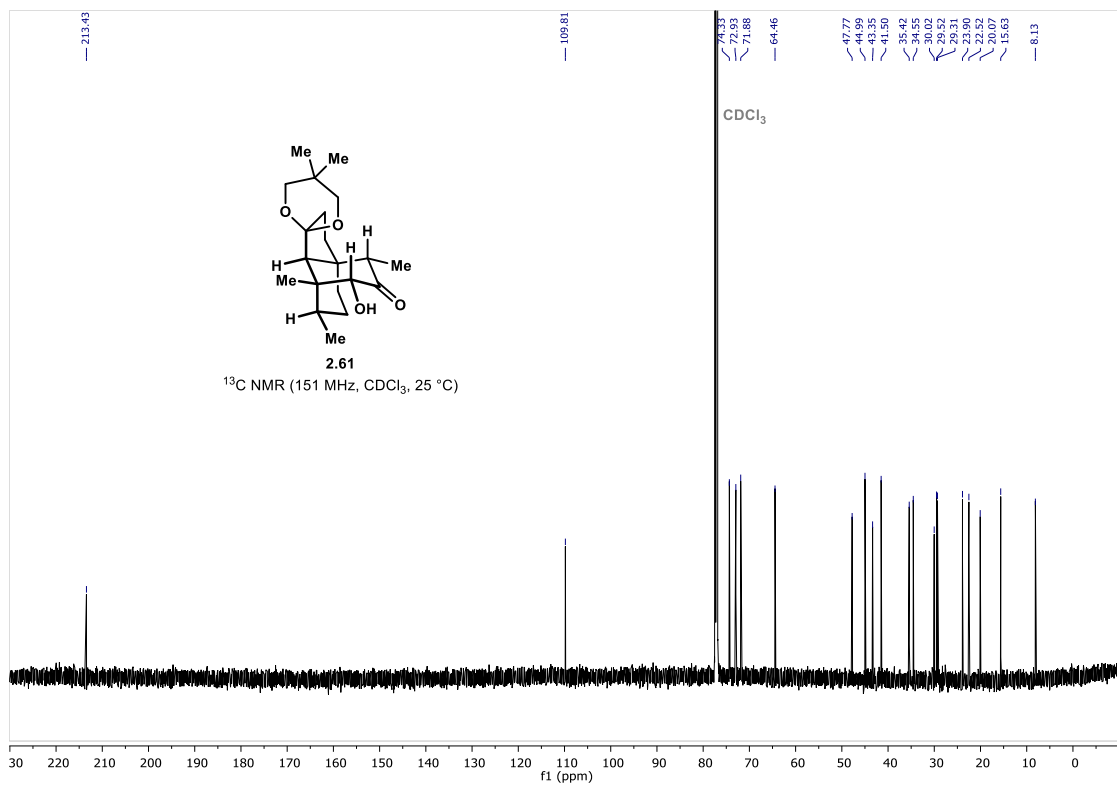
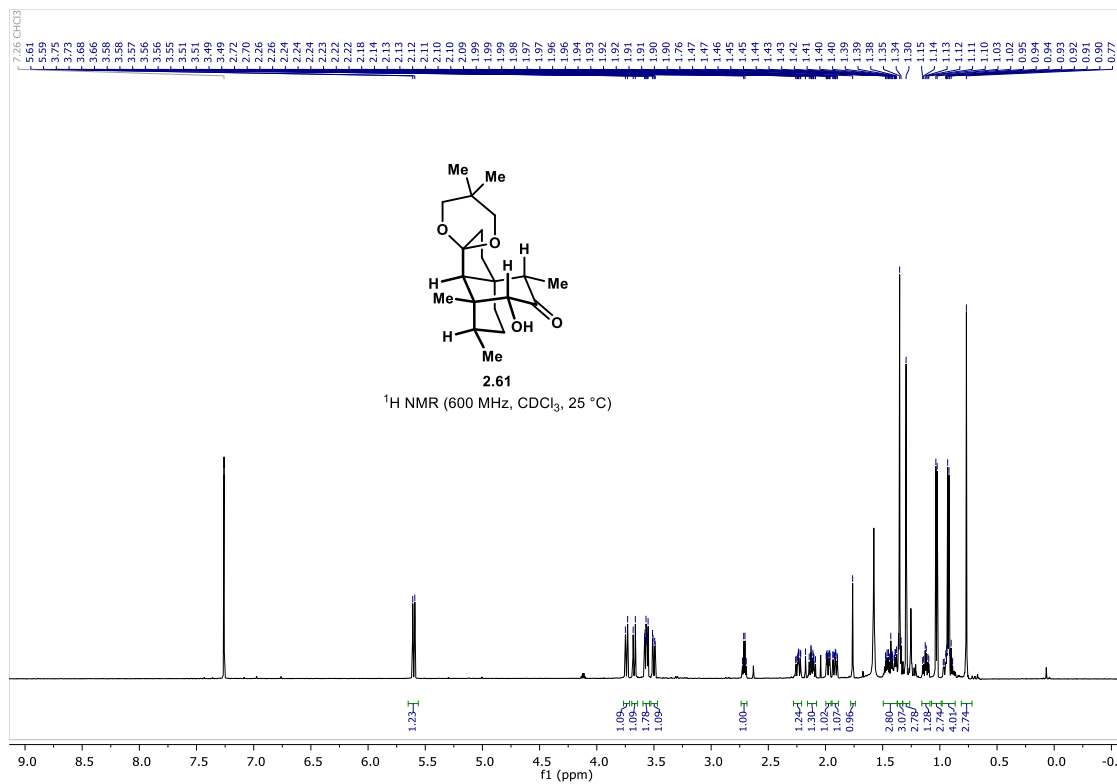


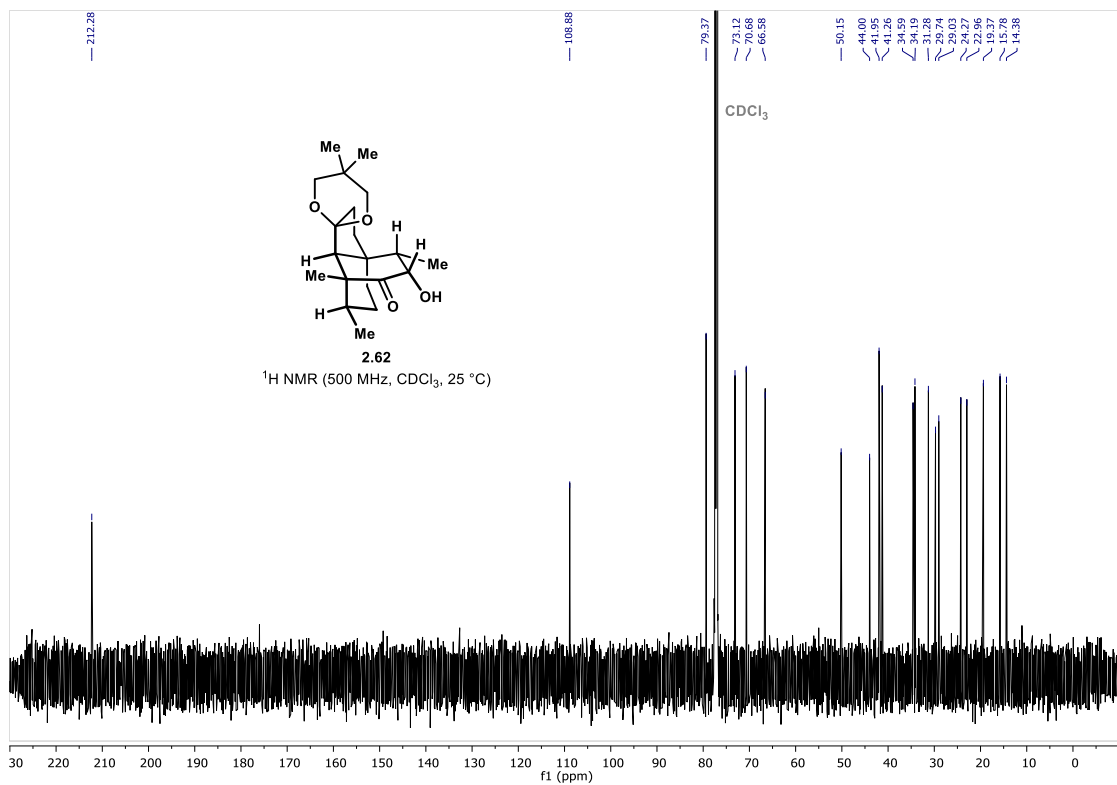
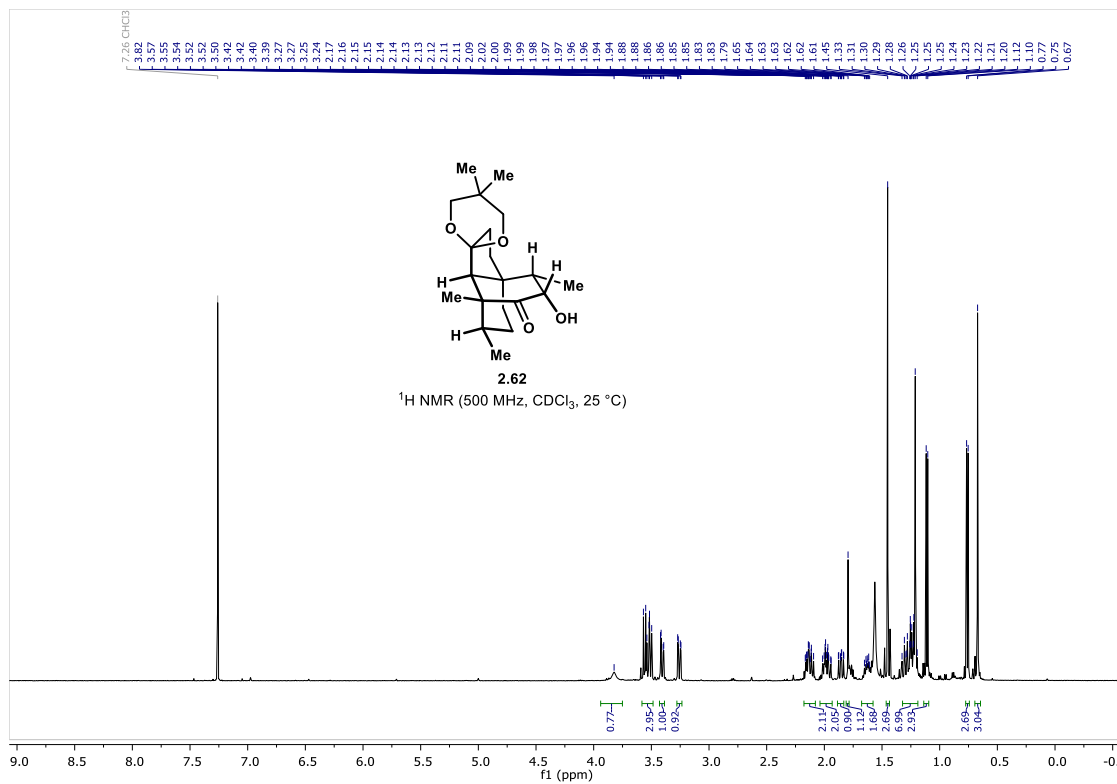


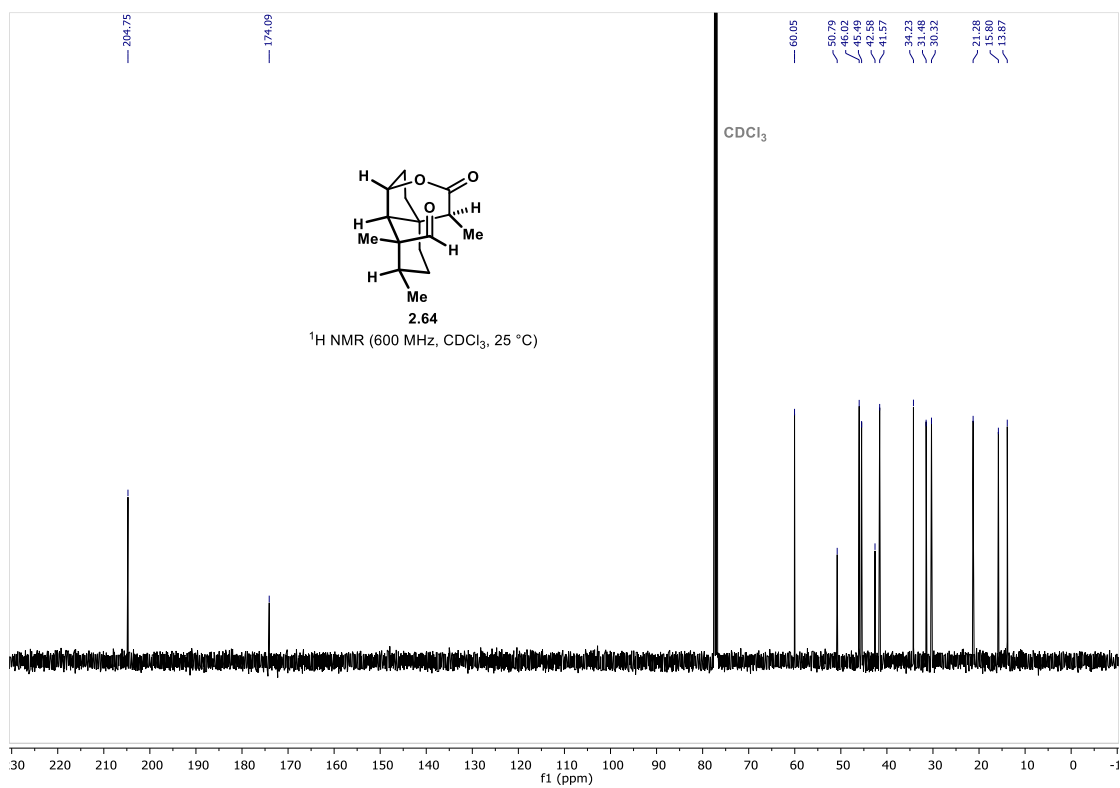
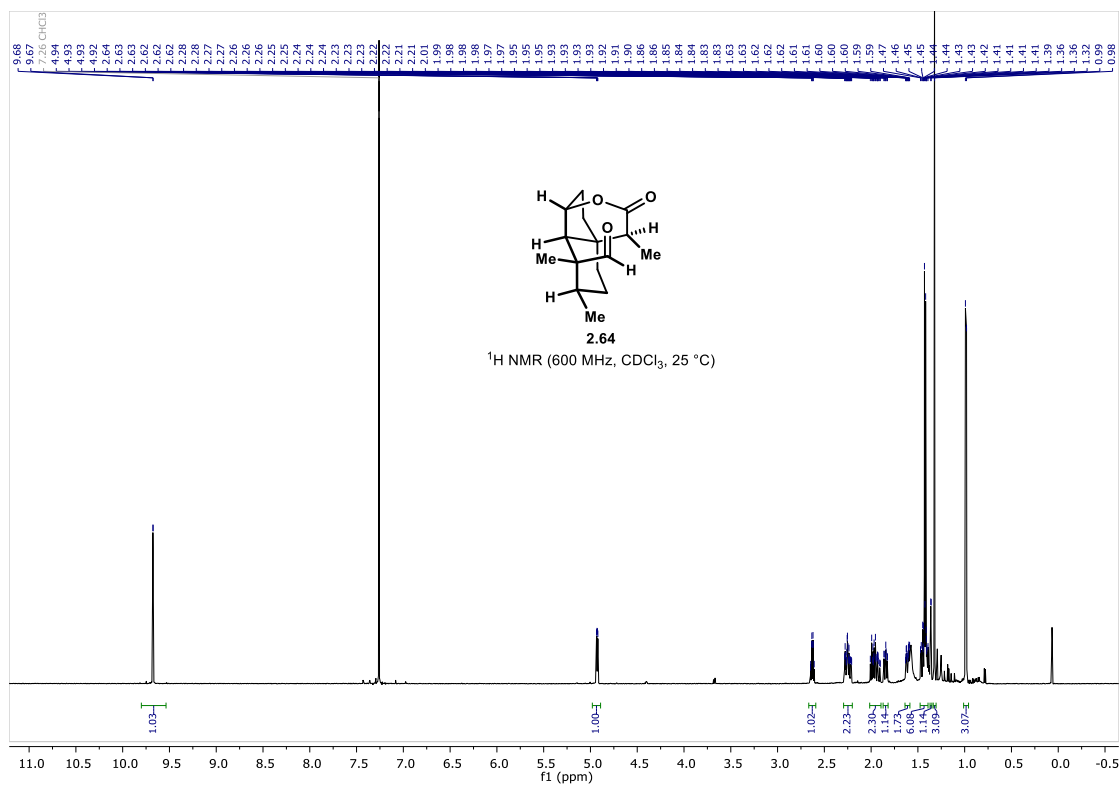






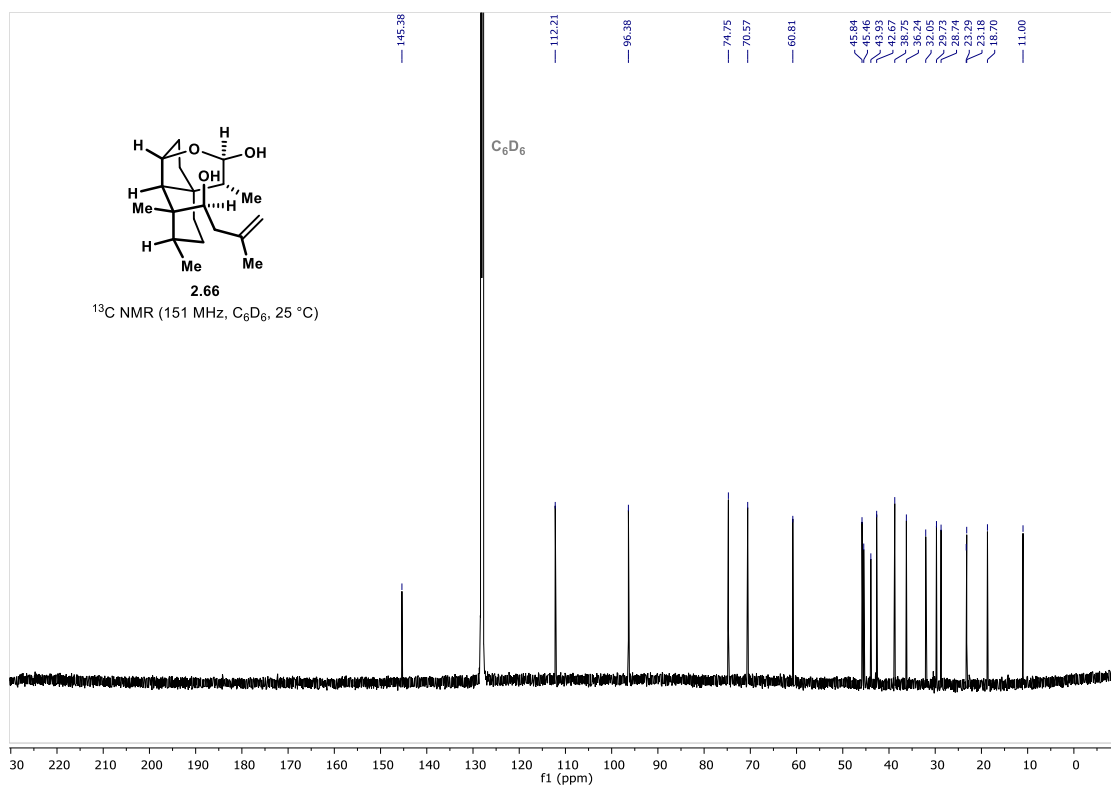
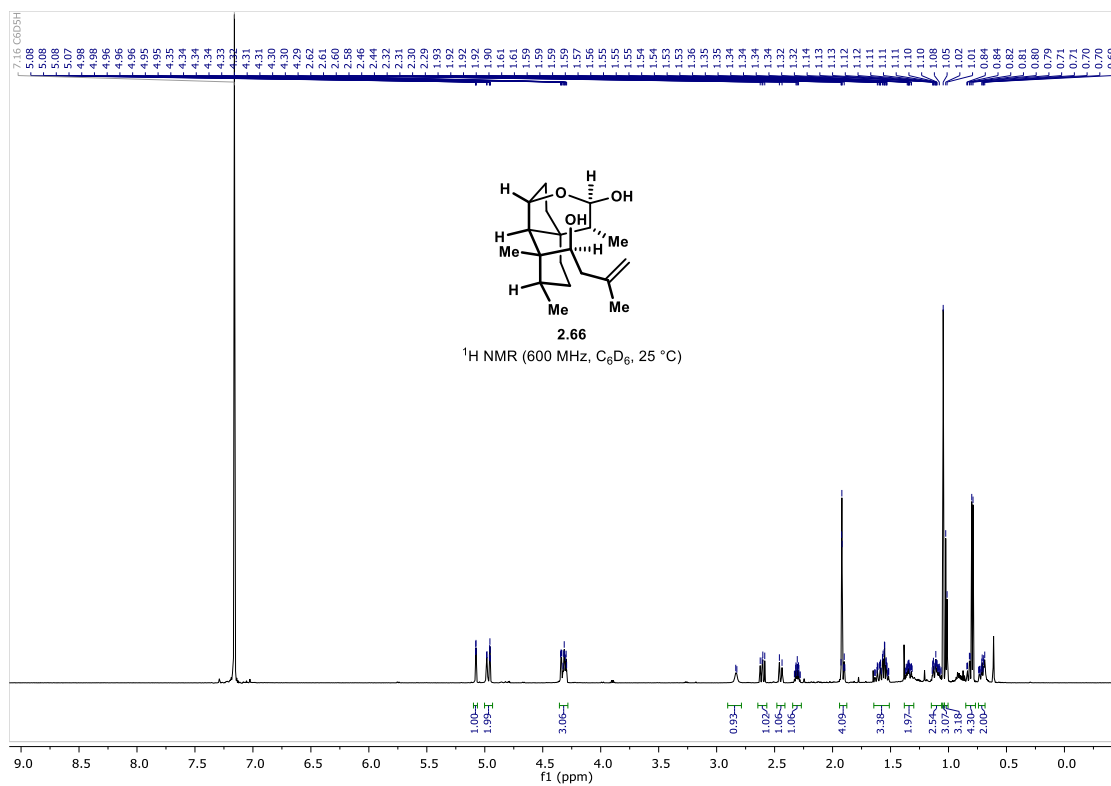




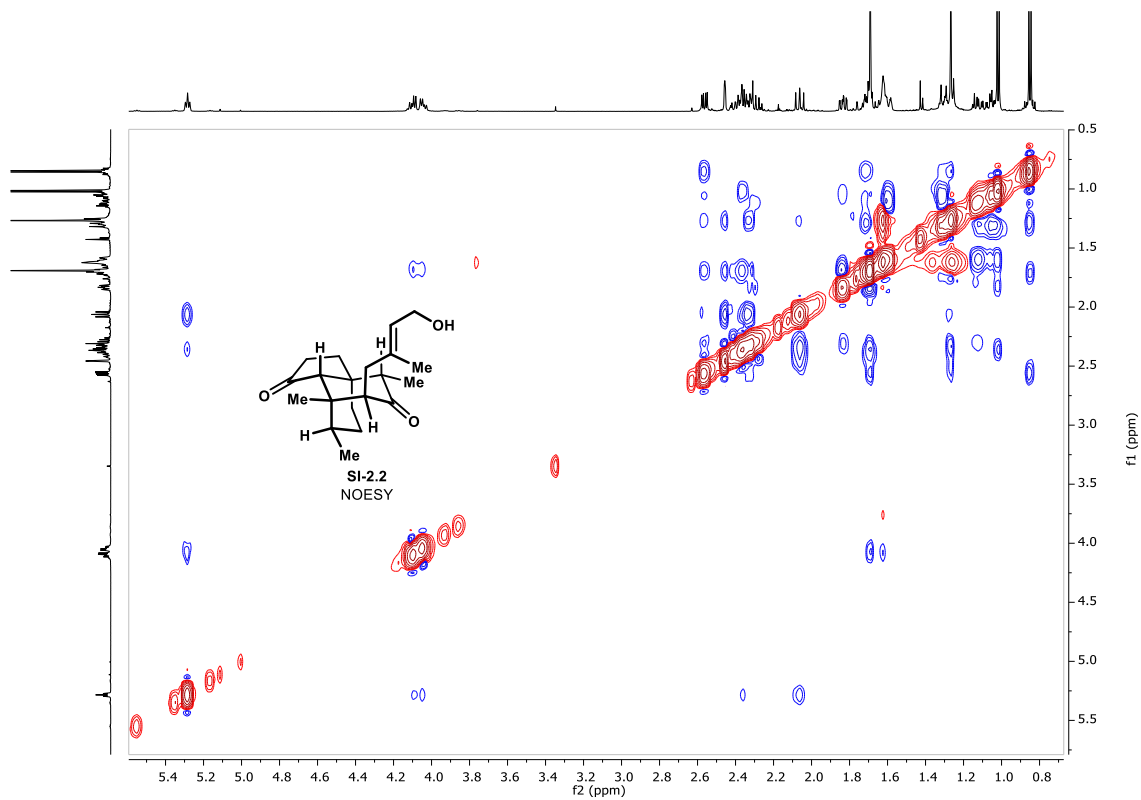
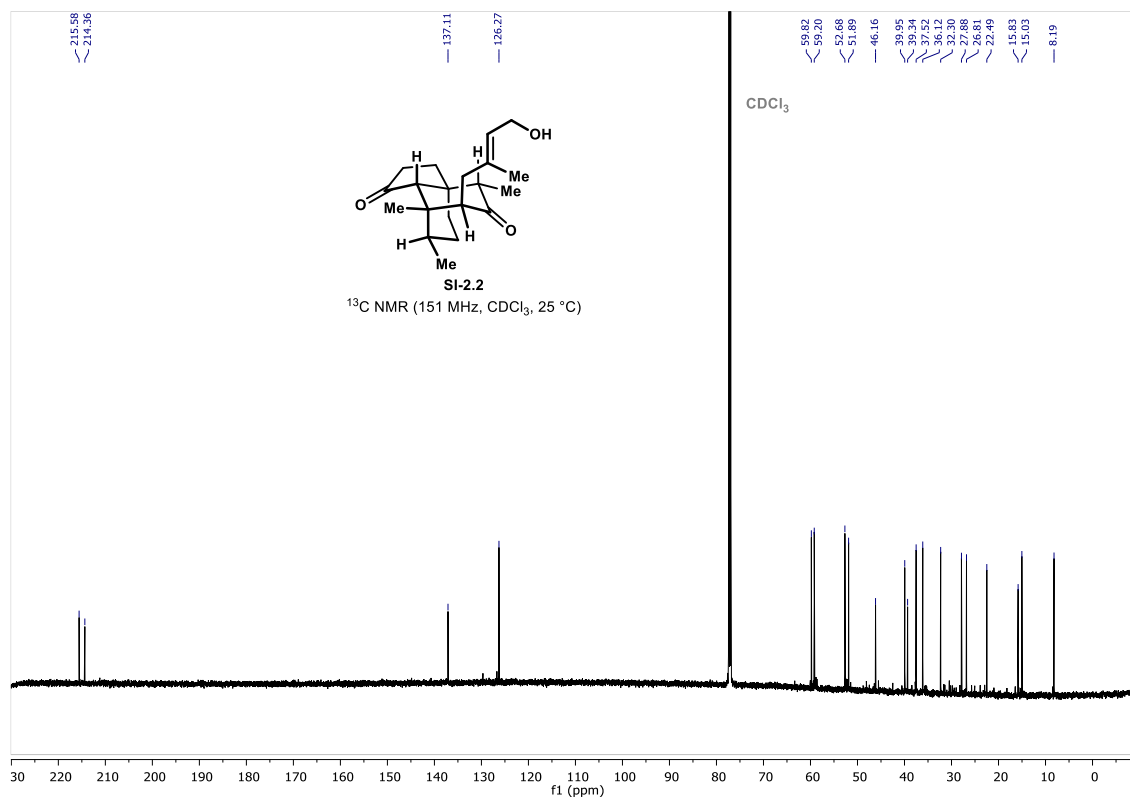


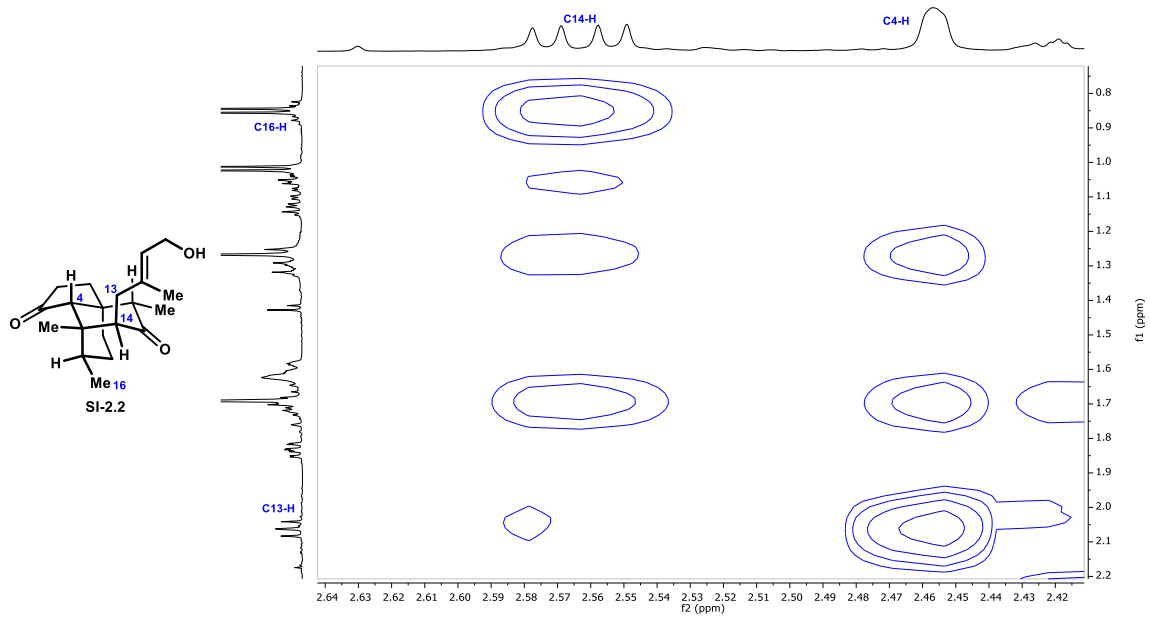




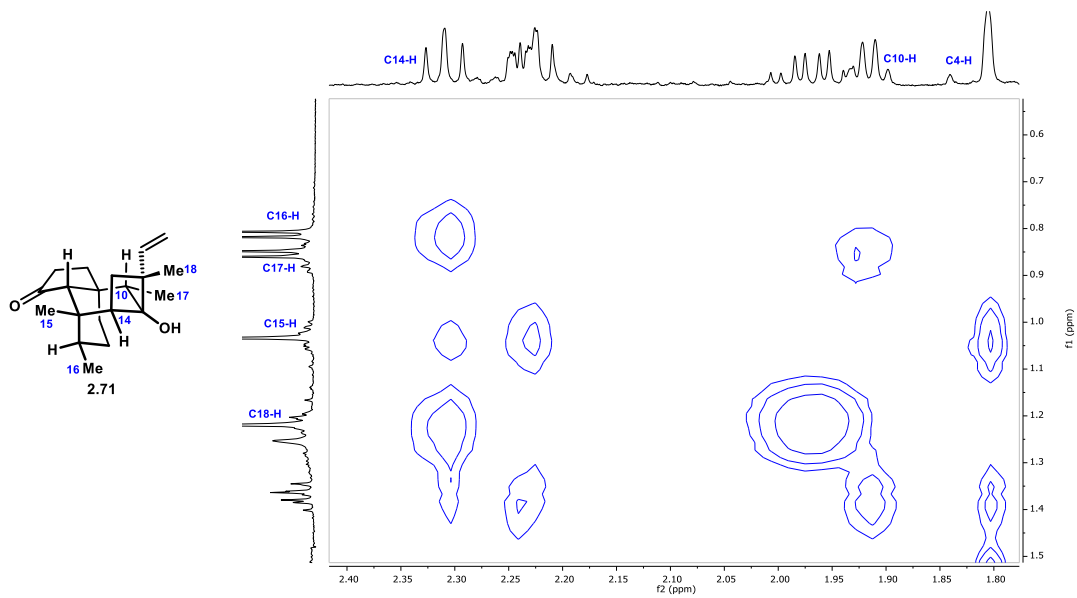
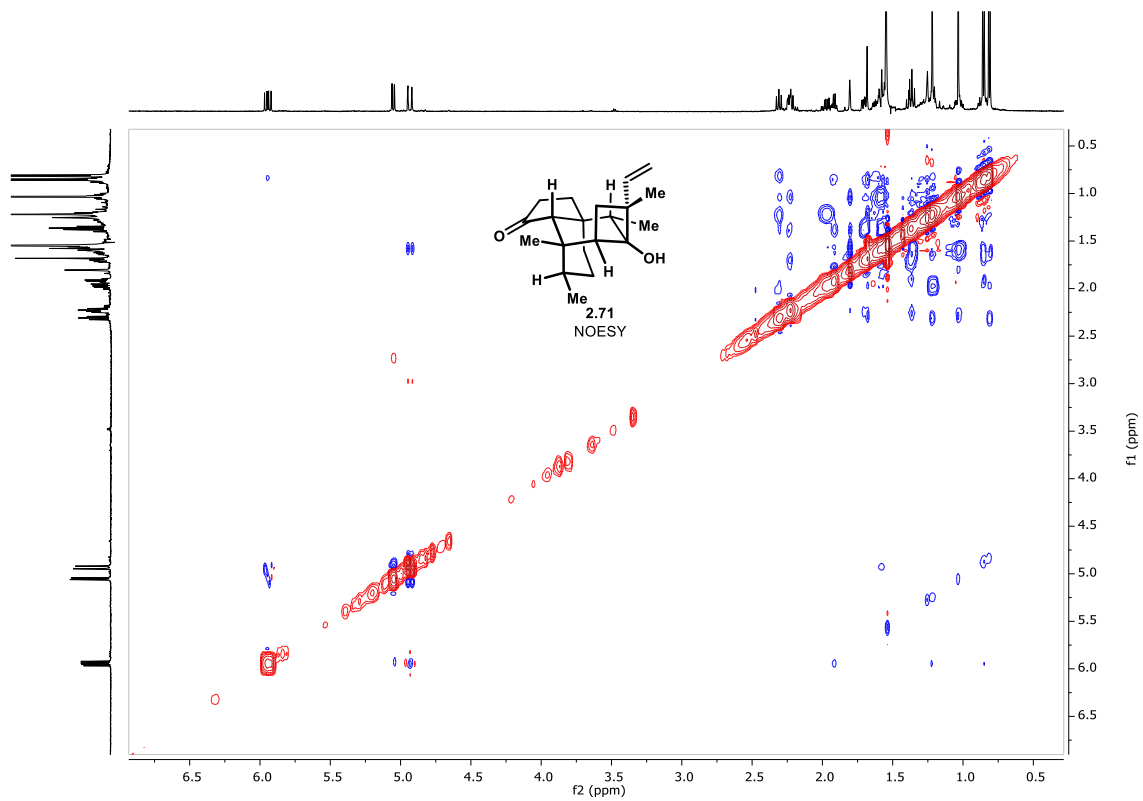


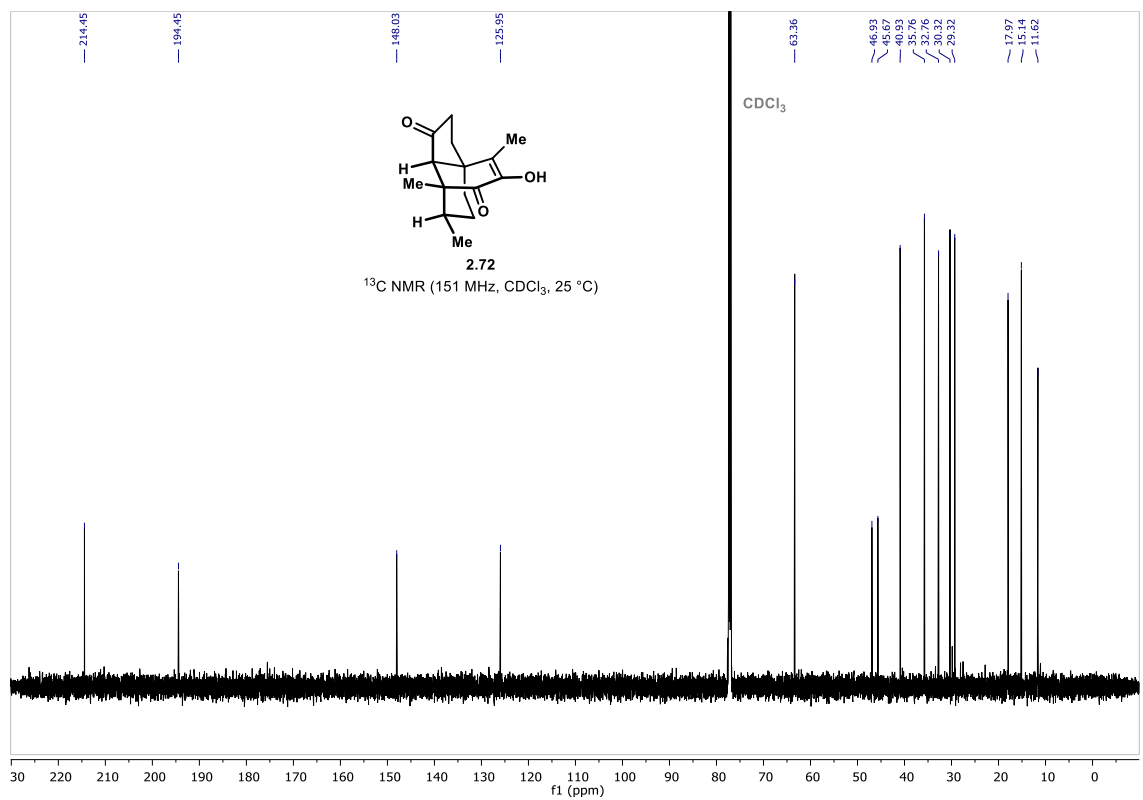
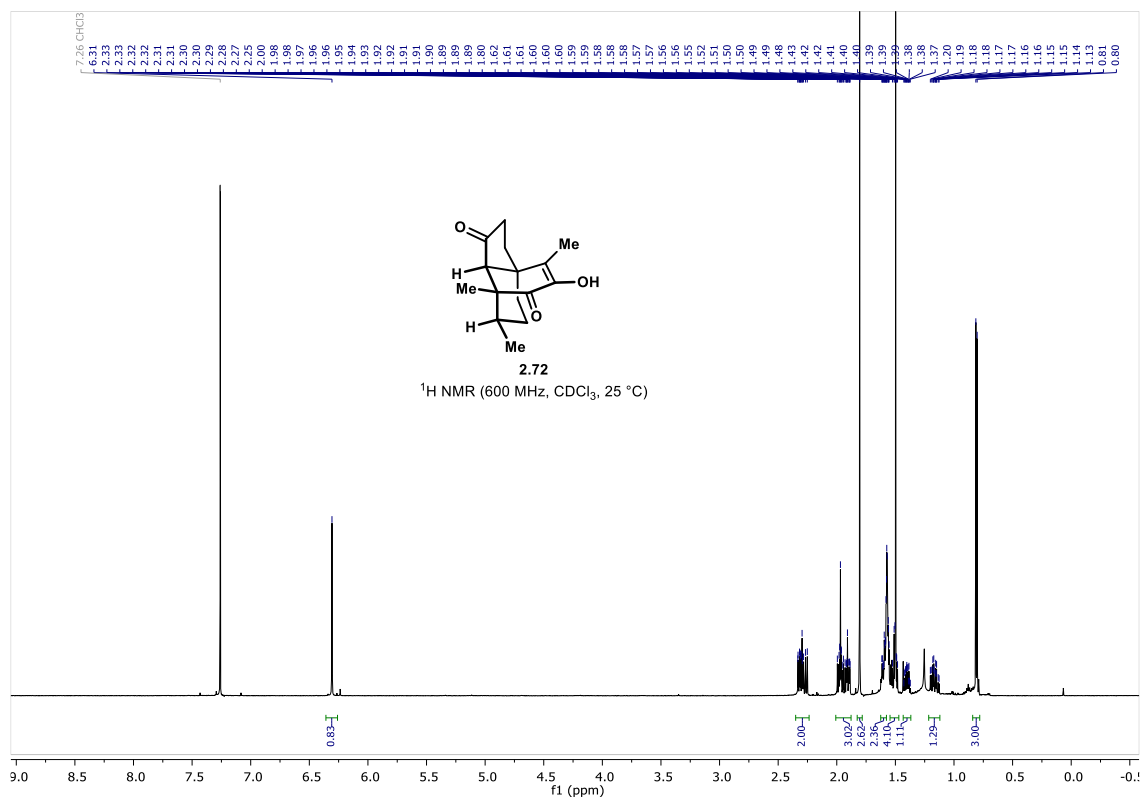


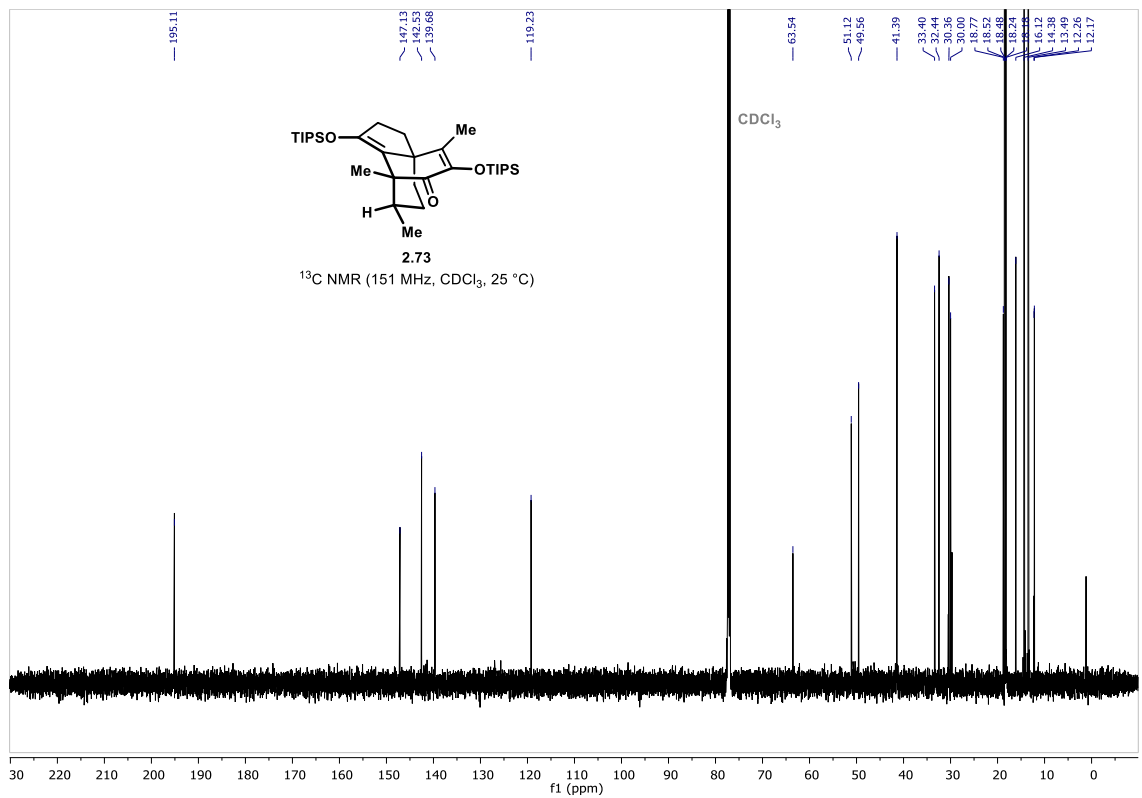
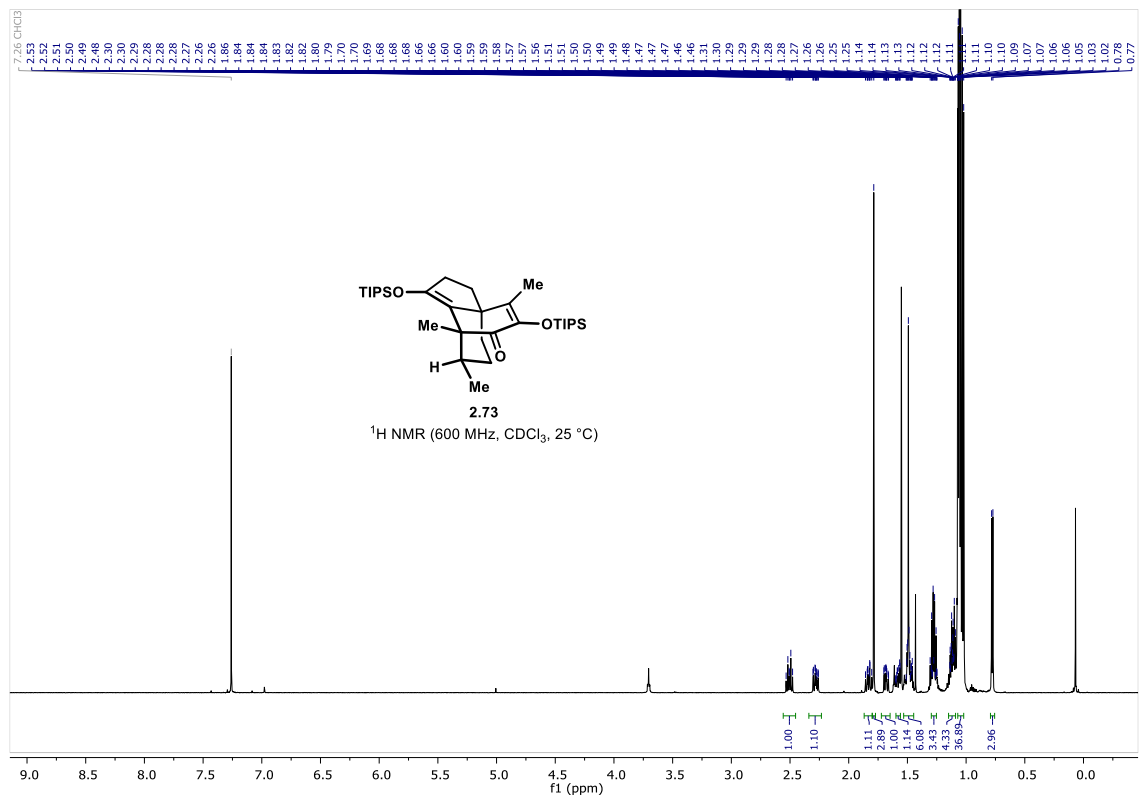




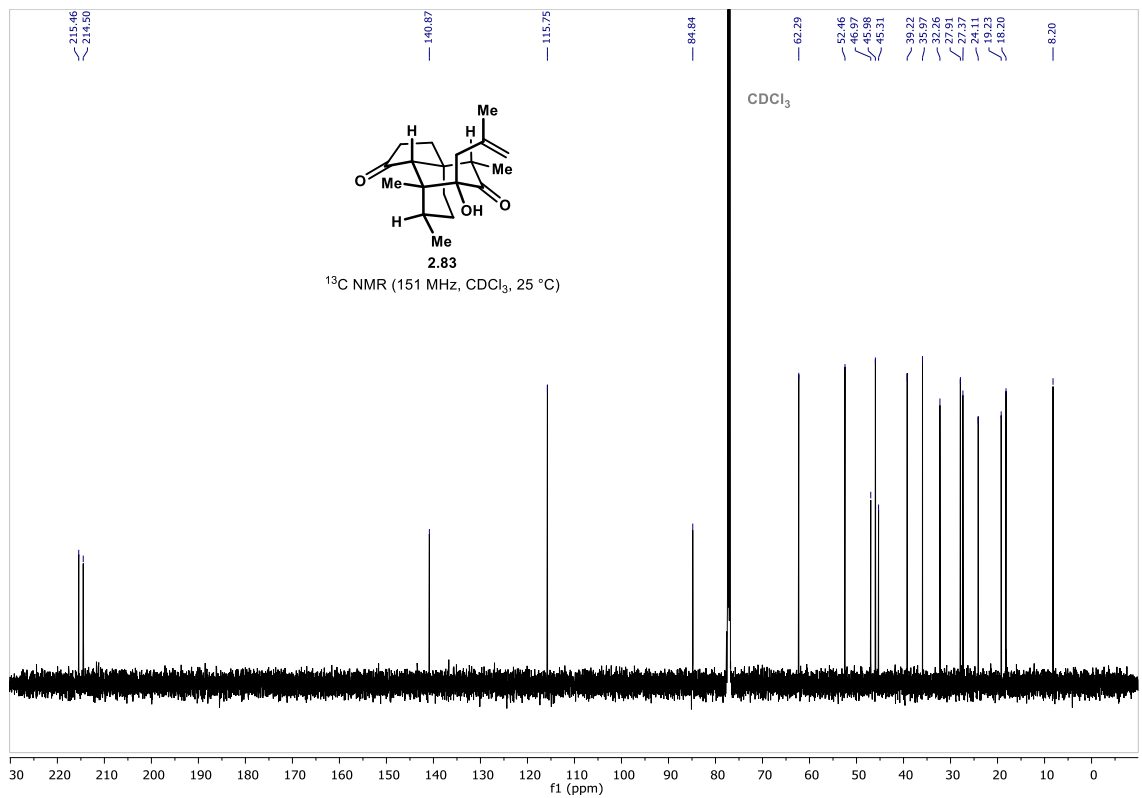
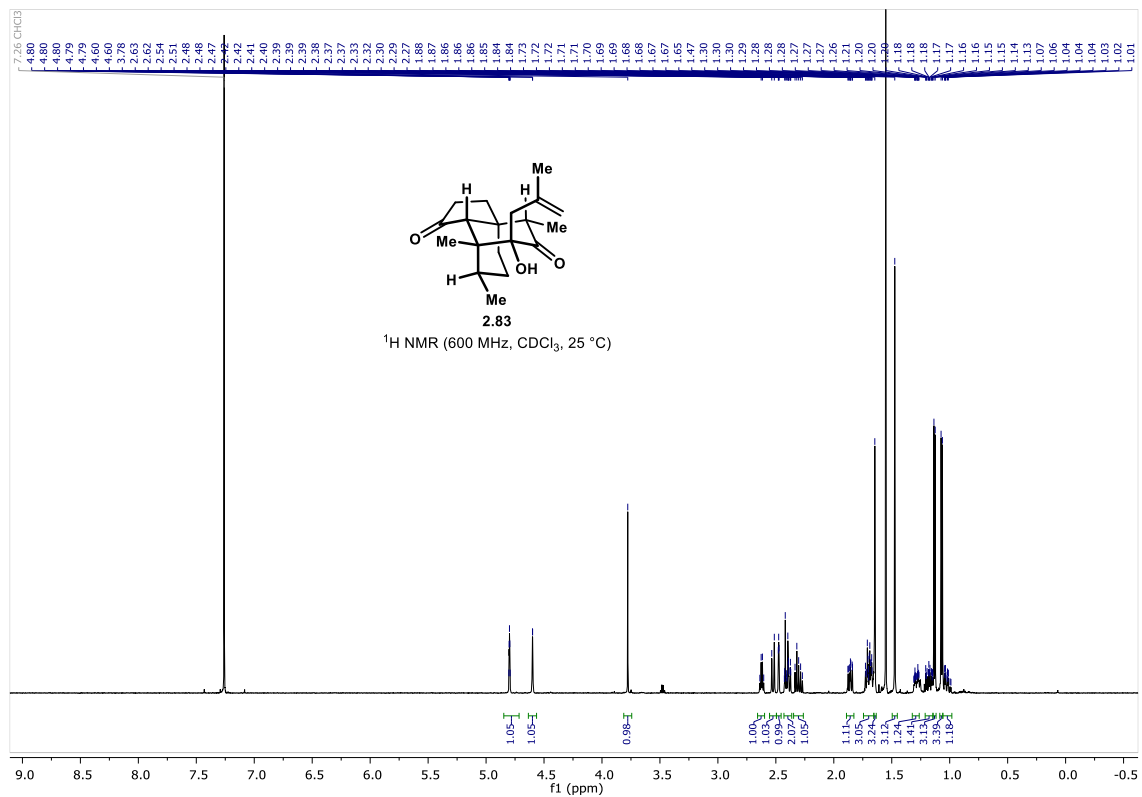


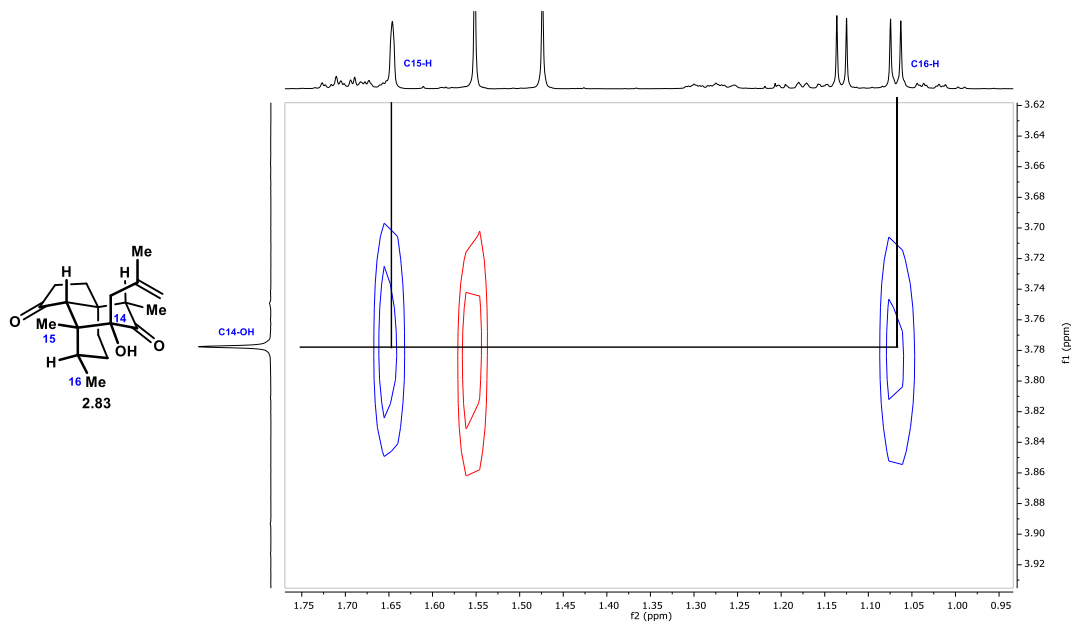
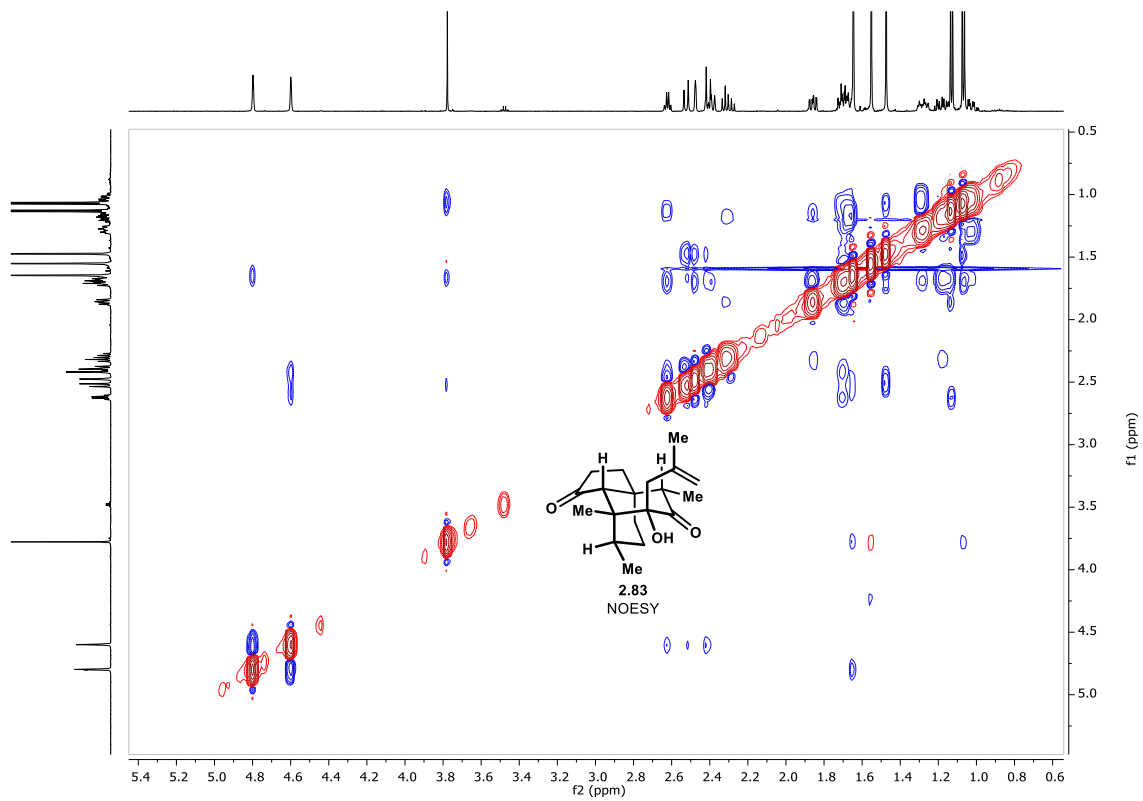


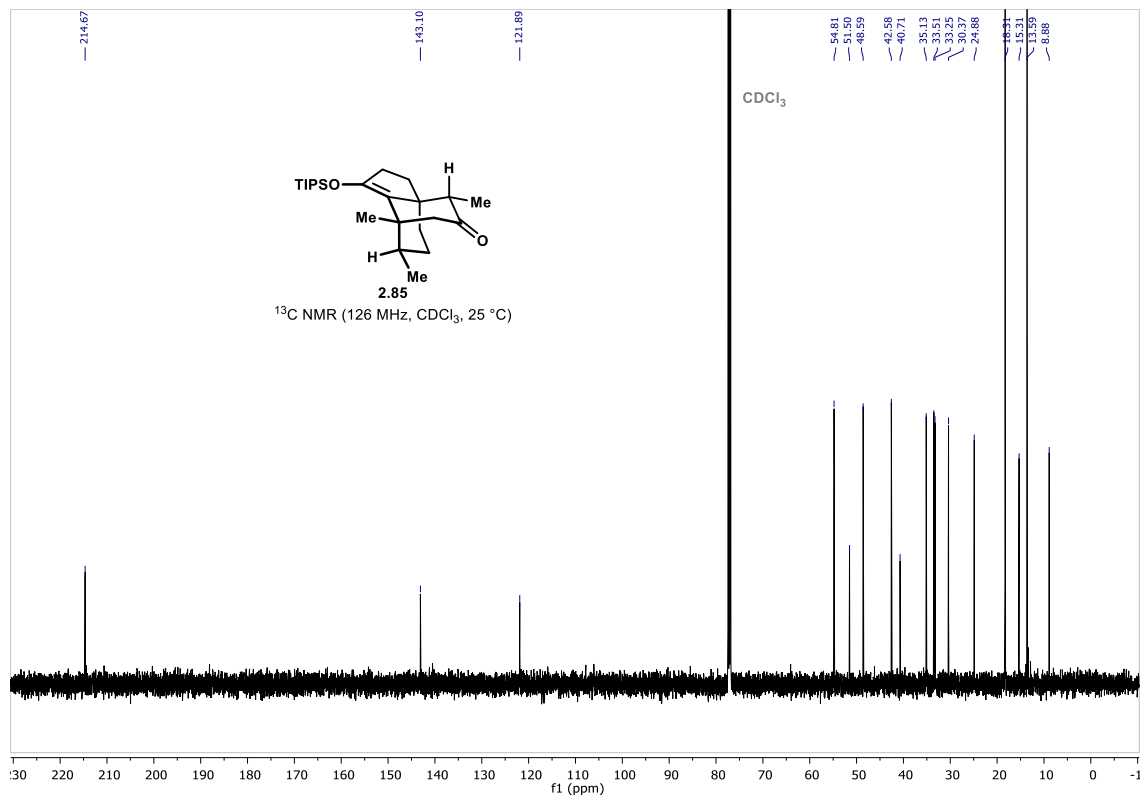
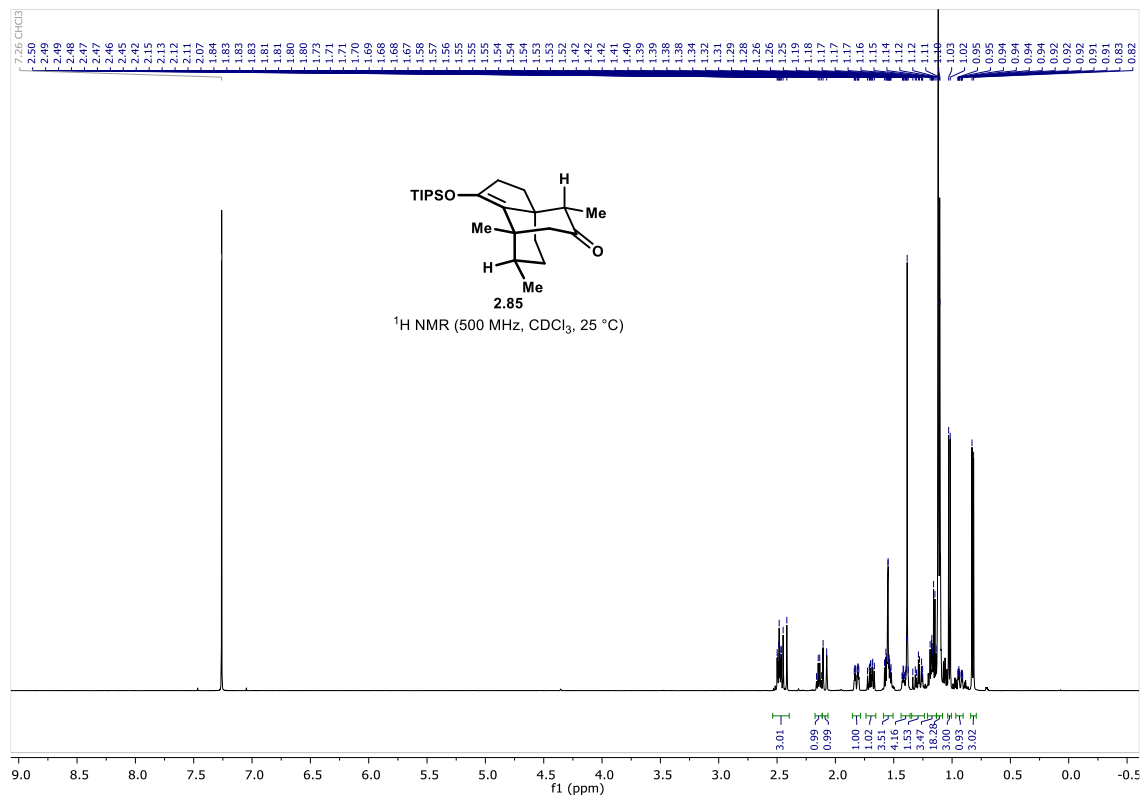


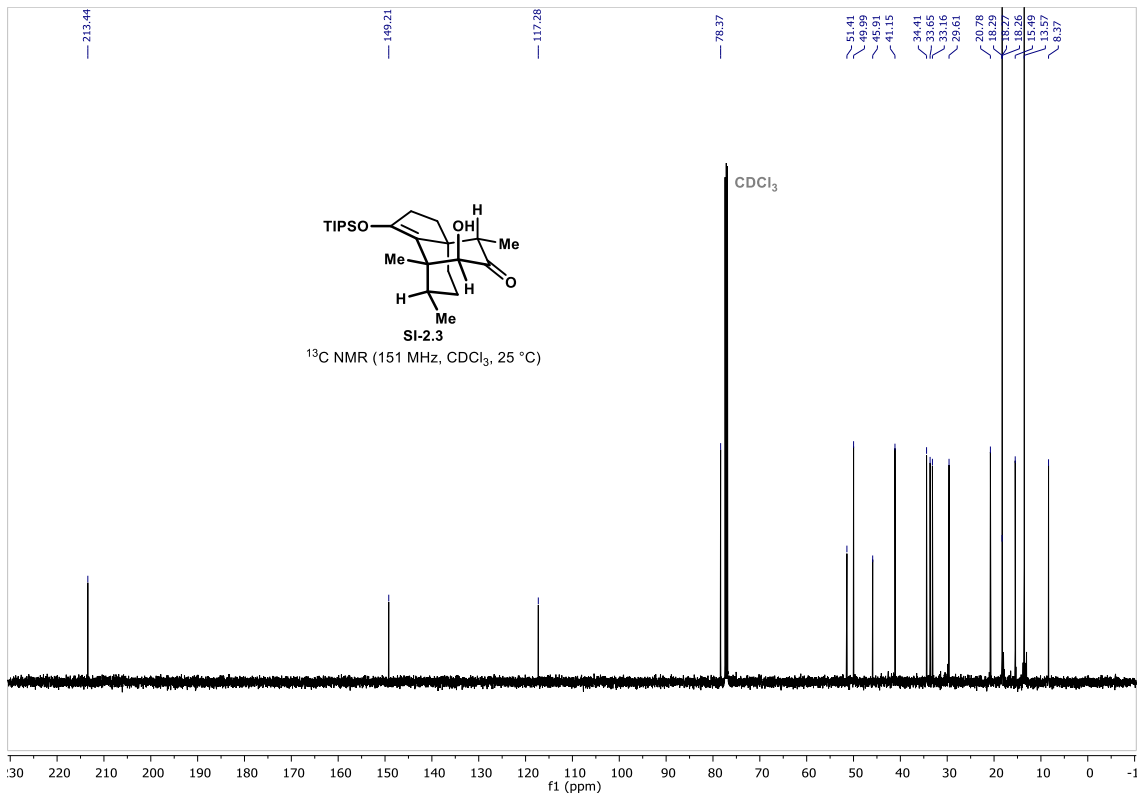
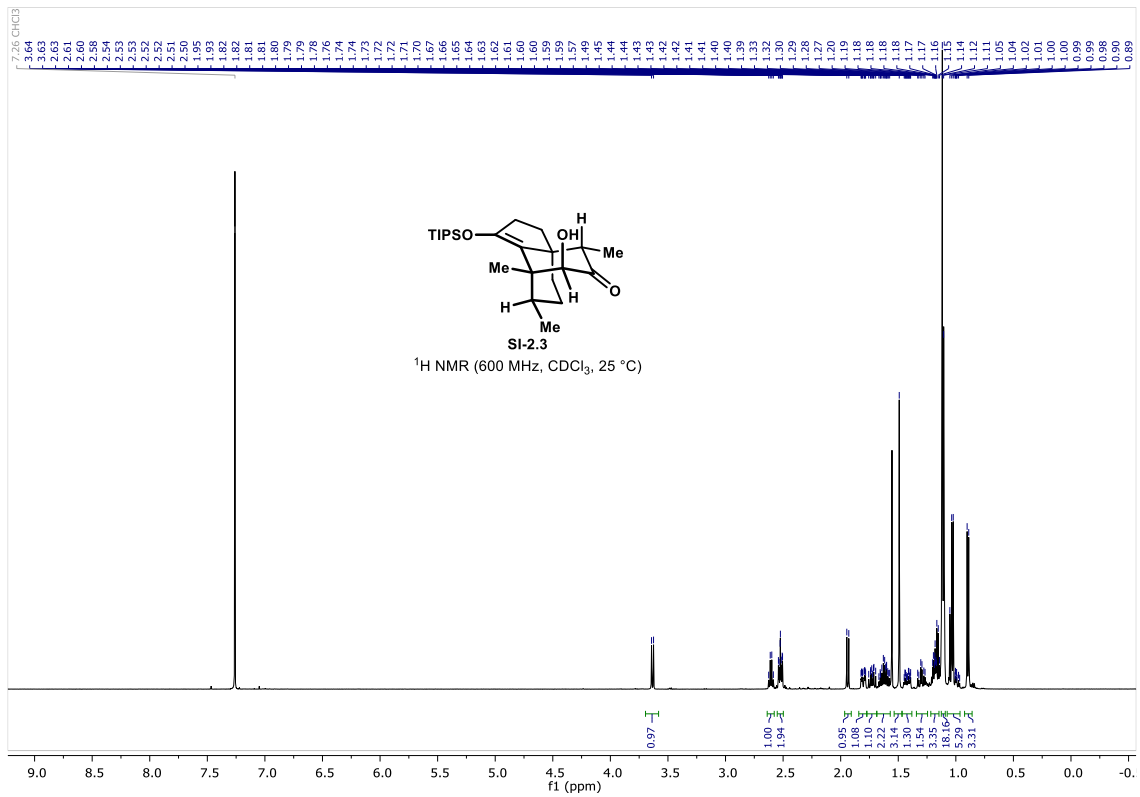


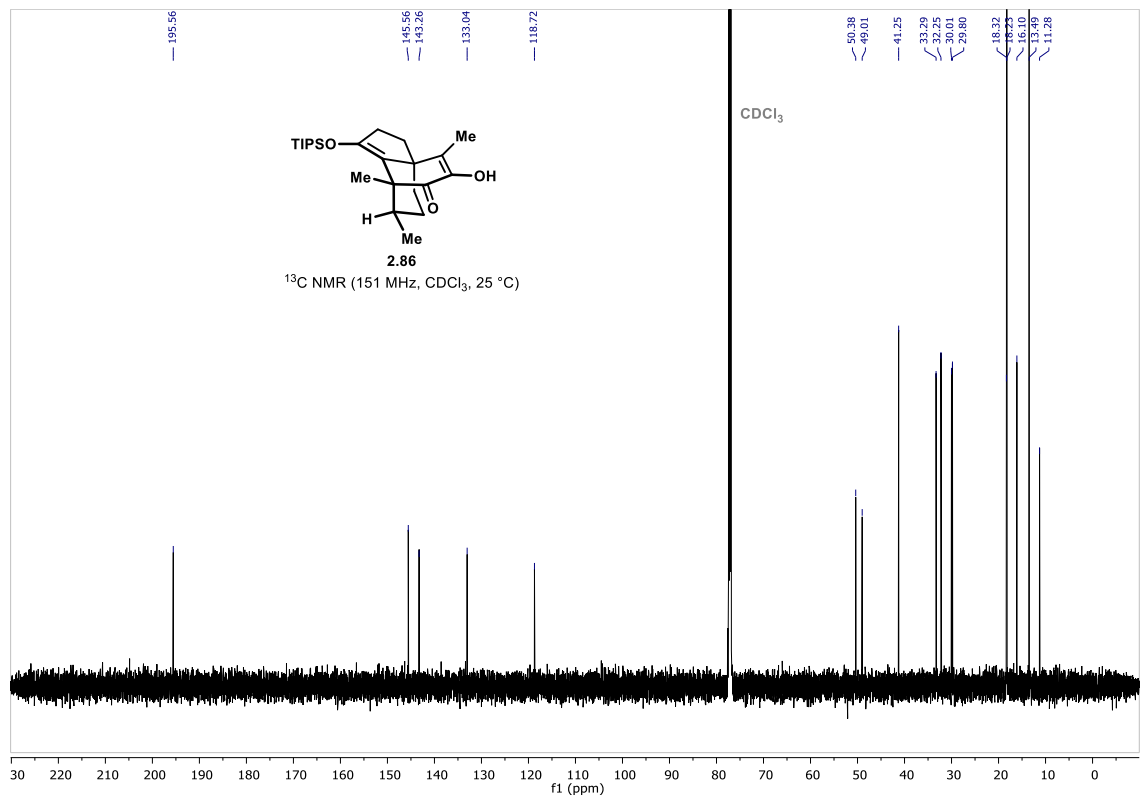
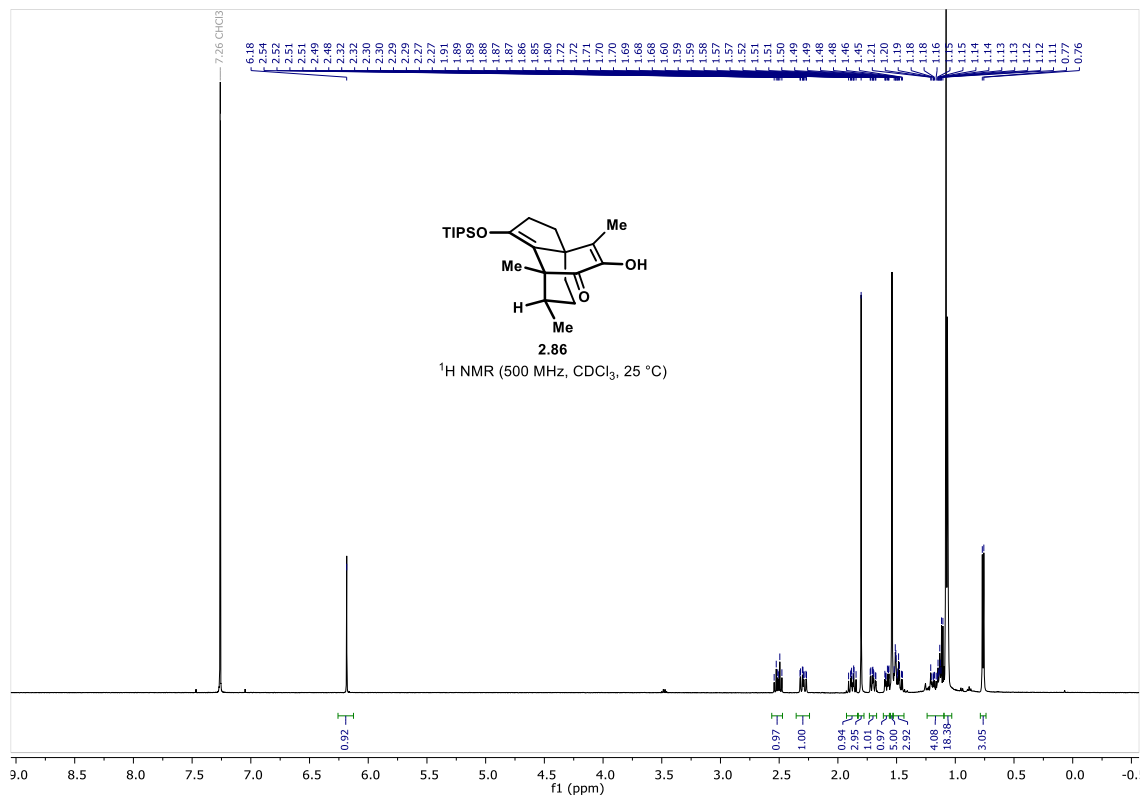


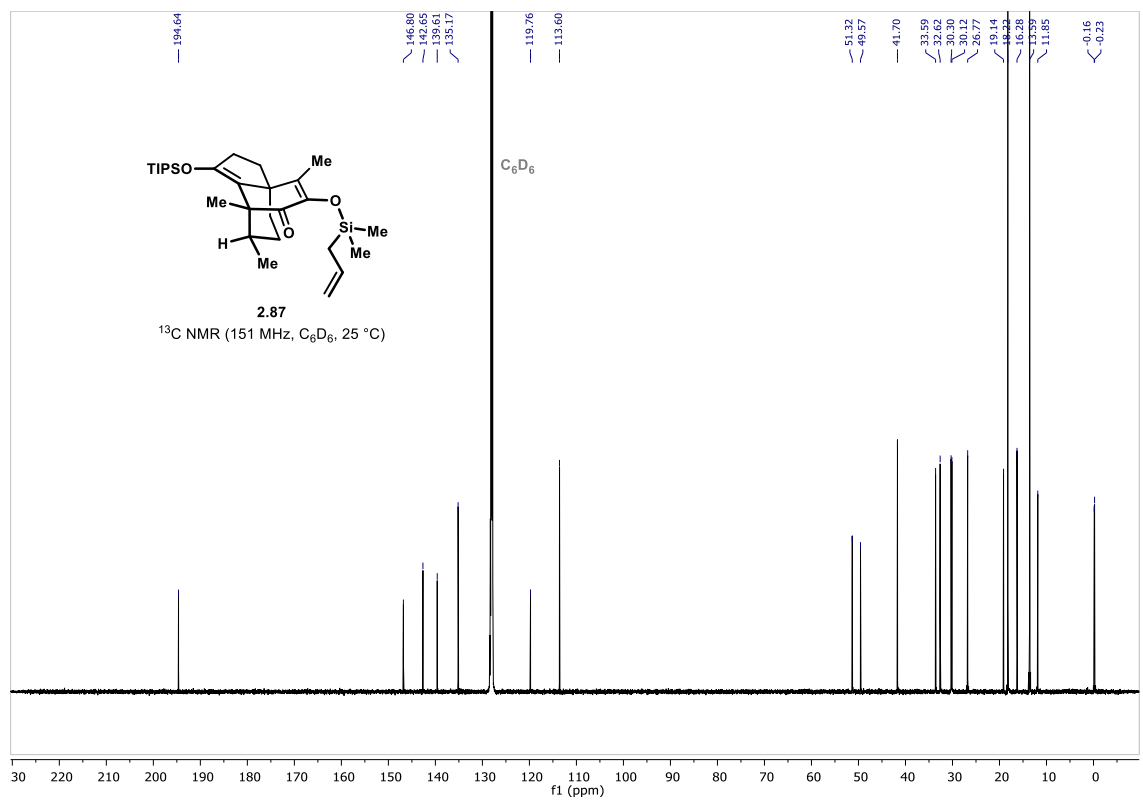
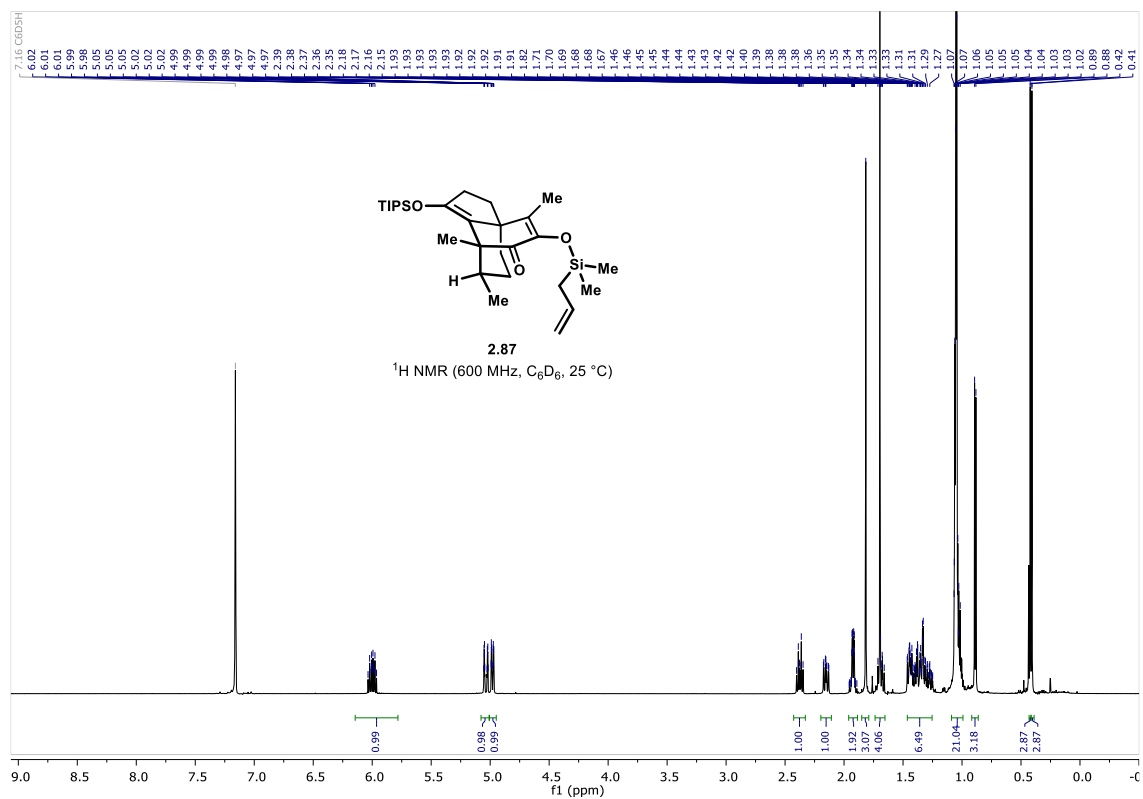




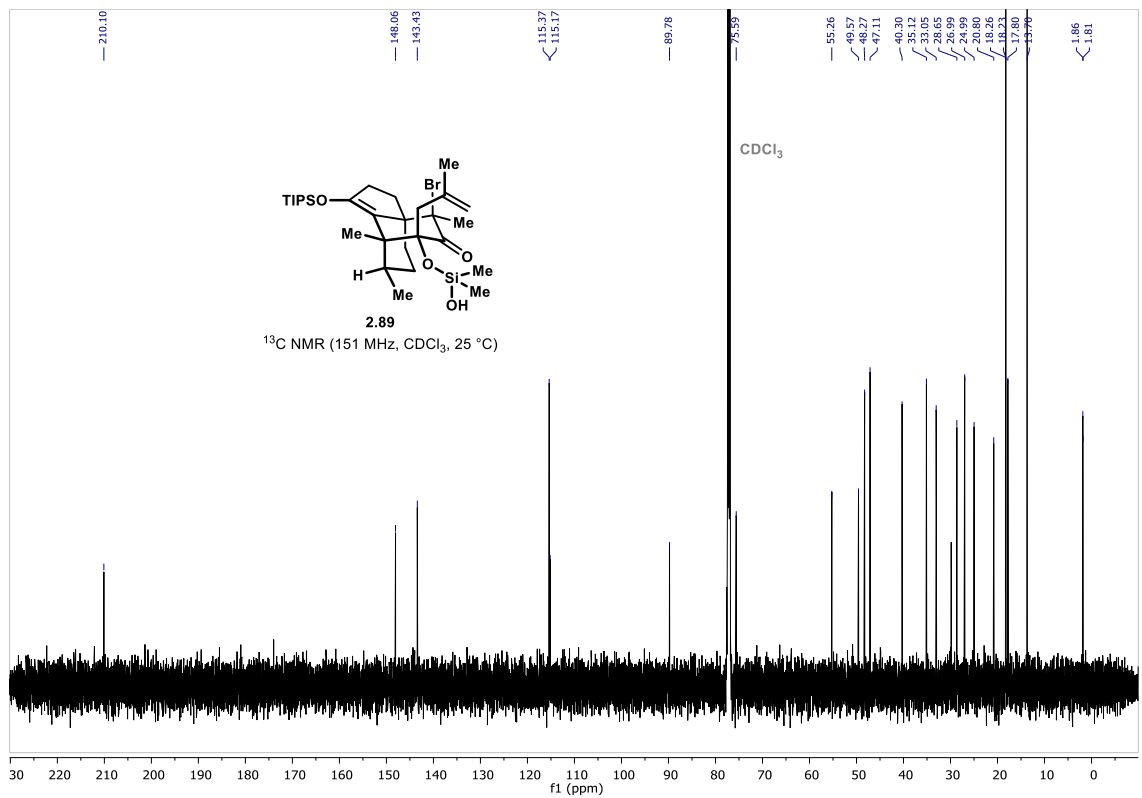
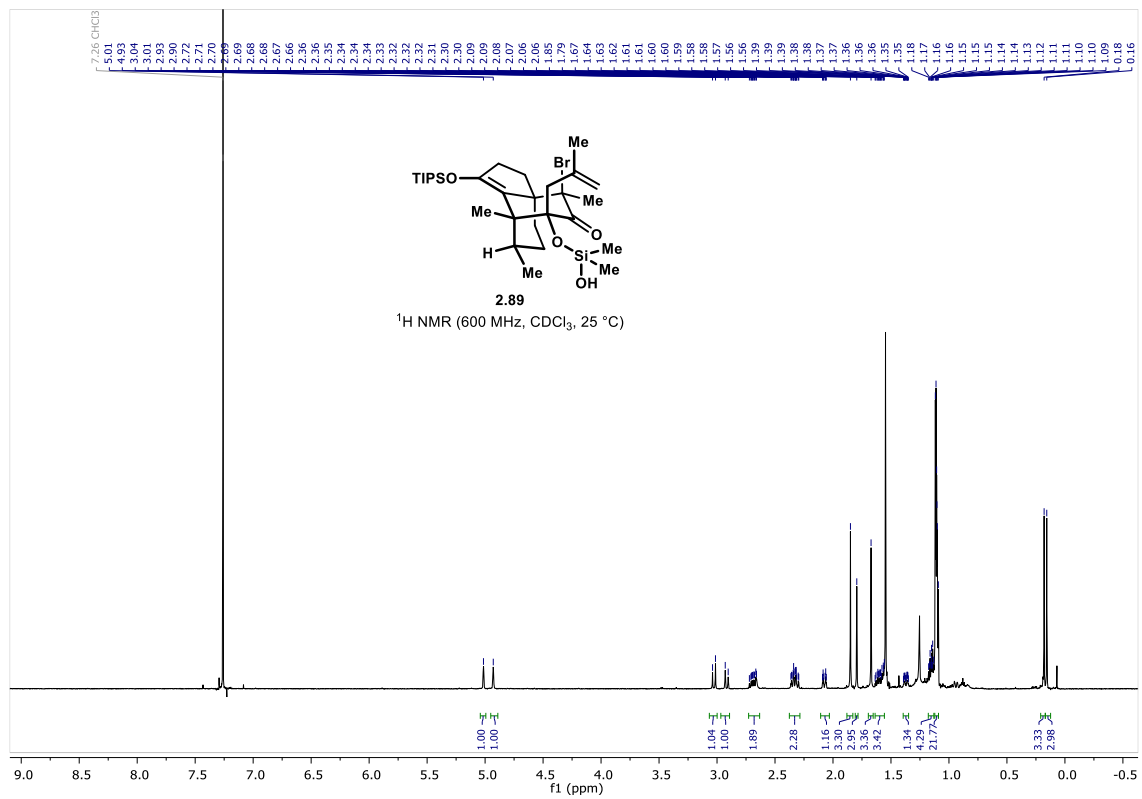






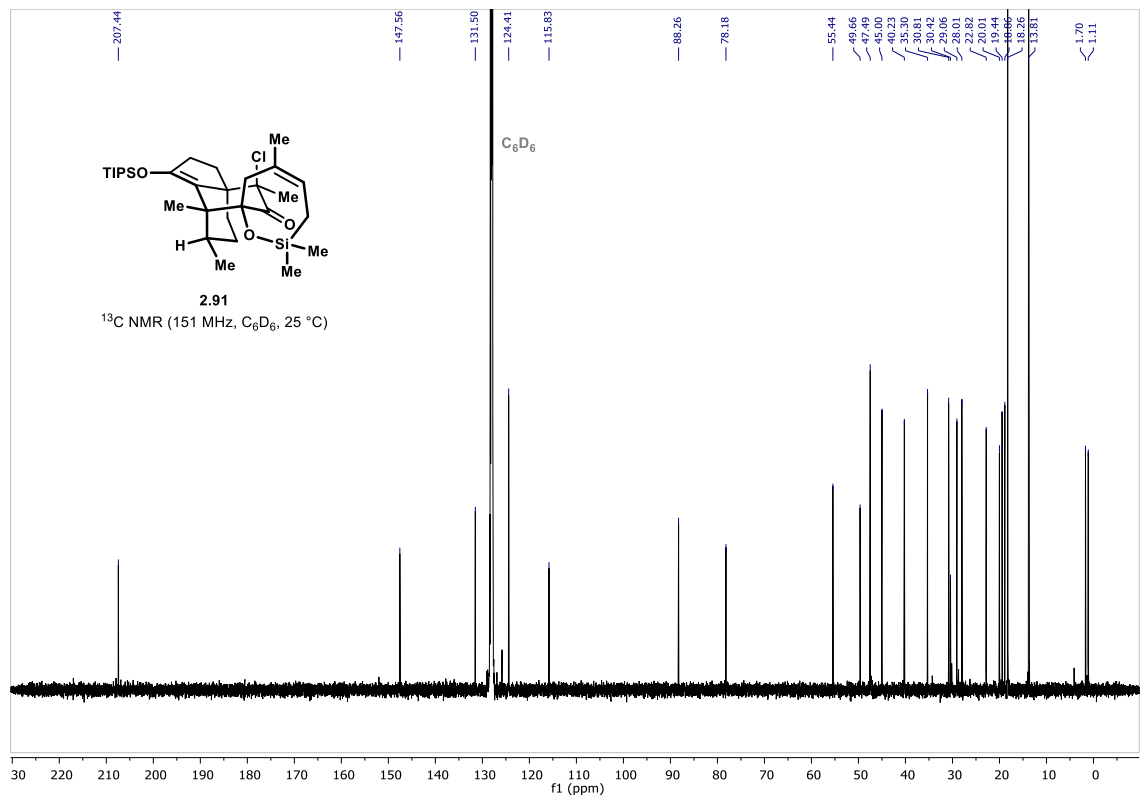
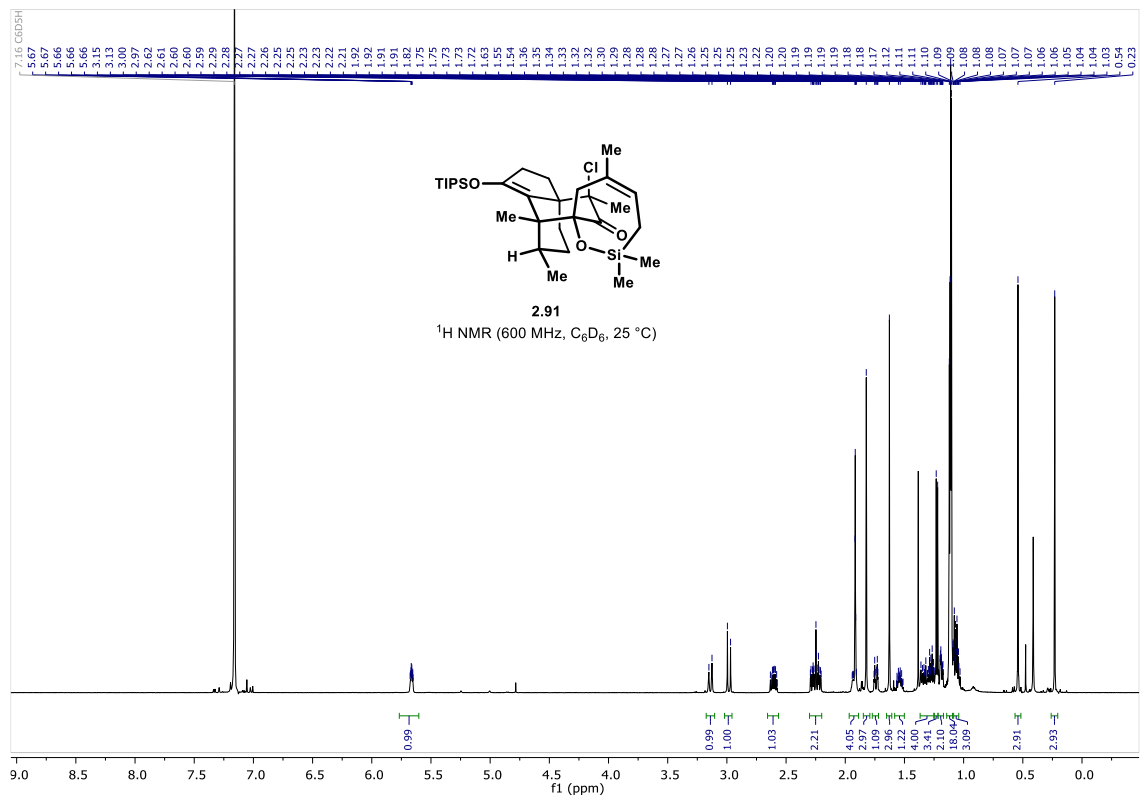


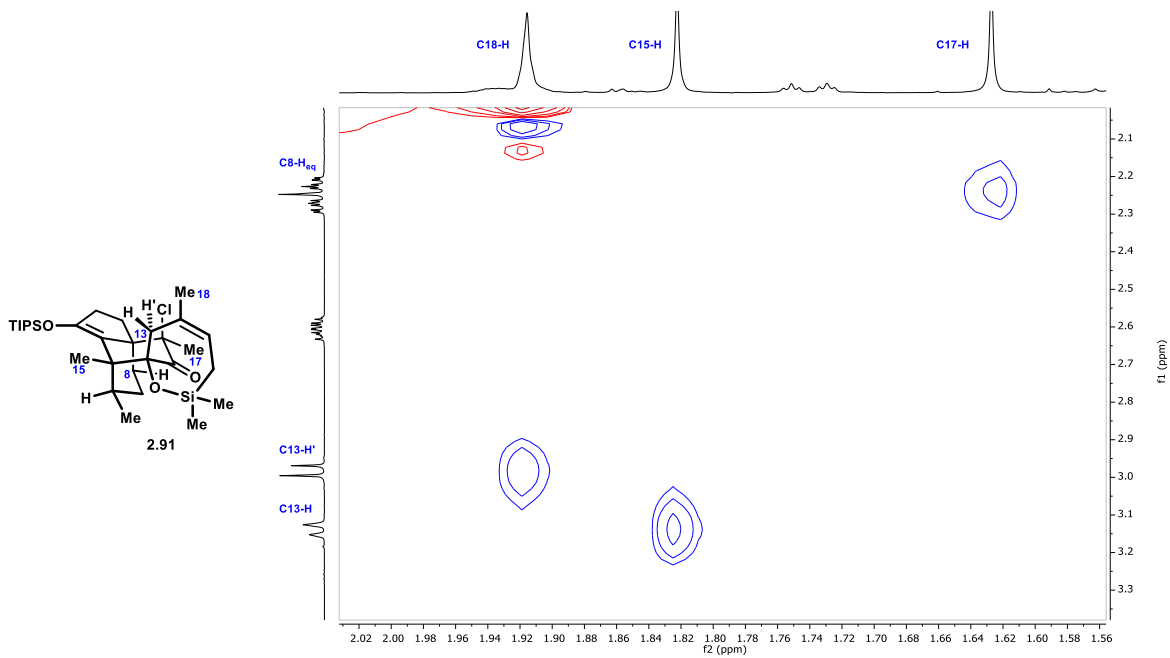
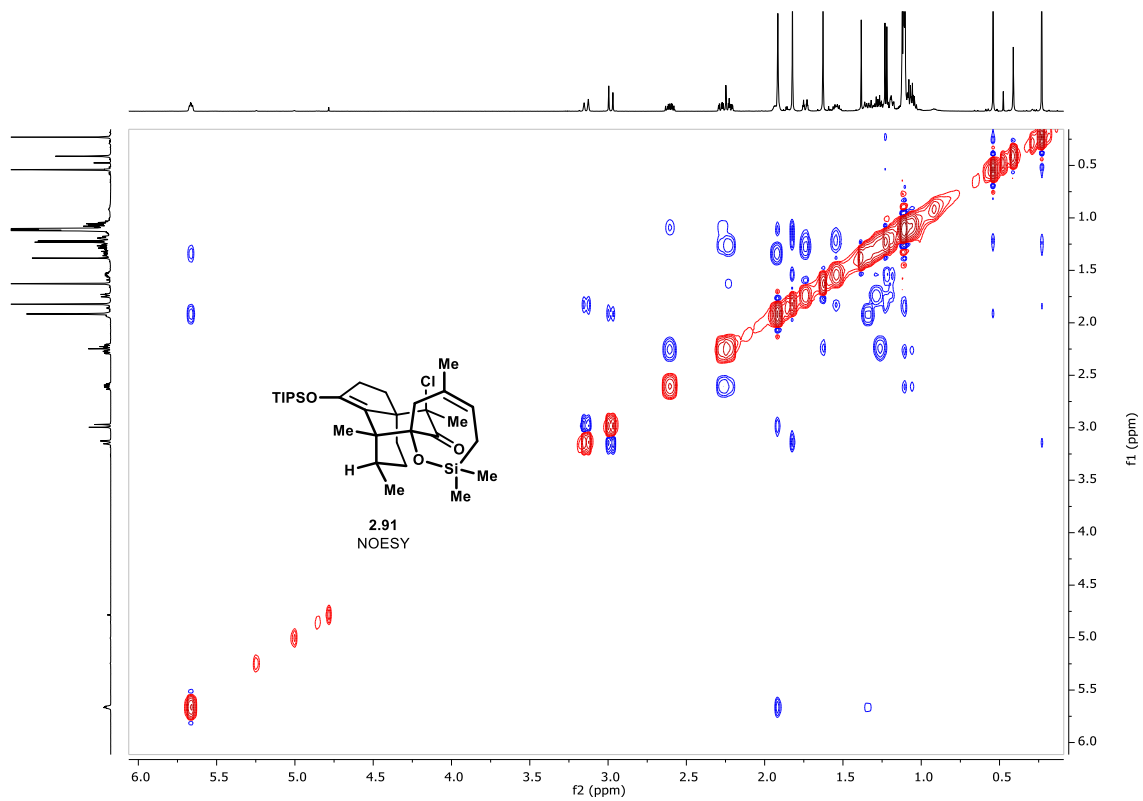


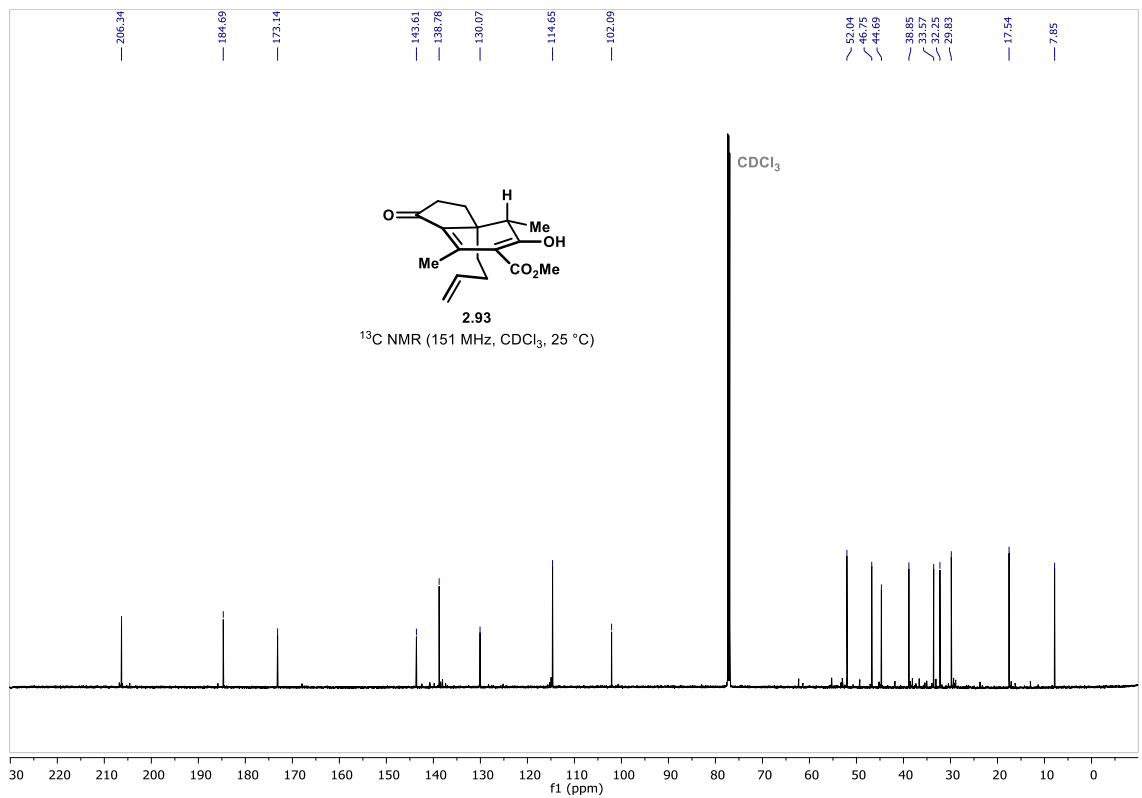
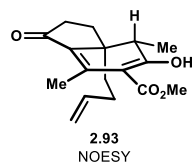
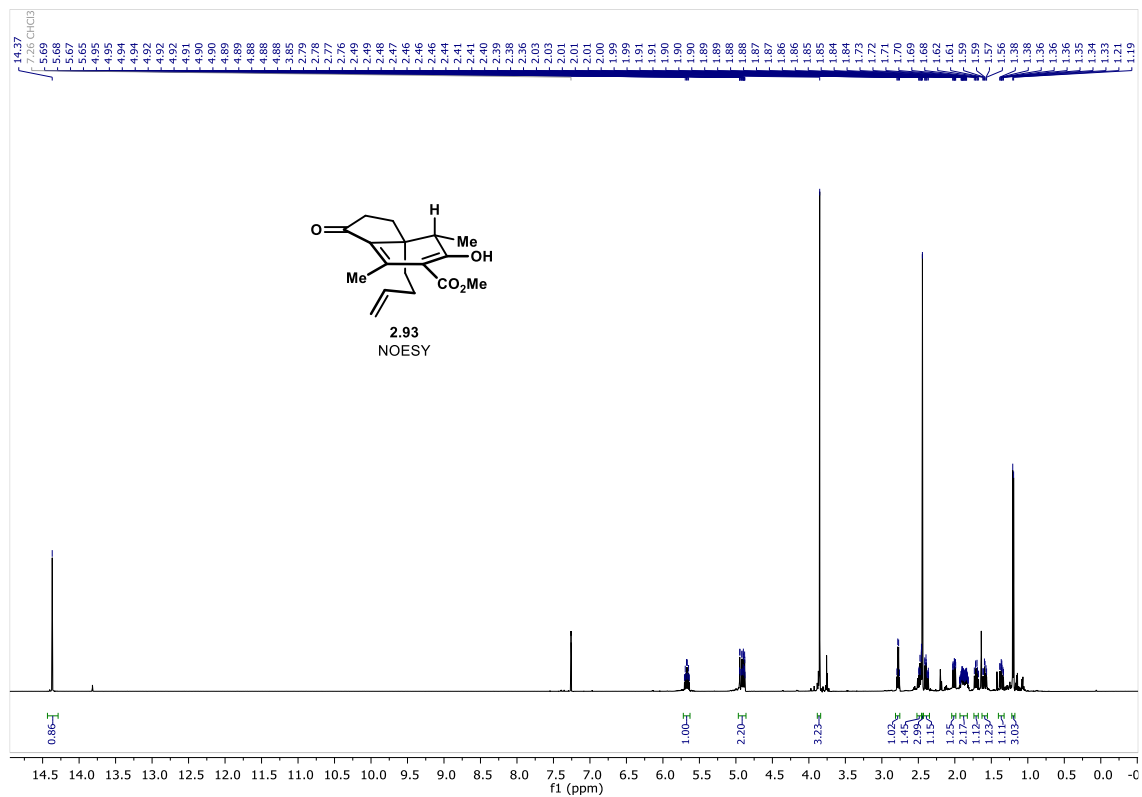


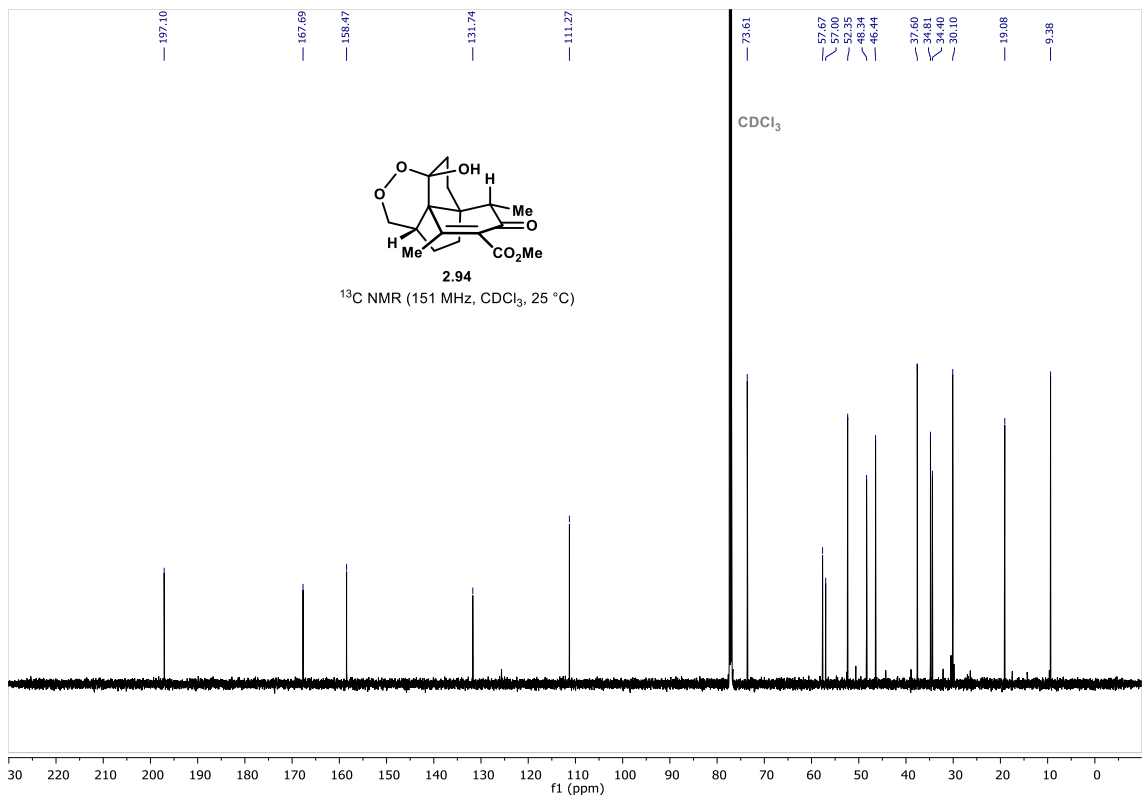
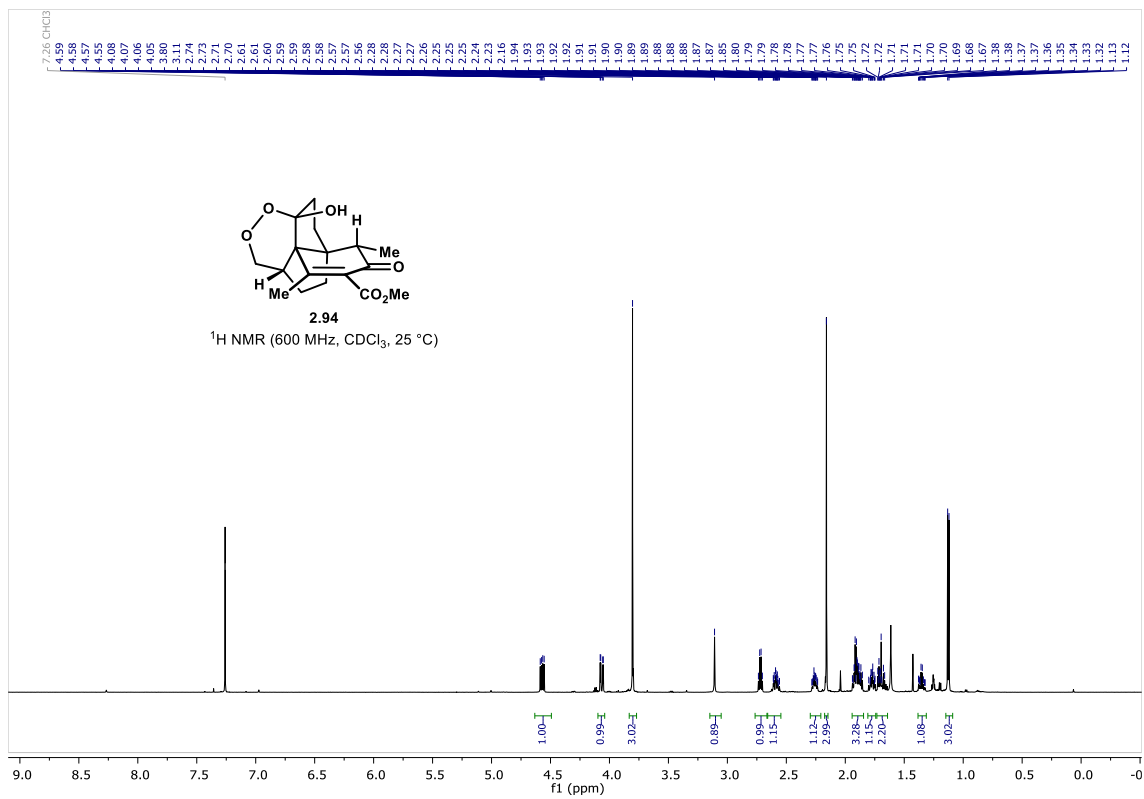


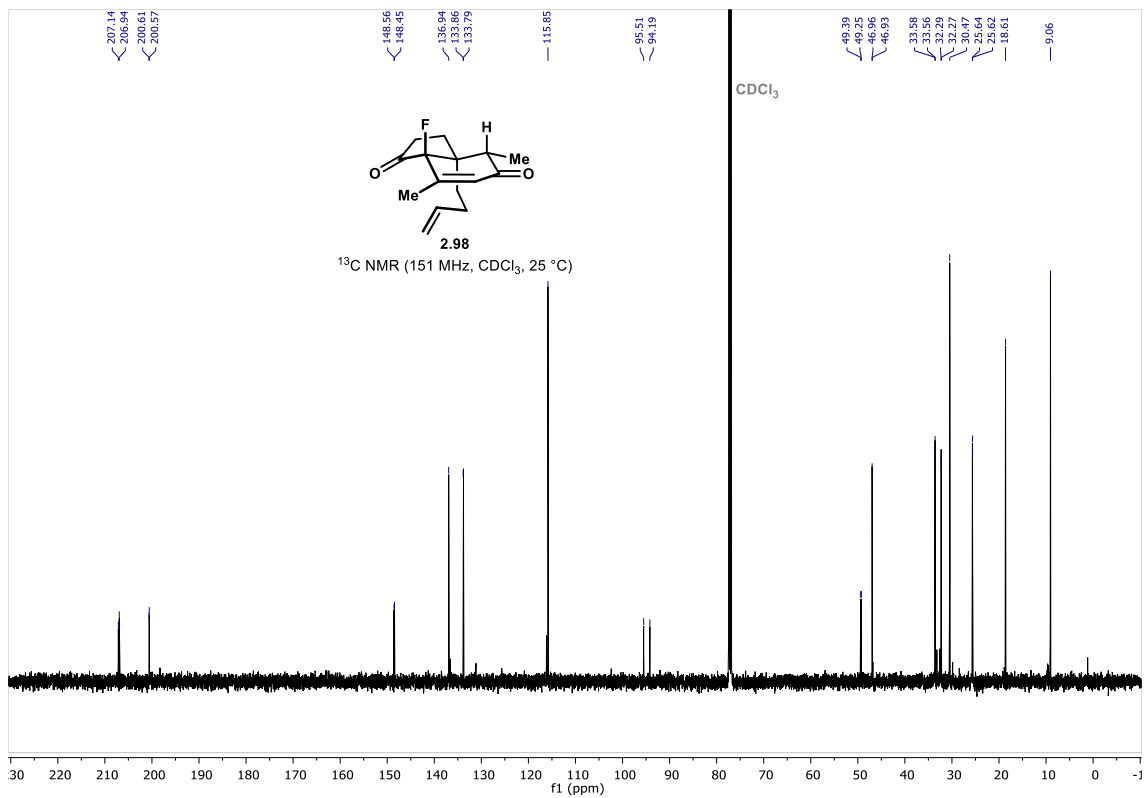
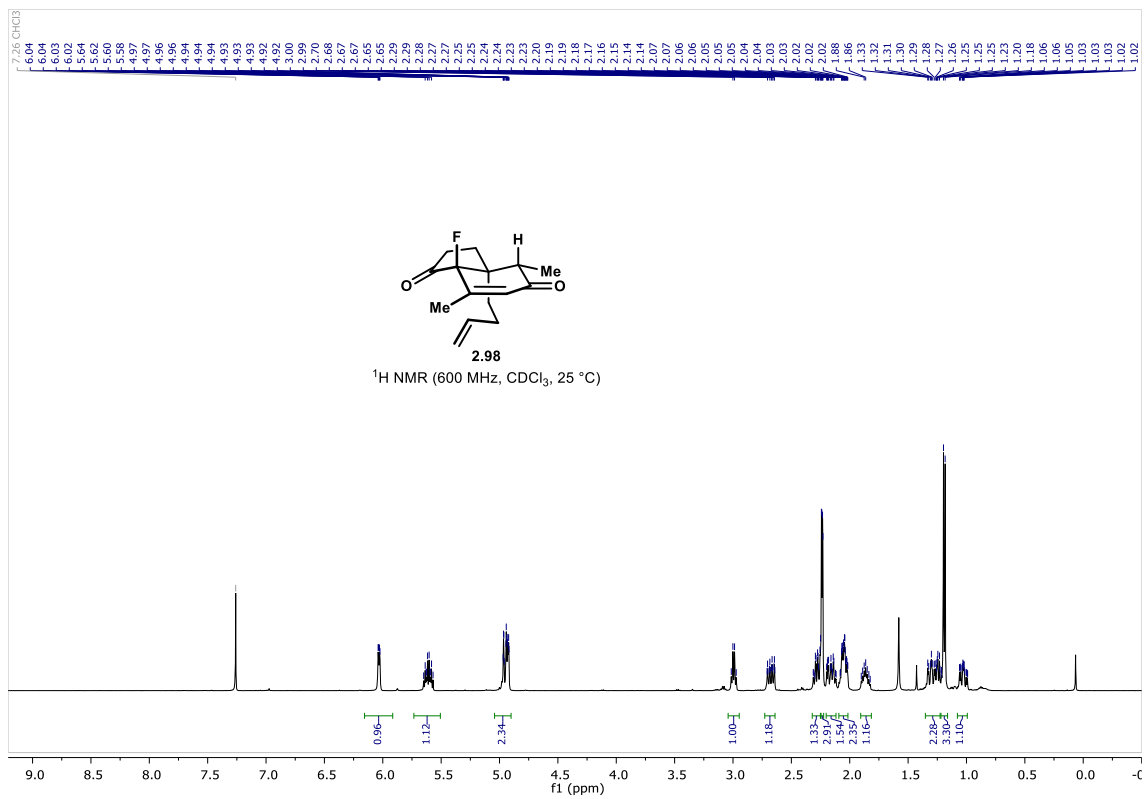


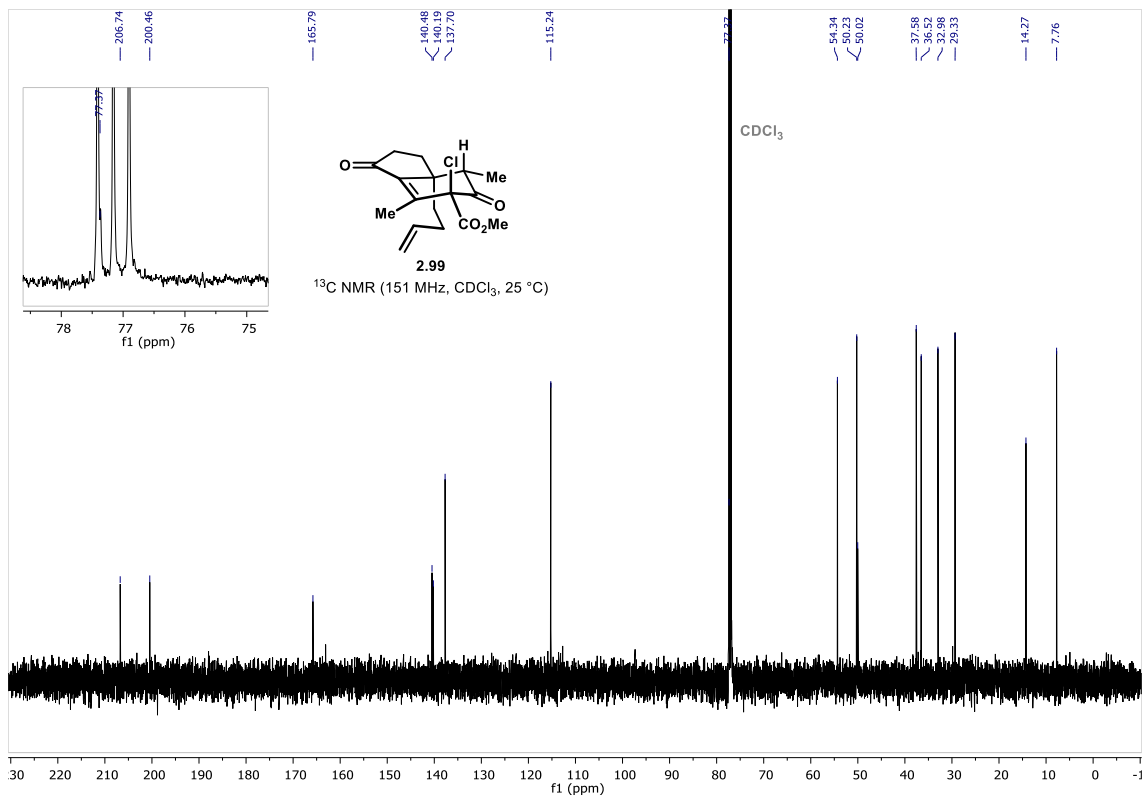
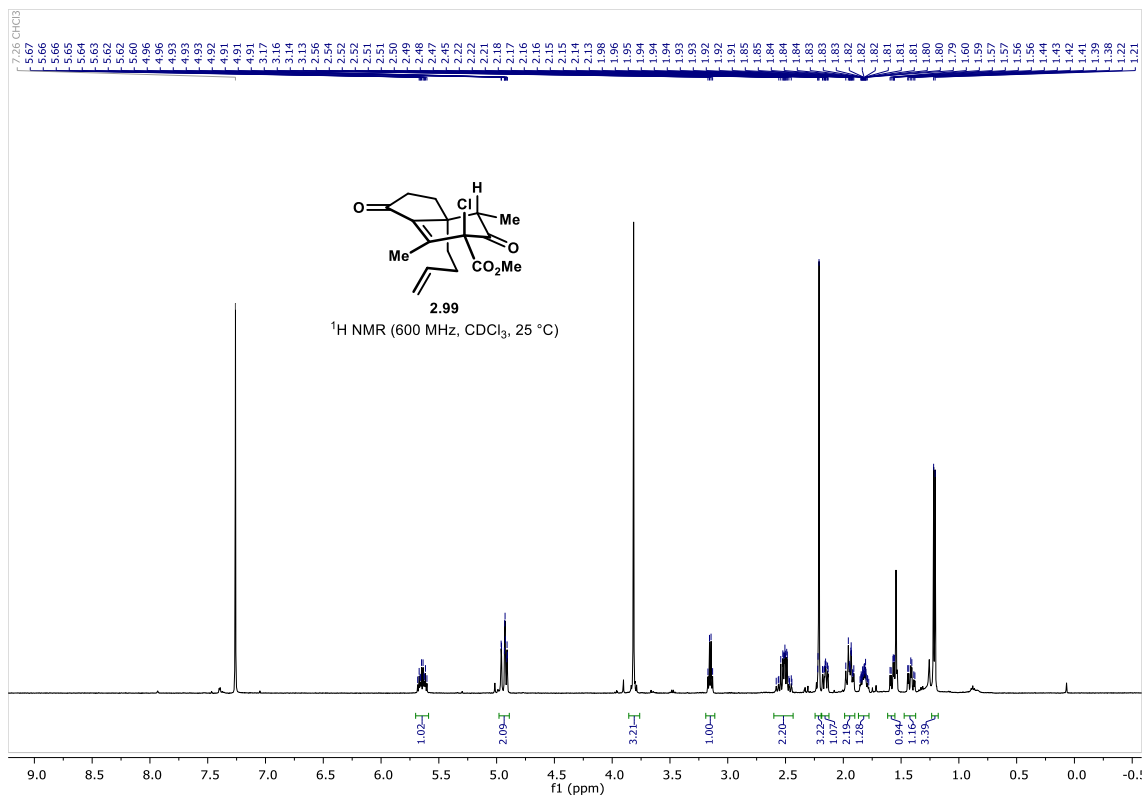


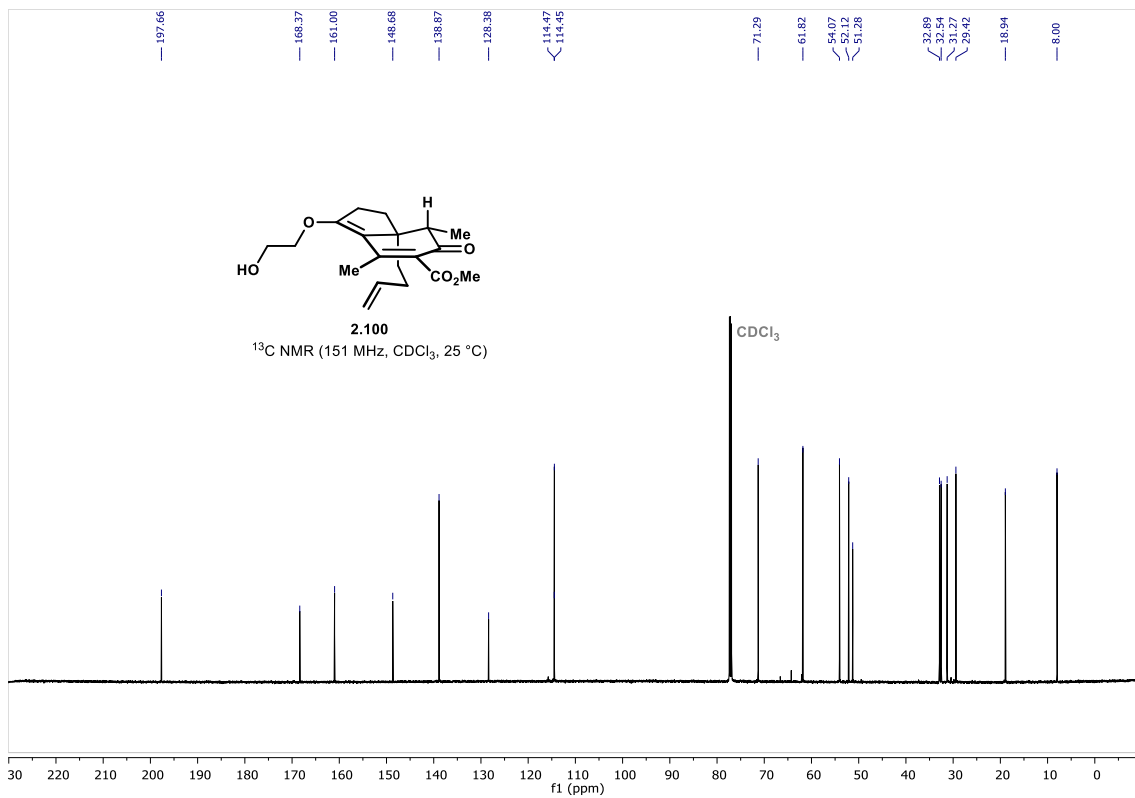
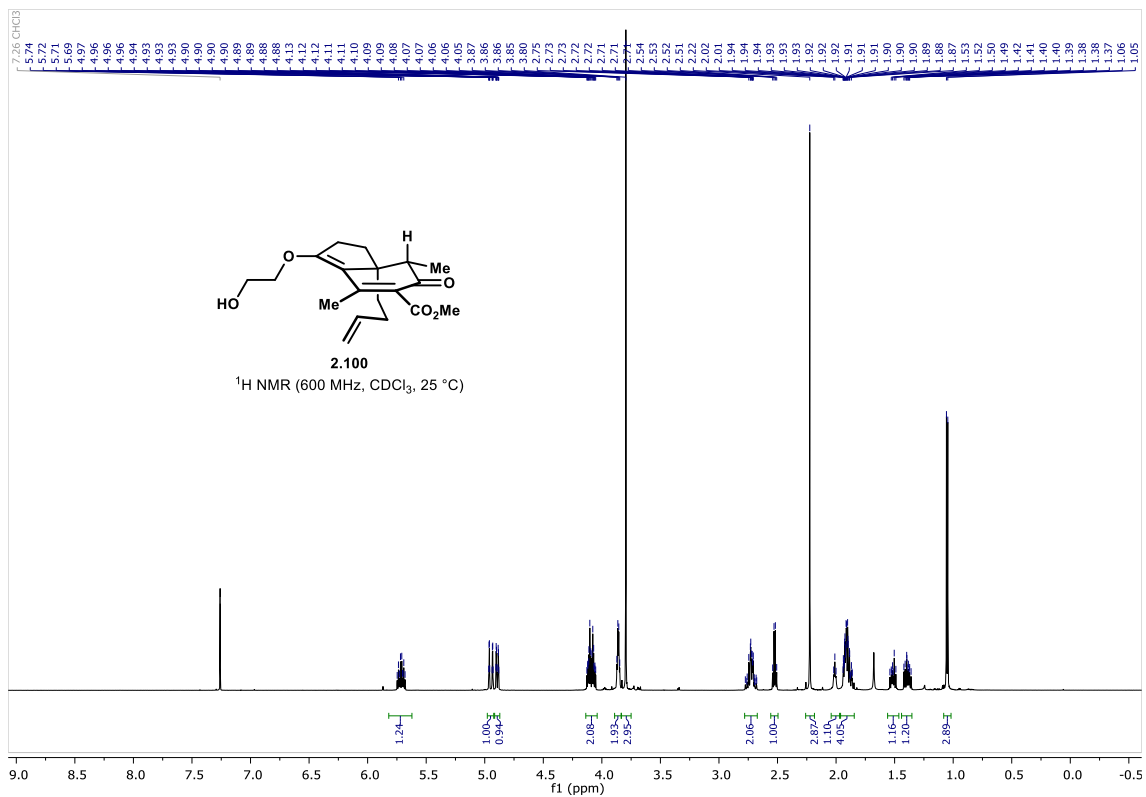




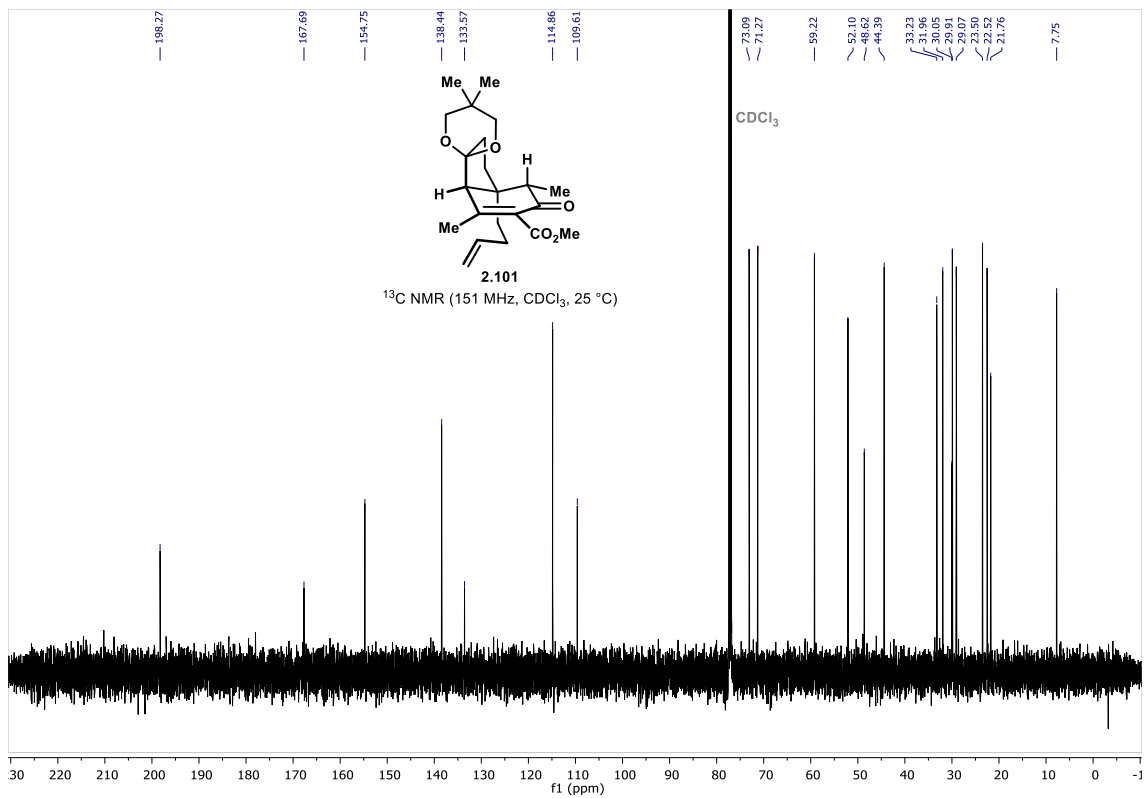
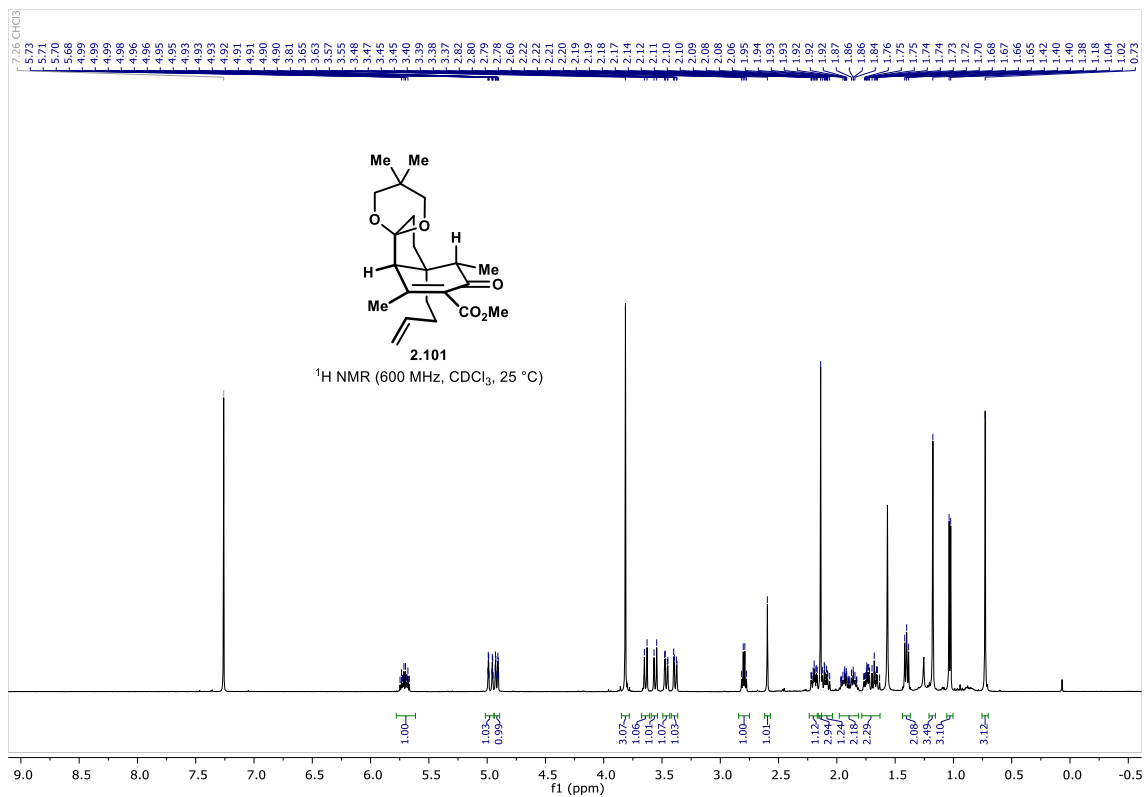


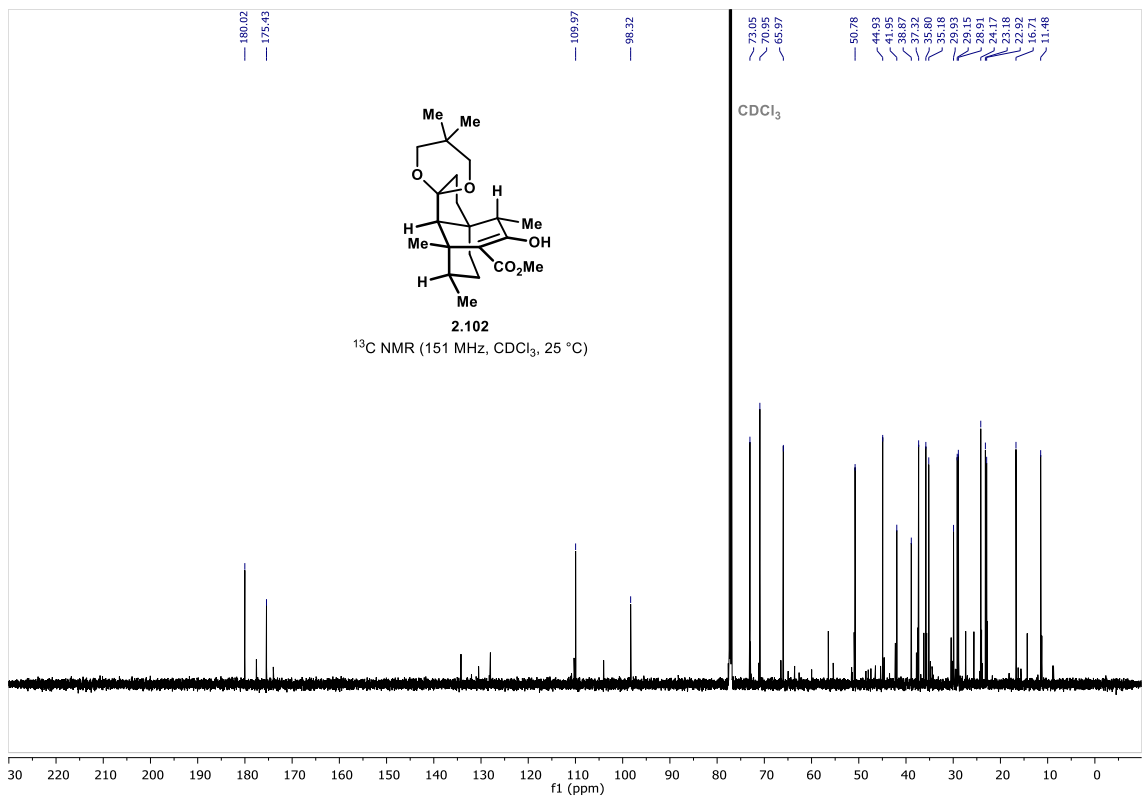
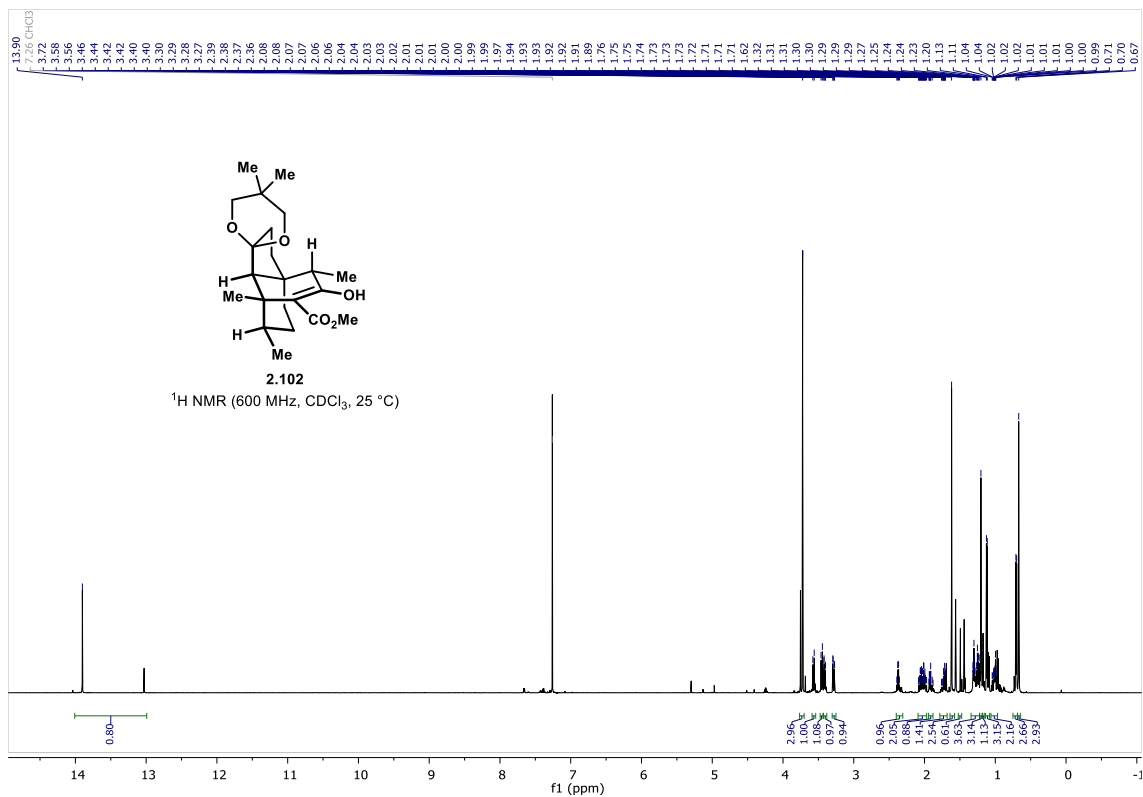




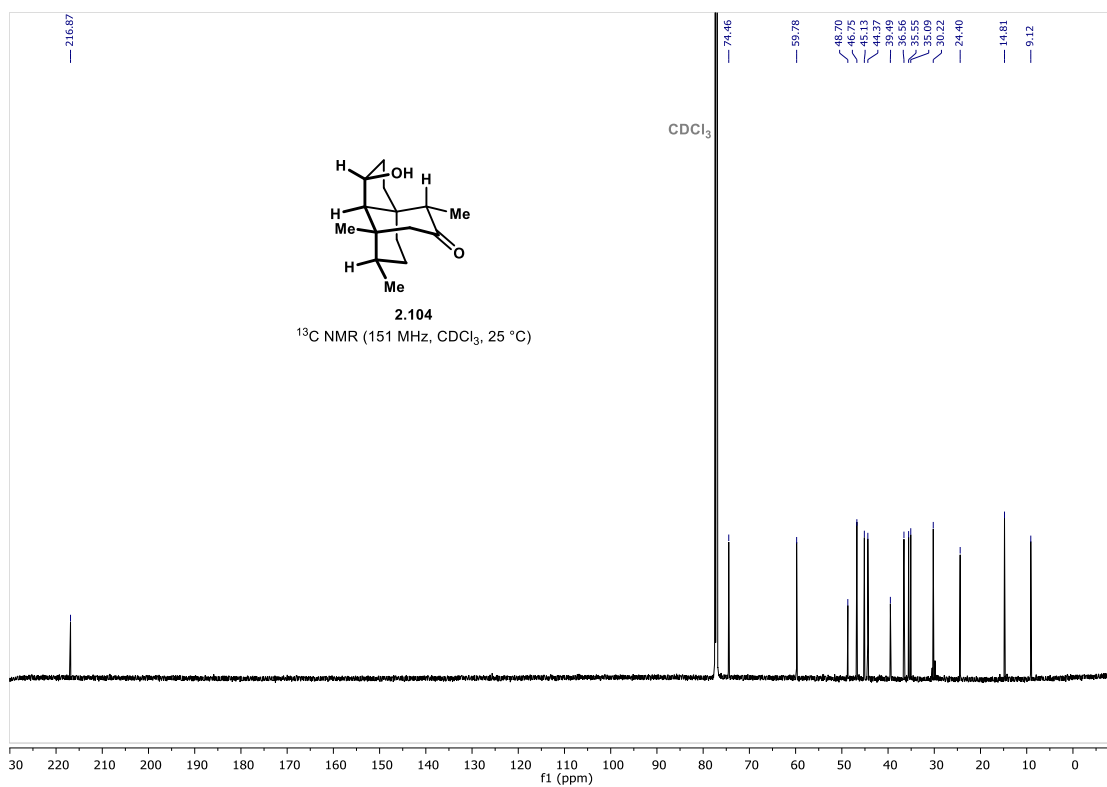
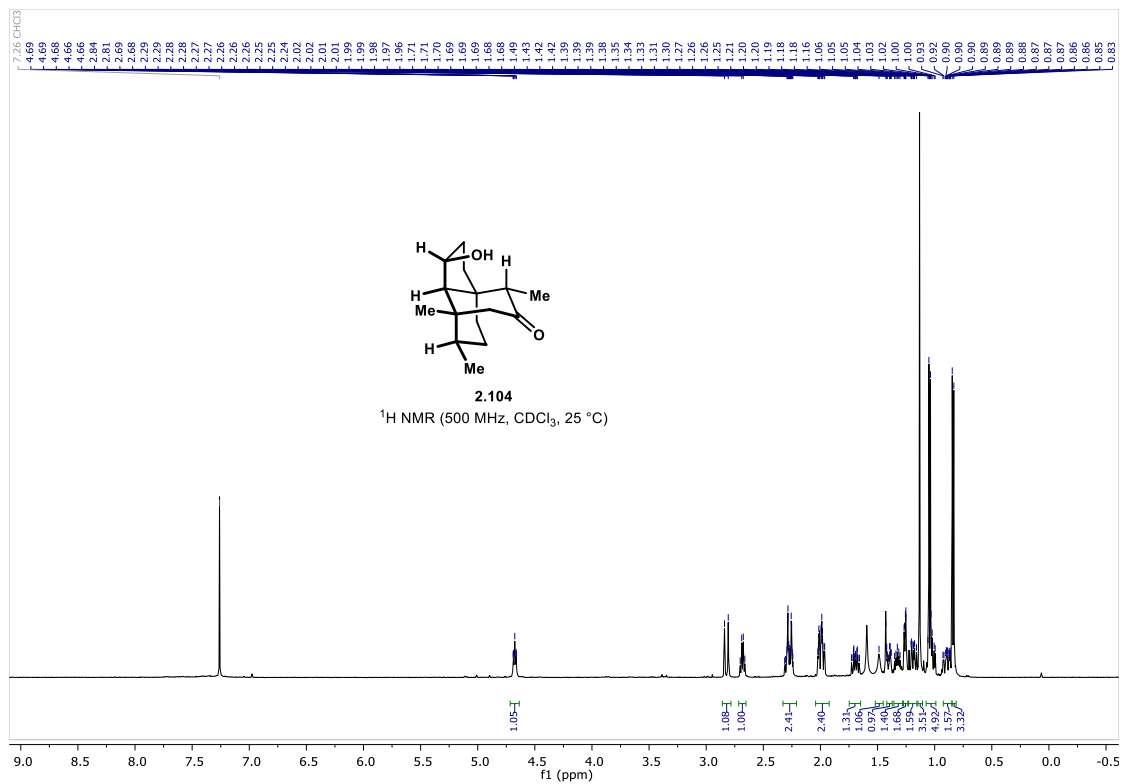




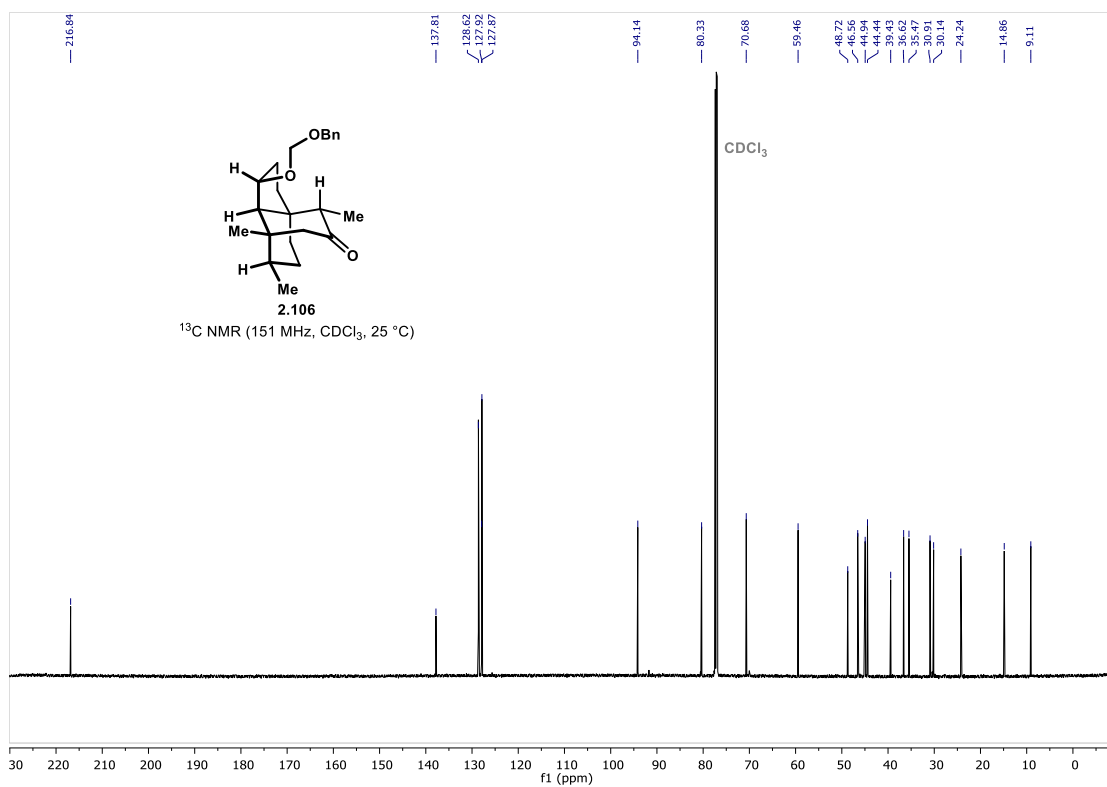
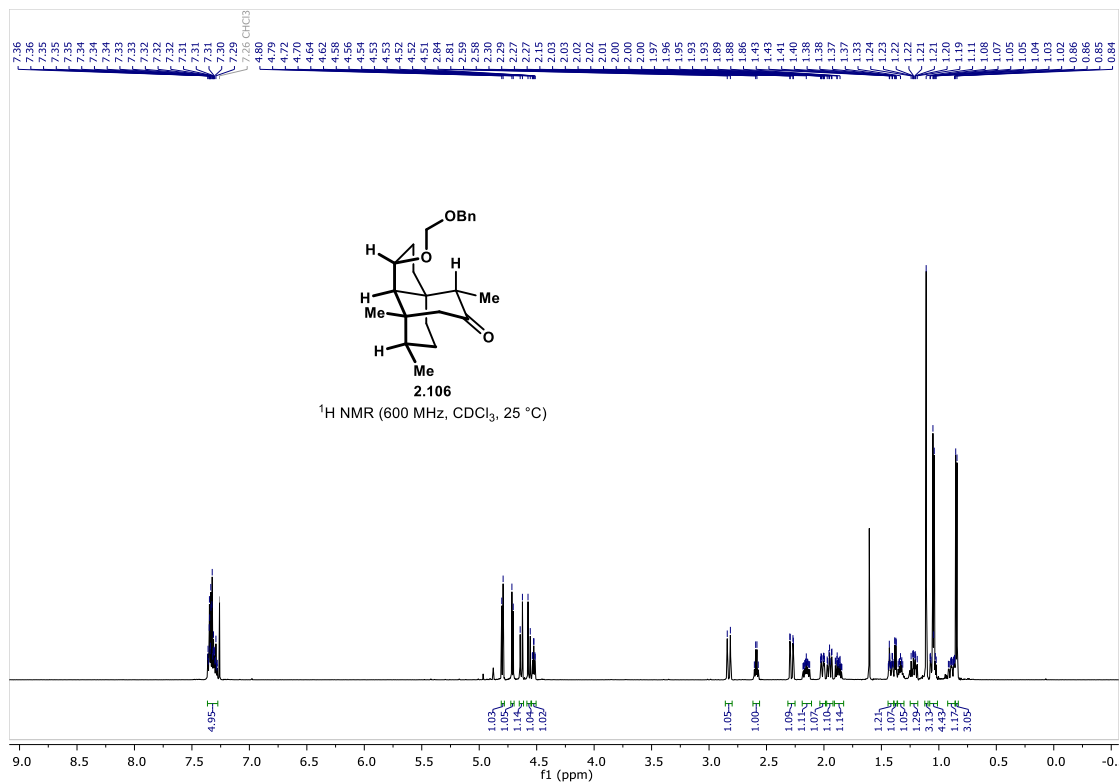


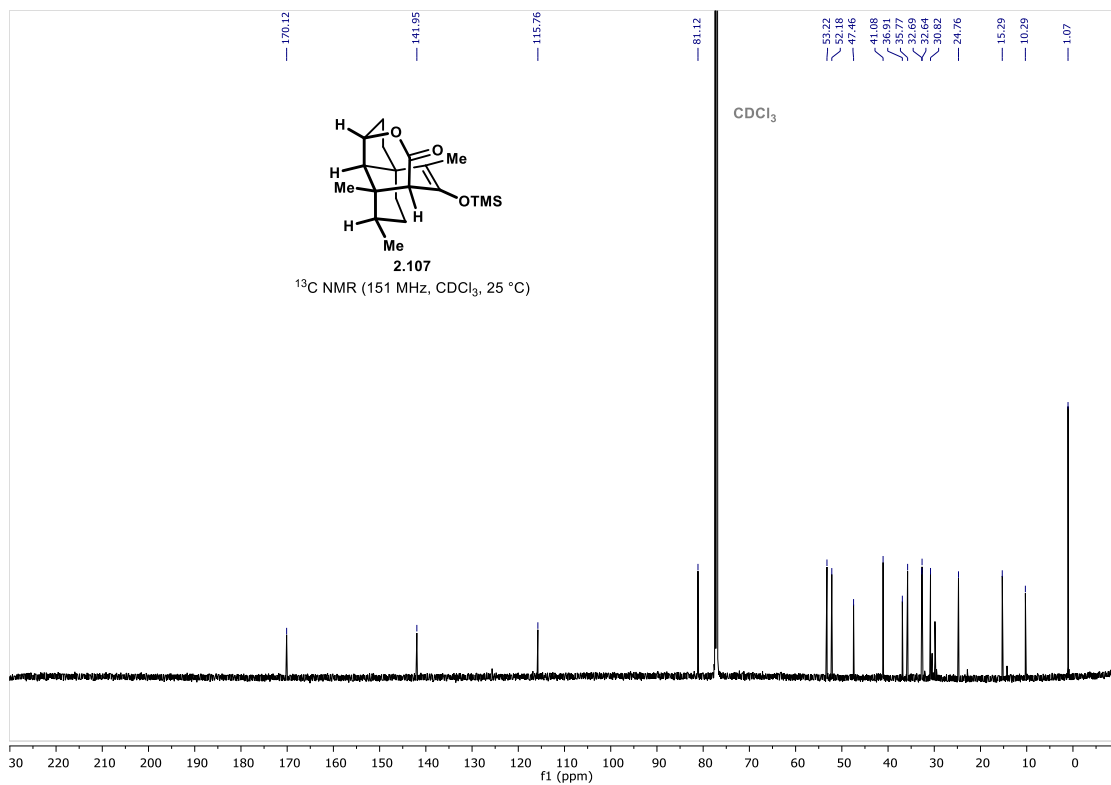
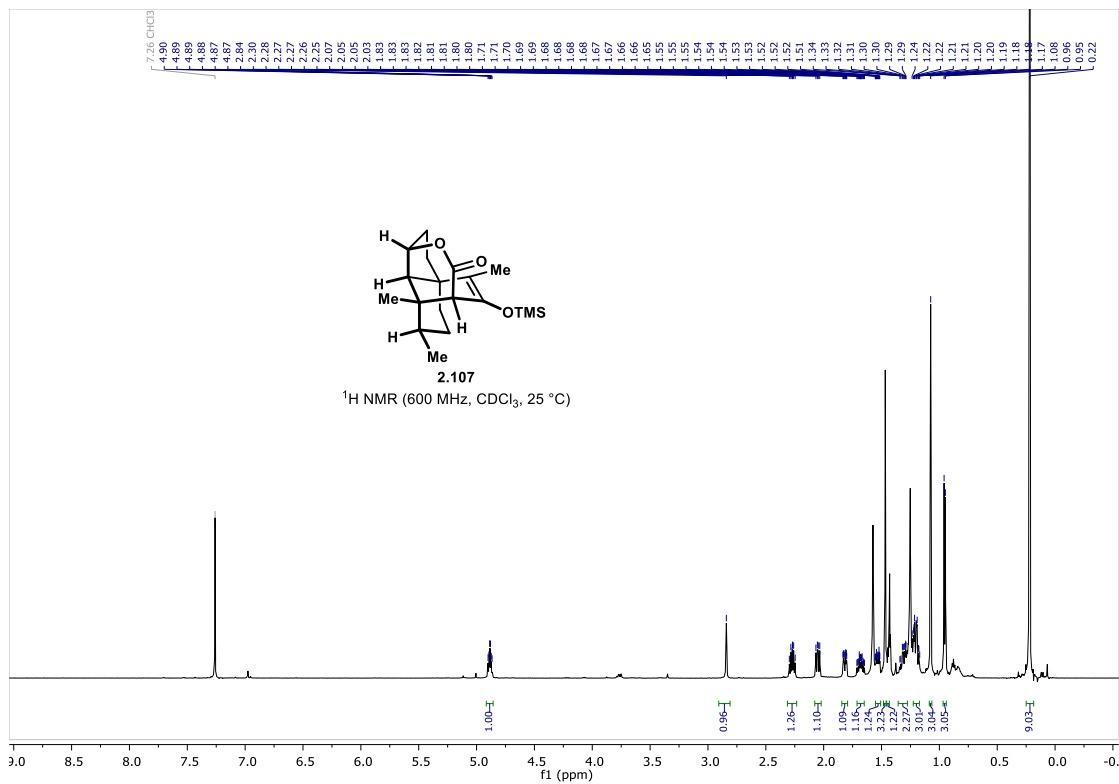


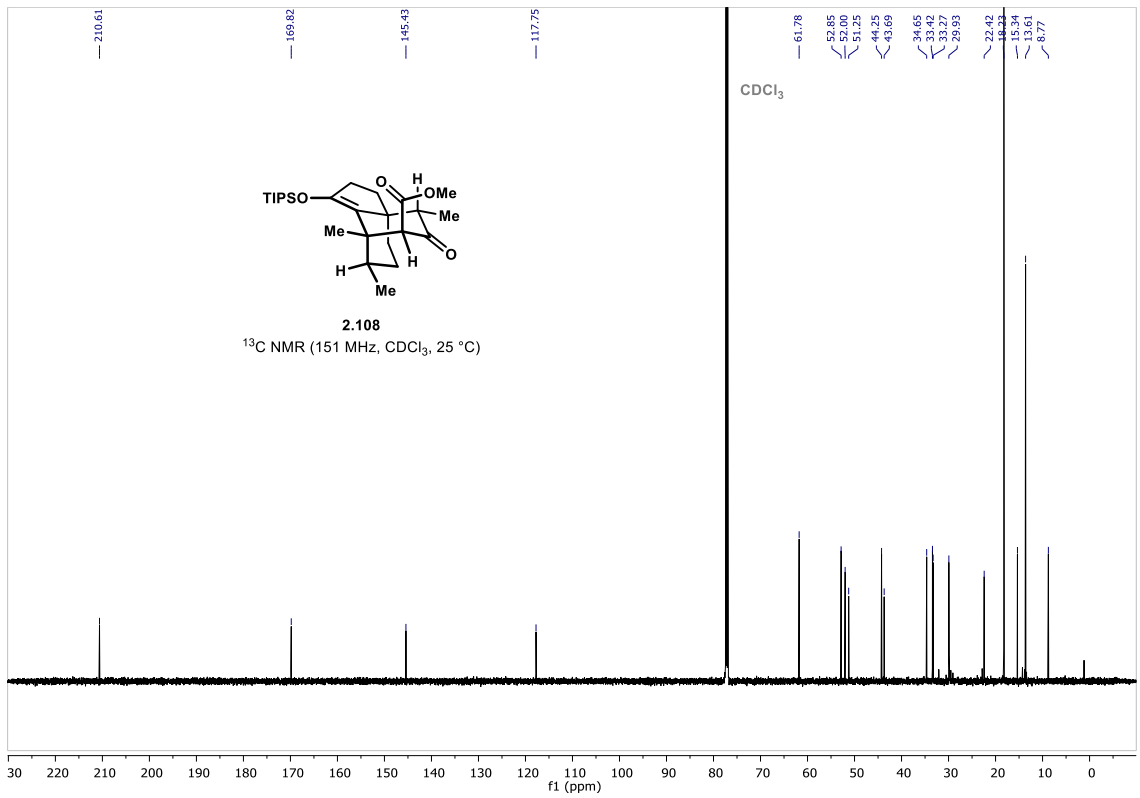
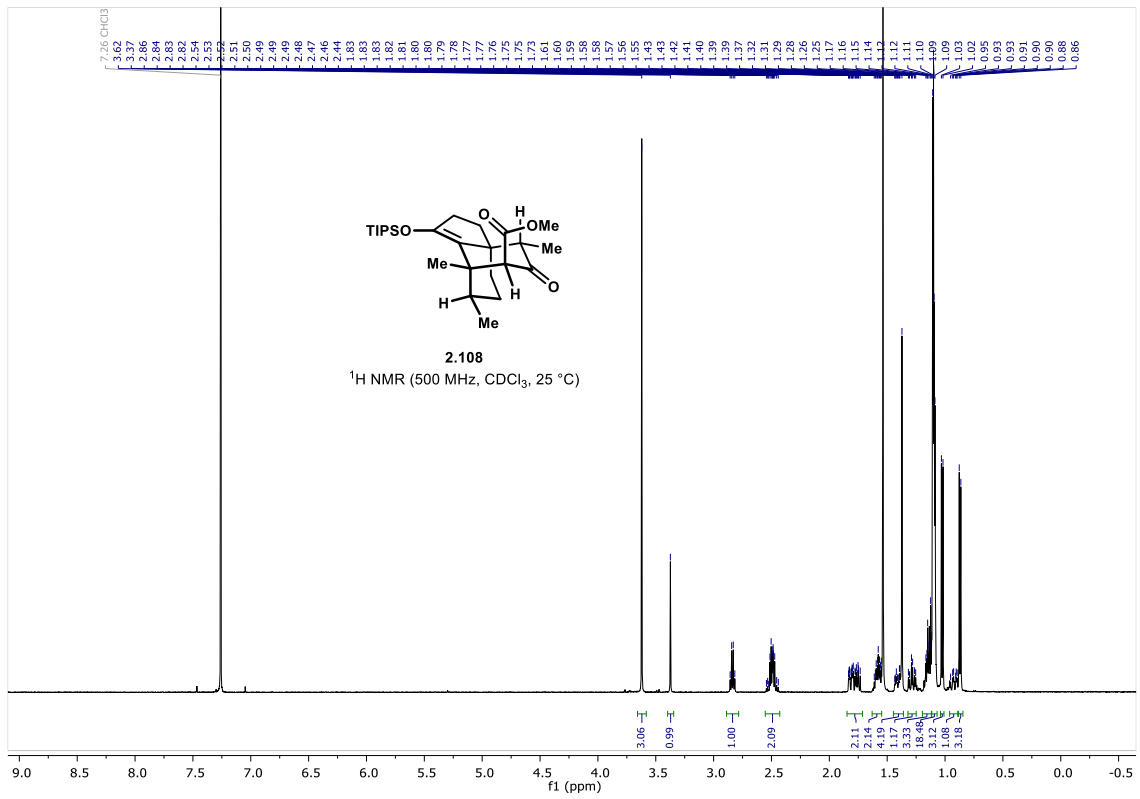




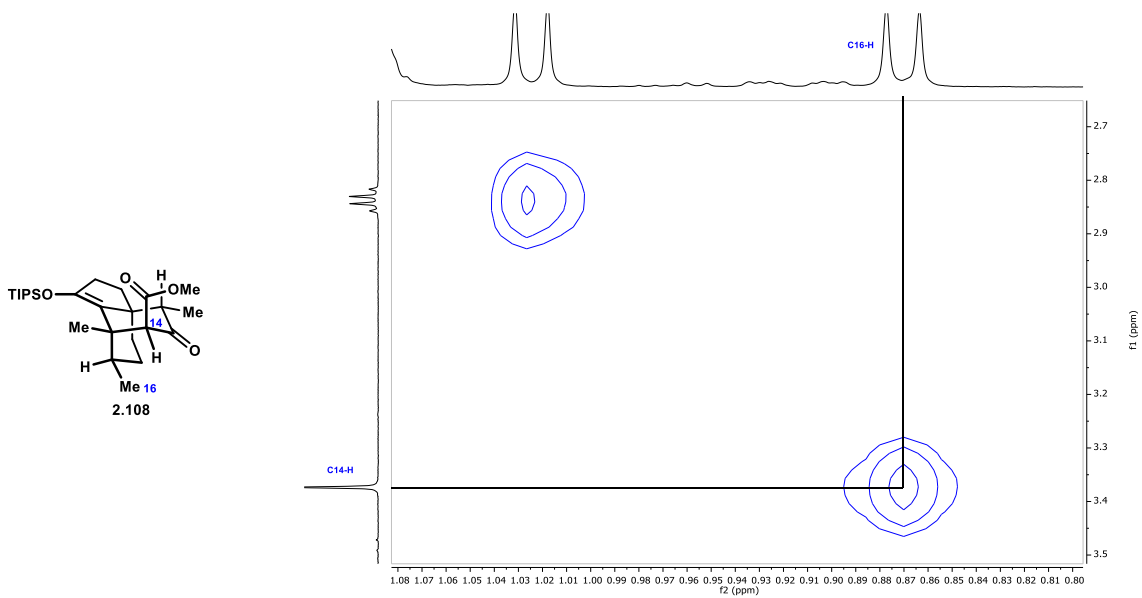
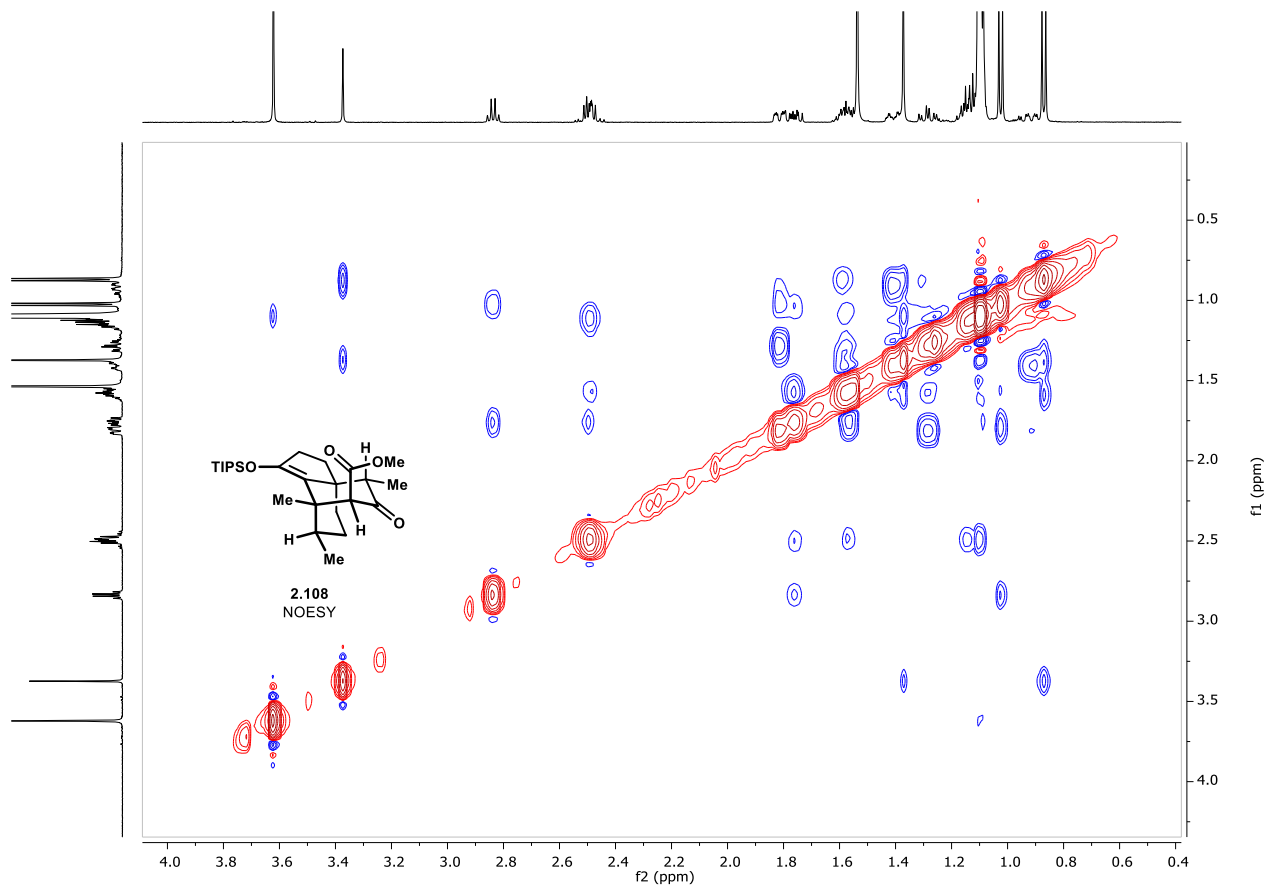


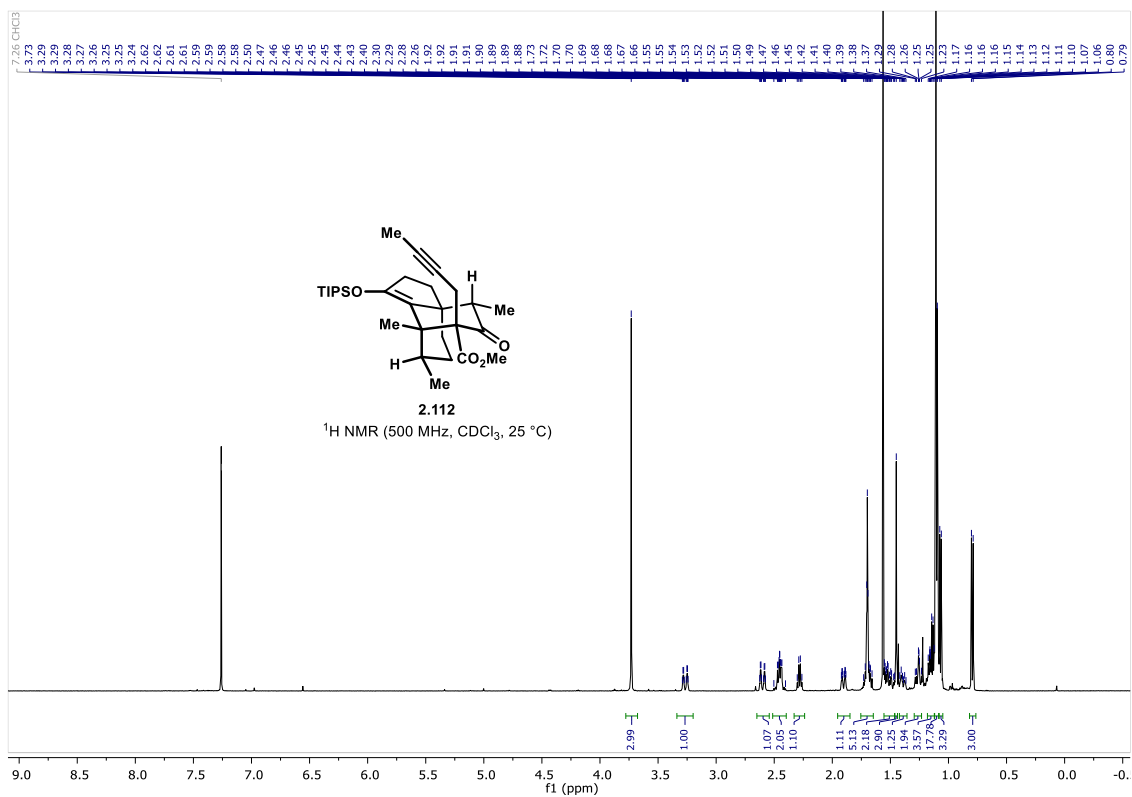
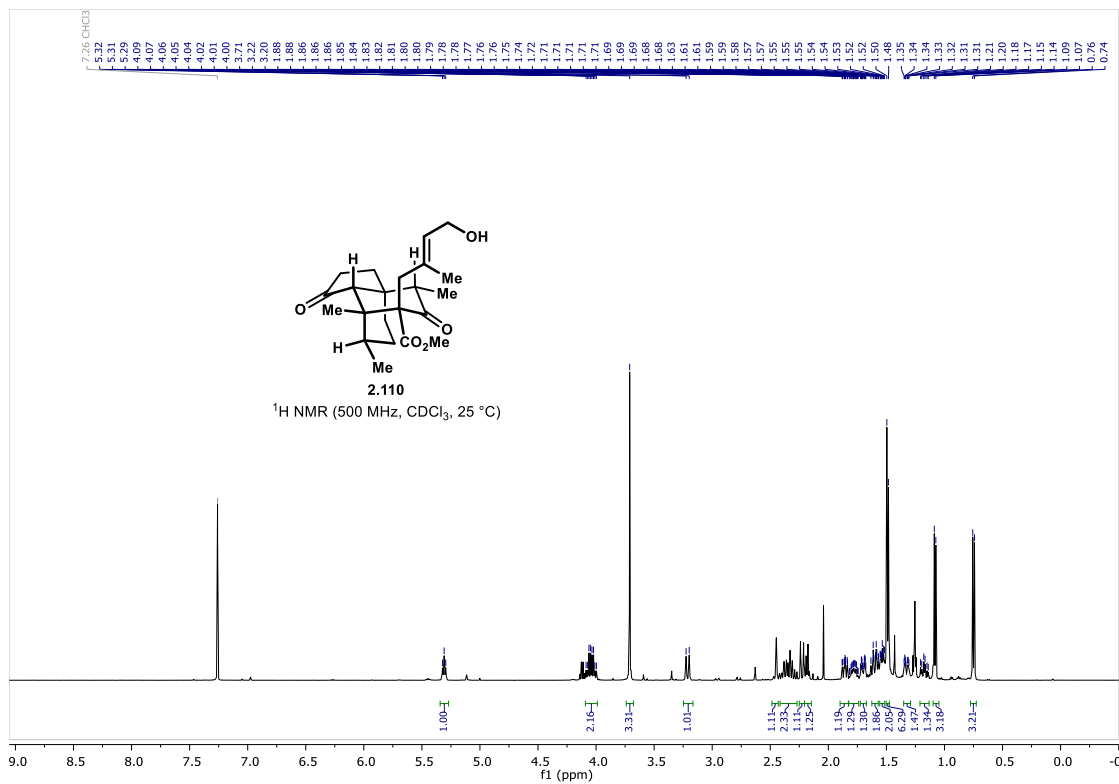




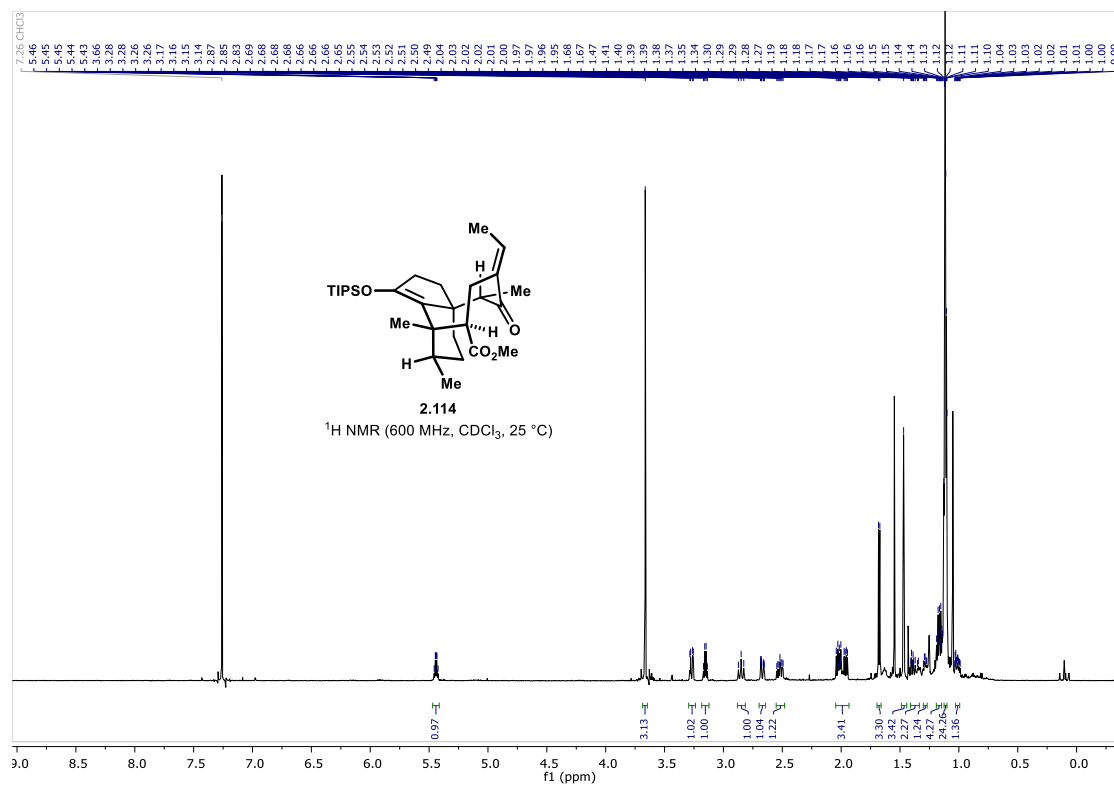
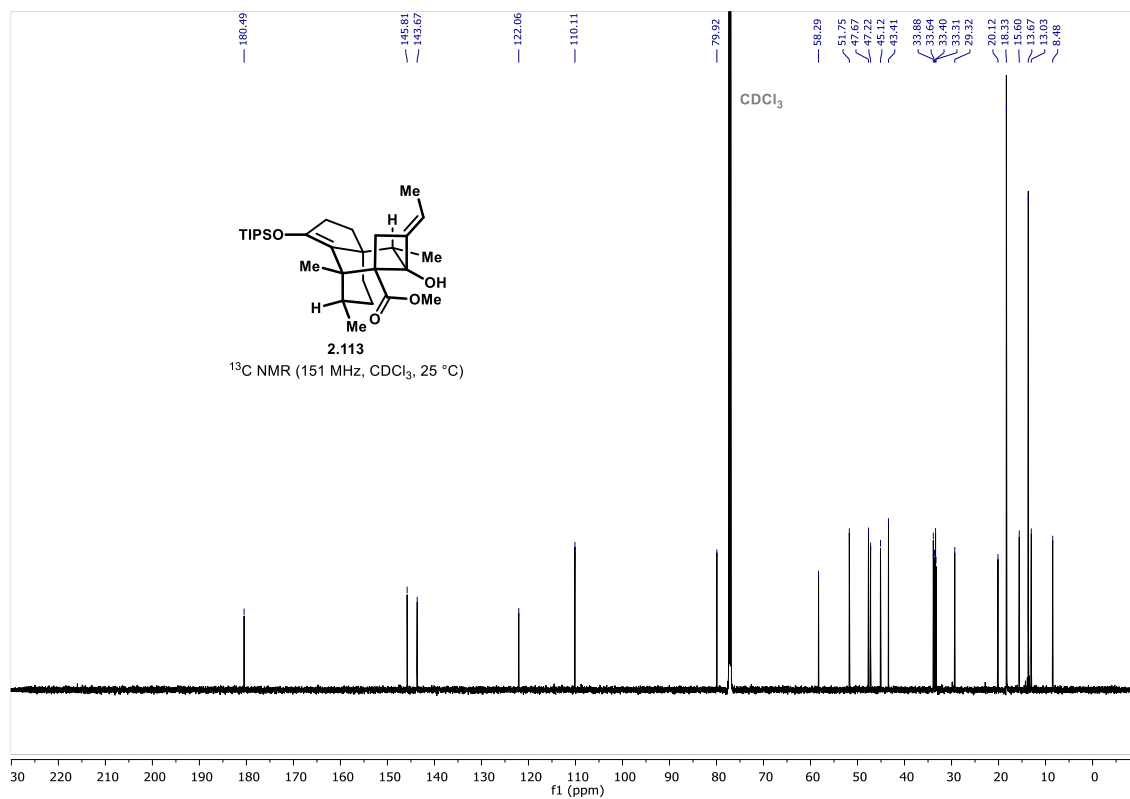


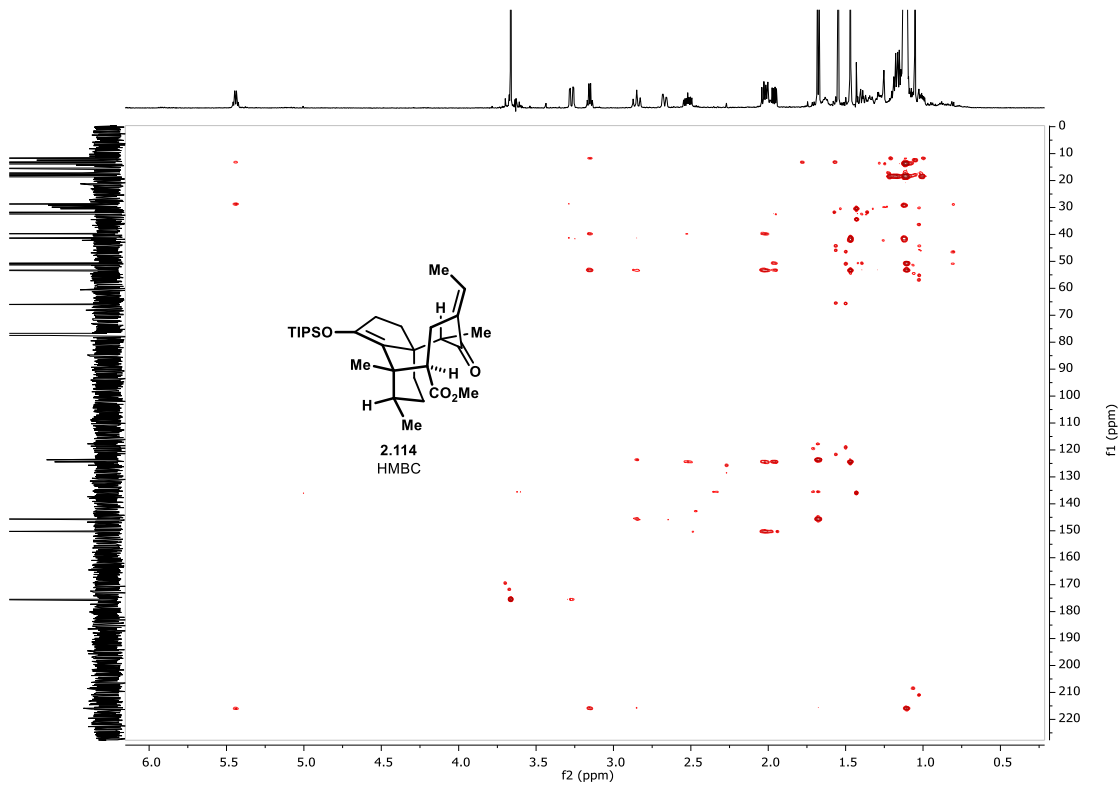
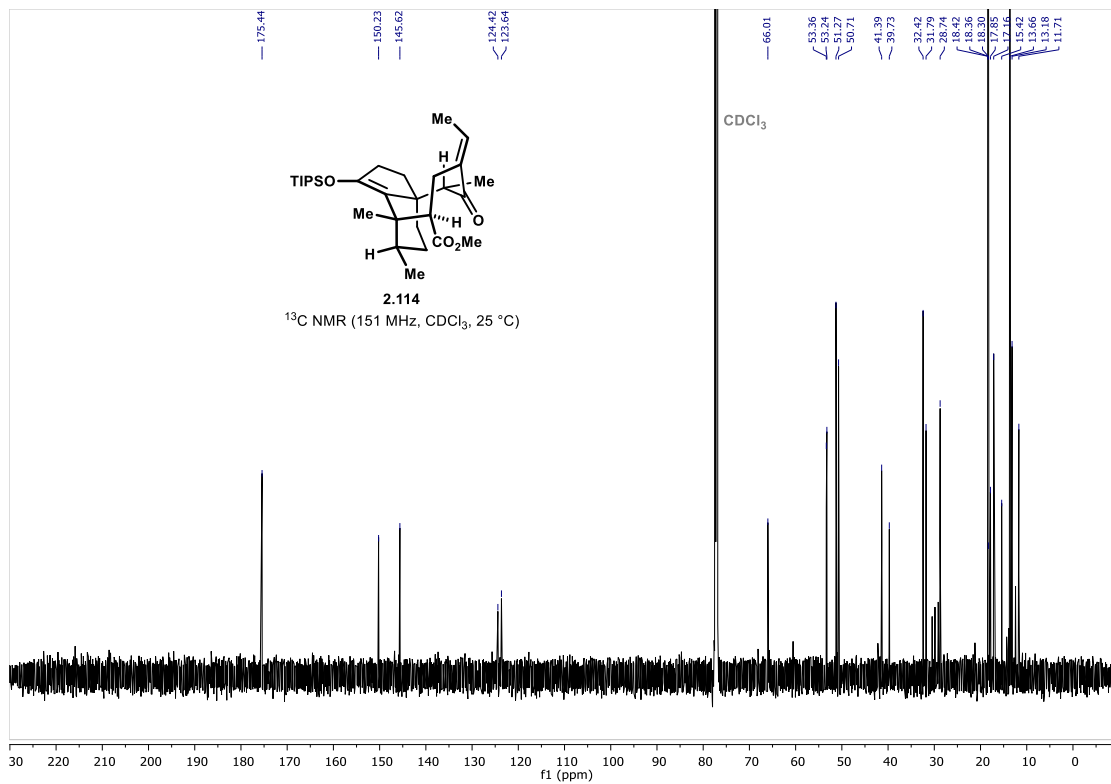


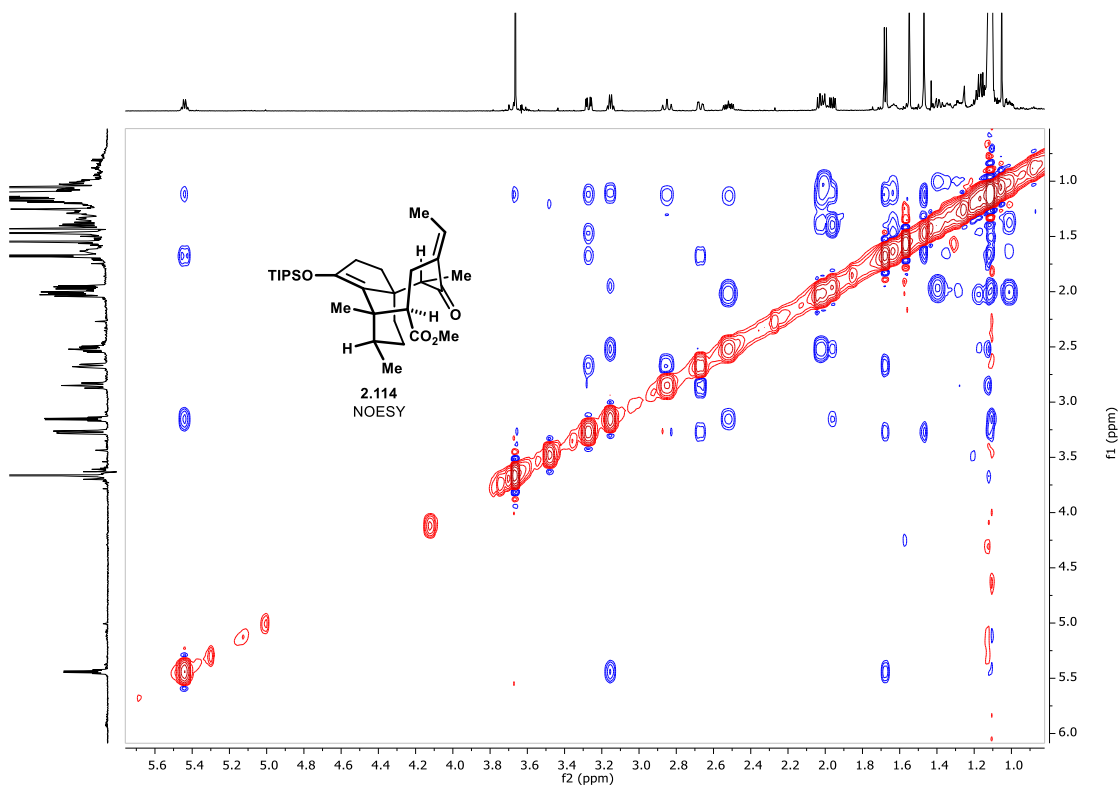
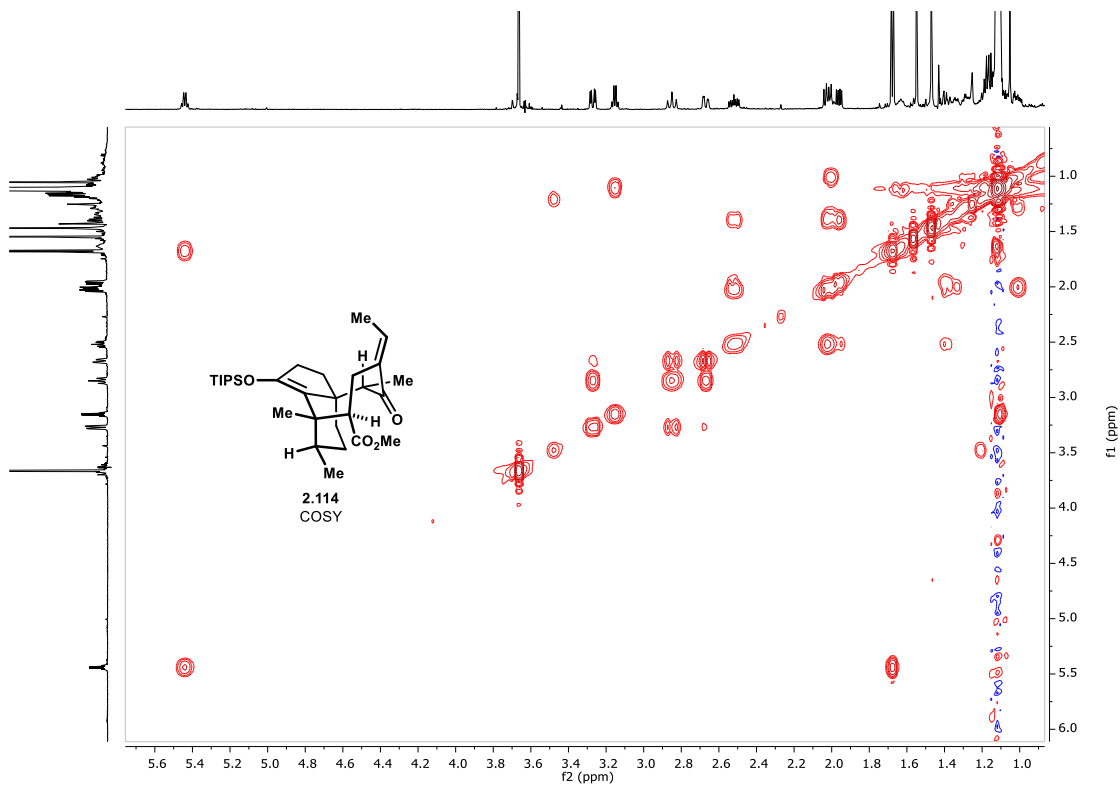


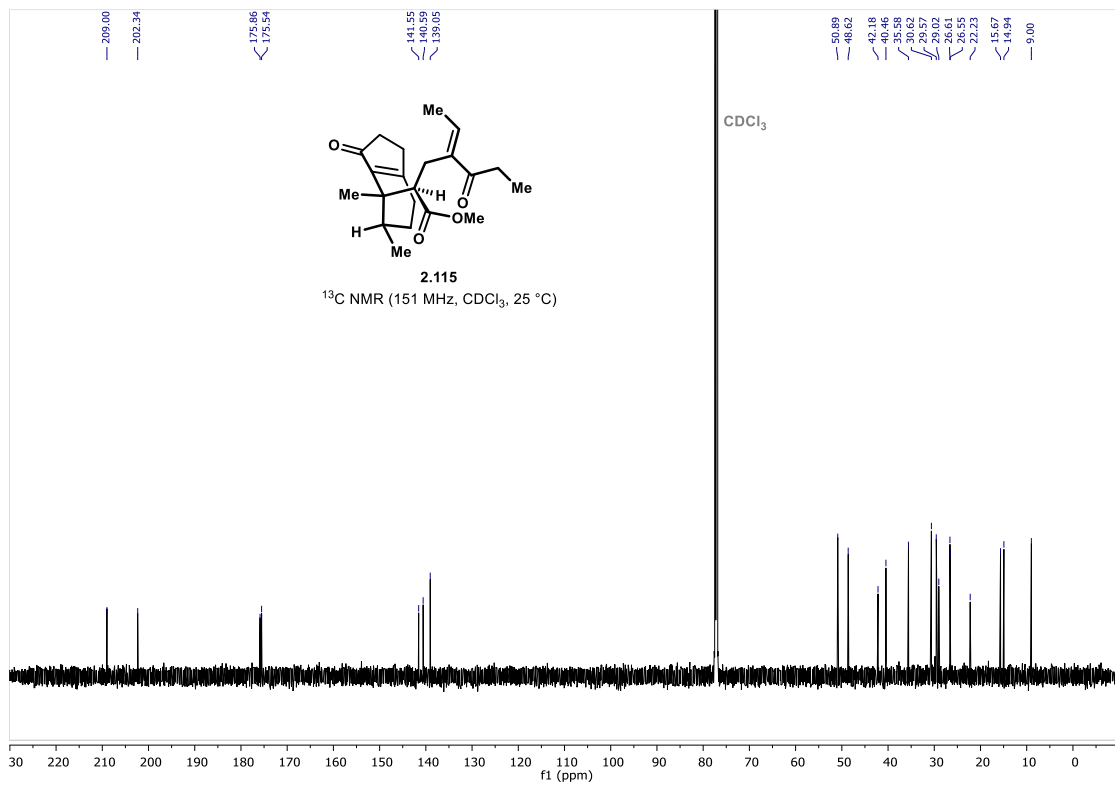
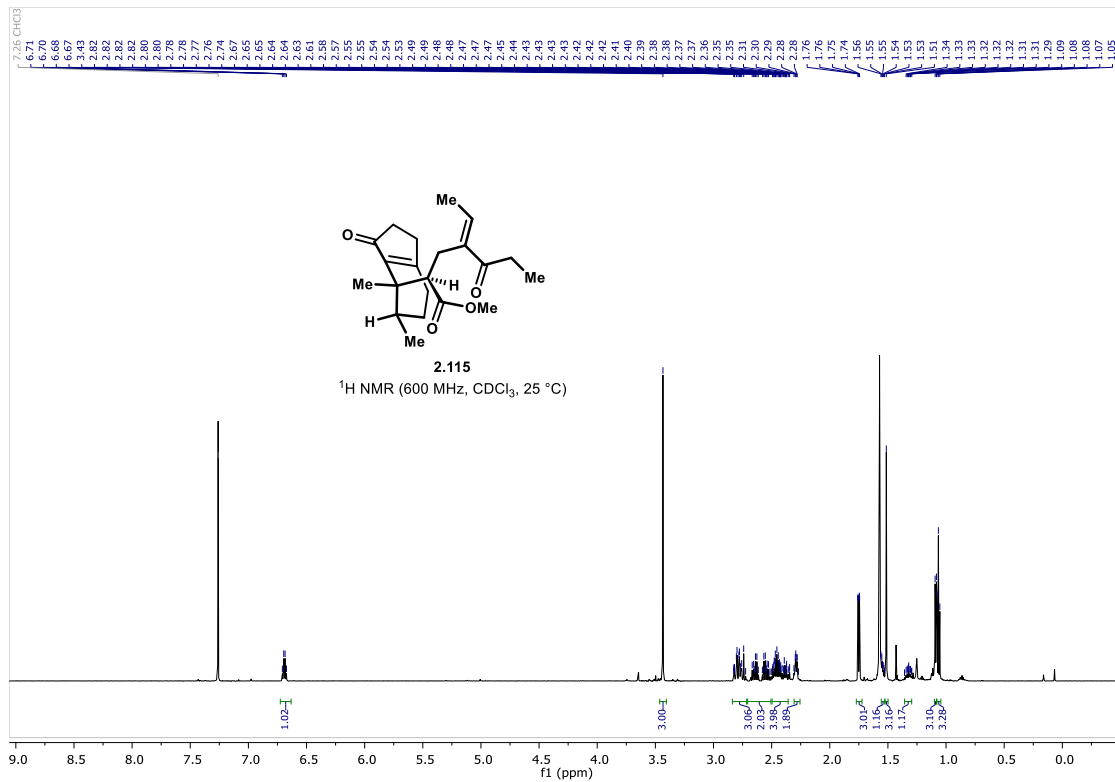


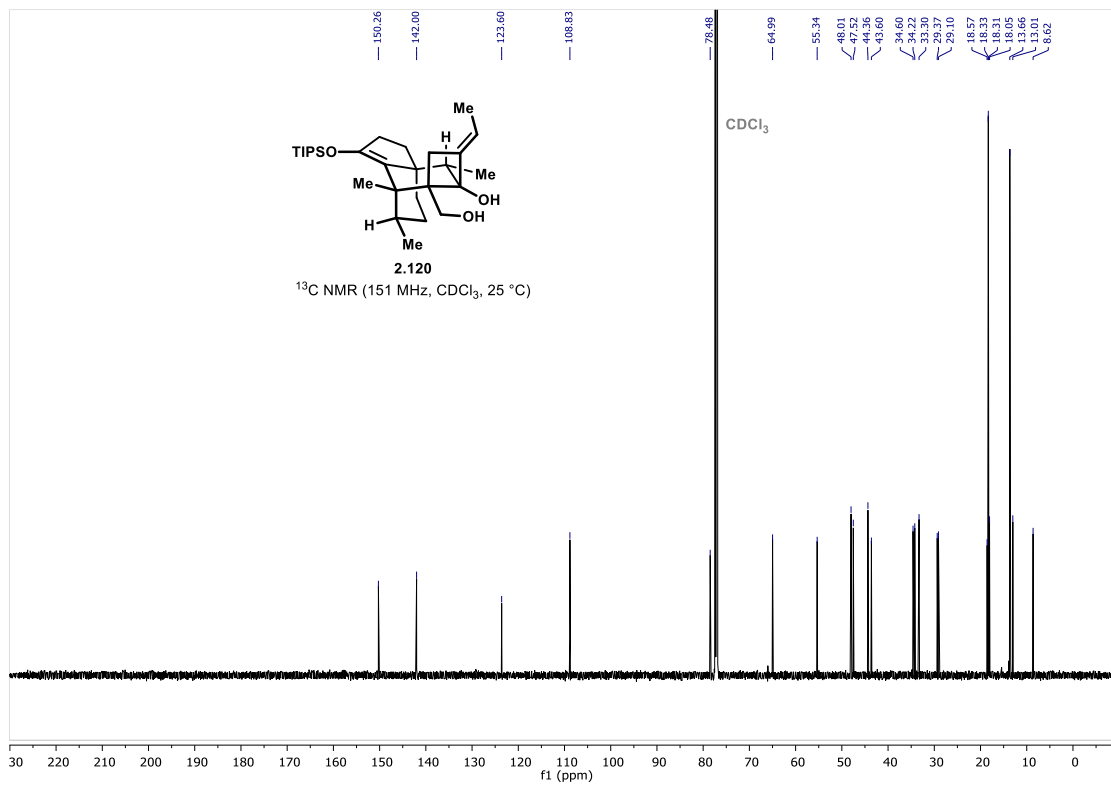
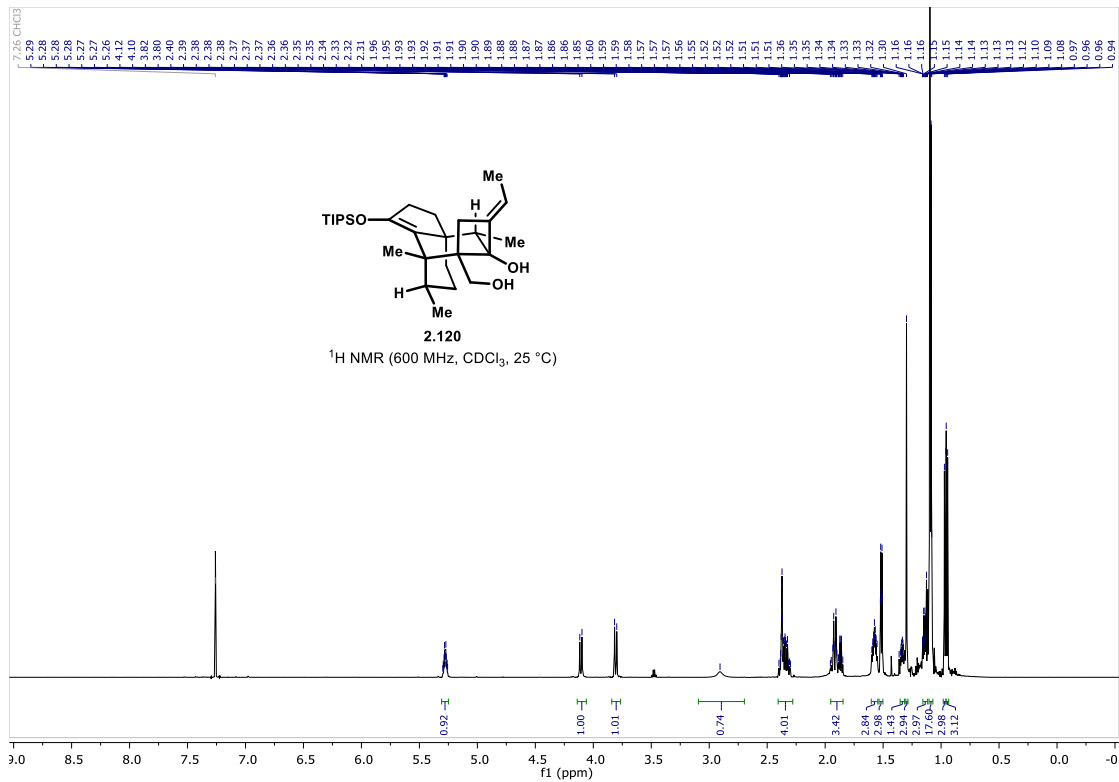




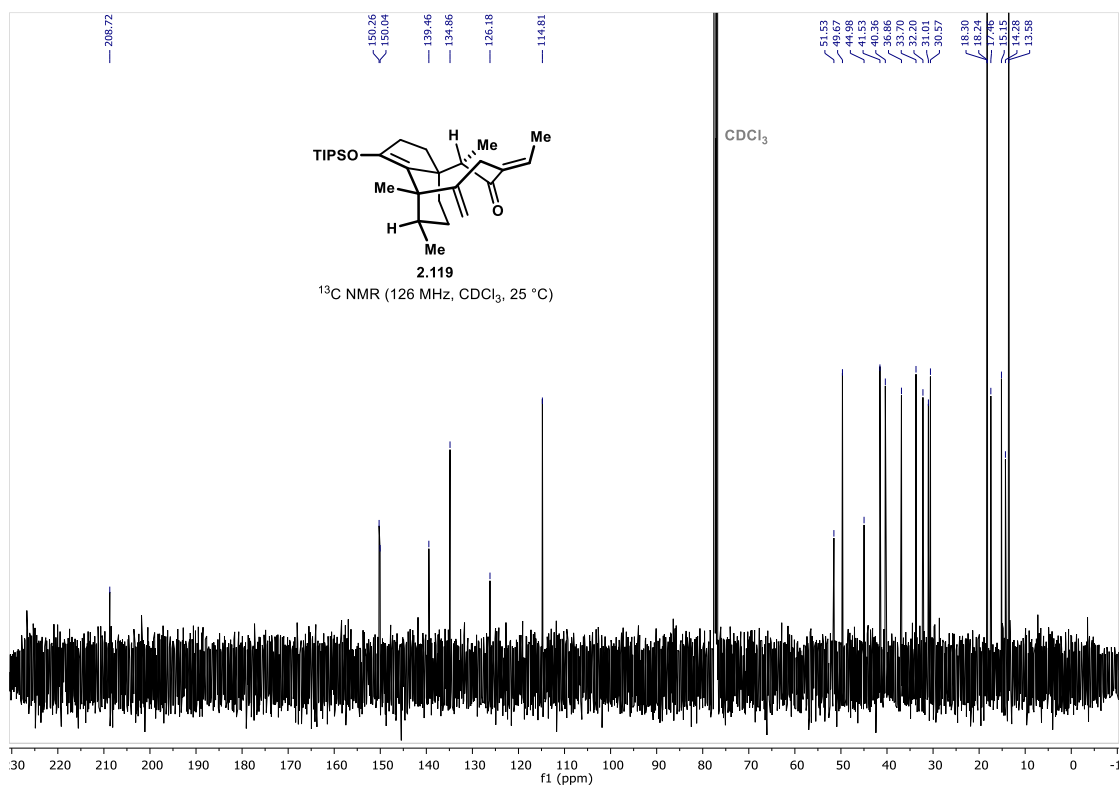
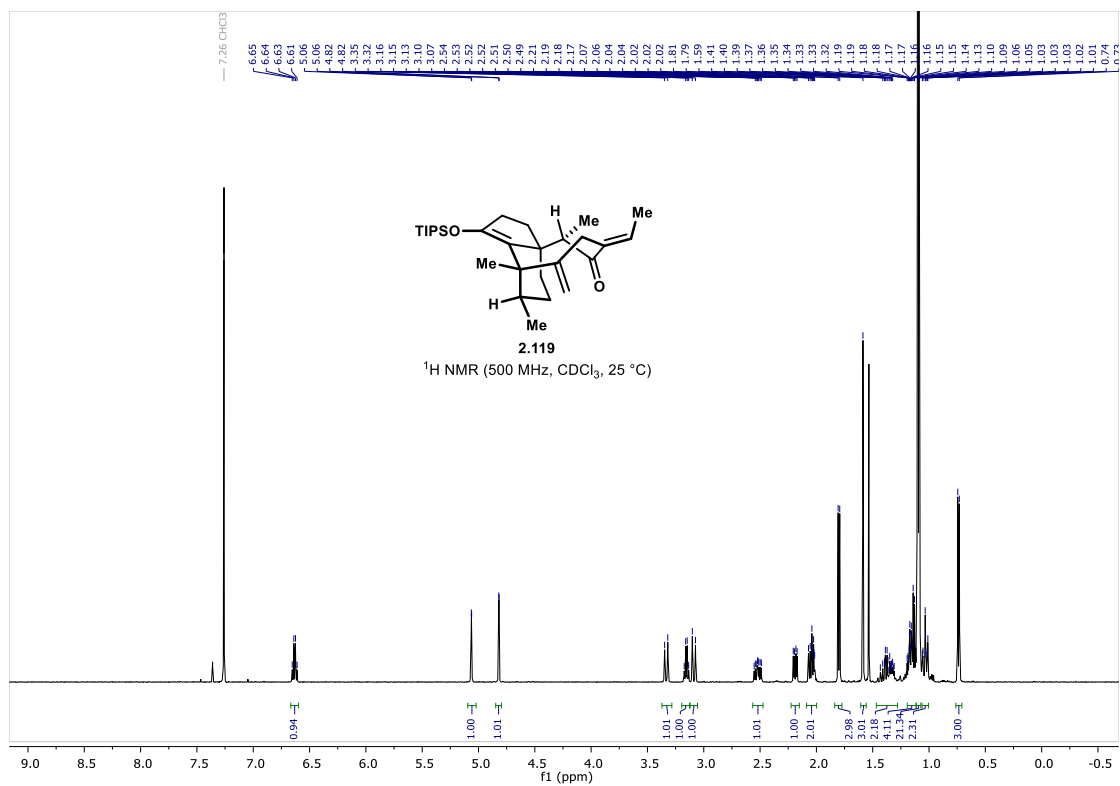


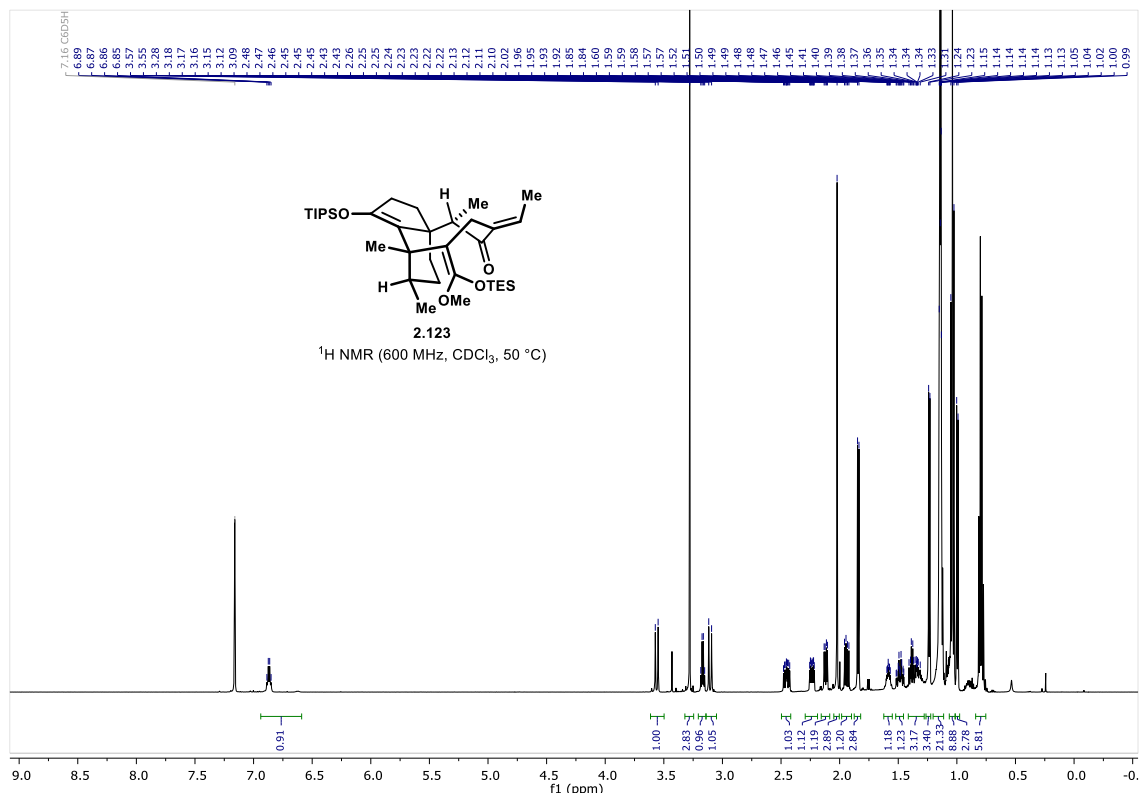
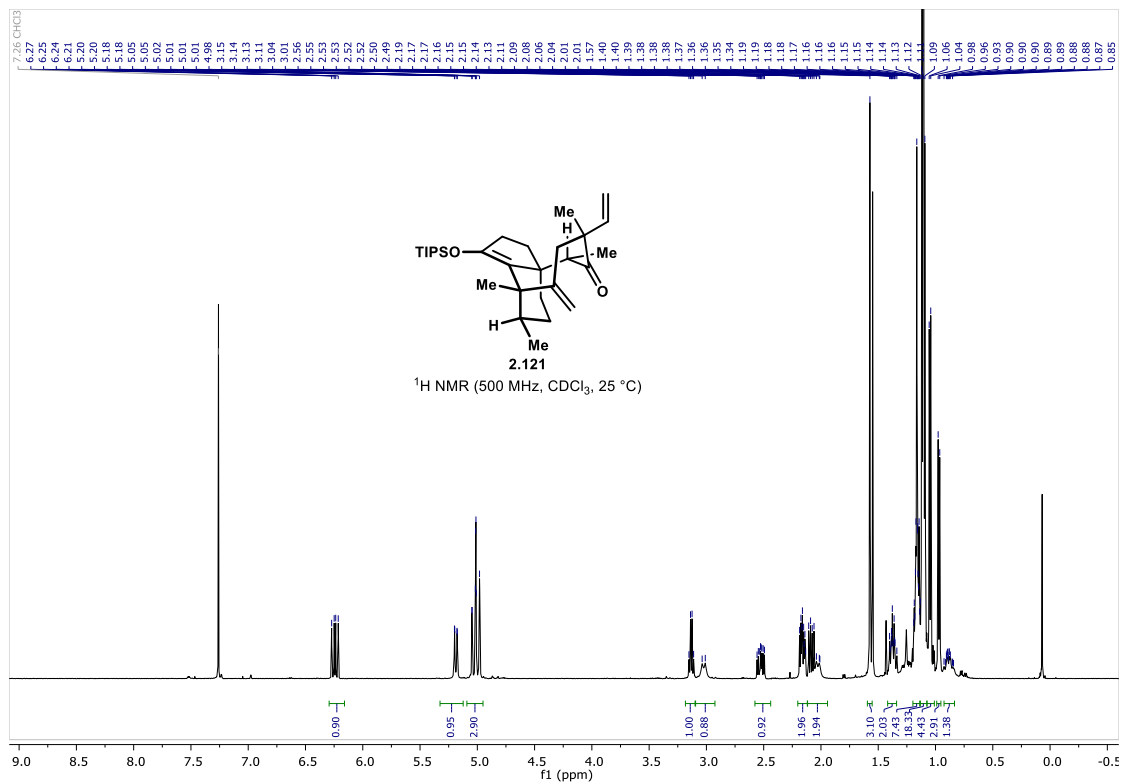


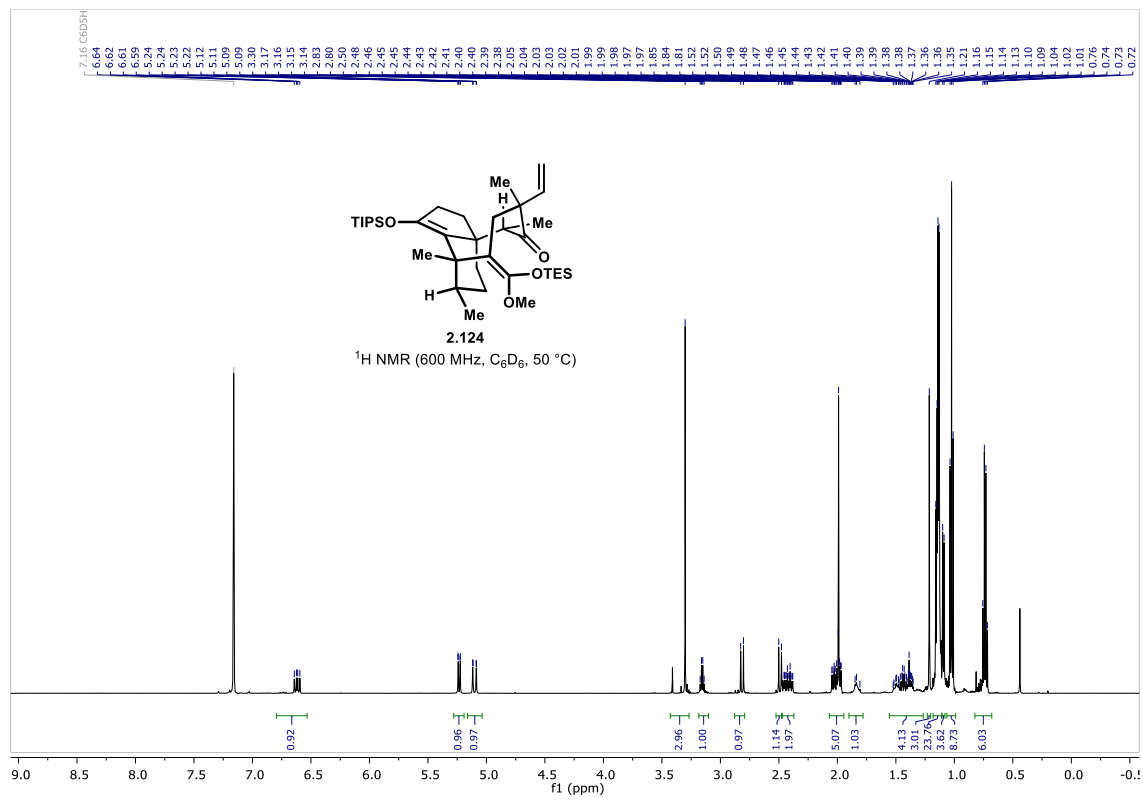
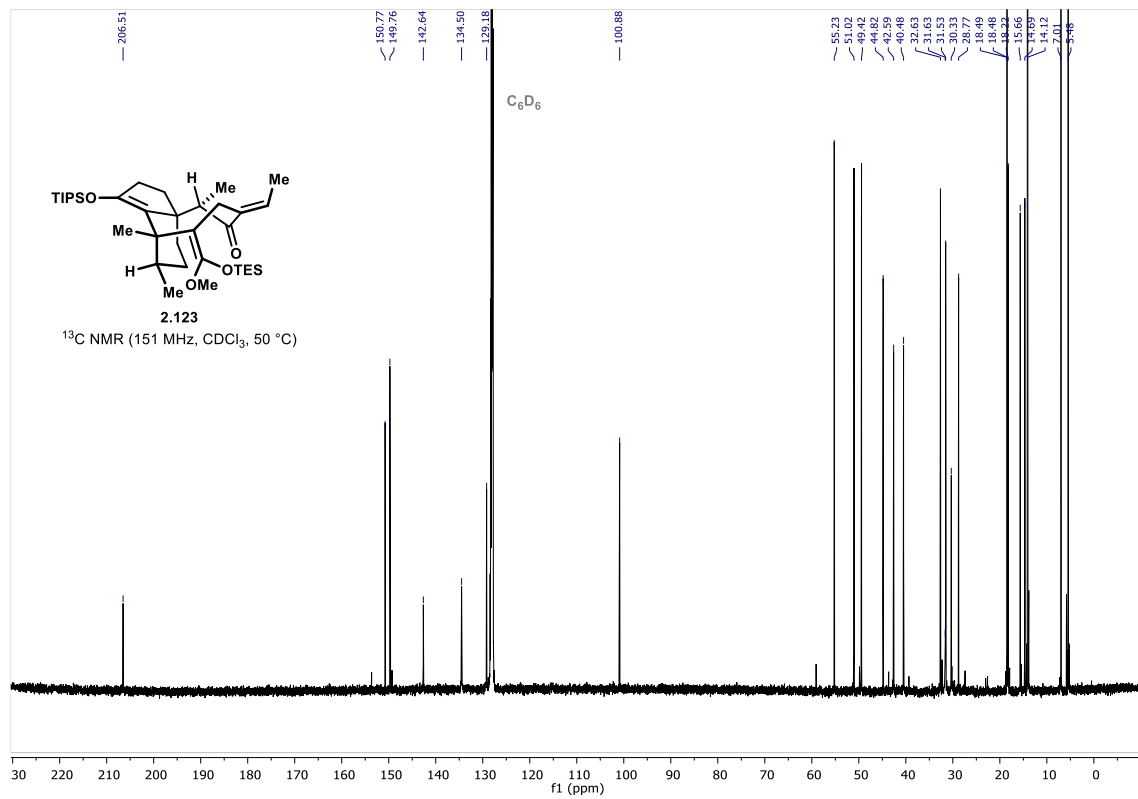




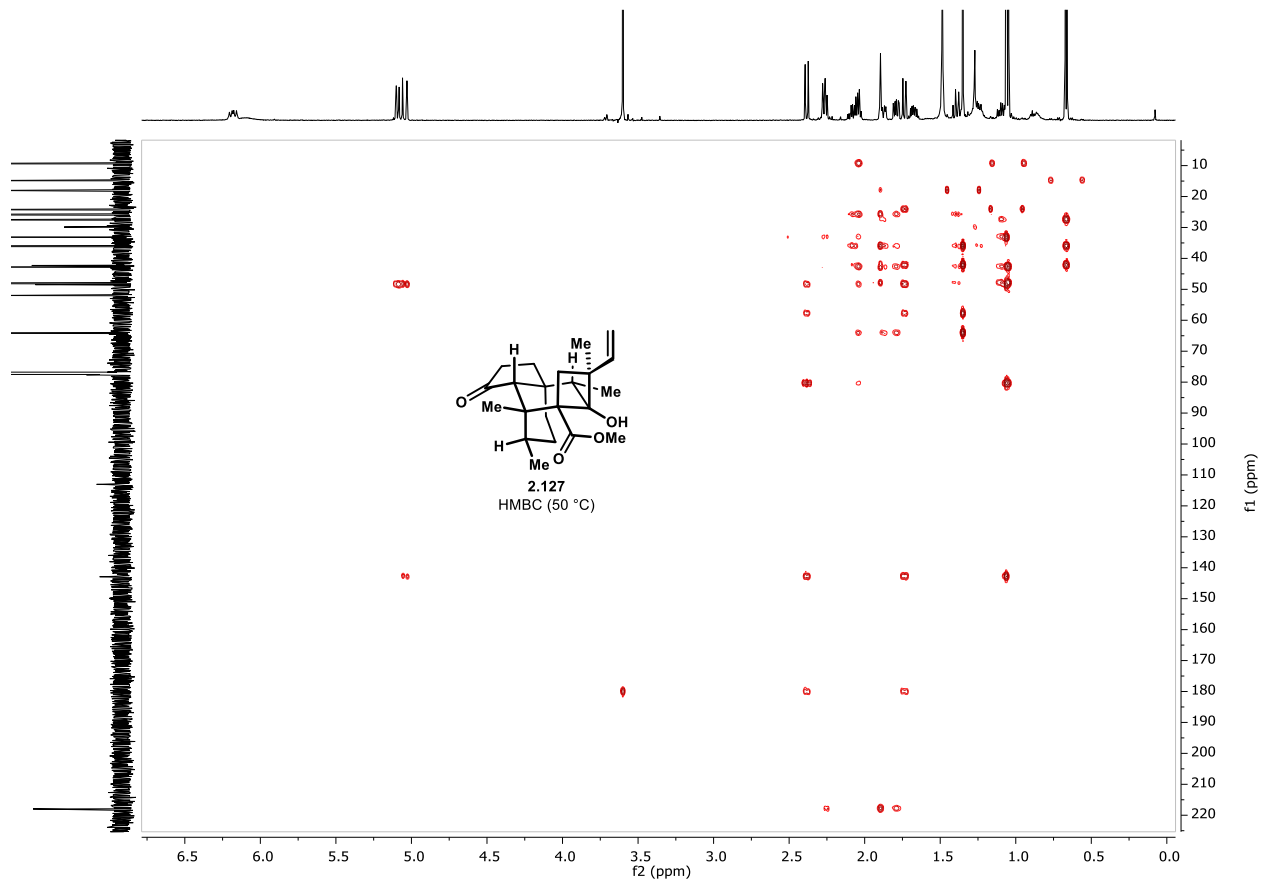
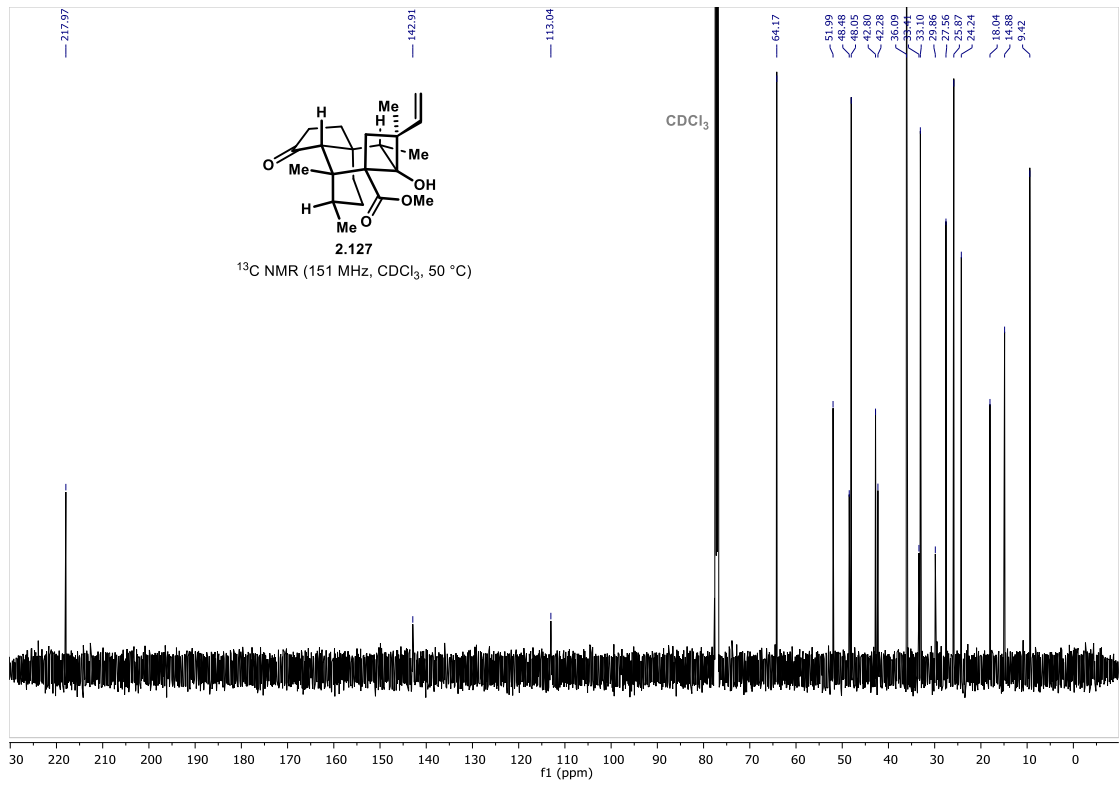


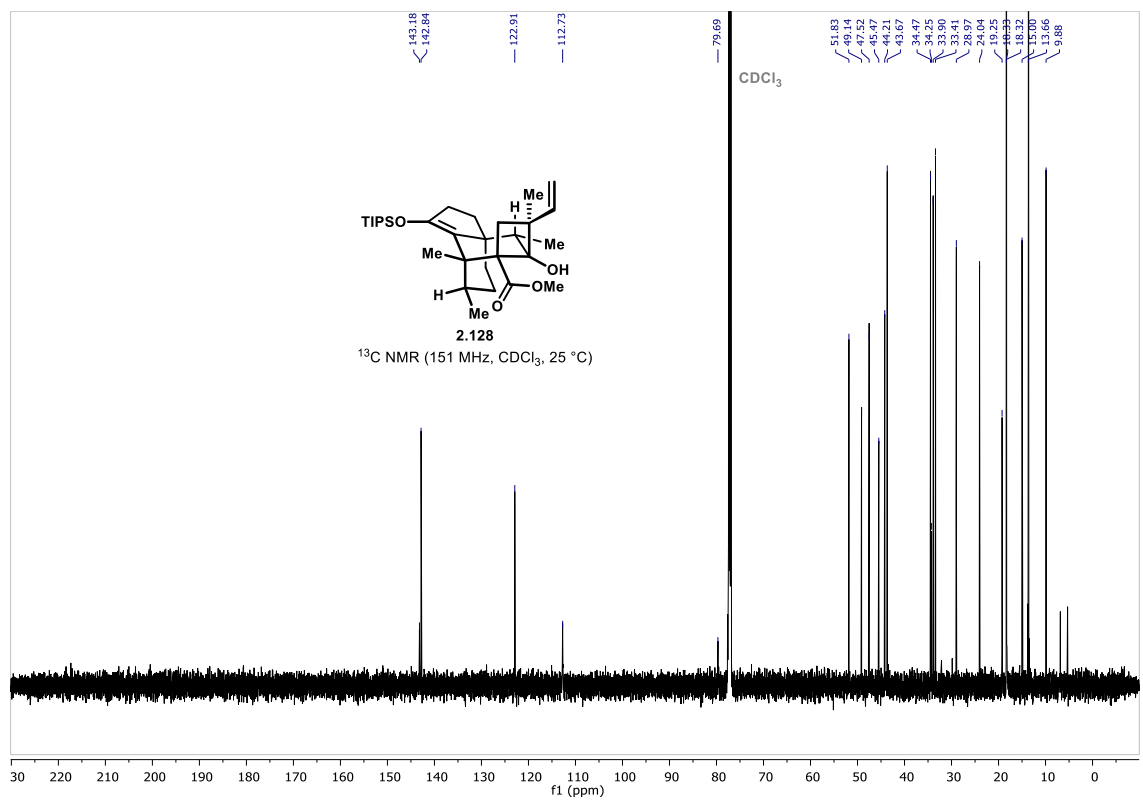
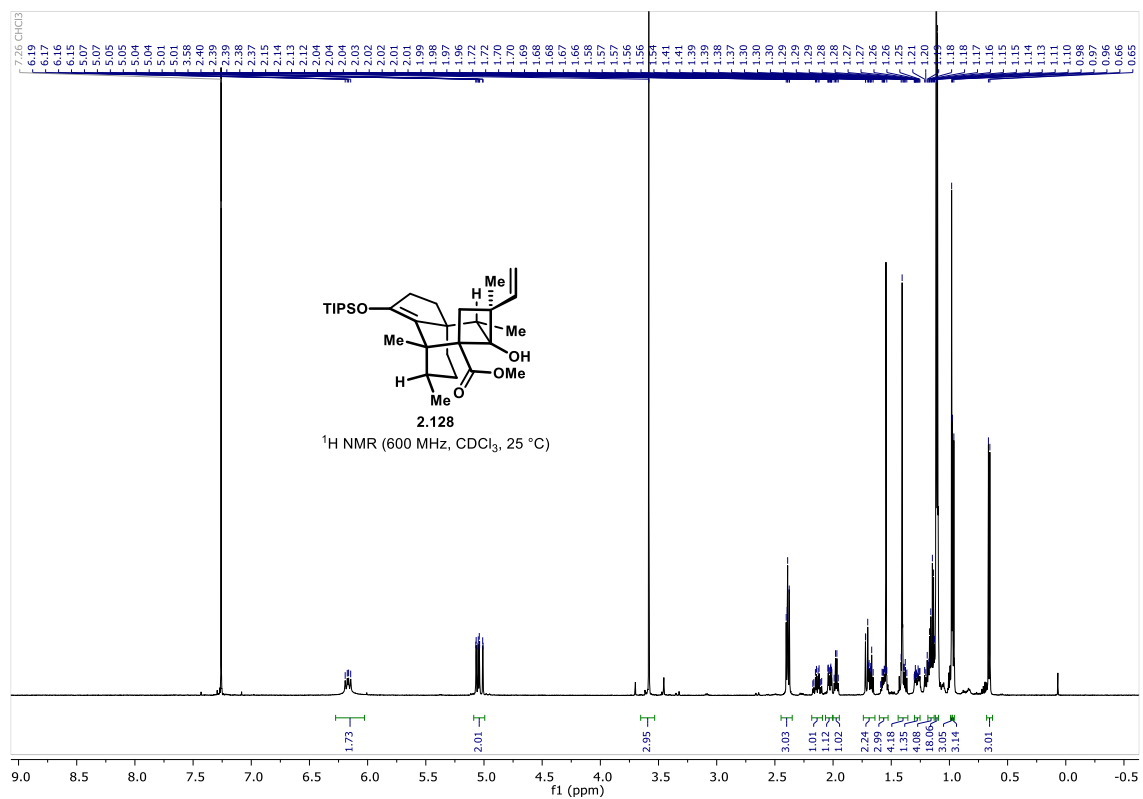


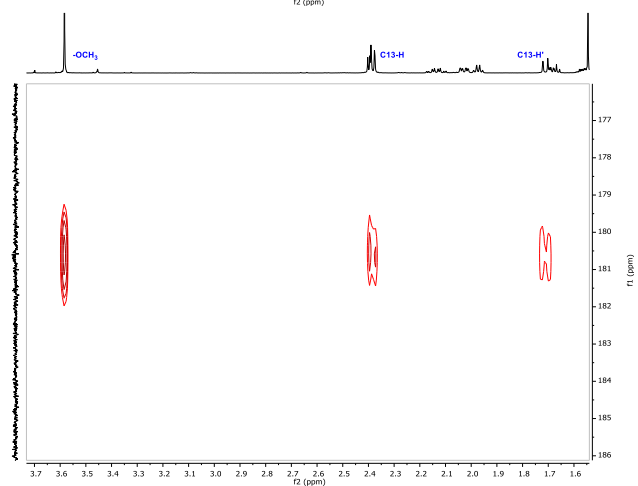
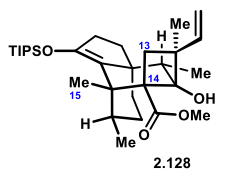
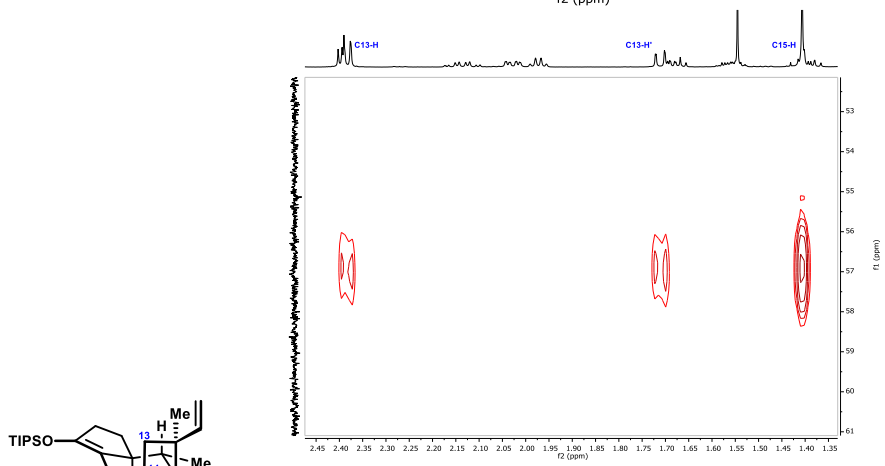
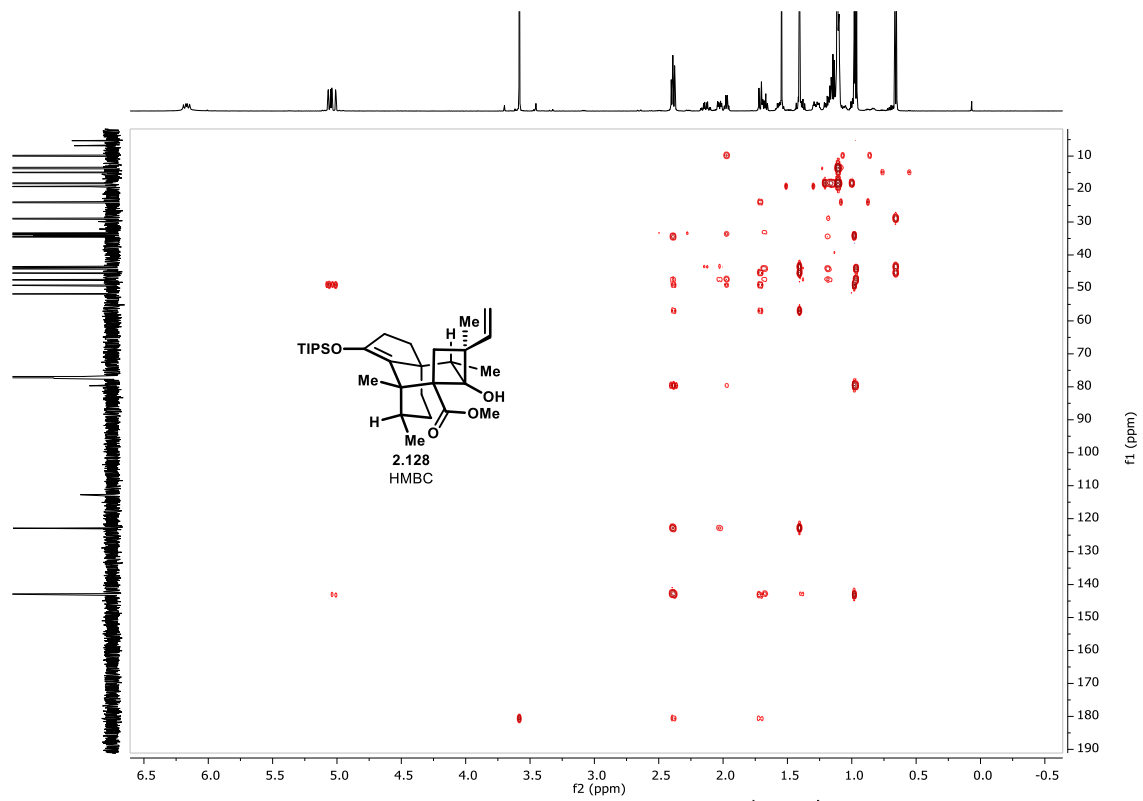


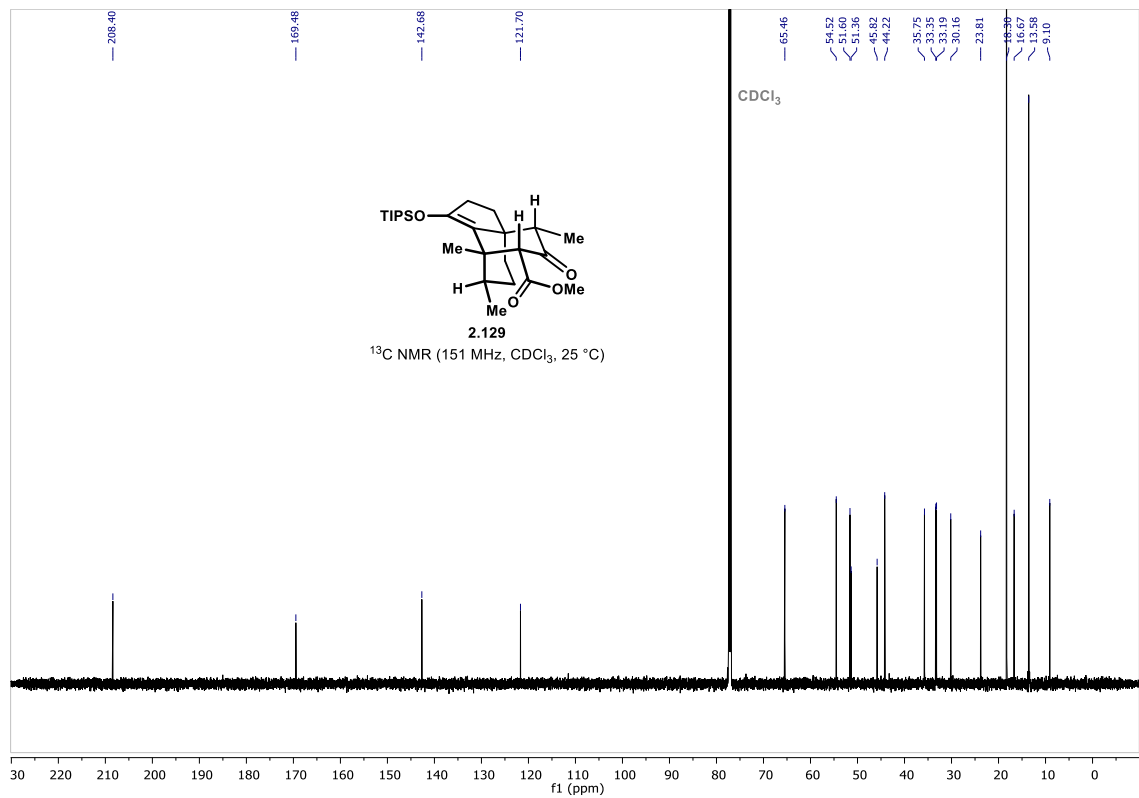
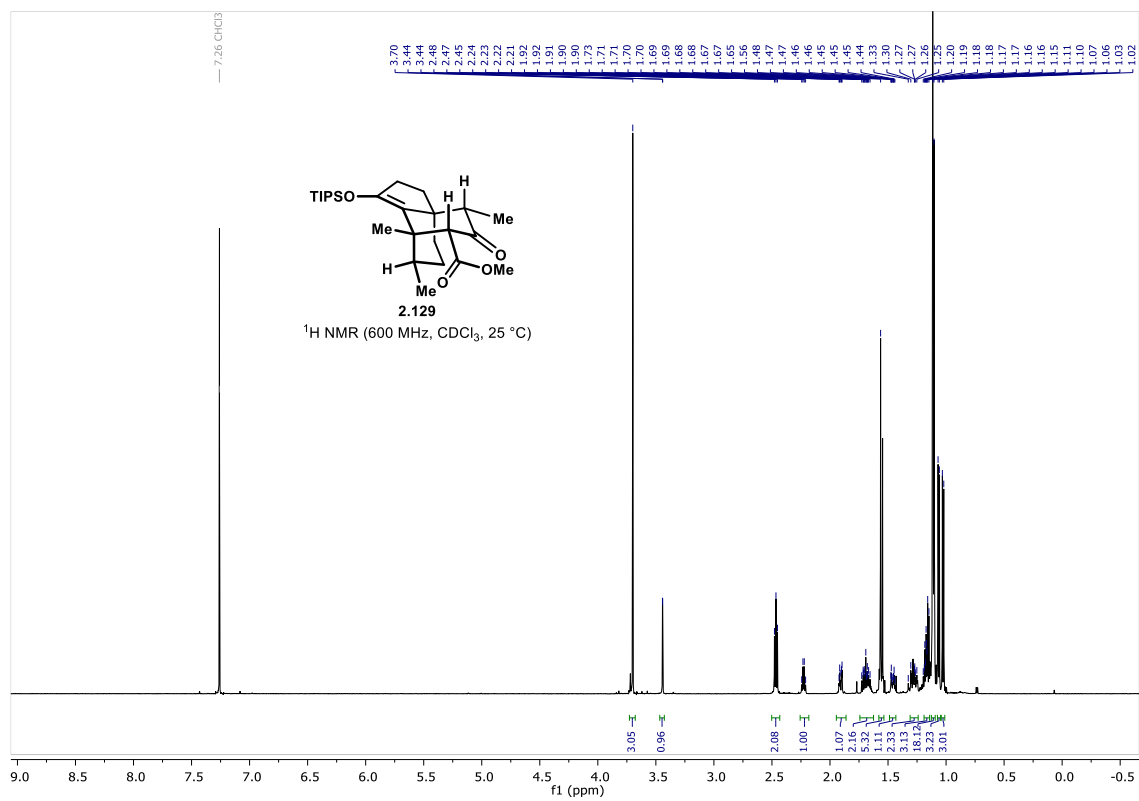




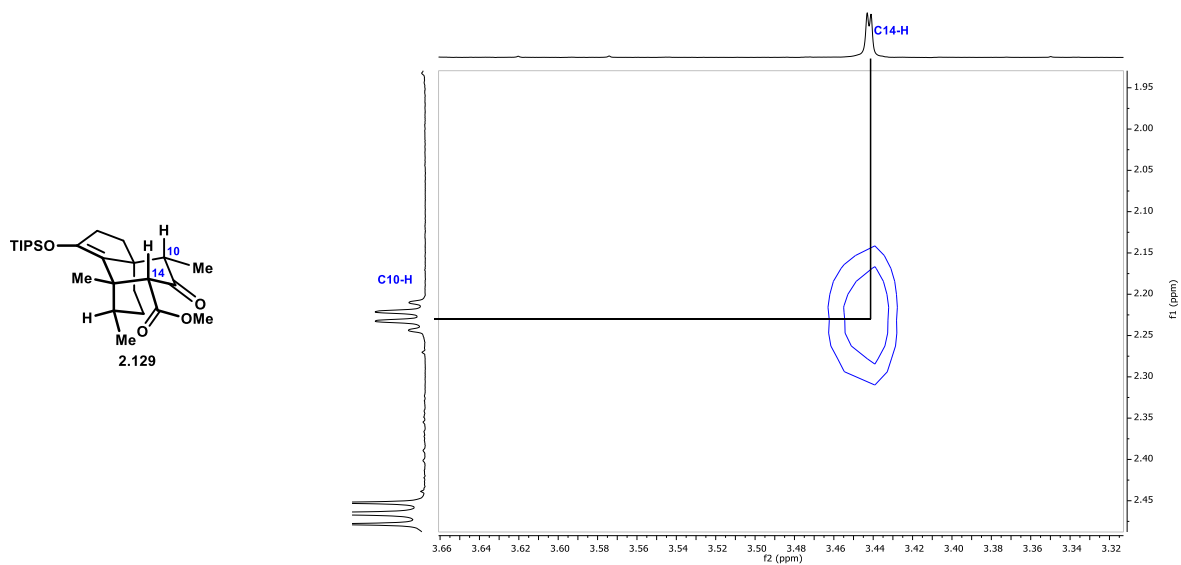
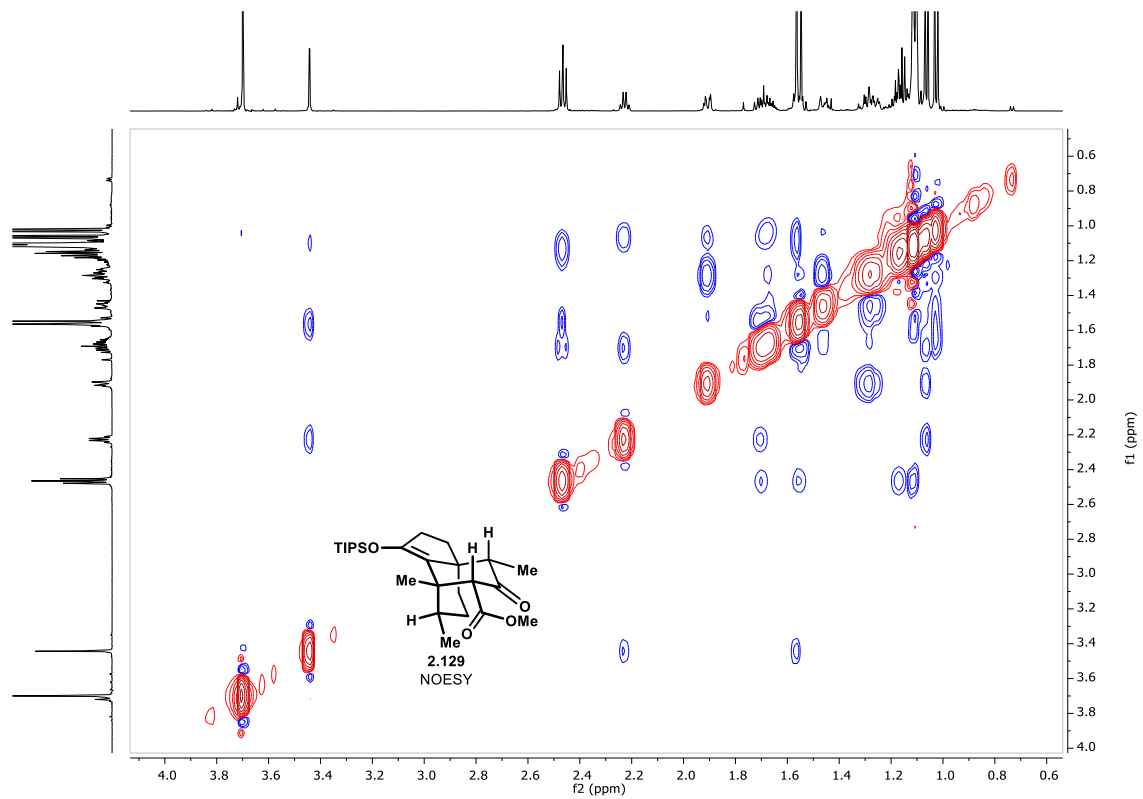




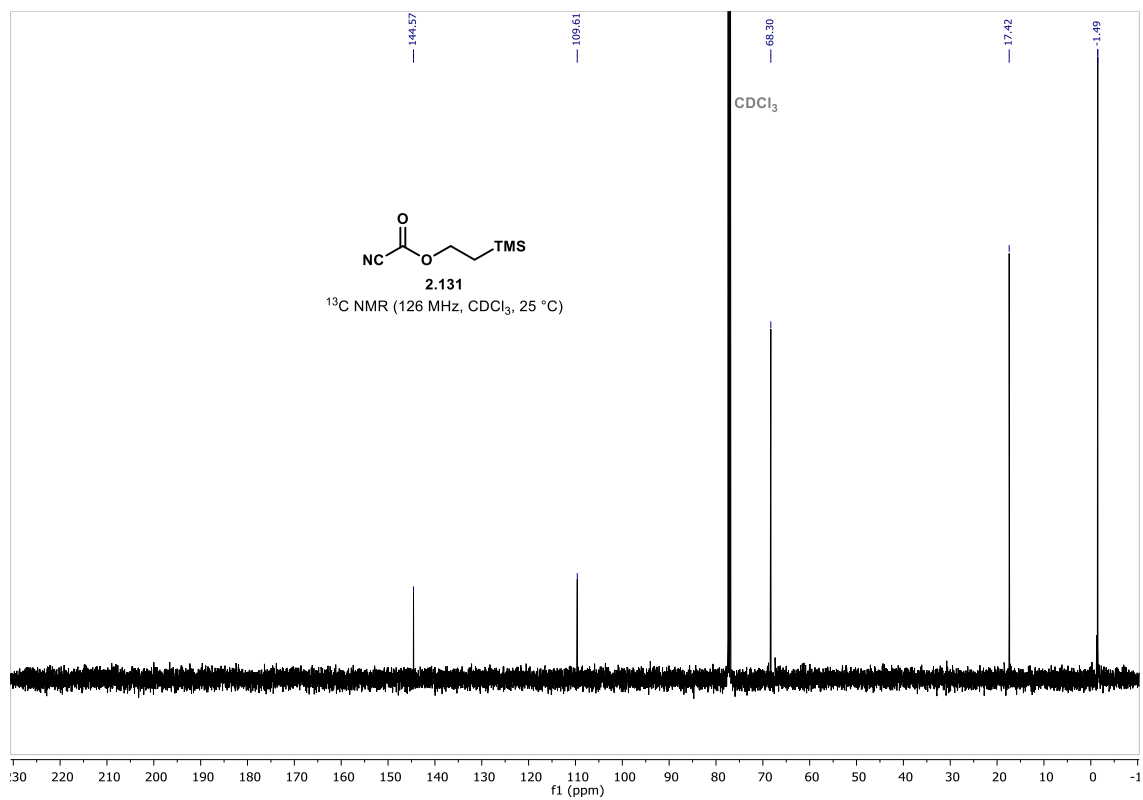
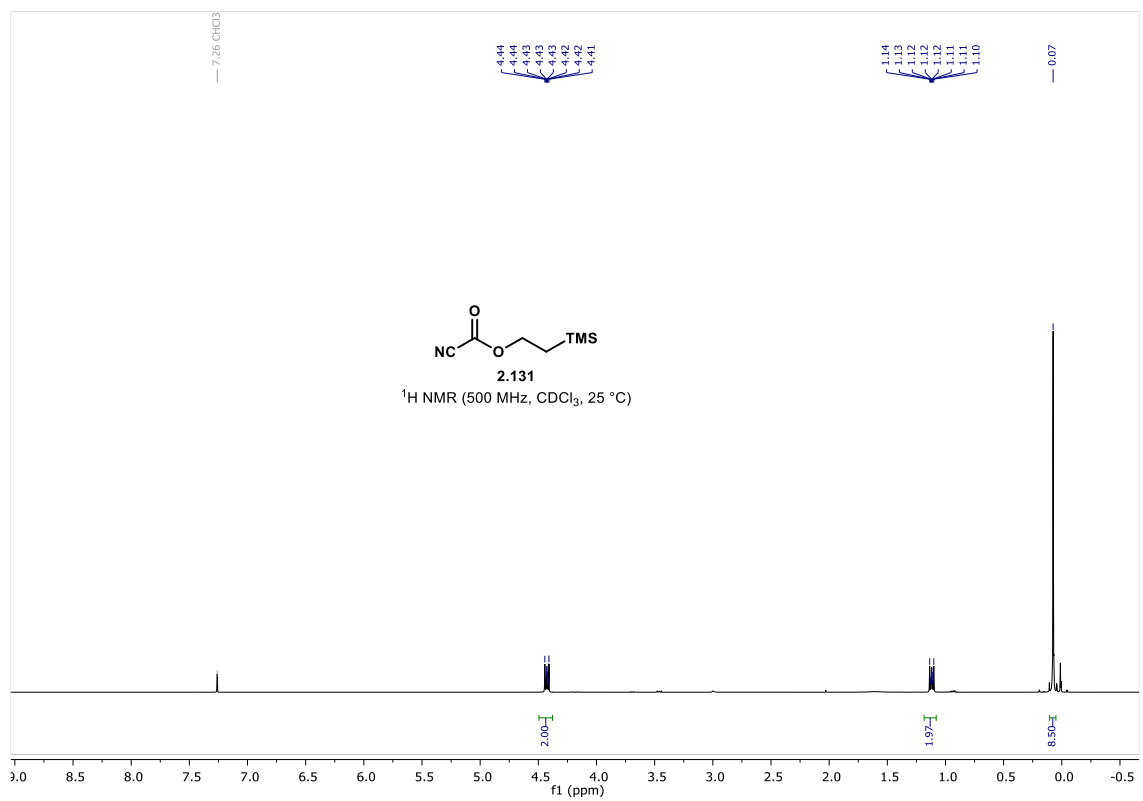


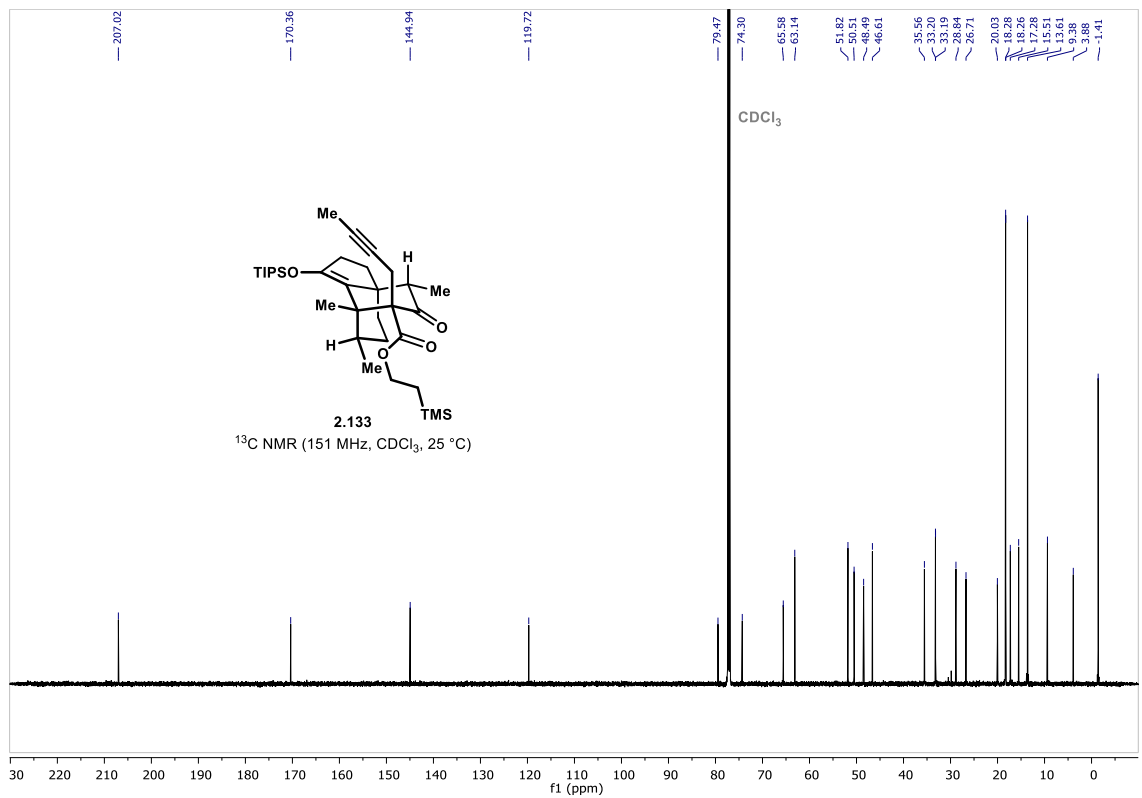
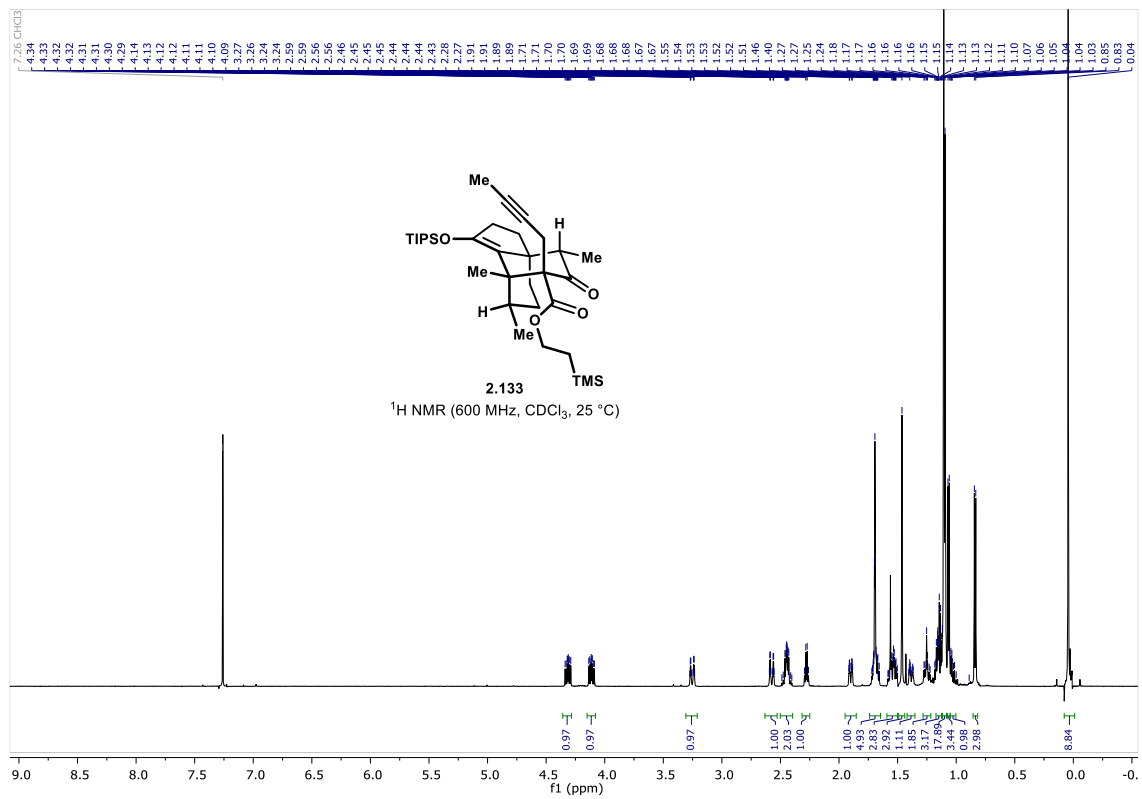


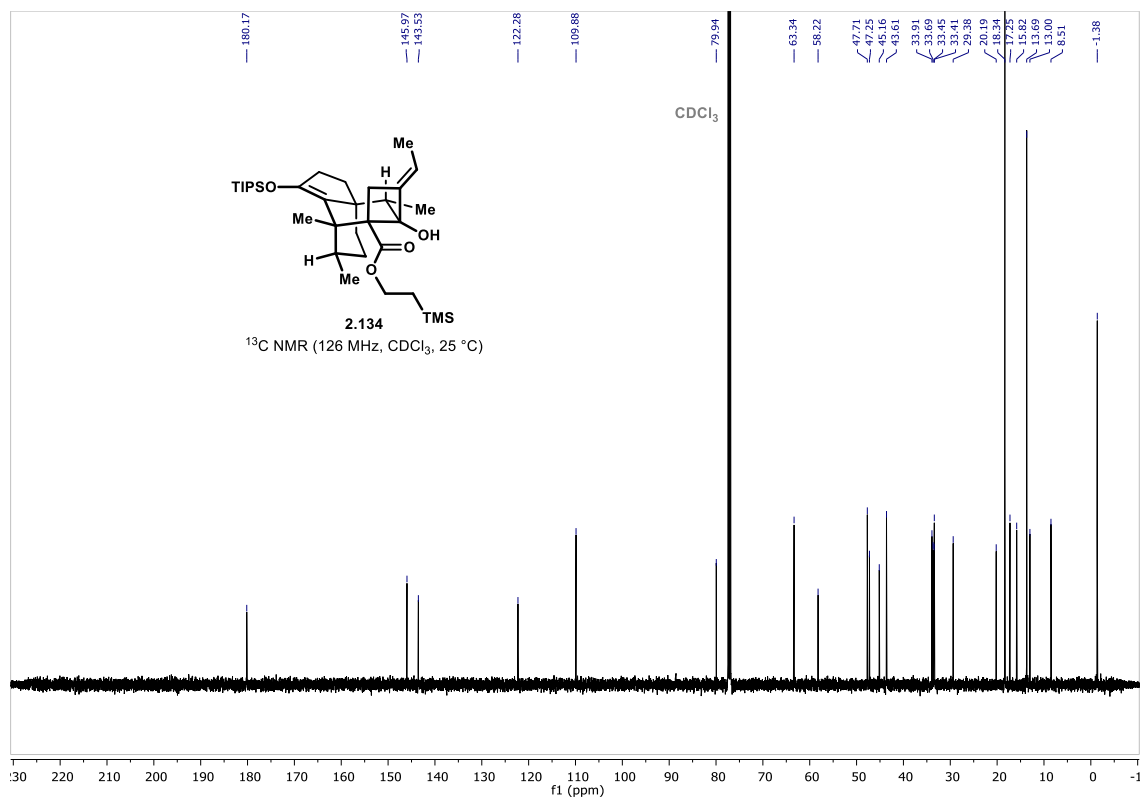
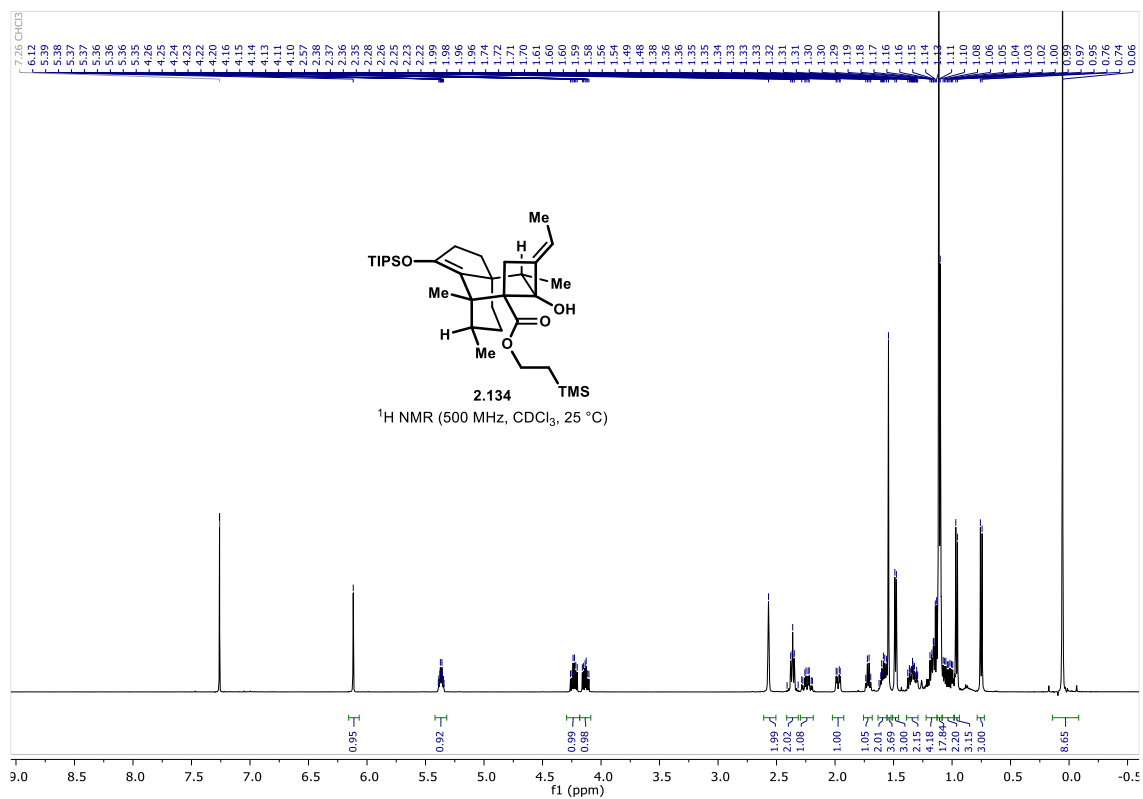


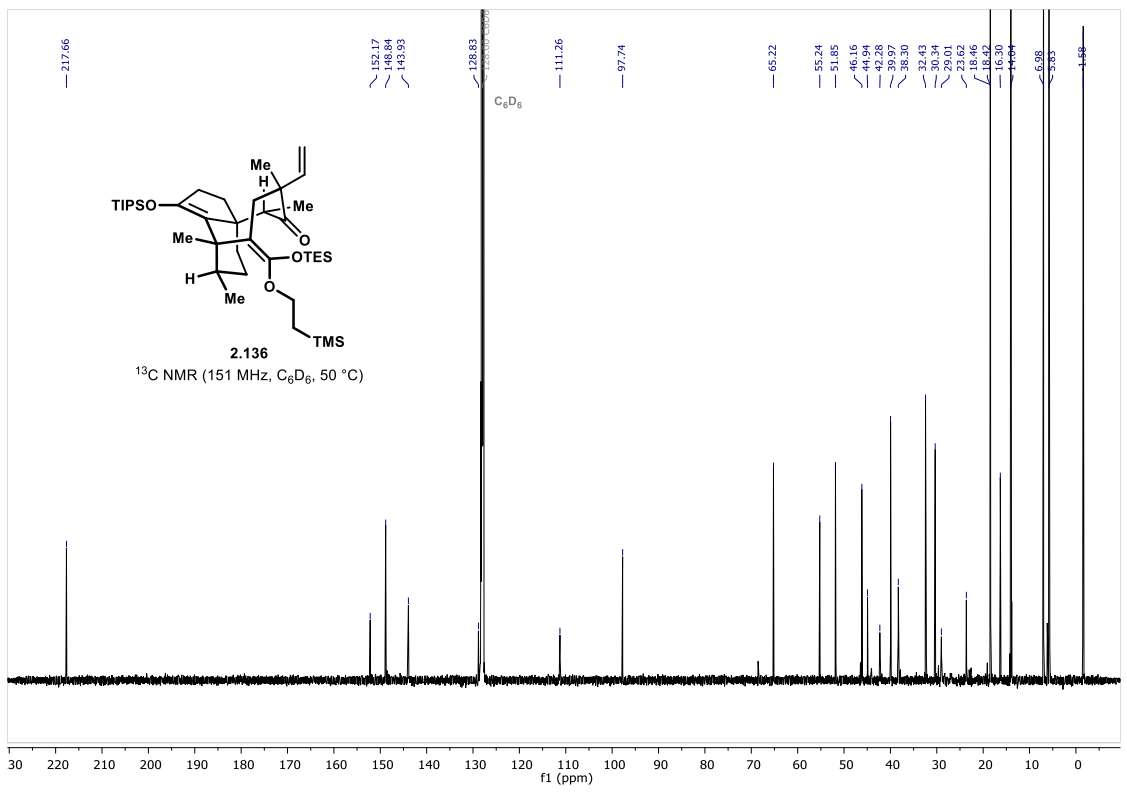
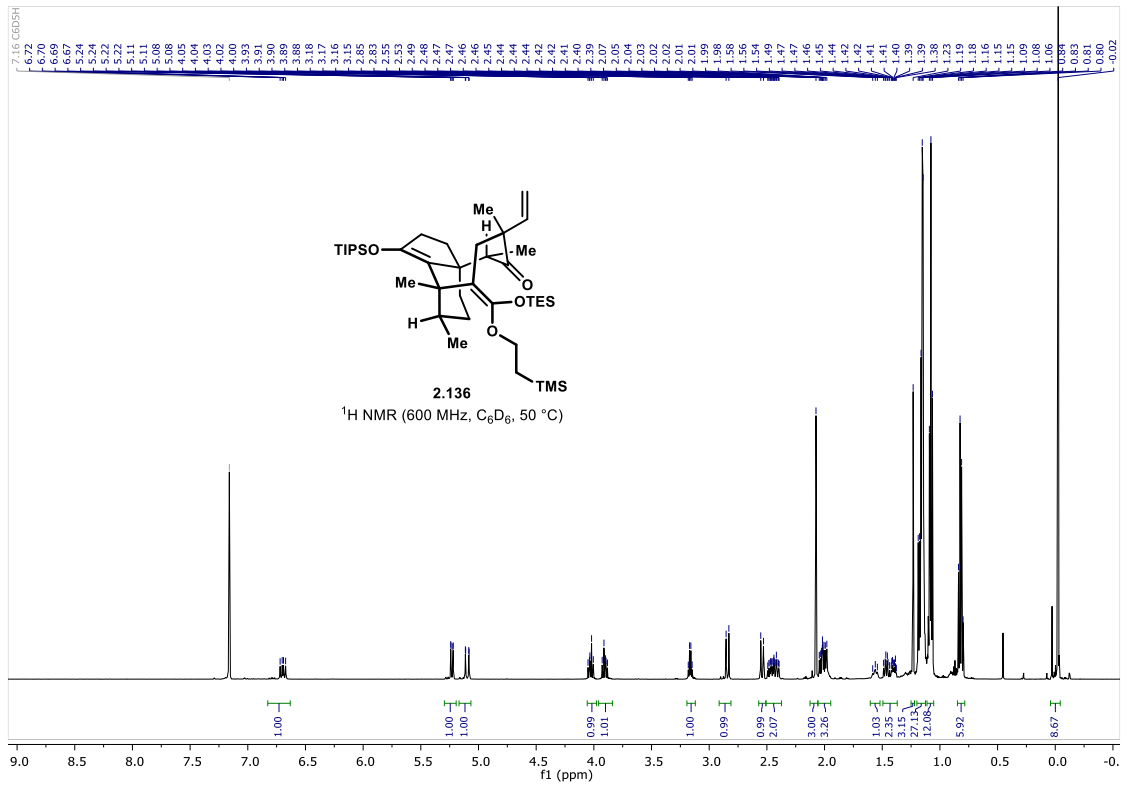


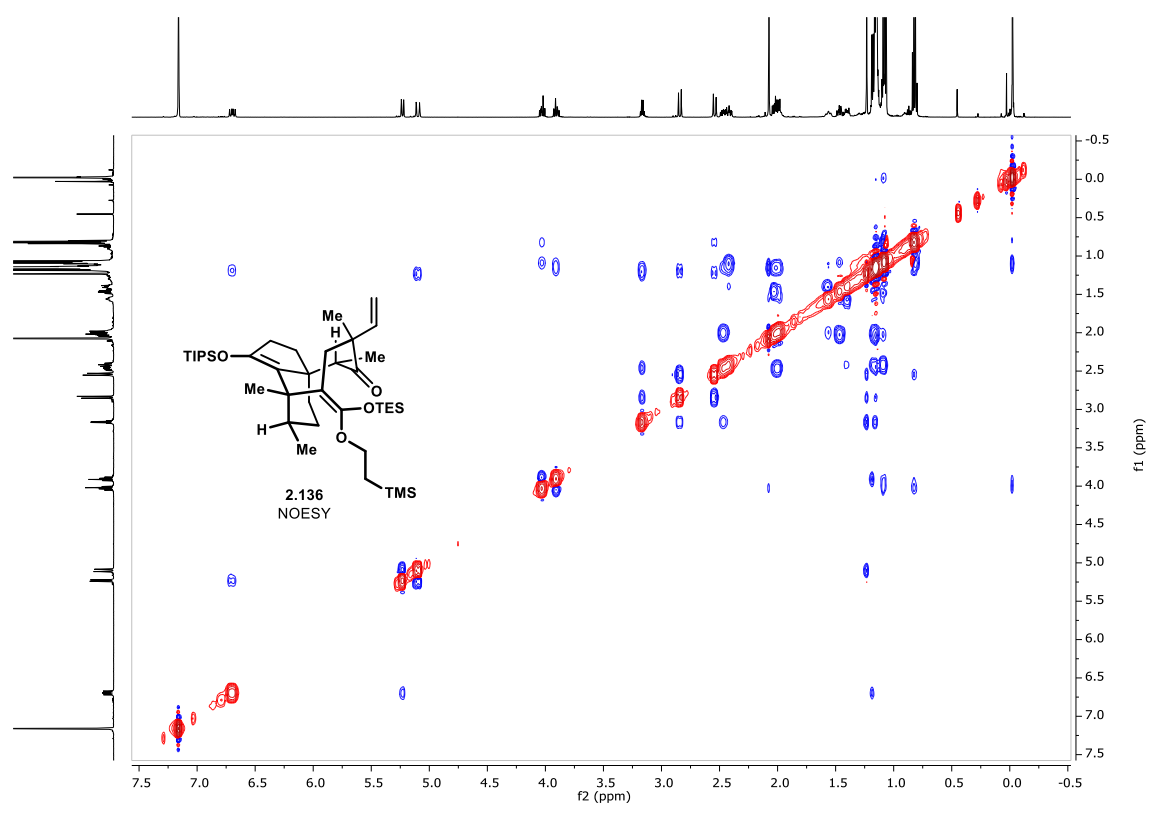
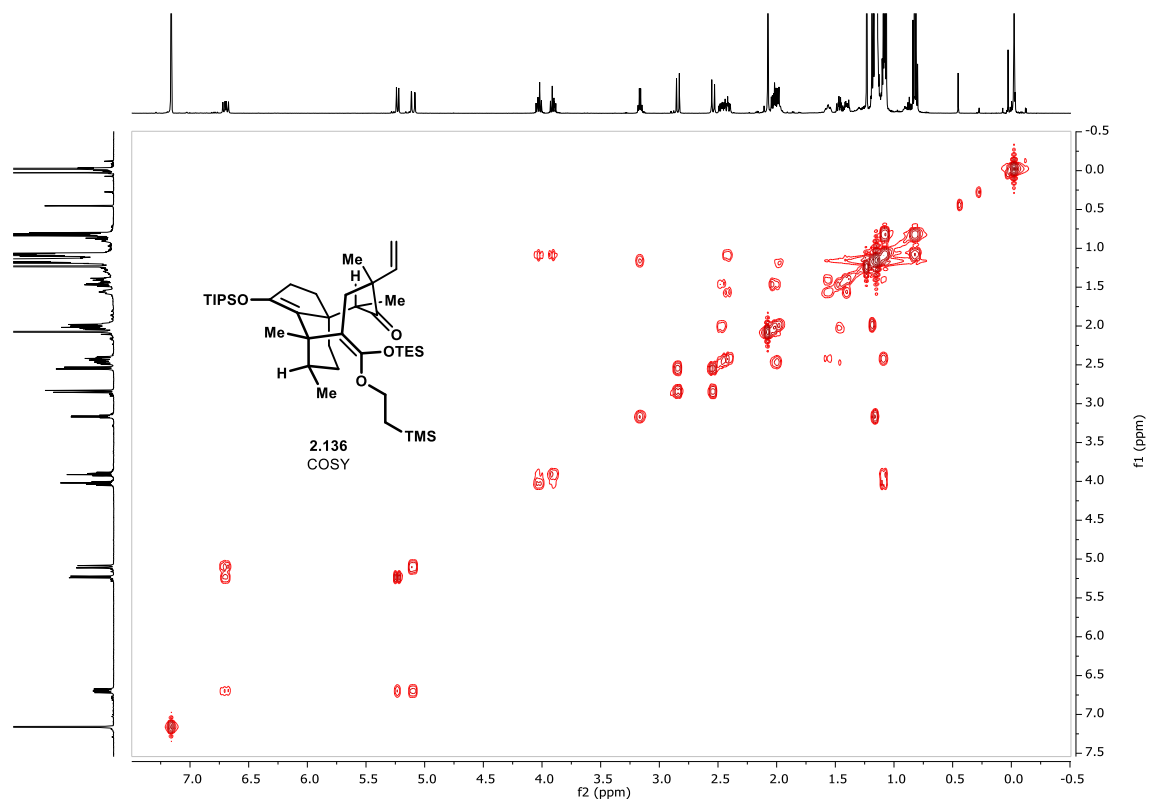


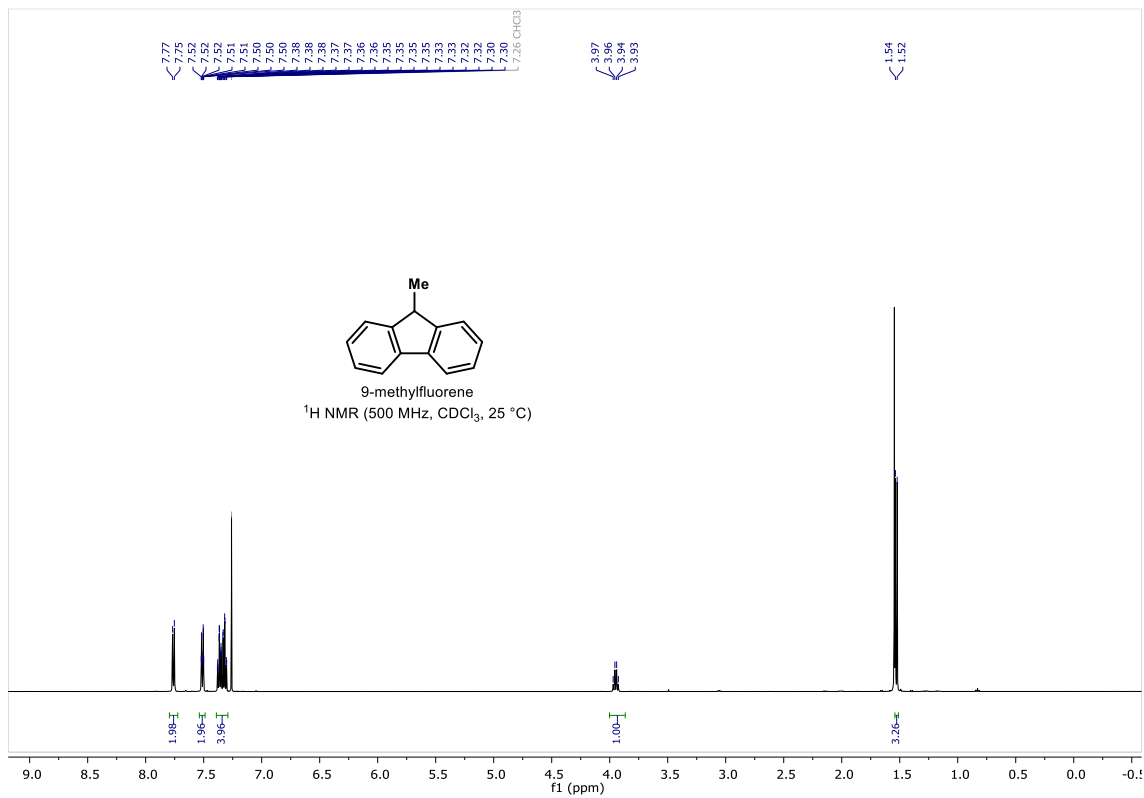
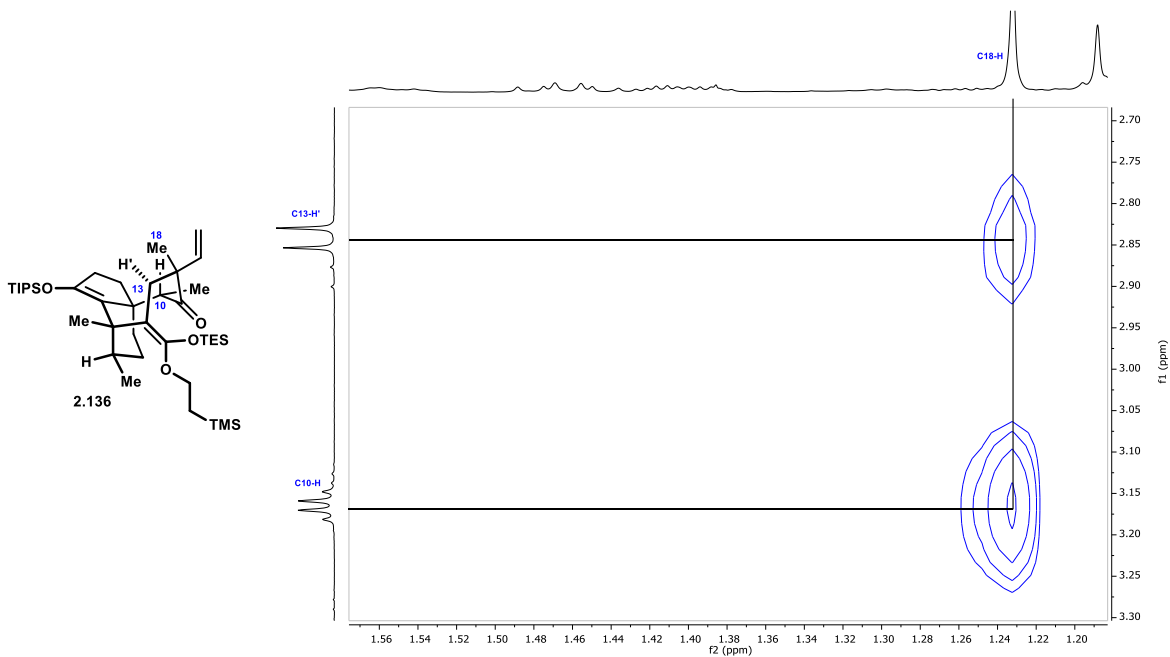




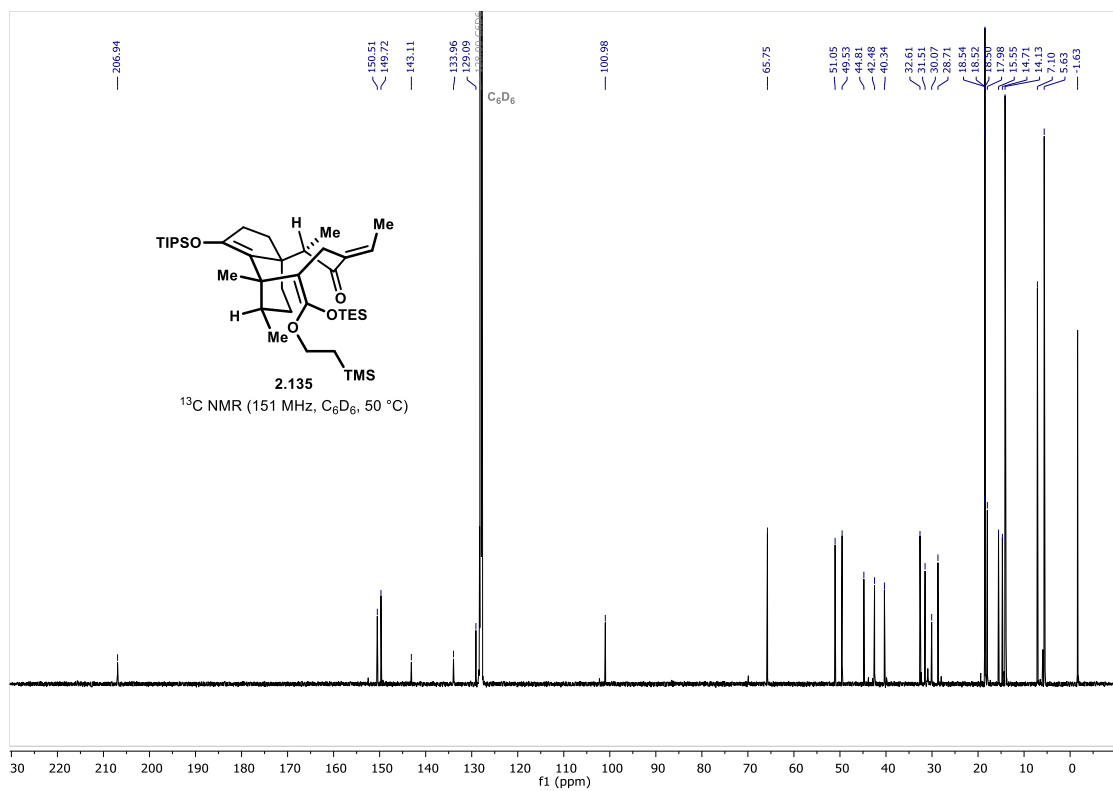
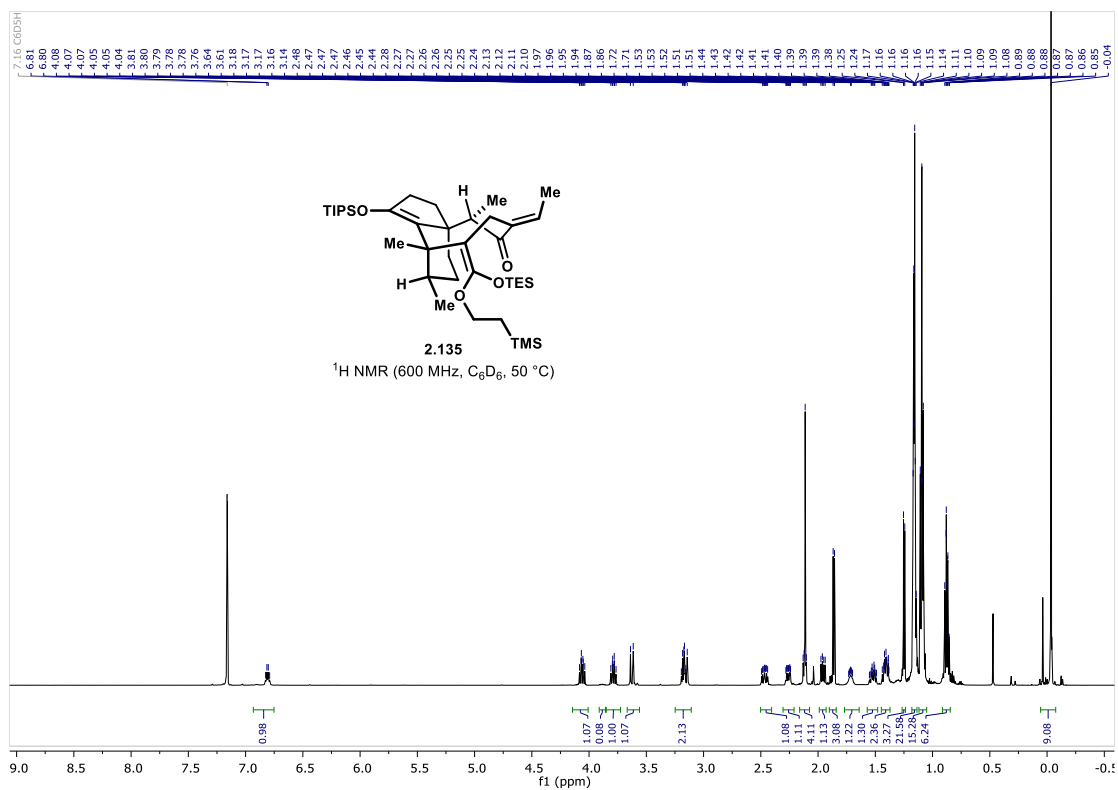


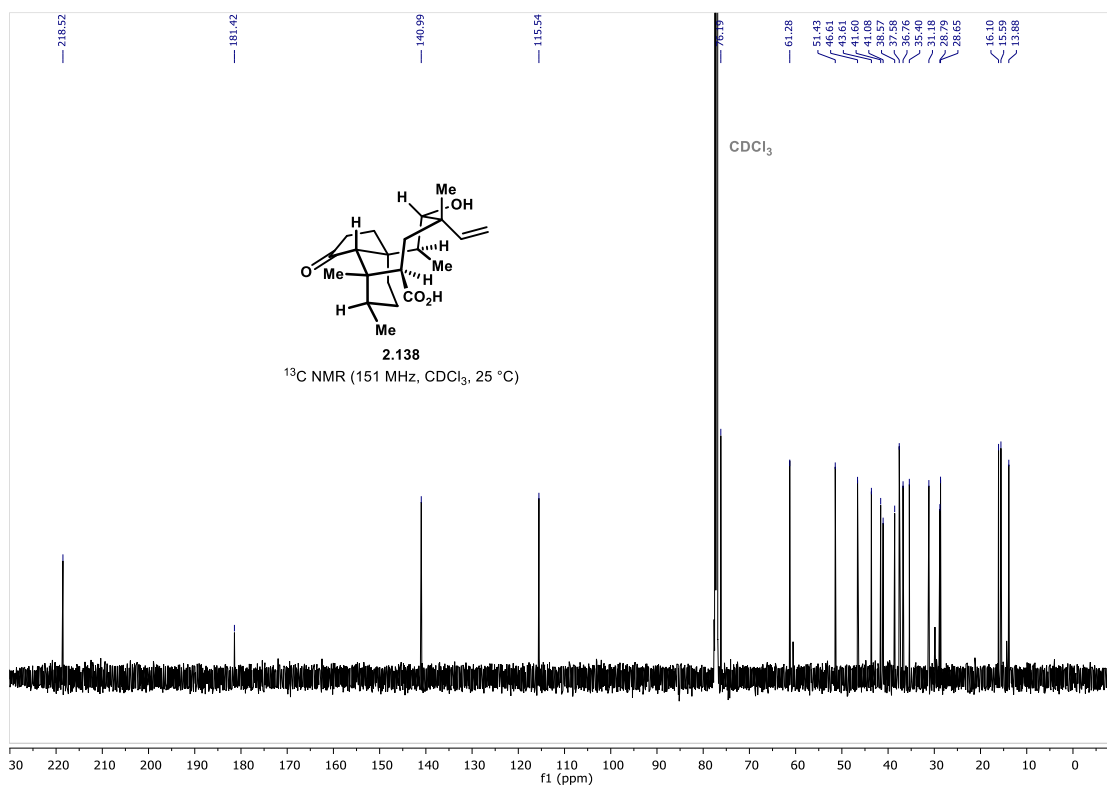
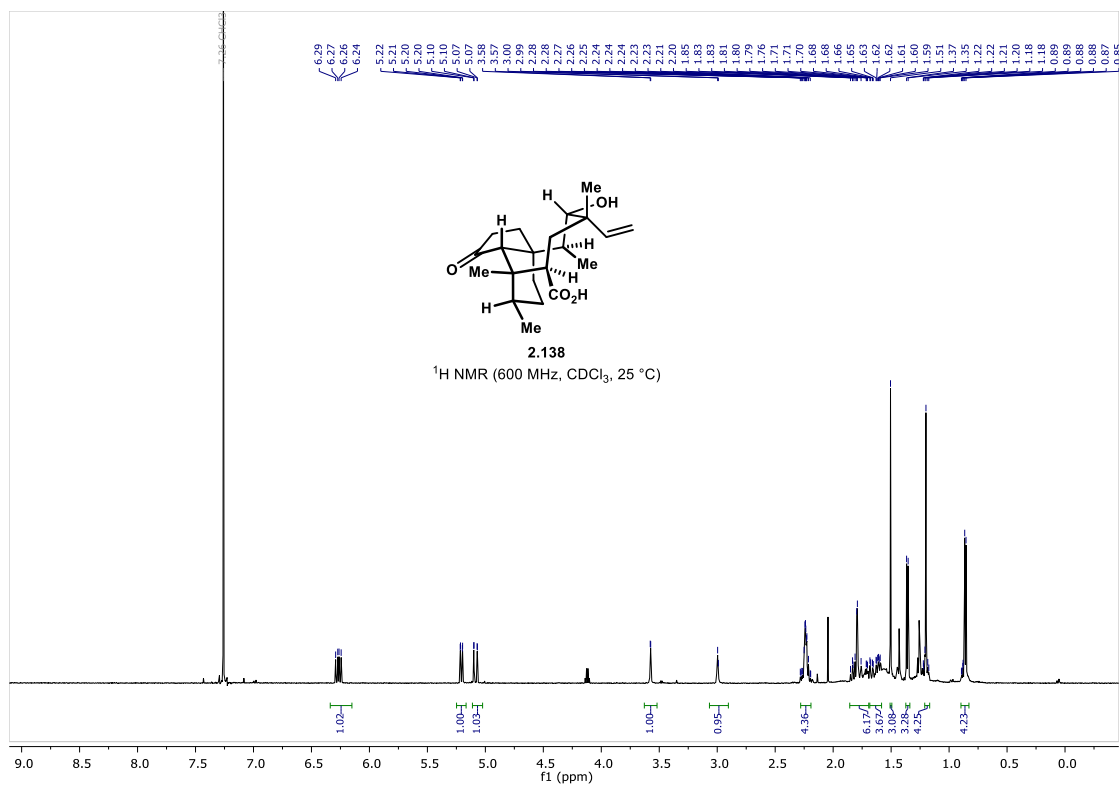


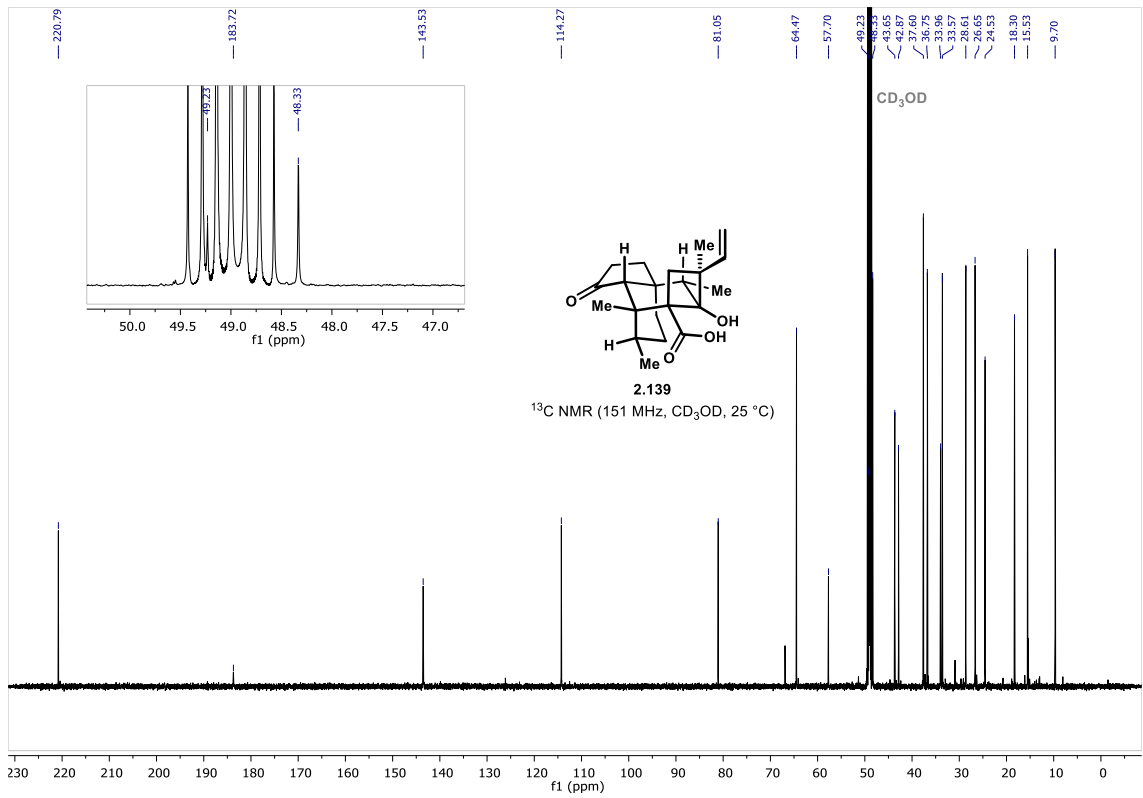
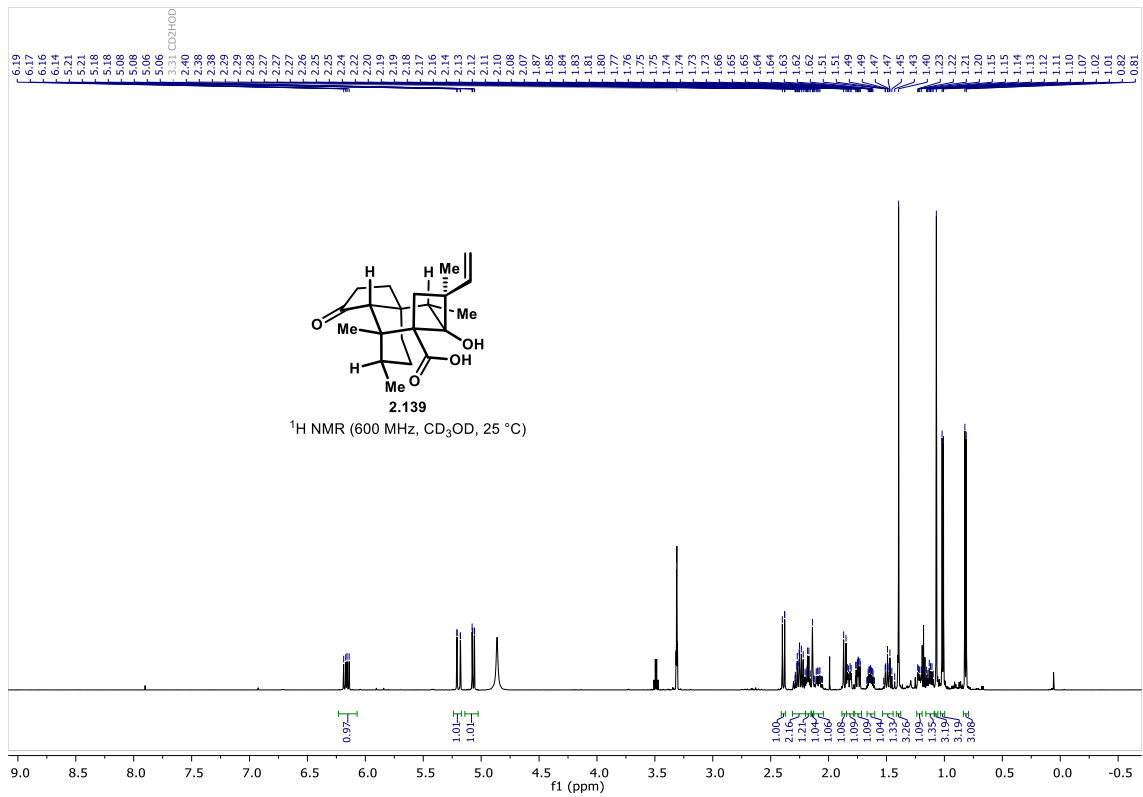


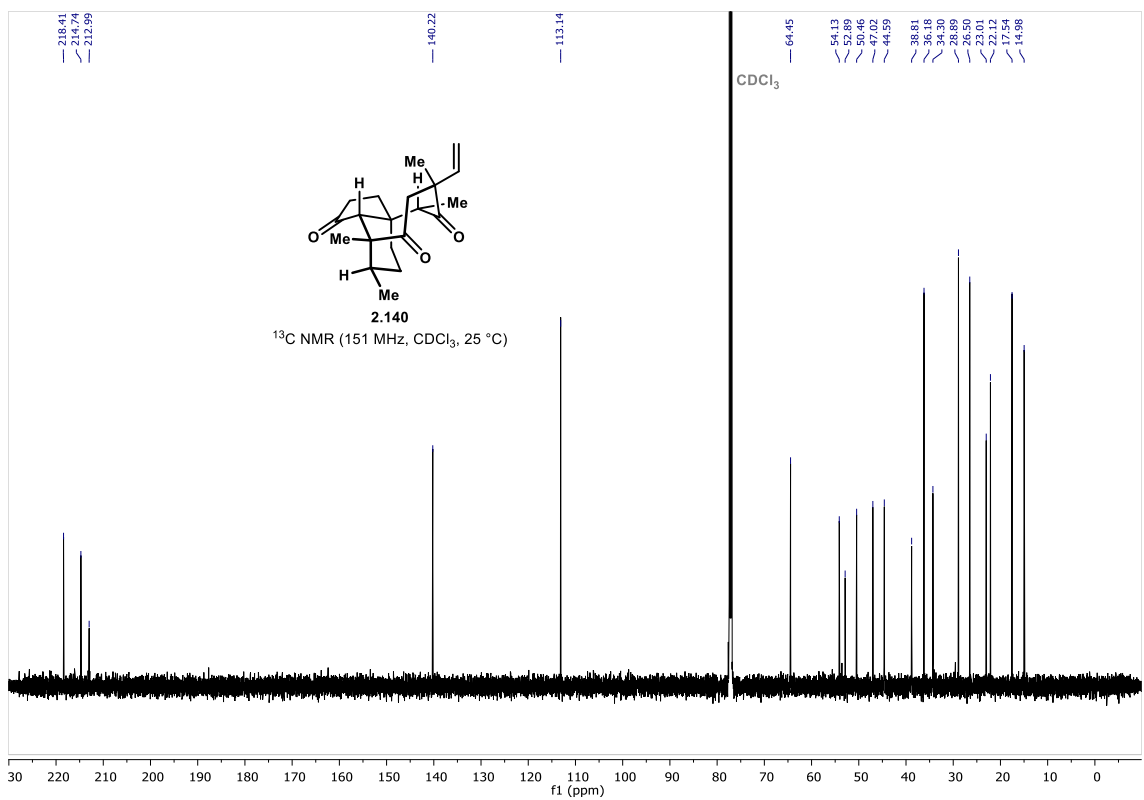
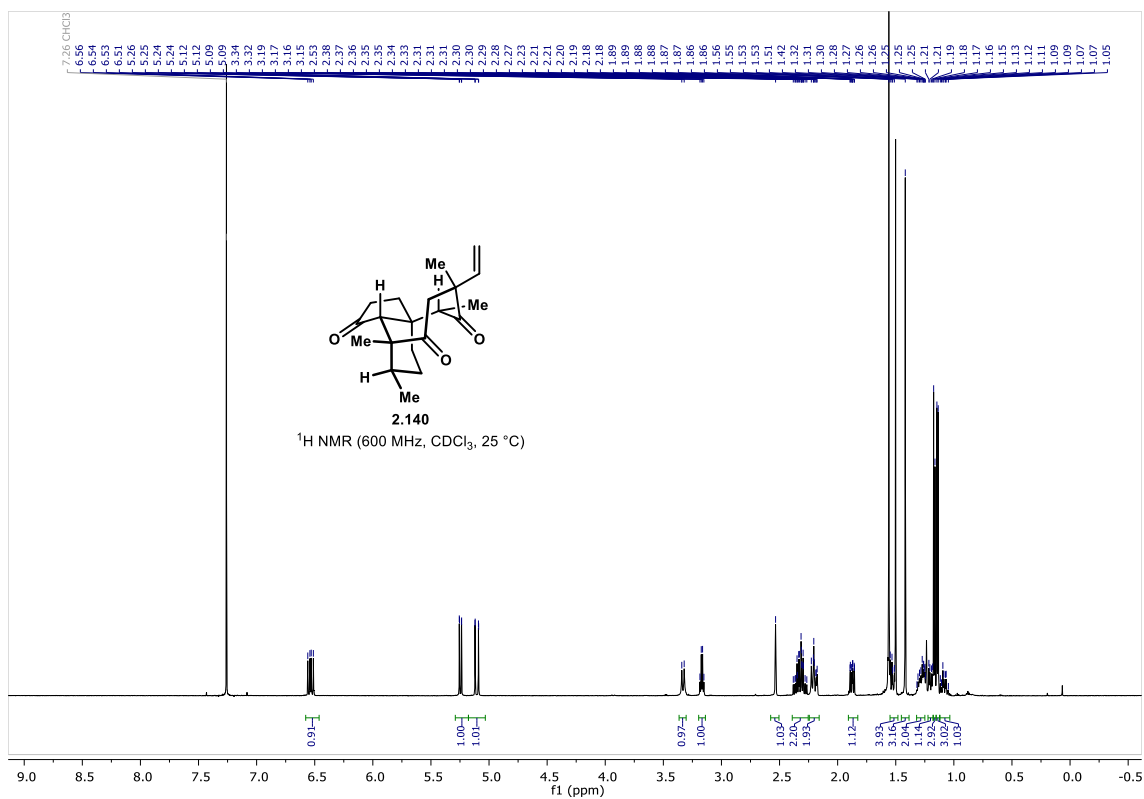


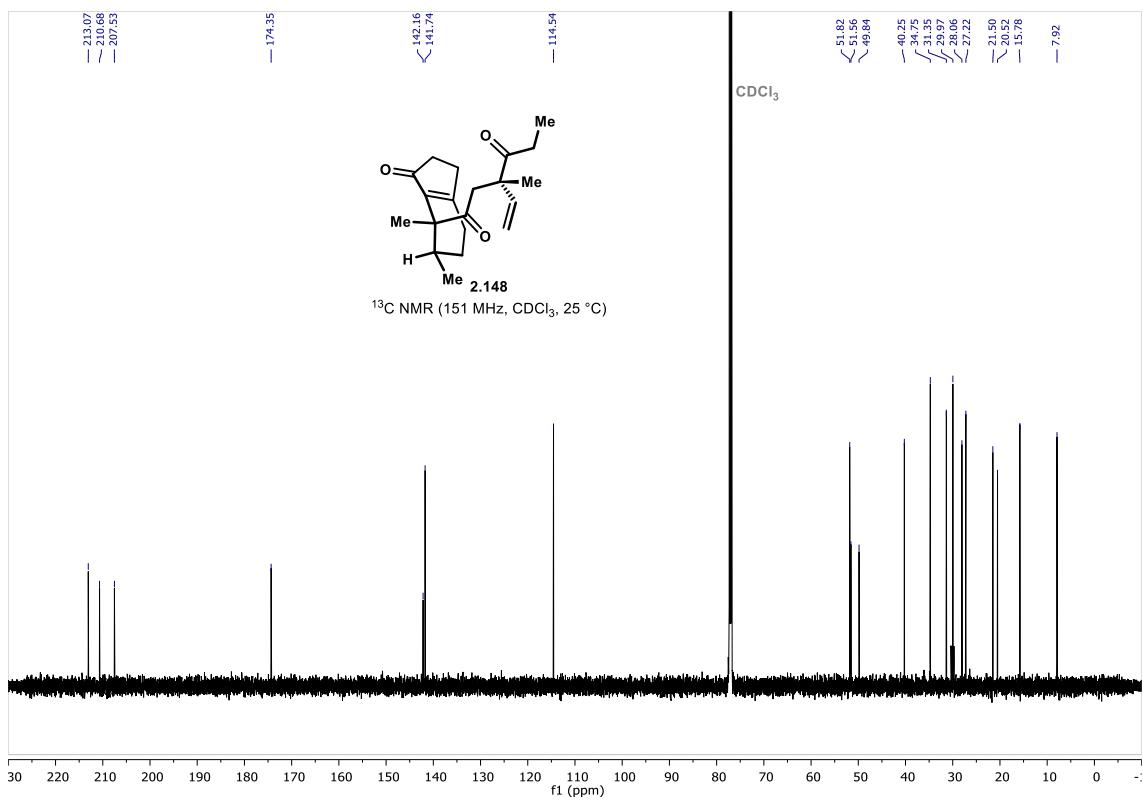
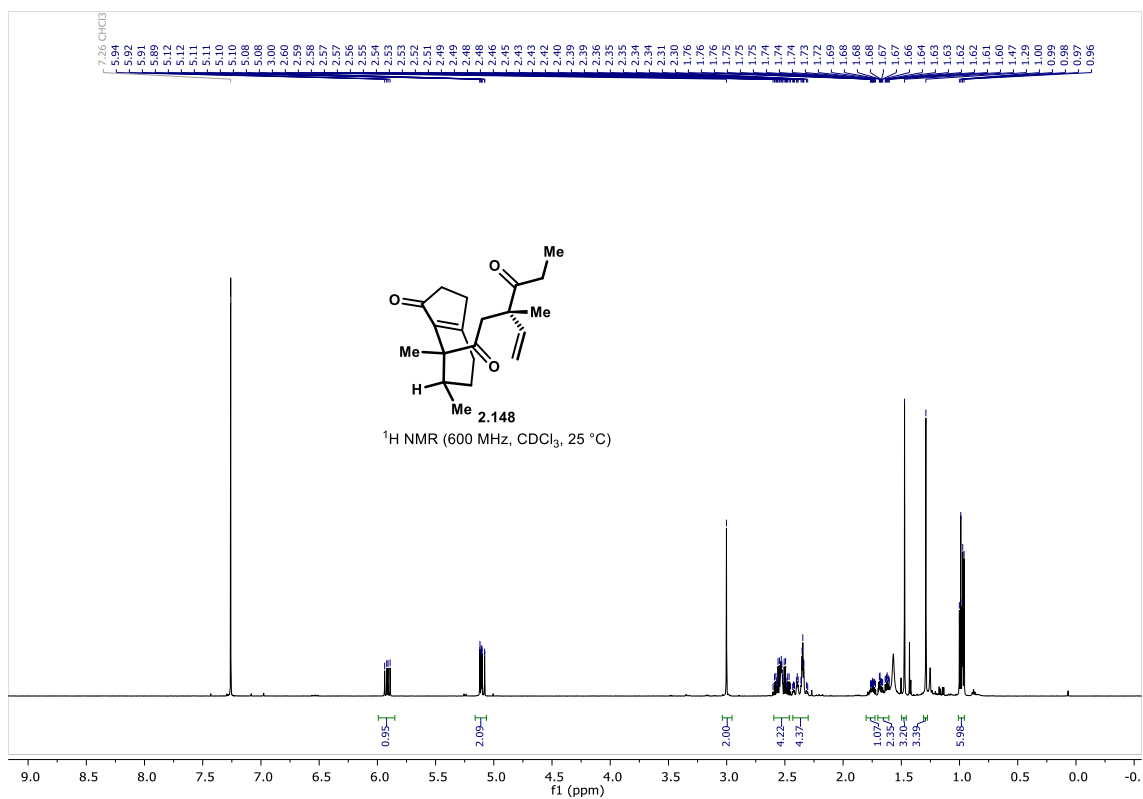


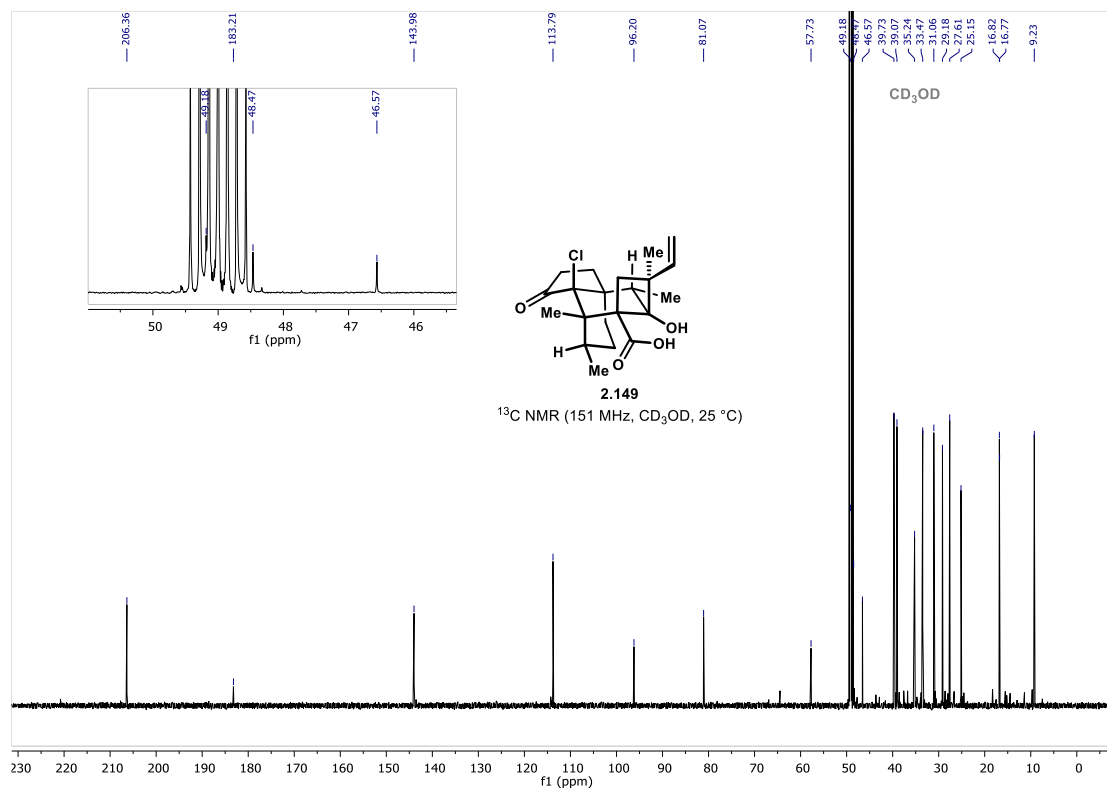
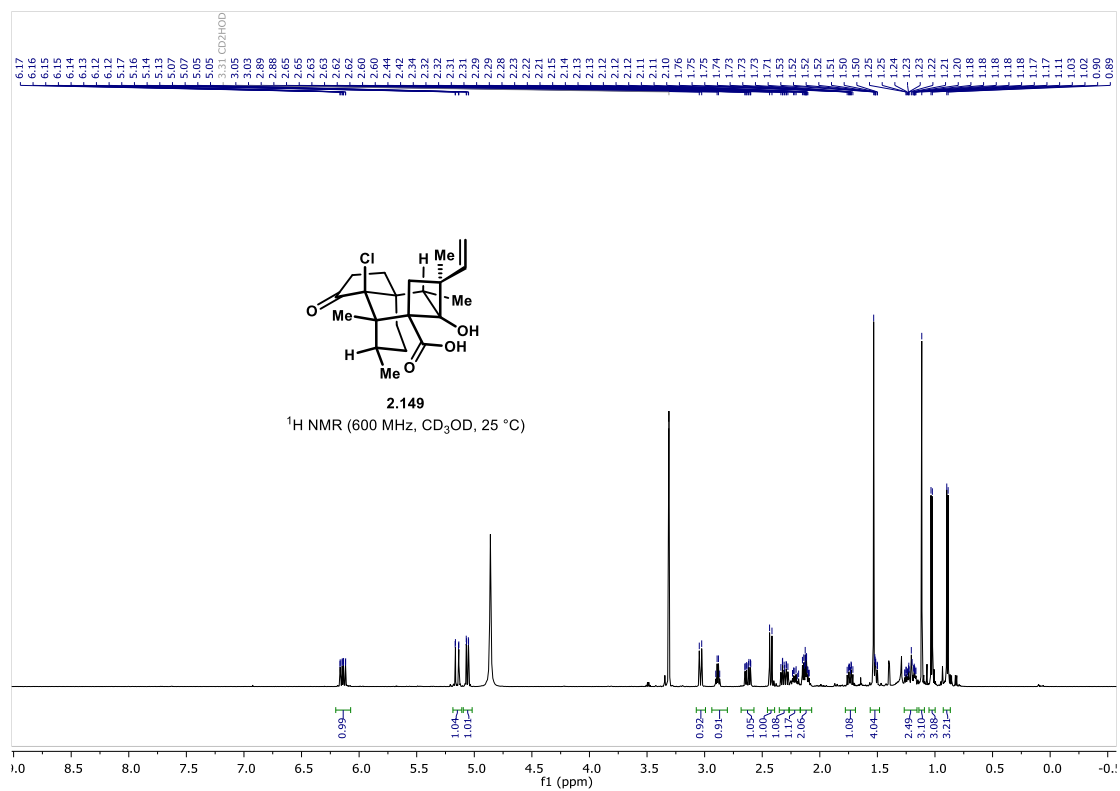


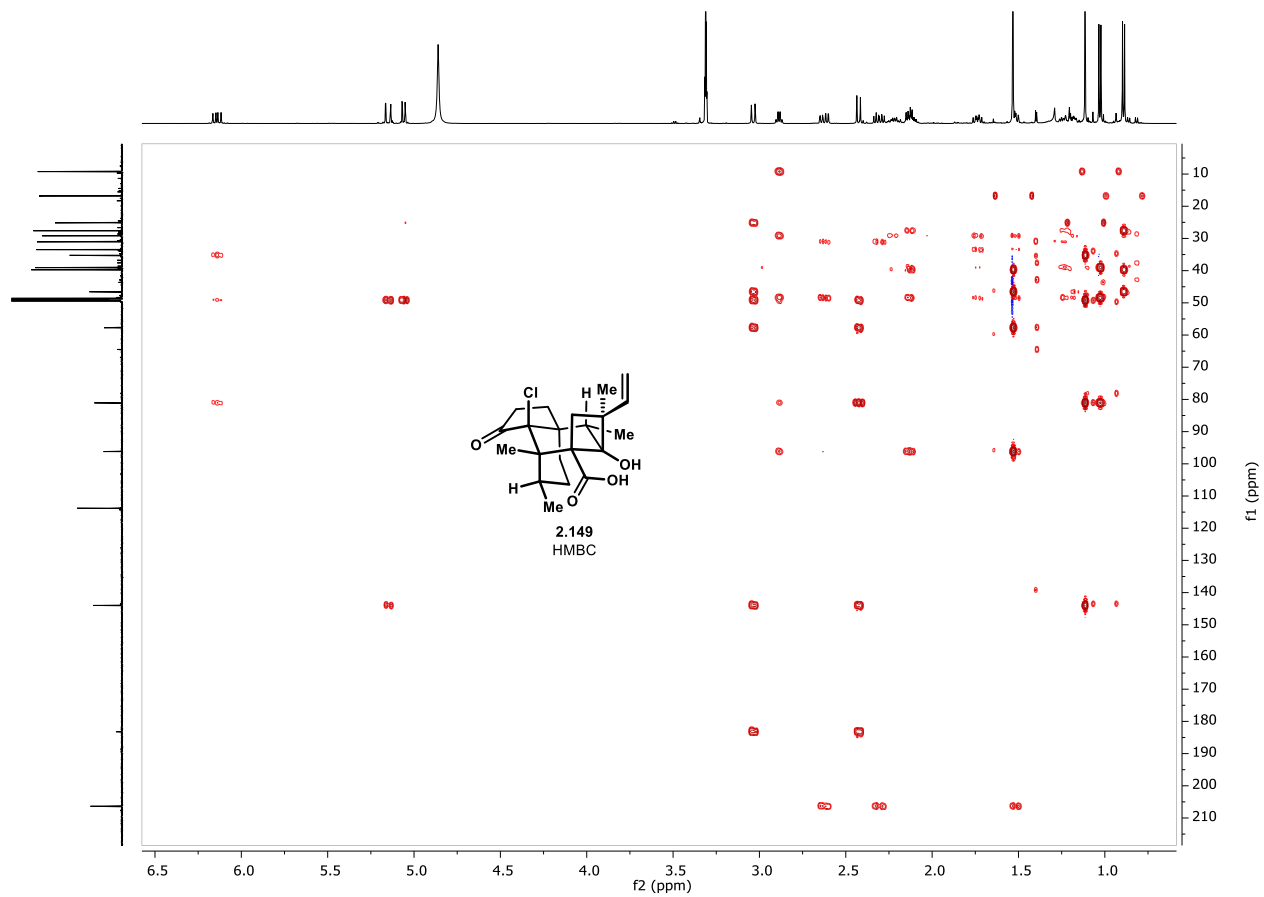


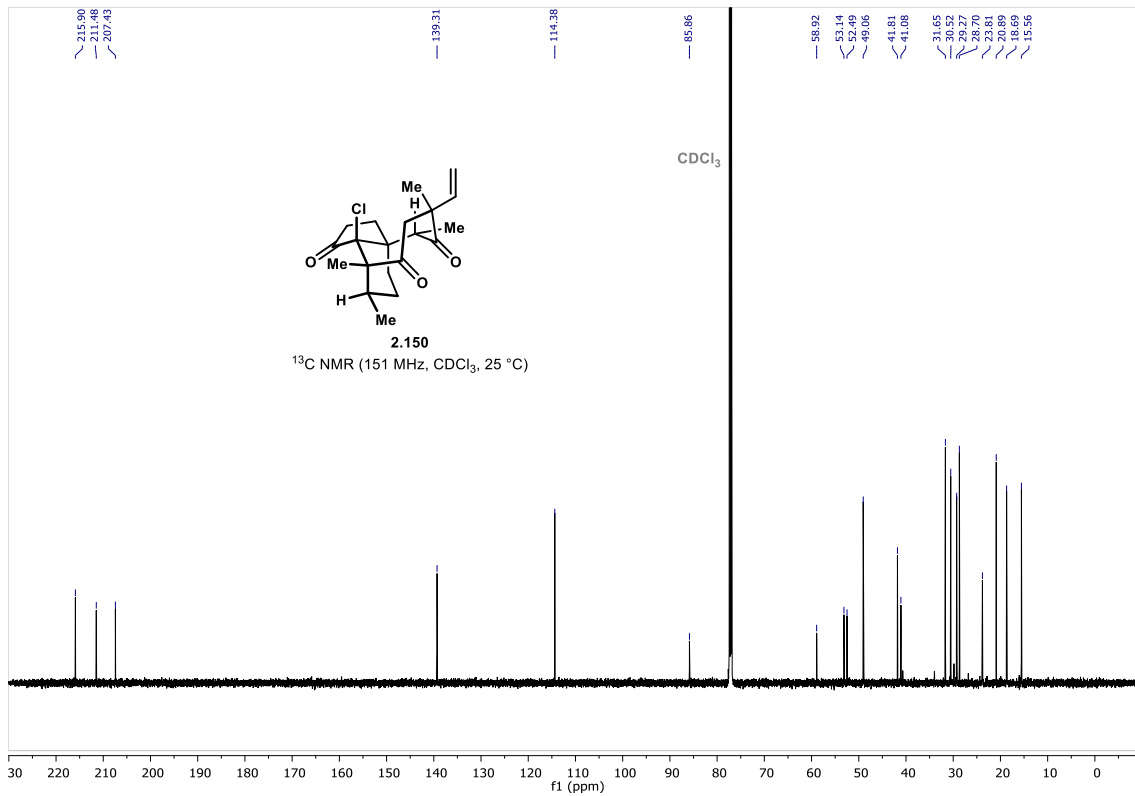
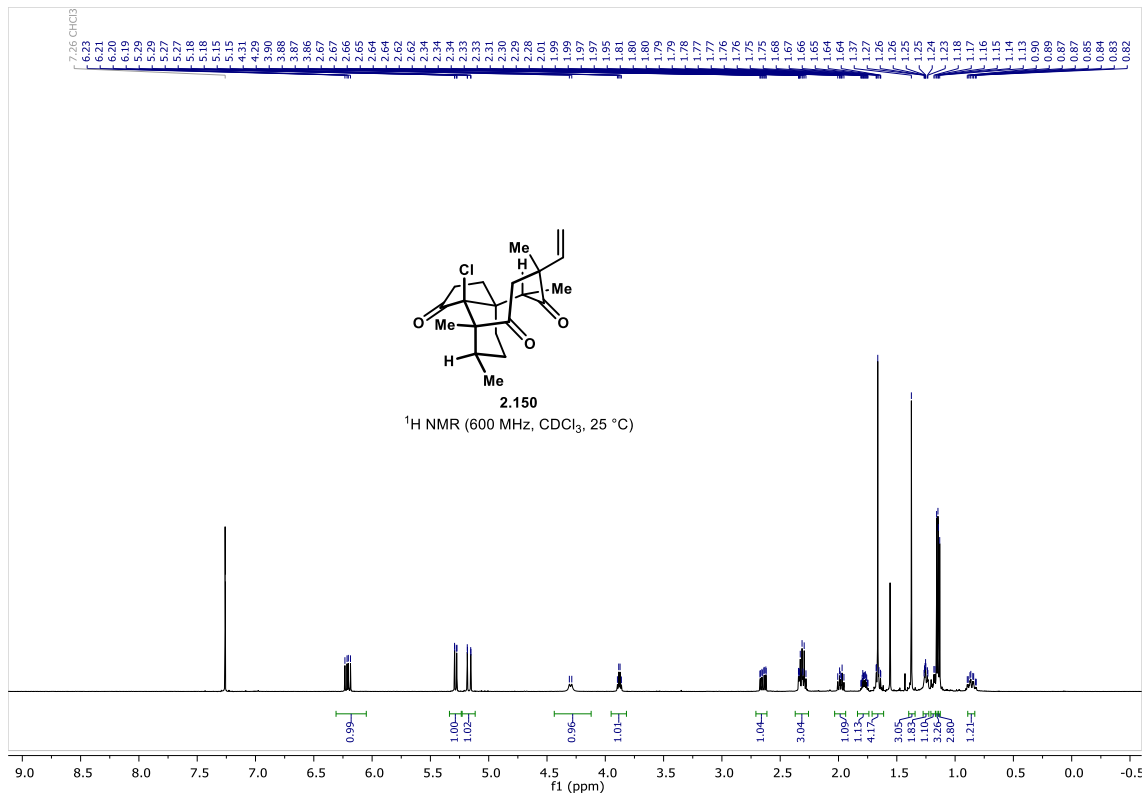




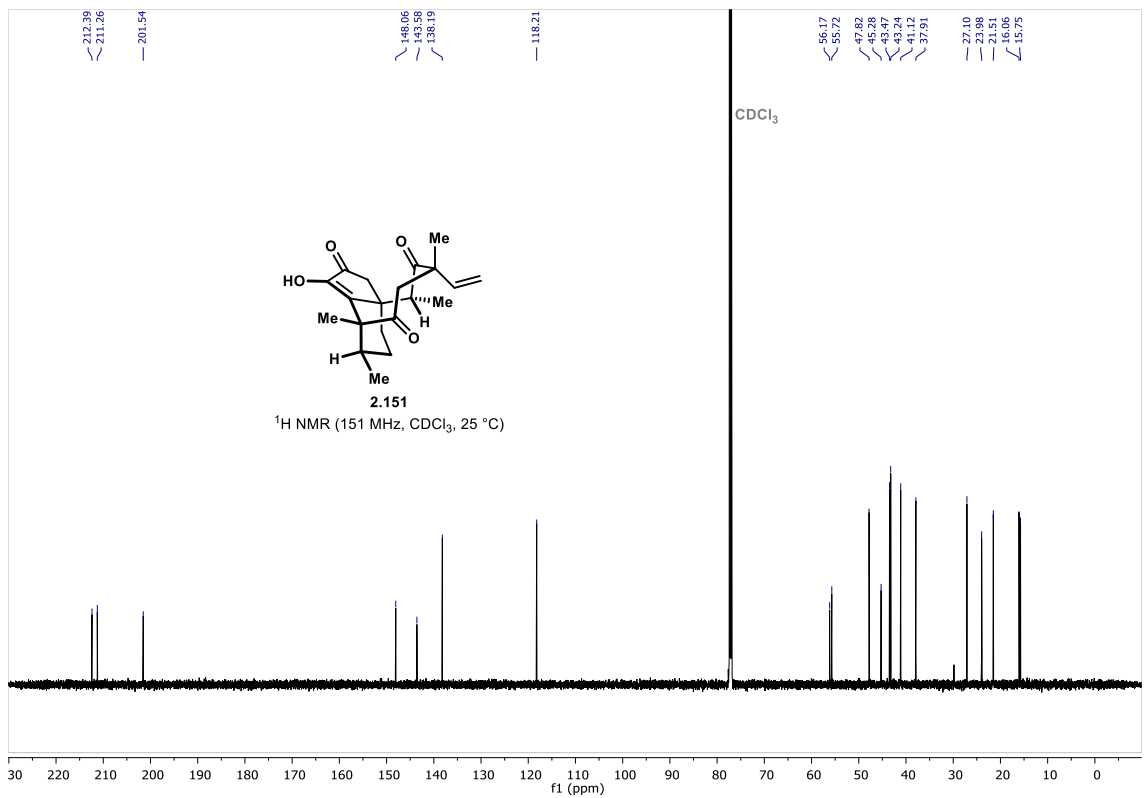
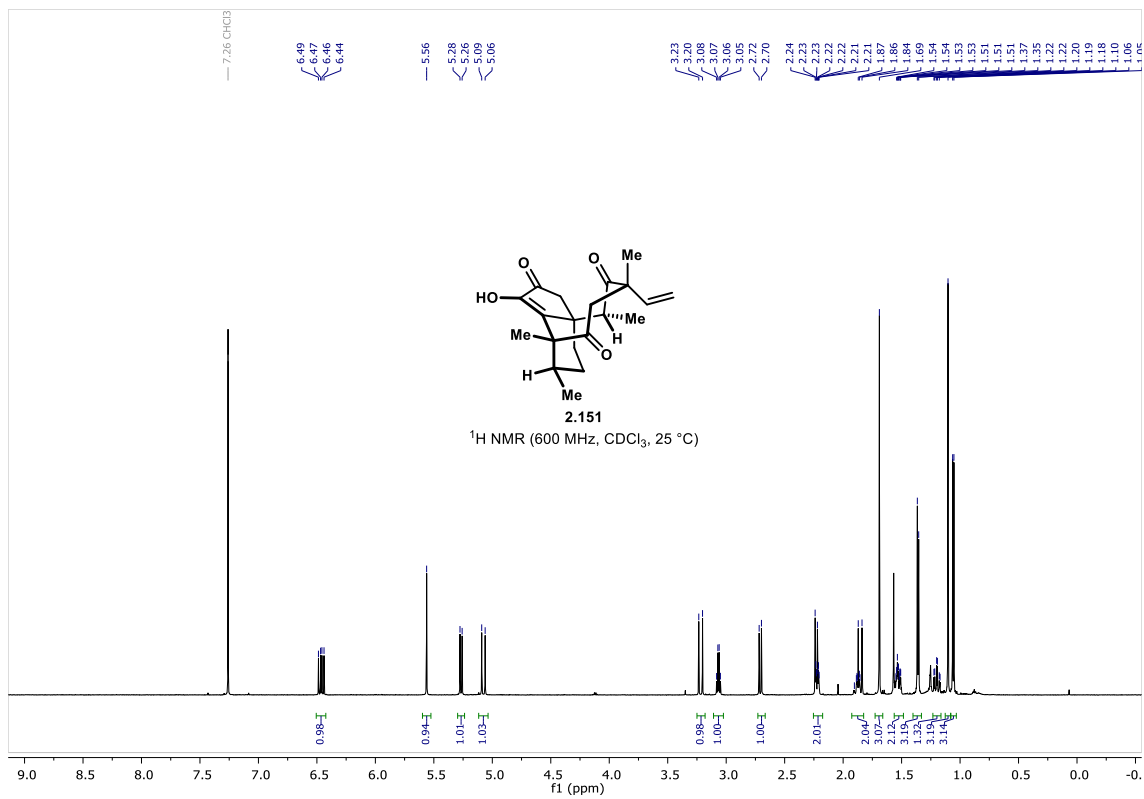


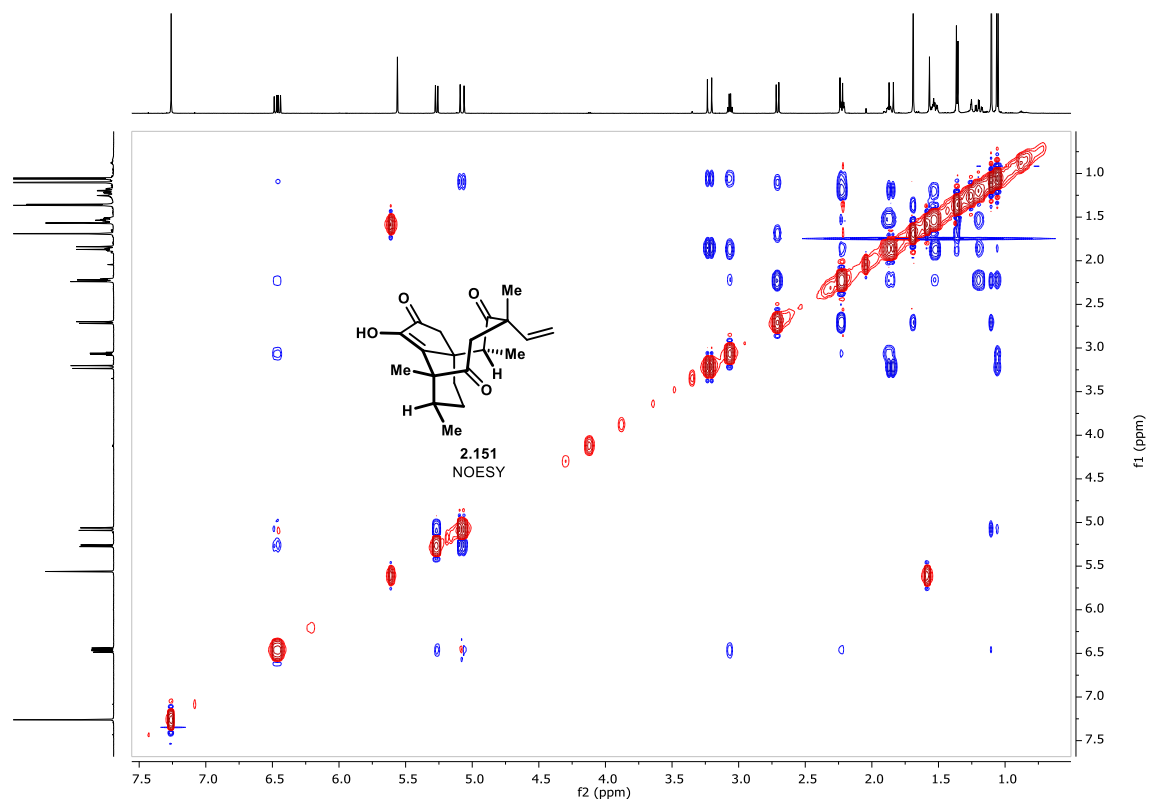
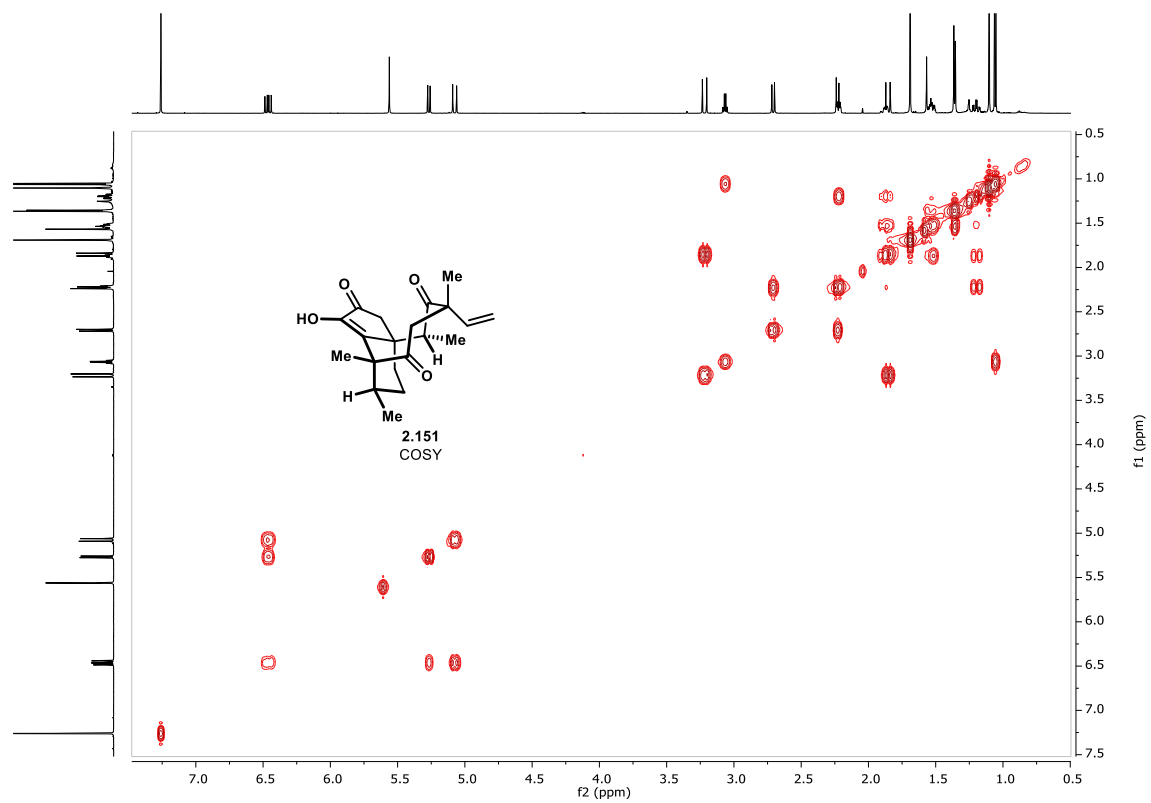


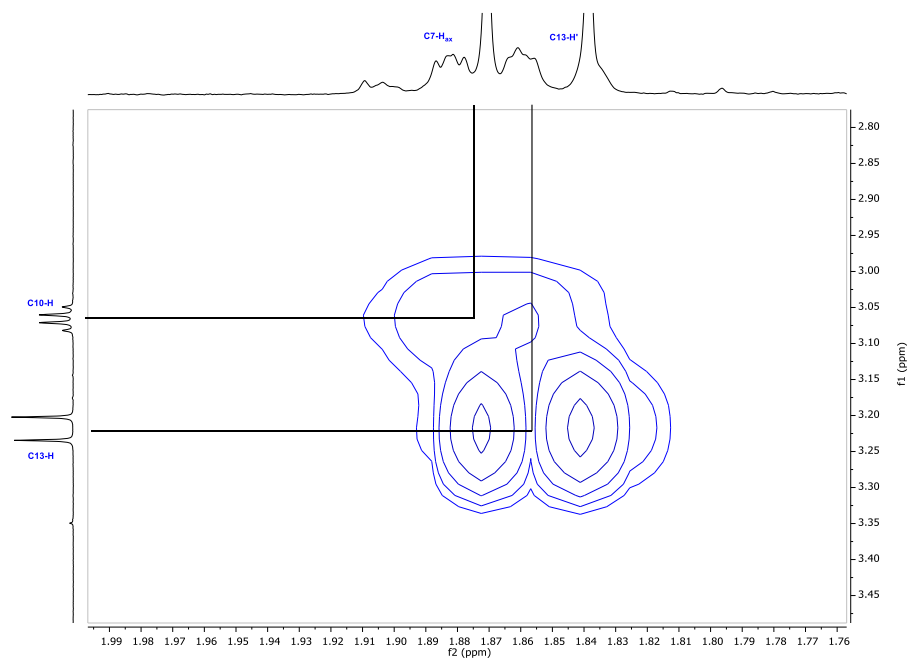
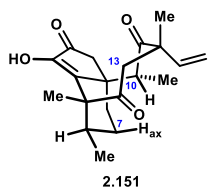
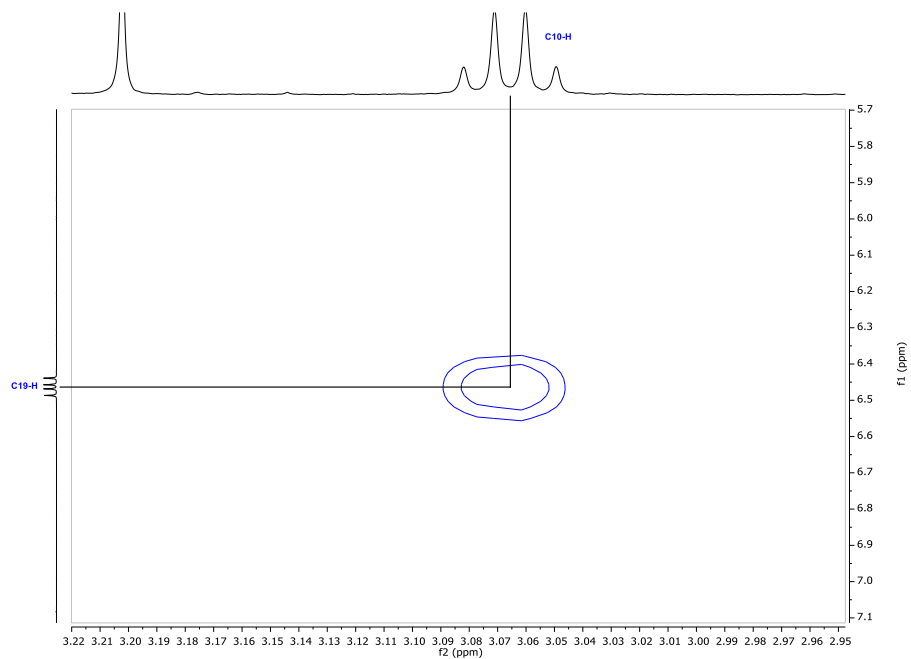
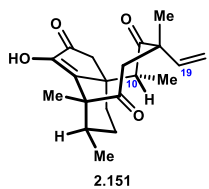


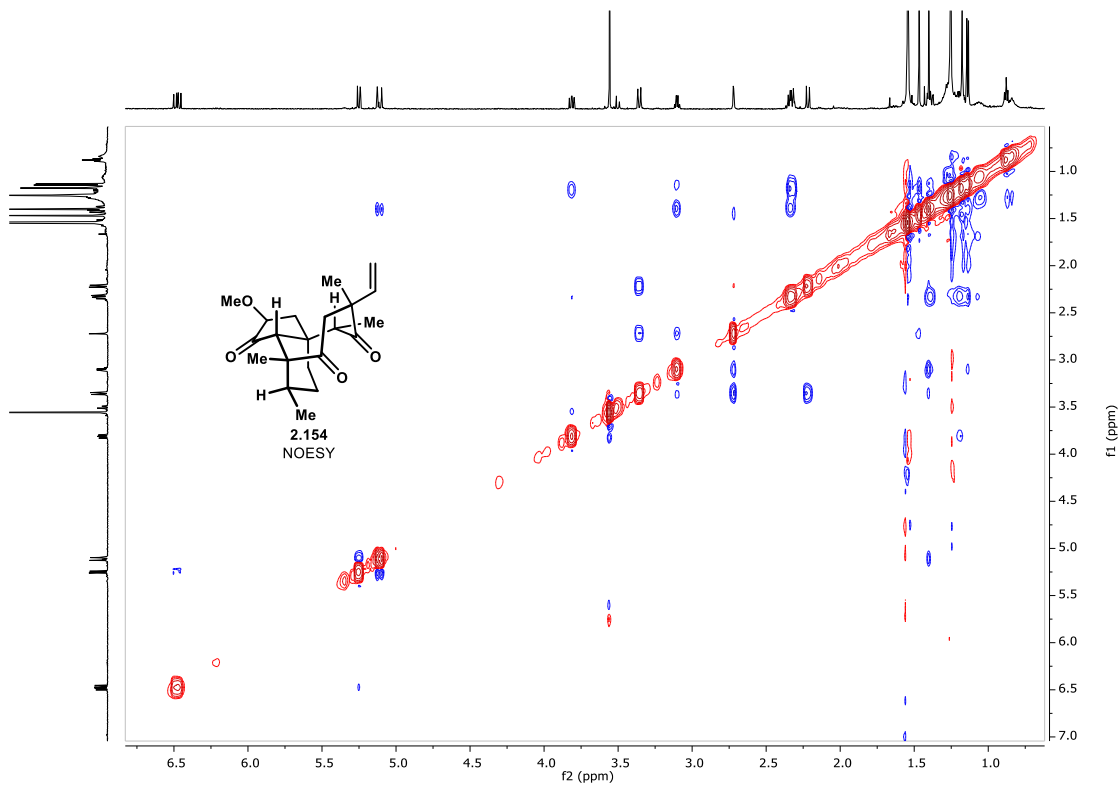
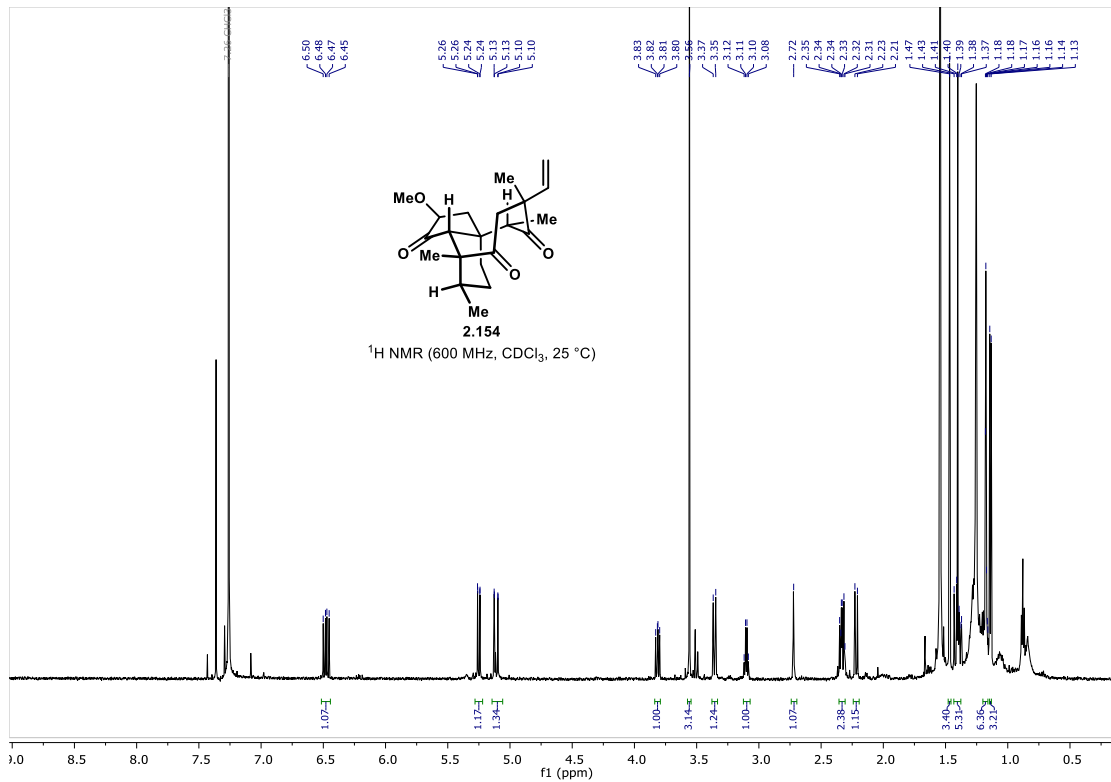


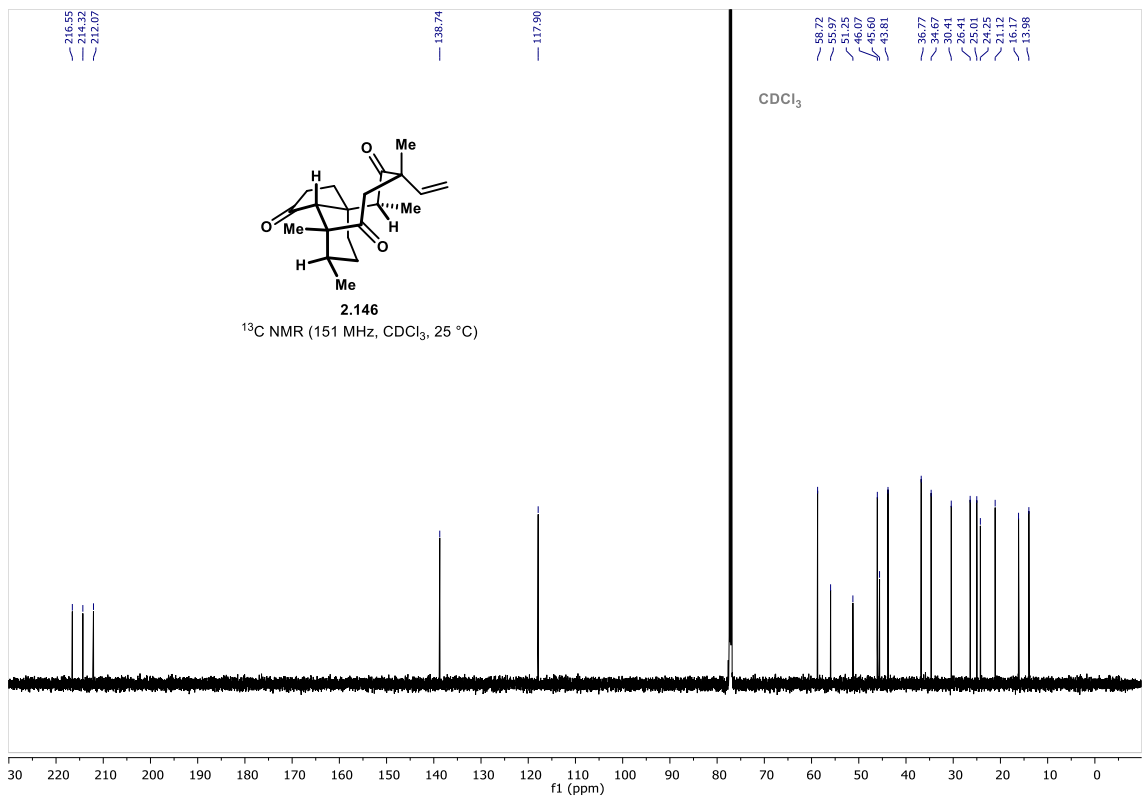
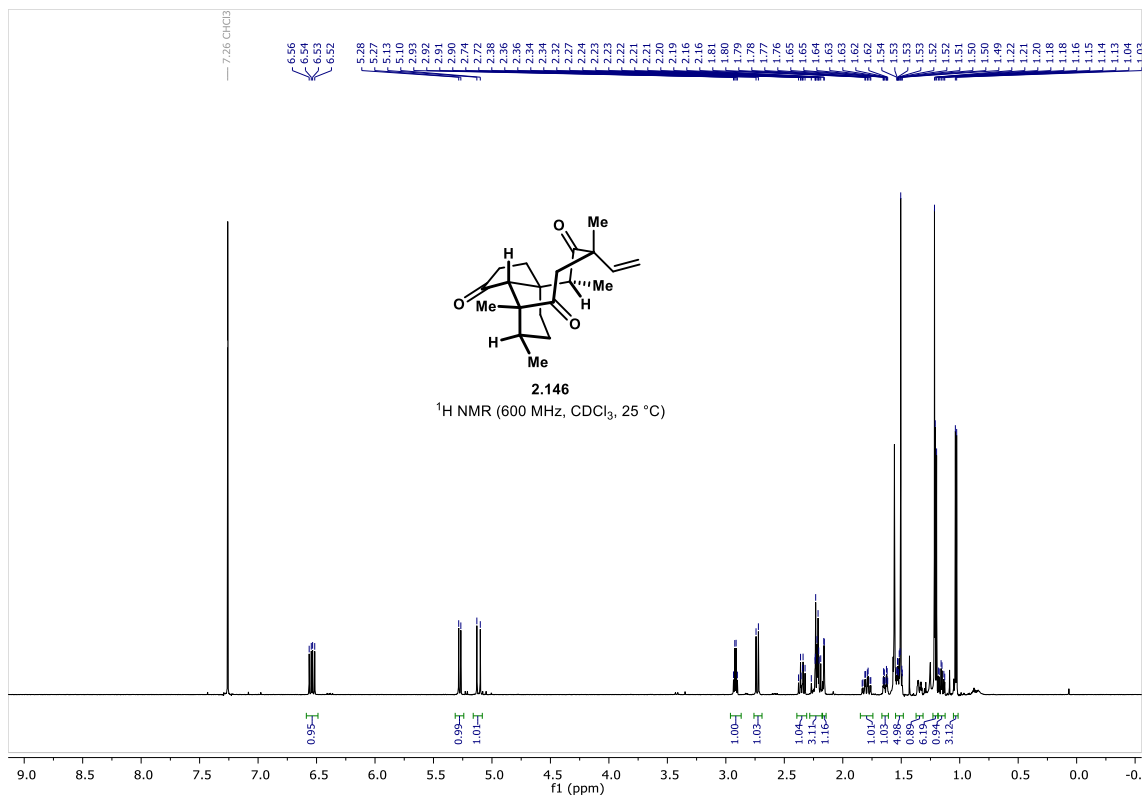


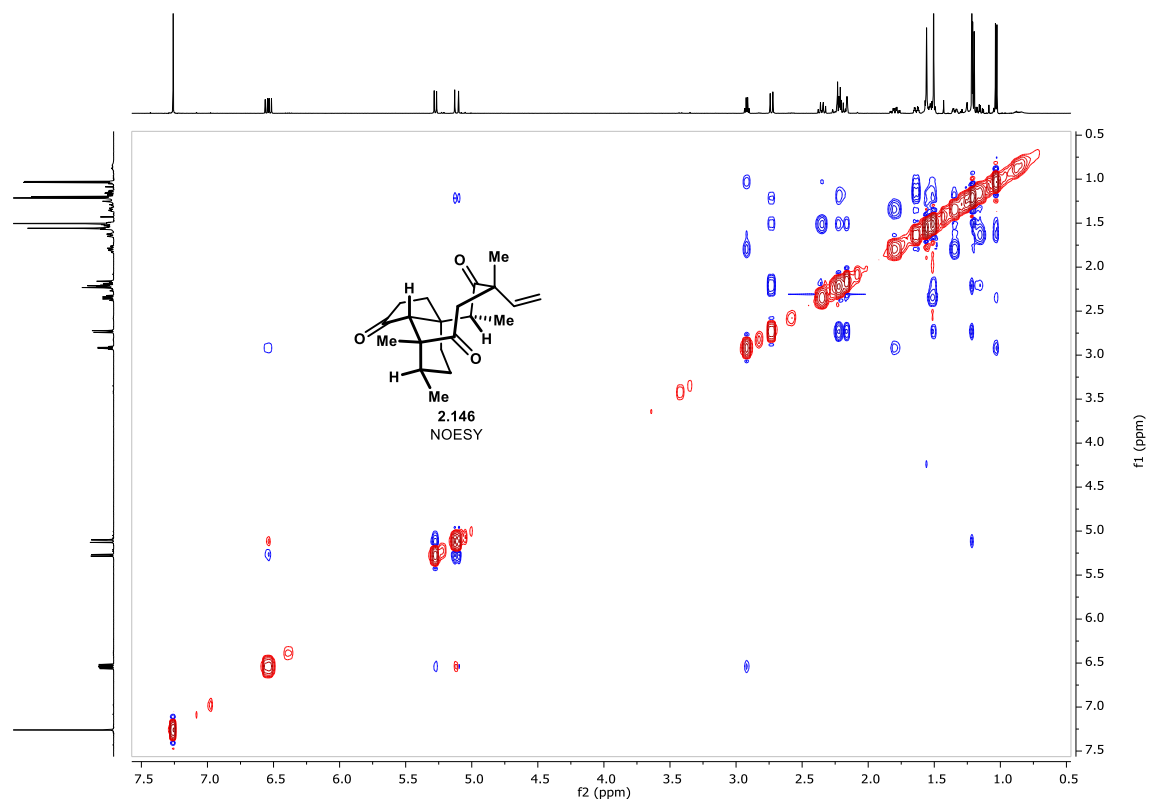
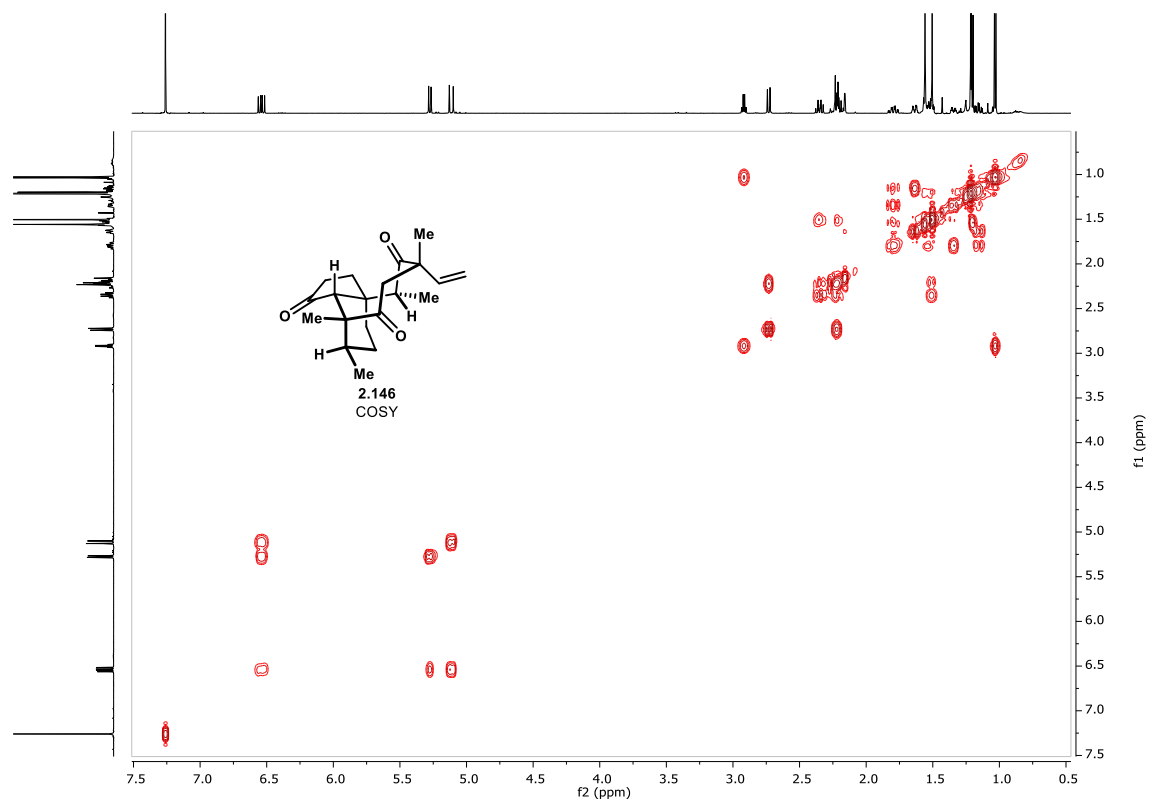


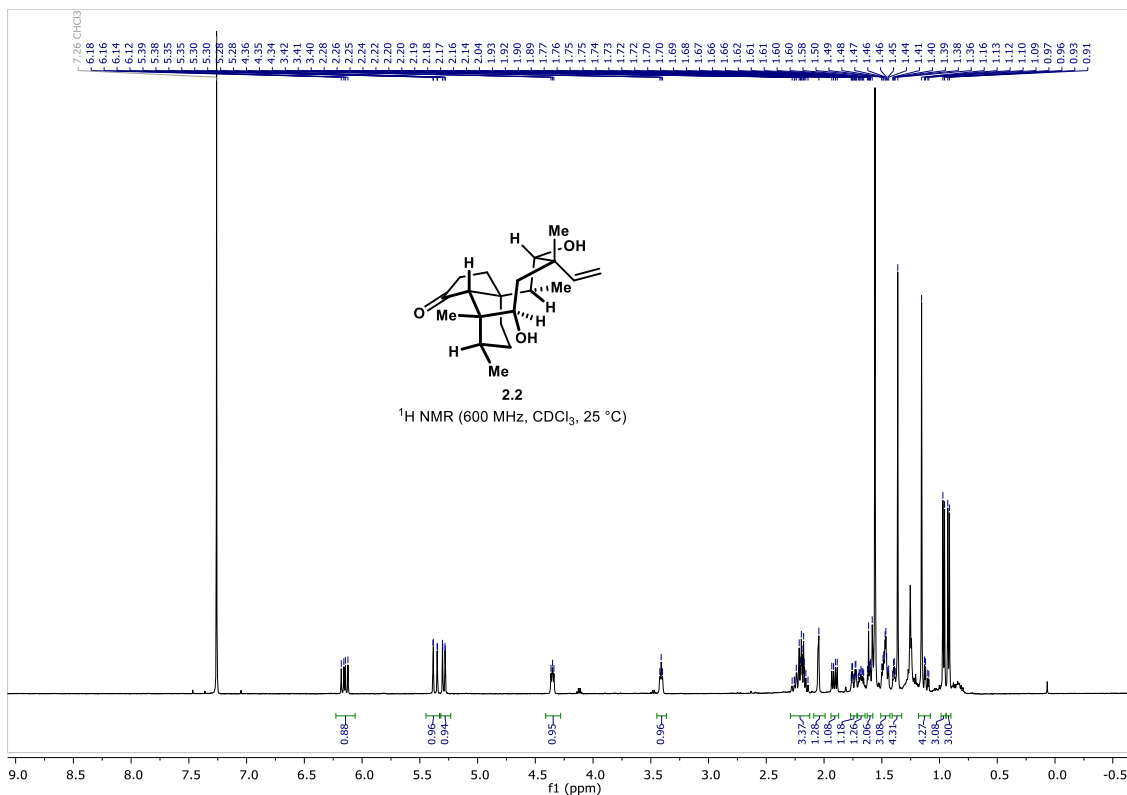
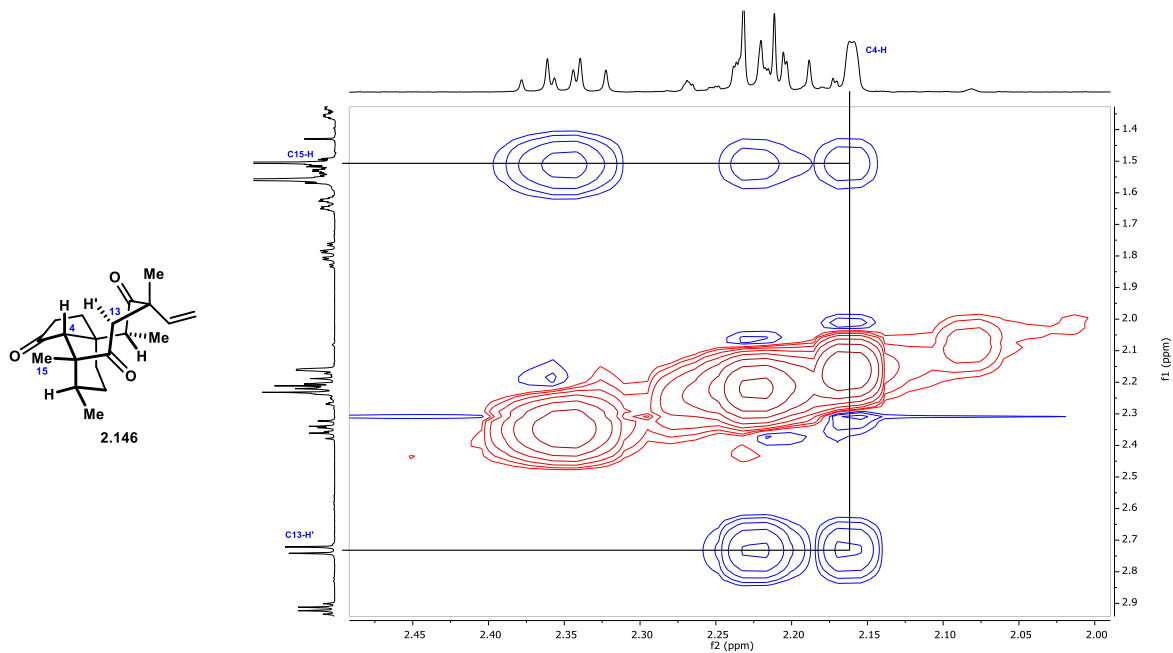


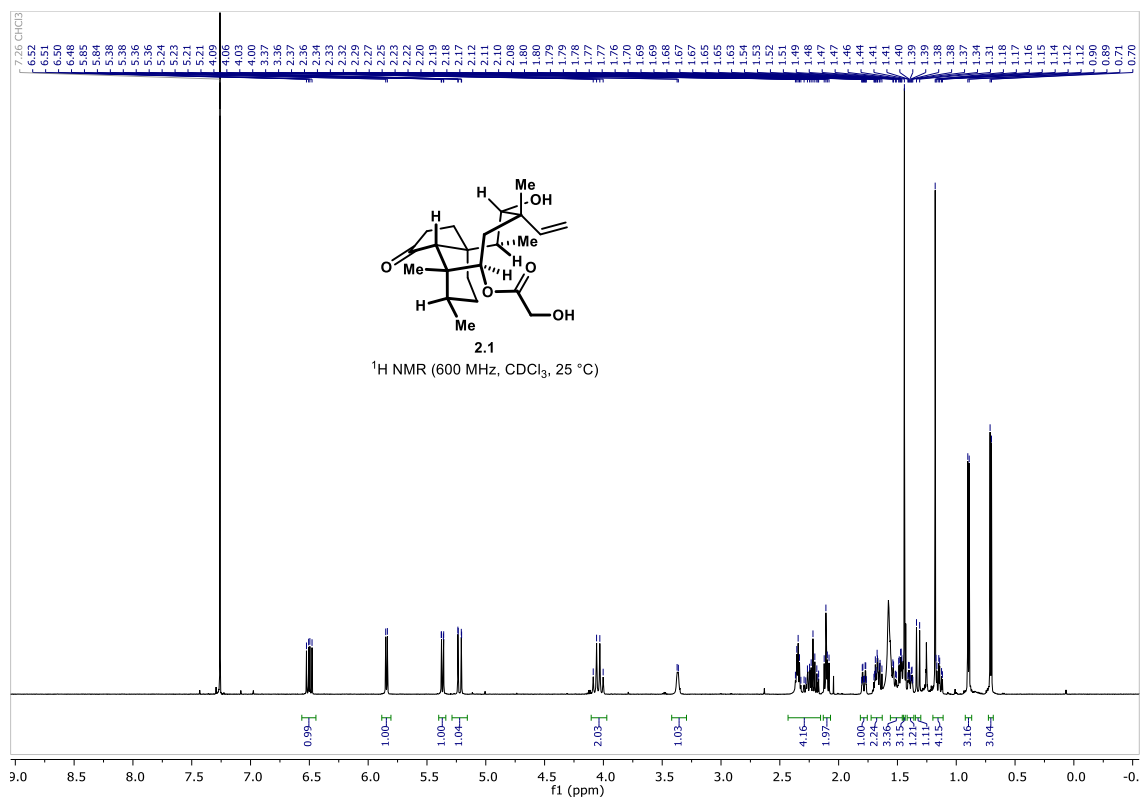
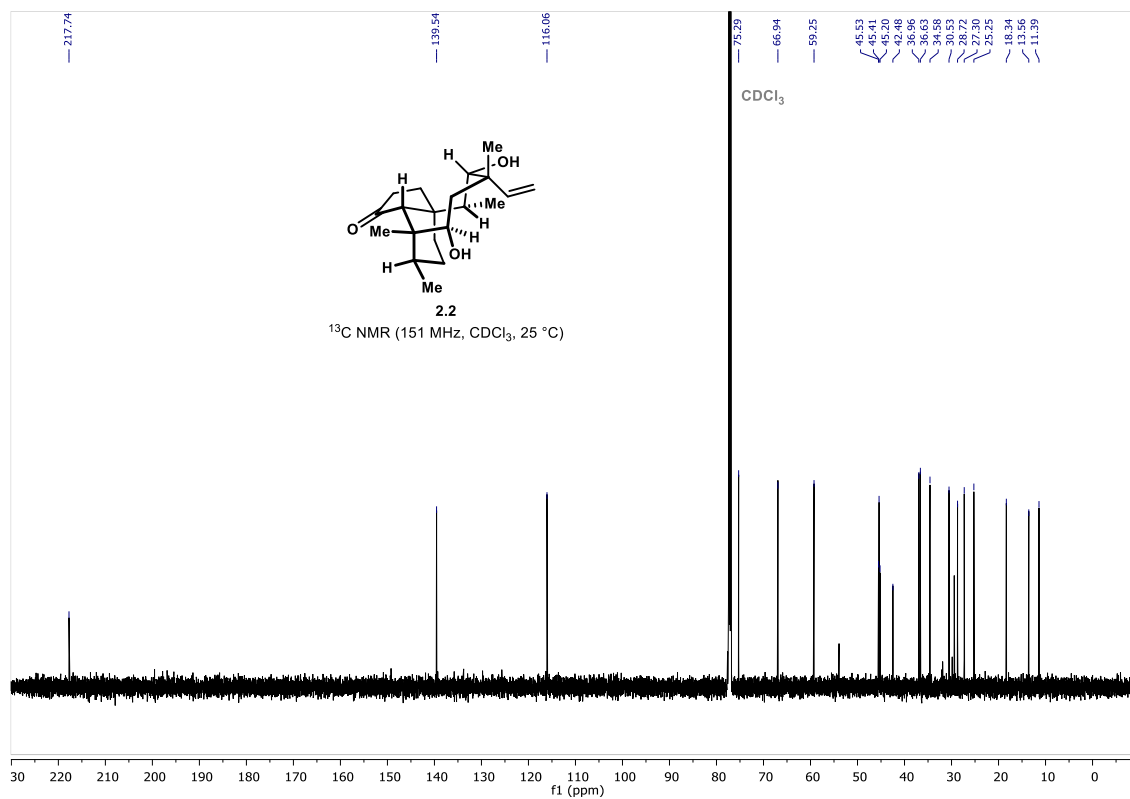




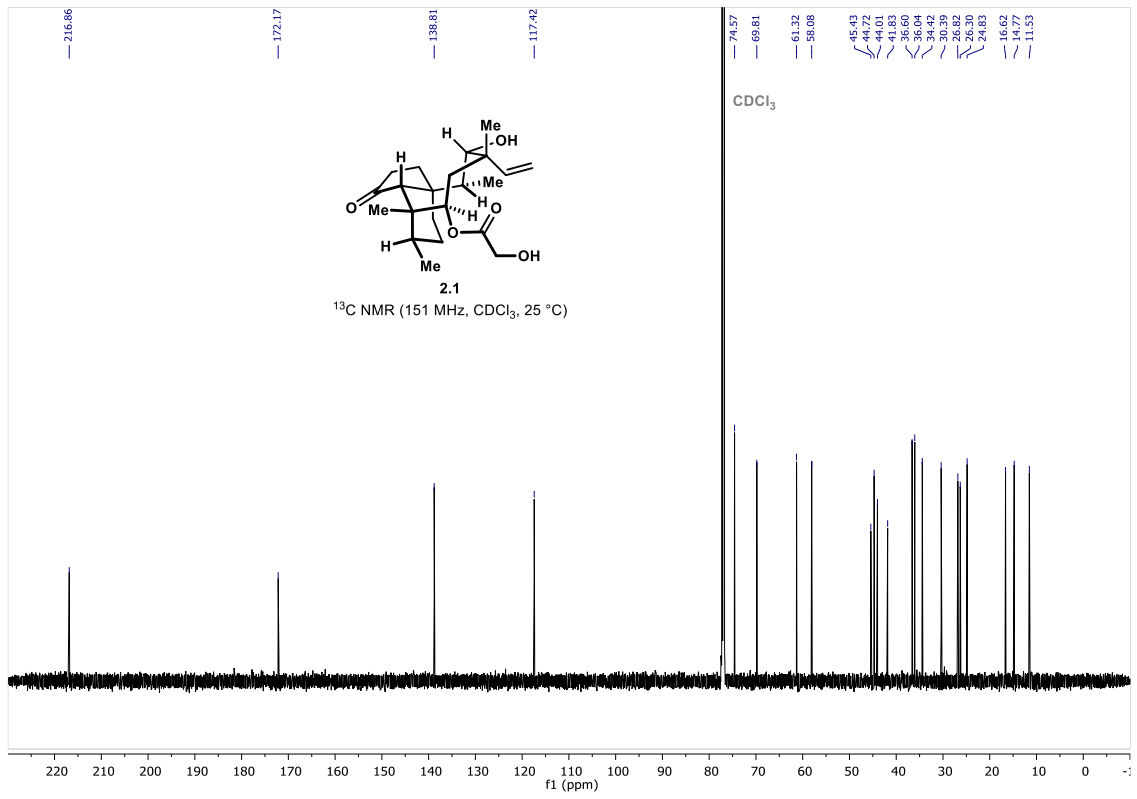




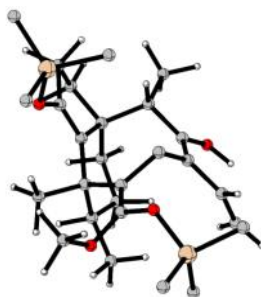








## Appendix B. Computational Data for Chapter 2



21-a

SPARTAN '18 Quantum Mechanics Program: (x86/Darwin)build 1.4.4

Job type: Geometry optimization. Method: RWB97X-D

Basis set: 6-31G(D)

Number of basis functions: 595

Number of electrons: 268

Atomic coordinates:

C	-1.400174	0.882746	-1.099460
C	-3.140711	-0.756436	-1.951070
C	-2.533518	-0.707118	0.539843
C	-2.934607	-1.562016	-0.668130
C	-1.376482	0.357290	0.336997
C	-1.936901	0.117884	-2.320518
C	0.045446	-0.162323	0.655373
C	0.889043	-0.694252	-0.493143
C	0.356591	-1.963196	-1.114292
C	-0.386150	-1.952084	-2.242100
C	0.617743	-0.138399	1.869779
C	0.704287	-3.204136	-0.410039
C	-0.780849	-0.712355	-3.017684
O	-0.875022	-3.085331	-2.812472
C	-0.048022	-4.297837	-0.208106
C	-2.300781	-1.617186	1.746420
C	-1.781171	1.535874	1.262268
C	-1.066334	-1.068786	-4.485063
C	-0.951330	2.078237	-1.509716
C	-1.257399	2.366630	-2.958553
C	-2.327543	1.306539	-3.235732
O	-0.325546	3.002594	-0.739000
Si	1.177573	3.707879	-0.986316
C	1.691482	4.284663	0.718029
C	2.396945	2.451517	-1.660643
C	1.003287	5.149617	-2.176467
O	1.906241	-0.531680	2.083192
O	-0.015135	0.238611	3.022574
C	0.531332	1.390756	3.650070

Si	2.328817	-1.774896	3.157399
C	3.848022	-2.554321	2.384097
C	0.916769	-2.990133	3.330809
C	2.776581	-1.051426	4.831124
H	-3.397615	-1.429722	-2.778111
H	-4.006146	-0.095673	-1.804954
H	-3.418017	-0.091023	0.758240
H	-3.880514	-2.059739	-0.416301
H	-2.212088	-2.362930	-0.823562
H	0.969588	0.088965	-1.249393
H	1.902869	-0.877160	-0.127318
H	1.711955	-3.211752	0.011313
H	0.095313	-0.053812	-3.021297
H	-0.484523	-3.846253	-2.353100
H	-1.094928	-4.358683	-0.497046
H	0.352789	-5.154887	0.324623
H	-1.478026	-2.312160	1.550357
H	-2.053958	-1.053280	2.649590
H	-3.201096	-2.208855	1.948221
H	-0.988835	2.278964	1.340900
H	-2.038744	1.181430	2.260967
H	-2.657514	2.033693	0.835321
H	-0.323392	-1.778810	-4.855706
H	-1.016050	-0.178146	-5.115824
H	-2.049721	-1.529798	-4.615329
H	-0.370066	2.242476	-3.599336
H	-1.615266	3.392624	-3.098263
H	-2.440527	1.047671	-4.290084
H	-3.292179	1.694430	-2.889865
H	1.833297	3.421228	1.377417
H	0.925210	4.928428	1.162736
H	2.631689	4.846687	0.689630
H	2.609165	1.673081	-0.920486
H	2.022973	1.962407	-2.567959
H	3.344006	2.941565	-1.916772
H	0.245652	5.857260	-1.823515
H	1.950221	5.692403	-2.276507
H	0.706426	4.811588	-3.175296
H	0.037848	1.478205	4.619302
H	1.611521	1.293003	3.796411
H	0.323977	2.285896	3.053453
H	4.636773	-1.808805	2.237467
H	3.620482	-2.994335	1.407655
H	4.251220	-3.347032	3.024954
H	0.623366	-3.410260	2.363962
H	0.037812	-2.498375	3.759085
H	1.204152	-3.815897	3.992436
H	1.897250	-0.634690	5.333426
H	3.526239	-0.257690	4.737361
H	3.194929	-1.829160	5.481727

A restricted hybrid HF-DFT SCF calculation will be performed using Pulay DIIS + Geometric Direct Minimization

Optimization:

Step	Energy	Max Grad.	Max Dist.
1	-1936.108006	0.021477	0.104599
2	-1936.110192	0.018104	0.110724
3	-1936.113847	0.016842	0.095576
4	-1936.116529	0.009687	0.081061
5	-1936.117278	0.004919	0.096520
6	-1936.117854	0.004722	0.078850
7	-1936.118117	0.003321	0.060763
8	-1936.118343	0.002321	0.105864
9	-1936.118189	0.006233	0.112180
10	-1936.118377	0.003854	0.133045
11	-1936.118315	0.004668	0.103648
12	-1936.118561	0.001419	0.137153
13	-1936.118433	0.004084	0.112200
14	-1936.118591	0.001850	0.098054
15	-1936.118457	0.003327	0.067687
16	-1936.118627	0.000557	0.040012
17	-1936.118584	0.001702	0.018622
18	-1936.118638	0.000412	0.008916
19	-1936.118639	0.000388	0.011040

Reason for exit: Successful completion

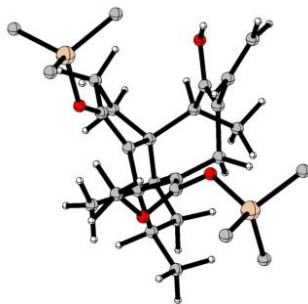
Quantum Calculation CPU Time : 16:30:42.04

Quantum Calculation Wall Time: 17:04:25.45

SPARTAN '18 Properties Program: (x86/Darwin) build 1.4.4

Reason for exit: Successful completion Properties CPU Time : 10.54

Properties Wall Time: 11.38



21-b

SPARTAN '18 Quantum Mechanics Program: (x86/Darwin)build 1.4.4

Job type: Geometry optimization. Method: RWB97X-D

Basis set: 6-31G(D)

Number of basis functions: 595

Number of electrons: 268

Atomic coordinates:

C	-1.660135	0.679357	-0.732137
C	-3.730530	-0.700429	-1.147873
C	-2.772425	-0.570181	1.200434
C	-3.443038	-1.459096	0.144415
C	-1.517390	0.275298	0.739362
C	-2.473406	-0.092247	-1.779784
C	-0.214894	-0.515234	0.909574
C	0.005234	-1.661929	-0.063111
C	0.644606	-1.290519	-1.385876
C	-0.094464	-1.016568	-2.478923
C	0.707665	-0.325386	1.862122
C	2.107400	-1.135700	-1.353096
C	-1.599741	-1.139959	-2.630823
O	0.455611	-0.566974	-3.646843
C	2.985350	-1.505842	-2.296742
C	-2.488642	-1.381471	2.465757
C	-1.583473	1.567033	1.587076
C	-2.010194	-2.625769	-2.626677
C	-1.107653	1.748726	-1.325855
C	-1.598587	1.962495	-2.738732
C	-2.837660	1.063273	-2.749054
O	-0.218930	2.599815	-0.756355
Si	1.029772	3.460398	-1.482994
C	2.023882	2.363784	-2.633146
C	0.358637	4.949442	-2.414482
C	2.083568	4.021641	-0.039092
O	1.898564	-0.992244	1.858916
O	0.553365	0.488439	2.944075
C	1.502604	1.538816	3.040681
Si	2.318945	-2.157115	3.014899
C	0.780189	-3.116780	3.485314

C	3.070184	-1.334191	4.523509
C	3.577613	-3.221166	2.128376
H	-4.271350	-1.331964	-1.861322
H	-4.408594	0.128041	-0.901245
H	-3.529638	0.184642	1.455926
H	-4.390340	-1.820648	0.565772
H	-2.851651	-2.358926	-0.048004
H	0.623630	-2.428360	0.413455
H	-0.957991	-2.133217	-0.245228
H	2.497356	-0.702463	-0.432212
H	-1.759054	-0.838704	-3.670011
H	1.398896	-0.399394	-3.486453
H	2.684818	-2.031936	-3.200311
H	4.050273	-1.339913	-2.163664
H	-1.846739	-2.241363	2.243800
H	-1.984707	-0.783973	3.231899
H	-3.423871	-1.763612	2.890742
H	-0.704613	2.193782	1.450514
H	-1.690684	1.343191	2.649575
H	-2.453985	2.146197	1.261384
H	-1.433947	-3.146007	-3.399054
H	-3.068917	-2.747486	-2.872698
H	-1.820008	-3.142440	-1.684407
H	-0.856861	1.642495	-3.481939
H	-1.837309	3.014507	-2.930188
H	-3.124694	0.715140	-3.746940
H	-3.681869	1.624961	-2.333588
H	1.429038	2.015769	-3.483839
H	2.403558	1.482994	-2.104366
H	2.884082	2.916243	-3.030512
H	-0.177497	4.659633	-3.323807
H	-0.327007	5.529439	-1.787450
H	1.180833	5.610535	-2.711521
H	2.601609	3.170317	0.414893
H	2.843194	4.743607	-0.359593
H	1.470740	4.498412	0.733424
H	1.258302	2.092235	3.948747
H	2.524378	1.151063	3.109660
H	1.422479	2.204739	2.173696
H	0.332604	-3.604752	2.612581
H	0.026096	-2.451284	3.918460
H	1.012068	-3.892054	4.224375
H	3.937246	-0.720921	4.253234
H	3.406993	-2.085273	5.247897
H	2.338045	-0.689569	5.021605
H	4.464852	-2.636568	1.862646
H	3.156344	-3.624481	1.200521
H	3.901868	-4.062352	2.750632

SCF model:

A restricted hybrid HF-DFT SCF calculation will be performed using Pulay DIIS + Geometric Direct Minimization

Optimization:

Step	Energy	Max Grad.	Max Dist.
1	-1936.100397	0.021557	0.070203
2	-1936.107506	0.013499	0.077074
3	-1936.109055	0.006810	0.090467
4	-1936.109895	0.006114	0.129375
5	-1936.110107	0.005940	0.133466
6	-1936.110134	0.006214	0.096937
7	-1936.110092	0.006831	0.077971
8	-1936.110666	0.004109	0.071839
9	-1936.110817	0.002613	0.122438
10	-1936.110964	0.002097	0.051684
11	-1936.110964	0.001889	0.055394
12	-1936.111055	0.001624	0.036713
13	-1936.111084	0.001371	0.043216
14	-1936.111129	0.002082	0.104523
15	-1936.111152	0.001317	0.041867
16	-1936.111159	0.001762	0.030712
17	-1936.111183	0.000777	0.026480
18	-1936.111187	0.001391	0.026635
19	-1936.111204	0.000532	0.031471

Reason for exit: Successful completion

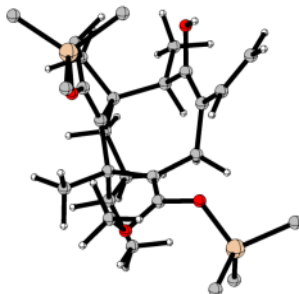
Quantum Calculation CPU Time : 16:40:30.21

Quantum Calculation Wall Time: 17:17:40.74

SPARTAN '18 Properties Program: (x86/Darwin) build 1.4.4

Reason for exit: Successful completion Properties CPU Time : 8.97

Properties Wall Time: 9.89



22-a

SPARTAN '18 Quantum Mechanics Program: (x86/Darwin)build 1.4.4

Job type: Geometry optimization. Method: RWB97X-D

Basis set: 6-31G(D)

Number of basis functions: 595

Number of electrons: 268

Atomic coordinates:

C	0.167754	0.406087	1.654473
C	1.134983	0.159213	2.882558
C	1.449880	-1.297813	3.247175
C	0.192038	-2.160135	3.338885
C	-0.832675	-0.746812	1.518278
C	-0.593233	-2.173076	2.020735
C	-2.036833	-0.695288	0.928595
C	-2.839395	-1.961502	1.100902
C	-2.044563	-2.675697	2.196812
C	0.214103	-3.050592	0.969895
C	0.945415	0.558370	0.336228
C	2.424951	0.973661	2.775114
C	-0.643606	1.662421	2.054514
O	-2.535559	0.364162	0.243896
Si	-3.687032	0.389783	-0.981892
C	0.024707	-2.624835	-0.467128
C	-3.320442	-0.902792	-2.291328
C	-3.527349	2.108030	-1.713966
C	-5.413946	0.142548	-0.284233
C	1.139290	1.705197	-0.330672
O	0.839722	2.946370	0.146782
O	1.721229	1.738873	-1.565771
C	-0.106194	3.669395	-0.629596
Si	3.247443	2.419527	-1.847960
C	4.350610	2.040680	-0.380850
C	3.098161	4.272249	-2.099724
C	3.826530	1.568048	-3.411283
C	1.599121	-0.689722	-0.242292
C	0.678810	-1.593943	-1.041684
C	0.436302	-1.168376	-2.427557
C	0.274656	-1.953901	-3.503031



O	-0.925186	-3.355725	-1.116213
C	0.007003	-4.561636	1.136429
H	0.578379	0.546490	3.747398
H	2.173346	-1.731181	2.546170
H	1.958668	-1.297492	4.219633
H	0.451148	-3.181033	3.647560
H	-0.454381	-1.748550	4.125813
H	-2.866911	-2.552250	0.177867
H	-3.872195	-1.748727	1.399642
H	-2.145934	-3.762448	2.168061
H	-2.406259	-2.338194	3.174850
H	1.268428	-2.874193	1.187750
H	3.087367	0.565645	2.003036
H	2.968739	0.954657	3.726958
H	2.224271	2.018790	2.517585
H	0.008875	2.481295	2.362281
H	-1.288940	1.393182	2.897623
H	-1.286896	2.011276	1.249056
H	-2.294432	-0.808635	-2.660793
H	-3.998410	-0.770139	-3.143267
H	-3.455108	-1.922954	-1.917445
H	-2.564141	2.224633	-2.221686
H	-3.599568	2.878987	-0.938848
H	-4.320199	2.296312	-2.448072
H	-6.165119	0.376464	-1.047832
H	-5.583306	-0.888741	0.039712
H	-5.591888	0.800651	0.573220
H	-0.252212	4.626231	-0.125933
H	0.258081	3.842500	-1.646860
H	-1.055952	3.125037	-0.670953
H	4.449213	0.960926	-0.226374
H	5.354529	2.454080	-0.528813
H	3.939404	2.471974	0.537665
H	4.075649	4.715046	-2.323535
H	2.707523	4.753339	-1.196961
H	2.426434	4.510505	-2.931771
H	4.820766	1.915567	-3.713474
H	3.873168	0.483911	-3.265182
H	3.136604	1.761850	-4.240016
H	2.059358	-1.247722	0.574545
H	2.425619	-0.388743	-0.890310
H	0.421381	-0.088078	-2.574565
H	0.371344	-3.036533	-3.456096
H	0.097162	-1.525878	-4.484724
H	-1.099359	-2.922387	-1.967524
H	0.099392	-4.852347	2.187765
H	0.767750	-5.108092	0.570075
H	-0.968083	-4.887804	0.770681

SCF model:

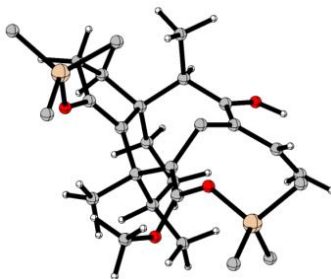
A restricted hybrid HF-DFT SCF calculation will be performed using Pulay DIIS + Geometric Direct Minimization

Optimization:

Step	Energy	Max Grad.	Max Dist.
1	-1936.110738	0.019005	0.100297
2	-1936.113738	0.023161	0.088799
3	-1936.115073	0.017382	0.091995
4	-1936.117094	0.012494	0.091998
5	-1936.116315	0.019413	0.127715
6	-1936.116120	0.020918	0.102457
7	-1936.118111	0.016131	0.115667
8	-1936.117632	0.013539	0.108776
9	-1936.118992	0.007956	0.075062
10	-1936.119311	0.006538	0.061120
11	-1936.120014	0.007094	0.047398
12	-1936.120101	0.005242	0.037902
13	-1936.120607	0.003112	0.127953
14	-1936.119782	0.009079	0.087645
15	-1936.120755	0.002121	0.043488
16	-1936.120588	0.003408	0.041417
17	-1936.120897	0.001844	0.052521
18	-1936.120812	0.002357	0.025183
19	-1936.120964	0.001278	0.035687
20	-1936.120960	0.002226	0.017491
21	-1936.121014	0.000805	0.025006
22	-1936.121028	0.000706	0.013443
23	-1936.121040	0.000751	0.027048
24	-1936.121041	0.000452	0.009700

Reason for exit: Successful completion  
Quantum Calculation CPU Time : 21:56:03.04  
Quantum Calculation Wall Time: 22:40:39.45

SPARTAN '18 Properties Program: (x86/Darwin) build 1.4.4  
Reason for exit: Successful completion Properties CPU Time : 11.01  
Properties Wall Time: 11.89



22-b

SPARTAN '18 Quantum Mechanics Program: (x86/Darwin) build 1.4.4

Job type: Geometry optimization. Method: RWB97X-D

Basis set: 6-31G(D)

Number of basis functions: 595

Number of electrons: 268

Atomic coordinates:

C	-0.597104	-0.143452	1.331548
C	0.200395	-0.335577	2.691914
C	0.945672	-1.658200	2.903874
C	0.098555	-2.874055	2.542734
C	-1.087089	-1.501452	0.803583
C	-0.410457	-2.844521	1.092588
C	-2.196972	-1.714699	0.080439
C	-2.543540	-3.169389	-0.104101
C	-1.586631	-3.841933	0.890860
C	0.758394	-3.261436	0.121255
C	0.208655	0.567550	0.222737
C	1.136564	0.831344	3.005932
C	-1.846594	0.676330	1.749868
O	-3.032762	-0.759947	-0.398156
Si	-3.470488	-0.455565	-1.989188
C	1.993424	-2.383065	0.139272
C	-4.947225	-1.522324	-2.440007
C	-2.035836	-0.797924	-3.148900
C	-3.904746	1.365794	-2.000765
C	0.293058	1.896583	0.055866
O	-0.230841	2.825805	0.912817
O	0.958106	2.463050	-0.991320
C	-1.251300	3.643237	0.354855
Si	2.224610	3.575263	-0.800838
C	1.560968	5.331537	-0.834409
C	3.310154	3.291065	-2.302693
C	3.131878	3.262931	0.806042
C	0.923443	-0.308536	-0.788008
C	2.093848	-1.090622	-0.235458
C	3.360513	-0.350639	-0.154216
C	4.297611	-0.408876	0.804078
O	3.061068	-3.112931	0.568753

C	0.356689	-3.580073	-1.331288
H	-0.589112	-0.336162	3.456708
H	1.891672	-1.661896	2.360668
H	1.211591	-1.717289	3.967449
H	0.655967	-3.800693	2.731237
H	-0.776004	-2.888903	3.207997
H	-2.394061	-3.500018	-1.140822
H	-3.598421	-3.346305	0.136099
H	-1.253109	-4.836557	0.578323
H	-2.105677	-3.963511	1.847390
H	1.116202	-4.210675	0.537245
H	0.638430	1.800150	2.910300
H	1.997485	0.828366	2.328532
H	1.514266	0.739185	4.031429
H	-1.562937	1.528076	2.369002
H	-2.514539	0.033535	2.331709
H	-2.407331	1.034387	0.888183
H	-4.697167	-2.588254	-2.388525
H	-5.292760	-1.309983	-3.457783
H	-5.783321	-1.342493	-1.756150
H	-1.743939	-1.853456	-3.141770
H	-1.160320	-0.197750	-2.879050
H	-2.313411	-0.541312	-4.178082
H	-4.339004	1.674199	-2.957305
H	-4.623329	1.602917	-1.209342
H	-3.002929	1.964626	-1.829755
H	-1.441570	4.437185	1.079220
H	-0.935621	4.082325	-0.596096
H	-2.167860	3.062385	0.202140
H	0.933430	5.511085	-1.714639
H	0.969295	5.554554	0.059580
H	2.393157	6.044711	-0.868699
H	2.742851	3.440645	-3.227850
H	3.715244	2.273991	-2.322375
H	4.155684	3.988956	-2.310751
H	3.522296	2.242369	0.859772
H	3.972399	3.959337	0.909901
H	2.462058	3.408215	1.660084
H	0.187099	-0.986912	-1.214937
H	1.281127	0.316349	-1.610475
H	3.531234	0.345510	-0.977025
H	4.176107	-0.998762	1.709102
H	5.199542	0.191690	0.737423
H	3.863529	-2.582884	0.436787
H	-0.288377	-4.461804	-1.377265
H	1.254484	-3.799045	-1.917449
H	-0.166369	-2.755360	-1.819804

SCF model:

A restricted hybrid HF-DFT SCF calculation will be performed using Pulay DIIS + Geometric Direct Minimization

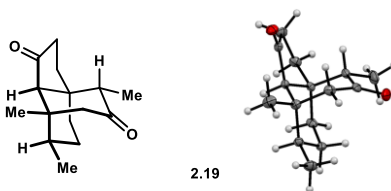
Optimization:

Step	Energy	Max Grad.	Max Dist.
1	-1936.107392	0.026031	0.103440
2	-1936.109329	0.019725	0.109108
3	-1936.113389	0.021627	0.083526
4	-1936.115829	0.011239	0.101226
5	-1936.116689	0.011021	0.104795
6	-1936.117091	0.006956	0.104154
7	-1936.117355	0.006084	0.079515
8	-1936.117810	0.002279	0.100374
9	-1936.117917	0.003176	0.057781
10	-1936.118114	0.002938	0.053017
11	-1936.118127	0.002830	0.085544
12	-1936.118206	0.002044	0.077021
13	-1936.118222	0.002829	0.072757
14	-1936.118251	0.002026	0.052829
15	-1936.118299	0.001666	0.031723
16	-1936.118327	0.000857	0.014986
17	-1936.118344	0.000948	0.012506
18	-1936.118360	0.000511	0.019174

Reason for exit: Successful completion  
Quantum Calculation CPU Time : 16:02:01.28  
Quantum Calculation Wall Time: 16:35:19.16

SPARTAN '18 Properties Program: (x86/Darwin) build 1.4.4  
Reason for exit: Successful completion Properties CPU Time : 10.85  
Properties Wall Time: 11.71

## Appendix C. X-Ray Crystallographic Data for Chapter 2



Crystal structure provided by Dr. Joseph Ziller (University of California, Irvine, California, United States of America). Thermal ellipsoids are drawn at 50% probability level.

Table 1. Crystal data and structure refinement for svp12.

Identification code	svp12 (Nick Foy)	
Empirical formula	C <sub>15</sub> H <sub>22</sub> O <sub>2</sub>	
Formula weight	234.32	
Temperature	133(2) K	
Wavelength	0.71073 Å	
Crystal system	Triclinic	
Space group	$P\bar{1}$	
Unit cell dimensions	$a = 7.0273(7)$ Å	$\alpha = 104.0991(12)^\circ$ .
	$b = 8.2582(8)$ Å	$\beta = 91.9119(11)^\circ$ .
	$c = 11.3832(11)$ Å	$\gamma = 93.6082(12)^\circ$ .
Volume	638.62(11) Å <sup>3</sup>	
Z	2	
Density (calculated)	1.219 Mg/m <sup>3</sup>	
Absorption coefficient	0.079 mm <sup>-1</sup>	
F(000)	256	
Crystal color	colorless	
Crystal size	0.408 x 0.338 x 0.222 mm <sup>3</sup>	
Theta range for data collection	1.847 to 28.905°	

Index ranges	$-9 \leq h \leq 9, -11 \leq k \leq 10, -15 \leq l \leq 15$
Reflections collected	7645
Independent reflections	3022 [R(int) = 0.0241]
Completeness to $\theta = 25.500^\circ$	99.8 %
Absorption correction	Semi-empirical from equivalents
Max. and min. transmission	0.8621 and 0.7994
Refinement method	Full-matrix least-squares on $F^2$
Data / restraints / parameters	3022 / 0 / 242
Goodness-of-fit on $F^2$	1.086
Final R indices [ $I > 2\sigma(I)$ = 2738 data]	R1 = 0.0375, wR2 = 0.1065
R indices (all data, 0.74 Å)	R1 = 0.0405, wR2 = 0.1094
Largest diff. peak and hole	0.408 and -0.164 e.Å <sup>-3</sup>

Table 2. Atomic coordinates ( $\times 10^4$ ) and equivalent isotropic displacement parameters ( $\text{Å}^2 \times 10^3$ ) for svp12. U(eq) is defined as one third of the trace of the orthogonalized  $U^{ij}$  tensor.

	x	y	z	U(eq)
O(1)	2844(1)	2759(1)	8051(1)	31(1)
O(2)	7560(1)	-462(1)	5073(1)	24(1)
C(1)	5315(1)	3445(1)	6811(1)	17(1)
C(2)	4337(1)	2390(1)	7576(1)	20(1)
C(3)	5248(1)	815(1)	7656(1)	20(1)
C(4)	7438(1)	1023(1)	7864(1)	15(1)

C(5)	8096(1)	2218(1)	9122(1)	16(1)
C(6)	7601(1)	4039(1)	9243(1)	17(1)
C(7)	8261(1)	4747(1)	8188(1)	17(1)
C(8)	7536(1)	3589(1)	6976(1)	13(1)
C(9)	8251(1)	1842(1)	6899(1)	13(1)
C(10)	7965(1)	1006(1)	5553(1)	17(1)
C(11)	8255(2)	2376(1)	4872(1)	22(1)
C(12)	8413(1)	4030(1)	5857(1)	20(1)
C(13)	4449(2)	5131(2)	6969(1)	31(1)
C(14)	8218(2)	-695(1)	7765(1)	26(1)
C(15)	7351(2)	1616(1)	10203(1)	25(1)

---

Table 3. Bond lengths [Å] and angles [°] for svp12.

O(1)-C(2)	1.2181(12)
O(2)-C(10)	1.2133(12)
C(1)-C(2)	1.5247(14)
C(1)-C(13)	1.5277(13)
C(1)-C(8)	1.5595(12)
C(2)-C(3)	1.5063(14)
C(3)-C(4)	1.5413(13)
C(4)-C(9)	1.5316(12)
C(4)-C(14)	1.5327(13)
C(4)-C(5)	1.5647(12)



C(5)-C(15)	1.5314(13)
C(5)-C(6)	1.5387(13)
C(6)-C(7)	1.5310(13)
C(7)-C(8)	1.5257(12)
C(8)-C(9)	1.5409(11)
C(8)-C(12)	1.5444(12)
C(9)-C(10)	1.5205(12)
C(10)-C(11)	1.5272(13)
C(11)-C(12)	1.5366(14)

C(2)-C(1)-C(13)	111.35(8)
C(2)-C(1)-C(8)	113.54(7)
C(13)-C(1)-C(8)	113.67(8)
O(1)-C(2)-C(3)	121.64(9)
O(1)-C(2)-C(1)	121.64(9)
C(3)-C(2)-C(1)	116.63(8)
C(2)-C(3)-C(4)	114.54(7)
C(9)-C(4)-C(14)	110.80(7)
C(9)-C(4)-C(3)	107.81(7)
C(14)-C(4)-C(3)	109.58(8)
C(9)-C(4)-C(5)	106.44(7)
C(14)-C(4)-C(5)	109.59(8)
C(3)-C(4)-C(5)	112.58(7)
C(15)-C(5)-C(6)	109.22(8)
C(15)-C(5)-C(4)	113.59(8)

C(6)-C(5)-C(4)	113.36(7)
C(7)-C(6)-C(5)	113.15(7)
C(8)-C(7)-C(6)	110.70(7)
C(7)-C(8)-C(9)	108.46(7)
C(7)-C(8)-C(12)	114.48(7)
C(9)-C(8)-C(12)	101.58(7)
C(7)-C(8)-C(1)	112.50(7)
C(9)-C(8)-C(1)	109.55(7)
C(12)-C(8)-C(1)	109.65(7)
C(10)-C(9)-C(4)	121.73(7)
C(10)-C(9)-C(8)	102.42(7)
C(4)-C(9)-C(8)	112.79(7)
O(2)-C(10)-C(9)	128.22(9)
O(2)-C(10)-C(11)	124.59(8)
C(9)-C(10)-C(11)	107.19(8)
C(10)-C(11)-C(12)	105.27(7)
C(11)-C(12)-C(8)	104.92(7)

---

Table 4. Anisotropic displacement parameters ( $\text{\AA}^2 \times 10^3$ ) for svp12. The anisotropic displacement factor exponent takes the form:  $-2\pi^2 [ h^2 a^{*2}U^{11} + \dots + 2 h k a^* b^* U^{12} ]$

---

$U^{11}$	$U^{22}$	$U^{33}$	$U^{23}$	$U^{13}$	$U^{12}$
----------	----------	----------	----------	----------	----------

---

O(1)	13(1)	49(1)	27(1)	0(1)	4(1)	1(1)
O(2)	28(1)	20(1)	20(1)	-1(1)	-1(1)	2(1)
C(1)	13(1)	19(1)	18(1)	2(1)	-2(1)	4(1)
C(2)	11(1)	28(1)	16(1)	0(1)	-2(1)	-2(1)
C(3)	18(1)	22(1)	19(1)	5(1)	1(1)	-7(1)
C(4)	18(1)	14(1)	15(1)	4(1)	2(1)	1(1)
C(5)	16(1)	19(1)	14(1)	5(1)	0(1)	0(1)
C(6)	18(1)	17(1)	14(1)	0(1)	-1(1)	1(1)
C(7)	19(1)	13(1)	18(1)	3(1)	-4(1)	-1(1)
C(8)	12(1)	13(1)	15(1)	4(1)	-1(1)	0(1)
C(9)	11(1)	14(1)	14(1)	4(1)	1(1)	2(1)
C(10)	14(1)	21(1)	16(1)	3(1)	2(1)	5(1)
C(11)	25(1)	26(1)	16(1)	7(1)	4(1)	5(1)
C(12)	21(1)	21(1)	19(1)	10(1)	-1(1)	-2(1)
C(13)	25(1)	29(1)	37(1)	6(1)	-4(1)	14(1)
C(14)	39(1)	16(1)	23(1)	7(1)	3(1)	7(1)
C(15)	29(1)	29(1)	17(1)	9(1)	2(1)	-2(1)

---

Table 5. Hydrogen coordinates ( $\times 10^4$ ) and isotropic displacement parameters ( $\text{\AA}^2 \times 10^3$ )

for svp12.

---

	x	y	z	U(eq)
--	---	---	---	-------

---

H(1A)	4987(18)	2754(15)	5977(12)	22(3)
H(3A)	4959(19)	-11(17)	6871(13)	29(3)
H(3B)	4630(20)	342(18)	8270(14)	35(4)
H(5A)	9506(18)	2218(15)	9166(11)	21(3)
H(6A)	6212(18)	4103(15)	9321(11)	19(3)
H(6B)	8213(19)	4739(16)	10021(12)	24(3)
H(7A)	7847(19)	5915(17)	8285(12)	26(3)
H(7B)	9690(20)	4832(16)	8195(12)	25(3)
H(9A)	9666(19)	2006(16)	7038(11)	22(3)
H(11A)	7170(20)	2295(17)	4286(13)	31(3)
H(11B)	9410(20)	2158(18)	4400(13)	34(4)
H(12A)	7771(18)	4923(16)	5590(12)	25(3)
H(12B)	9790(20)	4454(17)	6069(13)	30(3)
H(13A)	3090(20)	4950(20)	6723(15)	46(4)
H(13B)	5100(20)	5850(20)	6476(15)	44(4)
H(13C)	4560(20)	5760(20)	7827(15)	44(4)
H(14A)	7850(20)	-1448(19)	6955(15)	39(4)
H(14B)	7700(20)	-1220(20)	8378(14)	42(4)
H(14C)	9610(20)	-564(18)	7901(14)	36(4)
H(15A)	7930(20)	2378(18)	10960(14)	33(4)
H(15B)	7710(20)	441(19)	10204(14)	39(4)
H(15C)	5930(20)	1612(19)	10215(14)	39(4)

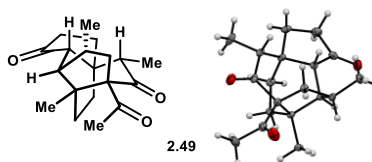
---

Table 6. Torsion angles [°] for svp12.

---

C(13)-C(1)-C(2)-O(1)	12.64(13)
C(8)-C(1)-C(2)-O(1)	142.47(9)
C(13)-C(1)-C(2)-C(3)	-170.79(8)
C(8)-C(1)-C(2)-C(3)	-40.96(11)
O(1)-C(2)-C(3)-C(4)	-139.32(9)
C(1)-C(2)-C(3)-C(4)	44.11(11)
C(2)-C(3)-C(4)-C(9)	-52.08(10)
C(2)-C(3)-C(4)-C(14)	-172.76(8)
C(2)-C(3)-C(4)-C(5)	65.02(10)
C(9)-C(4)-C(5)-C(15)	178.18(8)
C(14)-C(4)-C(5)-C(15)	-61.96(10)
C(3)-C(4)-C(5)-C(15)	60.27(10)
C(9)-C(4)-C(5)-C(6)	52.73(9)
C(14)-C(4)-C(5)-C(6)	172.60(8)
C(3)-C(4)-C(5)-C(6)	-65.18(10)
C(15)-C(5)-C(6)-C(7)	-179.02(7)
C(4)-C(5)-C(6)-C(7)	-51.27(10)
C(5)-C(6)-C(7)-C(8)	52.64(10)
C(6)-C(7)-C(8)-C(9)	-57.16(9)
C(6)-C(7)-C(8)-C(12)	-169.77(7)
C(6)-C(7)-C(8)-C(1)	64.18(9)
C(2)-C(1)-C(8)-C(7)	-73.79(9)
C(13)-C(1)-C(8)-C(7)	54.87(11)
C(2)-C(1)-C(8)-C(9)	46.93(10)

C(13)-C(1)-C(8)-C(9)	175.58(8)
C(2)-C(1)-C(8)-C(12)	157.59(8)
C(13)-C(1)-C(8)-C(12)	-73.76(10)
C(14)-C(4)-C(9)-C(10)	58.72(11)
C(3)-C(4)-C(9)-C(10)	-61.19(10)
C(5)-C(4)-C(9)-C(10)	177.80(7)
C(14)-C(4)-C(9)-C(8)	-178.99(7)
C(3)-C(4)-C(9)-C(8)	61.10(9)
C(5)-C(4)-C(9)-C(8)	-59.92(9)
C(7)-C(8)-C(9)-C(10)	-163.55(7)
C(12)-C(8)-C(9)-C(10)	-42.59(8)
C(1)-C(8)-C(9)-C(10)	73.32(8)
C(7)-C(8)-C(9)-C(4)	63.87(9)
C(12)-C(8)-C(9)-C(4)	-175.18(7)
C(1)-C(8)-C(9)-C(4)	-59.26(9)
C(4)-C(9)-C(10)-O(2)	-20.24(14)
C(8)-C(9)-C(10)-O(2)	-147.29(9)
C(4)-C(9)-C(10)-C(11)	158.92(8)
C(8)-C(9)-C(10)-C(11)	31.87(9)
O(2)-C(10)-C(11)-C(12)	171.01(9)
C(9)-C(10)-C(11)-C(12)	-8.19(10)
C(10)-C(11)-C(12)-C(8)	-18.78(10)
C(7)-C(8)-C(12)-C(11)	154.76(8)
C(9)-C(8)-C(12)-C(11)	38.12(9)
C(1)-C(8)-C(12)-C(11)	-77.72(9)



Crystal structure provided by Dr. Joseph Ziller (University of California, Irvine, California, United States of America). Thermal ellipsoids are drawn at 50% probability level.

Table 1. Crystal data and structure refinement for svp33.

Identification code	svp33 (Nick Foy)	
Empirical formula	$C_{19} H_{26} O_3$	
Formula weight	302.40	
Temperature	133(2) K	
Wavelength	0.71073 Å	
Crystal system	Monoclinic	
Space group	<i>Pn</i>	
Unit cell dimensions	$a = 7.0542(5)$ Å	$\alpha = 90^\circ$ .
	$b = 13.5509(10)$ Å	$\beta = 111.0502(11)^\circ$ .
	$c = 8.7184(6)$ Å	$\gamma = 90^\circ$ .
Volume	$777.78(10)$ Å <sup>3</sup>	
Z	2	
Density (calculated)	1.291 Mg/m <sup>3</sup>	
Absorption coefficient	0.085 mm <sup>-1</sup>	
F(000)	328	
Crystal color	colorless	
Crystal size	0.340 x 0.164 x 0.050 mm <sup>3</sup>	
Theta range for data collection	2.920 to 30.503°	

Index ranges	-10 ≤ h ≤ 10, -19 ≤ k ≤ 19, -12 ≤ l ≤ 11
Reflections collected	18388
Independent reflections	4535 [R(int) = 0.0379]
Completeness to theta = 25.242°	99.9 %
Absorption correction	Semi-empirical from equivalents
Max. and min. transmission	0.8622 and 0.8165
Refinement method	Full-matrix least-squares on F <sup>2</sup>
Data / restraints / parameters	4535 / 2 / 303
Goodness-of-fit on F <sup>2</sup>	1.038
Final R indices [I > 2σ(I) = 4056 data]	R1 = 0.0408, wR2 = 0.0931
R indices (all data, 0.70 Å)	R1 = 0.0489, wR2 = 0.0978
Largest diff. peak and hole	0.349 and -0.215 e.Å <sup>-3</sup>

Table 2. Atomic coordinates (x 10<sup>4</sup>) and equivalent isotropic displacement parameters (Å<sup>2</sup> x 10<sup>3</sup>) for svp33. U(eq) is defined as one third of the trace of the orthogonalized U<sup>ij</sup> tensor.

	x	y	z	U(eq)
O(1)	1847(2)	4076(1)	9730(2)	23(1)
O(2)	10610(2)	1650(1)	10451(2)	27(1)
O(3)	8167(3)	1461(1)	6183(2)	30(1)
C(1)	3532(3)	3837(2)	10618(3)	16(1)
C(2)	4403(3)	3937(2)	12468(3)	20(1)
C(3)	6529(3)	3483(2)	13006(3)	17(1)
C(4)	6547(3)	2818(2)	11561(2)	12(1)



C(5)	8737(3)	2688(2)	11594(2)	14(1)
C(6)	9007(3)	2064(2)	10213(2)	14(1)
C(7)	7372(3)	2020(2)	8497(2)	12(1)
C(8)	5185(3)	1772(1)	8549(2)	12(1)
C(9)	5248(3)	1199(1)	10096(3)	14(1)
C(10)	5540(3)	1828(2)	11624(3)	14(1)
C(11)	5145(3)	3385(1)	10045(2)	12(1)
C(12)	4257(3)	2815(1)	8414(2)	12(1)
C(13)	4889(3)	3305(2)	7083(2)	14(1)
C(14)	7164(3)	3061(2)	7692(3)	14(1)
C(15)	10182(3)	2304(2)	13255(3)	23(1)
C(16)	8034(3)	1244(2)	7484(3)	17(1)
C(17)	8466(4)	203(2)	8104(3)	22(1)
C(18)	3936(3)	1151(2)	7050(3)	17(1)
C(19)	4391(4)	4394(2)	6758(3)	21(1)

---

Table 3. Bond lengths [Å] and angles [°] for svp33.

O(1)-C(1)	1.206(3)
O(2)-C(6)	1.212(2)
O(3)-C(16)	1.207(3)
C(1)-C(2)	1.512(3)
C(1)-C(11)	1.525(3)
C(2)-C(3)	1.531(3)

C(2)-H(2A)	0.97(3)
C(2)-H(2B)	0.97(4)
C(3)-C(4)	1.552(3)
C(3)-H(3A)	0.96(2)
C(3)-H(3B)	0.92(3)
C(4)-C(10)	1.528(3)
C(4)-C(11)	1.542(3)
C(4)-C(5)	1.545(3)
C(5)-C(15)	1.532(3)
C(5)-C(6)	1.537(3)
C(5)-H(5A)	0.94(3)
C(6)-C(7)	1.528(3)
C(7)-C(16)	1.549(3)
C(7)-C(14)	1.558(3)
C(7)-C(8)	1.595(3)
C(8)-C(18)	1.539(3)
C(8)-C(9)	1.542(3)
C(8)-C(12)	1.544(3)
C(9)-C(10)	1.532(3)
C(9)-H(9A)	0.99(3)
C(9)-H(9B)	0.93(3)
C(10)-H(10A)	0.95(3)
C(10)-H(10B)	0.98(3)
C(11)-C(12)	1.540(3)
C(11)-H(11A)	0.98(3)

C(12)-C(13)	1.536(3)
C(12)-H(12A)	0.96(3)
C(13)-C(19)	1.520(3)
C(13)-C(14)	1.535(3)
C(13)-H(13A)	0.99(3)
C(14)-H(14A)	0.95(3)
C(14)-H(14B)	0.95(3)
C(15)-H(15A)	0.98(3)
C(15)-H(15B)	1.00(5)
C(15)-H(15C)	0.96(3)
C(16)-C(17)	1.503(3)
C(17)-H(17A)	0.97(4)
C(17)-H(17B)	0.89(4)
C(17)-H(17C)	1.01(4)
C(18)-H(18A)	0.90(3)
C(18)-H(18B)	0.93(3)
C(18)-H(18C)	0.99(3)
C(19)-H(19A)	0.94(3)
C(19)-H(19B)	0.98(3)
C(19)-H(19C)	0.94(3)
O(1)-C(1)-C(2)	126.09(19)
O(1)-C(1)-C(11)	125.23(19)
C(2)-C(1)-C(11)	108.69(17)
C(1)-C(2)-C(3)	105.56(17)

C(1)-C(2)-H(2A)	109.1(18)
C(3)-C(2)-H(2A)	114.8(18)
C(1)-C(2)-H(2B)	107(2)
C(3)-C(2)-H(2B)	114(2)
H(2A)-C(2)-H(2B)	106(3)
C(2)-C(3)-C(4)	106.12(16)
C(2)-C(3)-H(3A)	109.7(15)
C(4)-C(3)-H(3A)	108.4(15)
C(2)-C(3)-H(3B)	110.6(16)
C(4)-C(3)-H(3B)	111.3(16)
H(3A)-C(3)-H(3B)	111(2)
C(10)-C(4)-C(11)	107.76(16)
C(10)-C(4)-C(5)	111.99(16)
C(11)-C(4)-C(5)	113.68(16)
C(10)-C(4)-C(3)	109.95(16)
C(11)-C(4)-C(3)	102.49(16)
C(5)-C(4)-C(3)	110.52(16)
C(15)-C(5)-C(6)	109.01(17)
C(15)-C(5)-C(4)	112.18(17)
C(6)-C(5)-C(4)	116.89(16)
C(15)-C(5)-H(5A)	105.0(16)
C(6)-C(5)-H(5A)	103.1(16)
C(4)-C(5)-H(5A)	109.7(16)
O(2)-C(6)-C(7)	118.62(18)
O(2)-C(6)-C(5)	119.42(18)

C(7)-C(6)-C(5)	121.76(16)
C(6)-C(7)-C(16)	108.01(16)
C(6)-C(7)-C(14)	108.73(16)
C(16)-C(7)-C(14)	110.86(16)
C(6)-C(7)-C(8)	112.19(15)
C(16)-C(7)-C(8)	111.50(16)
C(14)-C(7)-C(8)	105.54(15)
C(18)-C(8)-C(9)	107.16(16)
C(18)-C(8)-C(12)	109.76(16)
C(9)-C(8)-C(12)	113.94(16)
C(18)-C(8)-C(7)	110.83(16)
C(9)-C(8)-C(7)	113.98(16)
C(12)-C(8)-C(7)	101.13(15)
C(10)-C(9)-C(8)	115.64(15)
C(10)-C(9)-H(9A)	108.7(16)
C(8)-C(9)-H(9A)	110.9(16)
C(10)-C(9)-H(9B)	106.5(18)
C(8)-C(9)-H(9B)	109.7(17)
H(9A)-C(9)-H(9B)	105(2)
C(4)-C(10)-C(9)	112.09(16)
C(4)-C(10)-H(10A)	111.1(15)
C(9)-C(10)-H(10A)	110.1(15)
C(4)-C(10)-H(10B)	105.1(16)
C(9)-C(10)-H(10B)	111.1(16)
H(10A)-C(10)-H(10B)	107(2)

C(1)-C(11)-C(12)	113.57(16)
C(1)-C(11)-C(4)	104.12(16)
C(12)-C(11)-C(4)	117.67(15)
C(1)-C(11)-H(11A)	102.6(14)
C(12)-C(11)-H(11A)	111.8(15)
C(4)-C(11)-H(11A)	105.6(15)
C(13)-C(12)-C(11)	110.39(16)
C(13)-C(12)-C(8)	102.91(15)
C(11)-C(12)-C(8)	111.58(15)
C(13)-C(12)-H(12A)	112.8(16)
C(11)-C(12)-H(12A)	108.2(16)
C(8)-C(12)-H(12A)	111.0(16)
C(19)-C(13)-C(14)	114.67(18)
C(19)-C(13)-C(12)	116.78(17)
C(14)-C(13)-C(12)	101.33(15)
C(19)-C(13)-H(13A)	111.2(15)
C(14)-C(13)-H(13A)	104.8(14)
C(12)-C(13)-H(13A)	106.9(15)
C(13)-C(14)-C(7)	105.61(16)
C(13)-C(14)-H(14A)	111.2(19)
C(7)-C(14)-H(14A)	110.6(19)
C(13)-C(14)-H(14B)	110.0(15)
C(7)-C(14)-H(14B)	112.4(15)
H(14A)-C(14)-H(14B)	107(2)
C(5)-C(15)-H(15A)	109.5(16)

C(5)-C(15)-H(15B)	109(3)
H(15A)-C(15)-H(15B)	105(3)
C(5)-C(15)-H(15C)	110.6(19)
H(15A)-C(15)-H(15C)	105(3)
H(15B)-C(15)-H(15C)	118(3)
O(3)-C(16)-C(17)	119.5(2)
O(3)-C(16)-C(7)	120.79(19)
C(17)-C(16)-C(7)	119.70(18)
C(16)-C(17)-H(17A)	107(2)
C(16)-C(17)-H(17B)	107(2)
H(17A)-C(17)-H(17B)	113(3)
C(16)-C(17)-H(17C)	116(2)
H(17A)-C(17)-H(17C)	105(3)
H(17B)-C(17)-H(17C)	109(3)
C(8)-C(18)-H(18A)	108.3(19)
C(8)-C(18)-H(18B)	112.0(18)
H(18A)-C(18)-H(18B)	110(2)
C(8)-C(18)-H(18C)	110.9(18)
H(18A)-C(18)-H(18C)	108(3)
H(18B)-C(18)-H(18C)	108(3)
C(13)-C(19)-H(19A)	113(2)
C(13)-C(19)-H(19B)	109.2(17)
H(19A)-C(19)-H(19B)	110(2)
C(13)-C(19)-H(19C)	113.3(19)
H(19A)-C(19)-H(19C)	103(3)

Table 4. Anisotropic displacement parameters ( $\text{\AA}^2 \times 10^3$ ) for svp33. The anisotropic displacement factor exponent takes the form:  $-2\pi^2 [h^2 a^{*2}U^{11} + \dots + 2 h k a^* b^* U^{12}]$

	$U^{11}$	$U^{22}$	$U^{33}$	$U^{23}$	$U^{13}$	$U^{12}$
O(1)	19(1)	27(1)	24(1)	0(1)	8(1)	9(1)
O(2)	13(1)	37(1)	26(1)	-5(1)	1(1)	8(1)
O(3)	48(1)	30(1)	22(1)	3(1)	23(1)	11(1)
C(1)	18(1)	14(1)	18(1)	-1(1)	9(1)	-1(1)
C(2)	22(1)	23(1)	16(1)	-3(1)	10(1)	1(1)
C(3)	19(1)	21(1)	11(1)	-2(1)	6(1)	-4(1)
C(4)	12(1)	16(1)	9(1)	0(1)	4(1)	-2(1)
C(5)	12(1)	17(1)	11(1)	1(1)	2(1)	-3(1)
C(6)	12(1)	15(1)	14(1)	3(1)	4(1)	-1(1)
C(7)	10(1)	15(1)	11(1)	0(1)	4(1)	1(1)
C(8)	9(1)	13(1)	11(1)	-1(1)	2(1)	-1(1)
C(9)	15(1)	12(1)	16(1)	0(1)	6(1)	-3(1)
C(10)	13(1)	17(1)	13(1)	2(1)	5(1)	-4(1)
C(11)	11(1)	12(1)	11(1)	0(1)	4(1)	-1(1)
C(12)	10(1)	14(1)	11(1)	-1(1)	2(1)	1(1)
C(13)	17(1)	15(1)	8(1)	1(1)	2(1)	3(1)
C(14)	16(1)	16(1)	13(1)	2(1)	7(1)	1(1)



C(15)	15(1)	38(1)	13(1)	6(1)	0(1)	1(1)
C(16)	15(1)	21(1)	18(1)	-1(1)	8(1)	3(1)
C(17)	24(1)	18(1)	26(1)	-2(1)	11(1)	7(1)
C(18)	15(1)	16(1)	16(1)	-5(1)	2(1)	-2(1)
C(19)	29(1)	17(1)	16(1)	5(1)	7(1)	6(1)

---

Table 5. Hydrogen coordinates ( $\times 10^4$ ) and isotropic displacement parameters ( $\text{\AA}^2 \times 10^3$ ) for svp33.

---

	x	y	z	U(eq)
H(2A)	4370(40)	4620(20)	12760(40)	28(8)
H(2B)	3500(50)	3600(30)	12900(40)	40(9)
H(3A)	7530(40)	3998(18)	13160(30)	10(6)
H(3B)	6800(40)	3123(19)	13960(30)	11(6)
H(5A)	9270(40)	3310(20)	11460(30)	16(6)
H(9A)	6320(40)	680(20)	10380(30)	18(6)
H(9B)	4040(40)	850(20)	9880(30)	20(7)
H(10A)	6290(40)	1471(18)	12590(30)	9(5)
H(10B)	4230(40)	2000(20)	11710(30)	16(6)
H(11A)	5920(40)	3962(19)	9940(30)	10(6)
H(12A)	2810(40)	2781(19)	8120(30)	15(6)
H(13A)	4280(40)	2911(19)	6070(30)	10(6)

H(14A)	7650(50)	3050(20)	6810(40)	27(7)
H(14B)	7920(40)	3552(19)	8450(30)	11(6)
H(15A)	11540(50)	2210(20)	13210(30)	23(7)
H(15B)	10370(70)	2830(30)	14100(60)	60(11)
H(15C)	9770(50)	1660(20)	13480(40)	22(7)
H(17A)	7700(50)	-230(30)	7210(40)	38(9)
H(17B)	9810(50)	120(30)	8420(40)	38(9)
H(17C)	8020(50)	20(30)	9050(40)	37(8)
H(18A)	2610(50)	1180(20)	6950(40)	25(7)
H(18B)	4080(40)	1370(20)	6090(40)	21(7)
H(18C)	4350(50)	450(30)	7210(40)	33(8)
H(19A)	4850(50)	4660(20)	5960(40)	32(8)
H(19B)	2920(40)	4490(20)	6430(30)	21(7)
H(19C)	5020(50)	4790(20)	7680(40)	31(8)

---

Table 6. Torsion angles [°] for svp33.

---

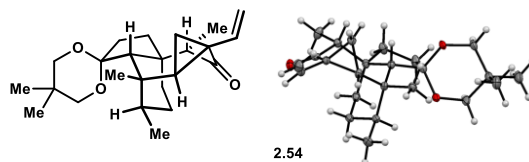
O(1)-C(1)-C(2)-C(3)	177.1(2)
C(11)-C(1)-C(2)-C(3)	-3.0(2)
C(1)-C(2)-C(3)-C(4)	-19.3(2)
C(2)-C(3)-C(4)-C(10)	-80.6(2)
C(2)-C(3)-C(4)-C(11)	33.8(2)
C(2)-C(3)-C(4)-C(5)	155.31(17)
C(10)-C(4)-C(5)-C(15)	-68.6(2)

C(11)-C(4)-C(5)-C(15)	168.96(18)
C(3)-C(4)-C(5)-C(15)	54.4(2)
C(10)-C(4)-C(5)-C(6)	58.3(2)
C(11)-C(4)-C(5)-C(6)	-64.1(2)
C(3)-C(4)-C(5)-C(6)	-178.70(17)
C(15)-C(5)-C(6)-O(2)	-25.6(3)
C(4)-C(5)-C(6)-O(2)	-154.13(19)
C(15)-C(5)-C(6)-C(7)	159.54(18)
C(4)-C(5)-C(6)-C(7)	31.1(3)
O(2)-C(6)-C(7)-C(16)	11.1(3)
C(5)-C(6)-C(7)-C(16)	-174.01(17)
O(2)-C(6)-C(7)-C(14)	-109.2(2)
C(5)-C(6)-C(7)-C(14)	65.6(2)
O(2)-C(6)-C(7)-C(8)	134.42(19)
C(5)-C(6)-C(7)-C(8)	-50.7(2)
C(6)-C(7)-C(8)-C(18)	-146.33(17)
C(16)-C(7)-C(8)-C(18)	-25.0(2)
C(14)-C(7)-C(8)-C(18)	95.42(19)
C(6)-C(7)-C(8)-C(9)	-25.4(2)
C(16)-C(7)-C(8)-C(9)	95.94(19)
C(14)-C(7)-C(8)-C(9)	-143.61(16)
C(6)-C(7)-C(8)-C(12)	97.34(18)
C(16)-C(7)-C(8)-C(12)	-141.36(16)
C(14)-C(7)-C(8)-C(12)	-20.91(18)
C(18)-C(8)-C(9)-C(10)	-153.76(17)

C(12)-C(8)-C(9)-C(10)	-32.1(2)
C(7)-C(8)-C(9)-C(10)	83.2(2)
C(11)-C(4)-C(10)-C(9)	61.1(2)
C(5)-C(4)-C(10)-C(9)	-64.7(2)
C(3)-C(4)-C(10)-C(9)	172.02(16)
C(8)-C(9)-C(10)-C(4)	-23.2(2)
O(1)-C(1)-C(11)-C(12)	-26.8(3)
C(2)-C(1)-C(11)-C(12)	153.42(17)
O(1)-C(1)-C(11)-C(4)	-156.0(2)
C(2)-C(1)-C(11)-C(4)	24.2(2)
C(10)-C(4)-C(11)-C(1)	81.00(18)
C(5)-C(4)-C(11)-C(1)	-154.27(16)
C(3)-C(4)-C(11)-C(1)	-34.97(19)
C(10)-C(4)-C(11)-C(12)	-45.7(2)
C(5)-C(4)-C(11)-C(12)	79.0(2)
C(3)-C(4)-C(11)-C(12)	-161.67(16)
C(1)-C(11)-C(12)-C(13)	116.78(18)
C(4)-C(11)-C(12)-C(13)	-121.26(17)
C(1)-C(11)-C(12)-C(8)	-129.43(17)
C(4)-C(11)-C(12)-C(8)	-7.5(2)
C(18)-C(8)-C(12)-C(13)	-74.34(19)
C(9)-C(8)-C(12)-C(13)	165.48(15)
C(7)-C(8)-C(12)-C(13)	42.76(18)
C(18)-C(8)-C(12)-C(11)	167.29(16)
C(9)-C(8)-C(12)-C(11)	47.1(2)

C(7)-C(8)-C(12)-C(11)	-75.60(18)
C(11)-C(12)-C(13)-C(19)	-54.9(2)
C(8)-C(12)-C(13)-C(19)	-174.05(17)
C(11)-C(12)-C(13)-C(14)	70.46(18)
C(8)-C(12)-C(13)-C(14)	-48.74(18)
C(19)-C(13)-C(14)-C(7)	161.18(17)
C(12)-C(13)-C(14)-C(7)	34.47(19)
C(6)-C(7)-C(14)-C(13)	-128.81(16)
C(16)-C(7)-C(14)-C(13)	112.60(17)
C(8)-C(7)-C(14)-C(13)	-8.3(2)
C(6)-C(7)-C(16)-O(3)	-124.8(2)
C(14)-C(7)-C(16)-O(3)	-5.8(3)
C(8)-C(7)-C(16)-O(3)	111.5(2)
C(6)-C(7)-C(16)-C(17)	56.8(2)
C(14)-C(7)-C(16)-C(17)	175.79(19)
C(8)-C(7)-C(16)-C(17)	-66.9(2)

---



Crystal structure provided by Dr. Joseph Ziller (University of California, Irvine, California, United States of America). Thermal ellipsoids are drawn at 50% probability level.

Table 1. Crystal data and structure refinement for svp31.

Identification code	svp31 (Nick Foy)
Empirical formula	C <sub>24</sub> H <sub>36</sub> O <sub>3</sub>

Formula weight	372.53	
Temperature	133(2) K	
Wavelength	0.71073 Å	
Crystal system	Orthorhombic	
Space group	$P2_12_12_1$	
Unit cell dimensions	$a = 10.1500(5) \text{ \AA}$	$\alpha = 90^\circ$ .
	$b = 10.7641(5) \text{ \AA}$	$\beta = 90^\circ$ .
	$c = 18.6866(9) \text{ \AA}$	$\gamma = 90^\circ$ .
Volume	2041.62(17) Å <sup>3</sup>	
Z	4	
Density (calculated)	1.212 Mg/m <sup>3</sup>	
Absorption coefficient	0.078 mm <sup>-1</sup>	
F(000)	816	
Crystal color	colorless	
Crystal size	0.379 x 0.268 x 0.226 mm <sup>3</sup>	
Theta range for data collection	2.180 to 30.503°	
Index ranges	$-14 \leq h \leq 14, -15 \leq k \leq 15, -26 \leq l \leq 26$	
Reflections collected	50926	
Independent reflections	6137 [R(int) = 0.0507]	
Completeness to theta = 25.242°	100.0 %	
Absorption correction	Semi-empirical from equivalents	
Max. and min. transmission	0.8622 and 0.8282	
Refinement method	Full-matrix least-squares on F <sup>2</sup>	
Data / restraints / parameters	6137 / 0 / 388	
Goodness-of-fit on F <sup>2</sup>	1.044	

Final R indices [ $I > 2\sigma(I)$  = 5512 data]      R1 = 0.0370, wR2 = 0.0864

R indices (all data, 0.70 Å)      R1 = 0.0454, wR2 = 0.0907

Largest diff. peak and hole      0.301 and -0.193 e.Å<sup>-3</sup>

Table 2. Atomic coordinates ( $\times 10^4$ ) and equivalent isotropic displacement parameters (Å<sup>2</sup>  $\times 10^3$ )

for svp31. U(eq) is defined as one third of the trace of the orthogonalized U<sup>ij</sup> tensor.

---

	x	y	z	U(eq)
O(1)	5928(1)	11140(1)	2158(1)	20(1)
O(2)	6328(1)	5073(1)	1531(1)	16(1)
O(3)	7889(1)	5940(1)	767(1)	17(1)
C(1)	7918(2)	8442(1)	2627(1)	14(1)
C(2)	6842(2)	8318(1)	3164(1)	15(1)
C(3)	7018(2)	9574(1)	2798(1)	13(1)
C(4)	6032(2)	10024(1)	2265(1)	14(1)
C(5)	5144(2)	9121(1)	1865(1)	14(1)
C(6)	5871(2)	8305(1)	1298(1)	13(1)
C(7)	6713(2)	9070(1)	775(1)	16(1)
C(8)	8048(2)	9477(1)	1067(1)	16(1)
C(9)	8848(2)	8388(1)	1368(1)	14(1)
C(10)	8056(2)	7663(1)	1944(1)	12(1)
C(11)	6704(2)	7252(1)	1643(1)	12(1)
C(12)	6659(2)	6134(1)	1106(1)	15(1)
C(13)	5570(2)	6456(2)	559(1)	22(1)

---

C(14)	4830(2)	7554(1)	880(1)	18(1)
C(15)	7699(2)	10587(1)	3195(1)	18(1)
C(16)	8196(2)	10528(2)	3843(1)	25(1)
C(17)	3983(2)	9850(2)	1551(1)	22(1)
C(18)	10188(2)	8864(2)	1624(1)	21(1)
C(19)	6279(2)	3934(1)	1131(1)	18(1)
C(20)	7562(2)	3680(1)	734(1)	18(1)
C(21)	7902(2)	4860(1)	320(1)	19(1)
C(22)	7350(2)	2617(2)	202(1)	26(1)
C(23)	8648(2)	3338(2)	1263(1)	24(1)
C(24)	8843(2)	6523(1)	2203(1)	16(1)

---

Table 3. Bond lengths [Å] and angles [°] for svp31.

---

O(1)-C(4)	1.2225(18)
O(2)-C(12)	1.4312(17)
O(2)-C(19)	1.4373(18)
O(3)-C(12)	1.415(2)
O(3)-C(21)	1.4315(17)
C(1)-C(2)	1.489(2)
C(1)-C(10)	1.5343(19)
C(1)-C(3)	1.556(2)
C(1)-H(1A)	0.968(19)
C(2)-C(3)	1.525(2)



C(2)-H(2A)	0.98(2)
C(2)-H(2B)	0.96(2)
C(3)-C(15)	1.488(2)
C(3)-C(4)	1.494(2)
C(4)-C(5)	1.522(2)
C(5)-C(17)	1.533(2)
C(5)-C(6)	1.562(2)
C(5)-H(5A)	0.973(19)
C(6)-C(7)	1.538(2)
C(6)-C(14)	1.543(2)
C(6)-C(11)	1.553(2)
C(7)-C(8)	1.525(2)
C(7)-H(7A)	1.00(2)
C(7)-H(7B)	0.99(2)
C(8)-C(9)	1.532(2)
C(8)-H(8A)	0.97(2)
C(8)-H(8B)	1.00(2)
C(9)-C(18)	1.530(2)
C(9)-C(10)	1.554(2)
C(9)-H(9A)	0.973(18)
C(10)-C(24)	1.542(2)
C(10)-C(11)	1.548(2)
C(11)-C(12)	1.569(2)
C(11)-H(11A)	0.972(18)
C(12)-C(13)	1.544(2)

C(13)-C(14)	1.524(2)
C(13)-H(13A)	0.98(2)
C(13)-H(13B)	0.99(2)
C(14)-H(14A)	0.99(2)
C(14)-H(14B)	0.96(2)
C(15)-C(16)	1.315(2)
C(15)-H(15A)	0.96(2)
C(16)-H(16A)	0.92(3)
C(16)-H(16B)	0.99(2)
C(17)-H(17A)	0.97(2)
C(17)-H(17B)	0.98(2)
C(17)-H(17C)	1.01(2)
C(18)-H(18A)	0.96(2)
C(18)-H(18B)	0.98(2)
C(18)-H(18C)	0.97(2)
C(19)-C(20)	1.523(2)
C(19)-H(19A)	0.98(2)
C(19)-H(19B)	0.96(2)
C(20)-C(23)	1.525(3)
C(20)-C(21)	1.526(2)
C(20)-C(22)	1.531(2)
C(21)-H(21A)	0.98(2)
C(21)-H(21B)	0.97(2)
C(22)-H(22A)	0.99(2)
C(22)-H(22B)	0.98(3)

C(22)-H(22C)	0.97(2)
C(23)-H(23A)	0.99(2)
C(23)-H(23B)	1.00(3)
C(23)-H(23C)	0.93(2)
C(24)-H(24A)	0.98(2)
C(24)-H(24B)	0.99(2)
C(24)-H(24C)	0.94(2)
C(12)-O(2)-C(19)	113.57(11)
C(12)-O(3)-C(21)	112.83(12)
C(2)-C(1)-C(10)	125.32(13)
C(2)-C(1)-C(3)	60.09(9)
C(10)-C(1)-C(3)	130.78(13)
C(2)-C(1)-H(1A)	113.4(10)
C(10)-C(1)-H(1A)	110.7(10)
C(3)-C(1)-H(1A)	107.8(11)
C(1)-C(2)-C(3)	62.14(10)
C(1)-C(2)-H(2A)	116.5(14)
C(3)-C(2)-H(2A)	113.5(13)
C(1)-C(2)-H(2B)	119.9(11)
C(3)-C(2)-H(2B)	115.6(11)
H(2A)-C(2)-H(2B)	117.2(18)
C(15)-C(3)-C(4)	113.92(12)
C(15)-C(3)-C(2)	118.77(13)
C(4)-C(3)-C(2)	120.52(13)

C(15)-C(3)-C(1)	113.80(13)
C(4)-C(3)-C(1)	120.67(12)
C(2)-C(3)-C(1)	57.78(9)
O(1)-C(4)-C(3)	119.04(14)
O(1)-C(4)-C(5)	119.79(14)
C(3)-C(4)-C(5)	121.16(12)
C(4)-C(5)-C(17)	108.43(12)
C(4)-C(5)-C(6)	114.36(12)
C(17)-C(5)-C(6)	113.07(12)
C(4)-C(5)-H(5A)	108.3(11)
C(17)-C(5)-H(5A)	106.9(12)
C(6)-C(5)-H(5A)	105.4(11)
C(7)-C(6)-C(14)	109.82(12)
C(7)-C(6)-C(11)	110.65(13)
C(14)-C(6)-C(11)	101.60(11)
C(7)-C(6)-C(5)	113.11(11)
C(14)-C(6)-C(5)	108.31(13)
C(11)-C(6)-C(5)	112.69(12)
C(8)-C(7)-C(6)	114.83(12)
C(8)-C(7)-H(7A)	107.8(14)
C(6)-C(7)-H(7A)	108.9(13)
C(8)-C(7)-H(7B)	112.0(12)
C(6)-C(7)-H(7B)	107.0(13)
H(7A)-C(7)-H(7B)	105.9(17)
C(7)-C(8)-C(9)	112.50(12)

C(7)-C(8)-H(8A)	110.7(13)
C(9)-C(8)-H(8A)	109.0(13)
C(7)-C(8)-H(8B)	109.6(12)
C(9)-C(8)-H(8B)	109.8(12)
H(8A)-C(8)-H(8B)	105.0(17)
C(18)-C(9)-C(8)	109.29(12)
C(18)-C(9)-C(10)	114.27(13)
C(8)-C(9)-C(10)	111.41(13)
C(18)-C(9)-H(9A)	108.0(12)
C(8)-C(9)-H(9A)	107.7(11)
C(10)-C(9)-H(9A)	106.0(11)
C(1)-C(10)-C(24)	102.76(12)
C(1)-C(10)-C(11)	112.14(12)
C(24)-C(10)-C(11)	110.27(12)
C(1)-C(10)-C(9)	110.40(11)
C(24)-C(10)-C(9)	110.50(12)
C(11)-C(10)-C(9)	110.53(12)
C(10)-C(11)-C(6)	115.15(11)
C(10)-C(11)-C(12)	118.47(13)
C(6)-C(11)-C(12)	106.15(11)
C(10)-C(11)-H(11A)	109.2(11)
C(6)-C(11)-H(11A)	104.9(11)
C(12)-C(11)-H(11A)	101.3(11)
O(3)-C(12)-O(2)	109.76(12)
O(3)-C(12)-C(13)	111.64(13)

O(2)-C(12)-C(13)	112.24(13)
O(3)-C(12)-C(11)	111.96(12)
O(2)-C(12)-C(11)	105.26(11)
C(13)-C(12)-C(11)	105.77(12)
C(14)-C(13)-C(12)	105.48(13)
C(14)-C(13)-H(13A)	110.1(14)
C(12)-C(13)-H(13A)	107.7(14)
C(14)-C(13)-H(13B)	112.7(15)
C(12)-C(13)-H(13B)	111.3(14)
H(13A)-C(13)-H(13B)	109.4(18)
C(13)-C(14)-C(6)	105.53(14)
C(13)-C(14)-H(14A)	108.7(13)
C(6)-C(14)-H(14A)	110.8(13)
C(13)-C(14)-H(14B)	112.1(12)
C(6)-C(14)-H(14B)	114.7(12)
H(14A)-C(14)-H(14B)	105.1(18)
C(16)-C(15)-C(3)	126.97(16)
C(16)-C(15)-H(15A)	119.4(14)
C(3)-C(15)-H(15A)	113.5(14)
C(15)-C(16)-H(16A)	123.4(16)
C(15)-C(16)-H(16B)	120.0(13)
H(16A)-C(16)-H(16B)	117(2)
C(5)-C(17)-H(17A)	109.3(13)
C(5)-C(17)-H(17B)	110.5(14)
H(17A)-C(17)-H(17B)	108.2(19)

C(5)-C(17)-H(17C)	111.7(15)
H(17A)-C(17)-H(17C)	109.1(18)
H(17B)-C(17)-H(17C)	108.0(18)
C(9)-C(18)-H(18A)	105.9(14)
C(9)-C(18)-H(18B)	113.0(14)
H(18A)-C(18)-H(18B)	108(2)
C(9)-C(18)-H(18C)	113.4(14)
H(18A)-C(18)-H(18C)	108.7(18)
H(18B)-C(18)-H(18C)	107.6(18)
O(2)-C(19)-C(20)	112.09(13)
O(2)-C(19)-H(19A)	110.2(11)
C(20)-C(19)-H(19A)	109.9(12)
O(2)-C(19)-H(19B)	106.5(12)
C(20)-C(19)-H(19B)	111.1(12)
H(19A)-C(19)-H(19B)	106.9(17)
C(19)-C(20)-C(23)	110.25(14)
C(19)-C(20)-C(21)	106.89(13)
C(23)-C(20)-C(21)	111.47(14)
C(19)-C(20)-C(22)	109.26(14)
C(23)-C(20)-C(22)	109.96(14)
C(21)-C(20)-C(22)	108.94(13)
O(3)-C(21)-C(20)	112.25(12)
O(3)-C(21)-H(21A)	105.3(12)
C(20)-C(21)-H(21A)	110.6(12)
O(3)-C(21)-H(21B)	108.9(14)

C(20)-C(21)-H(21B)	110.8(14)
H(21A)-C(21)-H(21B)	108.8(17)
C(20)-C(22)-H(22A)	110.9(14)
C(20)-C(22)-H(22B)	110.3(16)
H(22A)-C(22)-H(22B)	108(2)
C(20)-C(22)-H(22C)	110.7(14)
H(22A)-C(22)-H(22C)	108(2)
H(22B)-C(22)-H(22C)	109(2)
C(20)-C(23)-H(23A)	110.9(12)
C(20)-C(23)-H(23B)	110.0(15)
H(23A)-C(23)-H(23B)	109.4(19)
C(20)-C(23)-H(23C)	108.9(16)
H(23A)-C(23)-H(23C)	109.6(18)
H(23B)-C(23)-H(23C)	108(2)
C(10)-C(24)-H(24A)	110.6(14)
C(10)-C(24)-H(24B)	111.5(12)
H(24A)-C(24)-H(24B)	108.0(17)
C(10)-C(24)-H(24C)	110.1(13)
H(24A)-C(24)-H(24C)	107.6(18)
H(24B)-C(24)-H(24C)	109.0(18)

---

Table 4. Anisotropic displacement parameters ( $\text{\AA}^2 \times 10^3$ ) for svp31. The anisotropic displacement factor exponent takes the form:  $-2\sigma^2 [ h^2 a^{*2} U^{11} + \dots + 2 h k a^* b^* U^{12} ]$

---



	U <sup>11</sup>	U <sup>22</sup>	U <sup>33</sup>	U <sup>23</sup>	U <sup>13</sup>	U <sup>12</sup>
O(1)	24(1)	13(1)	22(1)	1(1)	-1(1)	2(1)
O(2)	21(1)	10(1)	16(1)	-1(1)	3(1)	-2(1)
O(3)	24(1)	12(1)	15(1)	-2(1)	6(1)	-3(1)
C(1)	15(1)	13(1)	13(1)	-1(1)	-1(1)	2(1)
C(2)	18(1)	14(1)	13(1)	1(1)	0(1)	0(1)
C(3)	15(1)	12(1)	12(1)	0(1)	0(1)	1(1)
C(4)	14(1)	15(1)	12(1)	0(1)	3(1)	2(1)
C(5)	14(1)	13(1)	14(1)	0(1)	-1(1)	2(1)
C(6)	16(1)	10(1)	12(1)	0(1)	-2(1)	1(1)
C(7)	20(1)	14(1)	13(1)	3(1)	1(1)	2(1)
C(8)	20(1)	12(1)	16(1)	2(1)	5(1)	-1(1)
C(9)	15(1)	12(1)	14(1)	-1(1)	3(1)	-1(1)
C(10)	13(1)	10(1)	13(1)	0(1)	0(1)	1(1)
C(11)	14(1)	10(1)	12(1)	0(1)	-1(1)	0(1)
C(12)	19(1)	10(1)	14(1)	0(1)	-1(1)	-1(1)
C(13)	31(1)	16(1)	20(1)	-4(1)	-12(1)	4(1)
C(14)	21(1)	14(1)	20(1)	0(1)	-8(1)	0(1)
C(15)	18(1)	16(1)	20(1)	-5(1)	1(1)	-1(1)
C(16)	30(1)	26(1)	20(1)	-7(1)	-2(1)	-5(1)
C(17)	19(1)	24(1)	21(1)	-4(1)	-7(1)	9(1)
C(18)	18(1)	20(1)	24(1)	-2(1)	1(1)	-6(1)
C(19)	23(1)	10(1)	22(1)	-1(1)	2(1)	-3(1)
C(20)	25(1)	11(1)	18(1)	-2(1)	2(1)	-1(1)

C(21)	30(1)	13(1)	16(1)	-3(1)	5(1)	-2(1)
C(22)	39(1)	15(1)	25(1)	-6(1)	1(1)	-1(1)
C(23)	29(1)	17(1)	27(1)	-2(1)	-3(1)	5(1)
C(24)	16(1)	14(1)	18(1)	1(1)	-1(1)	3(1)

Table 5. Hydrogen coordinates ( $\times 10^4$ ) and isotropic displacement parameters ( $\text{\AA}^2 \times 10^3$ ) for svp31.

	x	y	z	U(eq)
H(1A)	8772(19)	8598(17)	2839(9)	8(4)
H(2A)	7110(20)	8320(20)	3666(13)	28(6)
H(2B)	6050(20)	7874(17)	3042(10)	12(4)
H(5A)	4780(20)	8537(18)	2209(10)	13(4)
H(7A)	6870(20)	8570(20)	335(12)	28(6)
H(7B)	6170(20)	9783(19)	622(11)	22(5)
H(8A)	7940(20)	10100(20)	1436(11)	24(5)
H(8B)	8560(20)	9899(19)	682(11)	21(5)
H(9A)	9000(19)	7805(16)	979(10)	9(4)
H(11A)	6163(19)	6938(16)	2033(10)	8(4)
H(13A)	6010(20)	6710(20)	110(12)	28(6)
H(13B)	4990(30)	5730(20)	467(12)	34(6)
H(14A)	4140(30)	7230(20)	1207(12)	31(6)

H(14B)	4360(20)	8019(19)	523(11)	19(5)
H(15A)	7800(20)	11340(20)	2921(12)	33(6)
H(16A)	8120(30)	9840(20)	4134(14)	42(7)
H(16B)	8650(20)	11255(19)	4049(11)	24(5)
H(17A)	3580(20)	10350(20)	1926(11)	25(5)
H(17B)	3310(20)	9280(20)	1362(12)	30(6)
H(17C)	4270(20)	10410(20)	1149(13)	36(6)
H(18A)	10610(20)	9220(20)	1209(12)	29(6)
H(18B)	10760(20)	8200(20)	1804(12)	31(6)
H(18C)	10120(20)	9490(20)	1996(12)	26(5)
H(19A)	5540(20)	3953(18)	790(11)	17(5)
H(19B)	6090(20)	3283(18)	1471(10)	18(5)
H(21A)	8800(20)	4812(19)	129(11)	20(5)
H(21B)	7290(20)	4990(20)	-74(11)	25(5)
H(22A)	7060(30)	1850(20)	452(12)	33(6)
H(22B)	8180(30)	2430(30)	-49(15)	44(7)
H(22C)	6690(20)	2840(20)	-151(13)	30(6)
H(23A)	8770(20)	4000(20)	1625(11)	22(5)
H(23B)	9490(30)	3200(20)	1003(13)	39(7)
H(23C)	8420(30)	2600(20)	1490(13)	34(6)
H(24A)	8280(20)	5970(20)	2486(12)	32(6)
H(24B)	9600(20)	6771(19)	2504(11)	19(5)
H(24C)	9160(20)	6070(20)	1809(11)	22(5)

Table 6. Torsion angles [°] for svp31.

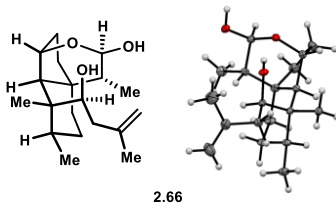
---

C(10)-C(1)-C(2)-C(3)	-121.05(16)
C(1)-C(2)-C(3)-C(15)	-101.42(15)
C(1)-C(2)-C(3)-C(4)	109.18(15)
C(2)-C(1)-C(3)-C(15)	110.11(14)
C(10)-C(1)-C(3)-C(15)	-137.27(16)
C(2)-C(1)-C(3)-C(4)	-108.91(15)
C(10)-C(1)-C(3)-C(4)	3.7(2)
C(10)-C(1)-C(3)-C(2)	112.61(18)
C(15)-C(3)-C(4)-O(1)	5.1(2)
C(2)-C(3)-C(4)-O(1)	155.91(14)
C(1)-C(3)-C(4)-O(1)	-135.81(15)
C(15)-C(3)-C(4)-C(5)	-173.74(13)
C(2)-C(3)-C(4)-C(5)	-23.0(2)
C(1)-C(3)-C(4)-C(5)	45.33(19)
O(1)-C(4)-C(5)-C(17)	-16.5(2)
C(3)-C(4)-C(5)-C(17)	162.32(13)
O(1)-C(4)-C(5)-C(6)	110.64(16)
C(3)-C(4)-C(5)-C(6)	-70.50(17)
C(4)-C(5)-C(6)-C(7)	-51.57(17)
C(17)-C(5)-C(6)-C(7)	73.19(17)
C(4)-C(5)-C(6)-C(14)	-173.53(12)
C(17)-C(5)-C(6)-C(14)	-48.78(17)
C(4)-C(5)-C(6)-C(11)	74.87(16)

C(17)-C(5)-C(6)-C(11)	-160.37(13)
C(14)-C(6)-C(7)-C(8)	-159.14(13)
C(11)-C(6)-C(7)-C(8)	-47.78(16)
C(5)-C(6)-C(7)-C(8)	79.74(16)
C(6)-C(7)-C(8)-C(9)	52.57(17)
C(7)-C(8)-C(9)-C(18)	177.96(13)
C(7)-C(8)-C(9)-C(10)	-54.82(16)
C(2)-C(1)-C(10)-C(24)	-87.74(17)
C(3)-C(1)-C(10)-C(24)	-166.44(15)
C(2)-C(1)-C(10)-C(11)	30.66(19)
C(3)-C(1)-C(10)-C(11)	-48.0(2)
C(2)-C(1)-C(10)-C(9)	154.39(14)
C(3)-C(1)-C(10)-C(9)	75.70(19)
C(18)-C(9)-C(10)-C(1)	53.77(16)
C(8)-C(9)-C(10)-C(1)	-70.71(16)
C(18)-C(9)-C(10)-C(24)	-59.23(16)
C(8)-C(9)-C(10)-C(24)	176.30(12)
C(18)-C(9)-C(10)-C(11)	178.43(12)
C(8)-C(9)-C(10)-C(11)	53.96(15)
C(1)-C(10)-C(11)-C(6)	71.71(15)
C(24)-C(10)-C(11)-C(6)	-174.43(12)
C(9)-C(10)-C(11)-C(6)	-51.96(16)
C(1)-C(10)-C(11)-C(12)	-161.12(12)
C(24)-C(10)-C(11)-C(12)	-47.26(17)
C(9)-C(10)-C(11)-C(12)	75.21(15)

C(7)-C(6)-C(11)-C(10)	48.17(16)
C(14)-C(6)-C(11)-C(10)	164.74(13)
C(5)-C(6)-C(11)-C(10)	-79.57(16)
C(7)-C(6)-C(11)-C(12)	-85.01(14)
C(14)-C(6)-C(11)-C(12)	31.56(15)
C(5)-C(6)-C(11)-C(12)	147.25(12)
C(21)-O(3)-C(12)-O(2)	58.49(15)
C(21)-O(3)-C(12)-C(13)	-66.62(15)
C(21)-O(3)-C(12)-C(11)	175.00(12)
C(19)-O(2)-C(12)-O(3)	-57.59(16)
C(19)-O(2)-C(12)-C(13)	67.18(17)
C(19)-O(2)-C(12)-C(11)	-178.24(12)
C(10)-C(11)-C(12)-O(3)	-21.83(17)
C(6)-C(11)-C(12)-O(3)	109.50(14)
C(10)-C(11)-C(12)-O(2)	97.37(14)
C(6)-C(11)-C(12)-O(2)	-131.30(12)
C(10)-C(11)-C(12)-C(13)	-143.64(14)
C(6)-C(11)-C(12)-C(13)	-12.31(16)
O(3)-C(12)-C(13)-C(14)	-134.39(14)
O(2)-C(12)-C(13)-C(14)	101.88(15)
C(11)-C(12)-C(13)-C(14)	-12.38(17)
C(12)-C(13)-C(14)-C(6)	32.94(17)
C(7)-C(6)-C(14)-C(13)	77.31(15)
C(11)-C(6)-C(14)-C(13)	-39.86(15)
C(5)-C(6)-C(14)-C(13)	-158.73(13)

C(4)-C(3)-C(15)-C(16)	151.99(18)
C(2)-C(3)-C(15)-C(16)	0.7(3)
C(1)-C(3)-C(15)-C(16)	-64.3(2)
C(12)-O(2)-C(19)-C(20)	55.72(18)
O(2)-C(19)-C(20)-C(23)	70.78(16)
O(2)-C(19)-C(20)-C(21)	-50.53(17)
O(2)-C(19)-C(20)-C(22)	-168.27(13)
C(12)-O(3)-C(21)-C(20)	-58.13(18)
C(19)-C(20)-C(21)-O(3)	51.87(19)
C(23)-C(20)-C(21)-O(3)	-68.67(18)
C(22)-C(20)-C(21)-O(3)	169.81(15)



Crystal structure provided by Dr. Joseph Ziller (University of California, Irvine, California, United States of America). Thermal ellipsoids are drawn at 50% probability level.

Table 1. Crystal data and structure refinement for svp26.

Identification code	svp26 (Nick Foy)
Empirical formula	$C_{19} H_{32} O_3 \cdot \frac{1}{2}(C_6H_6)$
Formula weight	347.50
Temperature	93(2) K
Wavelength	0.71073 Å
Crystal system	Monoclinic
Space group	$P2_1/n$

Unit cell dimensions	a = 13.0637(5) Å	α = 90°.
	b = 9.1907(4) Å	β = 108.7738(7)°.
	c = 17.2333(7) Å	γ = 90°.
Volume	1959.02(14) Å <sup>3</sup>	
Z	4	
Density (calculated)	1.178 Mg/m <sup>3</sup>	
Absorption coefficient	0.076 mm <sup>-1</sup>	
F(000)	764	
Crystal color	colorless	
Crystal size	0.525 x 0.399 x 0.254 mm <sup>3</sup>	
Theta range for data collection	1.716 to 31.544°	
Index ranges	-18 ≤ h ≤ 18, -13 ≤ k ≤ 13, -25 ≤ l ≤ 25	
Reflections collected	47570	
Independent reflections	6280 [R(int) = 0.0361]	
Completeness to theta = 25.242°	100.0 %	
Absorption correction	Semi-empirical from equivalents	
Max. and min. transmission	0.8623 and 0.8325	
Refinement method	Full-matrix least-squares on F <sup>2</sup>	
Data / restraints / parameters	6280 / 0 / 366	
Goodness-of-fit on F <sup>2</sup>	1.032	
Final R indices [I > 2σ(I) = 5001 data]	R1 = 0.0449, wR2 = 0.1059	
R indices (all data, 0.68 Å)	R1 = 0.0622, wR2 = 0.1183	
Largest diff. peak and hole	0.716 and -0.447 e.Å <sup>-3</sup>	

Table 2. Atomic coordinates (x 10<sup>4</sup>) and equivalent isotropic displacement parameters (Å<sup>2</sup> x 10<sup>3</sup>)



for svp26.  $U(\text{eq})$  is defined as one third of the trace of the orthogonalized  $U_{ij}$  tensor.

	x	y	z	$U(\text{eq})$
O(1)	8205(1)	5546(1)	1763(1)	14(1)
O(2)	8570(1)	3417(1)	2464(1)	17(1)
O(3)	8299(1)	6932(1)	3122(1)	14(1)
C(1)	8921(1)	4304(1)	1954(1)	14(1)
C(2)	10090(1)	4746(1)	2405(1)	13(1)
C(3)	10419(1)	6084(1)	1990(1)	14(1)
C(4)	11594(1)	6536(1)	2409(1)	18(1)
C(5)	11733(1)	7320(1)	3219(1)	17(1)
C(6)	11001(1)	8668(1)	3096(1)	15(1)
C(7)	9762(1)	8268(1)	2788(1)	12(1)
C(8)	9651(1)	7385(1)	1981(1)	13(1)
C(9)	8589(1)	6768(1)	1401(1)	15(1)
C(10)	8935(1)	6266(1)	670(1)	20(1)
C(11)	10137(1)	5806(1)	1054(1)	20(1)
C(12)	10824(1)	3418(1)	2484(1)	21(1)
C(13)	9384(1)	7474(1)	3448(1)	12(1)
C(14)	9360(1)	8406(1)	4189(1)	15(1)
C(15)	9527(1)	7482(1)	4946(1)	20(1)
C(16)	10479(1)	7491(2)	5546(1)	36(1)
C(17)	8613(2)	6600(2)	5001(1)	47(1)
C(18)	11432(1)	9692(1)	3832(1)	20(1)

C(19)	9088(1)	9664(1)	2523(1)	16(1)
C(20)	10534(1)	10498(1)	787(1)	24(1)
C(21)	9453(1)	10835(1)	410(1)	26(1)
C(22)	8917(1)	10335(1)	-378(1)	25(1)

---

Table 3. Bond lengths [Å] and angles [°] for svp26.

---

O(1)-C(1)	1.4448(12)
O(1)-C(9)	1.4501(12)
O(2)-C(1)	1.3819(12)
O(2)-H(2)	0.884(19)
O(3)-C(13)	1.4359(12)
O(3)-H(3)	0.847(17)
C(1)-C(2)	1.5288(14)
C(1)-H(1A)	1.007(13)
C(2)-C(12)	1.5317(14)
C(2)-C(3)	1.5506(14)
C(2)-H(2A)	0.984(13)
C(3)-C(4)	1.5290(14)
C(3)-C(11)	1.5560(15)
C(3)-C(8)	1.5572(14)
C(4)-C(5)	1.5296(15)
C(4)-H(4A)	1.014(15)
C(4)-H(4B)	1.022(15)

C(5)-C(6)	1.5375(15)
C(5)-H(5A)	0.987(15)
C(5)-H(5B)	1.003(14)
C(6)-C(18)	1.5334(15)
C(6)-C(7)	1.5762(13)
C(6)-H(6A)	1.005(14)
C(7)-C(19)	1.5397(14)
C(7)-C(13)	1.5603(13)
C(7)-C(8)	1.5760(14)
C(8)-C(9)	1.5335(14)
C(8)-H(8A)	0.987(14)
C(9)-C(10)	1.5394(15)
C(9)-H(9A)	0.969(13)
C(10)-C(11)	1.5533(17)
C(10)-H(10A)	0.992(16)
C(10)-H(10B)	0.970(15)
C(11)-H(11A)	0.978(15)
C(11)-H(11B)	1.001(15)
C(12)-H(12A)	0.986(16)
C(12)-H(12B)	0.986(17)
C(12)-H(12C)	0.968(17)
C(13)-C(14)	1.5449(14)
C(13)-H(13A)	0.985(13)
C(14)-C(15)	1.5124(15)
C(14)-H(14A)	0.990(14)

C(14)-H(14B)	0.985(15)
C(15)-C(16)	1.3381(18)
C(15)-C(17)	1.4706(18)
C(16)-H(16A)	0.97(2)
C(16)-H(16B)	0.977(19)
C(17)-H(17A)	0.97(2)
C(17)-H(17B)	1.02(3)
C(17)-H(17C)	1.00(2)
C(18)-H(18A)	1.004(15)
C(18)-H(18B)	0.994(15)
C(18)-H(18C)	0.995(16)
C(19)-H(19A)	0.987(15)
C(19)-H(19B)	0.987(15)
C(19)-H(19C)	0.982(15)
C(20)-C(21)	1.3865(18)
C(20)-C(22)#1	1.3855(17)
C(20)-H(20)	0.968(16)
C(21)-C(22)	1.3910(18)
C(21)-H(21)	0.974(17)
C(22)-C(20)#1	1.3855(17)
C(22)-H(22)	0.951(16)
C(1)-O(1)-C(9)	114.89(7)
C(1)-O(2)-H(2)	110.7(12)
C(13)-O(3)-H(3)	109.0(11)

O(2)-C(1)-O(1)	106.74(8)
O(2)-C(1)-C(2)	108.33(8)
O(1)-C(1)-C(2)	111.91(8)
O(2)-C(1)-H(1A)	108.7(8)
O(1)-C(1)-H(1A)	109.0(8)
C(2)-C(1)-H(1A)	112.0(8)
C(1)-C(2)-C(12)	109.14(8)
C(1)-C(2)-C(3)	110.87(8)
C(12)-C(2)-C(3)	114.48(8)
C(1)-C(2)-H(2A)	105.7(7)
C(12)-C(2)-H(2A)	107.2(8)
C(3)-C(2)-H(2A)	109.0(8)
C(4)-C(3)-C(2)	112.52(9)
C(4)-C(3)-C(11)	113.59(8)
C(2)-C(3)-C(11)	109.84(8)
C(4)-C(3)-C(8)	110.02(8)
C(2)-C(3)-C(8)	109.87(7)
C(11)-C(3)-C(8)	100.31(8)
C(5)-C(4)-C(3)	111.38(8)
C(5)-C(4)-H(4A)	108.0(8)
C(3)-C(4)-H(4A)	107.0(8)
C(5)-C(4)-H(4B)	112.0(8)
C(3)-C(4)-H(4B)	110.7(8)
H(4A)-C(4)-H(4B)	107.6(11)
C(4)-C(5)-C(6)	111.61(9)

C(4)-C(5)-H(5A)	109.0(9)
C(6)-C(5)-H(5A)	109.2(9)
C(4)-C(5)-H(5B)	110.1(8)
C(6)-C(5)-H(5B)	111.2(8)
H(5A)-C(5)-H(5B)	105.5(12)
C(18)-C(6)-C(5)	109.50(9)
C(18)-C(6)-C(7)	119.05(8)
C(5)-C(6)-C(7)	112.59(8)
C(18)-C(6)-H(6A)	106.4(8)
C(5)-C(6)-H(6A)	105.4(8)
C(7)-C(6)-H(6A)	102.6(8)
C(19)-C(7)-C(13)	108.70(8)
C(19)-C(7)-C(8)	106.66(8)
C(13)-C(7)-C(8)	116.21(8)
C(19)-C(7)-C(6)	109.46(8)
C(13)-C(7)-C(6)	113.27(8)
C(8)-C(7)-C(6)	102.14(7)
C(9)-C(8)-C(3)	99.63(8)
C(9)-C(8)-C(7)	124.92(8)
C(3)-C(8)-C(7)	120.71(8)
C(9)-C(8)-H(8A)	103.0(8)
C(3)-C(8)-H(8A)	104.4(8)
C(7)-C(8)-H(8A)	101.4(8)
O(1)-C(9)-C(8)	111.85(8)
O(1)-C(9)-C(10)	110.68(8)

C(8)-C(9)-C(10)	101.64(8)
O(1)-C(9)-H(9A)	103.9(8)
C(8)-C(9)-H(9A)	115.5(8)
C(10)-C(9)-H(9A)	113.6(8)
C(9)-C(10)-C(11)	104.84(8)
C(9)-C(10)-H(10A)	109.0(9)
C(11)-C(10)-H(10A)	110.8(9)
C(9)-C(10)-H(10B)	111.0(9)
C(11)-C(10)-H(10B)	113.9(9)
H(10A)-C(10)-H(10B)	107.2(12)
C(10)-C(11)-C(3)	105.42(8)
C(10)-C(11)-H(11A)	111.0(9)
C(3)-C(11)-H(11A)	109.0(9)
C(10)-C(11)-H(11B)	111.4(9)
C(3)-C(11)-H(11B)	113.1(8)
H(11A)-C(11)-H(11B)	106.9(12)
C(2)-C(12)-H(12A)	110.5(9)
C(2)-C(12)-H(12B)	111.9(10)
H(12A)-C(12)-H(12B)	106.8(13)
C(2)-C(12)-H(12C)	111.4(10)
H(12A)-C(12)-H(12C)	107.9(13)
H(12B)-C(12)-H(12C)	108.0(13)
O(3)-C(13)-C(14)	103.67(7)
O(3)-C(13)-C(7)	112.34(8)
C(14)-C(13)-C(7)	116.01(8)

O(3)-C(13)-H(13A)	108.0(8)
C(14)-C(13)-H(13A)	106.2(8)
C(7)-C(13)-H(13A)	110.1(7)
C(15)-C(14)-C(13)	111.44(8)
C(15)-C(14)-H(14A)	109.1(8)
C(13)-C(14)-H(14A)	110.9(8)
C(15)-C(14)-H(14B)	110.5(8)
C(13)-C(14)-H(14B)	107.0(8)
H(14A)-C(14)-H(14B)	107.8(12)
C(16)-C(15)-C(17)	121.70(13)
C(16)-C(15)-C(14)	120.24(11)
C(17)-C(15)-C(14)	118.06(11)
C(15)-C(16)-H(16A)	121.4(12)
C(15)-C(16)-H(16B)	121.4(10)
H(16A)-C(16)-H(16B)	117.2(16)
C(15)-C(17)-H(17A)	113.6(12)
C(15)-C(17)-H(17B)	109.9(14)
H(17A)-C(17)-H(17B)	109.7(19)
C(15)-C(17)-H(17C)	110.4(12)
H(17A)-C(17)-H(17C)	107.9(16)
H(17B)-C(17)-H(17C)	105.1(18)
C(6)-C(18)-H(18A)	108.1(9)
C(6)-C(18)-H(18B)	112.2(9)
H(18A)-C(18)-H(18B)	104.1(12)
C(6)-C(18)-H(18C)	113.3(9)



H(18A)-C(18)-H(18C)	108.2(12)
H(18B)-C(18)-H(18C)	110.5(12)
C(7)-C(19)-H(19A)	112.4(9)
C(7)-C(19)-H(19B)	110.6(9)
H(19A)-C(19)-H(19B)	109.3(12)
C(7)-C(19)-H(19C)	109.3(9)
H(19A)-C(19)-H(19C)	106.8(12)
H(19B)-C(19)-H(19C)	108.3(12)
C(21)-C(20)-C(22)#1	120.07(11)
C(21)-C(20)-H(20)	121.0(9)
C(22)#1-C(20)-H(20)	118.9(9)
C(20)-C(21)-C(22)	120.01(11)
C(20)-C(21)-H(21)	119.8(10)
C(22)-C(21)-H(21)	120.2(10)
C(20)#1-C(22)-C(21)	119.91(12)
C(20)#1-C(22)-H(22)	120.2(10)
C(21)-C(22)-H(22)	119.9(10)

---

Symmetry transformations used to generate equivalent atoms:

#1 -x+2,-y+2,-z

Table 4. Anisotropic displacement parameters ( $\text{\AA}^2 \times 10^3$ ) for svp26. The anisotropic displacement factor exponent takes the form:  $-2\pi^2 [h^2 a^{*2} U^{11} + \dots + 2 h k a^* b^* U^{12}]$

---

U <sup>11</sup>	U <sup>22</sup>	U <sup>33</sup>	U <sup>23</sup>	U <sup>13</sup>	U <sup>12</sup>
-----------------	-----------------	-----------------	-----------------	-----------------	-----------------

---

O(1)	11(1)	13(1)	16(1)	0(1)	3(1)	-1(1)
O(2)	16(1)	16(1)	18(1)	2(1)	4(1)	-3(1)
O(3)	11(1)	15(1)	18(1)	-3(1)	6(1)	-2(1)
C(1)	13(1)	12(1)	15(1)	-1(1)	4(1)	0(1)
C(2)	11(1)	13(1)	15(1)	-1(1)	4(1)	1(1)
C(3)	13(1)	16(1)	14(1)	-2(1)	6(1)	-1(1)
C(4)	12(1)	22(1)	24(1)	-4(1)	9(1)	-2(1)
C(5)	10(1)	21(1)	20(1)	-2(1)	4(1)	-2(1)
C(6)	12(1)	16(1)	16(1)	-1(1)	5(1)	-3(1)
C(7)	11(1)	11(1)	14(1)	0(1)	4(1)	-1(1)
C(8)	12(1)	14(1)	12(1)	1(1)	4(1)	-2(1)
C(9)	15(1)	15(1)	14(1)	2(1)	2(1)	-1(1)
C(10)	24(1)	24(1)	12(1)	0(1)	4(1)	-4(1)
C(11)	23(1)	24(1)	17(1)	-4(1)	11(1)	-4(1)
C(12)	17(1)	18(1)	28(1)	-3(1)	7(1)	5(1)
C(13)	10(1)	11(1)	14(1)	0(1)	4(1)	0(1)
C(14)	15(1)	14(1)	15(1)	-2(1)	6(1)	0(1)
C(15)	27(1)	20(1)	15(1)	-2(1)	11(1)	0(1)
C(16)	33(1)	50(1)	23(1)	10(1)	6(1)	1(1)
C(17)	49(1)	63(1)	30(1)	12(1)	13(1)	-26(1)
C(18)	17(1)	22(1)	21(1)	-5(1)	6(1)	-7(1)
C(19)	16(1)	12(1)	19(1)	3(1)	5(1)	1(1)
C(20)	32(1)	21(1)	19(1)	-1(1)	8(1)	-5(1)
C(21)	33(1)	24(1)	25(1)	-2(1)	15(1)	3(1)

C(22) 24(1) 28(1) 25(1) 2(1) 9(1) 0(1)

---

Table 5. Hydrogen coordinates ( $\times 10^4$ ) and isotropic displacement parameters ( $\text{\AA}^2 \times 10^3$ ) for svp26.

---

	x	y	z	U(eq)
H(2)	7935(16)	3030(20)	2197(11)	47(5)
H(3)	8265(13)	6342(18)	2736(10)	31(4)
H(1A)	8852(11)	3758(15)	1432(8)	16(3)
H(2A)	10109(10)	5016(14)	2962(8)	13(3)
H(4A)	11790(12)	7242(16)	2027(9)	23(4)
H(4B)	12098(12)	5658(17)	2484(9)	25(4)
H(5A)	12494(12)	7623(16)	3460(9)	26(4)
H(5B)	11595(11)	6630(16)	3625(9)	20(3)
H(6A)	11095(11)	9193(15)	2612(8)	18(3)
H(8A)	9848(11)	8130(15)	1642(8)	17(3)
H(9A)	7983(11)	7436(15)	1251(8)	15(3)
H(10A)	8866(12)	7095(18)	288(9)	29(4)
H(10B)	8468(12)	5495(17)	368(9)	25(4)
H(11A)	10607(12)	6405(16)	843(9)	25(4)
H(11B)	10251(12)	4772(16)	920(9)	24(4)
H(12A)	10500(12)	2556(18)	2654(9)	29(4)

H(12B)	11538(13)	3565(18)	2901(10)	34(4)
H(12C)	10938(13)	3193(18)	1969(10)	33(4)
H(13A)	9864(11)	6644(15)	3677(8)	14(3)
H(14A)	9922(11)	9172(16)	4309(8)	20(3)
H(14B)	8650(12)	8889(16)	4033(9)	23(4)
H(16A)	10620(17)	6850(20)	6017(13)	60(6)
H(16B)	11062(15)	8140(20)	5530(11)	42(5)
H(17A)	8770(16)	6060(20)	5509(13)	55(5)
H(17B)	8370(20)	5900(30)	4514(16)	86(8)
H(17C)	7973(17)	7230(20)	4948(12)	56(6)
H(18A)	12161(12)	10055(17)	3841(9)	28(4)
H(18B)	11579(12)	9172(17)	4363(9)	24(4)
H(18C)	10958(12)	10549(17)	3810(9)	27(4)
H(19A)	9169(12)	10338(17)	2985(9)	26(4)
H(19B)	8315(12)	9425(16)	2267(9)	25(4)
H(19C)	9335(12)	10188(17)	2120(9)	26(4)
H(20)	10914(12)	10815(17)	1340(10)	29(4)
H(21)	9068(13)	11408(18)	703(10)	36(4)
H(22)	8173(13)	10557(18)	-633(9)	31(4)

---

Table 6. Torsion angles [°] for svp26.

---

C(9)-O(1)-C(1)-O(2)	165.56(8)
C(9)-O(1)-C(1)-C(2)	47.20(11)
O(2)-C(1)-C(2)-C(12)	70.20(10)

O(1)-C(1)-C(2)-C(12)	-172.40(8)
O(2)-C(1)-C(2)-C(3)	-162.81(8)
O(1)-C(1)-C(2)-C(3)	-45.40(10)
C(1)-C(2)-C(3)-C(4)	-178.37(8)
C(12)-C(2)-C(3)-C(4)	-54.37(11)
C(1)-C(2)-C(3)-C(11)	-50.76(10)
C(12)-C(2)-C(3)-C(11)	73.23(11)
C(1)-C(2)-C(3)-C(8)	58.68(10)
C(12)-C(2)-C(3)-C(8)	-177.33(8)
C(2)-C(3)-C(4)-C(5)	-75.36(11)
C(11)-C(3)-C(4)-C(5)	159.05(9)
C(8)-C(3)-C(4)-C(5)	47.52(12)
C(3)-C(4)-C(5)-C(6)	-57.41(12)
C(4)-C(5)-C(6)-C(18)	-160.39(8)
C(4)-C(5)-C(6)-C(7)	64.76(11)
C(18)-C(6)-C(7)-C(19)	60.57(12)
C(5)-C(6)-C(7)-C(19)	-169.30(8)
C(18)-C(6)-C(7)-C(13)	-60.91(12)
C(5)-C(6)-C(7)-C(13)	69.22(10)
C(18)-C(6)-C(7)-C(8)	173.33(9)
C(5)-C(6)-C(7)-C(8)	-56.53(10)
C(4)-C(3)-C(8)-C(9)	169.55(8)
C(2)-C(3)-C(8)-C(9)	-66.03(9)
C(11)-C(3)-C(8)-C(9)	49.61(9)
C(4)-C(3)-C(8)-C(7)	-49.54(11)

C(2)-C(3)-C(8)-C(7)	74.88(11)
C(11)-C(3)-C(8)-C(7)	-169.49(8)
C(19)-C(7)-C(8)-C(9)	-62.69(11)
C(13)-C(7)-C(8)-C(9)	58.67(13)
C(6)-C(7)-C(8)-C(9)	-177.53(9)
C(19)-C(7)-C(8)-C(3)	166.62(8)
C(13)-C(7)-C(8)-C(3)	-72.03(11)
C(6)-C(7)-C(8)-C(3)	51.77(11)
C(1)-O(1)-C(9)-C(8)	-61.93(11)
C(1)-O(1)-C(9)-C(10)	50.63(11)
C(3)-C(8)-C(9)-O(1)	67.53(9)
C(7)-C(8)-C(9)-O(1)	-71.07(12)
C(3)-C(8)-C(9)-C(10)	-50.57(9)
C(7)-C(8)-C(9)-C(10)	170.83(9)
O(1)-C(9)-C(10)-C(11)	-87.39(10)
C(8)-C(9)-C(10)-C(11)	31.54(11)
C(9)-C(10)-C(11)-C(3)	-0.44(11)
C(4)-C(3)-C(11)-C(10)	-147.48(9)
C(2)-C(3)-C(11)-C(10)	85.51(10)
C(8)-C(3)-C(11)-C(10)	-30.15(10)
C(19)-C(7)-C(13)-O(3)	66.63(10)
C(8)-C(7)-C(13)-O(3)	-53.63(11)
C(6)-C(7)-C(13)-O(3)	-171.47(8)
C(19)-C(7)-C(13)-C(14)	-52.37(11)
C(8)-C(7)-C(13)-C(14)	-172.63(8)

C(6)-C(7)-C(13)-C(14)	69.53(11)
O(3)-C(13)-C(14)-C(15)	84.11(10)
C(7)-C(13)-C(14)-C(15)	-152.25(9)
C(13)-C(14)-C(15)-C(16)	104.16(13)
C(13)-C(14)-C(15)-C(17)	-76.55(15)
C(22)#1-C(20)-C(21)-C(22)	0.1(2)
C(20)-C(21)-C(22)-C(20)#1	-0.1(2)

Symmetry transformations used to generate equivalent atoms:

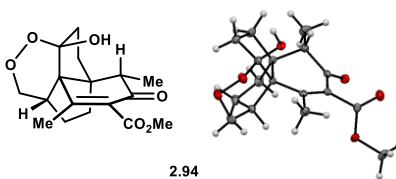
#1 -x+2,-y+2,-z

Table 7. Hydrogen bonds for svp26 [ $\text{\AA}$  and  $^\circ$ ].

D-H...A	d(D-H)	d(H...A)	d(D...A)	$\angle$ (DHA)
O(2)-H(2)...O(3)#2	0.884(19)	1.83(2)	2.6942(11)	165.2(18)
O(3)-H(3)...O(1)	0.847(17)	1.808(17)	2.6330(11)	164.1(16)

Symmetry transformations used to generate equivalent atoms:

#1 -x+2,-y+2,-z #2 -x+3/2,y-1/2,-z+1/2



Crystal structure provided by Dr. Joseph Ziller (University of California, Irvine, California, United States of America). Thermal ellipsoids are drawn at 50% probability level.

Table 1. Crystal data and structure refinement for svp21.

Identification code	svp21 (Nick Foy)	
Empirical formula	C <sub>17</sub> H <sub>22</sub> O <sub>6</sub>	
Formula weight	322.34	
Temperature	133(2) K	
Wavelength	0.71073 Å	
Crystal system	Orthorhombic	
Space group	<i>P</i> 2 <sub>1</sub> 2 <sub>1</sub> 2 <sub>1</sub>	
Unit cell dimensions	<i>a</i> = 7.697(2) Å	$\alpha = 90^\circ$ .
	<i>b</i> = 11.370(3) Å	$\beta = 90^\circ$ .
	<i>c</i> = 17.862(5) Å	$\gamma = 90^\circ$ .
Volume	1563.3(8) Å <sup>3</sup>	
Z	4	
Density (calculated)	1.370 Mg/m <sup>3</sup>	
Absorption coefficient	0.103 mm <sup>-1</sup>	
F(000)	688	
Crystal color	colorless	
Crystal size	0.263 x 0.141 x 0.108 mm <sup>3</sup>	
Theta range for data collection	2.123 to 28.867°	
Index ranges	-10 ≤ <i>h</i> ≤ 10, -14 ≤ <i>k</i> ≤ 15, -24 ≤ <i>l</i> ≤ 23	
Reflections collected	18815	
Independent reflections	3874 [R(int) = 0.0395]	
Completeness to theta = 25.500°	99.9 %	
Absorption correction	Semi-empirical from equivalents	
Max. and min. transmission	0.8621 and 0.8336	



Refinement method	Full-matrix least-squares on F <sup>2</sup>
Data / restraints / parameters	3874 / 0 / 296
Goodness-of-fit on F <sup>2</sup>	1.060
Final R indices [ $I > 2\sigma(I)$ = 3567 data]	R1 = 0.0362, wR2 = 0.0902
R indices (all data, 0.74 Å)	R1 = 0.0407, wR2 = 0.0926
Largest diff. peak and hole	0.326 and -0.197 e.Å <sup>-3</sup>

Table 2. Atomic coordinates ( $\times 10^4$ ) and equivalent isotropic displacement parameters ( $\text{Å}^2 \times 10^3$ ) for svp21. U(eq) is defined as one third of the trace of the orthogonalized  $U^{ij}$  tensor.

	x	y	z	U(eq)
O(1)	7242(2)	8409(1)	842(1)	19(1)
O(2)	6857(2)	7155(1)	728(1)	23(1)
O(3)	6741(2)	9960(1)	1587(1)	17(1)
O(4)	1190(2)	12212(1)	997(1)	26(1)
O(5)	114(2)	10676(1)	360(1)	22(1)
O(6)	-38(2)	10259(1)	2246(1)	18(1)
C(1)	5131(3)	7111(2)	431(1)	22(1)
C(2)	3785(3)	7526(2)	999(1)	16(1)
C(3)	3276(3)	6635(2)	1599(1)	20(1)
C(4)	2441(3)	7397(2)	2202(1)	19(1)
C(5)	3674(2)	8458(2)	2265(1)	13(1)
C(6)	5331(3)	8165(2)	2737(1)	20(1)
C(7)	6849(3)	8033(2)	2191(1)	18(1)

C(8)	6333(2)	8770(2)	1517(1)	14(1)
C(9)	4333(2)	8674(2)	1438(1)	12(1)
C(10)	3532(2)	9708(2)	1034(1)	12(1)
C(11)	2123(2)	10263(2)	1310(1)	13(1)
C(12)	1458(2)	10028(2)	2070(1)	13(1)
C(13)	2769(3)	9543(2)	2612(1)	14(1)
C(14)	4197(3)	9993(2)	262(1)	18(1)
C(15)	1126(3)	11177(2)	883(1)	15(1)
C(16)	-1016(3)	11475(2)	-43(2)	28(1)
C(17)	1987(3)	9324(2)	3383(1)	25(1)

---

Table 3. Bond lengths [ $\text{\AA}$ ] and angles [ $^\circ$ ] for svp21.

---

O(1)-C(8)	1.452(2)
O(1)-O(2)	1.471(2)
O(2)-C(1)	1.432(3)
O(3)-C(8)	1.395(2)
O(4)-C(15)	1.195(3)
O(5)-C(15)	1.343(3)
O(5)-C(16)	1.449(3)
O(6)-C(12)	1.222(2)
C(1)-C(2)	1.524(3)
C(2)-C(3)	1.527(3)
C(2)-C(9)	1.581(3)
C(3)-C(4)	1.524(3)

C(4)-C(5)	1.539(3)
C(5)-C(13)	1.546(3)
C(5)-C(6)	1.564(3)
C(5)-C(9)	1.580(3)
C(6)-C(7)	1.529(3)
C(7)-C(8)	1.520(3)
C(8)-C(9)	1.550(3)
C(9)-C(10)	1.511(3)
C(10)-C(11)	1.349(3)
C(10)-C(14)	1.505(3)
C(11)-C(12)	1.475(3)
C(11)-C(15)	1.501(3)
C(12)-C(13)	1.503(3)
C(13)-C(17)	1.525(3)
C(8)-O(1)-O(2)	106.97(14)
C(1)-O(2)-O(1)	105.79(15)
C(15)-O(5)-C(16)	115.28(17)
O(2)-C(1)-C(2)	111.92(17)
C(1)-C(2)-C(3)	115.90(18)
C(1)-C(2)-C(9)	113.90(17)
C(3)-C(2)-C(9)	105.50(16)
C(4)-C(3)-C(2)	103.17(16)
C(3)-C(4)-C(5)	103.70(16)
C(4)-C(5)-C(13)	112.12(16)

C(4)-C(5)-C(6)	112.03(17)
C(13)-C(5)-C(6)	108.74(16)
C(4)-C(5)-C(9)	104.59(16)
C(13)-C(5)-C(9)	113.22(15)
C(6)-C(5)-C(9)	105.98(15)
C(7)-C(6)-C(5)	107.49(16)
C(8)-C(7)-C(6)	104.55(16)
O(3)-C(8)-O(1)	103.87(15)
O(3)-C(8)-C(7)	113.86(16)
O(1)-C(8)-C(7)	112.07(16)
O(3)-C(8)-C(9)	107.44(15)
O(1)-C(8)-C(9)	112.61(15)
C(7)-C(8)-C(9)	107.02(16)
C(10)-C(9)-C(8)	113.20(16)
C(10)-C(9)-C(5)	115.94(15)
C(8)-C(9)-C(5)	104.19(15)
C(10)-C(9)-C(2)	107.22(15)
C(8)-C(9)-C(2)	111.55(15)
C(5)-C(9)-C(2)	104.48(15)
C(11)-C(10)-C(14)	120.57(18)
C(11)-C(10)-C(9)	121.09(17)
C(14)-C(10)-C(9)	117.81(17)
C(10)-C(11)-C(12)	122.13(17)
C(10)-C(11)-C(15)	123.27(17)
C(12)-C(11)-C(15)	114.59(16)

O(6)-C(12)-C(11)	121.60(18)
O(6)-C(12)-C(13)	123.15(17)
C(11)-C(12)-C(13)	115.19(16)
C(12)-C(13)-C(17)	112.11(17)
C(12)-C(13)-C(5)	109.76(15)
C(17)-C(13)-C(5)	114.19(18)
O(4)-C(15)-O(5)	124.07(19)
O(4)-C(15)-C(11)	125.05(19)
O(5)-C(15)-C(11)	110.87(17)

Table 4. Anisotropic displacement parameters ( $\text{\AA}^2 \times 10^3$ ) for svp21. The anisotropic displacement factor exponent takes the form:  $-2\pi^2 [h^2 a^{*2}U^{11} + \dots + 2 h k a^* b^* U^{12}]$

	$U^{11}$	$U^{22}$	$U^{33}$	$U^{23}$	$U^{13}$	$U^{12}$
O(1)	16(1)	20(1)	22(1)	-4(1)	4(1)	1(1)
O(2)	19(1)	19(1)	30(1)	-9(1)	0(1)	6(1)
O(3)	11(1)	15(1)	24(1)	-1(1)	-2(1)	-2(1)
O(4)	31(1)	14(1)	33(1)	-2(1)	-9(1)	3(1)
O(5)	24(1)	18(1)	24(1)	0(1)	-12(1)	4(1)
O(6)	12(1)	22(1)	21(1)	-4(1)	0(1)	1(1)
C(1)	21(1)	22(1)	25(1)	-10(1)	-2(1)	4(1)
C(2)	13(1)	14(1)	21(1)	-5(1)	-3(1)	1(1)
C(3)	17(1)	12(1)	33(1)	0(1)	-4(1)	0(1)

C(4)	17(1)	15(1)	25(1)	6(1)	1(1)	-3(1)
C(5)	11(1)	15(1)	14(1)	2(1)	0(1)	1(1)
C(6)	17(1)	24(1)	18(1)	3(1)	-4(1)	5(1)
C(7)	12(1)	19(1)	23(1)	1(1)	-3(1)	2(1)
C(8)	10(1)	15(1)	17(1)	-2(1)	0(1)	1(1)
C(9)	10(1)	11(1)	13(1)	-1(1)	0(1)	0(1)
C(10)	10(1)	13(1)	14(1)	-1(1)	-3(1)	-3(1)
C(11)	12(1)	12(1)	16(1)	-2(1)	-2(1)	-1(1)
C(12)	12(1)	11(1)	16(1)	-5(1)	-1(1)	0(1)
C(13)	13(1)	17(1)	13(1)	-1(1)	1(1)	0(1)
C(14)	18(1)	21(1)	14(1)	3(1)	1(1)	1(1)
C(15)	13(1)	15(1)	16(1)	1(1)	1(1)	1(1)
C(16)	26(1)	28(1)	29(1)	3(1)	-12(1)	9(1)
C(17)	23(1)	36(1)	15(1)	3(1)	4(1)	4(1)

---

Table 5. Hydrogen coordinates ( $\times 10^4$ ) and isotropic displacement parameters ( $\text{\AA}^2 \times 10^3$ ) for svp21.

---

	x	y	z	U(eq)
H(3)	7820(40)	10020(30)	1721(16)	33(8)
H(1A)	4970(30)	6290(20)	319(14)	19(6)
H(1B)	5020(40)	7610(30)	-50(19)	43(8)

H(2A)	2770(40)	7730(20)	740(15)	22(7)
H(3A)	2490(40)	6030(30)	1421(19)	42(9)
H(3B)	4280(40)	6240(30)	1800(18)	38(8)
H(4A)	2330(30)	7010(30)	2683(15)	22(7)
H(4B)	1270(40)	7670(20)	2034(15)	27(7)
H(6A)	5620(30)	8770(20)	3088(15)	19(6)
H(6B)	5140(40)	7450(20)	3045(15)	26(7)
H(7A)	8050(30)	8280(20)	2384(14)	17(6)
H(7B)	6920(30)	7240(20)	2033(14)	16(6)
H(13A)	3640(30)	10120(20)	2640(13)	13(5)
H(14A)	5480(40)	10010(20)	278(15)	26(7)
H(14B)	3700(30)	10720(30)	69(15)	23(6)
H(14C)	3770(40)	9380(30)	-96(15)	27(7)
H(16A)	-1660(40)	11010(30)	-360(17)	30(7)
H(16B)	-380(40)	12060(30)	-314(19)	42(9)
H(16C)	-1730(40)	11850(30)	323(17)	36(8)
H(17A)	3020(50)	8960(30)	3713(19)	47(9)
H(17B)	1050(40)	8710(30)	3370(17)	36(8)
H(17C)	1470(30)	10060(20)	3592(14)	21(6)

---

Table 6. Torsion angles [°] for svp21.

---

C(8)-O(1)-O(2)-C(1)	76.81(17)
O(1)-O(2)-C(1)-C(2)	-66.4(2)

O(2)-C(1)-C(2)-C(3)	-78.8(2)
O(2)-C(1)-C(2)-C(9)	43.9(3)
C(1)-C(2)-C(3)-C(4)	161.97(18)
C(9)-C(2)-C(3)-C(4)	35.0(2)
C(2)-C(3)-C(4)-C(5)	-43.9(2)
C(3)-C(4)-C(5)-C(13)	158.47(16)
C(3)-C(4)-C(5)-C(6)	-78.9(2)
C(3)-C(4)-C(5)-C(9)	35.4(2)
C(4)-C(5)-C(6)-C(7)	105.5(2)
C(13)-C(5)-C(6)-C(7)	-130.06(18)
C(9)-C(5)-C(6)-C(7)	-8.0(2)
C(5)-C(6)-C(7)-C(8)	25.5(2)
O(2)-O(1)-C(8)-O(3)	-179.51(13)
O(2)-O(1)-C(8)-C(7)	57.14(19)
O(2)-O(1)-C(8)-C(9)	-63.58(18)
C(6)-C(7)-C(8)-O(3)	84.7(2)
C(6)-C(7)-C(8)-O(1)	-157.76(16)
C(6)-C(7)-C(8)-C(9)	-33.9(2)
O(3)-C(8)-C(9)-C(10)	32.7(2)
O(1)-C(8)-C(9)-C(10)	-81.06(19)
C(7)-C(8)-C(9)-C(10)	155.36(16)
O(3)-C(8)-C(9)-C(5)	-94.11(17)
O(1)-C(8)-C(9)-C(5)	152.13(15)
C(7)-C(8)-C(9)-C(5)	28.55(19)
O(3)-C(8)-C(9)-C(2)	153.74(16)



O(1)-C(8)-C(9)-C(2)	40.0(2)
C(7)-C(8)-C(9)-C(2)	-83.61(19)
C(4)-C(5)-C(9)-C(10)	104.17(18)
C(13)-C(5)-C(9)-C(10)	-18.2(2)
C(6)-C(5)-C(9)-C(10)	-137.30(16)
C(4)-C(5)-C(9)-C(8)	-130.74(15)
C(13)-C(5)-C(9)-C(8)	106.90(17)
C(6)-C(5)-C(9)-C(8)	-12.2(2)
C(4)-C(5)-C(9)-C(2)	-13.58(19)
C(13)-C(5)-C(9)-C(2)	-135.94(16)
C(6)-C(5)-C(9)-C(2)	104.95(17)
C(1)-C(2)-C(9)-C(10)	95.22(19)
C(3)-C(2)-C(9)-C(10)	-136.56(17)
C(1)-C(2)-C(9)-C(8)	-29.2(2)
C(3)-C(2)-C(9)-C(8)	98.99(19)
C(1)-C(2)-C(9)-C(5)	-141.21(17)
C(3)-C(2)-C(9)-C(5)	-12.98(19)
C(8)-C(9)-C(10)-C(11)	-132.31(19)
C(5)-C(9)-C(10)-C(11)	-12.0(3)
C(2)-C(9)-C(10)-C(11)	104.2(2)
C(8)-C(9)-C(10)-C(14)	56.1(2)
C(5)-C(9)-C(10)-C(14)	176.39(16)
C(2)-C(9)-C(10)-C(14)	-67.4(2)
C(14)-C(10)-C(11)-C(12)	-178.50(18)
C(9)-C(10)-C(11)-C(12)	10.1(3)

C(14)-C(10)-C(11)-C(15)	0.3(3)
C(9)-C(10)-C(11)-C(15)	-171.07(17)
C(10)-C(11)-C(12)-O(6)	-159.05(19)
C(15)-C(11)-C(12)-O(6)	22.0(3)
C(10)-C(11)-C(12)-C(13)	23.6(3)
C(15)-C(11)-C(12)-C(13)	-155.39(17)
O(6)-C(12)-C(13)-C(17)	2.6(3)
C(11)-C(12)-C(13)-C(17)	180.00(18)
O(6)-C(12)-C(13)-C(5)	130.67(19)
C(11)-C(12)-C(13)-C(5)	-52.0(2)
C(4)-C(5)-C(13)-C(12)	-69.9(2)
C(6)-C(5)-C(13)-C(12)	165.72(16)
C(9)-C(5)-C(13)-C(12)	48.2(2)
C(4)-C(5)-C(13)-C(17)	57.0(2)
C(6)-C(5)-C(13)-C(17)	-67.4(2)
C(9)-C(5)-C(13)-C(17)	175.06(17)
C(16)-O(5)-C(15)-O(4)	-3.8(3)
C(16)-O(5)-C(15)-C(11)	175.01(19)
C(10)-C(11)-C(15)-O(4)	-104.8(3)
C(12)-C(11)-C(15)-O(4)	74.2(3)
C(10)-C(11)-C(15)-O(5)	76.5(2)
C(12)-C(11)-C(15)-O(5)	-104.6(2)

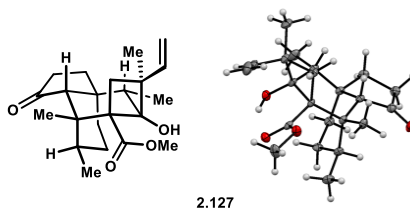
---

Table 7. Hydrogen bonds for svp21 [ $\text{\AA}$  and  $^\circ$ ].

D-H...A	d(D-H)	d(H...A)	d(D...A)	<(DHA)
O(3)-H(3)...O(6)#1	0.86(3)	1.92(3)	2.765(2)	166(3)

Symmetry transformations used to generate equivalent atoms:

#1 x+1,y,z



Crystal structure provided by Dr. Joseph Ziller (University of California, Irvine, California, United States of America). Thermal ellipsoids are drawn at 50% probability level.

Table 1. Crystal data and structure refinement for svp35.

Identification code	svp35 (Nick Foy)	
Empirical formula	C <sub>22</sub> H <sub>32</sub> O <sub>4</sub>	
Formula weight	360.47	
Temperature	133(2) K	
Wavelength	0.71073 Å	
Crystal system	Monoclinic	
Space group	<i>P</i> 2 <sub>1</sub> / <i>c</i>	
Unit cell dimensions	a = 8.2549(12) Å	α = 90°.
	b = 17.095(3) Å	β = 90.125(3)°.
	c = 13.487(2) Å	γ = 90°.
Volume	1903.2(5) Å <sup>3</sup>	

Z	4
Density (calculated)	1.258 Mg/m <sup>3</sup>
Absorption coefficient	0.085 mm <sup>-1</sup>
F(000)	784
Crystal color	colorless
Crystal size	0.413 x 0.234 x 0.072 mm <sup>3</sup>
Theta range for data collection	1.923 to 25.349°
Index ranges	-9 ≤ h ≤ 9, -20 ≤ k ≤ 20, -16 ≤ l ≤ 16
Reflections collected	19971
Independent reflections	3477 [R(int) = 0.0716]
Completeness to theta = 25.242°	100.0 %
Absorption correction	Semi-empirical from equivalents
Max. and min. transmission	0.8622 and 0.6535
Refinement method	Full-matrix least-squares on F <sup>2</sup>
Data / restraints / parameters	3477 / 0 / 363
Goodness-of-fit on F <sup>2</sup>	1.041
Final R indices [I > 2σ(I) = 2841 data]	R1 = 0.0485, wR2 = 0.1218
R indices (all data, 0.83 Å)	R1 = 0.0613, wR2 = 0.1304
Largest diff. peak and hole	0.383 and -0.246 e.Å <sup>-3</sup>

Table 2. Atomic coordinates (x 10<sup>4</sup>) and equivalent isotropic displacement parameters (Å<sup>2</sup> x 10<sup>3</sup>) for svp35. U(eq) is defined as one third of the trace of the orthogonalized U<sup>ij</sup> tensor.

---

	x	y	z	U(eq)
--	---	---	---	-------

---

O(1)	-371(1)	8051(1)	9242(1)	20(1)
O(2)	1895(2)	7843(1)	10100(1)	20(1)
O(3)	4396(2)	7185(1)	9216(1)	19(1)
O(4)	3197(2)	9965(1)	6247(1)	26(1)
C(1)	2029(2)	7880(1)	8290(1)	14(1)
C(2)	1134(2)	7256(1)	7648(1)	16(1)
C(3)	2257(2)	6606(1)	8056(1)	17(1)
C(4)	3524(2)	7274(1)	8322(1)	15(1)
C(5)	4772(2)	7414(1)	7496(1)	16(1)
C(6)	5066(2)	8285(1)	7279(1)	14(1)
C(7)	6125(2)	8403(1)	6348(1)	18(1)
C(8)	5597(2)	9193(1)	5913(2)	20(1)
C(9)	3949(2)	9362(1)	6360(1)	18(1)
C(10)	3439(2)	8644(1)	6963(1)	15(1)
C(11)	2234(2)	8728(1)	7825(1)	14(1)
C(12)	3004(2)	9338(1)	8545(1)	18(1)
C(13)	4613(2)	9032(1)	8953(1)	18(1)
C(14)	5790(2)	8775(1)	8138(1)	18(1)
C(15)	1223(2)	7920(1)	9304(1)	15(1)
C(16)	-1215(3)	8064(1)	10182(2)	27(1)
C(17)	1635(2)	6204(1)	8980(2)	21(1)
C(18)	115(3)	6069(1)	9222(2)	30(1)
C(19)	2748(3)	5964(1)	7323(2)	24(1)
C(20)	6337(2)	6949(1)	7682(2)	23(1)
C(21)	602(2)	9014(1)	7416(2)	18(1)

C(22)	1918(3)	9663(1)	9369(2)	23(1)
-------	---------	---------	---------	-------

---

Table 3. Bond lengths [Å] and angles [°] for svp35.

---

O(1)-C(15)	1.337(2)
O(1)-C(16)	1.449(2)
O(2)-C(15)	1.214(2)
O(3)-C(4)	1.410(2)
O(3)-H(3)	0.86(2)
O(4)-C(9)	1.213(2)
C(1)-C(15)	1.524(2)
C(1)-C(2)	1.560(2)
C(1)-C(11)	1.589(2)
C(1)-C(4)	1.612(2)
C(2)-C(3)	1.548(2)
C(2)-H(2A)	0.951(19)
C(2)-H(2B)	0.987(19)
C(3)-C(17)	1.514(3)
C(3)-C(19)	1.533(3)
C(3)-C(4)	1.590(2)
C(4)-C(5)	1.537(3)
C(5)-C(6)	1.536(2)
C(5)-C(20)	1.536(3)
C(5)-H(5A)	0.980(19)

C(6)-C(10)	1.536(2)
C(6)-C(7)	1.544(2)
C(6)-C(14)	1.549(2)
C(7)-C(8)	1.535(3)
C(7)-H(7A)	0.967(19)
C(7)-H(7B)	0.99(2)
C(8)-C(9)	1.517(3)
C(8)-H(8A)	0.97(2)
C(8)-H(8B)	0.95(2)
C(9)-C(10)	1.533(2)
C(10)-C(11)	1.538(2)
C(10)-H(10A)	1.000(19)
C(11)-C(21)	1.535(2)
C(11)-C(12)	1.558(2)
C(12)-C(13)	1.529(3)
C(12)-C(22)	1.534(3)
C(12)-H(12A)	0.97(2)
C(13)-C(14)	1.533(3)
C(13)-H(13A)	1.00(2)
C(13)-H(13B)	0.95(2)
C(14)-H(14A)	0.98(2)
C(14)-H(14B)	0.99(2)
C(16)-H(16A)	0.95(2)
C(16)-H(16B)	0.99(3)
C(16)-H(16C)	0.95(3)

C(17)-C(18)	1.317(3)
C(17)-H(17A)	0.95(2)
C(18)-H(18A)	0.98(3)
C(18)-H(18B)	1.00(2)
C(19)-H(19A)	1.00(2)
C(19)-H(19B)	0.98(2)
C(19)-H(19C)	1.00(2)
C(20)-H(20A)	0.98(2)
C(20)-H(20B)	1.01(3)
C(20)-H(20C)	1.00(2)
C(21)-H(21A)	0.99(2)
C(21)-H(21B)	0.98(2)
C(21)-H(21C)	0.99(2)
C(22)-H(22A)	0.98(3)
C(22)-H(22B)	1.01(2)
C(22)-H(22C)	0.98(2)
C(15)-O(1)-C(16)	114.98(14)
C(4)-O(3)-H(3)	105.6(15)
C(15)-C(1)-C(2)	108.79(14)
C(15)-C(1)-C(11)	111.18(13)
C(2)-C(1)-C(11)	117.10(14)
C(15)-C(1)-C(4)	109.88(14)
C(2)-C(1)-C(4)	86.40(13)
C(11)-C(1)-C(4)	120.96(14)



C(3)-C(2)-C(1)	90.62(13)
C(3)-C(2)-H(2A)	117.4(11)
C(1)-C(2)-H(2A)	115.0(11)
C(3)-C(2)-H(2B)	108.8(11)
C(1)-C(2)-H(2B)	111.4(11)
H(2A)-C(2)-H(2B)	111.9(15)
C(17)-C(3)-C(19)	107.22(15)
C(17)-C(3)-C(2)	114.54(15)
C(19)-C(3)-C(2)	116.33(16)
C(17)-C(3)-C(4)	111.41(15)
C(19)-C(3)-C(4)	119.05(15)
C(2)-C(3)-C(4)	87.58(13)
O(3)-C(4)-C(5)	107.13(14)
O(3)-C(4)-C(3)	116.70(14)
C(5)-C(4)-C(3)	112.95(14)
O(3)-C(4)-C(1)	118.78(14)
C(5)-C(4)-C(1)	113.27(14)
C(3)-C(4)-C(1)	87.25(12)
C(6)-C(5)-C(20)	113.54(15)
C(6)-C(5)-C(4)	113.29(14)
C(20)-C(5)-C(4)	111.48(15)
C(6)-C(5)-H(5A)	101.7(10)
C(20)-C(5)-H(5A)	108.8(10)
C(4)-C(5)-H(5A)	107.3(10)
C(10)-C(6)-C(5)	107.56(14)

C(10)-C(6)-C(7)	102.66(14)
C(5)-C(6)-C(7)	111.84(14)
C(10)-C(6)-C(14)	109.10(14)
C(5)-C(6)-C(14)	116.21(15)
C(7)-C(6)-C(14)	108.57(14)
C(8)-C(7)-C(6)	105.36(14)
C(8)-C(7)-H(7A)	111.9(11)
C(6)-C(7)-H(7A)	112.1(10)
C(8)-C(7)-H(7B)	110.0(12)
C(6)-C(7)-H(7B)	109.8(12)
H(7A)-C(7)-H(7B)	107.7(16)
C(9)-C(8)-C(7)	105.67(15)
C(9)-C(8)-H(8A)	109.7(13)
C(7)-C(8)-H(8A)	111.2(13)
C(9)-C(8)-H(8B)	109.4(12)
C(7)-C(8)-H(8B)	112.4(12)
H(8A)-C(8)-H(8B)	108.3(17)
O(4)-C(9)-C(8)	124.89(17)
O(4)-C(9)-C(10)	127.32(17)
C(8)-C(9)-C(10)	107.80(15)
C(9)-C(10)-C(6)	103.04(14)
C(9)-C(10)-C(11)	120.28(15)
C(6)-C(10)-C(11)	113.23(14)
C(9)-C(10)-H(10A)	101.9(11)
C(6)-C(10)-H(10A)	108.4(11)

C(11)-C(10)-H(10A)	108.9(11)
C(21)-C(11)-C(10)	109.09(14)
C(21)-C(11)-C(12)	111.52(15)
C(10)-C(11)-C(12)	105.70(14)
C(21)-C(11)-C(1)	109.77(14)
C(10)-C(11)-C(1)	106.38(13)
C(12)-C(11)-C(1)	114.08(14)
C(13)-C(12)-C(22)	111.79(16)
C(13)-C(12)-C(11)	110.37(14)
C(22)-C(12)-C(11)	117.10(15)
C(13)-C(12)-H(12A)	107.7(11)
C(22)-C(12)-H(12A)	106.3(12)
C(11)-C(12)-H(12A)	102.7(12)
C(12)-C(13)-C(14)	113.03(15)
C(12)-C(13)-H(13A)	108.3(12)
C(14)-C(13)-H(13A)	113.1(12)
C(12)-C(13)-H(13B)	110.2(12)
C(14)-C(13)-H(13B)	107.7(12)
H(13A)-C(13)-H(13B)	104.1(16)
C(13)-C(14)-C(6)	116.56(15)
C(13)-C(14)-H(14A)	110.3(11)
C(6)-C(14)-H(14A)	112.1(11)
C(13)-C(14)-H(14B)	108.9(12)
C(6)-C(14)-H(14B)	106.6(12)
H(14A)-C(14)-H(14B)	101.1(17)

O(2)-C(15)-O(1)	121.43(16)
O(2)-C(15)-C(1)	126.11(16)
O(1)-C(15)-C(1)	112.45(14)
O(1)-C(16)-H(16A)	105.6(13)
O(1)-C(16)-H(16B)	110.2(13)
H(16A)-C(16)-H(16B)	113.2(19)
O(1)-C(16)-H(16C)	109.9(14)
H(16A)-C(16)-H(16C)	111(2)
H(16B)-C(16)-H(16C)	107(2)
C(18)-C(17)-C(3)	127.47(19)
C(18)-C(17)-H(17A)	120.3(13)
C(3)-C(17)-H(17A)	112.2(13)
C(17)-C(18)-H(18A)	122.4(14)
C(17)-C(18)-H(18B)	122.8(14)
H(18A)-C(18)-H(18B)	115(2)
C(3)-C(19)-H(19A)	109.1(13)
C(3)-C(19)-H(19B)	108.7(13)
H(19A)-C(19)-H(19B)	112.8(18)
C(3)-C(19)-H(19C)	112.2(12)
H(19A)-C(19)-H(19C)	104.9(17)
H(19B)-C(19)-H(19C)	109.2(17)
C(5)-C(20)-H(20A)	109.4(12)
C(5)-C(20)-H(20B)	111.6(14)
H(20A)-C(20)-H(20B)	110.4(18)
C(5)-C(20)-H(20C)	112.3(13)

H(20A)-C(20)-H(20C)	108.3(18)
H(20B)-C(20)-H(20C)	104.6(19)
C(11)-C(21)-H(21A)	111.3(12)
C(11)-C(21)-H(21B)	111.5(11)
H(21A)-C(21)-H(21B)	107.9(16)
C(11)-C(21)-H(21C)	111.4(13)
H(21A)-C(21)-H(21C)	106.4(18)
H(21B)-C(21)-H(21C)	108.0(17)
C(12)-C(22)-H(22A)	108.8(14)
C(12)-C(22)-H(22B)	114.4(13)
H(22A)-C(22)-H(22B)	103.0(19)
C(12)-C(22)-H(22C)	111.8(12)
H(22A)-C(22)-H(22C)	109.4(19)
H(22B)-C(22)-H(22C)	109.0(18)

---

Table 4. Anisotropic displacement parameters ( $\text{\AA}^2 \times 10^3$ ) for svp35. The anisotropic displacement factor exponent takes the form:  $-2\pi^2 [h^2 a^{*2}U^{11} + \dots + 2 h k a^* b^* U^{12}]$

---

	$U^{11}$	$U^{22}$	$U^{33}$	$U^{23}$	$U^{13}$	$U^{12}$
O(1)	16(1)	22(1)	20(1)	4(1)	5(1)	2(1)
O(2)	21(1)	20(1)	18(1)	1(1)	0(1)	0(1)
O(3)	18(1)	19(1)	19(1)	2(1)	-2(1)	3(1)
O(4)	32(1)	15(1)	31(1)	8(1)	7(1)	5(1)

C(1)	13(1)	9(1)	19(1)	3(1)	-1(1)	0(1)
C(2)	14(1)	13(1)	20(1)	1(1)	0(1)	-3(1)
C(3)	18(1)	10(1)	23(1)	1(1)	-1(1)	-1(1)
C(4)	18(1)	9(1)	20(1)	0(1)	-3(1)	1(1)
C(5)	16(1)	11(1)	21(1)	-1(1)	-1(1)	1(1)
C(6)	14(1)	11(1)	18(1)	-1(1)	0(1)	-1(1)
C(7)	15(1)	15(1)	23(1)	-2(1)	1(1)	-2(1)
C(8)	23(1)	16(1)	21(1)	2(1)	4(1)	-5(1)
C(9)	23(1)	14(1)	17(1)	1(1)	-1(1)	-2(1)
C(10)	17(1)	10(1)	17(1)	0(1)	-1(1)	-2(1)
C(11)	14(1)	10(1)	19(1)	2(1)	1(1)	1(1)
C(12)	22(1)	10(1)	21(1)	-1(1)	2(1)	-1(1)
C(13)	19(1)	16(1)	20(1)	-4(1)	-1(1)	-5(1)
C(14)	14(1)	15(1)	23(1)	-1(1)	-2(1)	-2(1)
C(15)	17(1)	7(1)	22(1)	1(1)	-2(1)	-2(1)
C(16)	22(1)	35(1)	24(1)	7(1)	8(1)	3(1)
C(17)	27(1)	12(1)	25(1)	4(1)	-2(1)	-3(1)
C(18)	34(1)	20(1)	35(1)	8(1)	3(1)	-5(1)
C(19)	31(1)	11(1)	29(1)	-2(1)	0(1)	-2(1)
C(20)	20(1)	18(1)	30(1)	2(1)	4(1)	5(1)
C(21)	17(1)	15(1)	22(1)	4(1)	2(1)	2(1)
C(22)	25(1)	17(1)	27(1)	-5(1)	3(1)	1(1)

---

Table 5. Hydrogen coordinates ( $\times 10^4$ ) and isotropic displacement parameters ( $\text{\AA}^2 \times 10^3$ )

for svp35.

---

	x	y	z	U(eq)
H(3)	3720(30)	7293(13)	9682(17)	25(6)
H(2A)	10(20)	7208(10)	7774(13)	8(4)
H(2B)	1360(20)	7329(11)	6935(14)	9(4)
H(5A)	4280(20)	7236(10)	6874(14)	8(4)
H(7A)	7270(20)	8394(10)	6504(13)	7(4)
H(7B)	5910(20)	7979(13)	5865(15)	24(5)
H(8A)	6350(30)	9603(14)	6092(15)	27(6)
H(8B)	5510(20)	9179(12)	5210(16)	18(5)
H(10A)	2950(20)	8302(12)	6441(14)	13(5)
H(12A)	3240(20)	9776(12)	8107(14)	17(5)
H(13A)	4370(20)	8608(13)	9444(16)	25(5)
H(13B)	5140(20)	9426(12)	9336(14)	17(5)
H(16A)	-2330(30)	8128(13)	10022(16)	29(6)
H(16B)	-780(30)	8489(15)	10609(17)	35(6)
H(16C)	-1050(30)	7583(15)	10524(17)	35(6)
H(17A)	2490(30)	6018(13)	9390(16)	22(5)
H(18A)	-790(30)	6246(15)	8812(18)	39(7)
H(18B)	-200(30)	5782(14)	9842(18)	40(7)
H(19A)	1790(30)	5628(14)	7179(16)	29(6)
H(19B)	3660(30)	5668(13)	7606(16)	26(6)

H(19C)	3070(20)	6180(12)	6667(16)	19(5)
H(20A)	7030(30)	6980(13)	7093(16)	23(5)
H(20B)	6100(30)	6383(15)	7854(17)	39(7)
H(20C)	6960(30)	7153(13)	8263(17)	30(6)
H(21A)	690(30)	9548(14)	7136(16)	27(6)
H(21B)	-230(20)	9026(11)	7936(14)	14(5)
H(21C)	210(30)	8674(13)	6871(16)	27(6)
H(22A)	2480(30)	10099(15)	9691(18)	37(6)
H(22B)	1720(30)	9286(14)	9937(17)	31(6)
H(22C)	870(30)	9842(12)	9112(15)	23(5)
H(14A)	6740(20)	8527(11)	8429(14)	14(5)
H(14B)	6280(30)	9247(13)	7833(15)	24(5)

---

Table 6. Torsion angles [°] for svp35.

---

C(15)-C(1)-C(2)-C(3)	-88.23(15)
C(11)-C(1)-C(2)-C(3)	144.70(15)
C(4)-C(1)-C(2)-C(3)	21.55(13)
C(1)-C(2)-C(3)-C(17)	90.63(17)
C(1)-C(2)-C(3)-C(19)	-143.27(16)
C(1)-C(2)-C(3)-C(4)	-21.85(13)
C(17)-C(3)-C(4)-O(3)	26.7(2)
C(19)-C(3)-C(4)-O(3)	-98.9(2)
C(2)-C(3)-C(4)-O(3)	142.14(15)



C(17)-C(3)-C(4)-C(5)	151.50(15)
C(19)-C(3)-C(4)-C(5)	25.9(2)
C(2)-C(3)-C(4)-C(5)	-93.03(15)
C(17)-C(3)-C(4)-C(1)	-94.34(16)
C(19)-C(3)-C(4)-C(1)	140.09(17)
C(2)-C(3)-C(4)-C(1)	21.12(13)
C(15)-C(1)-C(4)-O(3)	-31.4(2)
C(2)-C(1)-C(4)-O(3)	-140.11(15)
C(11)-C(1)-C(4)-O(3)	100.25(19)
C(15)-C(1)-C(4)-C(5)	-158.45(14)
C(2)-C(1)-C(4)-C(5)	92.87(16)
C(11)-C(1)-C(4)-C(5)	-26.8(2)
C(15)-C(1)-C(4)-C(3)	87.70(15)
C(2)-C(1)-C(4)-C(3)	-20.98(12)
C(11)-C(1)-C(4)-C(3)	-140.62(15)
O(3)-C(4)-C(5)-C(6)	-94.68(16)
C(3)-C(4)-C(5)-C(6)	135.45(15)
C(1)-C(4)-C(5)-C(6)	38.2(2)
O(3)-C(4)-C(5)-C(20)	34.87(19)
C(3)-C(4)-C(5)-C(20)	-95.01(18)
C(1)-C(4)-C(5)-C(20)	167.79(15)
C(20)-C(5)-C(6)-C(10)	171.93(15)
C(4)-C(5)-C(6)-C(10)	-59.58(19)
C(20)-C(5)-C(6)-C(7)	59.9(2)
C(4)-C(5)-C(6)-C(7)	-171.57(15)

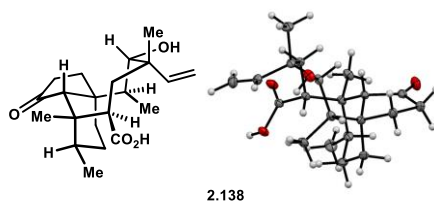
C(20)-C(5)-C(6)-C(14)	-65.5(2)
C(4)-C(5)-C(6)-C(14)	63.00(19)
C(10)-C(6)-C(7)-C(8)	35.84(18)
C(5)-C(6)-C(7)-C(8)	150.88(15)
C(14)-C(6)-C(7)-C(8)	-79.58(17)
C(6)-C(7)-C(8)-C(9)	-18.70(19)
C(7)-C(8)-C(9)-O(4)	174.28(18)
C(7)-C(8)-C(9)-C(10)	-5.8(2)
O(4)-C(9)-C(10)-C(6)	-152.10(18)
C(8)-C(9)-C(10)-C(6)	27.94(18)
O(4)-C(9)-C(10)-C(11)	-24.9(3)
C(8)-C(9)-C(10)-C(11)	155.10(16)
C(5)-C(6)-C(10)-C(9)	-156.77(14)
C(7)-C(6)-C(10)-C(9)	-38.67(16)
C(14)-C(6)-C(10)-C(9)	76.37(17)
C(5)-C(6)-C(10)-C(11)	71.73(18)
C(7)-C(6)-C(10)-C(11)	-170.17(14)
C(14)-C(6)-C(10)-C(11)	-55.13(19)
C(9)-C(10)-C(11)-C(21)	63.2(2)
C(6)-C(10)-C(11)-C(21)	-174.51(14)
C(9)-C(10)-C(11)-C(12)	-56.9(2)
C(6)-C(10)-C(11)-C(12)	65.47(17)
C(9)-C(10)-C(11)-C(1)	-178.50(15)
C(6)-C(10)-C(11)-C(1)	-56.16(18)
C(15)-C(1)-C(11)-C(21)	-76.93(17)

C(2)-C(1)-C(11)-C(21)	49.0(2)
C(4)-C(1)-C(11)-C(21)	151.95(16)
C(15)-C(1)-C(11)-C(10)	165.18(14)
C(2)-C(1)-C(11)-C(10)	-68.93(18)
C(4)-C(1)-C(11)-C(10)	34.1(2)
C(15)-C(1)-C(11)-C(12)	49.06(19)
C(2)-C(1)-C(11)-C(12)	174.95(14)
C(4)-C(1)-C(11)-C(12)	-82.07(19)
C(21)-C(11)-C(12)-C(13)	179.07(15)
C(10)-C(11)-C(12)-C(13)	-62.51(18)
C(1)-C(11)-C(12)-C(13)	54.0(2)
C(21)-C(11)-C(12)-C(22)	49.7(2)
C(10)-C(11)-C(12)-C(22)	168.08(16)
C(1)-C(11)-C(12)-C(22)	-75.4(2)
C(22)-C(12)-C(13)-C(14)	-174.54(15)
C(11)-C(12)-C(13)-C(14)	53.3(2)
C(12)-C(13)-C(14)-C(6)	-43.9(2)
C(10)-C(6)-C(14)-C(13)	43.1(2)
C(5)-C(6)-C(14)-C(13)	-78.7(2)
C(7)-C(6)-C(14)-C(13)	154.26(16)
C(16)-O(1)-C(15)-O(2)	-2.2(2)
C(16)-O(1)-C(15)-C(1)	177.67(15)
C(2)-C(1)-C(15)-O(2)	125.39(18)
C(11)-C(1)-C(15)-O(2)	-104.23(19)
C(4)-C(1)-C(15)-O(2)	32.4(2)

C(2)-C(1)-C(15)-O(1)	-54.51(18)
C(11)-C(1)-C(15)-O(1)	75.87(17)
C(4)-C(1)-C(15)-O(1)	-147.52(14)
C(19)-C(3)-C(17)-C(18)	-98.1(2)
C(2)-C(3)-C(17)-C(18)	32.6(3)
C(4)-C(3)-C(17)-C(18)	130.0(2)

Table 7. Hydrogen bonds for svp35 [ $\text{\AA}$  and  $^\circ$ ].

D-H...A	d(D-H)	d(H...A)	d(D...A)	$\angle$ (DHA)
O(3)-H(3)...O(2)	0.86(2)	1.86(2)	2.6382(18)	149(2)



Crystal structure provided by Dr. Joseph Ziller (University of California, Irvine, California, United States of America). Thermal ellipsoids are drawn at 50% probability level.

Table 1. Crystal data and structure refinement for svp37.

Identification code	svp37 (Nick Foy)
Empirical formula	$\text{C}_{21} \text{H}_{32} \text{O}_4$
Formula weight	348.46

Temperature	93(2) K	
Wavelength	1.54178 Å	
Crystal system	Monoclinic	
Space group	<i>P</i> 2 <sub>1</sub> / <i>c</i>	
Unit cell dimensions	<i>a</i> = 8.2013(4) Å	$\alpha = 90^\circ$ .
	<i>b</i> = 26.4165(11) Å	$\beta = 106.325(2)^\circ$ .
	<i>c</i> = 9.0570(4) Å	$\gamma = 90^\circ$ .
Volume	1883.09(15) Å <sup>3</sup>	
Z	4	
Density (calculated)	1.229 Mg/m <sup>3</sup>	
Absorption coefficient	0.664 mm <sup>-1</sup>	
F(000)	760	
Crystal color	colorless	
Crystal size	0.189 x 0.161 x 0.051 mm <sup>3</sup>	
Theta range for data collection	3.346 to 68.917°	
Index ranges	$-9 \leq h \leq 9, -31 \leq k \leq 29, -10 \leq l \leq 10$	
Reflections collected	35645	
Independent reflections	3485 [R(int) = 0.0387]	
Completeness to theta = 67.679°	100.0 %	
Absorption correction	Semi-empirical from equivalents	
Max. and min. transmission	0.8643 and 0.8179	
Refinement method	Full-matrix least-squares on F <sup>2</sup>	
Data / restraints / parameters	3485 / 0 / 354	
Goodness-of-fit on F <sup>2</sup>	1.036	
Final R indices [ $I > 2\sigma(I)$ = 3217 data]	R1 = 0.0357, wR2 = 0.0898	

R indices (all data, 0.83 Å)

R1 = 0.0384, wR2 = 0.0919

Largest diff. peak and hole

0.302 and -0.193 e.Å<sup>-3</sup>

Table 2. Atomic coordinates ( $\times 10^4$ ) and equivalent isotropic displacement parameters ( $\text{Å}^2 \times 10^3$ ) for svp37.  $U(\text{eq})$  is defined as one third of the trace of the orthogonalized  $U^{ij}$  tensor.

	x	y	z	U(eq)
O(1)	-40(1)	4420(1)	5521(1)	21(1)
O(2)	1915(1)	4771(1)	4549(1)	18(1)
O(3)	4447(1)	2783(1)	2906(1)	20(1)
O(4)	5171(1)	3274(1)	10244(1)	24(1)
C(1)	2508(1)	3951(1)	5618(1)	13(1)
C(2)	1555(1)	3463(1)	4925(1)	14(1)
C(3)	2174(2)	3225(1)	3629(1)	16(1)
C(4)	4089(2)	3056(1)	4158(1)	15(1)
C(5)	5580(2)	3433(1)	4824(1)	15(1)
C(6)	6073(1)	3512(1)	6634(1)	14(1)
C(7)	7007(2)	4016(1)	7178(1)	19(1)
C(8)	5863(2)	4476(1)	7150(1)	20(1)
C(9)	4552(2)	4374(1)	8029(1)	18(1)
C(10)	3445(2)	3901(1)	7380(1)	14(1)
C(11)	4678(1)	3449(1)	7485(1)	13(1)
C(12)	5663(2)	3265(1)	9099(1)	17(1)
C(13)	7344(2)	3043(1)	9042(1)	20(1)

C(14)	7305(2)	3072(1)	7349(1)	18(1)
C(15)	1336(2)	4400(1)	5240(1)	15(1)
C(16)	1805(2)	3560(1)	2212(1)	19(1)
C(17)	620(2)	3911(1)	1794(2)	24(1)
C(18)	1114(2)	2736(1)	3142(2)	23(1)
C(19)	5604(2)	3896(1)	3786(1)	18(1)
C(20)	3578(2)	4858(1)	8198(2)	26(1)
C(21)	2168(2)	3800(1)	8302(1)	19(1)

---

Table 3. Bond lengths [Å] and angles [°] for svp37.

---

O(1)-C(15)	1.2253(15)
O(2)-C(15)	1.3216(14)
O(3)-C(4)	1.4417(13)
O(4)-C(12)	1.2138(15)
C(1)-C(15)	1.5050(15)
C(1)-C(2)	1.5462(15)
C(1)-C(10)	1.5694(15)
C(2)-C(3)	1.5376(16)
C(3)-C(16)	1.5180(16)
C(3)-C(18)	1.5507(16)
C(3)-C(4)	1.5726(16)
C(4)-C(5)	1.5603(16)
C(5)-C(19)	1.5456(16)

C(5)-C(6)	1.5887(15)
C(6)-C(7)	1.5470(16)
C(6)-C(14)	1.5552(16)
C(6)-C(11)	1.5577(15)
C(7)-C(8)	1.5316(18)
C(8)-C(9)	1.5315(17)
C(9)-C(20)	1.5371(17)
C(9)-C(10)	1.5586(16)
C(10)-C(21)	1.5361(16)
C(10)-C(11)	1.5502(15)
C(11)-C(12)	1.5362(15)
C(12)-C(13)	1.5125(17)
C(13)-C(14)	1.5267(16)
C(16)-C(17)	1.3186(19)

C(15)-C(1)-C(2)	110.33(9)
C(15)-C(1)-C(10)	113.35(9)
C(2)-C(1)-C(10)	113.00(9)
C(3)-C(2)-C(1)	114.40(9)
C(16)-C(3)-C(2)	112.17(10)
C(16)-C(3)-C(18)	106.47(9)
C(2)-C(3)-C(18)	106.15(9)
C(16)-C(3)-C(4)	111.58(9)
C(2)-C(3)-C(4)	113.51(9)
C(18)-C(3)-C(4)	106.36(10)



O(3)-C(4)-C(5)	108.19(9)
O(3)-C(4)-C(3)	108.00(9)
C(5)-C(4)-C(3)	122.91(9)
C(19)-C(5)-C(4)	114.37(10)
C(19)-C(5)-C(6)	118.71(10)
C(4)-C(5)-C(6)	115.29(9)
C(7)-C(6)-C(14)	107.71(9)
C(7)-C(6)-C(11)	107.51(9)
C(14)-C(6)-C(11)	101.34(9)
C(7)-C(6)-C(5)	113.66(9)
C(14)-C(6)-C(5)	106.20(9)
C(11)-C(6)-C(5)	119.18(9)
C(8)-C(7)-C(6)	115.61(10)
C(9)-C(8)-C(7)	111.57(10)
C(8)-C(9)-C(20)	111.46(10)
C(8)-C(9)-C(10)	111.38(9)
C(20)-C(9)-C(10)	116.09(10)
C(21)-C(10)-C(11)	111.40(9)
C(21)-C(10)-C(9)	110.35(9)
C(11)-C(10)-C(9)	107.09(9)
C(21)-C(10)-C(1)	110.68(10)
C(11)-C(10)-C(1)	104.57(9)
C(9)-C(10)-C(1)	112.57(9)
C(12)-C(11)-C(10)	117.53(9)
C(12)-C(11)-C(6)	103.95(9)

C(10)-C(11)-C(6)	116.38(9)
O(4)-C(12)-C(13)	124.16(11)
O(4)-C(12)-C(11)	126.44(11)
C(13)-C(12)-C(11)	109.35(10)
C(12)-C(13)-C(14)	104.60(10)
C(13)-C(14)-C(6)	106.49(10)
O(1)-C(15)-O(2)	122.74(11)
O(1)-C(15)-C(1)	123.56(10)
O(2)-C(15)-C(1)	113.69(10)
C(17)-C(16)-C(3)	127.40(12)

Table 4. Anisotropic displacement parameters ( $\text{\AA}^2 \times 10^3$ ) for svp37. The anisotropic displacement factor exponent takes the form:  $-2\sigma^2 [h^2 a^{*2}U^{11} + \dots + 2 h k a^* b^* U^{12}]$

	$U^{11}$	$U^{22}$	$U^{33}$	$U^{23}$	$U^{13}$	$U^{12}$
O(1)	19(1)	16(1)	31(1)	6(1)	13(1)	3(1)
O(2)	19(1)	14(1)	24(1)	5(1)	10(1)	2(1)
O(3)	33(1)	16(1)	15(1)	-2(1)	11(1)	3(1)
O(4)	34(1)	27(1)	12(1)	2(1)	8(1)	3(1)
C(1)	14(1)	13(1)	13(1)	1(1)	6(1)	0(1)
C(2)	14(1)	14(1)	14(1)	1(1)	4(1)	-1(1)
C(3)	19(1)	14(1)	13(1)	-1(1)	3(1)	-2(1)
C(4)	22(1)	13(1)	11(1)	-1(1)	7(1)	1(1)

C(5)	16(1)	16(1)	14(1)	1(1)	7(1)	2(1)
C(6)	14(1)	16(1)	14(1)	2(1)	4(1)	-1(1)
C(7)	17(1)	22(1)	17(1)	1(1)	4(1)	-6(1)
C(8)	25(1)	15(1)	18(1)	-1(1)	4(1)	-8(1)
C(9)	25(1)	14(1)	14(1)	-3(1)	4(1)	-2(1)
C(10)	19(1)	13(1)	12(1)	0(1)	6(1)	0(1)
C(11)	16(1)	12(1)	11(1)	0(1)	4(1)	-2(1)
C(12)	22(1)	14(1)	14(1)	0(1)	3(1)	-4(1)
C(13)	19(1)	22(1)	17(1)	4(1)	1(1)	-2(1)
C(14)	15(1)	21(1)	18(1)	4(1)	5(1)	1(1)
C(15)	17(1)	14(1)	14(1)	0(1)	5(1)	-2(1)
C(16)	22(1)	21(1)	12(1)	-1(1)	3(1)	-3(1)
C(17)	28(1)	26(1)	17(1)	2(1)	2(1)	1(1)
C(18)	27(1)	18(1)	22(1)	-5(1)	4(1)	-6(1)
C(19)	22(1)	19(1)	15(1)	2(1)	9(1)	-2(1)
C(20)	38(1)	16(1)	22(1)	-5(1)	6(1)	1(1)
C(21)	25(1)	19(1)	17(1)	2(1)	12(1)	2(1)

---

Table 5. Hydrogen coordinates ( $\times 10^4$ ) and isotropic displacement parameters ( $\text{\AA}^2 \times 10^3$ )

for svp37.

---

	x	y	z	U(eq)
--	---	---	---	-------

---

H(1A)	3369(17)	4017(5)	5118(15)	9(3)
H(2)	1210(20)	5042(7)	4480(20)	39(5)
H(2A)	335(18)	3534(5)	4511(15)	13(3)
H(2B)	1653(17)	3211(5)	5734(16)	12(3)
H(3)	4740(20)	2987(7)	2300(20)	39(5)
H(4A)	4143(16)	2792(5)	4933(15)	11(3)
H(5A)	6558(17)	3242(5)	4720(15)	12(3)
H(7A)	7817(18)	4079(5)	6608(16)	17(3)
H(7B)	7700(18)	3963(5)	8275(17)	19(3)
H(8A)	5293(18)	4594(5)	6096(17)	18(3)
H(8B)	6580(20)	4767(6)	7637(18)	27(4)
H(9A)	5205(17)	4264(5)	9084(17)	14(3)
H(11A)	4046(17)	3141(5)	7090(15)	12(3)
H(13A)	7446(19)	2695(6)	9426(17)	21(4)
H(13B)	8280(20)	3248(6)	9688(19)	29(4)
H(14A)	6870(18)	2751(6)	6823(16)	17(3)
H(14B)	8430(20)	3137(6)	7173(17)	22(4)
H(16A)	2500(20)	3482(6)	1530(18)	26(4)
H(17A)	-150(20)	3996(6)	2396(19)	27(4)
H(17B)	430(20)	4100(6)	820(20)	29(4)
H(18A)	-100(20)	2822(6)	2882(19)	28(4)
H(18B)	1370(20)	2581(6)	2230(20)	32(4)
H(18C)	1390(20)	2484(6)	4021(19)	29(4)
H(19A)	5545(18)	3778(6)	2741(18)	21(4)
H(19B)	6670(20)	4080(6)	4170(18)	23(4)

H(19C)	4690(20)	4146(6)	3724(17)	23(4)
H(20A)	2800(20)	4801(6)	8850(20)	33(4)
H(20B)	4420(20)	5119(7)	8715(19)	33(4)
H(20C)	2980(20)	5007(7)	7190(20)	35(4)
H(21A)	1740(20)	3454(6)	8139(18)	25(4)
H(21B)	2730(20)	3841(6)	9381(19)	27(4)
H(21C)	1200(20)	4048(6)	8026(19)	31(4)

Table 6. Torsion angles [°] for svp37.

C(15)-C(1)-C(2)-C(3)	112.82(11)
C(10)-C(1)-C(2)-C(3)	-119.13(10)
C(1)-C(2)-C(3)-C(16)	-66.16(12)
C(1)-C(2)-C(3)-C(18)	177.94(10)
C(1)-C(2)-C(3)-C(4)	61.47(12)
C(16)-C(3)-C(4)-O(3)	-59.32(12)
C(2)-C(3)-C(4)-O(3)	172.74(9)
C(18)-C(3)-C(4)-O(3)	56.39(11)
C(16)-C(3)-C(4)-C(5)	67.63(13)
C(2)-C(3)-C(4)-C(5)	-60.30(13)
C(18)-C(3)-C(4)-C(5)	-176.65(10)
O(3)-C(4)-C(5)-C(19)	73.08(12)
C(3)-C(4)-C(5)-C(19)	-53.79(14)
O(3)-C(4)-C(5)-C(6)	-144.04(9)

C(3)-C(4)-C(5)-C(6)	89.09(12)
C(19)-C(5)-C(6)-C(7)	-16.35(14)
C(4)-C(5)-C(6)-C(7)	-157.54(10)
C(19)-C(5)-C(6)-C(14)	-134.59(10)
C(4)-C(5)-C(6)-C(14)	84.22(11)
C(19)-C(5)-C(6)-C(11)	112.04(12)
C(4)-C(5)-C(6)-C(11)	-29.14(14)
C(14)-C(6)-C(7)-C(8)	-157.05(10)
C(11)-C(6)-C(7)-C(8)	-48.56(13)
C(5)-C(6)-C(7)-C(8)	85.59(12)
C(6)-C(7)-C(8)-C(9)	53.16(14)
C(7)-C(8)-C(9)-C(20)	171.86(10)
C(7)-C(8)-C(9)-C(10)	-56.73(13)
C(8)-C(9)-C(10)-C(21)	178.78(10)
C(20)-C(9)-C(10)-C(21)	-52.23(14)
C(8)-C(9)-C(10)-C(11)	57.37(12)
C(20)-C(9)-C(10)-C(11)	-173.64(10)
C(8)-C(9)-C(10)-C(1)	-57.02(13)
C(20)-C(9)-C(10)-C(1)	71.97(13)
C(15)-C(1)-C(10)-C(21)	64.58(12)
C(2)-C(1)-C(10)-C(21)	-61.88(12)
C(15)-C(1)-C(10)-C(11)	-175.34(9)
C(2)-C(1)-C(10)-C(11)	58.20(11)
C(15)-C(1)-C(10)-C(9)	-59.44(12)
C(2)-C(1)-C(10)-C(9)	174.11(9)

C(21)-C(10)-C(11)-C(12)	-54.10(13)
C(9)-C(10)-C(11)-C(12)	66.65(12)
C(1)-C(10)-C(11)-C(12)	-173.69(9)
C(21)-C(10)-C(11)-C(6)	-178.29(9)
C(9)-C(10)-C(11)-C(6)	-57.54(12)
C(1)-C(10)-C(11)-C(6)	62.12(12)
C(7)-C(6)-C(11)-C(12)	-78.55(11)
C(14)-C(6)-C(11)-C(12)	34.32(11)
C(5)-C(6)-C(11)-C(12)	150.29(9)
C(7)-C(6)-C(11)-C(10)	52.36(12)
C(14)-C(6)-C(11)-C(10)	165.23(9)
C(5)-C(6)-C(11)-C(10)	-78.81(13)
C(10)-C(11)-C(12)-O(4)	32.08(17)
C(6)-C(11)-C(12)-O(4)	162.30(11)
C(10)-C(11)-C(12)-C(13)	-150.50(10)
C(6)-C(11)-C(12)-C(13)	-20.28(12)
O(4)-C(12)-C(13)-C(14)	174.60(11)
C(11)-C(12)-C(13)-C(14)	-2.89(12)
C(12)-C(13)-C(14)-C(6)	25.33(12)
C(7)-C(6)-C(14)-C(13)	75.35(11)
C(11)-C(6)-C(14)-C(13)	-37.37(11)
C(5)-C(6)-C(14)-C(13)	-162.54(9)
C(2)-C(1)-C(15)-O(1)	53.82(14)
C(10)-C(1)-C(15)-O(1)	-74.04(14)
C(2)-C(1)-C(15)-O(2)	-125.21(10)

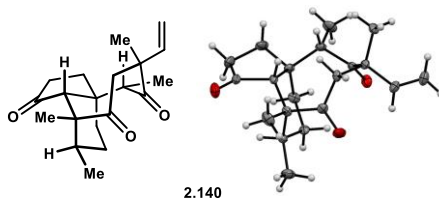
C(10)-C(1)-C(15)-O(2)	106.93(11)
C(2)-C(3)-C(16)-C(17)	-24.03(17)
C(18)-C(3)-C(16)-C(17)	91.68(15)
C(4)-C(3)-C(16)-C(17)	-152.67(12)

Table 7. Hydrogen bonds for svp37 [ $\text{\AA}$  and  $^\circ$ ].

D-H...A	d(D-H)	d(H...A)	d(D...A)	$\angle$ (DHA)
O(2)-H(2)...O(1)#1	0.907(19)	1.719(19)	2.6228(12)	174.4(17)
O(3)-H(3)...O(4)#2	0.86(2)	2.13(2)	2.9421(13)	159.6(17)

Symmetry transformations used to generate equivalent atoms:

#1 -x,-y+1,-z+1 #2 x,y,z-1



Crystal structure provided by Dr. Joseph Ziller (University of California, Irvine, California, United States of America). Thermal ellipsoids are drawn at 50% probability level.

Table 1. Crystal data and structure refinement for svp38.

Identification code	svp38 (Nick Foy)
Empirical formula	$\text{C}_{20} \text{H}_{28} \text{O}_3$



Formula weight	316.42	
Temperature	93(2) K	
Wavelength	1.54178 Å	
Crystal system	Monoclinic	
Space group	Cc	
Unit cell dimensions	a = 8.9985(6) Å	$\alpha = 90^\circ$ .
	b = 18.7587(12) Å	$\beta = 110.083(3)^\circ$ .
	c = 11.0000(7) Å	$\gamma = 90^\circ$ .
Volume	1743.9(2) Å <sup>3</sup>	
Z	4	
Density (calculated)	1.205 Mg/m <sup>3</sup>	
Absorption coefficient	0.626 mm <sup>-1</sup>	
F(000)	688	
Crystal color	colorless	
Crystal size	0.248 x 0.187 x 0.165 mm <sup>3</sup>	
Theta range for data collection	4.714 to 68.722°	
Index ranges	$-10 \leq h \leq 10, -22 \leq k \leq 22, -12 \leq l \leq 13$	
Reflections collected	26443	
Independent reflections	3063 [R(int) = 0.0336]	
Completeness to theta = 67.679°	100.0 %	
Absorption correction	Semi-empirical from equivalents	
Max. and min. transmission	0.8643 and 0.8119	
Refinement method	Full-matrix least-squares on F <sup>2</sup>	
Data / restraints / parameters	3063 / 2 / 212	
Goodness-of-fit on F <sup>2</sup>	1.056	

Final R indices [ $I > 2\sigma(I)$ ] = 3026 data]      R1 = 0.0283, wR2 = 0.0732  
R indices (all data, 0.83 Å)                      R1 = 0.0287, wR2 = 0.0737  
Absolute structure parameter                      -0.12(8)  
Largest diff. peak and hole                      0.157 and -0.141 e.Å<sup>-3</sup>

Table 2. Atomic coordinates ( $\times 10^4$ ) and equivalent isotropic displacement parameters (Å<sup>2</sup>  $\times 10^3$ ) for svp38. U(eq) is defined as one third of the trace of the orthogonalized U<sup>ij</sup> tensor.

	x	y	z	U(eq)
O(1)	2388(2)	3557(1)	5445(2)	36(1)
O(2)	3310(2)	2310(1)	3099(1)	26(1)
O(3)	8129(2)	4765(1)	6418(2)	42(1)
C(1)	6506(2)	3704(1)	5546(2)	19(1)
C(2)	4945(2)	4007(1)	5636(2)	19(1)
C(3)	3789(2)	3427(1)	5759(2)	21(1)
C(4)	4380(2)	2706(1)	6365(2)	20(1)
C(5)	3840(2)	2092(1)	5354(2)	19(1)
C(6)	4295(2)	2300(1)	4182(2)	18(1)
C(7)	6022(2)	2469(1)	4380(2)	21(1)
C(8)	6397(2)	3280(1)	4298(2)	20(1)
C(9)	8122(2)	3337(1)	4291(3)	33(1)
C(10)	8671(2)	4086(1)	4764(3)	37(1)
C(11)	7803(2)	4269(1)	5675(2)	29(1)
C(12)	5278(2)	3656(1)	3078(2)	24(1)

C(13)	3817(2)	4011(1)	3220(2)	22(1)
C(14)	4210(2)	4482(1)	4420(2)	21(1)
C(15)	2065(2)	1993(1)	4944(2)	24(1)
C(16)	1329(2)	1424(1)	5167(2)	30(1)
C(17)	4737(2)	1406(1)	5950(2)	27(1)
C(18)	6455(3)	2009(1)	3382(2)	33(1)
C(19)	2808(3)	4956(1)	4384(3)	34(1)
C(20)	5271(3)	4423(1)	6918(2)	32(1)

---

Table 3. Bond lengths [Å] and angles [°] for svp38.

---

O(1)-C(3)	1.212(2)
O(2)-C(6)	1.217(2)
O(3)-C(11)	1.206(3)
C(1)-C(11)	1.547(2)
C(1)-C(2)	1.550(2)
C(1)-C(8)	1.559(3)
C(2)-C(3)	1.543(3)
C(2)-C(20)	1.550(3)
C(2)-C(14)	1.553(3)
C(3)-C(4)	1.522(3)
C(4)-C(5)	1.558(3)
C(5)-C(15)	1.515(2)
C(5)-C(6)	1.530(3)

C(5)-C(17)	1.541(3)
C(6)-C(7)	1.527(3)
C(7)-C(18)	1.547(3)
C(7)-C(8)	1.568(2)
C(8)-C(12)	1.544(3)
C(8)-C(9)	1.558(2)
C(9)-C(10)	1.521(3)
C(10)-C(11)	1.506(3)
C(12)-C(13)	1.529(3)
C(13)-C(14)	1.525(3)
C(14)-C(19)	1.533(3)
C(15)-C(16)	1.323(3)
C(11)-C(1)-C(2)	114.44(15)
C(11)-C(1)-C(8)	104.31(15)
C(2)-C(1)-C(8)	117.31(14)
C(3)-C(2)-C(20)	101.42(15)
C(3)-C(2)-C(1)	113.58(15)
C(20)-C(2)-C(1)	110.52(16)
C(3)-C(2)-C(14)	112.27(15)
C(20)-C(2)-C(14)	112.73(15)
C(1)-C(2)-C(14)	106.45(15)
O(1)-C(3)-C(4)	118.49(17)
O(1)-C(3)-C(2)	120.01(17)
C(4)-C(3)-C(2)	121.34(15)

C(3)-C(4)-C(5)	111.59(15)
C(15)-C(5)-C(6)	109.91(15)
C(15)-C(5)-C(17)	111.67(16)
C(6)-C(5)-C(17)	108.56(16)
C(15)-C(5)-C(4)	109.95(15)
C(6)-C(5)-C(4)	107.75(14)
C(17)-C(5)-C(4)	108.90(15)
O(2)-C(6)-C(7)	119.97(18)
O(2)-C(6)-C(5)	120.87(17)
C(7)-C(6)-C(5)	119.13(15)
C(6)-C(7)-C(18)	105.94(16)
C(6)-C(7)-C(8)	114.97(14)
C(18)-C(7)-C(8)	112.88(17)
C(12)-C(8)-C(9)	108.56(16)
C(12)-C(8)-C(1)	110.99(14)
C(9)-C(8)-C(1)	101.98(16)
C(12)-C(8)-C(7)	113.81(16)
C(9)-C(8)-C(7)	107.52(15)
C(1)-C(8)-C(7)	113.15(15)
C(10)-C(9)-C(8)	105.61(17)
C(11)-C(10)-C(9)	104.80(17)
O(3)-C(11)-C(10)	124.37(19)
O(3)-C(11)-C(1)	126.3(2)
C(10)-C(11)-C(1)	109.30(17)
C(13)-C(12)-C(8)	115.91(15)

C(14)-C(13)-C(12)	112.91(15)
C(13)-C(14)-C(19)	111.68(17)
C(13)-C(14)-C(2)	108.47(14)
C(19)-C(14)-C(2)	117.30(17)
C(16)-C(15)-C(5)	125.96(19)

---

Table 4. Anisotropic displacement parameters ( $\text{\AA}^2 \times 10^3$ ) for svp38. The anisotropic displacement factor exponent takes the form:  $-2\pi^2 [h^2 a^{*2}U^{11} + \dots + 2 h k a^* b^* U^{12}]$

	U <sup>11</sup>	U <sup>22</sup>	U <sup>33</sup>	U <sup>23</sup>	U <sup>13</sup>	U <sup>12</sup>
O(1)	25(1)	29(1)	63(1)	10(1)	26(1)	7(1)
O(2)	29(1)	25(1)	21(1)	-2(1)	4(1)	-5(1)
O(3)	35(1)	29(1)	57(1)	-5(1)	7(1)	-13(1)
C(1)	17(1)	16(1)	23(1)	3(1)	5(1)	-2(1)
C(2)	22(1)	17(1)	21(1)	-1(1)	10(1)	0(1)
C(3)	22(1)	21(1)	23(1)	-1(1)	14(1)	2(1)
C(4)	21(1)	22(1)	18(1)	2(1)	8(1)	-3(1)
C(5)	17(1)	18(1)	21(1)	2(1)	5(1)	-1(1)
C(6)	21(1)	12(1)	22(1)	-2(1)	6(1)	1(1)
C(7)	22(1)	17(1)	28(1)	2(1)	12(1)	4(1)
C(8)	18(1)	19(1)	28(1)	3(1)	14(1)	2(1)
C(9)	23(1)	29(1)	55(2)	9(1)	24(1)	6(1)
C(10)	20(1)	31(1)	63(2)	10(1)	20(1)	-2(1)

C(11)	17(1)	20(1)	42(1)	7(1)	2(1)	-1(1)
C(12)	29(1)	24(1)	23(1)	3(1)	14(1)	0(1)
C(13)	21(1)	22(1)	21(1)	6(1)	3(1)	1(1)
C(14)	19(1)	17(1)	27(1)	4(1)	10(1)	2(1)
C(15)	19(1)	29(1)	24(1)	0(1)	6(1)	-1(1)
C(16)	23(1)	36(1)	32(1)	-3(1)	10(1)	-9(1)
C(17)	24(1)	21(1)	36(1)	8(1)	9(1)	0(1)
C(18)	41(1)	24(1)	45(1)	0(1)	28(1)	6(1)
C(19)	31(1)	27(1)	48(1)	9(1)	19(1)	11(1)
C(20)	46(1)	26(1)	28(1)	-7(1)	17(1)	-3(1)

---

Table 5. Hydrogen coordinates ( $\times 10^4$ ) and isotropic displacement parameters ( $\text{\AA}^2 \times 10^3$ ) for svp38.

---

	x	y	z	U(eq)
H(1A)	6940	3367	6289	23
H(4A)	3972	2615	7079	24
H(4B)	5550	2713	6735	24
H(7A)	6676	2297	5262	26
H(9A)	8810	2977	4875	39
H(9B)	8145	3263	3407	39
H(10A)	9830	4097	5220	44

H(10B)	8398	4426	4031	44
H(12A)	5891	4023	2808	29
H(12B)	4919	3300	2372	29
H(13A)	3293	4305	2443	27
H(13B)	3062	3637	3265	27
H(14A)	5069	4811	4388	25
H(15A)	1421	2375	4485	29
H(16A)	1924	1029	5622	36
H(16B)	206	1410	4872	36
H(17A)	5878	1487	6196	41
H(17B)	4420	1019	5313	41
H(17C)	4483	1275	6718	41
H(18A)	7607	1997	3611	50
H(18B)	5975	2217	2517	50
H(18C)	6056	1524	3386	50
H(19A)	3084	5234	5185	50
H(19B)	1886	4657	4301	50
H(19C)	2559	5281	3642	50
H(20A)	5827	4868	6883	48
H(20B)	5928	4132	7644	48
H(20C)	4266	4533	7038	48

---

Table 6. Torsion angles [°] for svp38.

---

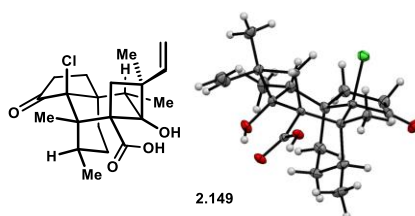


C(11)-C(1)-C(2)-C(3)	-169.33(17)
C(8)-C(1)-C(2)-C(3)	68.0(2)
C(11)-C(1)-C(2)-C(20)	-56.1(2)
C(8)-C(1)-C(2)-C(20)	-178.82(15)
C(11)-C(1)-C(2)-C(14)	66.61(19)
C(8)-C(1)-C(2)-C(14)	-56.09(19)
C(20)-C(2)-C(3)-O(1)	84.1(2)
C(1)-C(2)-C(3)-O(1)	-157.36(19)
C(14)-C(2)-C(3)-O(1)	-36.5(2)
C(20)-C(2)-C(3)-C(4)	-91.2(2)
C(1)-C(2)-C(3)-C(4)	27.3(2)
C(14)-C(2)-C(3)-C(4)	148.18(17)
O(1)-C(3)-C(4)-C(5)	70.8(2)
C(2)-C(3)-C(4)-C(5)	-113.86(18)
C(3)-C(4)-C(5)-C(15)	-68.4(2)
C(3)-C(4)-C(5)-C(6)	51.37(19)
C(3)-C(4)-C(5)-C(17)	168.94(15)
C(15)-C(5)-C(6)-O(2)	-5.8(2)
C(17)-C(5)-C(6)-O(2)	116.66(18)
C(4)-C(5)-C(6)-O(2)	-125.55(17)
C(15)-C(5)-C(6)-C(7)	176.53(15)
C(17)-C(5)-C(6)-C(7)	-61.1(2)
C(4)-C(5)-C(6)-C(7)	56.7(2)
O(2)-C(6)-C(7)-C(18)	-48.9(2)
C(5)-C(6)-C(7)-C(18)	128.85(17)

O(2)-C(6)-C(7)-C(8)	76.5(2)
C(5)-C(6)-C(7)-C(8)	-105.76(19)
C(11)-C(1)-C(8)-C(12)	-85.24(17)
C(2)-C(1)-C(8)-C(12)	42.5(2)
C(11)-C(1)-C(8)-C(9)	30.22(18)
C(2)-C(1)-C(8)-C(9)	157.98(15)
C(11)-C(1)-C(8)-C(7)	145.40(15)
C(2)-C(1)-C(8)-C(7)	-86.84(19)
C(6)-C(7)-C(8)-C(12)	-50.5(2)
C(18)-C(7)-C(8)-C(12)	71.2(2)
C(6)-C(7)-C(8)-C(9)	-170.76(18)
C(18)-C(7)-C(8)-C(9)	-49.1(2)
C(6)-C(7)-C(8)-C(1)	77.4(2)
C(18)-C(7)-C(8)-C(1)	-160.89(16)
C(12)-C(8)-C(9)-C(10)	79.2(2)
C(1)-C(8)-C(9)-C(10)	-38.0(2)
C(7)-C(8)-C(9)-C(10)	-157.27(19)
C(8)-C(9)-C(10)-C(11)	30.6(2)
C(9)-C(10)-C(11)-O(3)	166.3(2)
C(9)-C(10)-C(11)-C(1)	-11.0(2)
C(2)-C(1)-C(11)-O(3)	40.7(3)
C(8)-C(1)-C(11)-O(3)	170.22(19)
C(2)-C(1)-C(11)-C(10)	-142.07(17)
C(8)-C(1)-C(11)-C(10)	-12.6(2)
C(9)-C(8)-C(12)-C(13)	-148.12(18)

C(1)-C(8)-C(12)-C(13)	-36.8(2)
C(7)-C(8)-C(12)-C(13)	92.2(2)
C(8)-C(12)-C(13)-C(14)	48.7(2)
C(12)-C(13)-C(14)-C(19)	167.36(16)
C(12)-C(13)-C(14)-C(2)	-61.9(2)
C(3)-C(2)-C(14)-C(13)	-61.79(19)
C(20)-C(2)-C(14)-C(13)	-175.58(15)
C(1)-C(2)-C(14)-C(13)	63.08(18)
C(3)-C(2)-C(14)-C(19)	65.9(2)
C(20)-C(2)-C(14)-C(19)	-47.9(2)
C(1)-C(2)-C(14)-C(19)	-169.27(17)
C(6)-C(5)-C(15)-C(16)	126.9(2)
C(17)-C(5)-C(15)-C(16)	6.4(3)
C(4)-C(5)-C(15)-C(16)	-114.6(2)

---



Crystal structure provided by Dr. Joseph Ziller (University of California, Irvine, California, United States of America). Thermal ellipsoids are drawn at 50% probability level.

Table 1. Crystal data and structure refinement for svp39.

Identification code	svp39 (Nick Foy)
Empirical formula	C <sub>21</sub> H <sub>29</sub> Cl O <sub>4</sub>
Formula weight	380.89

Temperature	93(2) K	
Wavelength	1.54178 Å	
Crystal system	Monoclinic	
Space group	<i>C2/c</i>	
Unit cell dimensions	a = 26.331(2) Å	$\alpha = 90^\circ$ .
	b = 10.6739(8) Å	$\beta = 112.157(3)^\circ$ .
	c = 14.3569(10) Å	$\gamma = 90^\circ$ .
Volume	3737.0(5) Å <sup>3</sup>	
Z	8	
Density (calculated)	1.354 Mg/m <sup>3</sup>	
Absorption coefficient	2.004 mm <sup>-1</sup>	
F(000)	1632	
Crystal color	colorless	
Crystal size	0.241 x 0.206 x 0.106 mm <sup>3</sup>	
Theta range for data collection	3.625 to 68.798°	
Index ranges	$-31 \leq h \leq 31, -12 \leq k \leq 12, -16 \leq l \leq 17$	
Reflections collected	37465	
Independent reflections	3429 [R(int) = 0.0449]	
Completeness to theta = 67.679°	99.9 %	
Absorption correction	Semi-empirical from equivalents	
Max. and min. transmission	0.6614 and 0.5595	
Refinement method	Full-matrix least-squares on F <sup>2</sup>	
Data / restraints / parameters	3429 / 2 / 247	
Goodness-of-fit on F <sup>2</sup>	1.053	
Final R indices [ $I > 2\sigma(I)$ = 3347 data]	R1 = 0.0480, wR2 = 0.1290	

R indices (all data, 0.83 Å)

R1 = 0.0486, wR2 = 0.1295

Largest diff. peak and hole

0.721 and -0.667 e.Å<sup>-3</sup>

Table 2. Atomic coordinates ( $\times 10^4$ ) and equivalent isotropic displacement parameters ( $\text{Å}^2 \times 10^3$ )

for svp39. U(eq) is defined as one third of the trace of the orthogonalized  $U^{ij}$  tensor.

	x	y	z	U(eq)
Cl(1)	7376(1)	7891(1)	7752(1)	22(1)
O(1)	5201(1)	5663(1)	6061(1)	19(1)
O(2)	5728(1)	5416(1)	5174(1)	16(1)
O(3)	5637(1)	6144(2)	7999(1)	21(1)
O(4)	6781(1)	10395(2)	6523(1)	28(1)
C(1)	6148(1)	6398(2)	6776(1)	12(1)
C(2)	6611(1)	5378(2)	7060(2)	15(1)
C(3)	6441(1)	4891(2)	7914(2)	18(1)
C(4)	6144(1)	6197(2)	7880(1)	15(1)
C(5)	6505(1)	7151(2)	8654(2)	17(1)
C(6)	6468(1)	8481(2)	8223(2)	16(1)
C(7)	5893(1)	9099(2)	7849(2)	22(1)
C(8)	5478(1)	8688(2)	6821(2)	22(1)
C(9)	5733(1)	8595(2)	6028(2)	19(1)
C(10)	6260(1)	7742(2)	6412(1)	14(1)
C(11)	6655(1)	8468(2)	7336(1)	13(1)
C(12)	6801(1)	9864(2)	7248(2)	21(1)

C(13)	6983(1)	10409(2)	8310(2)	24(1)
C(14)	6874(1)	9397(2)	8970(2)	19(1)
C(15)	5644(1)	5799(2)	5977(2)	14(1)
C(16)	6917(1)	4494(2)	8881(2)	24(1)
C(17)	6035(1)	3819(2)	7628(2)	22(1)
C(18)	5988(1)	2938(2)	6957(2)	27(1)
C(19)	6398(1)	7116(2)	9633(2)	27(1)
C(20)	5296(1)	8282(2)	4987(2)	28(1)
C(21)	6502(1)	7621(2)	5599(2)	18(1)

---

Table 3. Bond lengths [Å] and angles [°] for svp39.

---

Cl(1)-C(11)	1.866(2)
O(1)-C(15)	1.225(3)
O(2)-C(15)	1.319(2)
O(2)-H(2)	0.821(18)
O(3)-C(4)	1.410(2)
O(3)-H(3)	0.823(17)
O(4)-C(12)	1.169(3)
C(1)-C(15)	1.529(3)
C(1)-C(2)	1.568(3)
C(1)-C(10)	1.592(3)
C(1)-C(4)	1.604(3)
C(2)-C(3)	1.545(3)

C(2)-H(2A)	0.9900
C(2)-H(2B)	0.9900
C(3)-C(17)	1.513(3)
C(3)-C(16)	1.537(3)
C(3)-C(4)	1.590(3)
C(4)-C(5)	1.542(3)
C(5)-C(19)	1.534(3)
C(5)-C(6)	1.537(3)
C(5)-H(5A)	1.0000
C(6)-C(11)	1.530(3)
C(6)-C(14)	1.545(3)
C(6)-C(7)	1.551(3)
C(7)-C(8)	1.532(3)
C(7)-H(7A)	0.9900
C(7)-H(7B)	0.9900
C(8)-C(9)	1.527(3)
C(8)-H(8A)	0.9900
C(8)-H(8B)	0.9900
C(9)-C(20)	1.541(3)
C(9)-C(10)	1.575(3)
C(9)-H(9A)	1.0000
C(10)-C(21)	1.532(3)
C(10)-C(11)	1.550(3)
C(11)-C(12)	1.555(3)
C(12)-C(13)	1.531(3)

C(13)-C(14)	1.533(3)
C(13)-H(13A)	0.9900
C(13)-H(13B)	0.9900
C(14)-H(14A)	0.9900
C(14)-H(14B)	0.9900
C(16)-H(16A)	0.9800
C(16)-H(16B)	0.9800
C(16)-H(16C)	0.9800
C(17)-C(18)	1.318(3)
C(17)-H(17A)	0.9500
C(18)-H(18A)	0.9500
C(18)-H(18B)	0.9500
C(19)-H(19A)	0.9800
C(19)-H(19B)	0.9800
C(19)-H(19C)	0.9800
C(20)-H(20A)	0.9800
C(20)-H(20B)	0.9800
C(20)-H(20C)	0.9800
C(21)-H(21A)	0.9800
C(21)-H(21B)	0.9800
C(21)-H(21C)	0.9800
C(15)-O(2)-H(2)	106(2)
C(4)-O(3)-H(3)	108.2(19)
C(15)-C(1)-C(2)	105.92(15)



C(15)-C(1)-C(10)	110.22(15)
C(2)-C(1)-C(10)	119.32(16)
C(15)-C(1)-C(4)	110.97(15)
C(2)-C(1)-C(4)	86.84(14)
C(10)-C(1)-C(4)	121.06(15)
C(3)-C(2)-C(1)	90.62(15)
C(3)-C(2)-H(2A)	113.5
C(1)-C(2)-H(2A)	113.5
C(3)-C(2)-H(2B)	113.5
C(1)-C(2)-H(2B)	113.5
H(2A)-C(2)-H(2B)	110.8
C(17)-C(3)-C(16)	106.70(18)
C(17)-C(3)-C(2)	115.17(17)
C(16)-C(3)-C(2)	115.37(17)
C(17)-C(3)-C(4)	111.47(17)
C(16)-C(3)-C(4)	119.54(17)
C(2)-C(3)-C(4)	88.13(15)
O(3)-C(4)-C(5)	107.07(16)
O(3)-C(4)-C(3)	116.03(16)
C(5)-C(4)-C(3)	113.23(17)
O(3)-C(4)-C(1)	119.03(16)
C(5)-C(4)-C(1)	113.06(15)
C(3)-C(4)-C(1)	87.72(14)
C(19)-C(5)-C(6)	112.69(18)
C(19)-C(5)-C(4)	111.59(17)

C(6)-C(5)-C(4)	113.03(16)
C(19)-C(5)-H(5A)	106.3
C(6)-C(5)-H(5A)	106.3
C(4)-C(5)-H(5A)	106.3
C(11)-C(6)-C(5)	109.62(16)
C(11)-C(6)-C(14)	103.18(16)
C(5)-C(6)-C(14)	112.49(17)
C(11)-C(6)-C(7)	107.17(16)
C(5)-C(6)-C(7)	115.95(17)
C(14)-C(6)-C(7)	107.56(17)
C(8)-C(7)-C(6)	117.35(17)
C(8)-C(7)-H(7A)	108.0
C(6)-C(7)-H(7A)	108.0
C(8)-C(7)-H(7B)	108.0
C(6)-C(7)-H(7B)	108.0
H(7A)-C(7)-H(7B)	107.2
C(9)-C(8)-C(7)	112.51(17)
C(9)-C(8)-H(8A)	109.1
C(7)-C(8)-H(8A)	109.1
C(9)-C(8)-H(8B)	109.1
C(7)-C(8)-H(8B)	109.1
H(8A)-C(8)-H(8B)	107.8
C(8)-C(9)-C(20)	111.05(19)
C(8)-C(9)-C(10)	110.66(17)
C(20)-C(9)-C(10)	116.84(17)

C(8)-C(9)-H(9A)	105.8
C(20)-C(9)-H(9A)	105.8
C(10)-C(9)-H(9A)	105.8
C(21)-C(10)-C(11)	110.81(16)
C(21)-C(10)-C(9)	110.24(16)
C(11)-C(10)-C(9)	103.24(15)
C(21)-C(10)-C(1)	110.86(16)
C(11)-C(10)-C(1)	108.51(15)
C(9)-C(10)-C(1)	112.92(16)
C(6)-C(11)-C(10)	113.17(16)
C(6)-C(11)-C(12)	103.04(16)
C(10)-C(11)-C(12)	121.08(17)
C(6)-C(11)-Cl(1)	110.16(13)
C(10)-C(11)-Cl(1)	112.52(13)
C(12)-C(11)-Cl(1)	95.15(12)
O(4)-C(12)-C(13)	126.5(2)
O(4)-C(12)-C(11)	127.4(2)
C(13)-C(12)-C(11)	106.10(17)
C(12)-C(13)-C(14)	106.65(17)
C(12)-C(13)-H(13A)	110.4
C(14)-C(13)-H(13A)	110.4
C(12)-C(13)-H(13B)	110.4
C(14)-C(13)-H(13B)	110.4
H(13A)-C(13)-H(13B)	108.6
C(13)-C(14)-C(6)	104.98(16)

C(13)-C(14)-H(14A)	110.8
C(6)-C(14)-H(14A)	110.8
C(13)-C(14)-H(14B)	110.8
C(6)-C(14)-H(14B)	110.8
H(14A)-C(14)-H(14B)	108.8
O(1)-C(15)-O(2)	121.93(18)
O(1)-C(15)-C(1)	124.40(18)
O(2)-C(15)-C(1)	113.66(16)
C(3)-C(16)-H(16A)	109.5
C(3)-C(16)-H(16B)	109.5
H(16A)-C(16)-H(16B)	109.5
C(3)-C(16)-H(16C)	109.5
H(16A)-C(16)-H(16C)	109.5
H(16B)-C(16)-H(16C)	109.5
C(18)-C(17)-C(3)	126.9(2)
C(18)-C(17)-H(17A)	116.6
C(3)-C(17)-H(17A)	116.6
C(17)-C(18)-H(18A)	120.0
C(17)-C(18)-H(18B)	120.0
H(18A)-C(18)-H(18B)	120.0
C(5)-C(19)-H(19A)	109.5
C(5)-C(19)-H(19B)	109.5
H(19A)-C(19)-H(19B)	109.5
C(5)-C(19)-H(19C)	109.5
H(19A)-C(19)-H(19C)	109.5

H(19B)-C(19)-H(19C)	109.5
C(9)-C(20)-H(20A)	109.5
C(9)-C(20)-H(20B)	109.5
H(20A)-C(20)-H(20B)	109.5
C(9)-C(20)-H(20C)	109.5
H(20A)-C(20)-H(20C)	109.5
H(20B)-C(20)-H(20C)	109.5
C(10)-C(21)-H(21A)	109.5
C(10)-C(21)-H(21B)	109.5
H(21A)-C(21)-H(21B)	109.5
C(10)-C(21)-H(21C)	109.5
H(21A)-C(21)-H(21C)	109.5
H(21B)-C(21)-H(21C)	109.5

---

Table 4. Anisotropic displacement parameters ( $\text{\AA}^2 \times 10^3$ ) for svp39. The anisotropic displacement factor exponent takes the form:  $-2\sigma^2 [ h^2 a^2 U^{11} + \dots + 2 h k a^* b^* U^{12} ]$

	$U^{11}$	$U^{22}$	$U^{33}$	$U^{23}$	$U^{13}$	$U^{12}$
Cl(1)	17(1)	24(1)	23(1)	-2(1)	5(1)	-2(1)
O(1)	13(1)	25(1)	19(1)	-9(1)	5(1)	-5(1)
O(2)	14(1)	20(1)	12(1)	-6(1)	2(1)	-4(1)
O(3)	18(1)	30(1)	18(1)	-9(1)	12(1)	-9(1)
O(4)	36(1)	17(1)	23(1)	-1(1)	3(1)	-4(1)

C(1)	12(1)	14(1)	10(1)	-3(1)	3(1)	-2(1)
C(2)	13(1)	17(1)	13(1)	0(1)	4(1)	1(1)
C(3)	20(1)	18(1)	12(1)	-1(1)	4(1)	-4(1)
C(4)	17(1)	19(1)	12(1)	-2(1)	7(1)	-6(1)
C(5)	21(1)	20(1)	10(1)	-4(1)	7(1)	-8(1)
C(6)	17(1)	18(1)	13(1)	-5(1)	7(1)	-6(1)
C(7)	20(1)	24(1)	24(1)	-7(1)	10(1)	-2(1)
C(8)	15(1)	22(1)	26(1)	-4(1)	5(1)	2(1)
C(9)	20(1)	15(1)	18(1)	-1(1)	1(1)	2(1)
C(10)	15(1)	14(1)	11(1)	-1(1)	3(1)	-3(1)
C(11)	12(1)	12(1)	14(1)	-1(1)	4(1)	-2(1)
C(12)	18(1)	18(1)	28(1)	-7(1)	12(1)	-7(1)
C(13)	28(1)	20(1)	23(1)	-6(1)	9(1)	-8(1)
C(14)	21(1)	20(1)	16(1)	-8(1)	7(1)	-7(1)
C(15)	14(1)	11(1)	13(1)	0(1)	2(1)	0(1)
C(16)	28(1)	24(1)	15(1)	4(1)	2(1)	-2(1)
C(17)	24(1)	21(1)	22(1)	3(1)	7(1)	-4(1)
C(18)	34(1)	18(1)	25(1)	0(1)	5(1)	-5(1)
C(19)	41(1)	30(1)	14(1)	-7(1)	14(1)	-14(1)
C(20)	26(1)	23(1)	22(1)	-1(1)	-4(1)	6(1)
C(21)	23(1)	19(1)	13(1)	-1(1)	8(1)	-4(1)

---

Table 5. Hydrogen coordinates ( $\times 10^4$ ) and isotropic displacement parameters ( $\text{\AA}^2 \times 10^3$ )

for svp39.

---

	x	y	z	U(eq)
H(2)	5442(9)	5080(30)	4810(20)	38(8)
H(3)	5401(9)	5910(30)	7463(15)	24(7)
H(2A)	6559	4755	6521	18
H(2B)	6986	5733	7302	18
H(5A)	6893	6873	8833	20
H(7A)	5729	8935	8356	26
H(7B)	5942	10017	7828	26
H(8A)	5325	7861	6890	26
H(8B)	5172	9296	6592	26
H(9A)	5866	9457	5967	23
H(13A)	6771	11176	8309	29
H(13B)	7377	10625	8567	29
H(14A)	6712	9768	9427	23
H(14B)	7219	8962	9379	23
H(16A)	7201	5142	9071	37
H(16B)	7071	3702	8764	37
H(16C)	6781	4384	9424	37
H(17A)	5789	3776	7969	27
H(18A)	6225	2938	6596	33
H(18B)	5718	2304	6835	33
H(19A)	6413	6248	9862	41

---

H(19B)	6035	7468	9513	41
H(19C)	6678	7612	10149	41
H(20A)	5470	8221	4493	42
H(20B)	5018	8945	4783	42
H(20C)	5122	7481	5021	42
H(21A)	6232	7229	4999	27
H(21B)	6833	7103	5852	27
H(21C)	6595	8455	5426	27

---

Table 6. Torsion angles [°] for svp39.

---

C(15)-C(1)-C(2)-C(3)	-91.36(16)
C(10)-C(1)-C(2)-C(3)	143.72(16)
C(4)-C(1)-C(2)-C(3)	19.56(14)
C(1)-C(2)-C(3)-C(17)	93.20(19)
C(1)-C(2)-C(3)-C(16)	-141.75(18)
C(1)-C(2)-C(3)-C(4)	-19.71(14)
C(17)-C(3)-C(4)-O(3)	24.3(2)
C(16)-C(3)-C(4)-O(3)	-101.0(2)
C(2)-C(3)-C(4)-O(3)	140.68(17)
C(17)-C(3)-C(4)-C(5)	148.71(17)
C(16)-C(3)-C(4)-C(5)	23.4(2)
C(2)-C(3)-C(4)-C(5)	-94.91(17)
C(17)-C(3)-C(4)-C(1)	-97.11(17)
C(16)-C(3)-C(4)-C(1)	137.58(19)



C(2)-C(3)-C(4)-C(1)	19.27(14)
C(15)-C(1)-C(4)-O(3)	-31.8(2)
C(2)-C(1)-C(4)-O(3)	-137.69(18)
C(10)-C(1)-C(4)-O(3)	99.7(2)
C(15)-C(1)-C(4)-C(5)	-158.80(17)
C(2)-C(1)-C(4)-C(5)	95.35(18)
C(10)-C(1)-C(4)-C(5)	-27.3(3)
C(15)-C(1)-C(4)-C(3)	86.86(17)
C(2)-C(1)-C(4)-C(3)	-18.99(14)
C(10)-C(1)-C(4)-C(3)	-141.63(17)
O(3)-C(4)-C(5)-C(19)	34.9(2)
C(3)-C(4)-C(5)-C(19)	-94.3(2)
C(1)-C(4)-C(5)-C(19)	167.91(18)
O(3)-C(4)-C(5)-C(6)	-93.38(19)
C(3)-C(4)-C(5)-C(6)	137.47(17)
C(1)-C(4)-C(5)-C(6)	39.7(2)
C(19)-C(5)-C(6)-C(11)	172.29(17)
C(4)-C(5)-C(6)-C(11)	-60.0(2)
C(19)-C(5)-C(6)-C(14)	58.1(2)
C(4)-C(5)-C(6)-C(14)	-174.22(17)
C(19)-C(5)-C(6)-C(7)	-66.3(2)
C(4)-C(5)-C(6)-C(7)	61.4(2)
C(11)-C(6)-C(7)-C(8)	44.6(2)
C(5)-C(6)-C(7)-C(8)	-78.2(2)
C(14)-C(6)-C(7)-C(8)	154.95(19)

C(6)-C(7)-C(8)-C(9)	-43.8(3)
C(7)-C(8)-C(9)-C(20)	-175.51(18)
C(7)-C(8)-C(9)-C(10)	53.0(2)
C(8)-C(9)-C(10)-C(21)	178.22(17)
C(20)-C(9)-C(10)-C(21)	49.8(2)
C(8)-C(9)-C(10)-C(11)	-63.4(2)
C(20)-C(9)-C(10)-C(11)	168.24(19)
C(8)-C(9)-C(10)-C(1)	53.6(2)
C(20)-C(9)-C(10)-C(1)	-74.8(2)
C(15)-C(1)-C(10)-C(21)	-74.4(2)
C(2)-C(1)-C(10)-C(21)	48.5(2)
C(4)-C(1)-C(10)-C(21)	153.81(17)
C(15)-C(1)-C(10)-C(11)	163.74(16)
C(2)-C(1)-C(10)-C(11)	-73.4(2)
C(4)-C(1)-C(10)-C(11)	31.9(2)
C(15)-C(1)-C(10)-C(9)	49.9(2)
C(2)-C(1)-C(10)-C(9)	172.75(16)
C(4)-C(1)-C(10)-C(9)	-81.9(2)
C(5)-C(6)-C(11)-C(10)	67.7(2)
C(14)-C(6)-C(11)-C(10)	-172.32(16)
C(7)-C(6)-C(11)-C(10)	-59.0(2)
C(5)-C(6)-C(11)-C(12)	-159.85(16)
C(14)-C(6)-C(11)-C(12)	-39.8(2)
C(7)-C(6)-C(11)-C(12)	73.55(19)
C(5)-C(6)-C(11)-C(1)	-59.29(18)

C(14)-C(6)-C(11)-Cl(1)	60.75(18)
C(7)-C(6)-C(11)-Cl(1)	174.11(13)
C(21)-C(10)-C(11)-C(6)	-173.03(17)
C(9)-C(10)-C(11)-C(6)	68.9(2)
C(1)-C(10)-C(11)-C(6)	-51.1(2)
C(21)-C(10)-C(11)-C(12)	64.0(2)
C(9)-C(10)-C(11)-C(12)	-54.1(2)
C(1)-C(10)-C(11)-C(12)	-174.10(16)
C(21)-C(10)-C(11)-Cl(1)	-47.35(19)
C(9)-C(10)-C(11)-Cl(1)	-165.36(13)
C(1)-C(10)-C(11)-Cl(1)	74.59(17)
C(6)-C(11)-C(12)-O(4)	-151.5(2)
C(10)-C(11)-C(12)-O(4)	-23.8(3)
Cl(1)-C(11)-C(12)-O(4)	96.4(2)
C(6)-C(11)-C(12)-C(13)	29.1(2)
C(10)-C(11)-C(12)-C(13)	156.78(18)
Cl(1)-C(11)-C(12)-C(13)	-83.00(16)
O(4)-C(12)-C(13)-C(14)	173.6(2)
C(11)-C(12)-C(13)-C(14)	-6.9(2)
C(12)-C(13)-C(14)-C(6)	-17.8(2)
C(11)-C(6)-C(14)-C(13)	36.0(2)
C(5)-C(6)-C(14)-C(13)	154.08(18)
C(7)-C(6)-C(14)-C(13)	-77.0(2)
C(2)-C(1)-C(15)-O(1)	121.3(2)
C(10)-C(1)-C(15)-O(1)	-108.4(2)

C(4)-C(1)-C(15)-O(1)	28.5(3)
C(2)-C(1)-C(15)-O(2)	-57.9(2)
C(10)-C(1)-C(15)-O(2)	72.5(2)
C(4)-C(1)-C(15)-O(2)	-150.65(17)
C(16)-C(3)-C(17)-C(18)	-98.3(3)
C(2)-C(3)-C(17)-C(18)	31.1(3)
C(4)-C(3)-C(17)-C(18)	129.5(2)

Table 7. Hydrogen bonds for svp39 [ $\text{\AA}$  and  $^\circ$ ].

D-H...A	d(D-H)	d(H...A)	d(D...A)	$\angle$ (DHA)
O(2)-H(2)...O(1)#1	0.821(18)	1.860(18)	2.6806(19)	178(3)
O(3)-H(3)...O(1)	0.823(17)	1.90(2)	2.629(2)	148(3)
O(3)-H(3)...O(3)#2	0.823(17)	2.57(2)	3.110(3)	124(2)

Symmetry transformations used to generate equivalent atoms:

#1 -x+1,-y+1,-z+1 #2 -x+1,y,-z+3/2

## Appendix D. Spectra for Chapter 3

